



National Library  
of Canada

Acquisitions and  
Bibliographic Services Branch

395 Wellington Street  
Ottawa, Ontario  
K1A 0N4

Bibliothèque nationale  
du Canada

Direction des acquisitions et  
des services bibliographiques

395, rue Wellington  
Ottawa (Ontario)  
K1A 0N4

*Your file* *Votre référence*

*Our file* *Notre référence*

## NOTICE

The quality of this microform is heavily dependent upon the quality of the original thesis submitted for microfilming. Every effort has been made to ensure the highest quality of reproduction possible.

If pages are missing, contact the university which granted the degree.

Some pages may have indistinct print especially if the original pages were typed with a poor typewriter ribbon or if the university sent us an inferior photocopy.

Reproduction in full or in part of this microform is governed by the Canadian Copyright Act, R.S.C. 1970, c. C-30, and subsequent amendments.

## AVIS

La qualité de cette microforme dépend grandement de la qualité de la thèse soumise au microfilmage. Nous avons tout fait pour assurer une qualité supérieure de reproduction.

S'il manque des pages, veuillez communiquer avec l'université qui a conféré le grade.

La qualité d'impression de certaines pages peut laisser à désirer, surtout si les pages originales ont été dactylographiées à l'aide d'un ruban usé ou si l'université nous a fait parvenir une photocopie de qualité inférieure.

La reproduction, même partielle, de cette microforme est soumise à la Loi canadienne sur le droit d'auteur, SRC 1970, c. C-30, et ses amendements subséquents.

**THE BEHAVIOUR OF MALLEABLE METALS  
IN TUMBLING MILLS**

**Mohammad Noaparast**

Department of Mining and Metallurgical Engineering  
McGill University  
Montreal, Canada

February, 1996

A thesis submitted to the Faculty of Graduate Studies and Research  
in partial fulfilment of the requirements for the degree of  
Doctor of Philosophy

©Mohammad Noaparast, 1996



National Library  
of Canada

Acquisitions and  
Bibliographic Services Branch

395 Wellington Street  
Ottawa, Ontario  
K1A 0N4

Bibliothèque nationale  
du Canada

Direction des acquisitions et  
des services bibliographiques

395, rue Wellington  
Ottawa (Ontario)  
K1A 0N4

*Your file* *Votre référence*

*Our file* *Notre référence*

The author has granted an irrevocable non-exclusive licence allowing the National Library of Canada to reproduce, loan, distribute or sell copies of his/her thesis by any means and in any form or format, making this thesis available to interested persons.

L'auteur a accordé une licence irrévocable et non exclusive permettant à la Bibliothèque nationale du Canada de reproduire, prêter, distribuer ou vendre des copies de sa thèse de quelque manière et sous quelque forme que ce soit pour mettre des exemplaires de cette thèse à la disposition des personnes intéressées.

The author retains ownership of the copyright in his/her thesis. Neither the thesis nor substantial extracts from it may be printed or otherwise reproduced without his/her permission.

L'auteur conserve la propriété du droit d'auteur qui protège sa thèse. Ni la thèse ni des extraits substantiels de celle-ci ne doivent être imprimés ou autrement reproduits sans son autorisation.

ISBN 0-612-12451-7

Canada

---

**Abstract**

The objective of this work was to investigate the behaviour of malleable metals in tumbling mills. Much of the work focused on lead: shots, flattened shots and fragments were ground in three different laboratory mills. Testwork with fragments was repeated in the presence of a brittle and harder mineral phase (95 % silica, 5 % lead) and for copper (100% copper). The transfer of particles across size classes and the loss of weight because of smearing on the mill shell and grinding media were measured. Microhardness tests confirmed that lead did not work-harden during grinding.

The transfer across size classes was modelled with various first order differential equations describing flattening, folding, cold-welding and actual breakage. Model parameters were estimated using a least-square minimization criterion. When more than one model was fitted to a given data set, the one whose phenomenological basis was closest to the dominant transfer mechanisms observed almost always yielded the best data fit. The dominant mechanism was very dependent on the type of metal ground, its particle size and shape, the grinding intensity generated by the tumbling mill and the presence of a hard, brittle phase. Flattening, responsible for the transfer to coarser size classes, generally dominated over folding, the mechanism accountable for the transfer to finer size classes (other than breakage). Breakage was favoured over flattening and folding when grinding finer and softer particles, in a high impact environment, or in the presence of a hard, brittle mineral phase. Loss of weight due to smearing significantly increased when grinding a softer mineral in a mill with a rough inner shell, or when particle breakage took place.

A methodology based on the Laboratory Knelson Concentrator was developed and tested to estimate the breakage function and gravity recoverability of gold flakes. Progeny from the breakage of gold particles was shown to be highly gravity recoverable, more than 90% above 0.025 mm. The breakage function was non-normalizable, with a large  $b_{i+1,i}$  component, because of folding.

---

## Résumé

Ce travail avait comme objectif l'étude du comportement des métaux malléables dans les broyeurs. Le gros du travail s'est fait avec des particules de plomb (sphères, sphères aplaties et fragments) qui furent broyées dans trois broyeurs de laboratoire.

Les essais faits avec les fragments de plomb le furent également en présence d'une phase dominante d'un minéral fragile et dur, de même qu'avec des fragments de cuivre, un métal plus dur que le plomb. On a mesuré la distribution granulométrique du produit de même que la perte de poids due au recouvrement du métal malléable à la surface des corps broyants et de la virole du broyeur. On a vérifié à l'aide d'essais de microdureté que le plomb ne s'était pas fragilisé durant le broyage.

Le transfert de poids d'une classe granulométrique à l'autre a été modélisé à l'aide d'équations différentielles de premier ordre qui décrivent les phénomènes d'aplatissement, pliage, soudage à froid et fragmentation. On a estimé les paramètres de ces modèles par la méthode des moindres carrés. Pour certains essais, on essaya de représenter les données par plus d'un modèle; ce fut alors presque toujours celui qui était basé sur le ou les mécanismes de transfert dominants qui a le mieux représenté les données. Ce mécanisme dominant dépend du type de métal broyé, de la taille et la forme des particules, l'intensité du broyage et la présence d'une phase dominante fragile et dure. L'aplatissement des particules (et par conséquent leur transfert à des classes plus grossières) se produit généralement de deux à trois plus souvent que leur pliage (responsable du transfert à des classes plus fines sans qu'il y ait fragmentation). Les particules se fragmentent davantage si elles sont plus fines ou moins dures, dans un environnement à énergie d'impact élevée, ou en présence d'une quantité importante d'un minéral dur et fragile. La perte de poids par revêtement des corps broyants devient plus importante lorsque qu'on broie un métal plus mou dans un broyeur à surface plus rugueuse, ou lorsqu'il y a fragmentation des particules.

On a développé et mis à l'essai une méthodologie axée sur l'utilisation du Knelson de laboratoire visant à déterminer la fonction de fragmentation et l'aptitude à la récupération gravimétrique des flocons d'or. La progéniture des flocons offre un excellente aptitude à la récupération gravimétrique, plus de 90% au-dessus de 0.025 mm. La fonction de fragmentation, non-normalisable, avait une composante  $b_{i+1,i}$  importante à cause du phénomène de pliage.

---

**Acknowledgements**

This thesis would hardly have been possible without the teaching and the unmeasurable assistance of a number of persons and organizations. I would like to take this opportunity to express to them my sincere appreciation and thanks.

- I would like to express my deepest appreciation to my supervisor Professor André R. Laplante for his strong guidance and advice, invaluable suggestions, constant encouragement and continued friendship throughout of this research, without which this studying would still be unfinished.

- I acknowledge Prof. S. Yue for many helpful discussions, and also would like to thank Professors J.A. Finch, Z. Xu, and R. Rao for their suggestions during this work.

- I thank Mr. R. Langlois and Mr. M. Leroux, mineral processing technicians, for their help. Ms. H. Campbell and Mr. M. Knoepfel were also very helpful with sample preparation and the scanning electron microscope. I am also indebted to all my colleagues and friends in the Mineral Processing Group, particularly my fellow graduate student Mr. A. Farzanegan. I also acknowledge personnel of the P.S. Library, particularly Mr. Henry Lim Soo. The author wishes to thank Casa Berardi, Snip, and Hemlo for providing gold samples and fire assaying services.

- I would like to extend my appreciation to the Iranian Ministry of Culture & Higher Education for making my post-graduate studies possible.

- I am very grateful for the unfailing support provided by my wife, S. Livani, for her understanding and patience during my studies.

---

**Table of Contents**

Abstract . . . . .	i
Résumé . . . . .	ii
Acknowledgements . . . . .	iii
Table of Contents . . . . .	iv
Nomenclature . . . . .	viii
List of Figures . . . . .	xii
List of Tables . . . . .	xxii
List of Appendices . . . . .	xxvi
<b>Chapter 1: Introduction . . . . .</b>	<b>1</b>
1.1 Scope of the Project . . . . .	2
1.2 Outline of Experimental Work . . . . .	4
1.3 Structure of the Thesis . . . . .	5
<b>Chapter 2: Theoretical Considerations . . . . .</b>	<b>7</b>
2.1 Introduction . . . . .	8
2.2 Mechanisms of Size Reduction . . . . .	8
2.3 Particle Size Distribution of Comminuted Product . . . . .	10
2.4 Comminution Laws (Energy-Size Reduction Relationships) . . . . .	14
2.5 Comminution Kinetics . . . . .	16
2.6 Batch Grinding Integro-Differential Equation . . . . .	18
2.7 The Practical Equation (The Size-Mass Balance Equation) . . . . .	20
2.8 The Rate Constant of Breakage or Selection Function . . . . .	21
2.9 Selection Function Determination . . . . .	24
2.9.1 The batch grinding test (The one-size-fraction test) . . . . .	25
2.9.2 The back-calculation method . . . . .	26
2.10 Breakage and Cumulative Breakage Functions . . . . .	28

---

2.11 Breakage Function Determination . . . . .	31
2.11.1 Single particle breakage method . . . . .	31
2.11.2 One-size-fraction test . . . . .	32
2.11.3 Back-calculation . . . . .	33
2.12 Malleability & Native Metals . . . . .	34
2.13 Metal Grinding . . . . .	36
<b>Chapter 3: Models of Malleable Metal Grinding . . . . .</b>	<b>42</b>
3.1 Introduction . . . . .	43
3.2 Classical Mathematical Model for Grinding . . . . .	43
3.3 Defining Models of Malleable Metal Grinding . . . . .	44
3.3.1 Case 1: Folding & flattening and no breakage . . . . .	44
3.3.2 Case 2: Folding & flattening and explicit breakage . . . . .	46
3.3.3 Case 3: Folding & flattening and limited breakage . . . . .	49
3.3.4 Case 4: Agglomeration . . . . .	51
3.4 Differential Equations: Solutions and Rate Constants Estimations . . . . .	53
<b>Chapter 4: The Behaviour of Coarse Lead in Tumbling Mills . . . . .</b>	<b>55</b>
4.1 Introduction . . . . .	56
4.2 Apparati . . . . .	56
4.3 Test 1 to 3: Grinding Lead Shots . . . . .	58
4.3.1 Procedure . . . . .	58
4.3.2 Results and discussion . . . . .	59
4.4 Test 4 to 6: Grinding Flattened Lead Shots . . . . .	79
4.4.1 Procedure . . . . .	79
4.4.2 Results and discussion . . . . .	79
4.5 Microhardness Tests . . . . .	96
4.5.1 Definitions . . . . .	96
4.5.2 Apparatus and procedure . . . . .	99
4.5.3 Results and discussion . . . . .	100

---

4.6 Conclusions .....	100
<b>Chapter 5: The Behaviour of Lead Fragments in Tumbling Mills .....</b>	<b>103</b>
5.1 Introduction .....	104
5.2 Experimental .....	104
5.3 Results and Discussion .....	106
5.3.1 First series of tests: Grinding lead fragments .....	106
5.3.2 Second series of tests: Grinding lead fragments mixed with silica .....	131
5.4 Conclusions .....	152
<b>Chapter 6: The Behaviour of Copper Fragments in Tumbling Mills .....</b>	<b>154</b>
6.1 Introduction .....	155
6.2 Experimental .....	155
6.3 Results and Discussion .....	156
6.4 Conclusions .....	171
<b>Chapter 7: Cascadography- An Attempt at Characterizing the Shape of Lead Fragments .....</b>	<b>173</b>
7.1 Introduction .....	174
7.2 Theory of Cascadography .....	175
7.3 Experimental Section .....	178
7.3.1 Apparatus & procedure .....	178
7.4 Results and Discussion .....	179
7.5 Conclusions .....	192
<b>Chapter 8: Breakage Function and Recoverability of Free Gold .....</b>	<b>194</b>
8.1 Introduction .....	195
8.2 Methodology .....	198
8.2.1 Isolating GRG .....	199
8.2.2 The grinding tests .....	199
8.2.3 Recovery of GRG .....	201

---

8.3 Results and Discussion . . . . .	201
8.3.1 Casa Berardi tests . . . . .	201
8.3.2 Snip tests . . . . .	205
8.3.3 Hemlo tests . . . . .	209
8.4 Conclusions . . . . .	221
<b>Chapter 9: Discussion and Conclusions . . . . .</b>	<b>223</b>
9.1 Overall Discussion . . . . .	224
9.2 Contributions to Knowledge . . . . .	234
9.3 Suggestions for Future Research . . . . .	235
<b>References . . . . .</b>	<b>237</b>
<b>Appendix I: Analytical &amp; Numerical Solutions of the Proposed Models . . . . .</b>	<b>A1</b>
1.1 Introduction . . . . .	A2
1.2 Analytical Solution . . . . .	A2
1.2.1 Case 1: Folding & flattening and no breakage . . . . .	A2
1.3 Numerical Solution . . . . .	A4
1.3.1 Case 1: Folding & flattening and no breakage . . . . .	A5
<b>Appendix II: Complete Set of the Estimated Rate Constants &amp; Fitted Curves of Chapters 5 &amp; 6 . . . . .</b>	<b>A7</b>
<b>Appendix III: Experimental Data &amp; Assaying Results, Charts and Tables of Chapters 4 &amp; 8 . . . . .</b>	<b>A56</b>

---

**Nomenclature**

$\alpha$	The distribution modulus.
$\alpha_1$	Characteristic of the material (Equation 2.26).
$\beta, \gamma, \phi$	Material characteristics (Equation 2.40).
$\epsilon$	Strain due to applied stress (Equation 4.1).
$\sigma$	Applied stress (Equation 4.1).
$\mu$	Particle size at which the $Q_i$ is 1/2 (Equation 2.29).
$\Lambda$	Characteristic of the material (Equations 2.28, 2.29).
$a$	Constant related with mill conditions (Equation 2.27).
$a_1, a_2, a_3$	Constants, having the dimension of length (Equation 2.5).
<b>AG</b>	Agglomeration model.
<b>b</b>	Breakage function.
<b>B</b>	Cumulative breakage function.
<b>Bre.</b>	Breakage rate constants.
<b>C</b>	Constant (Equation 2.9).
$C_1$	Constant depending on C (Equations 2.10, 2.11).
$C_2$	Constant of Rittinger's law (Equation 2.13).
$C_3$	Constant of Kick's law (Equation 2.13).
$C_4$	Constant of Bond's law, work index (Equation 2.14).
$C_5$	Constant related with material, units, etc. (Equation 2.16).
$C_6$	Constant of Charles equation (Equation 2.18).
$C_{11}, C_{12}, C_{13}, C_{14}$	Constants (Equation 2.31).
$C_{15}, C_{16}, C_{17}$	Constants (Equation 2.32).
$C_{18}, C_{19}, C_{110}, C_{111}$	Constants (Equation 2.41).
$C_{112}, C_{113}$	Constants (Equation 2.42).

---

<b>df.</b>	Degrees of freedom.
<b>E</b>	Energy input per unit volume (Equation 2.12).
<b>E<sub>1</sub></b>	Elasticity modulus (Equation 4.1).
<b>EBWOF</b>	Explicit breakage model with only flattening rate constant.
<b>FF</b>	Flattening and folding model.
<b>FFWEB</b>	Flattening, folding and explicit breakage model.
<b>FFWLB</b>	Flattening, folding and limited breakage model.
<b>Fla.</b>	Flattening rate constants.
<b>Fol.</b>	Folding rate constants.
<b>GRG</b>	Gravity recoverable gold.
<b>i,j</b>	Screen number i and j.
<b>k</b>	The size modulus.
<b>k<sub>1</sub>, k<sub>2</sub></b>	Constants of size distribution (Equations 2.9, 2.10).
<b>k<sub>3</sub></b>	Constant (Equations 2.19, 2.20).
<b>KC</b>	Knelson Concentrator.
<b>LKC</b>	Laboratory Knelson Concentrator.
<b>LSF</b>	Least square fit.
<b>m</b>	Number of screens in a set of screens.
<b>ML</b>	Mass loss (Weight loss).
<b>MSS</b>	Average lack of fit.
<b>n</b>	The number of size classes.
<b>n<sub>1</sub></b>	Exponent and order indicator of the process (Equation 2.16).
<b>n<sub>2</sub></b>	Increment of the grinding times (Equation 3.39).
<b>N</b>	The current number of particles on the sieve (Equation 7.1).
<b>N<sub>0</sub></b>	The amount of material in a pan below the sieves

---

	(Equations 7.2, 7.3).
$N_0$	The original number of particles on the sieves (Equations 7.1, 7.2, 7.3).
$P_i(t)$	Cumulative broken mass in fraction below $i$ (Equations 2.38, 2.39).
$Q_i$	Correction factor (Equation 2.27).
$r$	Rate constant of malleable material grinding equation (Equations 3.7, 3.14, 3.22, 3.32).
$r_{ij}$	Rate constant of mass reporting from size $i$ to size $j$ (Equations 3.7, 3.14, 3.22, 3.32).
$R$	Reduction ratio (Equation 2.17).
$Re$	<b>Reynolds number.</b>
$R_{GRG}$	Recovery of GRG (Equation 8.1).
$s$	Selection function.
$SS$	Lack of fit.
$S_r$	Standard error.
$S_{rc}$	Sieve rate constant (Equations 7.1, 7.2, 7.3).
$t$	Grinding time.
$u$	Kick's law deviation exponent (Equation 2.17).
$u_1, u_2, u_3$	Number of cuts occurring on fracture per length, surface, and volume (Equation 2.8).
$w_i(t)$	Fractional weight at screen number $i$ or size $x_i$ .
$w_i^{calc}(t)$	The predicted mass in size $i$ after $t$ grinding time (Equation 3.39).
$w_i^{Exp}(t)$	The measured mass in size $i$ after $t$ grinding time (Equation 3.39).
$w(x,t)$	Weight fraction of material in size $x$ .
$W$	The whole feed weight.

---

$W_i$	Work index (Equations 2.15, 2.17).
$W_t$	Total work input for comminution (Equations 2.15, 2.17).
$x$	Particle size.
$x_1, x_2$	Initial and final size (Equations 2.12, 2.13).
$x_f$	Feed size.
$x_i$	Size of i.
$x_j$	Size of j.
$x_m$	Particle size which its selection function is maximum (Equation 2.29).
$x_p$	Product size.
$Y(x)$	Fracture of material finer than x.

---

**List of Figures**

2.1	Representation of the mechanisms of particle fraction and the resulting product size distributions . . . . .	10
2.2	Breakage rates for two types of mill with different diameter . . . . .	23
2.3	Breakage rate of gold ore as a function of particle size . . . . .	24
2.4	First-order plot to estimate of selection function . . . . .	25
2.5	Weight fraction variation in a set of screen . . . . .	28
2.6	Normalizable cumulative breakage function for ball milling of quartz . . . . .	29
2.7	Non-normalizable cumulative breakage function plot . . . . .	30
2.8	Three different single particle test methods; 1) slow compression, 2) Impact by a falling media, 3) Impact at high particle speed . . . . .	31
2.9	Cumulative breakage function distribution plot . . . . .	34
3.1	Representation of a three size class model based on flattening, folding and no breakage . . . . .	45
3.2	Representation of a three size class model based on flattening, folding and explicit breakage . . . . .	47
3.3	Representation of a three size class model based on flattening, folding and limited breakage . . . . .	50
3.4	Representation of a three size class model based on agglomeration . . . . .	52
4.1	Lead shots used in different tests (scale in cm) . . . . .	57
4.2	Flattened lead shots used in different tests (scale in cm) . . . . .	57
4.3	Size distribution of lead particles as a function of grinding time in the Bond ball mill (Test 1); size class 1: +4.00 mm, 2: 3.35-4.00 mm, 3: 2.80-3.35 mm, 4: 2.38-2.80 mm, 5: -2.38 mm . . . . .	60
4.4	Weight of individual particles in the Bond ball mill test (Test 1); a: +4.00 mm, b: 3.35-4.00 mm, c: 2.80-3.35 mm, d: 2.38-2.80 mm . . . . .	61
4.5	Super-flakes produced in the phase II of the Bond ball mill test (Test 1) . . . . .	63

---

4.6	Weight distribution of super-flakes in size class 1, after 70 minutes of grinding in the Bond ball mill (Test 1) . . . . .	64
4.7	Lost weight in Test 1 . . . . .	64
4.8	Fit of the flattening and folding model (no breakage) for Test 1; three phases and a: 3 size classes, b: 4 size classes, c: 5 size classes . . . . .	68
4.9	Fit of the agglomeration model for the second phase of Test 1; a: 3 size classes, b: 4 size classes, c: 5 size classes . . . . .	69
4.10	Fit of the flattening, folding and limited breakage model for the third phase of Test 1; a: 3 size classes, b: 4 size classes, c: 5 size classes . . . . .	71
4.11	Size distribution of lead particles as a function of grinding time in the Bond ball mill test (Test 2); size class 1: +4.00 mm, 2: 3.35-4.00 mm, 3: 2.80-3.35 mm, 4: 2.38-2.80 mm, 5: -2.38 mm . . . . .	72
4.12	Size distribution of lead particles as a function of grinding time in the Bond rod mill test (Test 3); size class 1: +4.00 mm, 2: 3.35-4.00 mm, 3: 2.80-3.35 mm, 4: 2.38-2.80 mm, 5: 2.00-2.38 mm, pan: -2.00 mm . . . . .	73
4.13	Lost weight in Test 3 . . . . .	74
4.14	Fines production as a function of time in the Bond rod mill (Test 3) . . . . .	74
4.15	Fit of the flattening and folding model (no breakage) for Test 3; two phases and a: 3 size classes, b: 4 size classes, c: 5 size classes . . . . .	77
4.16	Fit of the flattening, folding and limited breakage model for the second phase of Test 3 and a: 3 size classes, b: 4 size classes, c: 5 size classes . . . . .	78
4.17	Size distribution of lead particles as a function of grinding time in the Bond ball mill (Test 4); size class 1: a: 4.75 mm, 2: 4.00-4.75 mm, 3: 3.35-4.00 mm, 4: 2.80-3.35 mm, 5: -2.80 mm . . . . .	80
4.18	Lost weight in Test 4 (Bond ball mill) . . . . .	81
4.19	Fines production as a function of time in the Bond ball mill (Test 4) . . . . .	81
4.20	Fit of the flattening and folding model (no breakage) for the two phases of Test 4; a: 3 size classes, b: 4 size classes, c: 5 size classes . . . . .	83

---

4.21	Fit of the flattening , folding and limited breakage model for the second phase of Test 4; a: 3 size classes, b: 4 size classes, c: 5 size classes . . . . .	84
4.22	Fit of the conventional breakage model for the second phase of Test 4; a: 3 size classes, b: 4 size classes, c: 5 size classes . . . . .	86
4.23	Size distribution of lead particles as a function of grinding time in the Bond rod mill (Test 5); size class 1: +5.60 mm, 2: 4.75-5.60 mm, 3: 4.00-4.75 mm, 4: 3.35-4.00 mm, 5: 2.80-3.35 mm, pan: -2.80 mm . . . . .	88
4.24	Fines production as a function of time in the Bond rod mill (Test 5) . . . . .	88
4.25	Lost weight in Test 5 (Bond rod mill) . . . . .	89
4.26	Fit of the flattening and folding model (no breakage) for Test 5; a: 3 size classes, b: 4 size classes, c: 5 size classes . . . . .	89
4.27	Fit of the flattening, folding and limited breakage model for Test 5; a: 3 size classes, b: 4 size classes, c: 5 size classes . . . . .	92
4.28	Cumulative histograms of the weight of individual particle for Test 6; after a: 0.5 minute, b: 1 minute, c: 2 minutes, d: 4 minutes . . . . .	93
4.29	Size distribution of flattened lead shot as a function of grinding time in Test 6 (Bond rod mill) . . . . .	94
4.30	Lost weight in Test 6 (Bond rod mill) . . . . .	94
4.31	Weight percent of unbroken particles and percent particles remaining in the coarsest size class in Test 6 (Bond rod mill) . . . . .	95
4.32	Hardness of different lead particles (measured with a: lead shots, b: flattened lead shots, c: semi-flattened lead shots, d: lead flakes) . . . . .	102
5.1	A cylindrical lead fragment recovered from the Bond ball mill (feed size: 0.850-1.000 mm) . . . . .	108
5.2	A spherical lead fragment recovered from the Bond ball mill (feed size: 1.18-1.40 mm) . . . . .	109
5.3	A flattened lead fragment with serrated shape recovered from the Bond ball mill (feed size: 0.425-0.500 mm) . . . . .	109

---

5.4	A flattened lead fragment with a serrated shape recovered from the Bond ball mill (feed size: 0.425-0.500 mm) . . . . .	110
5.5	A flattened lead fragment recovered from the Bond ball mill (feed size: 1.18-1.40 mm) . . . . .	110
5.6	Size distribution of lead fragments as a function of grinding time in the Bond ball mill tests; a: 1.18-1.40 mm, b: 0.850-1.000 mm, c: 0.600-0.710 mm, d: 0.425-0.500 mm . . . . .	111
5.7	Fines production as a function of time in the Bond ball mill (Feed: lead fragments; a: 1.18-1.40 mm, b: 0.850-1.000 mm, c: 0.600-0.710 mm, d: 0.425-0.500 mm) . . . . .	112
5.8	Lost weight of lead fragments as a function of grinding time in the Bond ball mill tests; a: 1.18-1.40 mm, b: 0.850-1.000 mm, c: 0.600-0.710 mm, d: 0.425-0.500 mm . . . . .	113
5.9	Fit of the flattening, folding and limited breakage model for the Bond ball mill test (feed: 0.425-0.500 mm lead fragments); a: 3 size classes, b: 4 size classes, c: 5 size classes . . . . .	114
5.10	A spherical lead fragment recovered from the small ball mill (feed size: 1.18-1.40 mm) . . . . .	116
5.11	A cylindrical lead fragment recovered from the small ball mill (feed size: 0.425-0.500 mm) . . . . .	117
5.12	A cylindrical lead fragment recovered from the small ball mill (feed size: 1.18-1.40 mm) . . . . .	117
5.13	A flattened lead fragment with smooth shape recovered from the small ball mill (feed size: 0.850-1.000 mm) . . . . .	118
5.14	A flattened lead fragment with smooth shape recovered from the small ball mill (feed size: 0.850-1.000 mm) . . . . .	118
5.15	Size distribution of lead fragments as a function of grinding time in the small ball mill tests; a: 1.18-1.40 mm, b: 0.850-1.000 mm, c: 0.600-0.710 mm, d: 0.425-	

---

	0.500 mm . . . . .	119
<b>5.16</b>	Fines production as a function of time in the small ball mill (Feed: lead fragments; a: 1.18-1.40 mm, b: 0.850-1.000 mm, c: 0.600-0.710 mm, d: 0.425-0.500 mm) . . . . .	120
<b>5.17</b>	Lost weight of lead fragments as a function of grinding time in the small ball mill tests; a: 1.18-1.40 mm, b: 0.850-1.000 mm, c: 0.600-0.710 mm, d: 0.425-0.500 mm . . . . .	121
<b>5.18</b>	Fit of the flattening and folding model (no breakage) for the small ball mill test (feed: 0.600-0.710 mm lead fragments); a: 3 size classes, b: 4 size classes, c: 5 size classes . . . . .	122
<b>5.19</b>	A flattened lead fragment recovered from the Bond rod mill (feed size: 0.850-1.000 mm) . . . . .	124
<b>5.20</b>	A cylindrical lead fragment recovered from the Bond rod mill (feed size: 1.18-1.40 mm) . . . . .	124
<b>5.21</b>	A flattened lead fragment recovered from the Bond rod mill (feed size: 0.600-0.710 mm) . . . . .	125
<b>5.22</b>	A folded and flattened lead fragment recovered from the Bond rod mill (feed size: 0.850-1.000 mm) . . . . .	125
<b>5.23</b>	Size distribution of lead fragments as a function of grinding time in the Bond rod mill tests; a: 1.18-1.40 mm, b: 0.850-1.000 mm, c: 0.600-0.710 mm, d: 0.425-0.500 mm . . . . .	126
<b>5.24</b>	Fines production as a function of time in the Bond rod mill (Feed: lead fragments; a: 1.18-1.40 mm, b: 0.850-1.000 mm, c: 0.600-0.710 mm, d: 0.425-0.500 mm) . . . . .	127
<b>5.25</b>	Lost weight of lead fragments as a function of grinding time in the Bond rod mill tests; a: 1.18-1.40 mm, b: 0.850-1.000 mm, c: 0.600-0.710 mm, d: 0.425-0.500 mm . . . . .	128
<b>5.26</b>	Fit of the flattening, folding and explicit breakage model for the Bond rod mill	

---

	test (feed: 1.18-1.40 mm lead fragments); a: 3 size classes, b: 4 size classes, c: 5 size classes . . . . .	129
5.27	A lead fragment recovered from the Bond ball mill (feed size: 1.18-1.40 mm) . . . . .	132
5.28	A lead fragment recovered from the Bond ball mill (feed size: 0.600-0.710 mm) . . . . .	132
5.29	Size distribution of lead fragments as a function of grinding time in the Bond ball mill tests (lead fragments mixed with silica); a: 1.18-1.40 mm, b: 0.850-1.000 mm, c: 0.600-0.710 mm, d: 0.425-0.500 mm . . . . .	133
5.30	Fines production as a function of time in the Bond ball mill (Feed: lead fragments mixed with silica; a: 1.18-1.40 mm, b: 0.850-1.000 mm, c: 0.600-0.710 mm, d: 0.425-0.500 mm) . . . . .	134
5.31	Lost weight of lead as a function of grinding time in the Bond ball mill (lead fragments mixed with silica); a: 1.18-1.40 mm, b: 0.850-1.000 mm, c: 0.600-0.710 mm, d: 0.425-0.500 mm . . . . .	135
5.32	Fit of the flattening, folding and explicit breakage model for the Bond ball mill test (feed: 0.850-1.000 mm lead fragments mixed with silica); a: 3 size classes, b: 4 size classes, c: 5 size classes . . . . .	138
5.33	Size distribution of lead fragments as a function of grinding time in the small ball mill tests (lead fragments mixed with silica); a: 1.18-1.40 mm, b: 0.850-1.000 mm, c: 0.600-0.710 mm, d: 0.425-0.500 mm . . . . .	139
5.34	Fines production as a function of time in the small ball mill (Feed: lead fragments mixed with silica; a: 1.18-1.40 mm, b: 0.850-1.000 mm, c: 0.600-0.710 mm, d: 0.425-0.500 mm) . . . . .	140
5.35	Lost weight of lead fragments as a function of grinding time in the small ball mill tests (lead fragments mixed with silica); a: 1.18-1.40 mm, b: 0.850-1.000 mm, c: 0.600-0.710 mm, d: 0.425-0.500 mm . . . . .	141
5.36	Fit of the flattening, folding and explicit breakage model for the small ball mill	

---

	test (feed: 1.18-1.40 mm lead fragments mixed with silica); a: 3 size classes, b: 4 size classes, c: 5 size classes . . . . .	142
5.37	A lead fragment recovered from the Bond rod mill (feed size: 0.850-1.000 mm) . . . . .	144
5.38	A lead fragment recovered from the Bond rod mill (feed size: 0.850-1.000 mm) . . . . .	145
5.39	A lead fragment recovered from the Bond rod mill (feed size: 1.18-1.40 mm) . . . . .	145
5.40	A lead fragment recovered from the Bond rod mill (feed size: 1.18-1.40 mm) . . . . .	146
5.41	A lead fragment recovered from the Bond rod mill (feed size: 0.600-0.710 mm) . . . . .	146
5.42	Size distribution of lead fragments as a function of grinding time in the Bond rod mill tests (lead fragments mixed with silica); a: 1.18-1.40 mm, b: 0.850-1.000 mm, c: 0.600-0.710 mm, d: 0.425-0.500 mm . . . . .	147
5.43	Fines production as a function of time in the Bond rod mill (Feed: lead fragments mixed with silica; a: 1.18-1.40 mm, b: 0.850-1.000, c: 0.600-0.710, d: 0.425-0.500 mm) . . . . .	148
5.44	Lost weight of lead fragments as a function of grinding time in the Bond rod mill tests (lead fragments mixed with silica); a: 1.18-1.40 mm, b: 0.850-1.000 mm, c: 0.600-0.710 mm, d: 0.425-0.500 mm . . . . .	149
5.45	Fit of the flattening, folding and explicit breakage model for the Bond rod mill test (feed: 1.18-1.40 mm lead fragments mixed with silica); a: 3 size classes, b: 4 size classes, c: 5 size classes . . . . .	151
6.1	Size distribution of copper fragments as a function of grinding time in the Bond ball mill tests; a: 1.18-1.40 mm, b: 0.850-1.000 mm, c: 0.600-0.710 mm, d: 0.425-0.500 mm . . . . .	157
6.2	Fines production as a function of time in the Bond ball mill (Feed: copper	

---

	fragments; a: 1.18-1.40 mm, b: 0.850-1.000 mm, c: 0.600-0.710 mm, d: 0.425-0.500 mm) . . . . .	158
<b>6.3</b>	Lost weight of copper fragments as a function of grinding time in the Bond ball mill tests; a: 1.18-1.40 mm, b: 0.850-1.000 mm, c: 0.600-0.710 mm, d: 0.425-0.500 mm . . . . .	159
<b>6.4</b>	Fit of the flattening and folding without breakage model for the Bond ball mill test (feed: 0.425-0.500 mm copper fragments); a: 3 size classes, b: 4 size classes, c: 5 size classes . . . . .	161
<b>6.5</b>	Size distribution of copper fragments as a function of grinding time in the small ball mill tests; a: 1.18-1.40 mm, b: 0.850-1.000 mm, c: 0.600-0.710 mm, d: 0.425-0.500 mm . . . . .	162
<b>6.6</b>	Fines production as a function of time in the small ball mill (Feed: copper fragments; a: 1.18-1.40 mm, b: 0.850-1.000 mm, c: 0.600-0.710 mm, d: 0.425-0.500 mm) . . . . .	163
<b>6.7</b>	Lost weight of copper fragments as a function of grinding time in the small ball mill tests; a: 1.18-1.40 mm, b: 0.850-1.000 mm, c: 0.600-0.710 mm, d: 0.425-0.500 mm . . . . .	164
<b>6.8</b>	Fit of the flattening and folding without breakage model for the small ball mill test (feed: 0.600-0.710 mm copper fragments); a: 3 size classes, b: 4 size classes, c: 5 size classes . . . . .	166
<b>6.9</b>	Size distribution of copper fragments as a function of grinding time in the Bond rod mill tests; a: 1.18-1.40 mm, b: 0.850-1.000 mm, c: 0.600-0.710 mm, d: 0.425-0.500 mm . . . . .	167
<b>6.10</b>	Fines production as a function of time in the Bond rod mill (Feed: copper fragments; a: 1.18-1.40 mm, b: 0.850-1.000 mm, c: 0.600-0.710 mm, d: 0.425-0.500 mm) . . . . .	168
<b>6.11</b>	Lost weight of copper fragments as a function of grinding time in the Bond rod mill tests; a: 1.18-1.40 mm, b: 0.850-1.000 mm, c: 0.600-0.710 mm, d: 0.425-	

---

0.500 mm	169
<b>6.12</b> Fit of the flattening, folding and explicit breakage model for the Bond rod mill test (feed: 0.600-0.710 mm copper fragments); a: 3 size classes, b: 4 size classes, c: 5 size classes	170
<b>7.1</b> A schematic of a cascadograph	176
<b>7.2</b> A typical plot of mass flowrate vs. residence time of a cascadograph test	177
<b>7.3</b> An elongated particle, 3 <sup>rd</sup> concentrate of MLS test, (feed: 0.710-0.850 mm)	179
<b>7.4</b> An elongated particle, 1 <sup>st</sup> concentrate of MLS test, (feed: 0.710-0.850 mm)	180
<b>7.5</b> A flattened particle, tail of MLS test, (feed: 0.710-0.850 mm)	180
<b>7.6</b> A flattened particle, 3 <sup>rd</sup> concentrate of MLS test, (feed: 0.710-0.850 mm)	181
<b>7.7</b> An elongated particle, 1 <sup>st</sup> concentrate of MLS test, (feed: 1.00-1.18 mm)	181
<b>7.8</b> An elongated particle, 3 <sup>rd</sup> concentrate of MLS test, (feed: 1.00-1.18 mm)	182
<b>7.9</b> A flattened particle, 2 <sup>nd</sup> concentrate of MLS test, (feed: 1.00-1.18 mm)	182
<b>7.10</b> A flattened particle, 3 <sup>rd</sup> concentrate of MLS test, (feed: 1.00-1.18 mm)	183
<b>7.11</b> Mass flowrate percent in pan vs. sieving time in cascadography tests (feed: 0.710-0.850 mm), for four different products of Mozley Laboratory Separator; a: Tail, b: 3 <sup>rd</sup> concentrate, c: 2 <sup>nd</sup> concentrate, d: 1 <sup>st</sup> concentrate	189
<b>7.12</b> Mass flowrate percent in pan vs. sieving time in cascadography tests (feed: 1.00-1.18 mm), for four different products of Mozley Laboratory Separator; a: Tail, b: 3 <sup>rd</sup> concentrate, c: 2 <sup>nd</sup> concentrate, d: 1 <sup>st</sup> concentrate	190
<b>7.13</b> Mass left in stack vs. sieving time in cascadography tests; a: 2 <sup>nd</sup> assumption, and 0.710-0.850 mm feed, b: 2 <sup>nd</sup> assumption, and 1.000-1.180 mm feed, c: 1 <sup>st</sup> assumption, and 0.710-0.850 mm, d: 1 <sup>st</sup> assumption, and 1.000-1.180 mm feed.	191
<b>7.14</b> Average weight of particles in cascadography test (feed: 1.00-1.18 mm)	192
<b>8.1</b> The schematic diagram of the Knelson Concentrator	197
<b>8.2</b> The schematic of the methodology of the tests	197
<b>8.3</b> A typical flowsheet of Casa Berardi sample tests	198

---

8.4	Calculated cumulative breakage functions for the Casa Berardi tests . . . . .	204
8.5	Estimated selection functions for the Casa Berardi tests . . . . .	204
8.6	Calculated cumulative breakage functions for the Snip tests . . . . .	208
8.7	Estimated selection functions for the Snip tests . . . . .	208
8.8	Recovery of the progeny as a function of particle size for the Hemlo tests	212
8.9	The variation of silica selection functions in grinding increments for the Hemlo samples . . . . .	214
8.10	Estimated selection functions for gold and silica for the Hemlo tests . . .	215
8.11	Calculated cumulative breakage functions for the Hemlo tests . . . . .	216
8.12	Gold flake, originally in 0.150-0.212 mm, moved into two coarser size class, 0.300-0.425 mm, after flattening . . . . .	218
8.13	Gold flake, originally in 0.300-0.425 mm, moved into two coarser size class, 0.600-0.850 mm, after flattening . . . . .	218
8.14	Gold flake, originally in 0.300-0.425 mm, moved into two finer size class, 0.150-0.212 mm, after folding and possibly breakage . . . . .	219
8.15	Gold flake, originally in 0.300-0.425 mm, moved into two finer size class, 0.150-0.212 mm, after folding and possibly breakage . . . . .	219
8.16	Gold flake, originally in 1.18-1.70 mm, moved into one finer size class, 0.850-1.180 mm, after folding and possibly breakage . . . . .	220
8.17	Gold flake, originally in 1.18-1.70 mm, moved into two finer size class, 0.600-0.850 mm, after folding and possibly breakage . . . . .	220
9.1	A conceptual view of the transfers across size classes . . . . .	230
9.2	A conceptual view of smearing . . . . .	231
9.3	Fit of the cascadowgraphy response of the 1 <sup>st</sup> concentrate of MLS product of the 0.710-0.850 mm sample to Equation 7.2 using a) one, b) two and c) three particle types (each with a single screening rate constant) . . . . .	232

---

**List of Tables**

2.1	The variation of selection function (SF) with collision and existence flaws . . . . .	22
2.2	Variation of different methods to estimate selection function (SF) . . . . .	27
4.1	Apparati used for Tests 1 to 6 . . . . .	58
4.2	Weight distribution of particles in different size classes in the Bond ball mill after 24 minutes grinding (Test 1) . . . . .	62
4.3	Weight distribution of the super-flakes in size class 1, after 70 minutes of grinding in the Bond ball mill (Test 1) . . . . .	63
4.4	Estimated rate constants for Test 1 (all in $\text{min}^{-1}$ ); flattening and folding model (no breakage) . . . . .	67
4.5	Estimated rate constants for the second phase of Test 1; agglomeration model . . . . .	69
4.6	Estimated rate constants (all in $\text{min}^{-1}$ ) for the third phase of Test 1; flattening and folding and limited breakage model . . . . .	70
4.7	Estimated rate constants (all in $\text{min}^{-1}$ ) for Test 3; flattening and folding model (no breakage) . . . . .	76
4.8	Estimated rate constants for the second phase of Test 3; flattening, folding and limited breakage . . . . .	78
4.9	Estimated rate constants (all in $\text{min}^{-1}$ ) for Test 4; flattening and folding model (no breakage) . . . . .	82
4.10	Estimated rate constants (all in $\text{min}^{-1}$ ) of the second phase of Test 4, with the flattening, folding and limited breakage model . . . . .	85
4.11	Estimated breakage and cumulative breakage functions (BF, CBF) of lead . . . . .	86
4.12	Estimated rate constants (all in $\text{min}^{-1}$ ) for the second phase of Test 4; conventional breakage model . . . . .	87
4.13	Estimated rate constants (all in $\text{min}^{-1}$ ) for Test 5; flattening and folding model (no breakage) . . . . .	90

---

4.14	Estimated rate constants (all in $\text{min}^{-1}$ ) for Test 5; flattening, folding and limited breakage model . . . . .	91
4.15	Estimated breakage function (BF) and Cumulative breakage function (CBF) of lead in Test 6 (Bond rod mill) . . . . .	96
4.16	Hardness, recrystallization and melting temperatures, and activation energy of some malleable metals . . . . .	98
5.1	Specification of three mills, used in different tests . . . . .	105
5.2	Estimated rate constants (all in $\text{min}^{-1}$ ) for the Bond ball mill test, flattening, folding and limited breakage model (feed: 0.425-0.500 mm lead fragments) . . . . .	114
5.3	Estimated rate constants (all in $\text{min}^{-1}$ ) for the small ball mill test, flattening and folding without breakage model (feed: 0.600-0.710 mm lead fragments) . . . . .	122
5.4	Estimated breakage function (BF) of lead for the Bond rod mill tests . . . . .	129
5.5	Estimated rate constants (all in $\text{min}^{-1}$ ) for the Bond rod mill test, flattening, folding and explicit breakage model (feed: 1.18-1.40 mm lead fragments) . . . . .	130
5.6	Estimated breakage function (BF) of lead for the Bond ball mill tests (lead fragments mixed with silica) . . . . .	136
5.7	Estimated rate constants (all in $\text{min}^{-1}$ ) for the Bond ball mill test, flattening, folding and explicit breakage model (feed: 0.850-1.000 mm lead fragments mixed with silica) . . . . .	137
5.8	Estimated breakage function (BF) of lead for the small ball mill tests (lead fragments mixed with silica) . . . . .	142
5.9	Estimated rate constants (all in $\text{min}^{-1}$ ) for the small ball mill test, flattening, folding and explicit breakage model (feed: 1.18-1.40 mm lead fragments mixed with silica) . . . . .	143
5.10	Estimated breakage function (BF) of lead for the Bond rod mill tests (lead fragments mixed with silica) . . . . .	150
5.11	Estimated rate constants (all in $\text{min}^{-1}$ ) for the Bond rod mill test, flattening, folding and explicit breakage model (feed: 1.18-1.40 mm lead fragments mixed	

---

	with silica) . . . . .	151
5.12	Estimated rate constants (all in $\text{min}^{-1}$ ) for the Bond rod mill test, flattening, folding and explicit breakage model with only $r_{2,1}$ and breakage rate constants (feed: 1.18-1.40 mm lead fragments mixed with silica) . . . . .	152
6.1	Estimated rate constants (all in $\text{min}^{-1}$ ) for the Bond ball mill test, flattening and folding without breakage model (feed: 0.425-0.500 mm copper fragments) . . . . .	160
6.2	Estimated rate constants (all in $\text{min}^{-1}$ ) for the small ball mill test, flattening and folding without breakage model (feed: 0.600-0.710 mm copper fragments) . . . . .	165
6.3	Estimated breakage function (BF) of copper for the Bond rod mill tests . . . . .	170
6.4	Estimated rate constants (all in $\text{min}^{-1}$ ) for the Bond rod mill test, flattening, folding and explicit breakage model (feed: 0.600-0.710 mm copper fragments) . . . . .	171
7.1	The results of MLS tests for each sample . . . . .	183
7.2	Cascadography tests results on MLS products, (feed: 0.710-0.850 mm) . . . . .	185
7.3	Cascadography tests results on MLS products, (feed: 1.00-1.18 mm) . . . . .	186
7.4	Weight left in stack, based on the first assumption, for both two feeds . . . . .	187
7.5	Weight left in stack, based on the second assumption, for both two feeds . . . . .	188
8.1	Incremental grinding times for the Snip tests . . . . .	200
8.2	Table concentrate weight used for the Hemlo tests . . . . .	201
8.3	A typical metallurgical balance for the Casa Berardi first test . . . . .	202
8.4	The distribution of recoveries to the concentrate and feed distribution of the Casa Berardi tests . . . . .	203
8.5	The distribution of concentrates recoveries for the Snip tests . . . . .	205
8.6	The distribution of feeds for the Snip tests . . . . .	206
8.7	The distribution of recoveries to the concentrate and feed distribution for the Snip tests with the Bond ball mill . . . . .	207
8.8	The distribution of recoveries to the concentrate for the Hemlo tests . . . . .	209
8.9	The feed distribution for the Hemlo tests . . . . .	210

---

8.10	Amount of GRG predicted by Equation 8.2 . . . . .	212
8.11	Calculated head grades of the Hemlo tests . . . . .	213
8.12	Estimates of average selection functions of silica used in the Hemlo tests .	214
8.13	Estimated values of $\phi$ , $\beta$ , and $\gamma$ on the basis of breakage function calculation for the Hemlo tests . . . . .	217
9.1	Summary of the results . . . . .	225

---

**List of Appendices**

<b>Appendix I</b>	Analytical & Numerical Solutions of the Proposed Models .	A1
<b>Appendix II</b>	Complete Set of Estimated Rate Constants & Fitted Curves of Chapters 5 & 6 . . . . .	A7
<b>Appendix III</b>	Experimental Data & Assaying Results, Charts and Tables of Chapters 4 & 8 . . . . .	A56

## **Chapter 1: Introduction**

## 1.1 Scope of the Project

The term of malleability comes from Latin word "malleus" which means "hammer" or "mallet" <sup>(1, 2)</sup>. A mineral or metal is malleable if it can be flattened under the blow of a hammer without breaking or crumbling into fragments <sup>(3, 4, 5)</sup>. In nature, most elements combine to form compounds, but approximately twenty native elements can be found in their uncombined states as minerals <sup>(6, 3)</sup>. About half of these are metals, which are malleable, with the exception of bismuth <sup>(7)</sup> (which is brittle) and mercury (liquid at room temperature) <sup>(8)</sup>.

Although comminution is widely practised in mineral processing, most rocks and ores behave as non-homogeneous brittle substances, as the vast majority of minerals are brittle. As a result, very little is known about the behaviour of malleable native metals in grinding units, more specifically tumbling mills. Gold, the most malleable of metals, may be the exception, as its economic importance and common occurrence as a native element (unlike copper and lead, far more often found as sulphide) has attracted a lot of attention.

Gold has a very distinct behaviour in grinding circuits <sup>(9, 10)</sup>. Its malleability and high density (19.3 g/cm<sup>3</sup>) both contribute to its accumulation in grinding circuits, as it grinds very slowly and preferentially reports to cyclone underflow. Very large circulating loads of gold, up to 6700%, have been reported <sup>(9)</sup>. These can be put to good use with gravity circuits, capable of recovering a significant proportion of the gold in the ore even when only a small bleed (5 to 20%) of the circulating load is treated.

On the down side, gold recovery might suffer because of smearing, pounding into the mill liners and shell, settling into dead areas, or theft (these phenomena are inter-related). Accumulation of gold into the grinding circuit also makes head grade

estimations difficult. This unique behaviour and its engineering and economic implications have prompted this study. More specifically, a model of gold gravity recovery, based on the concept of *Gravity Recoverable Gold* (GRG), requires a description of gold's grinding kinetics. Although early versions of the algorithm have yielded acceptable predictions of the circulating load of GRG<sup>(11, 12)</sup>, the need for a more thorough investigation of gold's grinding kinetics has been identified.

Interest in a study of the grinding of malleable metals is not only limited to the grinding of gold ores. Metal powders can be used in the production of reagents, pigments, coating, and brazes<sup>(13, 14)</sup>. In particular, fine aluminum powder is widely used in a variety of industries such as the manufacturing of paints, printing inks, pyrotechnic chemicals, slurry explosives, light weight concrete blocks<sup>(13, 15, 16)</sup>. Copper powder is mixed with carbon for making contact brushes and bronze powders used in decorative paints and printing inks<sup>(17)</sup>. Lead, cadmium, and silver powders are used as active masses for galvanic cells and in lead accumulators and lead batteries<sup>(15, 18)</sup>, and iron powders are used in the production of welding rods<sup>(15)</sup>. Metal powders, especially gold, copper, and bronze, have been used for decorative purposes in ceramics, as basis for paints and inks, and in cosmetics. As far back as the historic records goes, powdered gold has been used to adorn some of the earliest manuscripts<sup>(17)</sup>. As malleable metals do not grind easily, surface active agents are occasionally used as grinding aids to minimize flake-flake interaction<sup>(19, 20)</sup> and to increase the number of breakage events.

For the present work, the idea of using a malleable metal other than gold (with physico-mechanical properties as close as possible to gold's) as a substitute for gold is attractive. Apart from the mere economic savings (one gram of gold shot, 6.38 mm and 99.95 % pure, is worth \$87.00, whereas one gram of lead shot, 4 mm and 99% pure, is worth \$0.0618)<sup>(21)</sup>, the risk of cross-contamination with actual gold ores is minimized. This is critical, as samples assaying in the 0.1 to 10 g/t Au are routinely treated in the

---

mineral processing laboratory. Recent cases of contamination by as little as 0.1 g/t have been reported <sup>(22)</sup>. Lead and copper are obvious candidate; they are, as gold, very malleable, have the same face-centered cubic structure, and a relatively high density (11.35 and 8.96 g/cm<sup>3</sup>, respectively), which makes gravity separation from low density gangues possible. Further, a better understanding of the breakage of lead and copper can be interesting because of practical applications, such as the decontamination of soils and other environments contaminated with lead (e.g. old firing ranges or battery recycling sites) <sup>(18, 23, 24)</sup> and the grinding of malleable copper contained in ores or converter slags.

Because this project aims at a practically virgin field, the approach will be primarily exploratory. Most of the test work will be performed with lead particles ground in different environments (i.e. various laboratory tumbling mills), with and without the presence of a second phase (silica sand) used to mimic gangue minerals. To analyze results in a more formal way, the data thus generated will be fitted to various grinding models, some conventional, some novel, but each focusing on different grinding mechanisms.

## 1.2 Outline of Experimental Work

Most of the experimental work will be performed using lead, and to a lesser extent, copper, as substitutes for gold, because of their price and availability. First the generation of lead fragments from spheres (shot) will be characterized in different grinding environments. Second, the behaviour of these fragments in the same grinding units will be researched. Mechanisms responsible for transfers between size classes will be emphasized with both conventional breakage and selection functions as well as novel concepts of flattening and folding rate constants. Traditional studies have focused on a characterization based on particle size alone (i.e. screening). In this study, specific attention will be paid to additional characterization techniques, such as cascadowgraphy

and weighing individual particles.

Because many of the technological applications that motivated this work call for the grinding of malleable metals in the presence of another species (e.g. gangue, slag, soil), a third segment of the thesis will repeat the grinding work, but in the presence of silica. After grinding, the two phases will be separated gravimetrically, and the lead phase characterized. For the fourth part of the work, the behaviour of copper in the same grinding units will be compared to that of lead.

The fifth and last segment of the research program will be the gold breakage function estimation. The breakage function is one of the key parameters in the traditional description of grinding. Different gold samples in various levels of grades are used in experiments to estimate gold's breakage function. To do that, a specific methodology is required because of the malleability of gold and its low grinding kinetics in regular grinding environments. As gold gravity recovery was the major impetus for this study, the breakage function will also be linked to recovery by gravity<sup>(11, 12)</sup>.

### **1.3 Structure of the Thesis**

This thesis consists of 9 chapters. In chapter 1, the rationale for the project, an outline of the experimental work and the structure of the thesis are presented.

In chapter 2, the classical representation of mineral grinding is described. Both the classical energy approach and population balance model (PBM) are reviewed. Malleability, malleable materials classification and metal grinding are also surveyed in this chapter. In chapter 3, novel mathematical models for malleable material grinding are introduced; solutions, both analytical and numerical, are presented.

In chapter 4, the results of the grinding of lead shots and flattened lead shots in two laboratory tumbling mills (Bond ball and rod mills) is presented and discussed. In chapter 5, three laboratory mills (Bond ball and rod mills and small ball mill) are used to grind lead fragments (similar to gold flakes recovered from industrial grinding circuits) with and without silica gangue. Chapter 6 presents the copper work, also performed as fragments, in the same mills. Cascadography is used to characterize the particle shape of the products of gravity separation tests and the results are given in chapter 7.

Chapter 8 links fragmentation and gravity recoverability, but for gold flakes from three mills. The monosized samples are incrementally ground and screened, and a Laboratory Knelson Concentrator (LKC) is used to assess recoverability. In chapter 9, the salient findings of the previous chapters are reviewed and discussed. Important conclusions, including claims to the original research, and suggestions for future research are presented.

## **Chapter 2: Theoretical Considerations**

## 2.1 Introduction

In recent decades, a great deal of effort has been invested in the mathematical description of size reduction, or comminution, of solid materials<sup>(25, 26)</sup>. The uses of comminution can be summarized as<sup>(27, 28, 29)</sup> a) decreasing the material size, b) increasing surface area for further treatment, and c) liberating material from its matrix. A description of comminution can be based on weight, grinding size, specific area, distribution of grind size, energy consumption, classification, and operating efficiency, all of which have been used<sup>(30)</sup>. The application of chemical reactor theory to the mathematical modelling of comminution processes<sup>(31, 32, 33)</sup> has led to an increased understanding of process behaviour and provides a logical basis to the design and analysis of comminution circuits. Both mathematical descriptions and accumulated industrial experience are important to design, operate and optimize grinding circuits.

A wide variety of factors such as machine type design (ball and rod mill), particle characteristics and properties<sup>(26)</sup> and conditions of comminution process (wet or dry grinding)<sup>(34, 35)</sup> will influence grinding performance. Each type of ore or material shows a particular behaviour in different grinding circuits. Optimum circuit selection must therefore focus on the material to be ground, which must be properly characterized.

## 2.2 Mechanisms of Size Reduction

A particle fractures when a stress or force higher than its fracture strength is applied. How this stress is exerted and the nature of the particles to be broken are the main parameters which determine how it will fracture<sup>(36, 37, 38)</sup>. When compressive and/or shear forces<sup>(38, 39, 40)</sup> are applied either at a fast or slow rate, fracture results from tensile stresses which arise.

The product from a comminution process will be considered to be the sum of contributions resulting from the action of several mechanisms. Three basic mechanisms are used to describe single particle fracture: impact grinding and two forms of attrition, namely abrasion and cleavage (chipping) grinding<sup>(36, 38, 39, 41)</sup>. Each mechanism takes place in a particular range of applied energy, and is also a function of the type of material broken.

Fracture by impact or shatter occurs when the applied energy on a material or particle is sufficient to cause breaking into fragments. Under these conditions many areas in the particle are overloaded and the result is a large number of particles with a wide range of size (Figure 2.1). This occurs when a rapid loading takes place such as in a high velocity impact<sup>(37, 38)</sup>. It has been reported that impact fracture of single particles of different composition and shape results in a distribution modulus of unity<sup>(36)</sup>.

Abrasion fracture occurs when insufficient energy to cause significant fracture of the particle is applied. In other words, abrasion occurs when two particles or surfaces slide on, or rub against each other, or against balls or the mill liner. Minerals' hardness is one of the factors which influences the rate of abrading. For particles initially of uniform size two distinct size ranges of product will form, the coarse, near the initial size, and the very fine<sup>(36, 37, 38)</sup>. Figure 2.1 shows the different mechanisms of particle fracture and the resulting product size distributions.

Another mechanism of fracture is cleavage or chipping. These two terms are classified in the same category, because particles which tend to cleave preferentially might be expected to be highly susceptible to chipping<sup>(36)</sup>. Since chipping is the breakage of edges or corners of a particle, therefore it is probably considered to be a case of cleavage<sup>(39)</sup>. Fracture by cleavage or chipping occurs when the energy applied is insufficient to produce complete fracture of the particles, or is just sufficient to load few

regions of the particles to the fracture point. This may happen if the particle is too large to be broken by the grinding medium, and as a result, the product size of cleavage or chipping is close to the original particle size<sup>(36, 39)</sup> (Figure 2.1).



**Figure 2.1:** Representation of the mechanisms of particle fraction and the resulting product size distributions (reprinted with permission from Kelly and Spottiswood<sup>(39)</sup>).

### 2.3 Particle Size Distribution of Comminuted Product

Since the primary effect of comminution is a decrease in particle size, determination of the product size is necessary. Several empirical size-distribution equations such as the Gaudin-Schuhmann, and the Rosin-Rammler have been proposed to describe the size distribution of broken materials<sup>(42)</sup>.

Gaudin and Schuhmann showed that the size distribution of a comminuted material can be expressed by the following empirical relationship<sup>(43, 44, 45, 46)</sup>:

$$Y = \left(\frac{x}{k}\right)^\alpha \quad (2.1)$$

where  $Y$  is the cumulative fraction finer than the stated particle size  $x$ . The  $\alpha$  and  $k$  are the distribution and size moduli (theoretical maximum size), respectively. The Rosin-Rammler empirical equation<sup>(47, 48, 49, 50)</sup>, which relates the same relative fraction of undersize to the relative size modulus, is as follows<sup>(44)</sup>:

$$Y = 1 - e^{-\left(\frac{x}{k}\right)^\alpha} \quad (2.2)$$

Gaudin and Meloy<sup>(44)</sup> have given an equation based on the single fracture and breakage, as follows:

$$Y = 1 - \left(1 - \frac{x}{x_f}\right)^\alpha \quad (2.3)$$

where  $x_f$  is the feed or initial and or maximum size and  $u$  is the size ratio which is a measure of the number of breaks in the particle and  $x$  is the size considered. It has been demonstrated that the Gaudin-Meloy distribution for single fracture is equally applicable to multiple fracture and is related to the Gaudin-Schuhmann distribution at least when the distribution modulus  $\alpha$  is close to unity<sup>(51)</sup>.

In 1956 Broadbent and Callcott<sup>(52, 53)</sup> described a method to analyze comminution products. They postulated that the size distribution from the breakage of a single particle is as follows:

$$Y = \frac{1 - e^{-\left(\frac{x}{x_0}\right)}}{1 - e^{-1}} \quad (2.4)$$

They attempted an experimental verification of the theory using an assumed primary breakage distribution, but the results were not very satisfactory.

Gilvarry <sup>(45, 54, 55)</sup> gave a new theoretical concept based on the existence and importance of the edge flaws in a solid material as postulated by Griffith <sup>(56, 57)</sup>. The equation obtained is as follows:

$$Y = 1 - e^{-\left[\frac{x}{a_1} - \left(\frac{x}{a_2}\right)^2 - \left(\frac{x}{a_3}\right)^3\right]} \quad (2.5)$$

where  $a_1$ ,  $a_2$ ,  $a_3$  are constants which include the mean density of stress activated flaws and shape factor. For small values of  $x$  the tail of the distribution goes to:

$$Y = 1 - e^{-\left(\frac{x}{a_1}\right)} \quad (2.6)$$

which is the Rosin-Rammler equation with an exponent of 1, and yields a logarithmic  $x$  value of:

$$Y = \left(\frac{x}{a_1}\right) \quad (2.7)$$

which is the Gaudin-Schuhmann law with an exponent of 1. The main disadvantage of this approach is that it can only be applied when the maximum fragment size of product is much smaller than the initial particle size <sup>(52)</sup>.

Klimpel and Austin <sup>(52)</sup> derived an equation which contains the earlier equations as special or approximate cases based on single fracture where overbreakage is avoided. The basis of the model is as that of Gilvarry. It is proposed that a volume within the

original particle is bounded by fractures and requires only one further fracture surface to make it a fragment. This equation is presented as follows:

$$Y = 1 - \left[ 1 - \left( \frac{x}{x_f} \right)^1 \right]^{\mu_1} \left[ 1 - \left( \frac{x}{x_f} \right)^2 \right]^{\mu_2} \left[ 1 - \left( \frac{x}{x_f} \right)^3 \right]^{\mu_3} \quad (2.8)$$

where  $u_1$ ,  $u_2$  and  $u_3$  are parameters related to the probability of the number of cuts occurring in fracture per length, surface and volume, respectively. It is defined<sup>(52)</sup> that for a particle to break [ $u_1 + u_2 + u_3$ ] must be at least unity.

Harris<sup>(47, 58)</sup> proposed an equation in differential form expressing the relationship of  $[dY/dx]$  with  $x$ , in particular representing the upper and lower limiting particle sizes and the skewed nature of the distribution as follows:

$$\frac{dY}{dx} = C (x - x_p)^{k_1} (x_f - x)^{k_2} \quad (2.9)$$

where  $C$ ,  $k_1$  and  $k_2$  are constants;  $x_f$  and  $x_p$  are the maximum and minimum of feed and product sizes, respectively. The shape of the distribution curve is determined by  $k_1$  and  $k_2$ , and it has a maximum when both  $k_1$  and  $k_2$  are positive. If both are null, the curve degenerates to a horizontal line, and when  $k_1$  and  $k_2$  are negative, the two branches asymptote upwards to two vertical lines  $x = x_f$  and  $x = x_p$ . In the case of small  $x_p$ , it can be neglected, and Equation 2.9 is written as follows:

$$\frac{dY}{dx} = C_1 x^{k_1} \left( 1 - \frac{x}{x_f} \right)^{k_2} \quad (2.10)$$

where  $C_1$  is a new constant related to  $C$ ,  $x_f$  and  $k_2$  as follows:

$$C_1 = (Cx_f)^{k_2} \quad (2.11)$$

Harris's method has a statistical basis<sup>(58)</sup> with the necessary form and flexibility to

describe the major features of size distribution curves.

## 2.4 Comminution Laws (Energy-Size Reduction Relationships)

A number of attempts have been made to formulate a general law of comminution. Obviously the ease with which substances may be comminuted varies considerably from material to material. In 1867 Rittinger<sup>(59, 60)</sup> stated that the energy required for size reduction of a solid is directly proportional to the new surface area created during the size reduction process. Rittinger's hypothesis can mathematically be stated as follows:

$$E = C_2 \left( \frac{1}{x_2} - \frac{1}{x_1} \right) \quad (2.12)$$

where E is energy input per unit volume,  $C_2$  is a constant,  $x_1$  and  $x_2$  are initial and final size, respectively. In 1885 Kick<sup>(59, 60, 61)</sup> suggested that for geometrically similar shape reduction, the energy varies as a function of the volumes or weights of the broken particles and the energy per unit volume is otherwise constant. The Kick concept may be expressed as follows:

$$E = C_3 \log \left( \frac{x_1}{x_2} \right) \quad (2.13)$$

where  $C_3$  is a constant.

Bond in 1952<sup>(57, 60, 62)</sup> proposed the third theory of comminution, and stated that "the total work useful in breakage which has been applied to a stated weight of homogeneous broken material is inversely proportional to the square root of the diameter of the product particles"<sup>(63, 64, 65)</sup>, i.e.:

$$W_t = \frac{C_4}{\sqrt{x_p}} \quad (2.14)$$

where  $W_t$  is the total work input and  $C_4$  represents a proportionality constant and  $x_p$  is the product size or the 80% passing size on a screen analysis plot. Since the purpose of this estimation is to relate the work input to the produced particle size, Bond introduced  $C_4$  as the experimental work index,  $W_i$ . It is defined as the number of kilowatt-hours required to reduce a ton of material from theoretically infinite size to 80% passing of 100 microns. Thus, this yields:

$$W_t = 10 W_i \left( \frac{1}{\sqrt{x_p}} - \frac{1}{\sqrt{x_f}} \right) \quad (2.15)$$

All the previous theories of comminution can generally be expressed in a differential equation form <sup>(66, 67, 68)</sup>:

$$\frac{dE}{dx} = - \left( \frac{C_5}{x^{n_1}} \right) \quad (2.16)$$

where  $x$  is the product size,  $C_5$  and  $n_1$  are constants,  $C_5$  being related to the material or unit chosen and  $n_1$  being an exponent indicating the order of the comminution process. It has been pointed out <sup>(66, 68)</sup> that by choosing some simple values of  $n_1$  and integrating Equation 2.16, all the previous theories can be found. If  $n_1=1$  this gives Kick's law; with  $n_1$  equals 2, integration gives Rittinger's law; and  $n_1=1.5$  leads to the third theory of comminution by Bond.

Further developments have been made by Holmes <sup>(61)</sup> and Charles <sup>(43, 59)</sup>. Holmes

employed a modified form of Kick's law, to suit the general characteristics of inhomogeneous brittle materials, and suggested the work input for comminution,  $W_i$ , in terms of reduction ratio,  $R$ , and product size as follows:

$$W_i = W_i \left[ 1 - \left( \frac{1}{R} \right)^u \right] \left( \frac{100}{x_p} \right)^u \quad (2.17)$$

where  $W_i$  is the work index, and  $u$  is Kick's law deviation exponent. It varies for different materials and different conditions of stress application and is related to deviations of the comminution system from an ideal Kick's law behaviour. Charles<sup>(43, 59)</sup> developed a general energy-size reduction equation for materials following the Gaudin-Schuhmann size distribution (Equation 2.1):

$$E = C_6 k^{(1-n)} \quad (2.18)$$

where  $C_6$  and  $n$  are constants. It has been shown<sup>(43)</sup> that the constants  $\alpha$  and  $n$  (Equations 2.1 and 2.18) are both dependent on the nature of materials and on the comminution devices. Berlioz and Fuerstenau<sup>(69)</sup> stated that in Charles' relation, if there is to be any fundamental basis for the  $E$  versus  $k$  relationship,  $E$  must be a measure of the useful work and not the total work input. Accordingly, they used a special batch ball mill which the power drawn could be determined with torque measuring apparatus.

## 2.5 Comminution Kinetics

Comminution kinetics looks at how the size distribution of a material evolves with grinding time. It is related to the rates at which feed (coarse) particles are ground and fines are produced, i.e. the disappearance from coarse sizes and appearance into finer sizes. The relationship among three variables, energy input (which can explicitly or implicitly be a function of grinding time), the mass being broken and its size distribution are described. Typical applications are the sizing, the optimization and automatic control

of crushing and grinding circuits<sup>(70, 71, 72, 73)</sup>, which are best achieved when comminution processes are simulated as close to reality as possible<sup>(74, 75, 76, 77, 78)</sup>.

Roberts<sup>(79, 80)</sup> used the probability theory approach and applied a first-order kinetics to the rate of size reduction. He introduced the mill power intensity as a part of the rate constant and stated that it is independent of the mill size. He presented the first-order equation as follow:

$$-\frac{dw(x,t)}{dt} = k_3 \left[ \frac{\text{Power}}{\text{Ton}} \right] w(x,t) \quad (2.19)$$

or,

$$w(x,t) = w(x,0) e^{\left( -k_3 \left[ \frac{\text{Power}}{\text{Ton}} \right] t \right)} \quad (2.20)$$

where  $w(x,t)$  is the cumulative mass coarser than size  $x$ , at  $t$  grinding time and  $w(x,0)$  is the same at time equal zero, and  $k_3$  is a constant for any size of density of solid and moisture content of pulp, and particles.

Bowdish<sup>(81)</sup> in theoretical and experimental studies, investigated the rate of breaking of oversized particles. In a further development of Roberts theory, he stated that a change in the area of the balls in a mill should make a change in the rate at which oversized particles are broken, which he tried to describe with first-order, second-order and zero-order models<sup>(81)</sup>. Arbiter and Bhrany<sup>(80, 82)</sup> experimentally showed that the rate of production for finer size fractions is constant (with time) and exponentially dependent on screen size. They observed that the fine particles production follows a zero-order kinetic, and its amount is directly proportional to the grinding time<sup>(83)</sup>. Fuerstenau and Somasundaran<sup>(25, 83)</sup>, observed this zero-order of fine particles production and in 1968 Herbst and Fuerstenau attempted to depict the interrelationship between selection function and breakage function<sup>(25)</sup>.

Harris<sup>(84)</sup> explained the three main research groups and frameworks which have been used to describe grinding kinetics namely, the creation of finer sizes, the distribution of coarser fractions, and the selection and breakage functions. He labelled the first one the Fahrenwald-Arbiter-Bhrany<sup>(84)</sup> approach, which essentially leads to fines production that follows zero-order kinetics. The second approach, the disappearance kinetics of the coarser fractions, and is a first-order kinetics phenomenon. The third one is the prediction of the size distribution equation via the selection and breakage function<sup>(85, 86)</sup>, using computerized solutions of the integro-differential equation of batch grinding, and both analytical and numerical solutions have been proposed<sup>(87, 88, 89)</sup>.

## 2.6 Batch Grinding Integro-Differential Equation

Epstein<sup>(49, 90, 91)</sup> formulated a description of breakage processes in terms of two parameters, the selection and distribution functions. The selection function,  $s$ , is the fraction by weight of a given particle size,  $x$ , which is broken per breakage event. The breakage or distribution function,  $B$ , describes the size distribution of the products of the breakage upon single breakage. The two concepts are combined in a series of mass balance equation (one per size class) that describes material appearing in a given size class upon breakage from coarser ones, and leaving because of breakage.

Broadbent and Callcott<sup>(53, 92, 93)</sup> accepted the proposed definition of  $s$  and  $B$  by Epstein and developed the matrix methodology of mathematical analysis. They made an assumption that the distribution function is the same for all coals, machines and particle sizes and defined it as:

$$B = \frac{\left[ 1 - e^{-\left(\frac{x}{x_n}\right)} \right]}{\left[ 1 - e^{-1} \right]} \quad (2.21)$$

When they attempted to determine the  $s$  and  $B$  values experimentally, they did not obtain

very satisfactory results <sup>(52, 94)</sup>.

Sedlatschek and Bass <sup>(87, 89, 95)</sup> in 1953 proposed a set of differential equations to describe the batch grinding process and a series of experiments to yield the unknown coefficients. In 1954 Bass <sup>(84, 89, 91)</sup> presented a mathematical theory for milling processes and was the first who derived the fundamental mass balance for batch grinding as an integro-differential equation as follows:

$$\frac{\partial^2 Y(x,t)}{\partial x \partial t} = -s(x) \frac{\partial Y(x,t)}{\partial t} + \int_x^{x_m} \frac{\partial B(x,z)}{\partial x} s(z) \frac{\partial Y(z,t)}{\partial z} dz \quad (2.22)$$

In 1962 Gardner and Austin <sup>(32, 87, 88, 96)</sup> proposed an equivalent equation to that of Bass in the cumulative form and presented two computer solutions to the integro-differential equation of batch grinding:

$$Y(x,t) = Y(x,0) + \int_0^t \int_x^{x_m} B(x,z) s(z) \frac{\partial Y(z,t)}{\partial z} dz dt \quad (2.23)$$

where  $Y(x,t)$  is the cumulative weight fraction of material finer than size  $x$  after grinding time  $t$ , a feed material having size distribution  $Y(x,0)$ . The maximum particle size is  $x_m$ .  $B(x,z)$  and  $s(x)$  are the breakage function and selection function, respectively. Many researchers have solved Equations 2.22 or 2.23 numerically and have shown that there is good agreement between calculated and experimental results. However, the analytical solutions were attempted by making several assumptions to simplify the equations. A simple analytical solution was presented <sup>(97, 98, 99)</sup> where the selection and breakage functions were introduced as a function of a new parameter. This assumption has no physical basis and has just been employed for mathematical simplicity.

Gaudin and Meloy<sup>(44, 91)</sup> used the matrix analysis to solve the batch grinding equation numerically, and presented calculated results for several theoretical batch grinds with different probabilities of breakage and breakage distribution functions which their calculated size distributions showed to be very similar to the same as experimental results<sup>(91)</sup>. The work on batch grinding equation was extended by other researchers who tried to achieve a better understanding and a more accurate mathematical representation.

## 2.7 The Practical Equation (The Size-Mass Balance Equation)

The integro-differential batch grinding equation (Equations 2.22 or 2.23) is not easily solved. It is thus easier to use an equation based on practical parameters which have physical meanings, and can be determined directly by experimentation. This is best achieved with a size-discretized representation. Consider a set of  $m$  screens numbered from the coarsest at the top of the set to the finest at the bottom. The general screen,  $i$ , has an aperture of size  $x_i$  and the sizes of the next coarser and finer screens are  $x_{i-1}$  and  $x_{i+1}$ , respectively. If a mass  $W$  is fed to the screen set, then the material retained on the screen  $i$  after passing through screen  $i-1$  has a size range from  $x_i$  to  $x_{i-1}$ , and has a fractional weight  $w_i(t)$  at time  $t$ <sup>(100)</sup>.

The mass balance equation is established<sup>(91)</sup> from the fractional weight passing the finest screen,  $w_{res}(t)$ , and the sum of fractional weights in size  $i$ , as follows:

$$w_{res}(t) + \sum_{i=1}^m w_i(t) = 100\% \quad (2.24)$$

It is obviously understood that for any size  $i$ , mass change through grinding is described by two terms, a positive mass change from coarser sizes (appearance term) and a negative one for mass reporting to finer sizes (disappearance term). The breakage function,  $b_{i,j}$ , is the fractional weight retained on a finer screen,  $i$ , which has been

produced by a single breakage from coarser size  $j$ <sup>(100)</sup>. The mass balance equation is as follows<sup>(25, 91)</sup>:

$$\frac{dw_i(t)}{dt} = -s_i w_i(t) + \sum_{j=1}^{i-1} b_{ij} s_j w_j(t) \quad (2.25)$$

This equation is a particular finite difference form of Equation 2.22<sup>(91)</sup> and can be solved analytically and/or numerically to yield the mass in different size classes.

## 2.8 The Rate Constant of Breakage or Selection Function

The selection function is dependent on the material hardness, and the equipment, and particularly the number of fracture events generated per unit time<sup>(39)</sup>. For specific ball mill and material, ball size<sup>(101, 102, 103, 104)</sup>, mill speed<sup>(105, 106)</sup>, ball loading<sup>(105, 107, 108)</sup>, reduction of the specific gravity of the grinding media<sup>(39, 109)</sup>, media shape<sup>(110, 111)</sup>, mill diameter<sup>(112, 113)</sup>, and the nature of mill contents<sup>(26)</sup> and powder filling<sup>(114, 115, 116, 117, 118, 119)</sup> are various parameters which affect the selection function. Austin and Klimpel presented a procedure to predict the specific rate of breakage in a ball mill containing a mixture of balls, from breakage parameters measured with a single diameter of ball<sup>(120)</sup>. It has empirically been found<sup>(11, 100)</sup> that the selection function is proportional to particle size up to a maximum value and then it falls off. The relation of selection function and particle size for small range of particles size<sup>(121, 122, 123)</sup> is as follows:

$$s_i = a x_i^{a_1} \quad (2.26)$$

For large particles a correction factor is added as below:

$$s_i = a x_i^{a_1} Q_i \quad (2.27)$$

and,

$$Q_i = \frac{1}{\left[1 + \left(\frac{x_i}{\mu}\right)^\Lambda\right]} \quad (2.28)$$

where  $a$ ,  $\alpha_1$ ,  $\mu$ , and  $\Lambda$  are descriptive parameters, and  $\Lambda \geq 0$ . The factor  $Q_i$  (correction factor) is 1 for small  $x_i$  and tends to zero as  $x_i$  increases. The maximum selection function occurs at a particle size  $x_m$  related to  $\mu$  and  $\Lambda$  by<sup>(100)</sup>:

$$x_m = \mu \left(\frac{\Lambda - \alpha_1}{\alpha_1}\right)^{-\left(\frac{1}{\Lambda}\right)}, \quad \Lambda > \alpha_1 > 0 \quad (2.29)$$

Various phenomenological explanations for the relationship between the selection function and particle size have been proposed. As shown in Table 2.1, they can be divided into energy and geometry based considerations.

**Table 2.1:** The variation of selection function (SF) with collision and existence flaws.

Phenomena	Geometry Based	Energy Based
Decrease in SF with decreasing size (fine end)	Lower ball-particle-ball collision probability	Smaller Griffith flaws
Decrease in SF with increasing size (coarse end)	Nipping	Energy released upon collision too low

Below  $x_m$  is generally the most important part of the curve, where most material is found and most energy consumed. The decrease in selection function with decreasing particle size stems from the higher strength of small particles, as their Griffith flaws are also smaller<sup>(124, 125)</sup>. Geometrically, smaller particles also have a lower probability of ball-particle-ball collision.

Above  $x_m$ , the selection function decreases with increasing particle size. Although the probability of collision is extremely high, the probability of breakage decreases substantially as particle size increases. This is largely due to a mismatch between the energy required for breakage, and that released by the grinding media upon single collisions, which is much lower. A geometry based explanation has also been proposed: as particle size increases, the nipping angle formed between two balls colliding with this particle also increases. If it exceeds a critical angle corresponding to the dynamic coefficient of friction, mineral particles slide out rather than be compressed. The value of this critical angle is geometry and mineral specific<sup>(28)</sup> between metal and mineral.

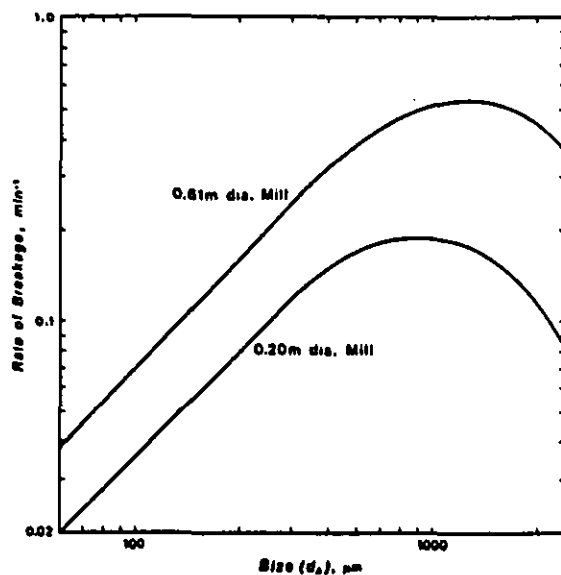


**Figure 2.2:** Breakage rates for two types of mill with different diameter (reprinted with permission from Kelly and Spottiswood<sup>(39)</sup>).

Figure 2.2 shows the variation of breakage rate for two mills with different diameters. It has been stated<sup>(106)</sup> that to scale-up mills the dependence of grinding kinetics parameters (selection and breakage functions) on the mill conditions such as mill diameter, mill speed, media load, size, particle hold-up must be known. Hodouin, Bérubé, and Everell<sup>(126)</sup> reported that an extrapolation technique can be used for the

selection function,  $s$ , measured with a laboratory ball mill to be applied in industrial-size mill. The breakage function, considered independent of environment, does not require scale-up.

For large particles, the disappearance of material from a given top size interval is often not first order<sup>(127, 128, 129)</sup>. This has been attributed<sup>(130)</sup> to the fact that large particles have two components, one hard part with a low breakage rate and a soft fraction with a high breakage rate<sup>(131)</sup>. Figure 2.3 shows the selection function of a gold ore which has different components in the coarse sizes.

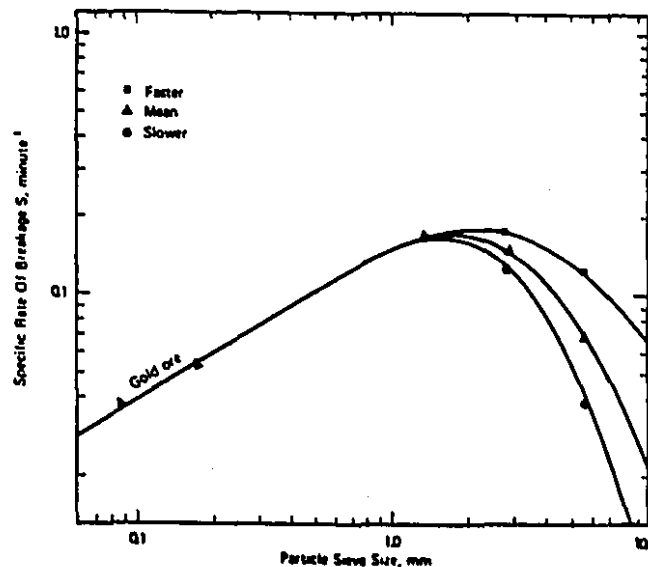


Figure 2.3: Breakage rate of gold ore as a function of particle size (reprinted with permission from Austin, Klimpel and Luckie<sup>(100)</sup>).

## 2.9 Selection Function Determination

The selection function is usually determined using two methods, laboratory batch grinding test (one-size-fraction method) and back-calculation techniques.

### 2.9.1 The batch grinding test (The one-size-fraction test)

This method is applied for material in one size class and for this reason it is called "one-size-fraction" test or method. Selected material is ground in each grinding time for different times and the mass remaining in this size class is monitored. Mathematically, first-order grinding yields:

$$S_i = \frac{\text{Ln} \left( \frac{w_i(t)}{w_i(0)} \right)}{t} \quad (2.30)$$

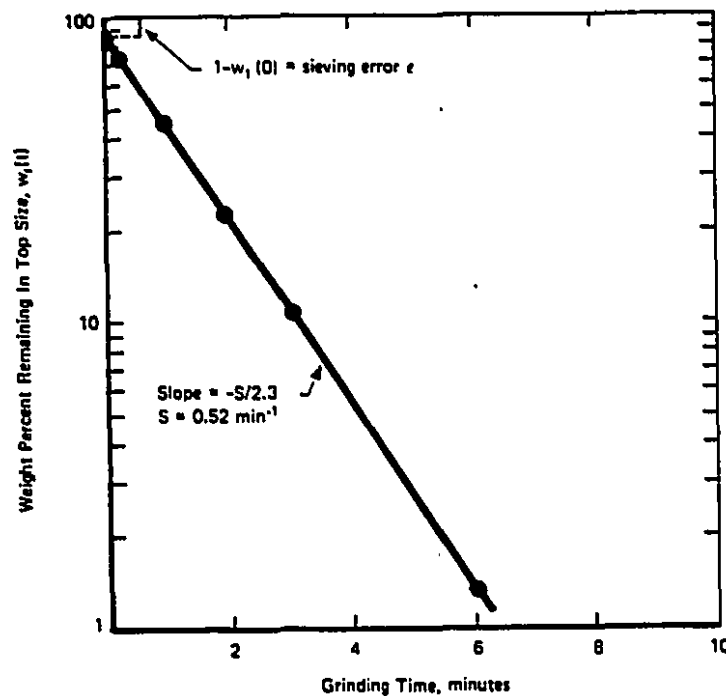


Figure 2.4: First-order plot to estimate of selection function (reprinted with permission from Austin, Klimpel and Luckie<sup>(100)</sup>).

Graphically a plot of the weight fraction remaining in the top size,  $w_i(t)$ , on a vertical log scale versus grinding time,  $t$ , on a linear scale, yields a straight line whose

slope is the negative of the selection function<sup>(106, 132, 133)</sup> (Figure 2.4). Although this method offers a powerful illustration of first-order disappearance kinetics, it is time consuming<sup>(100)</sup>, restricted to laboratory units, and can not be used when studying interaction between various size classes in the feed, which can affect the selection function. Its interest is mostly didactic.

### 2.9.2 The back-calculation method

For most applications, the selection function is indirectly determined by back-calculation techniques from experimental data. Two methods, one based on a single data set and the other on multiple sets<sup>1</sup>, can be used. In both cases, a computerized algorithm is used to estimate the selection function, by non-linear optimization<sup>(108, 134)</sup>.

Table 2.2 summarizes the possible approaches, which can yield an exact or least square fit (LSF). In each case the degrees of freedom (df.) is shown based on  $p$  sets of data,  $n$  size classes, and  $m$  parameters. The simplest and least reliable approach is to fit a single data set with a vector of selection function values, one for each size class. This method yields a single unique solution; therefore, model validation can only be achieved if many data sets are thus fitted, and the selection function vectors compared<sup>(135)</sup>. Even with a single data set, partial model validation can be obtained if a functional relationship is assumed between particle and the selection function (these will be reviewed below), as suggested by Hodouin<sup>(136)</sup>. Better reliability is achieved when multiple data sets are fitted with either a functional relationship or a vector of selection function values. In this work, multiple data sets will always be fitted, typically with a vector (i.e. selection function, flattening and folding rate constants).

---

<sup>1</sup>A data set is described as a set of measured feed and discharge size distributions (continuous grinding), or size distributions before grinding and after a grinding time  $t$  (batch mill).

Table 2.2: Variation of different methods to estimate selection function (SF).

No. of Data Set: → SF Condition: ↓	Single Data Set (p=1)	Multiple Data Set (p > 1)
Individual SF, (No functional form)	Exact Fit, df.:0	LSF, df.:n(p-1)
Functional description, m parameters	LSF, df.:(n-m)	LSF, df.:np-m

Klimpel and Austin used Equation 2.26 and the following equation to estimate selection function, using the back-calculation method<sup>(33, 132, 137)</sup>.

$$\log(s_i) = C_{11} + C_{12} (\log x_i)^1 + C_{13} (\log x_i)^2 + C_{14} (\log x_i)^3 + \dots \quad (2.31)$$

where  $x_i$  is the lower particle size and the  $C_{1i}$  values are constants. It has been reported that the estimated  $s$  values by Equation 2.31, sometimes give illogical shapes for the  $s$  versus  $x$  curves, especially when the breakage function is non-normalizable<sup>(132, 137)</sup>. This problem can be minimized if a more phenomenological relation is assumed between the selection function and particle size<sup>(136)</sup>, such as:

$$s_i = \frac{(C_{14} x_i^{C_{15}})}{(1 + C_{16} x_i^{C_{17}})} \quad (3.32)$$

where the  $C_{14}$ ,  $C_{15}$ ,  $C_{16}$ , and  $C_{17}$  are constants. The flexibility of using all available data or a limited data subset and application to continuous full-scale data are the advantages of this method, whereas its main disadvantage is that it is not always possible to detect when certain assumptions (e.g. normalized breakage function, section 2-10, or single selection function values for a huge data set) are not valid<sup>(100)</sup>.

## 2.10 Breakage and Cumulative Breakage Functions

As briefly mentioned in sections 2.7 and 2.8, the cumulative breakage function,  $B_{i,j}$ , is the weight fraction of material which, when broken once from size class  $j$ , is finer than size class  $i$ . In the size-discretized formulation, the breakage function,  $b_{i,j}$ , is the proportion of broken material which appears in size class  $i$  upon single breakage from size class  $j$ <sup>(39, 138)</sup>. Figure 2.5 presents a schematic view of the breakage and cumulative breakage functions for different size classes in a set of screens, for material broken from size class  $j$ .

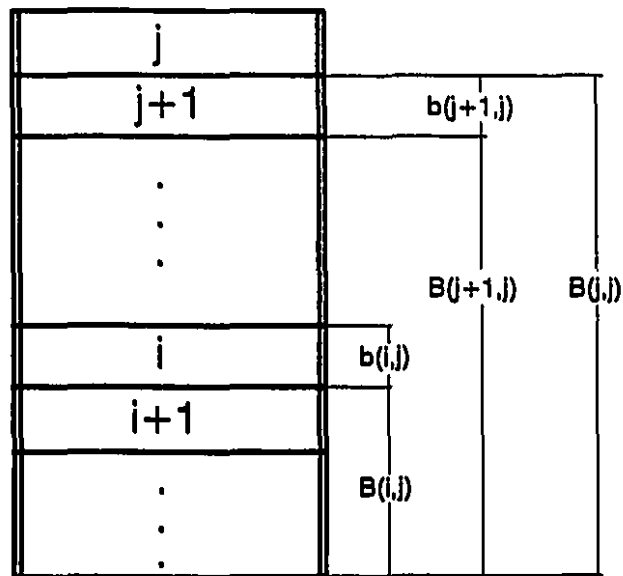


Figure 2.5: Weight fraction variation in a set of screen.

Since it is difficult to measure fragments broken from size class  $j$  into size class  $j$ , most researchers consider as broken only that part of the material which leaves the size class it is broken from; therefore it is understood<sup>(31, 139)</sup> that:

$$B_{jj} = 1 \quad (2.33)$$

$$b_{ij} = B_{i-1,j} - B_{i,j} \quad (2.34)$$

and in matrix form:

$$B = \begin{bmatrix} 0 & 0 & 0 & \dots & 0 \\ b_{2,1} & 0 & 0 & \dots & 0 \\ b_{3,1} & b_{3,2} & 0 & \dots & 0 \\ b_{4,1} & b_{4,2} & b_{4,3} & \dots & 0 \\ \vdots & \vdots & \vdots & \ddots & \vdots \\ b_{n-1,1} & b_{n-2,2} & b_{n-3,3} & \dots & 0 \end{bmatrix} \quad (2.35)$$

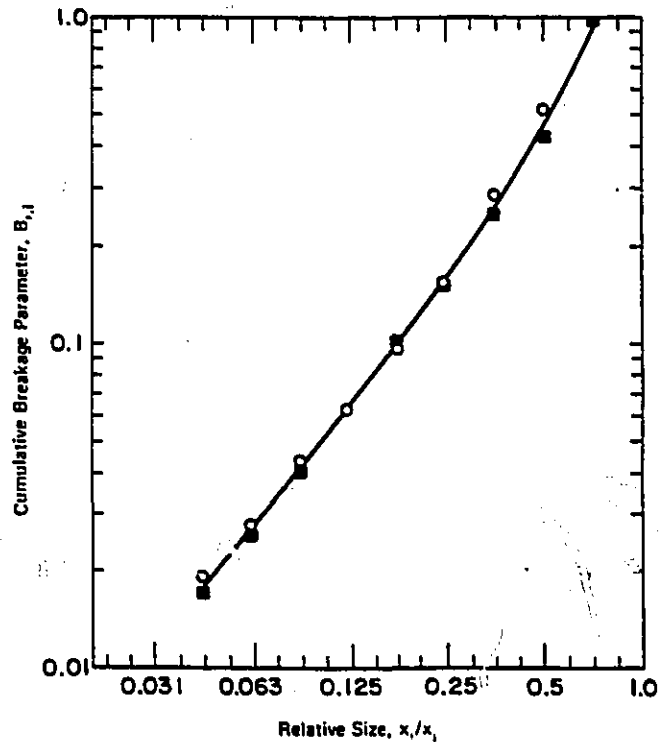


**Figure 2.6:** Normalizable cumulative breakage function for ball milling of quartz; ■: dry grinding, ○: wet grinding (reprinted with permission from Austin, Klimpel and Luckie (100)).

A breakage function is considered normalizable when it is independent of initial particle size; it then needs to be determined for just a single initial particle size. Figure 2.6 presents a typical normalizable breakage function. For normalizable breakage functions, the B matrix can be defined with a single column vector, and  $b_{i,j}$  can be replaced with  $b_{i,j}$  yielding:

$$\begin{aligned} b_{2,1} &= b_{3,2} = b_{4,3} = \dots = b_{j-1,j} \\ b_{3,1} &= b_{4,2} = b_{5,3} = \dots = b_{j-2,j} \\ &\dots \\ b_{i,1} &= b_{i+1,2} = b_{i+2,3} = \dots = b_{i+j-1,j} \end{aligned} \quad (2.36)$$

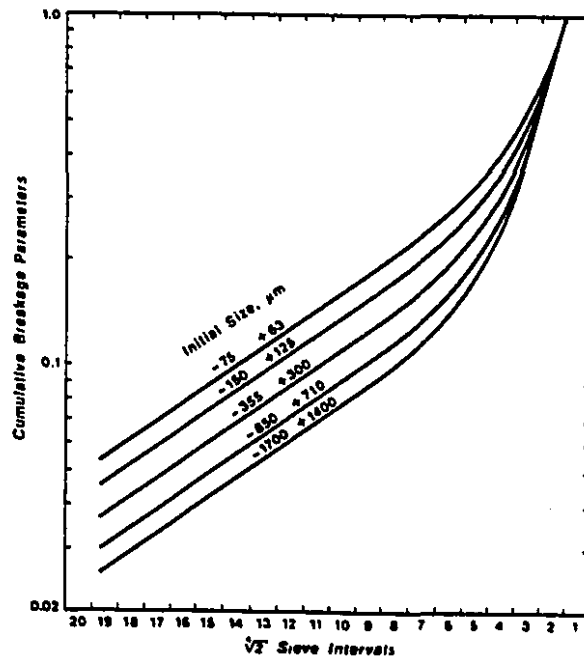


**Figure 2.7:** Non-normalizable cumulative breakage function plot (reprinted with permission from Kelly and Spottiswood<sup>(39)</sup>).

Normalizable breakage function values are usually plotted on a relative size basis,  $x_i/x_j$ , as shown in Figure 2.6. If spread in the product size distribution decreases as the initial particle size increases, the breakage function is non-normalizable. It can also be said that the larger particles produce a fewer fines, and or the smaller the breaking size,

the larger the amount of fines. Figure 2.7 shows a set of non-normalizable cumulative breakage function plot.

## 2.11 Breakage Function Determination

To estimate the breakage function distribution of materials, three main methods have been used <sup>(100, 132)</sup>:

- Single particle breakage test
- One-size-fraction test
- Back-calculation technique

### 2.11.1 Single particle breakage method

In this method, breakage of single particles is measured <sup>(140)</sup>. Comminution characteristics are also related to the energy input. Therefore, the required energy to break single particles can yield the basic data needed to estimate to the energy consumption in a practical comminution unit.

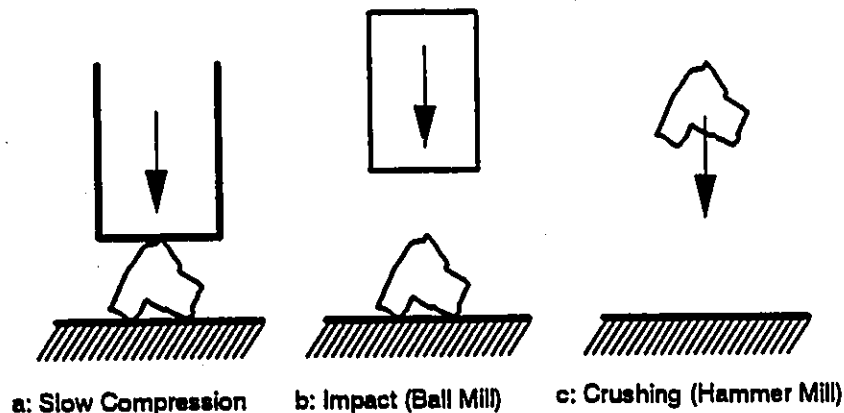


**Figure 2.8:** Three different single particle test methods; 1) slow compression, 2) Impact by a falling media, 3) Impact at high particle speed (Adapted from Krogh <sup>(141)</sup>).

The single particle tests are classified into three different types of tests<sup>(141)</sup>; slow compression, impact crushing, and abrasion. Figure 2.8 shows several types of single particle test method. The impact or falling media method is classified into single impact, double impact and pendulum tests<sup>(132, 142, 143)</sup>.

### 2.11.2 One-size-fraction test

In batch grinding tests, feed materials in one size fraction are ground for one or many short incremental times. The smaller the amount of material broken out of the initial size, the more accurate the breakage function values estimates are. It has been reported<sup>(100)</sup> that good results are obtained when the grinding time is chosen to give an amount of broken material out of the top size interval of about 20-30%. Klimpel and Austin also stated<sup>(100)</sup> that in order to get reliable values of the breakage function it is necessary to grind the one size fraction material (feed) for short times. By definition the values of  $b$  and  $B$  are calculated from:

$$b_{i,1} = \frac{w_i(t)}{w_1(0) - w_1(t)}, \quad i \geq 2 \quad (2.37)$$

$$B_{i,1} = \frac{P_i(t) - P_i(0)}{P_2(t) - P_2(0)}, \quad t \rightarrow 0, \quad i > 1, \quad \text{Method BI} \quad (2.38)$$

To get more accurate  $B$  values and use a procedure to correct for errors produced by secondary breakage, the solution of the batch grinding equation leads to method II, as Equation 2.39<sup>(100, 144)</sup>. It has been reported<sup>(100)</sup> that the BI method only works for a very small degree of grinding, and the BII method gives reasonable values up to about 30% of the top size broken out. Another method, BIII, is, in fact, the back-calculation method which requires an estimate of  $s$ .

$$B_{i,1} = \frac{\log \left[ \frac{(1 - P_i(0))}{(1 - P_i(t))} \right]}{\log \left[ \frac{(1 - P_2(0))}{(1 - P_2(t))} \right]}, \quad i > 1, \quad \text{Method BII} \quad (2.39)$$

### 2.11.3 Back-calculation

In the back-calculation method a computerized search procedure is attempted to obtain breakage parameters from size distribution produced by batch or continuous grinding<sup>(33)</sup>, based on a defined function. Klimpel and Austin reported that the value of  $B_{ij}$  can be fitted by an empirical function<sup>(100, 137, 145)</sup> made up of the sum of two straight lines on log-log scale plot, as follows:

$$B_{ij} = \phi_j \left( \frac{x_{i-1}}{x_j} \right)^\gamma + (1 - \phi_j) \left( \frac{x_{i-1}}{x_j} \right)^\beta, \quad 0 \leq \phi_j \leq 1 \quad (2.40)$$

where  $\phi_j$ ,  $\gamma$  and  $\beta$ , defined in Figure 2.9, are material specific. Other functions that have also been found to be quite suitable for representing the breakage function for various materials<sup>(136)</sup> are as follows:

$$B_{ij} = C_{18} \left( \frac{1}{x_j} \right)^{C_{19}} \left( \frac{x_i}{x_j} \right)^{C_{110}} + [1 - C_{18} \left( \frac{1}{x_j} \right)^{C_{19}}] \left( \frac{x_i}{x_j} \right)^{C_{111}} \quad (2.41)$$

$$B_{ij} = C_{18} \left( \frac{1}{x_j} \right)^{(C_{19} + C_{112})} \left( \frac{x_i}{x_j} \right)^{C_{110}} + [1 - C_{18} \left( \frac{1}{x_j} \right)^{C_{19}}] \left( \frac{x_i}{x_j} \right)^{(C_{111} + C_{113})} \quad (2.42)$$

where  $C_{12}$ ,  $C_{19}$ ,  $C_{110}$ ,  $C_{111}$ ,  $C_{112}$ , and  $C_{113}$  are constants.

When back calculating from batch grinding data sets, the size distribution of the feed and a minimum of two other grinding times is used as input and the computer program searches for the best values of the required parameters while minimizing the error between experimental and calculated values<sup>(100)</sup>. The continuous mill data are used based on the same criterion of error estimation (sum of least squares), knowing the residence time distribution.

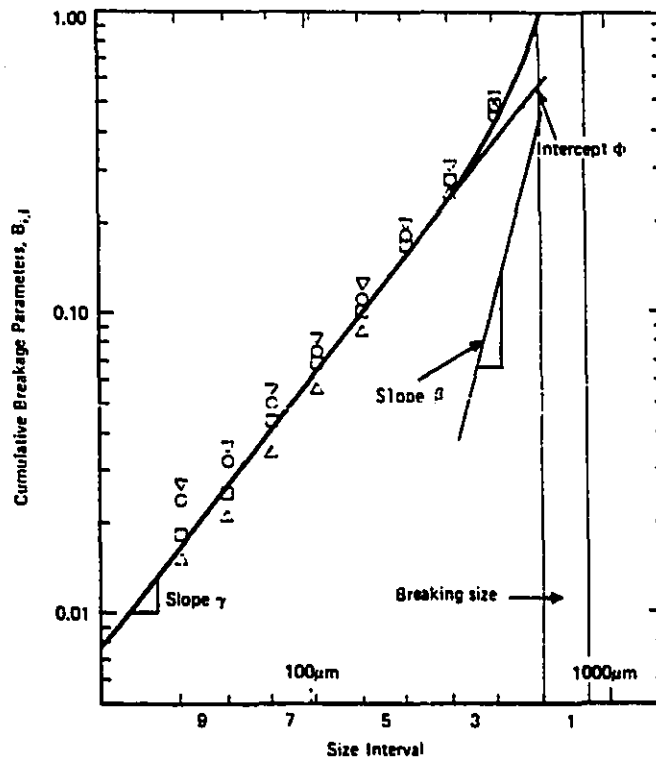


Figure 2.9: Cumulative breakage function distribution plot (reprinted with permission from Austin, Klimpel and Luckie<sup>(100)</sup>).

## 2.12 Malleability & Native Metals

There are many physical properties that characterize and aid to identify minerals.

Most of these properties can be divided into three groups <sup>(146)</sup>, based on a) cohesive forces, b) density, c) the action of light. Some other properties are less frequently used in the identification of minerals, such as response to heat, electrical conductivity and magnetism. The following properties depend on cohesive atomic forces: cleavage, fracture, hardness, tenacity, and elasticity. Some properties also related to the cohesive forces of minerals are classified under the tenacity group such as ductility, sectility, flexibility, brittleness and malleability <sup>(2, 146, 147)</sup>.

All solid materials show deformation, using an external load; some can recover their original dimensions or shape when the load is removed and some not. The recovery of the original shape of a deformed material when the load is removed is known as elastic behaviour <sup>(125)</sup>. The limiting load beyond which materials no longer show elastic behaviour is their elastic limit, they then undergo plastic deformation. Most minerals will break rather than undergo plastic deformation; most metals show plastic deformation, because of their metallic bonds <sup>(5)</sup>.

The metallic bond is a characteristic of ordinary metals and responsible for the cohesion of a metal. Electrons in metallic atoms are free to move, and by their movement, enable metals to carry electricity and heat <sup>(60)</sup>. The lack of attraction force between atoms allows entire blocks to slip easily in opposite directions when a strong force is applied <sup>(6)</sup>, but the atoms tend to re-bond as soon as the force is removed and the metal mass remains in one piece. As a result, metals are noted for their ability to be beaten into thin sheets, or to be bent or twisted repeatedly without breaking.

There are three iso-structural sub-groups of native metals; a) the gold group, including gold, silver, copper and lead, b) the platinum group, including platinum, palladium, iridium and osmium, and c) the iron group, including iron and nickel-iron <sup>(3, 148)</sup>. The elements of the gold group are similar in structure, with the atoms lying on the

points of a face-centered cubic lattice. In the platinum group, the structure is hexagonal close-packed, except platinum and palladium which have a cubic close-packed structure similar to the gold group. Crystals in the iron group metals have a body-centered cubic lattice <sup>(148)</sup>.

### 2.13 Metal Grinding

Milling is one of the methods to produce metallic powder <sup>(17, 149, 150)</sup>, and is being increasingly used in industry, particularly in aluminum and paint paste technologies <sup>(19, 20, 151)</sup> as a comparatively new technique (as of 1983). Metals, on account of their ductility, grind more slowly than brittle materials, resulting in increased energy consumption. A study of the literature suggests that it is not a widely investigated field. Previous work has focused on aluminum, copper, iron, zinc, tungsten, brass, and bronze.

When grinding ductile metal powders, a potential problem is the ability of particles to cold weld and agglomerate <sup>(14)</sup>, which is delayed or inhibited when grinding aids are employed <sup>(14, 152)</sup>. Rehbinder <sup>(12, 153)</sup>, in describing the mechanism of surface active or grinding aids, has mentioned that, when present in small quantities, affect the surface mechanical and electrical properties of metals. It has also been reported that the plastic flow of lead, tin and copper specimens increased under a given stress using the surface active liquid <sup>(153)</sup>.

The active mechanism of grinding aids has not been scientifically explained yet <sup>(100)</sup>. Rehbinder suggested that presence of grinding additives lowers the cohesive forces of solid molecules, and therefore adsorption of grinding aids in a flaw may weaken the bonding energies and therefore initiates the fracture. Some other researchers have suggested that the adsorbed grinding aids molecules pin the dislocations in the solids under the stress. These pins prevent the easy movement of dislocations or in fact prevent

plasticity<sup>(100, 154)</sup>, and causing a more brittle behaviour in that region of the solid. It has been mentioned that the grinding aids can change the fluidity of slurries and the flowability of dry powders, therefore affecting mass transfer through the grinding unit. Thus the effect of mass transfer or mass distribution changes may alter the particles which are to be nipped or broken<sup>(100, 154)</sup>.

Austin, Kilmpel, and Luckie<sup>(100)</sup>, in describing of acting mechanism of grinding aids, reported that two key factors can yield the optimum breakage rate; slurry density, and viscosity. These factors act against each other: higher slurry density increases the breakage rate, while the resulting higher slurry viscosity lowers it. The higher slurry density increases the lift of balls, and therefore the rate of breakage, whereas the higher slurry viscosity reduces the impact of balls. They explained that grinding aids act to take advantage of the higher density by reducing the effect of the higher viscosity. In the case of dry grinding aids, although they hypothesized that the effect of grinding aids is to change the cohesive forces of the particles, they conceded that the mechanism had not been explained<sup>(100)</sup>.

Hall<sup>(155)</sup> has patented in 1926 a method of metal grinding using oil-based grinding aids. For the grinding of nickel, iron and chromium-silver-copper, aids such as ethyl alcohol, water, cyclohexane, n-heptane, methylene chloride<sup>(13, 14)</sup> and lubricating oil<sup>(156)</sup> are used. In 1944, Olbrich<sup>(16)</sup> studied the grinding of compressed aluminum in a ball mill in the presence of grinding aids. He investigated three different grinding environments: porcelain balls and porcelain liner, steel balls and liner, and steel balls and liners with addition of grease and stearin to the charge of the mill. Grease and stearin considerably improved the grinding performance and increased the fineness of the product. The weight of added grinding aids were 0.1-0.3% of the weight of the aluminum charge.

Huttig and Sales<sup>(15, 157)</sup> in 1954 found that copper, zinc, aluminum, iron, tungsten and various alloys behave quite differently in grinding circuits. They presented three types of behaviour of metal powders during milling: brittle metals such as tungsten and Fe-Co-Al alloys ground readily, producing size distributions that could be fitted with a Rosin-Rammler law; tough materials, such as an alloy of chromium of nickel and carbon, abraded slowly; and large grains of soft metals such as copper, zinc, aluminum and partly with iron, were flattened rather broken.

Smith<sup>(158)</sup> in 1970 worked on the grinding of silver as a soft material in a vibration ball mill. His interest was in the grinding of soft materials of which malleable materials were a subgroup. A second subgroup was made of materials with excellent cleavage of which graphite was Smith's focus. Silver was chosen for its malleability and resistance to oxidation. In the grinding of silver he found that the initial particles were of a flaky character, which the flattened or plate-like form was retained throughout the grinding, and in graphite the rate of grinding exponentially decreased with time.

In 1972, Rees and Young<sup>(159)</sup> explained the processes which occur during the milling of combined of brittle tungsten carbide and ductile cobalt powder. They reported that a decrease in size of the tungsten carbide particles during grinding occurs and cobalt changes from a predominantly cubic to an hexagonal close packed structure. In 1976, Hopkins and Brooks<sup>(160)</sup> used cobalt powder in vibrational ball mill. They explained that initially the individual powder particles are flattened having a breadth/thickness ratios of 3:1. Size reduction took place with further grinding due to the propagation of cracks developed at the edge of particles and produced fine flakes.

Hashimoto and Watanabe<sup>(161)</sup> studied the impact of balls during vibratory ball milling of a mix of copper and 5% by volume of graphite powders. The motion of balls in a one-dimensional vibratory mill was analyzed by means of model simulation and

estimation of the energy consumption during impact. They found that the microhardness of the copper particles increased with an increase in the average energy consumption per collision.

Tripathi and Groszek <sup>(162, 163)</sup> in 1973 investigated the grinding of aluminum powder in the presence of five various types of hydrocarbons: tetraline, decalin, n-heptane, toluene and spindle oil. They reported that the processes of fragmentation and cold welding are affected by the nature of the hydrocarbons used in milling. They observed that a carbon-rich surface layer is produced on the surface of particles and powders due to the interaction between the freshly deformed surface and the hydrocarbons. This minimizes or prevents agglomeration.

In 1979, Vedaraman and Chandrasekaran <sup>(20)</sup> worked on the wet and dry grinding of aluminum powders by vibration and ball mills using stearic acid as a grinding aid, with a concentration between 0.05 to 4% of the weight of the aluminum charge. They intended to: a) study the effect of grinding characteristics such as feed weight (feed flowrate), grinding aid concentration, weight ratio and ball material density, and b) to compare the vibration and ball mills' performances. They found that under comparable operating conditions the rate of dry grinding in the vibration mill was higher. They also concluded that vibrating mills consume less energy than ball mills, for the same work.

Surshan, Vedaraman and Ramanujam <sup>(15, 20)</sup> in 1982 studied the mechanisms of grinding of aluminum, copper, and brass in a vibration mill, using relatively coarse materials. They used distilled stearic acid as grinding aid. They reported that, based on visual observations, adding the grinding aid is useful to prevent cold welding. They explained that the size distribution of metals used in grinding processes is based on the combination of two mechanisms: flattening followed by breakage, and abrasion. Flattening, which is followed by breakage, was dominant for aluminum, whereas for

---

copper (although the particles are flattened to a certain extent), abrasion seemed to be the dominant mechanism. For brass, flattening was almost negligible and abrasion was the main mechanism.

In 1990 and 1993, Moothedath and Sastry<sup>(164, 165)</sup> presented the functional forms of the rate parameters and the population balance models (PBM) for vibration milling of metal powders. They reported that grinding of metal powders takes place based on a combination of flattening, attrition and breakage mechanisms. They introduced two independent variables as the projected area diameter and thickness and developed a mathematical model for milling of metal powders by incorporating all these mechanisms, in contrast to the traditional grinding model for brittle materials which only includes breakage.

On gold grinding or gold breakage parameters estimation there is not a wide range of work. In 1985, the physical breakdown and abrasion rates of gold were studied using a tumbler to simulate natural high-energy environments<sup>(166)</sup>. The experimental work was done by tumbling of gold fragments for 30 to 240 hours with different combinations of sand, cobbles, and water. The results showed a very slow rate of physical breakdown of the gold fragments due to their malleability. It has also been reported that gold can absorb the impact and abrasive forces exerted by other minerals so that physical changes produced in the fragments are preliminary changes in shape. These experiments were meant to simulate alluvial environments, not tumbling mills.

In 1989, in a research program the performance of the gold gravity circuit at Les Mines Camchib Inc.<sup>(167, 168)</sup> was completed at McGill. Various streams of the grinding circuit (rod mill feed, ball mill discharge and cyclone overflow and underflow) were sampled and after calculations the grinding kinetics of the ore and gold were evaluated and compared. The selection function of gold was found equal to that of the ore above

0.212 mm, and slightly higher below. The author pointed out that the results were not totally conclusive, because of sampling and assaying errors and the poor liberation of gold above 0.212 mm.

In 1990, the breakage of gold flakes (from Les Mines Camchib Inc.) in the 0.850-1.200 mm size class in a 23 cm diameter by 20 cm long porcelain mill with steel balls, was studied<sup>(9)</sup>. It was reported that flakes could assume spherical or cylindrical shapes because of folding. It was also shown that the disappearance of flakes from the parent size class could be described with a first-order kinetics equation, as used for brittle materials.

The breakage rate constant of gold in the Hemlo (Golden Giant Mine) secondary mill was also measured and reported<sup>(9)</sup> to be 6 to 20 times smaller than that of the ore; the gap became wider with increasing particle size. Similar results were later reported at Casa Berardi Mines<sup>(169)</sup> and Agnico-Eagle (LaRonde Division)<sup>(170)</sup>. Indirect evidence of the slower grinding kinetics of gold in industrial tumbling mills is also abundant, in that the high circulating loads of gold measured in a number of plants can only be simulated if the selection function of gold is assumed much lower than that of the ore<sup>(11, 12, 171)</sup>.

## **Chapter 3: Models of Malleable Metal Grinding**

### 3.1 Introduction

As a substitute for gold, lead, and to a lesser extent copper, will be used in this work. Its behaviour in laboratory tumbling mills will be modelled mathematically, as an additional tool to understand flattening, folding and breaking mechanisms. The mathematical models to be tested will now be presented.

### 3.2 Classical Mathematical Model for Grinding

In the classical model of brittle material grinding, material appears as fragments (progeny) from coarser size classes or fractions and disappears when broken (Equation 2.25). This can be defined as follows:

$$\frac{dw_i(t)}{dt} = -s_i w_i(t) + \sum_{j=1, j>i}^{i-1} b_{ij} s_j w_j(t), \quad n \geq i \geq j \geq 1 \quad (3.1)$$

This equation enables one to calculate the mass fraction in any size class at any given time. A system of  $n$  size classes (excluding the pan) is defined by  $n$  differential equations. This system is known as the batch grinding equation. As an example, a batch system of two equations is given here:

$$\frac{dw_1(t)}{dt} = -s_1 w_1 \quad (3.2)$$

$$\frac{dw_2(t)}{dt} = -s_2 w_2 + b_{2,1} s_1 w_1 \quad (3.3)$$

This two-equation system is solved using the initial conditions, which yield:

$$w_1(t) = w_1(0)e^{(-s_1 t)} \quad (3.4)$$

$$w_2(t) = \left[ \frac{b_{2,1} s_1 w_1(0)}{(s_2 - s_1)} \right] e^{(-s_1 t)} + \left[ w_2(0) - \frac{b_{2,1} s_1 w_1(0)}{(s_2 - s_1)} \right] e^{(-s_2 t)} \quad (3.5)$$

### 3.3 Defining Models of Malleable Metal Grinding

A model of malleable metals grinding is first defined from a strict definition of malleability i.e. the ability to withstand a blow without any breakage, hence breakage is first omitted. In a batch system, the same mass conservation equation can be written (as for actual breakage) for any size class as the sum of two terms, disappearance and appearance:

$$\frac{dw_i(t)}{dt} = -[\text{Mass disappearing}] + [\text{Mass appearing}] \quad (3.6)$$

This statement of mass conservation is fundamental when defining mathematical models. It will be the basis of four different models, each derived from a specific set of assumptions. For all models, the various transfers are assumed to follow first-order kinetics.

#### 3.3.1 Case 1: Folding & flattening and no breakage

In this first model, it is assumed that no breakage takes place; particles are just folded and flattened. Folded particles move into finer size classes while flattened particles report to coarser sizes. To simplify the model, it is assumed that mass transfers only across adjacent size classes. Thus, the mass equation is defined for any size class such as  $i$ :

$$\frac{dw_i(t)}{dt} = r_{i-1,i} w_{i-1} - (r_{i,i-1} + r_{i,i+1}) w_i + r_{i+1,i} w_{i+1} \quad (3.7)$$

where  $w_i$  is the retained mass in size class  $i$  after grinding time of  $t$ , and  $r_{ij}$  defines the mass transfer rate from size class  $i$  to size class  $j$  (for  $i > j$ , folding and  $i < j$ , flattening). Therefore, for a simple system consisting of three size classes, four rate constants define the mass transfers, presented in Figure 3.1.

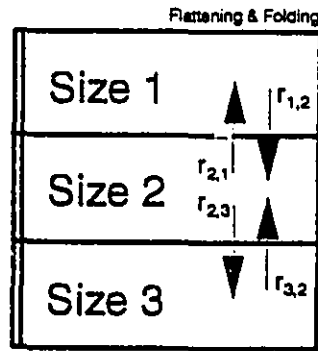


**Figure 3.1:** Representation of a three size class model based on flattening, folding and no breakage.

The mass equations or differential equations for a set of three size classes are <sup>(22)</sup>:

$$\frac{dw_1(t)}{dt} = -r_{1,2} w_1 + r_{2,1} w_2 \quad (3.8)$$

$$\frac{dw_2(t)}{dt} = r_{1,2} w_1 - (r_{2,1} + r_{2,3}) w_2 + r_{3,2} w_3 \quad (3.9)$$

$$\frac{dw_3(t)}{dt} = -r_{3,2} w_3 + r_{2,3} w_2 \quad (3.10)$$

To simplify, the third differential equation can be replaced by:

$$w_1 + w_2 + w_3 = 100\% \quad (3.11)$$

The solution for this system of differential equations (analytical solution) is derived (Appendix I):

$$w_1 = c_1 e^{-r_1 t} + c_2 e^{-r_2 t} + l_1 \quad (3.12)$$

$$w_2 = c_3 e^{-r_1 t} + c_4 e^{-r_2 t} + l_2 \quad (3.13)$$

where  $r_1$  and  $r_2$  are the roots of the representative equation of the differential equations. If we choose as initial conditions [ $w_1(0)=0$ ,  $w_2(0)=100\%$ ,  $w_3(0)=0$ ], the coefficients of the two above equations are:

$$l_1 = [(r_{2,1}r_{3,2})/(r_{1,2}r_{2,3} + r_{1,2}r_{3,2} + r_{2,1}r_{3,2})]$$

$$l_2 = [(r_{1,2}r_{3,2})/(r_{1,2}r_{2,3} + r_{1,2}r_{3,2} + r_{2,1}r_{3,2})]$$

$$c_1 = [-l_1 + ((r_1 l_1 + r_{2,1})/(r_1 - r_2))]$$

$$c_2 = [(-r_1 l_1 - r_{2,1})/(r_1 - r_2)]$$

$$c_3 = [1 - l_2 - ((r_1 - r_1 l_2 + r_{2,1} + r_{2,3})/(r_1 - r_2))]$$

$$c_4 = [(r_1 - r_1 l_2 + r_{2,1} + r_{2,3})/(r_1 - r_2)]$$

### 3.3.2 Case 2: Folding & flattening and explicit breakage

In this model a breakage term is added to the previous model to describe all possible breakages. Folding and flattening are as in section 3.3.1. It is assumed that particle breakage follows the traditional grinding equation (Equations 2.25, 3.1) and the broken particles may return to coarser size classes when flattened except when broken into the pan. Therefore, the mass equations are the summation of folding, flattening (Equation 3.7) and breakage (Equation 3.1) for any size class  $i$ , as follows:

$$\frac{dw_i(t)}{dt} = r_{i-1,i} w_{i-1} - (r_{i,i-1} + r_{i,i+1} - s_i) w_i + r_{i+1,i} w_{i+1} + \sum_{j=i+1}^{n-1} b_{i,j} s_j w_j \quad (3.14)$$

where  $n$  is the number of size classes,  $w_i$  is the mass in size  $i$ , and  $r_{i,j}$  defines the rate constant of mass transfer from size class  $i$  to size class  $j$  by flattening ( $i > j$ ) or folding ( $i < j$ ).  $b_{i,j}$  and  $s_i$  are the breakage and selection function values.

A simple example of this model is a system consisting of three size classes, as shown below in Figure 3.2. For this system, Equation 3.14 can be expanded as follows:

$$\frac{dw_1(t)}{dt} = -(r_{1,2} + s_1) w_1 + r_{2,1} w_2 \quad (3.15)$$

$$\frac{dw_2(t)}{dt} = (r_{1,2} + b_{2,1}s_1) w_1 - (r_{2,1} + r_{2,3} + s_2) w_2 + r_{3,2} w_3 \quad (3.16)$$

$$\frac{dw_3(t)}{dt} = b_{3,1} s_1 w_1 + (r_{2,3} + b_{3,2}s_2) w_2 - (r_{3,2} + s_3) w_3 \quad (3.17)$$

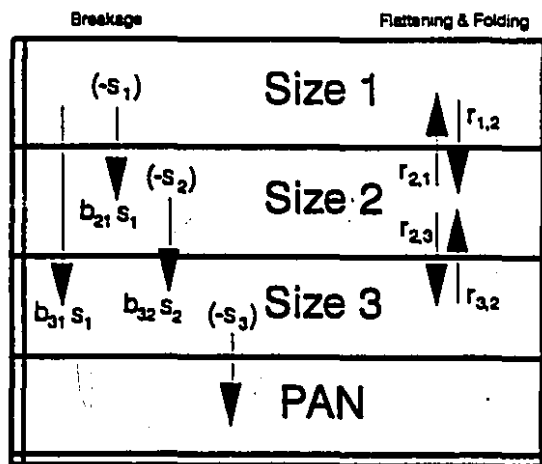


Figure 3.2: Representation of a three size class model based on flattening, folding and explicit breakage (Note: material also transfers to the pan from size classes 1, and 2, not shown).

To simplify, the overall mass balance equation can be used to solve the differential equations:

$$w_1 + w_2 + w_3 + \text{pan} = 100\% \quad (3.18)$$

The solution for this system of differential equations is derived (Appendix I):

$$w_1 = c_1 e^{-r_1 t} + c_2 e^{-r_2 t} + c_3 e^{-r_3 t} + l_1 \quad (3.19)$$

$$w_2 = c_4 e^{-r_1 t} + c_5 e^{-r_2 t} + c_6 e^{-r_3 t} + l_2 \quad (3.20)$$

$$w_3 = c_7 e^{-r_1 t} + c_8 e^{-r_2 t} + c_9 e^{-r_3 t} + l_3 \quad (3.21)$$

where  $r_1$ ,  $r_2$ , and  $r_3$  are the roots of the representative equation of the differential equations. If we choose as initial conditions [ $w_1(0)=l_4$ ,  $w_2(0)=l_5$ ,  $w_3(0)=l_6$ ], the coefficients of the three above equations are:

$$l_1 = 0, l_2 = 0, l_3 = 0$$

$$A = [-(r_{1,2} + s_1)l_4 + r_{2,1}l_5]$$

$$B = [(r_{1,2} + b_{2,1}s_1)l_4 - (r_{2,1} + r_{2,3} + s_2)l_5 + r_{3,2}l_6]$$

$$C = [b_{3,1}s_1l_4 + (r_{2,3} + b_{3,2}s_2)l_5 - (r_{3,2} + s_3)l_6]$$

$$c_1 = [l_4 - l_1 - c_2 - c_3]$$

$$c_2 = [(A - r_1 l_4 + r_1 l_1 - c_3(r_3 - r_1)) / (r_2 - r_1)]$$

$$c_3 = [((r_2 - r_1)(A - r_1^2 l_4 + r_1^2 l_1) - (A - r_1 l_4 + r_1 l_1)(r_2^2 - r_1^2)) / ((r_3 - r_1)(r_2 - r_1) - (r_3 - r_1)(r_2^2 - r_1^2))]$$

$$c_4 = [l_5 - l_2 - c_5 - c_6]$$

$$c_5 = [(B - r_1 l_5 + r_1 l_2 - c_6(r_3 - r_1)) / (r_2 - r_1)]$$

$$c_6 = [((r_2 - r_1)(B - r_1^2 l_5 + r_1^2 l_2) - (B - r_1 l_5 + r_1 l_2)(r_2^2 - r_1^2)) / ((r_3 - r_1)(r_2 - r_1) - (r_3 - r_1)(r_2^2 - r_1^2))]$$

$$c_7 = [l_6 - l_3 - c_8 - c_9]$$

$$c_8 = [(C - r_1 l_6 + r_1 l_3 - c_9(r_3 - r_1)) / (r_2 - r_1)]$$

$$c_9 = [((r_2 - r_1)(C - r_1^2 l_6 + r_1^2 l_3) - (C - r_1 l_6 + r_1 l_3)(r_2^2 - r_1^2)) / ((r_3 - r_1)(r_2 - r_1) - (r_3 - r_1)(r_2^2 - r_1^2))]$$

### 3.3.3 Case 3: Folding & flattening and limited breakage

This model uses the flattening and folding terms of the previous two models (Equation 3.7) and a breakage term which is different from that of the previous model (Equation 3.14). In this case, it is assumed that when material breaks, it does so either in the adjacent finer size class (and is incorporated in the folding term, i.e.  $r_{i,i+1}$ , or directly into the pan). The transfer of material directly into other finer size classes is assumed negligible, and is not explicitly described. Therefore, the mass equations are the summation of folding, flattening (Equation 3.7) and a breakage term representing the broken mass in pan, as follows for any size class  $i$ :

$$\frac{dw_i(t)}{dt} = r_{i-1,i} w_{i-1} - (r_{i,i-1} + r_{i,i+1} + r_{i,p}) w_i + r_{i+1,i} w_{i+1} \quad (3.22)$$

$$\frac{dw_p(t)}{dt} = \sum_{i=1}^{n-1} r_{i,p} w_i \quad (3.23)$$

where  $n$  is the number of size classes (inclusive of the pan).  $r_{i,p}$  is the rate constant for the transfer of broken particles to the finest size class or (the pan).

A simple example of this model is a system consisting of three size classes and a pan, as shown in Figure 3.3. Note that the rate constant  $r_{3,p}$  represents both breakage and folding from size class 3 to the pan. It is assumed that material either folded into the pan from size class 3 or broken from size classes 1 to 3 into the pan can not flatten back into size class 3. For this system, Equations 3.22 and 3.23 can be expanded as follows:

$$\frac{dw_1(t)}{dt} = -(r_{1,2} + r_{1,p}) w_1 + r_{2,1} w_2 \quad (3.24)$$

$$\frac{dw_2(t)}{dt} = r_{1,2} w_1 - (r_{2,1} + r_{2,3} + r_{2,p}) w_2 + r_{3,2} w_3 \quad (3.25)$$

$$\frac{dw_3(t)}{dt} = r_{2,3} w_2 - (r_{3,2} + r_{3,p}) w_3 \quad (3.26)$$

$$\frac{dw_p(t)}{dt} = r_{1,p} w_1 + r_{2,p} w_2 + r_{3,p} w_3 \quad (3.27)$$

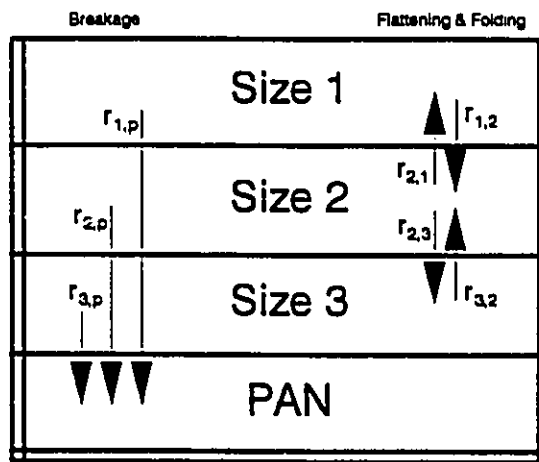


**Figure 3.3:** Representation of a three size class model based on flattening, folding and limited breakage.

To simplify, the mass balance equation can be used to solve the differential equations:

$$w_1 + w_2 + w_3 + pan = 100\% \quad (3.28)$$

The solution for this system of differential equations is derived (Appendix I):

$$w_1 = c_1 e^{-r_1 t} + c_2 e^{-r_2 t} + c_3 e^{-r_3 t} + I_1 \quad (3.29)$$

where  $r_1$ ,  $r_2$ , and  $r_3$  are the roots of the representative equation of the differential

$$w_2 = c_4 e^{-r_1 t} + c_5 e^{-r_2 t} + c_6 e^{-r_3 t} + l_2 \quad (3.30)$$

$$w_3 = c_7 e^{-r_1 t} + c_8 e^{-r_2 t} + c_9 e^{-r_3 t} + l_3 \quad (3.31)$$

equations. If we choose as initial conditions [ $w_1(0)=l_4$ ,  $w_2(0)=l_5$ ,  $w_3(0)=l_6$ ], the coefficients of the three above equations are:

$$l_1 = 0, l_2 = 0, l_3 = 0$$

$$A = [-(r_{1,2} + r_{1,p})l_4 + r_{2,1}l_5]$$

$$B = [r_{1,2}l_4 - (r_{2,1} + r_{2,3} + r_{2,p})l_5 + r_{3,2}l_6]$$

$$C = [r_{2,3}l_5 - (r_{3,2} + r_{3,p})l_6]$$

$$c_1 = [l_4 - l_1 - c_2 - c_3]$$

$$c_2 = [(A - r_1 l_4 + r_1 l_1 - c_3(r_3 - r_1)) / (r_2 - r_1)]$$

$$c_3 = [((r_2 - r_1)(A - r_1^2 l_4 + r_1^2 l_1) - (A - r_1 l_4 + r_1 l_1)(r_2^2 - r_1^2)) / ((r_3 - r_1)(r_2 - r_1) - (r_3 - r_1)(r_2^2 - r_1^2))]$$

$$c_4 = [l_5 - l_2 - c_5 - c_6]$$

$$c_5 = [(B - r_1 l_5 + r_1 l_2 - c_6(r_3 - r_1)) / (r_2 - r_1)]$$

$$c_6 = [((r_2 - r_1)(B - r_1^2 l_5 + r_1^2 l_2) - (B - r_1 l_5 + r_1 l_2)(r_2^2 - r_1^2)) / ((r_3 - r_1)(r_2 - r_1) - (r_3 - r_1)(r_2^2 - r_1^2))]$$

$$c_7 = [l_6 - l_3 - c_8 - c_9]$$

$$c_8 = [(C - r_1 l_6 + r_1 l_3 - c_9(r_3 - r_1)) / (r_2 - r_1)]$$

$$c_9 = [((r_2 - r_1)(C - r_1^2 l_6 + r_1^2 l_3) - (C - r_1 l_6 + r_1 l_3)(r_2^2 - r_1^2)) / ((r_3 - r_1)(r_2 - r_1) - (r_3 - r_1)(r_2^2 - r_1^2))]$$

### 3.3.4 Case 4: Agglomeration

The fourth model is defined when only agglomeration takes place. In tumbling mills, this takes place because of cold welding. Agglomeration and consolidation of particles produces large-surface-weight particles which move from any size class to coarser size classes. If it is assumed that particles just move upward to the adjacent size class, the appropriate model in this case is defined as follows:

$$\frac{dw_i(t)}{dt} = -r_{i,i-1} w_i + r_{i+1,i} w_{i+1} \quad (3.32)$$

For simplicity's sake, this model does not include possible agglomeration of a fine particle to a larger one which would result in a mass transfer across more than one size class. Figure 3.4 shows the agglomerating phenomenon for a system of three size classes.

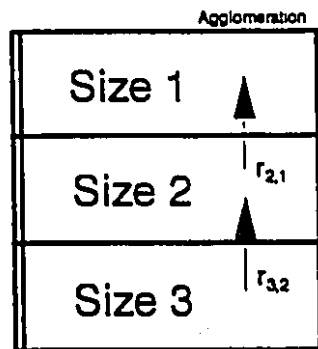


Figure 3.4: Representation of a three size class model based on agglomeration.

As a result, the mass equations of this system of three size classes can be written as follows:

$$\frac{dw_1(t)}{dt} = r_{2,1} w_2 \quad (3.33)$$

$$\frac{dw_2(t)}{dt} = -r_{2,1} w_2 + r_{3,2} w_3 \quad (3.34)$$

$$\frac{dw_3(t)}{dt} = -r_{3,2} w_3 \quad (3.35)$$

$$w_1 + w_2 + w_3 = 100\% \quad (3.36)$$

The analytical solution (Appendix I) of this set of differential equations is as follows:

$$w_1 = c_1 e^{-r_1 t} + c_2 e^{-r_2 t} + l_1 \quad (3.37)$$

$$w_2 = c_3 e^{-r_1 t} + c_4 e^{-r_2 t} + l_2 \quad (3.38)$$

where  $r_1$  and  $r_2$  are the roots of the representative equation of the differential equations. If we choose as initial conditions [ $w_1(0)=l_3$ ,  $w_2(0)=l_4$ ,  $w_3(0)=l_5$ ], the coefficients of the two above equations are:

$$l_1 = 1, l_2 = 0$$

$$c_1 = [((r_2 - r_1)(l_3 - 1) - r_{2,1}l_4 + r_1(l_3 - 1))/(r_2 - r_1)]$$

$$c_2 = [(r_{2,1}l_4 - r_1(l_3 - 1))/(r_2 - r_1)]$$

$$c_3 = [(-r_{2,1}l_4 + (r_{3,2} - r_1)(1 - l_3 - l_4))/(r_2 - r_1)]$$

$$c_4 = [((r_2 - r_{3,2})(1 - l_3 - l_4) + r_{2,1}l_4)/(r_2 - r_1)]$$

### 3.4 Differential Equations: Solutions & Rate Constant Estimations

The systems of differential equations that represent the various models can be solved analytically or numerically. Analytical solution for three size classes for the first model (flattening and folding without breakage) was presented in Appendix I. These become practically unmanageable for systems of four size classes or more. Clearly, numerical solutions are preferable. For the first model (flattening and folding without breakage) the numerical solution for the fourth-order of Runge-Kutta method<sup>(172)</sup> is presented in Appendix I (three size classes).

Even numerical solutions can be unwieldy, especially when they are to be used to estimate multiple rate constants simultaneously from multiple data sets. For the present work, an optimization technique is used, which minimizes the sum of the squared differences between predicted and measured mass in each of size classes, by adjusting the model's rate constants. For three size classes and  $n_2$  incremental grinding times, the

following criterion will be minimized:

$$Criterion = SS = \sum_{t=1}^{n_2} \sum_{i=1}^3 [w_i^{exp}(t) - w_i^{calc}(t)]^2 \quad (3.39)$$

The goodness of fit is best measured by computing the average least square, the sum of squares divided by degrees of freedom. The square root of the mean least square is the standard error. The least square fit and simplex<sup>(173)</sup> method are used to achieve the optimum values of rates constants with the "DIFFEQ" version 1.0 and "SCIENTIST" versions 1.0 and 2.0. Using these software enables us to fit multiple time increments simultaneously, yielding a more reliable estimation of the rate constants.

**Chapter 4: The Behaviour of Coarse Lead in  
Tumbling Mills**

## 4.1 Introduction

In this chapter the behaviour of coarse pure lead particles in different dry grinding environments is investigated. This study is divided into three parts; first, lead shots (3-4 mm in diameter) are ground in ball and rod mills. Second, the same lead shots are flattened to diameters of 5-6 mm and ground in the same mills. Third, microhardness tests on ground and unground lead flakes and shots are used to evaluate the extent of work hardening. The models used to describe folding, flattening, breakage and agglomeration were presented in chapter 3 (Equations 3.7, 3.14, 3.22, 3.23, and 3.32).

## 4.2 Apparati

In first series of tests (Tests 1, 2, and 3), standard commercial lead shots, shown in Figure 4.1,  $3.5 \pm 0.3$  mm in diameter,  $0.17 \pm 0.004$  g in weight, were used as feed. In the second series of tests (Tests 4, 5) the same lead shots were used, but they were first manually flattened into discs as shown in Figure 4.2, 5-6 mm in diameter and  $0.5 \pm 0.04$  mm in thickness, with a Arbour Press (Dake Corporation Model No. 1-1/2). Flattened lead shot in the size class 5.60-6.75 mm,  $0.28 \pm 0.01$  g in weight, were used as feed in Test 6, to estimate their breakage and selection function parameters. Testwork in the Bond ball mill<sup>(60)</sup> was performed using steel balls 5.0-7.5 cm in diameter, but with its standard ball weight (20.1 kg). In the Bond rod mill<sup>(60)</sup> tests were done with its standard steel rod charge (33 kg), six rods, 4 cm in diameter, and two rods, 3 cm in diameter (all 53 cm in length). Products were screened using a 2<sup>0.25</sup> Tyler geometric progression with a standard Ro-Tap machine. Table 4.1 summarises the units and charges of Tests 1 to 6.

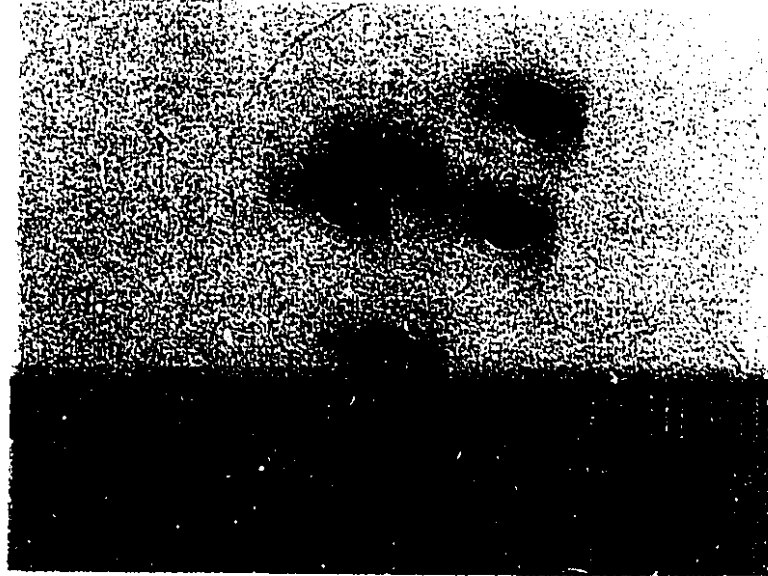


Figure 4.1: Lead shots used in different tests (scale in cm).

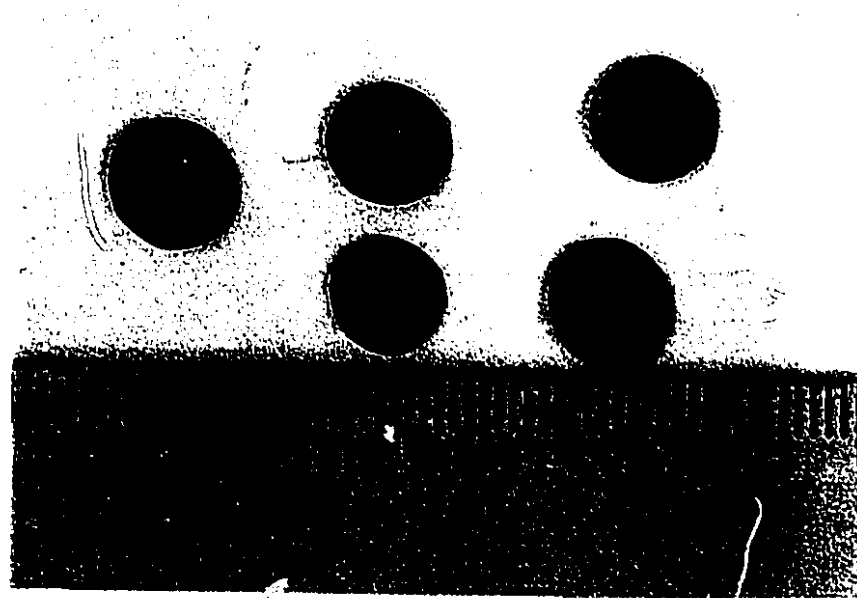


Figure 4.2: Flattened lead shots used in different tests (scale in cm).

Table 4.1: Apparati used for Tests 1 to 6.

Tests No.	Feed Type	Particle Weight (g)	Mill	Grinding Media
1	Lead shot	0.17	Bond ball mill	5-7.5 cm
2	Lead shot	0.17	Bond ball mill	5-7.5 cm
3	Lead shot	0.17	Bond rod mill	standard rods
4	Flattened lead shot	0.17	Bond ball mill	5-7.5 cm
5	Flattened lead shot	0.17	Bond rod mill	standard rods
6	Flattened lead shot	0.28	Bond rod mill	standard rods

### 4.3 Tests 1 to 3: Grinding Lead Shots

#### 4.3.1 Procedure

In the first test with the Bond ball mill (Test 1), 100 g of the lead shots, 100% in 2.80-3.35 mm size class, were ground to a total time of 120 minutes. After each grinding increment, particles from all size classes were individually weighed to determine mass loss. Grinding increments of 8 minutes were generally used up to 60 minutes, and size classes from previous increments were individually ground and screened. Before the next grinding increment all mass of the same size class was recombined in the five size classes<sup>1</sup>. From 60 to 120 minutes, all size classes were ground together in 15 minute increments.

Test 2 was a simplified repeat of the first test, to assess its reproducibility, to a

<sup>1</sup>The five size classes were: +4.00 mm, 3.35-4.00 mm, 2.80-3.35 mm, 2.38-2.80 mm, and 2.00-2.38 mm.

maximum grinding time of 100 minutes. Again, after an initial grinding of 4 minutes, increments of 8 minutes were used up to 40 minutes, and increments of 15 minutes up to 100 minutes. However, size classes were not individually ground.

In the rod mill test (Test 3), 100 g of lead shots 3.35-4.00 mm in diameter were used. They were ground for a total of 20 minutes, starting first with very small increments, 10 to 40 s, up to 3 to 5 minute increments.

### 4.3.2 Results and discussion

**Test 1:** In this test, size class 3 refers to the original size class, 2.80-3.35 mm. Size classes 1 and 2 are, respectively, the +4.00 mm and 3.35-4.00 mm. Size classes 4 and 5 are the 2.38-2.80 and -2.38 mm<sup>2</sup>, respectively. The weight percent in size class  $i$ , calculated on the basis of the total weight recovered, is  $w_i$ .

Visual observation of the grinding products showed three different grinding phases. In the first 30 minutes of grinding (phase I), particles started to exhibit bending, sometimes adopting needle (cigar) shapes and therefore moving into finer size classes. Other particles started to flatten and moved into size class 2 almost immediately, and after about 15 minutes, into size class 1. Figure 4.3 shows the size distribution of the mill product for the five size classes. In this figure, as in most of the figures used in this document to present raw data, no lines are drawn between data points. The intent is at first to examine the data as objectively as possible. The absence of lines does not force any interpretation, and also yields a clearer presentation. The data are also shown in the modelling section, with the corresponding model response. At first, material moves more rapidly into size class 4, for about 10 minutes; thereafter, and up to the end of

---

<sup>2</sup>"-2.38 mm" refers to all material finer than 2.38 mm --i.e. 0.00-2.38 mm.

phase II, the mass in the coarser size classes exceeds that in the finer classes. Flattening is therefore more prevalent than bending.

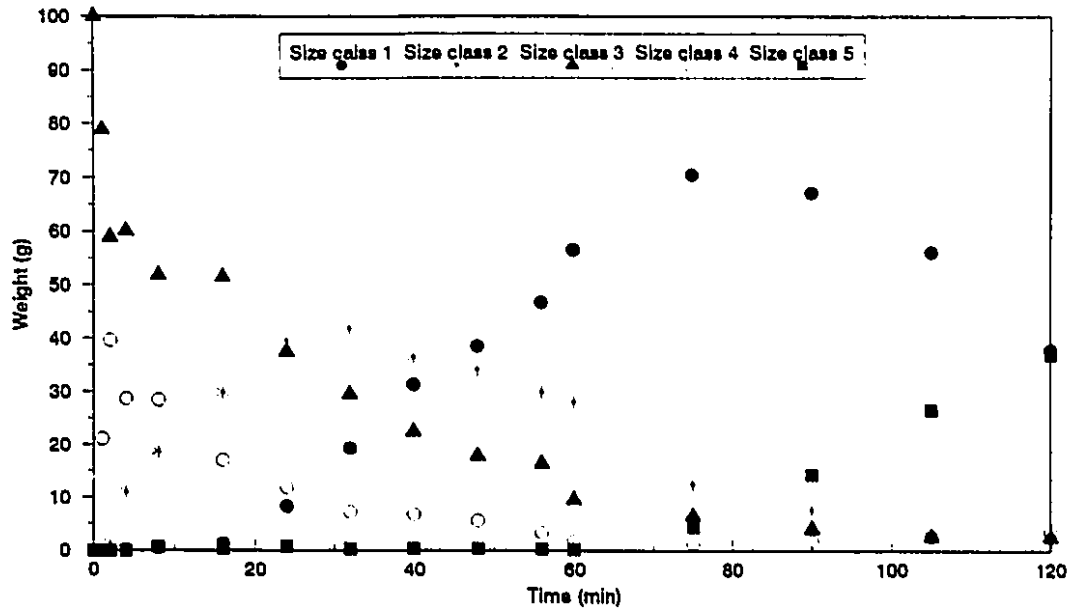


**Figure 4.3:** Size distribution of lead particles as a function of grinding time in the Bond ball mill (Test 1); size class 1: +4.00 mm, 2: 3.35-4.00 mm, 3: 2.80-3.35 mm, 4: 2.38-2.80 mm, 5: -2.38 mm.

Figures 4.4(a), (b), (c) and (d) show the weight distribution of individual particles in the main four size classes ( $w_1$  to  $w_4$ ) after 2 to 24 minutes of grinding. The graphs suggest a normal distribution for all size classes, with very little variation in average weight in the four different size classes as a function of grinding time. Table 4.2 shows how individual particles of size classes  $w_2$  to  $w_4$  are distributed in weight after 24 minutes of ball milling. The average weights are extremely similar, with a relative difference of only 1%. They are also very narrowly distributed, with standard deviations of 0.005 to 0.006 g (relative standard deviation of 2.8 to 3.8%). Statistically, the highest and lowest variances and averages are marginally different at 95%, but the overwhelming conclusion is that no breakage took place.

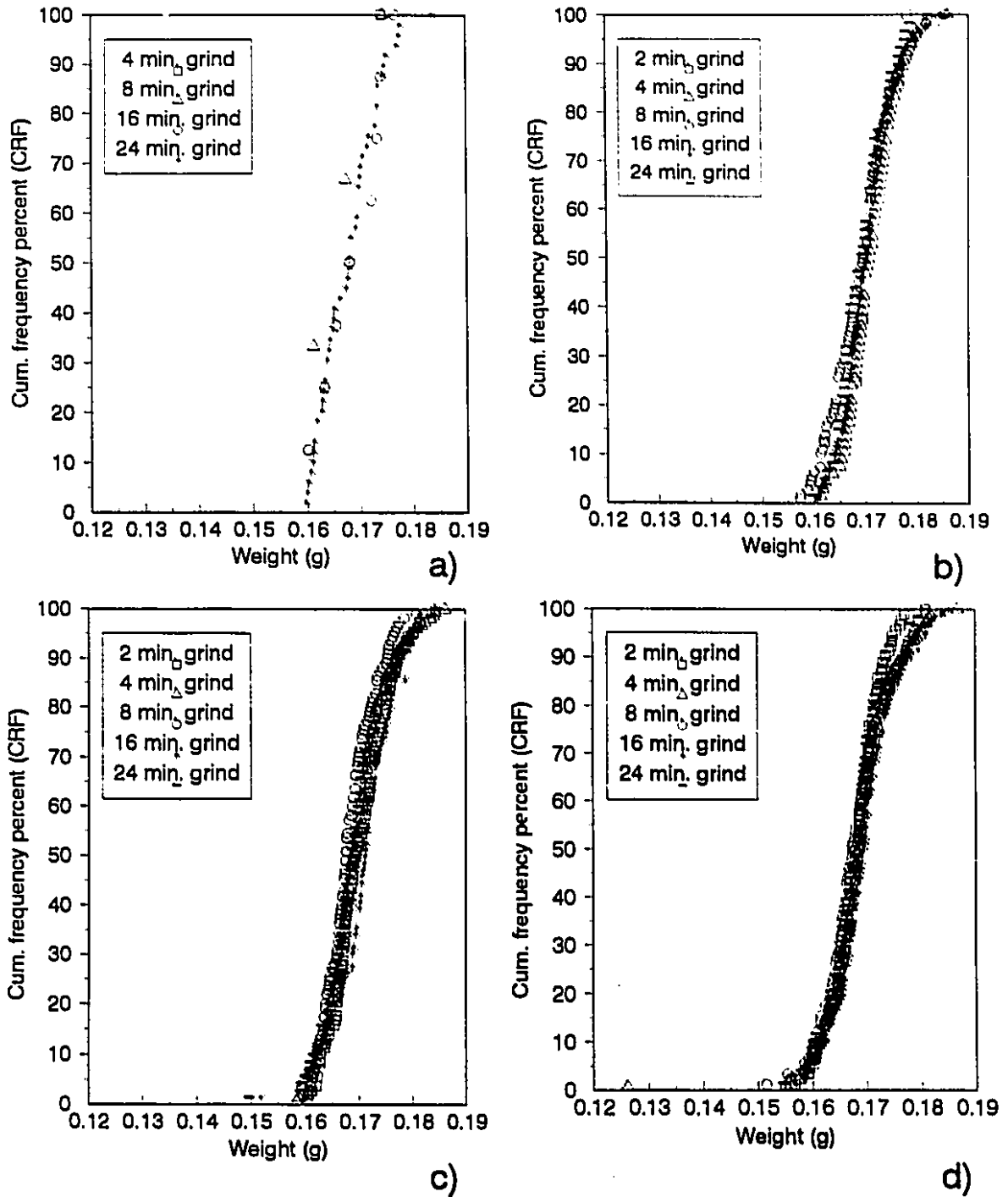


Figure 4.4: Weight of individual particles in the Bond ball mill test (Test 1); a: +4.00 mm, b: 3.35-4.00 mm, c: 2.80-3.35 mm, d: 2.38-2.80 mm.

**Table 4.2:** Weight distribution of particles in different size classes in the Bond ball mill after 24 minutes grinding (Test 1).

Size class (mm)	+4.00		3.35-4.00		2.80-3.35		2.38-2.80	
Weight (g)	Frequency		Frequency		Frequency		Frequency	
	No.	%	No.	%	No.	%	No.	%
0.1550-0.1599	2	4.1	1	1.7	4	5.7	5	7.4
0.1600-0.1649	16	32.7	9	15.3	12	17.1	13	19.1
0.1650-0.1699	15	30.6	23	39.0	26	37.1	31	45.6
0.1700-0.1749	12	24.5	18	30.5	13	18.6	15	22.1
0.1750-0.1799	3	6.1	7	11.9	10	14.3	3	4.4
0.1800-0.1849	1	2.0	1	1.7	5	7.1	1	1.5
Average	0.168		0.170		0.169		0.168	
Standard Dev.	0.006		0.005		0.006		0.005	
Variance	0.00003		0.00002		0.00004		0.00003	

In the second phase (phase II), from 30 to 70 minutes of grinding, the dominant mechanism is agglomeration to produce huge particles or "super-flakes", a form of cold welding, as shown in Figure 4.5. Weighing individual particles shows that after 70 minutes of grinding all particles in size class 1 are "super-flakes", aggregates of two or more flakes. At the end of this phase, after 70 minutes of grinding, 70% of the mass has reported into the coarsest size class as super-flakes (Figure 4.3).

Weight data shown in Table 4.3 confirm that the average weight, 0.66 g, is approximately four times that of the original particles, and is quite variable, with a standard deviation of 0.26 g (a relative 39%). Its distribution is no longer normal, but skewed to the right, not unlike a Poisson distribution. Figure 4.6 shows the distribution of particles weight in size class +4.00 mm.

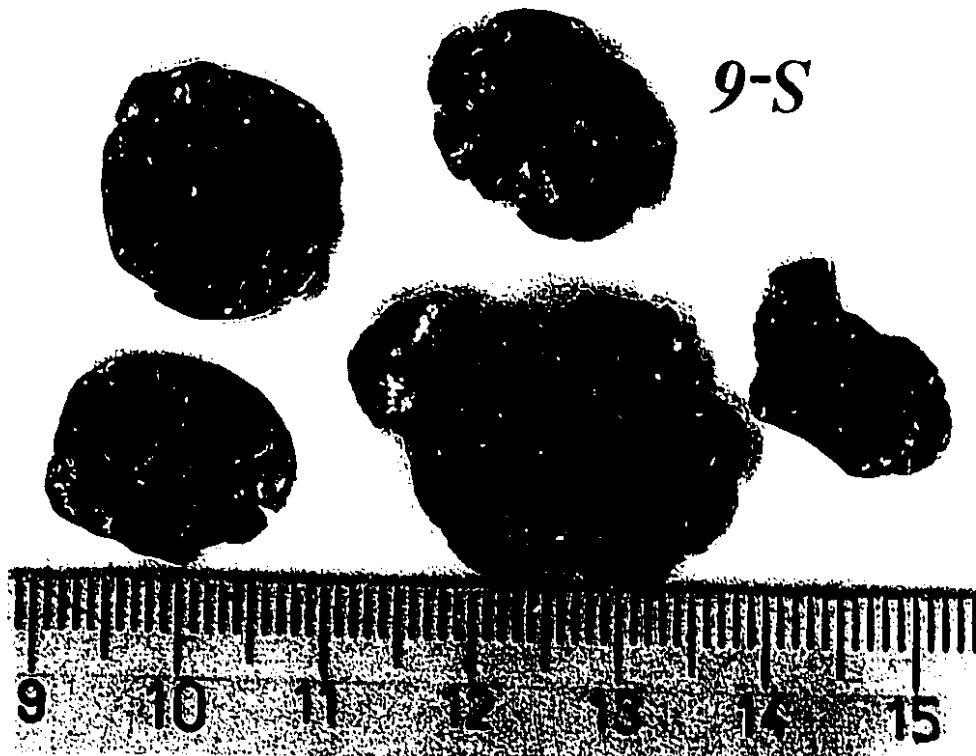


Figure 4.5: Super-flakes produced in the phase II of the Bond ball mill test (Test 1).

Table 4.3: Weight distribution of the super-flakes in size class 1, after 70 minutes of grinding in the Bond ball mill (Test 1).

Size class: +4.00 mm Weight (g) ↓	Frequency	
	No.	%
0.000-0.249	0	0.0
0.250-0.499	11	30.6
0.500-0.749	16	44.4
0.750-0.999	4	11.1
1.000-1.249	3	8.3
1.250-1.499	2	5.6
Average	0.661	
Standard Dev.	0.257	
Variance	0.066	

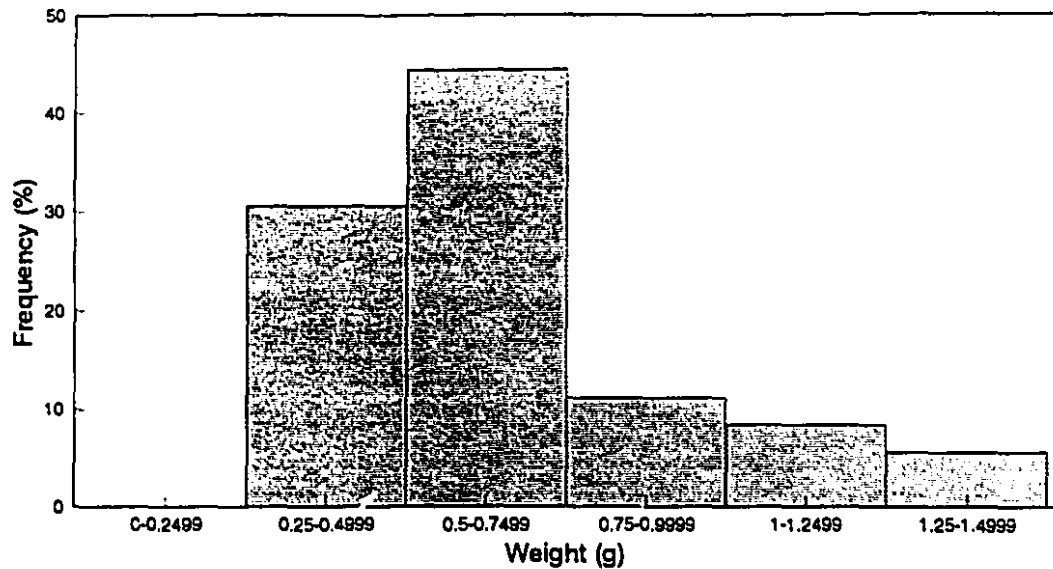


Figure 4.6: Weight distribution of super-flakes in size class 1, after 70 minutes of grinding in the Bond ball mill (Test 1).

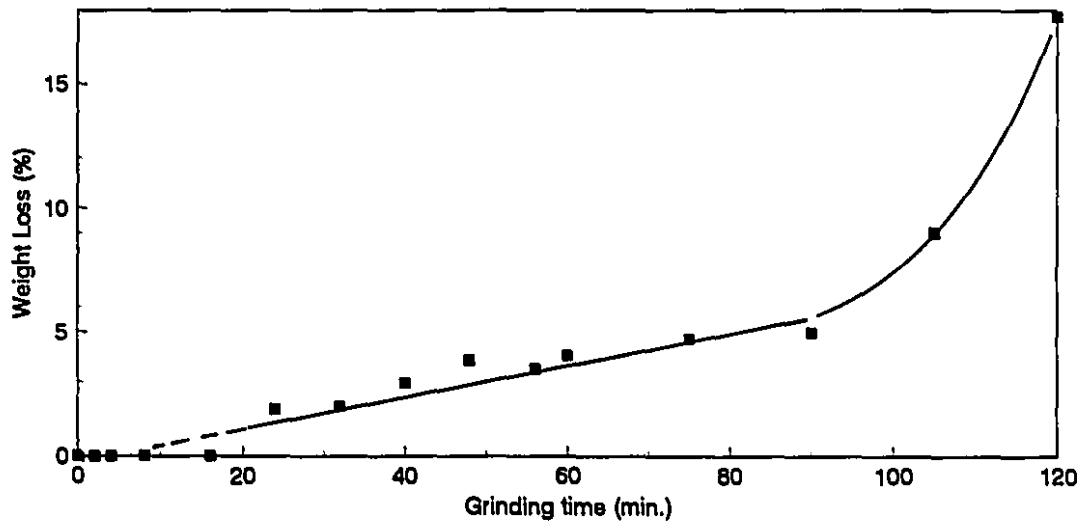


Figure 4.7: Lost weight in Test 1.

In the third phase (phase III), after 70 minutes of grinding, the super-flakes begin to break generally from fissures at their edges and produce flaky fragments similar to the gold flakes observed in industrial grinding circuits. As a result, the mass in finer size class (size class 5) increases and that in coarser ones (size classes 1 to 4) decreases, as

shown in Figure 4.3.

After 120 minutes of grinding about 18% of weight was lost, because of smearing of lead particles onto the grinding media and mill shell. This mass loss, undetectable until a grinding time of 24 minutes, increased slowly at the beginning of the second phase, but was 5% only after 90 minutes grinding (Figure 4.7). However, it dramatically increased from 5 to 18% between 90 and 120 minutes, which roughly corresponds to the period of breakage of the superflakes.

The size distribution data were first fitted to the folding and flattening model (Equation 3.7), using the sum of least squared differences criterion (Equation 3.39). Experimental points are the normalized weights (to a total weight of 100%) in five size classes,  $w_1$  (+4 mm),  $w_2$  (3.35-4 mm),  $w_3$  (2.80-3.35 mm),  $w_4$  (2.38-2.80 mm) and  $w_5$  (-2.38 mm). Normalization on the basis of weight rather than surface was chosen, as it does not require any assumption about particle shape variations (i.e. specific surface changes) with particle size, information which would be difficult to generate.

Initially, a simpler model was used, whereby only three size classes were considered, the original size class 3, or  $w_3$ , all coarser material,  $W_2^3$  ( $w_1 + w_2$ ), and all finer material,  $W_4$  ( $w_4 + w_5$ ). In a second step, two coarsest size classes were distinguished (to separate flattening from agglomeration), thereby yielding four size classes. Finally, data were fitted to all five size classes. Figure 4.8(a) shows the model fit for three size classes. Figures 4.8(b) and 4.8(c) present similar information for four and five size classes, respectively. The three size class model generally shows a good fit, although, for phase I, it can not account for the "induction time" of about 2 minutes

---

<sup>3</sup> $W_2$  is the material in size classes coarser than size class 3 ( $w_1 + w_2$ ), and  $W_4$  is material finer than size class 3 ( $w_4 + w_5$ ). In this document the upper case "W" is used to describe the weight in several coarser or finer size classes.

before the appearance of material in size class 2. The lack-of-fit of size class 4 is very probably due to experimental scatter. Phases II, and III are fitted acceptably. When modelling four size classes, the induction time denoting the appearance of lead particles in size class 1, about 16 minutes, cannot be fitted by the model. Much the same is observed when all five size classes are modelled separately.

The least squares fit also provides estimates of the rate constants which are shown in Table 4.4, and quantifies the lack-of-fit, in a manner analogous to a multilinear regression. Thus, a first criterion is sum of the squared residuals (SS). An average value (MSS), based on the degrees of freedom of the fit, is in fact more informative, its square root ( $S_e$ ), often called the "standard error", is an accepted measure of the average difference measured and fitted data.

Interpretation of the rate constants is difficult, because of their large number (albeit, there is some duplication, especially between when additional size classes are added). Each should be evaluated separately. For phase I, there is more interaction between size classes 3 and 4 than 2 to 3. In fact,  $r_{1,2}$  and  $r_{2,3}$  have negligible estimates, which suggests that folding of particles in size classes 1 and 2 is almost insignificant. Most interaction takes place between size classes 3 and 4, and the flattening rate constant is about twice as large as the folding one. For phase II, superflake formation, the rate constants for flattening are all of the same order of magnitude, 0.02 to 0.04  $\text{min}^{-1}$ , except for  $r_{5,4}$ , whose value is based on very low weight percents in size class 5 (and is therefore unreliable). Virtually all folding rate constants yield zero estimates, as one would expect from the dominance of agglomeration. In phase III, breakage is modelled by an increase in the folding rate constants (although folding is obviously not the mechanism responsible for mass transfer to finer size classes). Unsurprisingly, the flattening rate constants values are now negligible.

The lack-of-fit values confirm that phase I is the most difficult to model, with standard errors of 3.6 to 4.7%. Phase II yields much lower errors, 2.1 to 2.7%, because a single mechanism dominates (agglomeration). For phase III, the model of flattening and folding without breakage yields a surprisingly good fit, 3.1 to 3.8%, despite its obvious phenomenological inappropriateness.

**Table 4.4:** Estimated rate constants for Test 1 (all in  $\text{min}^{-1}$ ); flattening and folding model (no breakage).

Size classes	Three Size classes: ( $W_2, w_3, W_4$ )			Four size classes: ( $w_1, w_2, w_3, W_4$ )			Five size classes: ( $w_1, w_2, w_3, w_4, W_5$ )		
	Phases			Phases			Phases		
	(I)	(II)	(III)	(I)	(II)	(III)	(I)	(II)	(III)
$r_{2,3}$	0.00 <sup>4</sup>	0.00	0.01	0.00	0.00	0.12	0.00	0.00	0.12
$r_{3,2}$	0.04	0.04	0.00	0.04	0.04	0.00	0.04	0.05	0.00
$r_{3,4}$	0.46	0.00	0.18	0.89	0.00	0.16	0.91	0.00	0.17
$r_{4,3}$	1.00	0.02	0.00	1.90	0.02	0.00	1.95	0.04	0.00
$r_{1,2}$	-	-	-	0.00	0.00	0.01	0.00	0.00	0.09
$r_{2,1}$	-	-	-	0.02	0.04	0.00	0.02	0.04	0.00
$r_{4,5}$	-	-	-	-	-	-	0.00	0.03	0.23
$r_{5,4}$	-	-	-	-	-	-	0.00	0.26	0.00
SS	422	59	91	397	133	146	416	133	115
MSS <sup>5</sup>	21.1	4.2	11.4	22.1	7.4	14.6	13.0	6.1	9.6
$S_r$ <sup>6</sup>	4.6	2.1	3.4	4.7	2.7	3.8	3.6	2.5	3.1

<sup>4</sup>The rate constant estimate is negligible.

<sup>5</sup>Average lack-of-fit (MSS) is equal to overall lack-of-fit divided by degrees of freedom (df.) which is the number of data points minus the number of model parameters.

<sup>6</sup>The standard error ( $S_r$ ) is the square root of the average lack-of-fit (MSS).

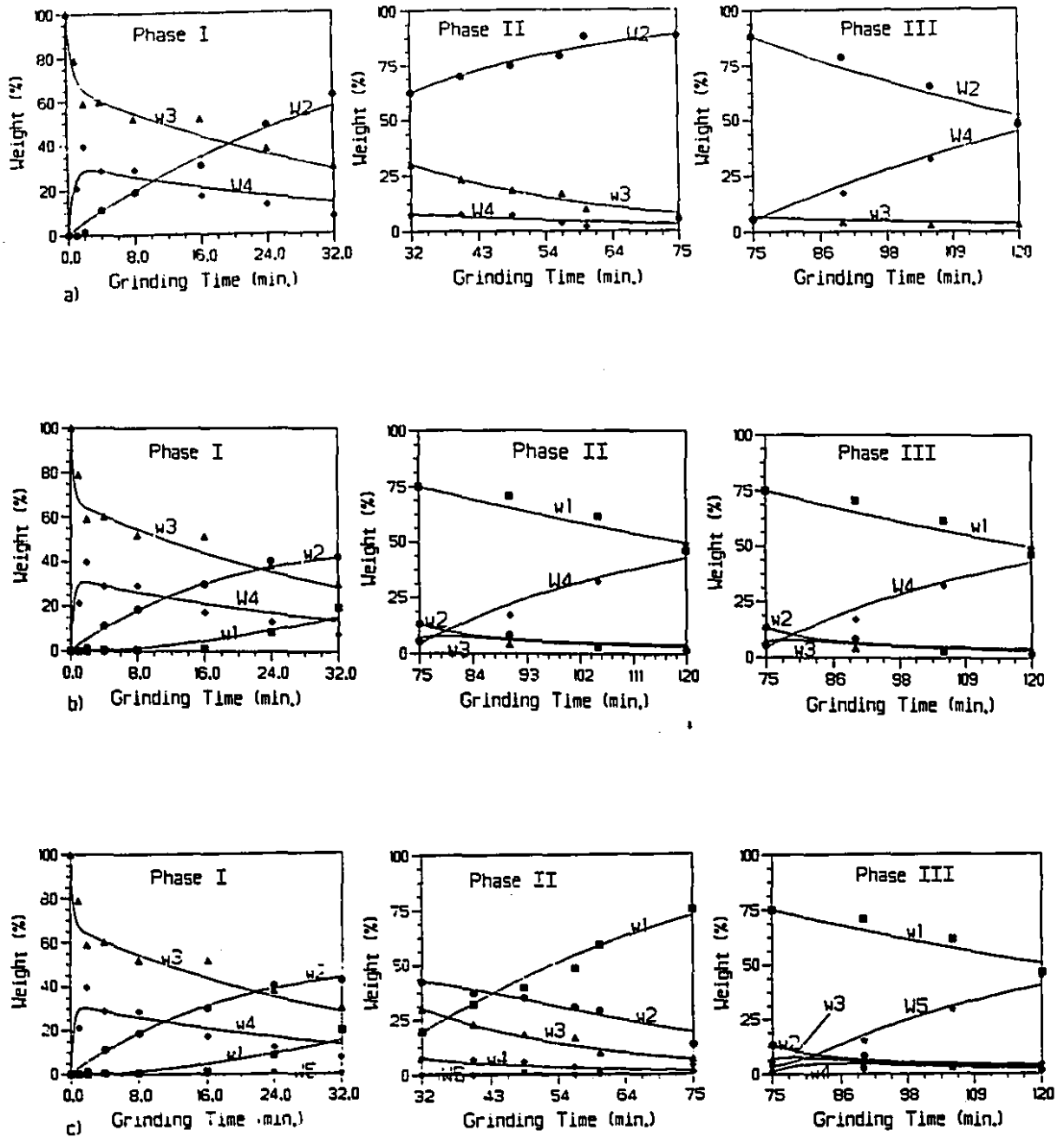
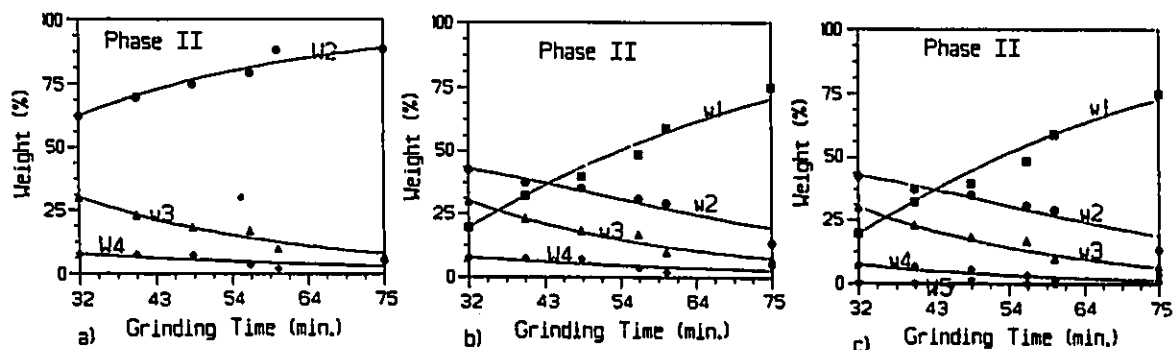


Figure 4.8: Fit of the flattening and folding model (no breakage) for Test 1; three phases and a: 3 size classes, b: 4 size classes, c: 5 size classes.

For the second modelling step, the data of the second phase (agglomeration) were fitted to the agglomeration model (Equation 3.32). Table 4.5 shows rate constants estimates with the lack-of-fit and Figure 4.9(a), 4.9(b), and 4.9(c) show the fitted curves. The lack-of-fit is comparable to that of the flattening and folding model, but with only half as many rate constants, it yields a lower average lack-of-fit, with standard errors of 1.9 to 2.5%.

**Table 4.5:** Estimated rate constants for the second phase of Test 1; agglomeration model.

Size classes	Phase II		
	Three Size classes: ( $W_2, w_3, W_4$ )	Four size classes: ( $w_1, w_2, w_3, W_4$ )	Five size classes: ( $w_1, w_2, w_3, w_4, W_5$ )
$r_{2,1}$	-	0.04	0.04
$r_{3,2}$	0.38	0.04	0.04
$r_{4,3}$	0.21	0.24	0.04
$r_{5,4}$	-	-	0.00
SS	59	133	131
MSS	3.7	6.3	5.1
$S_r$	1.9	2.5	2.3



**Figure 4.9:** Fit of the agglomeration model for the second phase of Test 1; a: 3 size classes, b: 4 size classes, c: 5 size classes.

**Table 4.6:** Estimated rate constants (all in  $\text{min}^{-1}$ ) for the third phase of Test 1; flattening, folding and limited breakage model.

Size classes	Phase III		
	Three size classes: ( $W_2, w_3, w_4, W_p$ )	Four size classes: ( $w_1, w_2, w_3, w_4, W_p$ )	Five size classes: ( $w_1, w_2, w_3, w_4, w_5, W_p$ )
$\Gamma_{1,p}$	-	0.01	0.01
$\Gamma_{2,p}$	0.01	0.00	0.00
$\Gamma_{3,p}$	0.00	0.00	0.00
$\Gamma_{4,p}$	0.08	0.17	0.00
$\Gamma_{5,p}$	-	-	0.03
$\Gamma_{1,2}$	-	0.00	0.00
$\Gamma_{2,1}$	-	0.08	0.09
$\Gamma_{2,3}$	0.00	0.00	0.01
$\Gamma_{3,2}$	0.00	0.00	0.00
$\Gamma_{3,4}$	0.07	0.02	0.04
$\Gamma_{4,3}$	0.08	0.00	0.00
$\Gamma_{4,5}$	-	-	0.07
$\Gamma_{5,4}$	-	-	0.04
SS	71	101	51
MSS	7.9	11.2	7.3
$S_r$	2.8	3.3	2.7

Although it is mathematically possible to get a relatively good fit for the third phase using the Equation 3.7 (flattening and folding), breakage also takes place, and should be modelled (Equations 3.14 or 3.22, and 3.23). Because breakage takes place

by abrasion, very fine fragments are detached from parent particle and report to the pan. The parent particles themselves eventually transfer to the adjacent finer size class. As a result, it makes sense to use the model of flattening, folding and limited breakage (Equations 3.22, and 3.23). The procedure of fitting the curves was as the previous phases for three, four and five size classes, and the rate constant estimates are tabulated in Table 4.6 and the fitted curves are shown in Figure 4.10. The rate constant estimates indicate that transfer of broken particles from the first class to the pan was dominant. However, the larger number of fitted parameters considerably lowers the reliability of individual estimates. The overall lack-of-fit (irrespective of the number of size classes used) was lower than with flattening and folding alone.

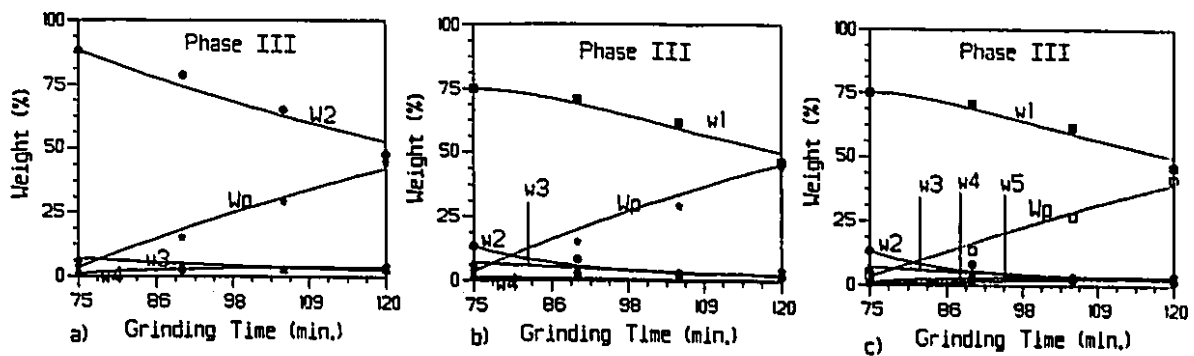


**Figure 4.10:** Fit of the flattening, folding and limited breakage model for the third phase of Test 1; a: 3 size classes, b: 4 size classes, c: 5 size classes.

**Test 2:** The main objective of Test 2 was to verify the results of Test 1, despite a simpler experimental procedure. Figure 4.11 shows that it was the case.

In the second test the same three phases were observed: particles in the first phase folded and flattened; in the second phase super-flakes were produced and these particles started breaking in the third phase. In Test 2, phase II or creation of super-flakes started after a shorter grinding time than the one in Test 1. This is probably due to the fact that in Test 1, material from the beginning up to 60 minutes of grinding was ground in

individual size classes whereas in Test 2 after each grinding cycle all size classes were combined prior to the next grinding increment (thus promoting more particle interaction). As a result, the super-flakes also began to break sooner (grinding time 55-60 minutes) than in Test 1 (70 minutes).

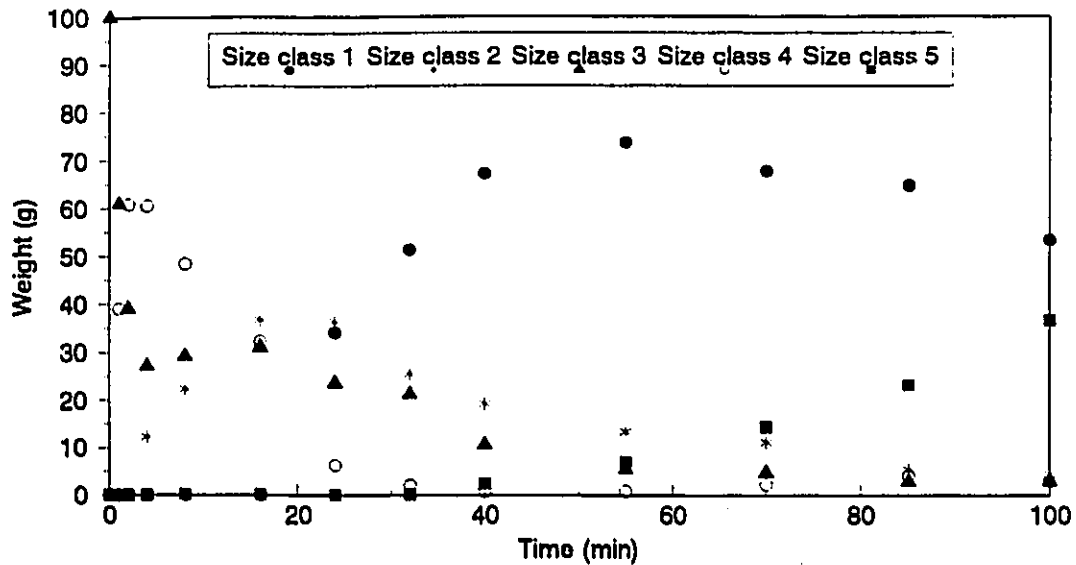


**Figure 4.11:** Size distribution of lead particles as a function of grinding time in the Bond ball mill test (Test 2); size class 1: +4.00 mm, 2: 3.35-4.00 mm, 3: 2.80-3.35 mm, 4: 2.38-2.80 mm, 5: -2.38 mm.

**Test 3:** The Bond rod mill test yielded results quite different from those of the ball mill, as significant breakage was achieved, even after only 20 minutes of grinding. Figure 4.12 presents the size distribution of the material recovered from the mill at different grinding times; clearly, not only breakage, but also folding and flattening occurred, as evidenced by the appearance of material in size class 1 (+4.00 mm).

The onset of particle breakage which can be identified by the arrival of fragments in the pan and size class 5 took place after 2.5 minutes of grinding. The importance of

this production clearly shows that from then on, breakage was the dominant mechanism. In fact, after 12 minutes of grinding, approximately 80% of the mass is either in the pan as fragments, or in size class 1 as flakes. No super-flakes were observed at any time.

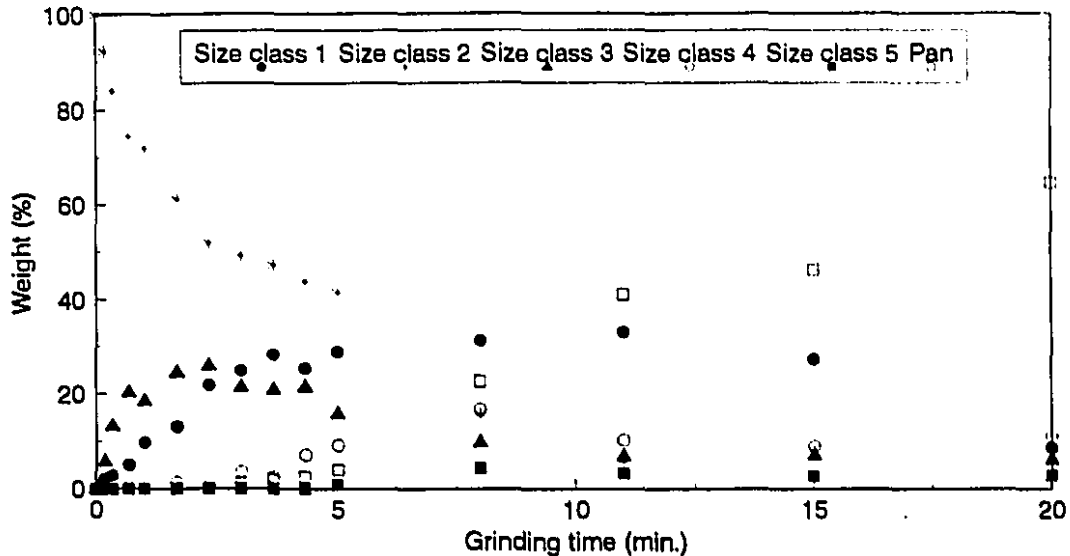


**Figure 4.12:** Size distribution of lead particles as a function of grinding time in the Bond rod mill test (Test 3); size class 1: +4.00 mm, 2: 3.35-4.00 mm, 3: 2.80-3.35 mm, 4: 2.38-2.80 mm, 5: 2.00-2.38 mm, pan: -2.00 mm.

The high impact energy of rods tumbling produced breakage of flattened particles, and was also responsible for a significant weight loss to the mill, as shown in Figure 4.13. As for the ball mill, the onset of significant mass loss roughly corresponds to the onset of breakage, which suggests that it is easier to coat the liners and grinding medium by impacting fine lead fragments than by smearing part of coarser particles.

Figure 4.14 shows the size distribution of the mill product, but as cumulative percent finer versus time. Such graphs can be used, when grinding monosized brittle material, to estimate the breakage function, from the linear section of each curve<sup>(25)</sup>. Figure 4.14 does identify such a section (from 5 minutes on) for the finest size classes,

but not so clearly for size classes approaching the initial one (+4.00 mm), as folding and flattening then overshadow breakage.

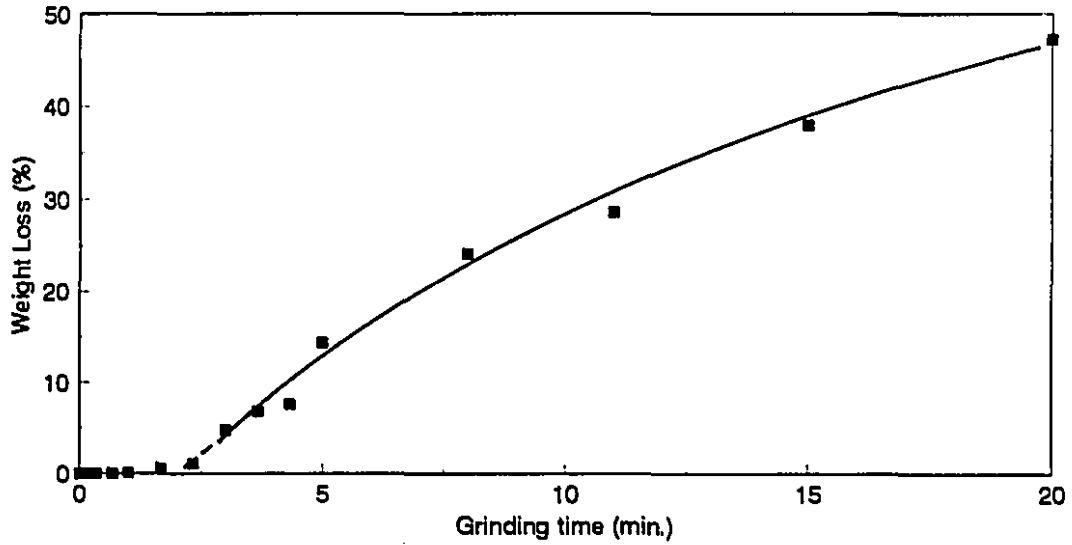


Figure 4.13: Lost weight in Test 3.

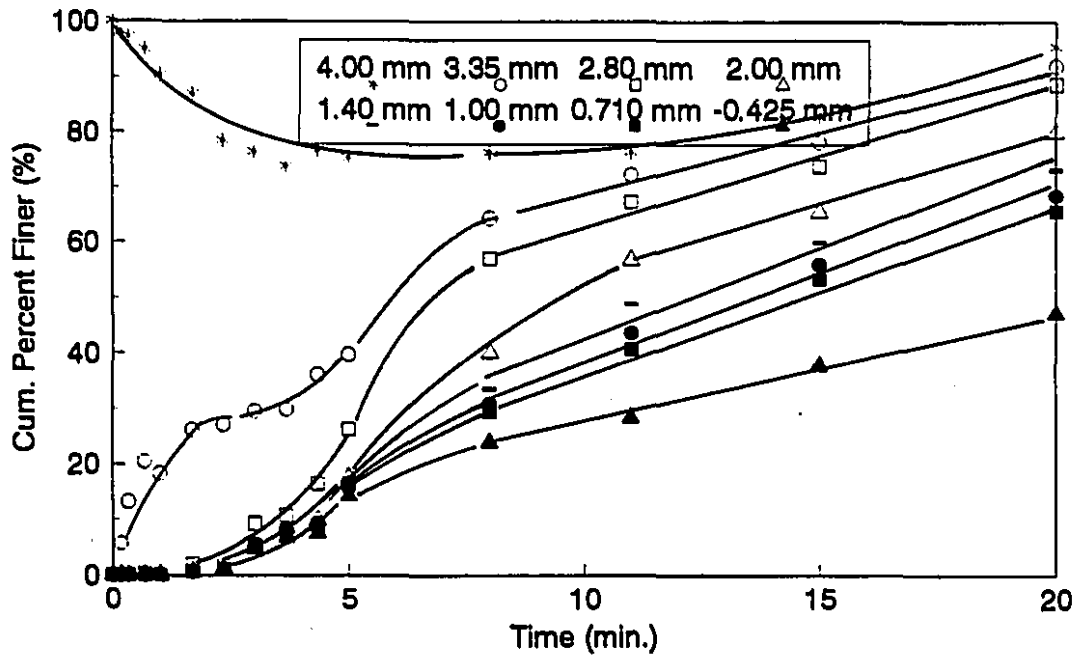


Figure 4.14: Fines production as a function of time in the Bond rod mill (Test 3).

The data were first fitted to the model of folding and flattening without breakage (Equation 3.7), for both the flattening and folding phase (0-5 minutes) and breakage phase (5-20 minutes). Three size classes were fitted as an initial and simple model,  $w_2$  (3.35-4.00 mm),  $w_1$  (+4.00 mm),  $W_3$  (2.80-3.35 mm) as  $w_3 + w_4 + w_5$ . In a second step,  $W_3$  was divided into two size classes,  $w_3$  (2.80-3.35 mm) and  $W_4$  (2.38-2.80) as  $w_4 + w_5$ . Finally, five size classes were fitted,  $w_1$  (+4.00 mm),  $w_2$  (3.35-4.00 mm),  $w_3$  (2.80-3.35 mm),  $w_4$  (2.38-2.80 mm),  $W_5$  (-2.38 mm). Table 4.7 shows the results of these calculations for the three steps and for two phases, and Figure 4.15 presents the fitted curves of the model of flattening, and folding without breakage.

Figure 4.15 shows an excellent fit for phase I (irrespective of the number of size classes used). This is confirmed in Table 4.7, with standard errors that decrease from 2.0 to 1.4% as the number of size classes increases. The lack-of-fit of phase II is much higher, 3.7 to 4.0%, but examination of Figure 4.15 suggests that at least part of it is due to experimental scatter (e.g. the 15.0 and 20.0 minutes points for  $w_4$ ). A higher lack-of-fit would be expected for phase II, because breakage is so significant.

Table 4.7 also gives the rate constant estimates. For phase I, flattening is more significant than folding, in approximately a 2:1 ratio (as for the Bond ball mill, Test 1). The little mass present in size class 4 and 5 make the estimates of the corresponding rate constant unreliable. For phase II, the dominance of breakage yields null estimates for the flattening rate constants, except for  $r_{2,1}$ .

In phase II, significant breakage calls for this phenomenon to be explicitly modelled. To do this, the model of flattening, folding and limited breakage was used. Results are shown in Figure 4.16 and Table 4.8. The three size class model used the coarsest size classes, all finer size classes being lumped in the pan. For four size classes, the 2.38-2.80 mm size class was added; for five size classes, the 2.00-2.38 mm

was added. From Figure 4.16, it is difficult to appreciate whether this model yields a better fit than flattening and folding alone. However, Table 4.8 shows lower standard errors, which decrease as the number of size classes of the model increases. For five size classes, the standard error is 3.3%, as opposed to 4.1% for flattening and folding. The lack-of-fit remains higher than in phase I, partly because of experimental scatter.

**Table 4.7:** Estimated rate constants (all in  $\text{min}^{-1}$ ) for Test 3; flattening and folding model (no breakage).

Size Classes	Three Size classes: ( $w_1, w_2, W_3$ )		Four Size classes: ( $w_1, w_2, w_3, W_4$ )		Five Size classes: ( $w_1, w_2, w_3, w_4, W_5$ )	
	Phase		Phase		Phase	
	I	II	I	II	I	II
$r_{1,2}$	0.00	0.16	0.07	0.17	0.06	0.19
$r_{2,1}$	0.11	0.31	0.11	0.32	0.13	0.37
$r_{2,3}$	0.36	0.30	0.47	0.30	0.42	0.26
$r_{3,2}$	0.63	0.00	1.05	0.00	0.93	0.00
$r_{3,4}$	-	-	0.10	0.90	0.10	0.56
$r_{4,3}$	-	-	0.00	0.06	0.00	0.00
$r_{4,5}$	-	-	-	-	33.30	0.41
$r_{5,4}$	-	-	-	-	72.26	0.00
SS	161	185	154	193	134	291
MSS	3.9	16.8	2.9	13.8	2.0	17.1
$S_r$	2.0	4.1	1.7	3.7	1.4	4.1

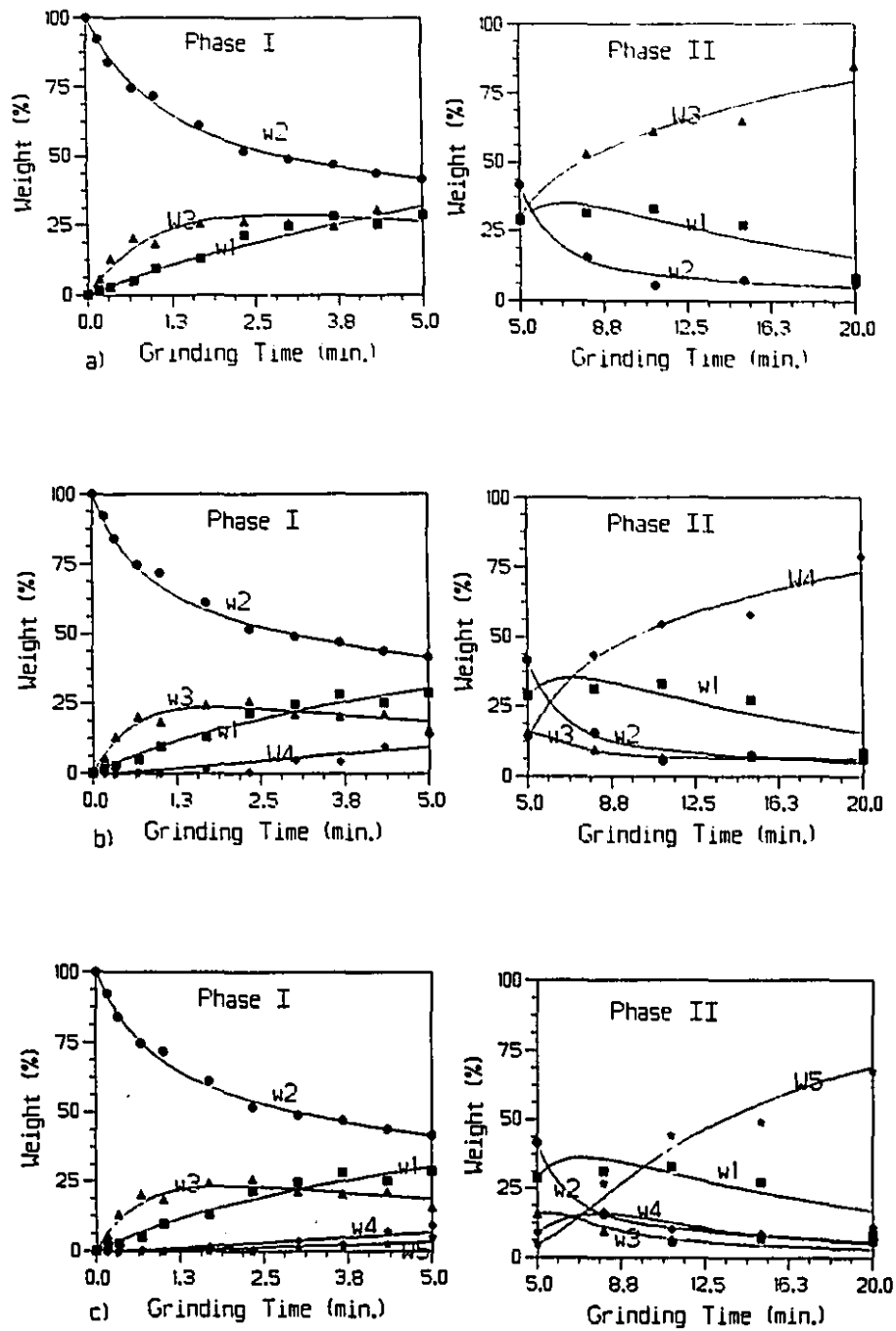


Figure 4.15: Fit of the flattening and folding model (no breakage) for Test 3; two phases and a: 3 size classes, b: 4 size classes, c: 5 size classes.

Table 4.8: Estimated rate constants for the second phase of Test 3; flattening, folding and limited breakage.

Size classes	Phase II		
	Three size classes: ( $w_1, w_2, w_3, W_p$ )	Four size classes: ( $w_1, w_2, w_3, w_4, W_p$ )	Five size classes: ( $w_1, w_2, w_3, w_4, w_5, W_p$ )
$\Gamma_{1,p}$	0.01	0.05	0.05
$\Gamma_{2,p}$	0.37	0.18	0.13
$\Gamma_{3,p}$	0.00	0.08	0.00
$\Gamma_{4,p}$	-	0.00	0.08
$\Gamma_{5,p}$	-	-	0.00
$\Gamma_{1,2}$	0.14	0.09	0.09
$\Gamma_{2,1}$	0.27	0.26	0.27
$\Gamma_{2,3}$	0.00	0.00	0.05
$\Gamma_{3,2}$	0.09	0.00	0.00
$\Gamma_{3,4}$	-	0.91	0.97
$\Gamma_{4,3}$	-	0.67	0.65
$\Gamma_{4,5}$	-	-	0.13
$\Gamma_{5,4}$	-	-	0.26
SS	204	176	181
MSS	15.7	11.7	10.7
$S_r$	4.0	3.4	3.3

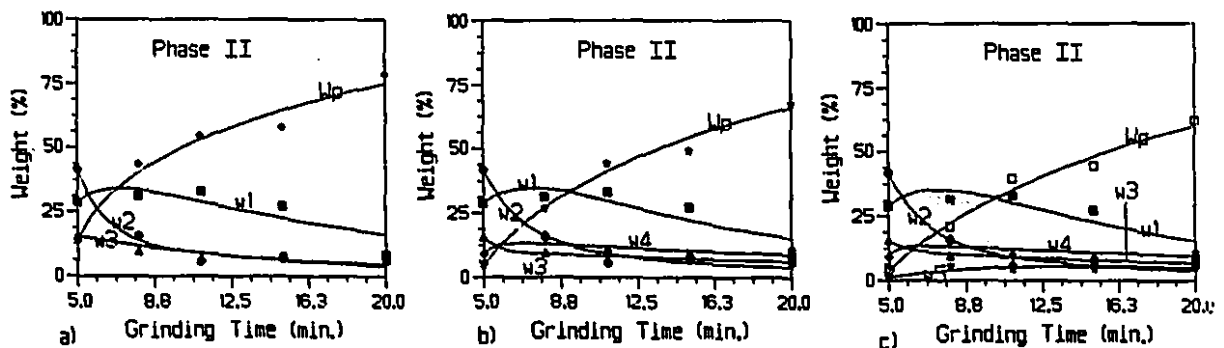


Figure 4.16: Fit of the flattening, folding and limited breakage model for the second phase of Test 3 and a: 3 size classes, b: 4 size classes, c: 5 size classes.

## 4.4 Tests 4 to 6: Grinding Flattened Lead Shots

### 4.4.1 Procedure

For Test 4, 100 g of flattened shots, in +4.75 mm size class (size class 1), were ground for 5, 10, 20, 30, 40, 50, 65 and 80 minutes in the Bond ball mill. Large grinding balls were used to achieve impact energy levels comparable to those of industrial mills (Table 4.1). After each grinding increment the mill product was screened from +4.75 mm to 0.425 mm.

For Test 5, 100 g of flakes (rolled shots) were ground for 10 minutes, in a single 5-minute increment followed by three one minute and one 2-minute increments in the Bond rod mill. The original mass was made from three different size classes, 18% in +5.60 mm ( $w_1$ ) which is the coarsest size class, 78% in 4.75-5.60 mm ( $w_2$ ), and 4% in the 4.00-4.75 mm ( $w_3$ ).

To complement Tests 4 and 5, an additional test was focused on weight rather than particle size considerations. Test 6 was performed with a relatively low number of particles: 55 flattened lead shots, 5.60-6.70 mm in diameter, were ground incrementally in the Bond rod mill. After each increment, all particles were weighed and fragments (identified by their lower weight) set aside. Parent particles were returned to the mill for the next increment.

### 4.4.2 Results and discussion

**Test 4:** Figure 4.17 shows the evolution of the size distribution of the material recovered from the mill for Test 4. Visual observation of the grinding products showed two different grinding phases. In the first 20 minutes of grinding most of the mass

remained in the original size class although some folding and flattening occurred. Superflakes was also observed, but because of the original size class is the coarsest one, the effect of super-flake formation is not shown in Figure 4.17.

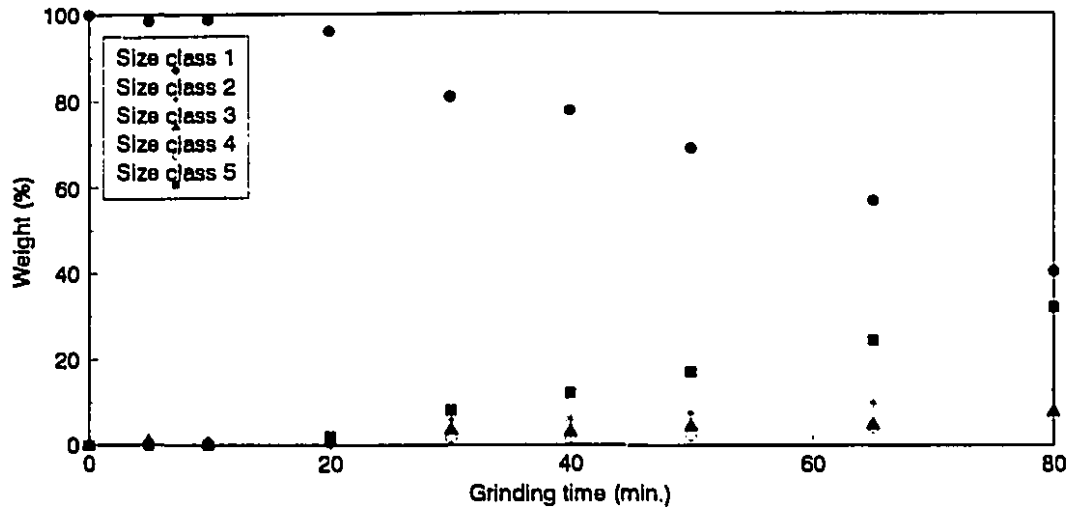


**Figure 4.17:** Size distribution of lead particles as a function of grinding time in the Bond ball mill (Test 4); size class 1: +4.75 mm, 2: 4.00-4.75 mm, 3: 3.35-4.00 mm, 4: 2.80-3.35 mm, 5: -2.80 mm.

After 20 minutes, particles started folding and breaking and reported to size classes finer than  $w_1$  (+4.75 mm), and  $w_1$  decreased, from almost 100% at 20 minutes to 40% at 80 minutes. The increase in  $w_5$  (-2.80 mm) is more than that of other size classes, strongly suggesting that breakage dominated over folding. However, some flattening of fragments was also observed.

Figure 4.18 shows the weight loss as a function of grinding time, which totalled 35% after 80 minutes. As for the previous tests, the rate of weight loss significantly increased at the onset of particle breakage. Figure 4.19 presents the fines production plot of Test 4. In first 20 minutes of grinding superflakes were produced and little breakage and folding took place; less than 5% of mass was finer than 4.75 mm. As breakage

began taking place, after 20 minutes of grinding, fines were created. After 80 minutes of grinding, 74% of mass was finer than 4.75 mm, and 35% finer than 0.425 mm.

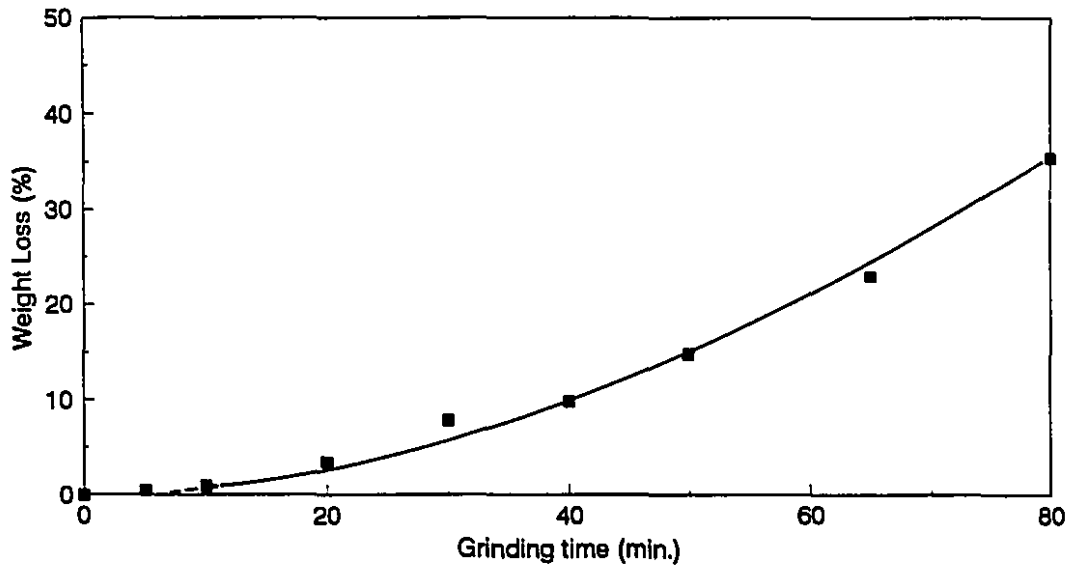


Figure 4.18: Lost weight in Test 4 (Bond ball mill).

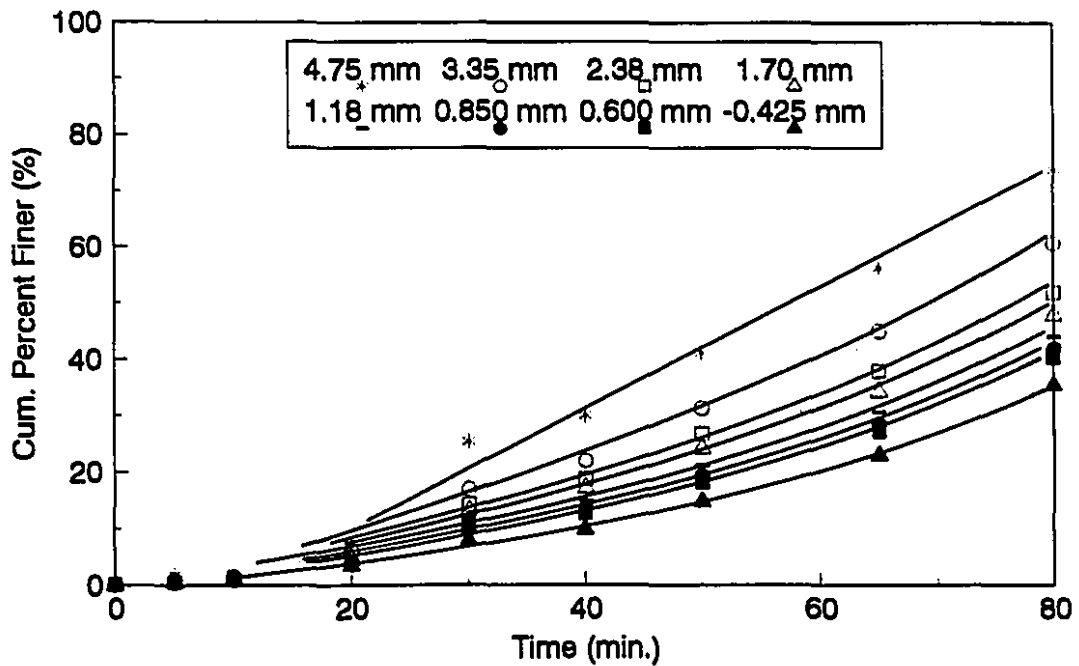


Figure 4.19: Fines production as a function of time in the Bond ball mill (Test 4).

The data were first fitted to the folding and flattening model without breakage (Equation 3.7), for both phases (phase I from 0 to 20 minutes, and phase II from 20 to 80 minutes). Experimental points are the weight percent in five size classes,  $w_1$  (+4.75 mm),  $w_2$  (4.00-4.75 mm),  $w_3$  (3.35-4.00 mm),  $w_4$  (2.80-3.35 mm) and  $w_5$  (-2.80 mm). The total weight was normalized to 100% to eliminate the effect of weight loss due to smearing. As for previous tests the results will be presented for three, four, and five size classes, in Table 4.9 and Figure 4.20(a) to 4.20(c). In three size classes  $W_3$  is mass in all size classes finer than 3.35 mm,  $W_4$  and  $W_5$  in the four and five size class model are the -2.80 mm and -2.38 mm, respectively.

**Table 4.9:** Estimated rate constants (all in  $\text{min}^{-1}$ ) for Test 4; flattening and folding model (no breakage).

Size classes	Three Size classes: $w_1, w_2, W_3$		Four size classes: $w_1, w_2, w_3, W_4$		Five size classes: $w_1, w_2, w_3, w_4, W_5$	
	Phases		Phases		Phases	
	(I)	(II)	(I)	(II)	(I)	(II)
$r_{1,2}$	0.00	0.01	0.00	0.01	0.00	0.12
$r_{2,1}$	0.00	0.00	0.00	0.00	0.00	0.00
$r_{2,3}$	0.55	0.32	0.59	0.08	0.65	0.32
$r_{3,2}$	0.00	0.07	0.00	0.00	0.00	0.42
$r_{3,4}$	-	-	0.20	0.15	0.21	0.12
$r_{4,3}$	-	-	0.00	0.00	0.00	0.00
$r_{4,5}$	-	-	-	-	0.20	0.22
$r_{5,4}$	-	-	-	-	0.00	0.00
SS	2.0	98.0	1.0	171.0	2.0	170.0
MSS	0.3	7.0	0.1	9.5	0.2	7.7
$S_r$	0.5	2.6	0.3	3.1	0.4	2.8

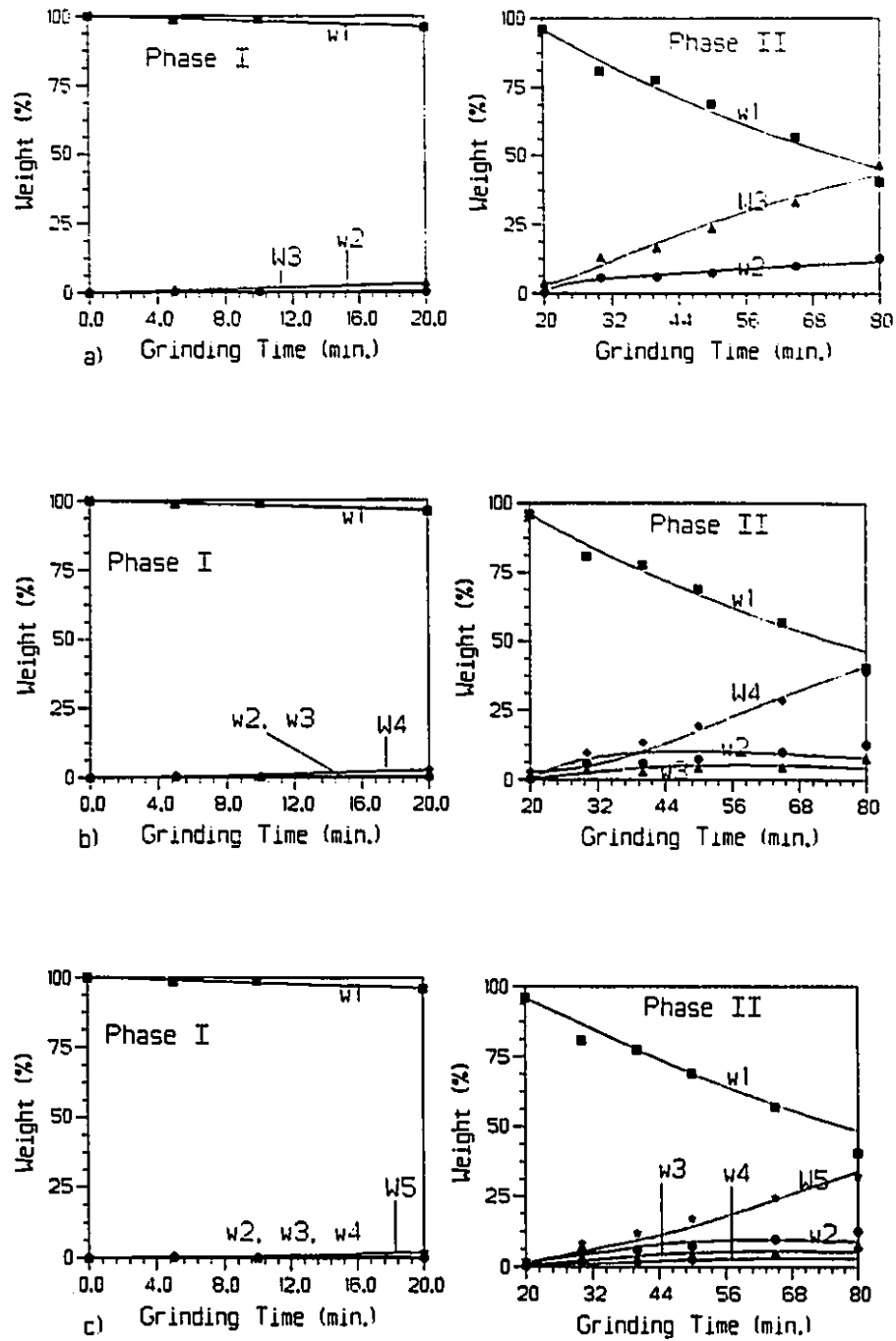
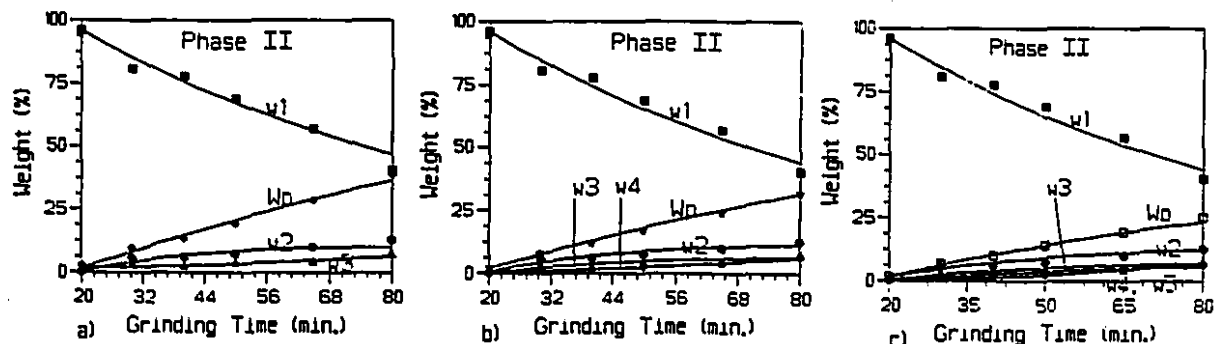


Figure 4.20: Fit of the flattening and folding model (no breakage) for the two phases of Test 4; a: 3 size classes, b: 4 size classes, c: 5 size classes.

Both Table 4.9 and Figure 4.20 show that the folding and flattening model yields an excellent fit for phase I, albeit over very small changes in size distribution. Because there is virtually no mass in size classes 2 to 5, the flattening rate constants ( $r_{i,i-1}$ ) can not be estimated. For phase II, the lack-of-fit is higher, but this stems in part from a greater scatter in the data and more significant changes in size distribution. The model, however, fails to represent the evolution of mass in size classes 2, 3, and 4 adequately (the increase of mass observed during the test is not reflected in the fit). The overall lack-of-fit is not higher because the changes in weight percent in those intermediate size classes are low.

To achieve a better fit of phase II, the folding, flattening and limited breakage model (Equation 3.22, 3.23) was used. The -3.35 mm, -2.80 mm, and -2.38 mm size classes are considered as pan ( $W_p$ ) for the three, four, and five size class fit, respectively. Results are presented in Table 4.10 and Figure 4.21. The average lack-of-fit values are lower than those of the flattening and folding (no breakage) model. More importantly, the model is now capable of trending the mass in size classes 2, 3, and 4 more adequately (compare Figure 4.21(b) and (c) to Figure 4.20(b) and (c) (phase II)).



**Figure 4.21:** Fit of the flattening, folding and limited breakage model for the second phase of Test 4; a: 3 size classes, b: 4 size classes, c: 5 size classes.

**Table 4.10:** Estimated rate constants (all in  $\text{min}^{-1}$ ) of the second phase of Test 4, with the flattening, folding and limited breakage model.

Size classes	Phase II		
	Three size classes: ( $w_1, w_2, w_3, W_p$ )	Four size classes: ( $w_1, w_2, w_3, w_4, W_p$ )	Five size classes: ( $w_1, w_2, w_3, w_4, w_5, W_p$ )
$\Gamma_{1,p}$	0.01	0.01	0.01
$\Gamma_{2,p}$	0.01	0.01	0.00
$\Gamma_{3,p}$	0.00	0.00	0.00
$\Gamma_{4,p}$	-	0.00	0.00
$\Gamma_{5,p}$	-	-	0.00
$\Gamma_{1,2}$	0.01	0.01	0.01
$\Gamma_{2,1}$	0.00	0.00	0.00
$\Gamma_{2,3}$	0.01	0.81	0.82
$\Gamma_{3,2}$	0.00	1.43	1.42
$\Gamma_{3,4}$	-	0.02	0.16
$\Gamma_{4,3}$	-	0.00	0.15
$\Gamma_{4,5}$	-	-	0.03
$\Gamma_{5,4}$	-	-	0.00
SS	88.0	77.0	77.0
MSS	5.2	3.9	3.4
$S_r$	2.3	2.0	1.8

Because breakage appears to be the dominant mechanism for phase II, the conventional breakage model (Equation 3.1) was also tested. Figure 4.19 shows an apparent constant rate of fines production from 20 minutes on (zero order kinetics); the breakage function of lead was estimated from these data using Herbst and Fuerstenau's

approach<sup>(25)</sup>, and is shown in Table 4.11. From this breakage function, the selection function was then estimated using the "SCIENTIST" software. Results are shown in Table 4.12 and Figure 4.22. Although the overall lack-of-fit values of this model for three, four, and five size class fit are higher than previous models (except for the three size classes of folding and flattening with limited breakage), the average lack-of-fit values are almost equal in all cases, as that the number of rate constants used is much lower.

**Table 4.11:** Estimated breakage and cumulative breakage functions (BF, CBF) of lead.

Size classes (mm)	BF values	CBF values
4.75	-	1.000
4.00	0.460	0.540
3.35	0.082	0.160
2.80	0.070	0.390
2.38	0.080	0.310
2.00	0.033	0.280
1.70	0.041	0.240
1.40	0.037	0.200
1.18	0.036	0.160

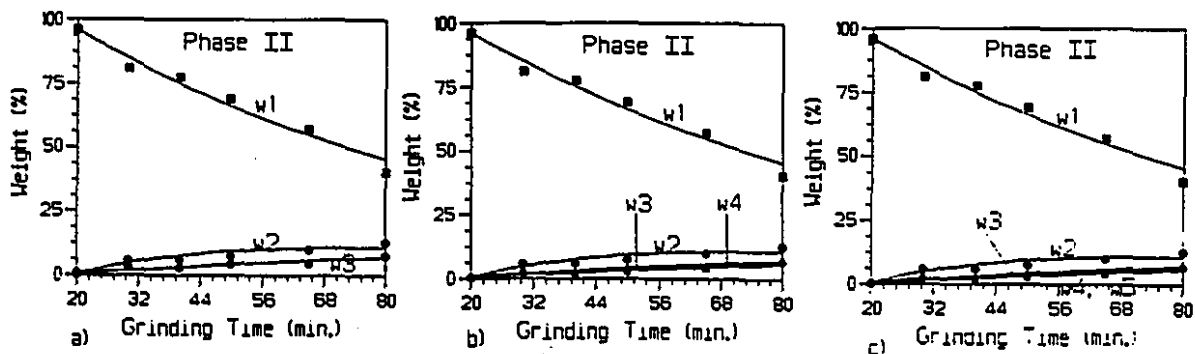


**Figure 4.22:** Fit of the conventional breakage model for the second phase of Test 4; a: 3 size classes, b: 4 size classes, c: 5 size classes.

**Table 4.12:** Estimated rate constants (all in  $\text{min}^{-1}$ ) for the second phase of Test 4; conventional breakage model.

Size classes	Phase II		
Rate constants	Three size classes: $w_1, w_2, w_3, W_p$	Four size classes: $w_1, w_2, w_3, w_4, W_p$	Five size classes: $w_1, w_2, w_3, w_4, w_5, W_p$
$s_1$	0.01	0.01	0.01
$s_2$	0.03	0.03	0.03
$s_3$	0.02	0.02	0.02
$s_4$	-	0.01	0.01
$s_5$	-	-	0.00
SS	78.0	81.0	81.0
MSS	5.2	4.1	3.2
$S_r$	2.3	2.0	1.8

**Test 5:** This test was exploratory, which explains why the first grinding increment, 5 minutes, yielded far too much grinding, as shown in Figure 4.23. Grinding increments were then decreased, up to a total grinding time of 10 minutes. After only 5 minutes significant grinding had been achieved. After 10 minutes of grinding virtually all mass was finer than 2.80 mm (i.e. in the pan), and 65% of the product recovered from the mill was finer than 0.600 mm (Figure 4.24). The mass in the coarsest size class, initially at 18%, decreased to less than 1% after 5 minutes of grinding. This is a strong indication that flattening (in this case from size class 2, containing initially 78% of the mass) was not a dominant phenomenon.

Figure 4.25 shows that 8% of the original mass is lost after 5 minutes, and 19%

after 10 minutes. The higher rate of weight loss in the second half of the test could stem from increased manipulation (i.e. three grinding increments instead of one).

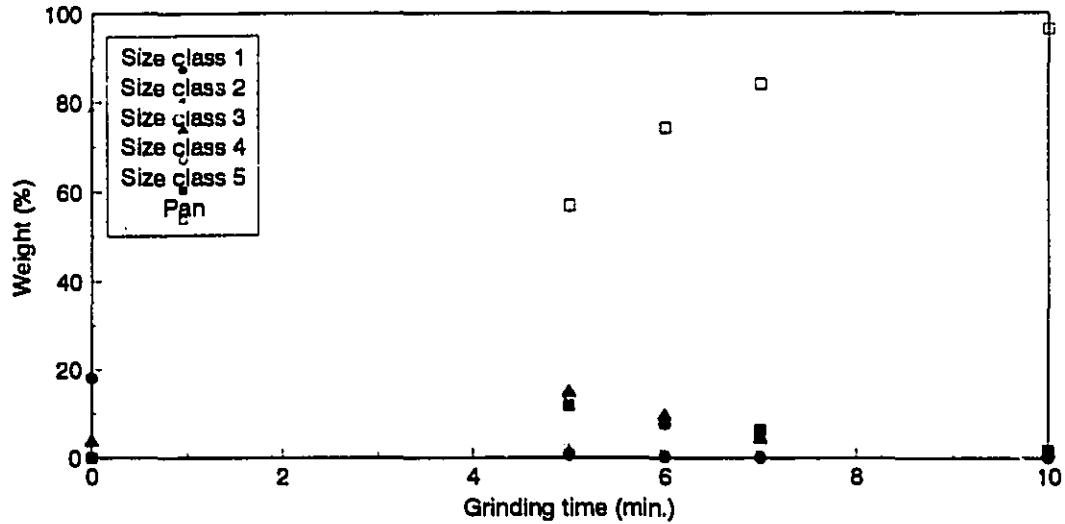


Figure 4.23: Size distribution of lead particles as a function of grinding time in the Bond rod mill (Test 5); size class 1: +5.60 mm, 2: 4.75-5.60 mm, 3: 4.00-4.75 mm, 4: 3.35-4.00 mm, 5: 2.80-3.35 mm, pan: -2.80 mm.

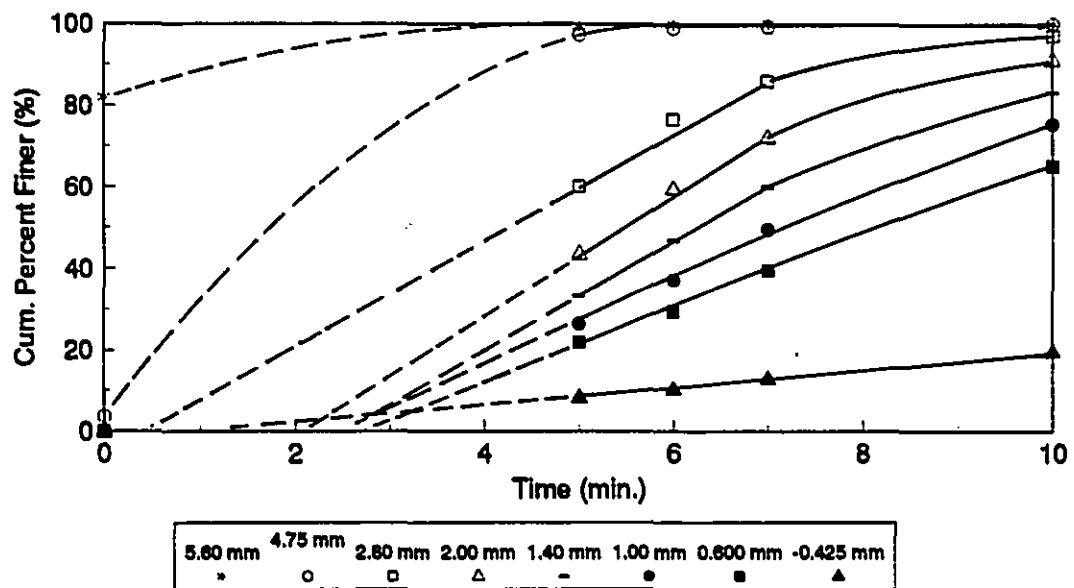


Figure 4.24: Fines production as a function of time in the Bond rod mill (Test 5).

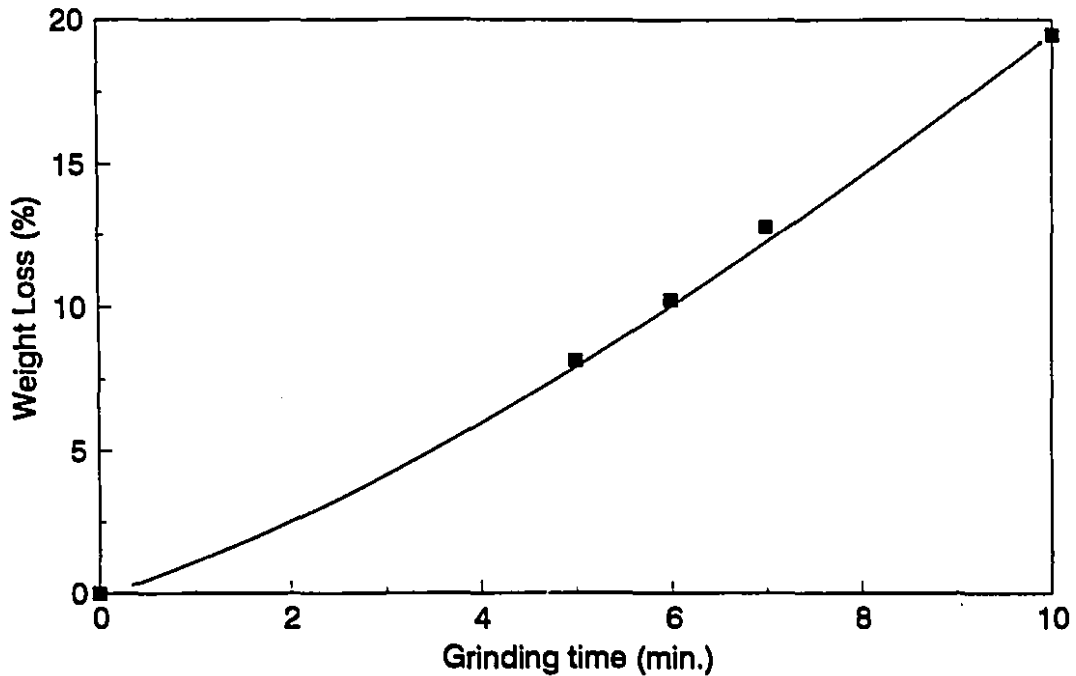


Figure 4.25: Lost weight in Test 5 (Bond rod mill).

The full data set was first fitted to the flattening and folding model (Equation 3.7). Figure 4.26 and Table 4.13 display the good fit of the model, although the lack of data between 0 to 5 minutes weakens this conclusion significantly. Table 4.13 confirms the observation that flattening is insignificant, as all estimates of the flattening rate constant are either very small or null.

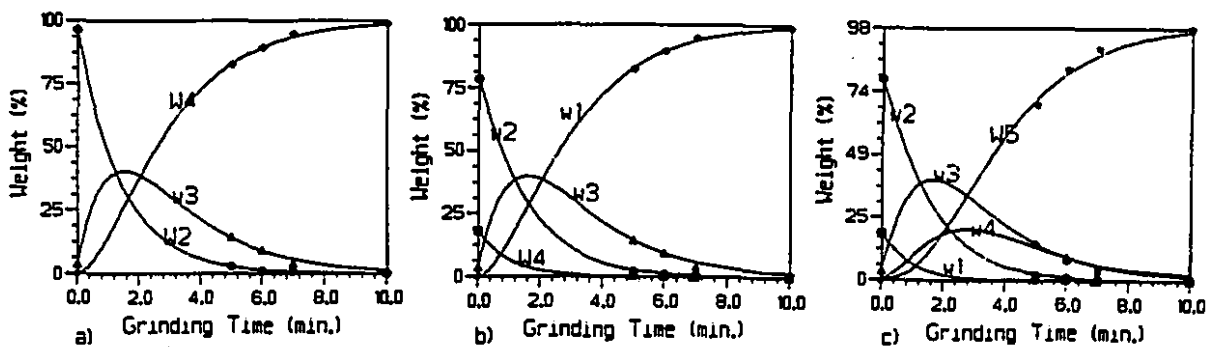


Figure 4.26: Fit of the flattening and folding model (no breakage) for Test 5; a: 3 size classes, b; 4 size classes, c: 5 size classes.

**Table 4.13:** Estimated rate constants (all in  $\text{min}^{-1}$ ) for Test 5; flattening and folding model (no breakage).

Rate Constants	Three Size classes $W_2, W_3, W_4$	Four Size classes $W_1, W_2, W_3, W_4$	Five Size classes $W_1, W_2, W_3, W_4, W_5$
$r_{1,2}$	-	1.04	1.11
$r_{2,1}$	-	0.00	0.00
$r_{2,3}$	0.71	0.79	0.79
$r_{3,2}$	0.00	0.00	0.00
$r_{3,4}$	0.58	0.59	0.59
$r_{4,3}$	0.00	0.00	0.00
$r_{4,5}$	-	-	0.98
$r_{5,4}$	-	-	0.00
SS	4.0	4.0	18.0
MSS	0.4	0.3	1.1
$S_r$	0.6	0.5	1.0

It is understood that given the importance of breakage, the folding rate constants (i.e.  $r_{i,i+1}$ ) represent breakage rather than folding. It is somewhat surprising that describing breakage as simply as a transfer to the adjacent finer size class can yield such a good fit. This may well be an artifice of the data set; choosing to include pan material in the finest size class further limits the lack-of-fit.

To represent breakage, obviously the dominant phenomenon of Test 5, the folding, flattening and limited breakage model was used. Figure 4.27 and Table 4.14 show a fit which is not as good as that of the folding and flattening model, but remains acceptable. The model in fact is more informative, as it discriminates between material going to the finest size class and the pan.

**Table 4.14:** Estimated rate constants (all in  $\text{min}^{-1}$ ) for Test 5; flattening, folding and limited breakage model.

Size classes	Three size classes: ( $W_2, w_3, w_4, W_p$ )	Four size classes: ( $w_1, w_2, w_3, w_4, W_p$ )	Five size classes: ( $w_1, w_2, w_3, w_4, w_5, W_p$ )
Rate constants			
$\Gamma_{1,p}$	-	0.00	0.53
$\Gamma_{2,p}$	0.00	0.00	0.00
$\Gamma_{3,p}$	0.00	0.00	0.00
$\Gamma_{4,p}$	0.97	0.97	0.00
$\Gamma_{5,p}$	-	-	1.13
$\Gamma_{1,2}$	-	1.12	0.00
$\Gamma_{2,1}$	-	0.00	0.00
$\Gamma_{2,3}$	0.71	0.79	0.73
$\Gamma_{3,2}$	0.00	0.00	0.00
$\Gamma_{3,4}$	0.58	0.59	0.53
$\Gamma_{4,3}$	0.00	0.00	0.00
$\Gamma_{4,5}$	-	-	0.87
$\Gamma_{5,4}$	-	-	0.00
SS	19.0	18.0	45.0
MSS	1.5	1.2	2.7
$S_r$	1.2	1.1	1.6

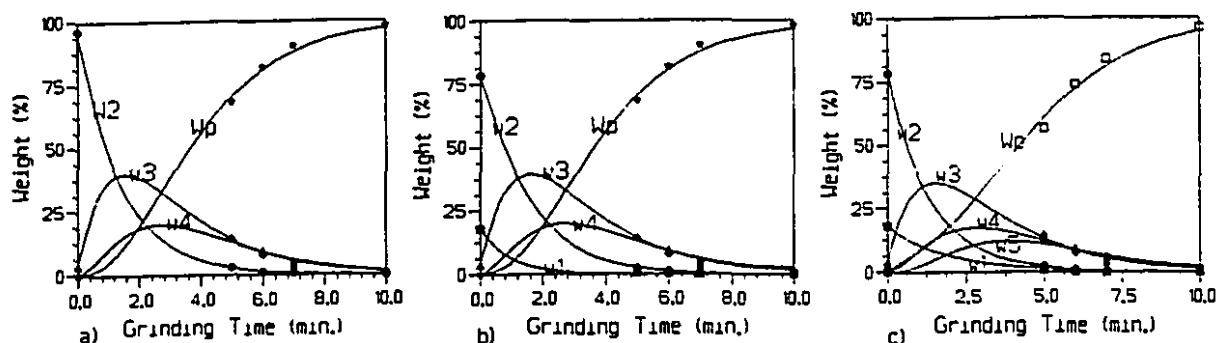


**Figure 4.27:** Fit of the flattening, folding and limited breakage model for Test 5; a: 3 size classes, b: 4 size classes, c: 5 size classes.

**Test 6:** Test 6 was meant to clarify some questions raised by Test 5, such as a) when does breakage begin, b) is there one or two grinding phases, and c) can we estimate the breakage function of fragments?

Figure 4.28 shows histograms of particle weight in the size classes where particles reported after 0.5, 1, 2, and 4 minutes of grinding. No breakage took place after 0.5 minute, and very limited breakage after 1 minute. However, breakage after 2 and 4 minutes is extremely significant, and there is a definite correlation between particle size and weight, especially in the finer size classes. Figure 4.29 shows the size distribution of the lead particles recovered from the mill, but the trend is in part misleading, as broken fragments (as determined by their weight) were removed as soon as they encountered --i.e. after each grinding increment.

Figure 4.30 presents weight loss percent versus grinding time for Test 6. It shows that the lost weight increased with grinding time, up to less than 35%, which corresponds to particle breakage. In the first increments of grinding, where folding and flattening were dominant, the weight loss was low; it increased significantly at the onset of breakage.

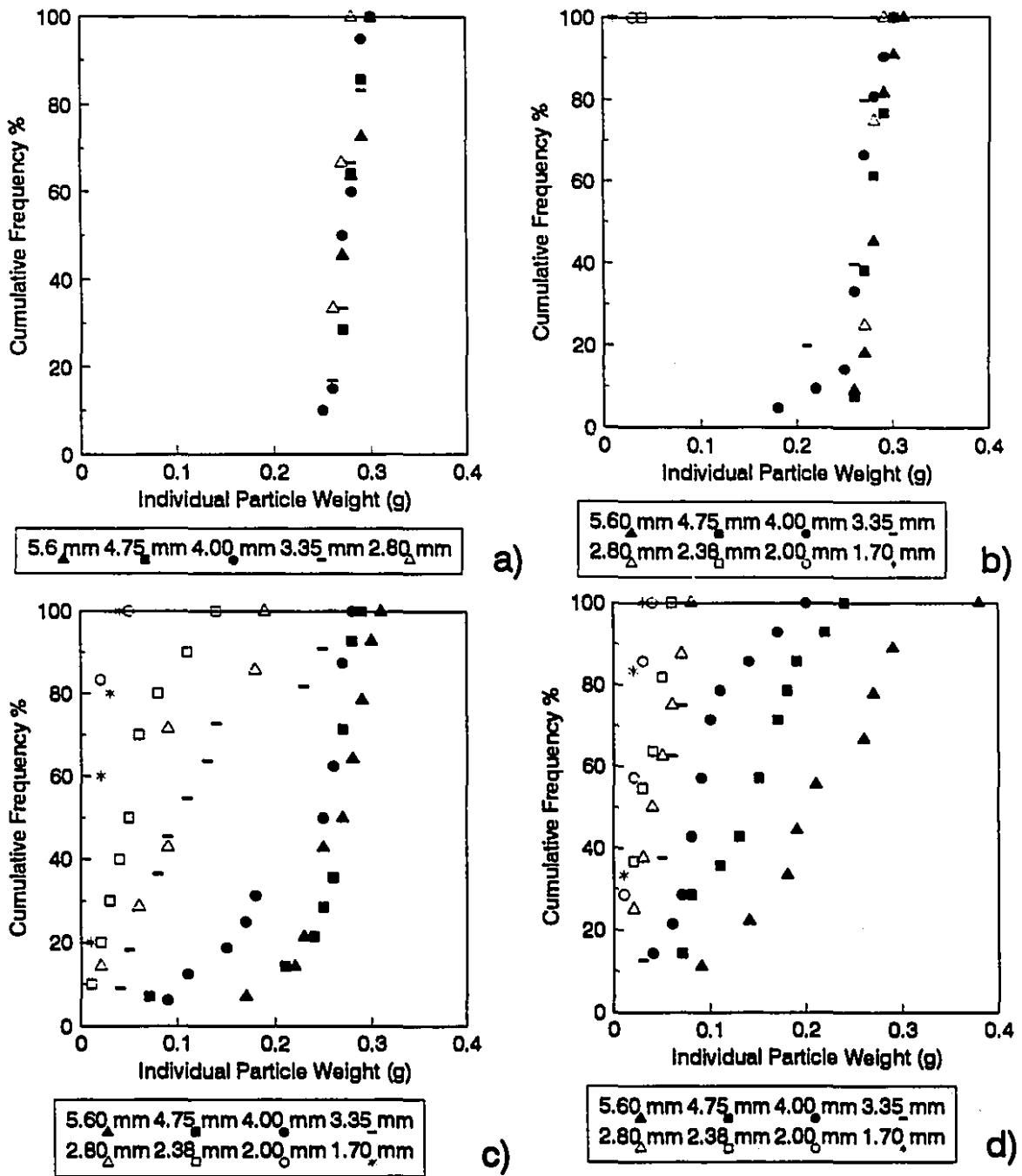


Figure 4.28: Cumulative histograms of the weight of individual particle for Test 6; after a: 0.5 minute, b: 1 minute, c: 2 minutes, d: 4 minutes.

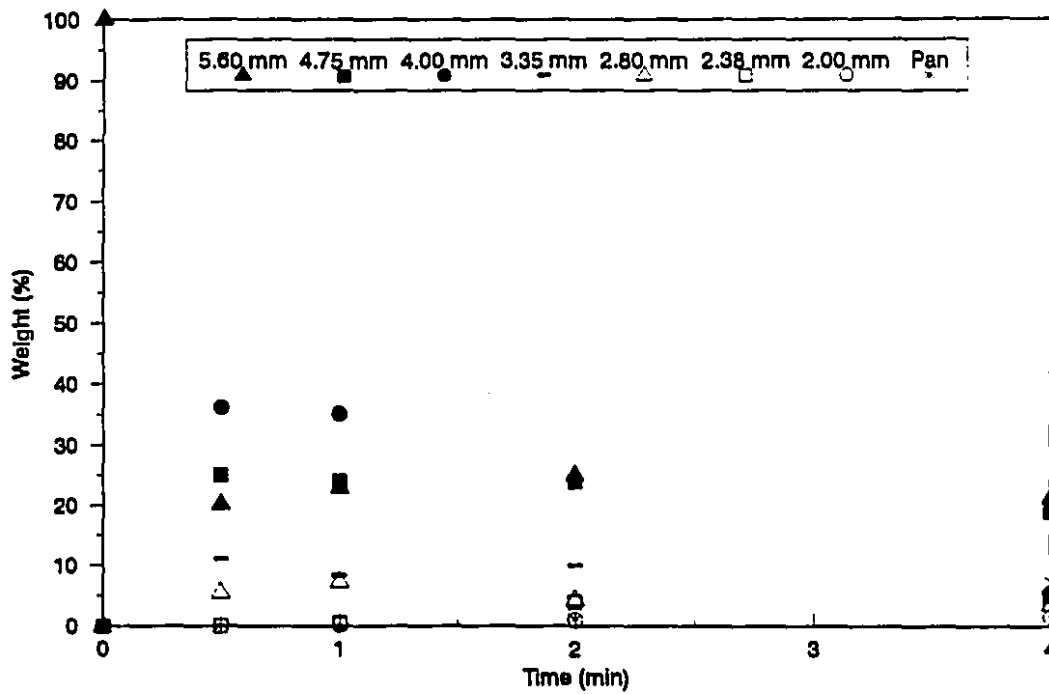


Figure 4.29: Size distribution of flattened lead shot as a function of grinding time in Test 6 (Bond rod mill).

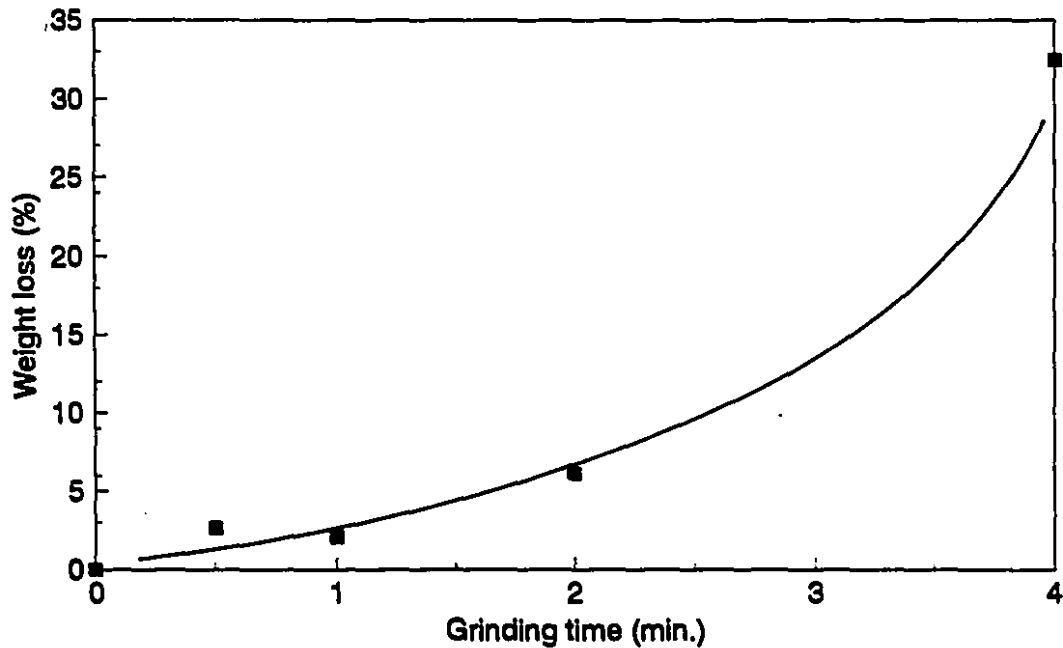
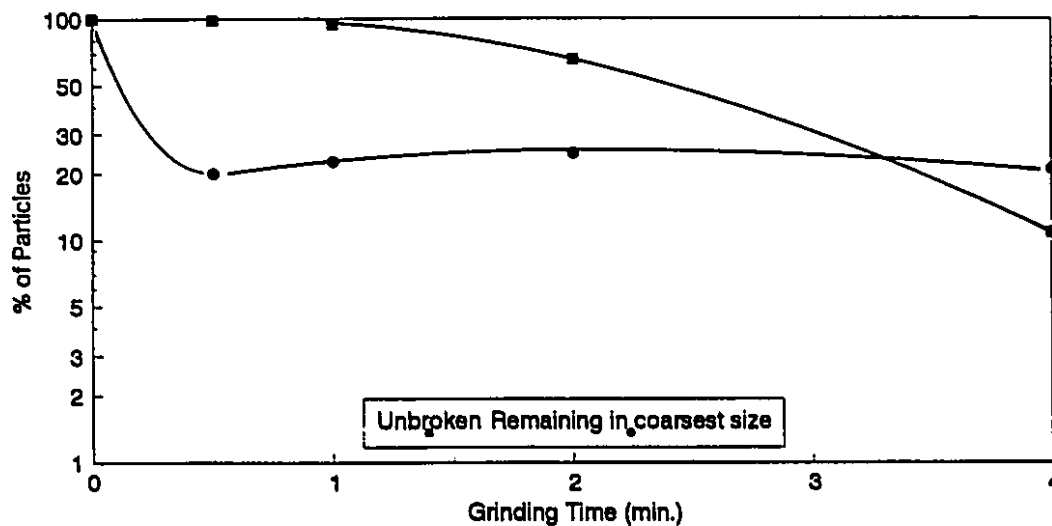


Figure 4.30: Lost weight in Test 6 (Bond rod mill).

When grinding material from a single size class, its selection function can be estimated from the slope of the weight left in this size class, on a logarithmic scale, as a function of time (linear scale). Such plots should be linear. For malleable materials, it may be appropriate to consider the weight or number of unbroken particles (as determined by their weight), irrespective of the size class they report to. Figure 4.31 shows both options, neither of which yields a linear plot. This is a good illustration of the complexity of the mechanisms governing the breakage of malleable materials.



**Figure 4.31:** Weight percent of unbroken particles and percent particles remaining in the coarsest size class in Test 6 (Bond rod mill).

Removing fragments after small grinding increments minimizes the probability of secondary breakage (i.e. the production of secondary fragments from primary fragments). Under such circumstances, the weight distribution of fragments in the various size classes should approach the breakage function. Using this assumption, the data of Test 6 were used to estimate the breakage function in the Bond rod mill, and are shown in Table 4.15. Data are erratic (as only 55 flattened lead shots were used), and definitely atypical of published data either for brittle<sup>(115)</sup> or malleable minerals<sup>(10)</sup>.

**Table 4.15:** Estimated breakage function (BF) and Cumulative breakage function (CBF) of lead in Test 6 (Bond rod mill).

Size class (mm)	BF	CBF
5.60	-	1.00
4.75	0.15	0.85
4.00	0.05	0.80
3.35	0.15	0.65
2.80	0.08	0.57
2.38	0.08	0.49
2.00	0.03	0.46
1.70	0.02	0.44
1.40	0.01	0.43

## 4.5 Microhardness Tests

### 4.5.1 Definitions

Many materials, when formed in different processes, are subjected to forces or loads. These forces can be tensile, compressive and/or shear. In such situations it is necessary to know the mechanical behaviour of materials, showing how they respond to forces<sup>(174)</sup>.

Hooke's law<sup>(174, 175)</sup> presents the relationship between stress and strain as follows:

$$\sigma = E_1 \epsilon \quad (4.1)$$

where  $\sigma$  is the applied stress and  $\epsilon$  is the strain and  $E_1$  is the modulus of elasticity or Young's modulus. Deformation in which stress and strain are proportional is called

elastic deformation, and corresponds to the linear part of the stress-strain curve whose slope is the modulus of elasticity. Deformation disappears completely once the stress is removed.

As a material is deformed beyond its elastic limit then deformation is called plastic and is no longer recoverable<sup>(174, 175)</sup>. The transition from elastic to plastic is a gradual one for most metals, and it is simply defined the "strength point" (as also called the yield point). Beyond the yield point additional stress will cause an increase of plastic deformation up to a maximum load, which then decreases to the eventual fracture point. The tensile strength is the stress at the maximum on the stress-strain curve.

Hardness is one of the mechanical property which is a measure of a material's resistance to localized plastic deformation. Several hardness tests are used: Rockwell<sup>(176)</sup>, Brinell<sup>(177)</sup>, Knoop<sup>(178, 179)</sup> and Vickers<sup>(179, 180)</sup>. The results of different hardness tests are not directly comparable but are well correlated. As tensile strength and hardness are both indicators of the resistance to plastic deformation, they are also correlated:

Strain hardening, work hardening or cold working are the different names of a phenomenon whereby a metal becomes harder and stronger as it is plastically deformed<sup>(174, 175, 181, 182)</sup>. Plastic deformation in metals is also the cause of ductility loss. A metal is work-hardened when work is done at a temperature below that at which recrystallization takes place<sup>(183)</sup>, a phenomenon called cold working. Most metals are work-hardened at room temperature; notable exceptions are zinc, tin, and lead, whose recrystallization temperature is  $-4\text{ }^{\circ}\text{C}$ <sup>(175, 184, 185, 186)</sup>.

Table 4.16 presents the recrystallization and melting temperatures, hardness values and activation energy of some malleable metals, gathered from different sources<sup>(175, 186, 187, 188, 189, 190)</sup>.

**Table 4.16:** Hardness, recrystallization and melting temperatures, and activation energy of some malleable metals.

Property: → Metal: ↓	Hardness (Vickers)	Temperature of:		Activation Energy (kcal/mol.)
		Rec. (°C)	Melting (°C)	
Lead	20	-4	327	25.7
Copper	35	121	1981	50.4
Gold	25	200	1064	41.7
Silver	27	200	962	45.2
Platinum	48	450	1769	68.1

The recrystallization temperature is defined as the lowest temperature at which recrystallization occurs completely<sup>(189, 191)</sup>, and typically is between one third and one half of the absolute melting temperature<sup>(174)</sup>. The activation energy is the energy required to initiate a reaction such as diffusion<sup>(174)</sup> which leads to grain boundary movement, and therefore recrystallization in a metal with a higher activation energy needs more energy to occur. If the energy level is sufficient, nucleating sites begin to form in areas of highest strain energy and recrystallization begins. This energy comes from strain (which can come from cold working), and is activated by heat (e.g. in heat treatment processes). Thus, recrystallization requires cold working, temperature and time. Since cold working and the number of nucleating sites are directly related and the number of nuclei and grain size have an inverse relationship, therefore the amount of cold working and recrystallized grain size are inversely related<sup>(191)</sup>.

Some other factors, such as impurities (solute atoms or insoluble) and the original grain size (before cold working), can change the recrystallization temperature and rate. The presence of other atoms increases the crystallization temperature, and as a result it is lowest for the pure metals<sup>(174, 189, 191)</sup>. It has been reported that pure gold (99.999%)

and silver recrystallize and can be hot worked at room temperature<sup>(184, 185)</sup>. This differs from the commercial gold and silver recrystallization temperatures reported in Table 4.16. Insoluble impurities such as oxides and gases cannot directly change the recrystallization temperature but they can enhance nucleation and therefore the number of smaller grains (increasing the surface of grain boundaries). Grain size before cold working can also influence the recrystallization temperature in that smaller grains have a higher boundary energy density than a specimen with larger grains. Therefore, recrystallization temperature for small grain size specimens is lower and, recrystallization faster<sup>(191)</sup>.

We will use microhardness tests to measure the hardness of different types of lead particles which have been used in the different grinding tests. We expect to be able to identify under which conditions, and to which extent, work hardening has taken.

#### 4.5.2 Apparatus and procedure

Hardness was measured on four different types of lead particles. The first was the lead shots themselves (3-4 mm in diameter), the second flattened lead shots (5-6 mm in diameter) which were produced using the manual hand press machine described in section 4.2. The third type was lead shots partially flattened (to a thickness of 2 mm) with the same press machine (section 4.2). Finally, lead flakes extracted from the Bond rod mill, 0.850-1.00 mm in diameter, were tested. A microhardness tester, LECO Corporation model M-400-G2 with a vickers diamond indenter, was used in these series of tests. Test load were placed on 3 (low system) and the hardness of 90 points for each sample (lead shots, flattened lead shots, semi flattened lead shots and lead flakes) was measured.

### 4.5.3 Results and discussion

Figure 4.32 presents all hardness measurements as cumulative histograms for the four types of particles. Hardness values have similar ranges, 9.7-19.1 for shots, 9.8-17.8 for flattened shots, 9.5-18.1 for semi-flattened shots and 9.0-21.3 for flakes. The average hardness varies between 13.1 and 13.9, with standard deviations of 1.6 to 2.7 (relative standard deviation of 12% to 19%). The highest and lowest variances and averages are not statistically different (at 95%) and the overall hardness is 13.7, with a standard deviation of 0.3 (between the average of the four particle types).

Results strongly suggest that neither the flattening, nor the grinding of shots affected particle hardness. This is without doubt related to the low recrystallization temperature of lead,  $-4^{\circ}\text{C}$ , significantly below room temperature, and its low activation energy (Table 4.16).

### 4.6 Conclusions

Test work with lead shots, though exploratory, yielded valuable insight into the grinding of malleable metals. First, the very different results obtained with the rod and ball mills highlight the importance of the grinding environment. In the Bond rod mill, much more energy is released upon impact of the rods (again the mill shell or each other), resulting in much more significant breakage and smearing. In the Bond ball mill, despite the large size of the balls used (5.0-7.5 cm, unlike the standard charge, 1.50 to 3.70 cm), the lower energy density limits the occurrence of breakage, until superflakes form and cracks at their edges propagate.

Another useful observation is that the correct phenomenological model, be it flattening and folding; flattening, folding and limited breakage; or agglomeration,

---

consistently displayed the best fit. This is not to say that the models are totally accurate. The lack-of-fit remains significant, the presence of "induction times" suggests that non-first-order phenomena take place (such as "multi-impact" transfers), and the models fail to predict transition from one phase to the next (e.g. flattening to agglomeration; flattening and folding to flattening, folding and limited breakage). Still, the models shed more light into the various phenomena. For example, the probability of flattening (i.e. moving to a coarser size class) is generally twice that of folding (i.e. moving to a finer size class).

Tests 4 to 6 confirmed some of the observations of Tests 1 to 3. For example, all tests showed an induction time before the onset of breakage. Test 4, with the Bond ball mill, was the only test during which superflakes were formed. Significant smearing of lead corresponded to the breakage phase, and was at a more significant rate in the rod mill than the ball mills.

Test 6 showed that strict breakage could be very complex, and not necessarily associated to distinct parent and progeny size classes. The concept of first order kinetics, when examined in detail for breakage, was very approximate. It also showed that weight loss due to smearing could affect parent particles as much as progeny.

Hardness studies suggested that no detectable work hardening had taken place either during sample preparation or grinding. This is consistent with lead's mechanical properties, in particular its low recrystallization temperature and activation energy. The absence of work hardening for lead is a contributing factor in malleability. Until cracks form at their edges, propagate and release fragments, particles can repeatedly fold and flatten.

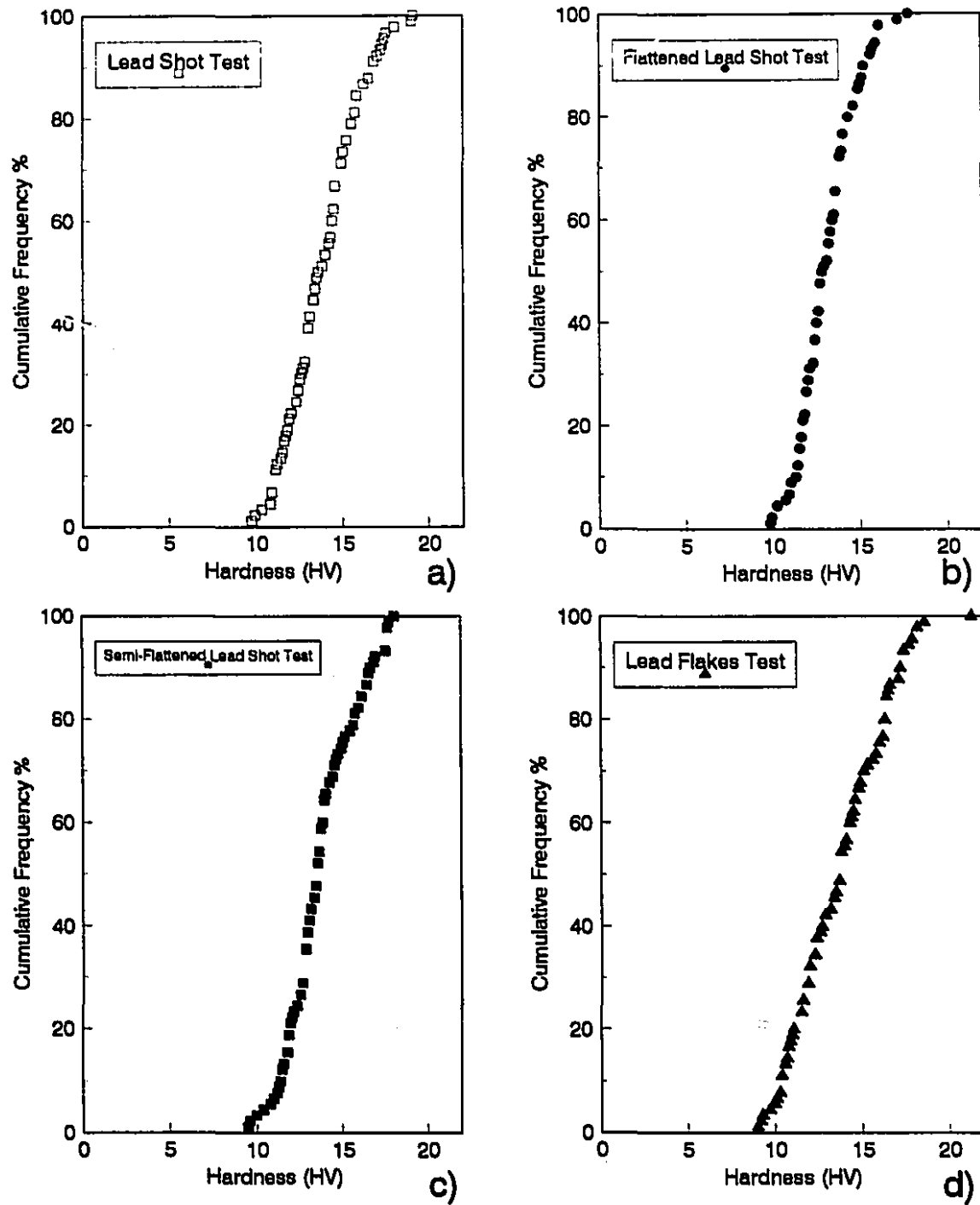


Figure 4.32: Hardness of different lead particles (measured with a: lead shots, b: flattened lead shots, c: semi-flattened lead shots, d: lead flakes).

**Chapter 5: The Behaviour of Lead Fragments in  
Tumbling Mills**

## 5.1 Introduction

In the last chapter, the grinding of lead shots, both spherical and flattened, was described. Irrespective of the system studied (i.e. mill and grinding medium), the final product was largely made up of irregularly shaped fragments similar to gold fragments recovered by gravity from industrial grinding circuits. This chapter describes the characterization of these fragments subjected to additional grinding, in a range of particle sizes closer to that of gold in industrial tumbling mills.

A first series of tests will focus on the lead fragments themselves. In a second series, the fragments will be ground in the presence of silica of similar size. This will be an attempt to further mimic the behaviour of gold flakes when gold ores, where very often silicates predominate, undergo grinding.

Data will be analyzed as it was in chapter 4, with the "DIFFEQ" and "SCIENTIST" software from MicroMath Scientific Software. The same models and criteria used in chapter 4, Equations 3.1, 3.7, 3.14, 3.22, 3.23 and 3.32, will also be tested. Because of the large number of tests, only salient results will be presented and discussed. All other data are shown in Appendix II.

## 5.2 Experimental

**Sample Preparation:** To produce lead fragments in various size classes, coarse lead particles were ground in a Bond rod mill and fragments in four specific size classes, 1.18-1.40 mm, 0.850-1.000 mm, 0.600-0.710 and 0.425-0.500 mm, were recovered. The silica sample used in the second series of tests was from Daubois Inc.; it was dry screened to obtain monosized fractions in the same size classes.

**Apparati:** Three different mills were used which could apply different energy levels on particles: the Bond ball, and Bond rod mills with their standard Bond charges<sup>(60)</sup>, and a small ball mill (18 cm in diameter and 18 cm in length), with a 10.4 kg graded charge of balls, 1.5 to 2.7 cm in diameter. Table 5.1 shows the specification of these three mills. A set of screens with  $2^{0.25}$  Tyler geometric progression was used. For the second series of tests, with lead fragments and silica, a Mozley Laboratory Separator (MLS) from Richard Mozley Limited was employed to separate them after each grinding increment.

**Table 5.1:** Specification of three mills, used in different tests.

Mills' Specification: → Types of Mills: ↓	Ball/Rod Charge (kg)	Mill Size dia. * length (cm*cm)	Ball(dia.)/Rod dia. * length (cm*cm)	Rev. (rpm)
Bond Rod Mill	33	30, 60	6 rods: 3, 53 2 rods: 4, 53	46
Bond Ball Mill	20.10	30, 30	1.5-3.7**	75
Small Ball Mill	10.40	18, 18	1.5-2.7	68

(\* standard charge for Bond test)

**Methodology:** In the first series, a total of 12 tests were performed for each of the four lead fragment size classes, in each of the three mills. Feed weight in the small ball, and Bond ball and rod mills was 10, 25, and 50 g, respectively. The experimental procedure, particularly in the first series of test, was very simple. The lead fragments were ground incrementally; between increments the size distribution of the lead recovered from the mill and the loss of weight were determined. The material was then entirely returned to the mill for the next grinding increment. To clean the mill shell and medium surface from the coated and smeared lead particles, 1 kg of 1.18-1.40 mm silica was ground for 5 minutes. This procedure was performed before each test in both the first and second series.

For the Bond ball mill, slower grinding kinetics required longer grinding times, 120 to 160 minutes, in increments of 10 up to 40 minutes. In the small ball mill total grinding time was 30 minutes for the 1.18-1.40 mm size class. This resulted in very significant weight loss; thus, total grinding and incremental grinding times were reduced for the other three size classes, down to 10 and 0.5 minutes, respectively. For the Bond rod mill, because of the fast grinding and smearing kinetics, total grinding times were low, 1.5 to 2.0 minutes; grinding increments were either 0.25 or 0.5 minute.

In the second series of tests, the same mills were used and feed for each test was made up of the lead fragments mixed with silica from the same size class. To maximize interaction of lead particles with silica (rather than lead-lead interaction), the weight ratio was set to 19:1 (95% silica). For all tests, the same weight of lead fragments as in the first series of tests was used. Individual size classes were then processed with the MLS, using the v-shaped tray, to separate lead from silica. Both products were dried and weighed; all size classes were then recombined for the next grinding increment.

The total grinding time for the Bond ball mill was 20 minutes with 5 minute increments, except the first test, using 1.18-1.40 mm of lead fragments, which was 30 minutes with 2, 7, and 10 minute increments. In the small ball mill total grinding time was 20 minutes for the all tests with 5 minute increments. For the Bond rod mill the grinding time for all tests was 10 minutes with 2, 3, and 4 minute increments.

### **5.3 Results and Discussion**

#### **5.3.1 First series of tests: Grinding lead fragments**

**Bond Ball Mill:** Figure 5.6 shows the size distributions observed for the Bond ball mill tests. In general, at first weight in the parent size class decreases very rapidly (class 2 for all tests). Most weight reports to size class 1 because of flattening, but some also

reports to finer size classes because of folding, especially for the first test (Figure 5.6(a)), with 1.18-1.40 mm fragments. Weight percent in the first size class eventually levels off, and even decreases slightly for Test 4 (Figure 5.6(d)), with 0.425-0.500 mm fragments. For the second phase of the test, weight percent in size class 2 still decreases, but the weight gain is most important in the finest size class, presumably because of breakage both from size classes 1 and 2.

Figure 5.7 details the appearance of material in the finer size classes. Material appearing in size class five is in fact significantly finer than the top size of size class five<sup>1</sup>, which confirms the observation of actual breakage. Appearance in these finer size classes roughly follows zero order kinetics for the last three tests.

Figure 5.8 presents the weight loss in the different Bond ball mill tests. Weight loss due to coating of medium and mill shell increased with time for all tests, but in a seemingly inconsistent pattern. For example, loss is much more significant for Test 1, minimum for Test 2, but then increases again from 2 to 4. The explanation resides in the methodology, and the chronological order, from Test 1 to Test 4. For Test 1, the mill had been scrubbed extensively before with conventional Bond tests. Most cavities were therefore available for lead coating. The mill was cleaned between tests, but to a lesser extent. Thus the number of smearing sites was lower than for Test 1, hence the lower weight loss. Because the cleaning methodology was identical between tests, the increase in weight loss from Test 2 to 4 must be related to fragment size i.e. losses are more significant for smaller fragments.

Figures 5.1 to 5.5 show scanning electron microscope (SEM) photographs of flattened and folded lead fragments with different shapes; folded particles such as in

---

<sup>1</sup>For example, in Figure 5.7(d), 10% of the recovered mass reports to size class 5, -0.300 mm. Figure 5.7(d) shows that of that 10%, 8% is finer than 0.150 mm.

Figure 5.1<sup>2</sup> reported to a finer size class whereas flattened particles such as Figures 5.3, and 5.4 moved to coarser size classes. Particles with spherical, cylindrical (Figures 5.1 and 5.2) and serrated shapes (Figure 5.3, 5.4, and 5.5) were visible in the Bond ball mill product. As reported by Hopkins and Brooks<sup>(160)</sup>, cracks indeed form at flake edges and propagate.

The flattening, folding and limited breakage model gives the best phenomenological fit for this first series of tests. As in chapter 4, three to five size class models (plus the pan) were tested. Estimated rate constants and fitted curves for the twelve tests are presented in Appendix II; results of one test, with a feed size of 0.425-0.500 mm in the Bond ball mill, are shown in this section. Table 5.2 and Figure 5.9 present the estimated rate constants and fitted curves, respectively.

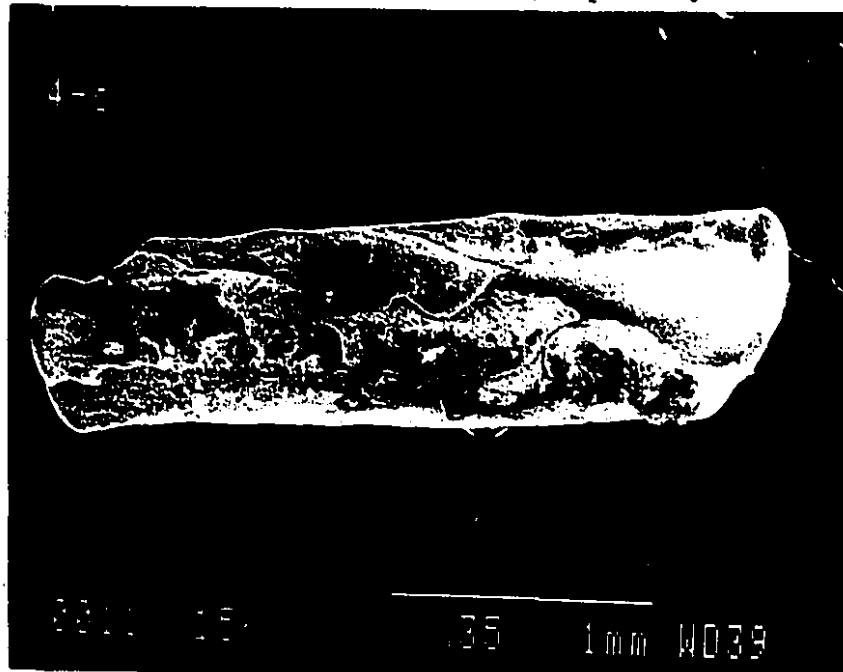


**Figure 5.1:** A cylindrical lead fragment recovered from the Bond ball mill (feed size: 0.850-1.000 mm).

<sup>2</sup>All SEM photos taken with Scanning Electric Microscope model JEOL JSM-840A.



Figure 5.2: A spherical lead fragment recovered from the Bond ball mill (feed size: 1.18-1.40 mm).

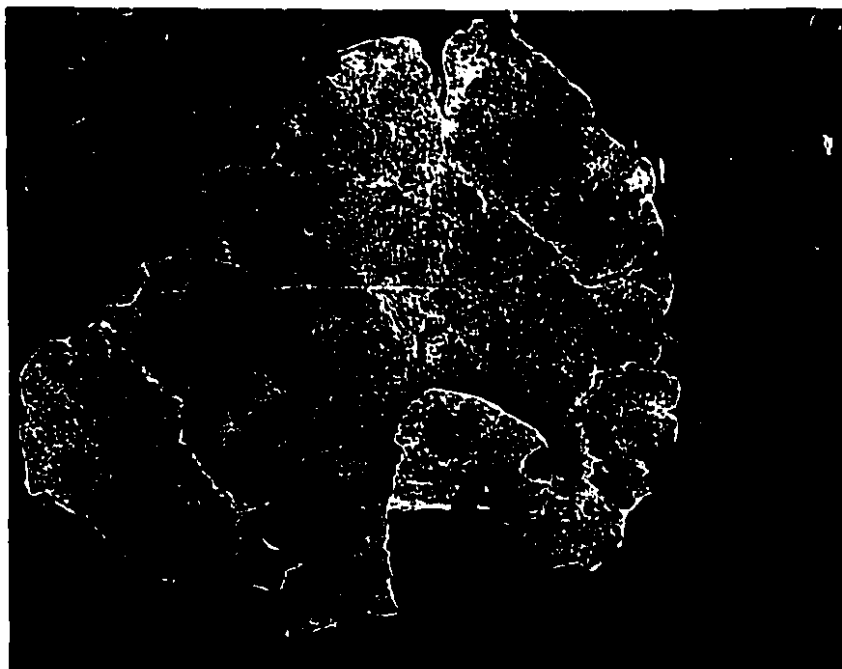
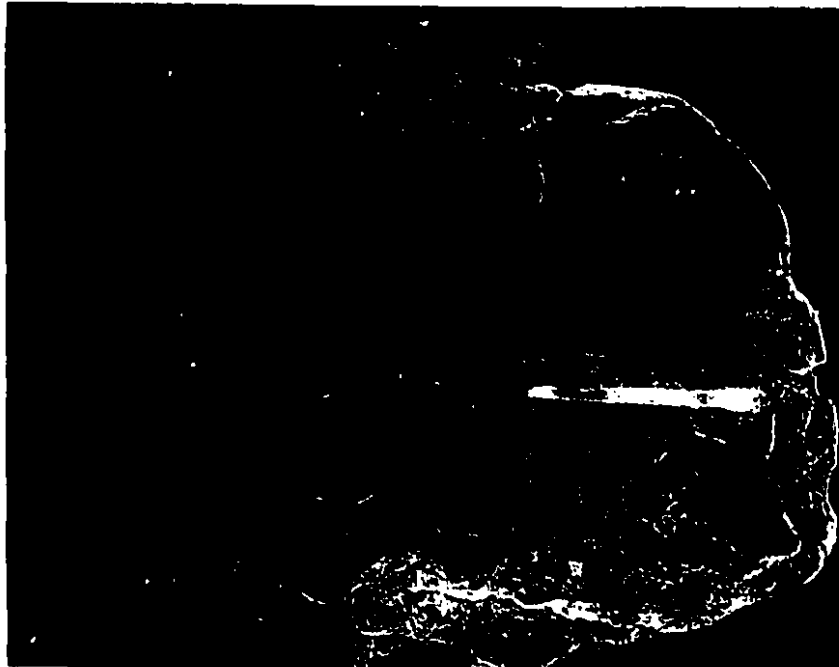


Figure 5.3: A flattened lead fragment with serrated shape recovered from the Bond ball mill (feed size: 0.425-0.500 mm).



**Figure 5.4:** A flattened lead fragment with a serrated shape recovered from the Bond ball mill (feed size: 0.425-0.500 mm).



**Figure 5.5:** A flattened lead fragment recovered from the Bond ball mill (feed size: 1.18-1.40 mm).

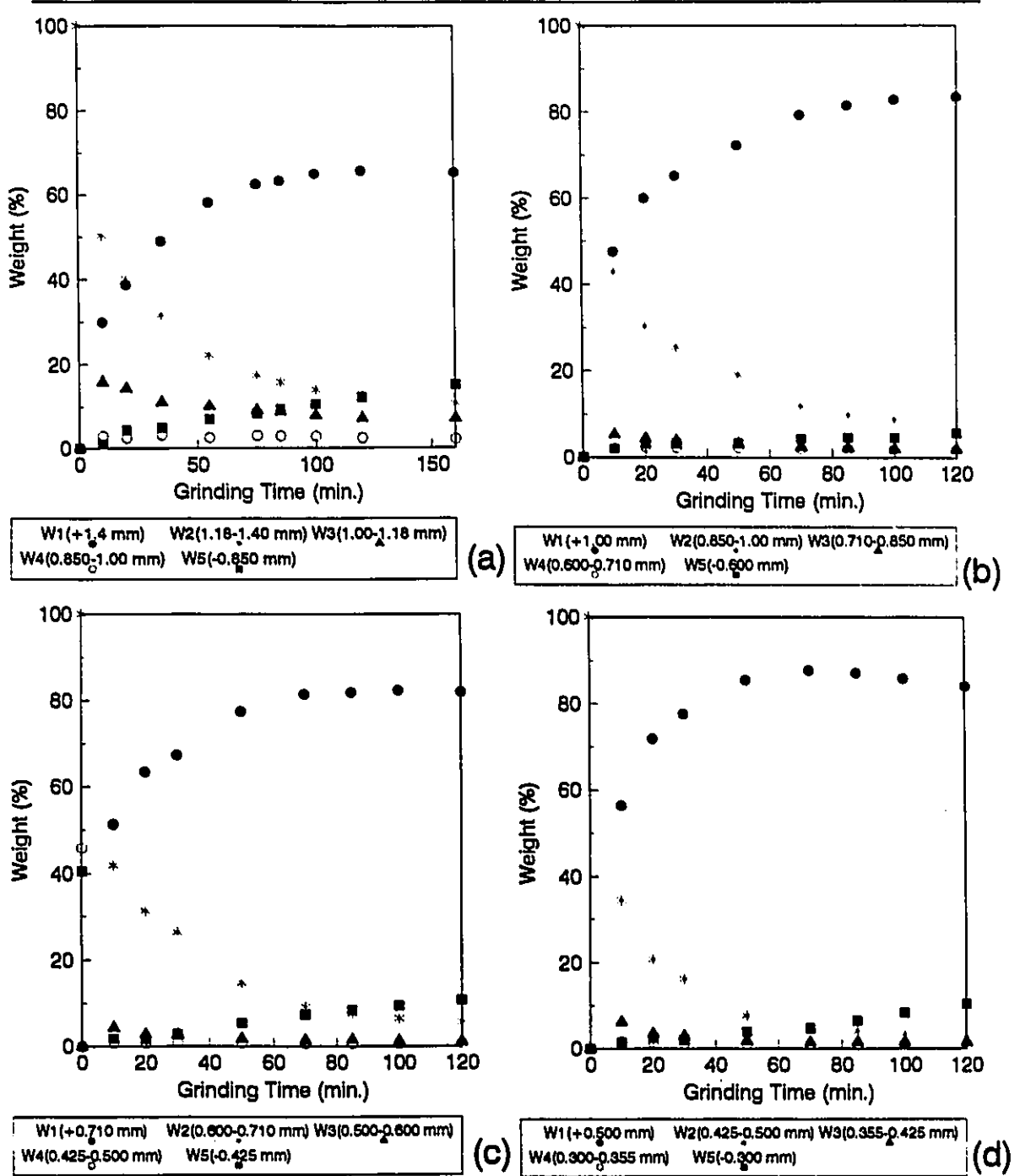


**Figure 5.6:** Size distribution of lead fragments as a function of grinding time in the Bond ball mill tests; a: 1.18-1.40 mm, b: 0.850-1.000 mm, c: 0.600-0.710 mm, d: 0.425-0.500 mm.

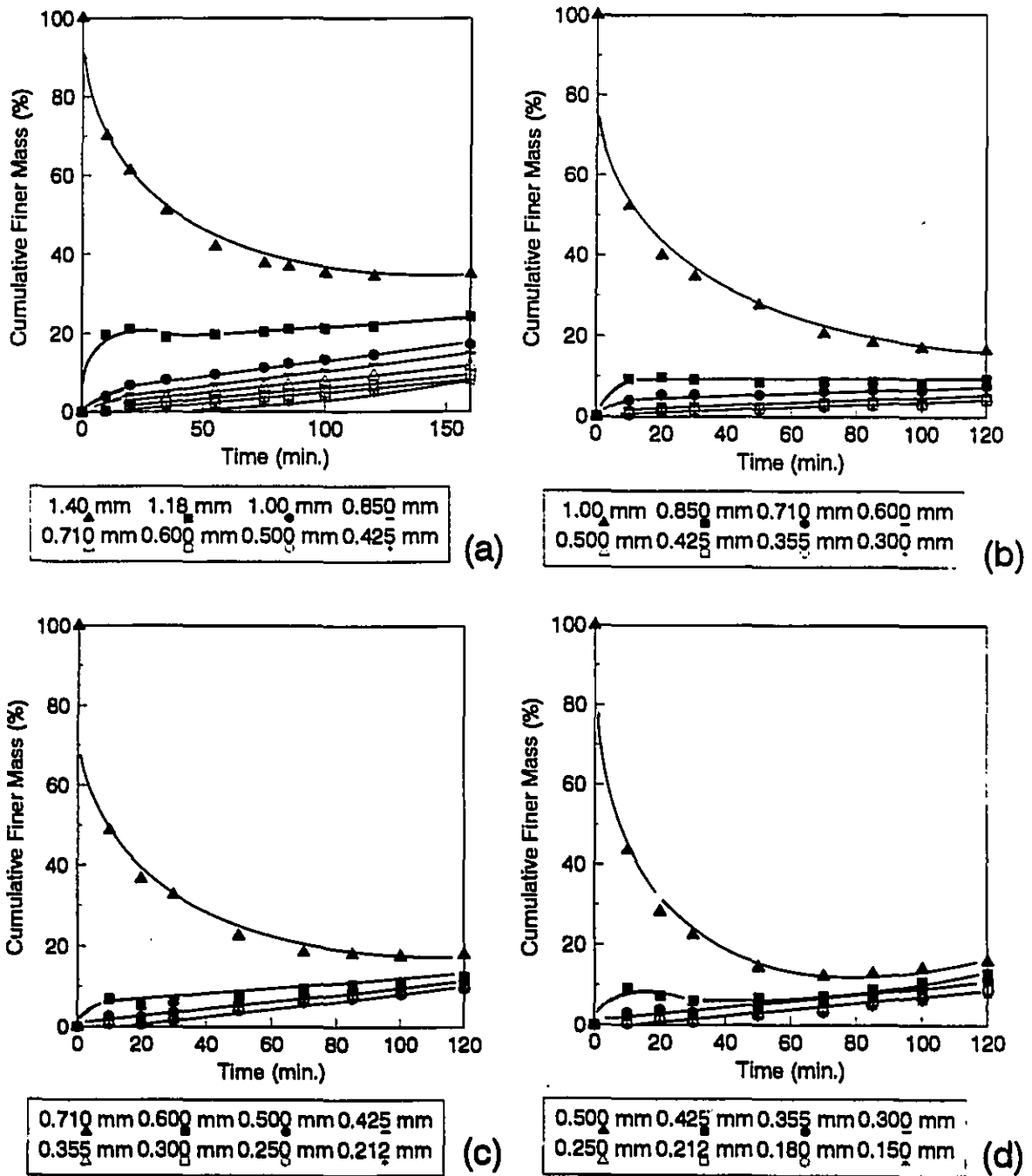


**Figure 5.7:** Fines production as a function of time in the Bond ball mill (Feed: lead fragments; a: 1.18-1.40 mm, b: 0.850-1.000 mm, c: 0.600-0.710 mm, d: 0.425-0.500 mm).

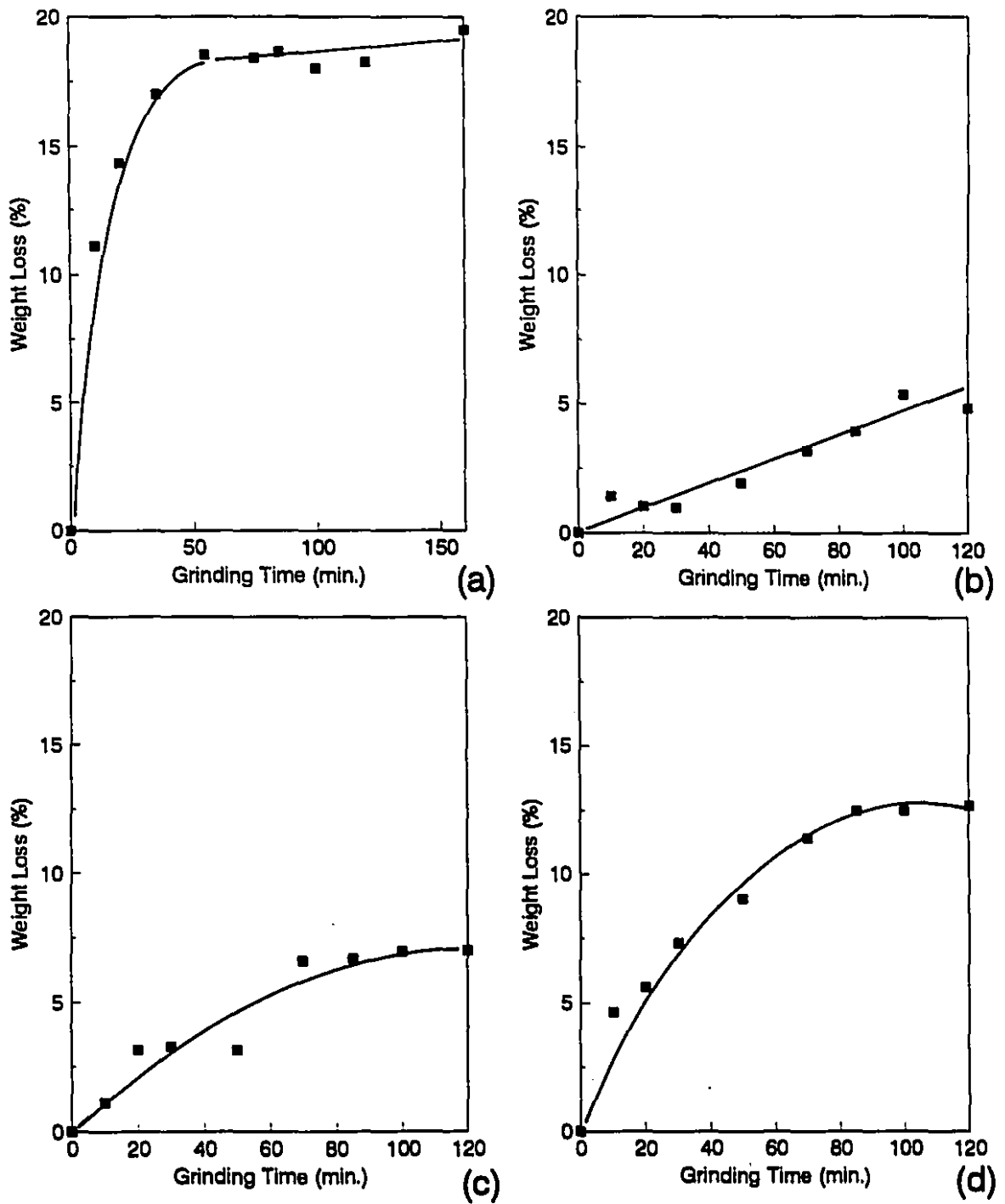
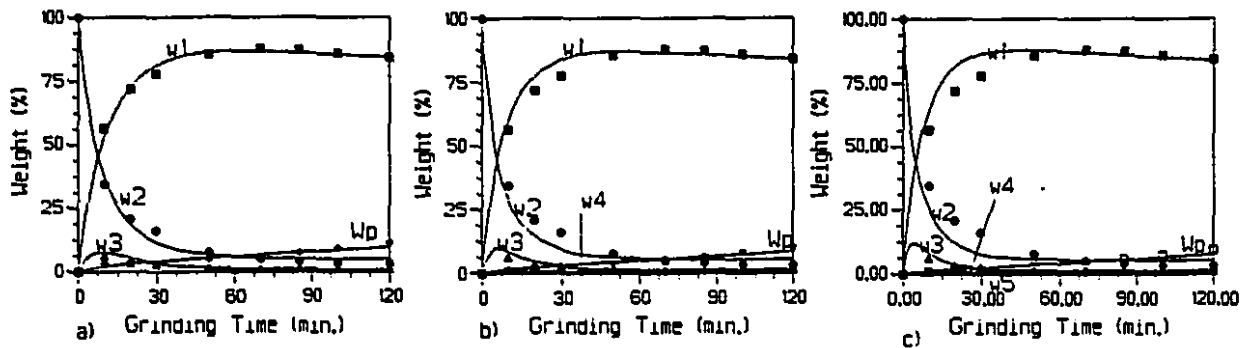


Figure 5.8: Lost weight of lead fragments as a function of grinding time in the Bond ball mill tests; a: 1.18-1.40 mm, b: 0.850-1.000 mm, c: 0.600-0.710 mm, d: 0.425-0.500 mm.

**Table 5.2:** Estimated rate constants (all in  $\text{min}^{-1}$ ) for the Bond ball mill test, flattening, folding and limited breakage model (feed: 0.425-0.500 mm lead fragments).

Size classes	Three Size classes: $w_1, w_2, w_3, W_p$	Four size classes: $w_1, w_2, w_3, w_4, W_p$	Five size classes: $w_1, w_2, w_3, w_4, w_5, W_p$
Rate constants			
$r_{1,p}$	0.001	0.001	0.001
$r_{2,p}$	0.003	0.003	0.002
$r_{3,p}$	0.000	0.000	0.000
$r_{4,p}$	-	0.000	0.000
$r_{5,p}$	-	-	-
$r_{1,2}$	0.005	0.009	0.009
$r_{2,1}$	0.089	0.139	0.139
$r_{2,3}$	0.026	0.333	0.086
$r_{3,2}$	0.138	0.004	0.346
$r_{3,4}$	-	0.000	0.007
$r_{4,3}$	-	0.001	0.000
$r_{4,5}$	-	-	0.010
$r_{5,4}$	-	-	0.000
SS	86.0	136.0	138.0
MSS	3.0	3.9	3.4
$S_r$	1.7	2.0	1.8



**Figure 5.9:** Fit of the flattening, folding and limited breakage model for the Bond ball mill test (feed: 0.425-0.500 mm lead fragments); a: 3 size classes, b: 4 size classes, c: 5 size classes.

Although the standard errors are reasonable, 1.8 to 2.0%, Figure 5.9 suggests that model fit is poor for size classes 1 and 2, especially between 20 and 30 minutes. Table 5.2 shows breakage rate constants ( $r_{i,p}$ ) which are much lower numerically than the flattening and folding rate constants. Again, the flattening rate constants are generally higher than their folding counterparts.

Overall results are shown in Appendix II (Table II.1). The three size classes not presented here displayed very similar results to the 0.425-0.500 mm. There was no detectable trend in the values of the rate constants.

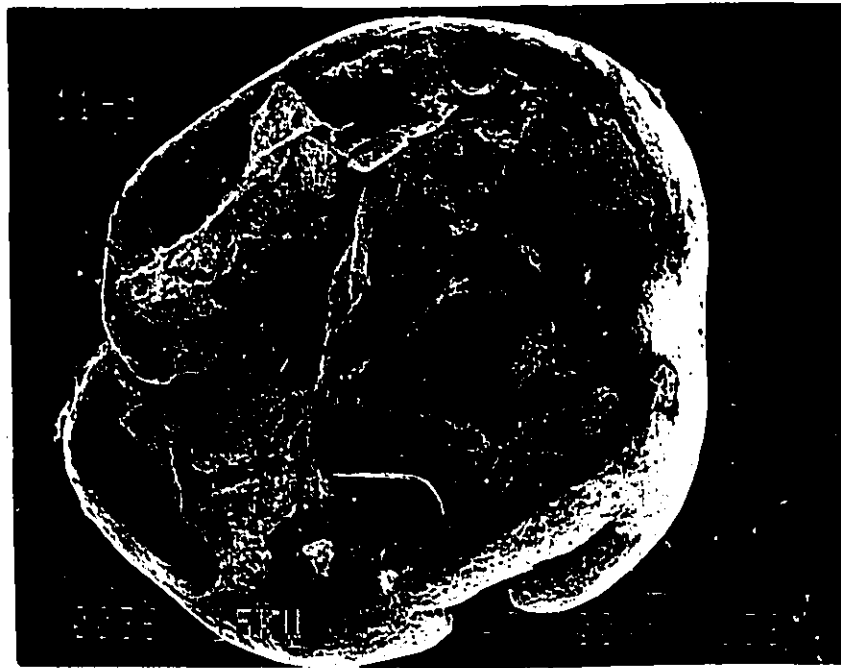
**Small Ball Mill:** Figure 5.15 shows the size distribution of the product of the small ball mill tests. As for the Bond ball mill, all of the weight is in size class 2 at time zero, and much of it rapidly flattens into size class 1. Unlike the Bond ball mill tests, there is significant folding into size class 3, and no evidence of significant breakage into size class 5. The lack of breakage is confirmed by Figure 5.16, which presents the cumulative percent finer as a function of grinding times.

Figure 5.17 illustrates the weight loss, which is very significant in a very short time. Tests 1 to 3 were performed on the same day, and show a pattern of increasing losses (e.g. after 10 minutes of grinding) with decreasing fragment size. Test 4, performed on a different day, exhibited much more spectacular losses, presumably because of a cleaner shell inner surface. This smearing can not be linked with particle breakage, which did not occur in the small ball mill.

Figures 5.10 to 5.14 show SEM photographs of lead fragments retrieved from the small ball mill. Particles with spherical and cylindrical shapes (Figures 5.10, and 5.11) were found, similar to some recovered from the Bond ball mill. The rough and serrated configuration was not visible as much as in the Bond ball mill. This is probably related

with the fact that the Bond ball mill can release more energy upon individual ball impact than the small ball mill, effecting breakage first at the edge of particles and eventually of the particles themselves. Rough and serrated flakes such as those retrieved from the Bond ball mill (Figures 5.3, and 5.4) could not be found.

The same modelling approach was used, obviously with the flattening and folding model. Results were particularly good, as shown in Figure 5.18 and Table 5.3. Except for the two coarsest size classes, the flattening rate constants are again higher than their folding counterparts. Modelling results for all four size classes are shown in Appendix II (Table II.2). The standard error for the other three size classes are slightly higher (1.2-1.8%) than for the 0.600-0.710 mm.



**Figure 5.10:** A spherical lead fragment recovered from the small ball mill (feed size: 1.18-1.40 mm).



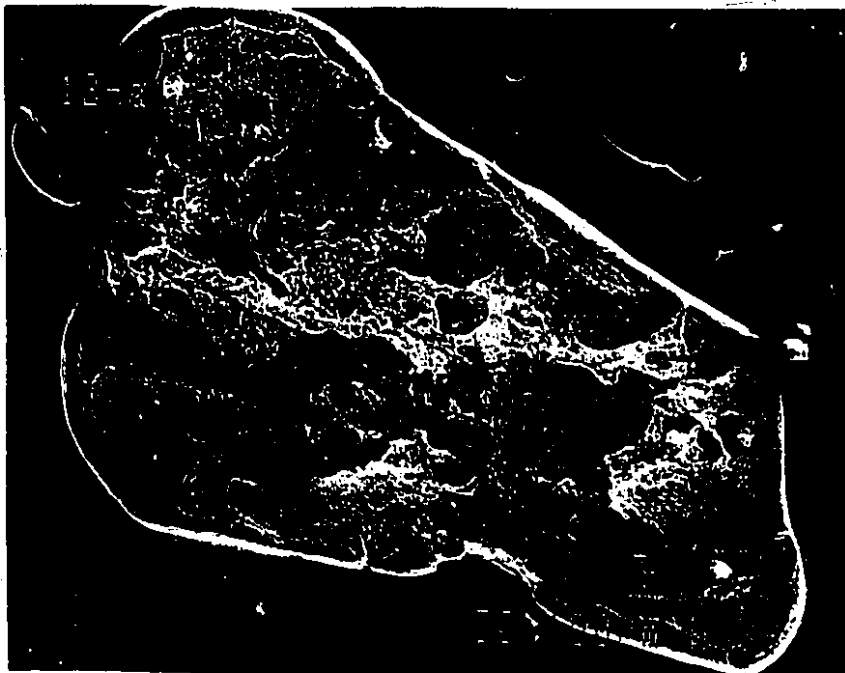
Figure 5.11: A cylindrical lead fragment recovered from the small ball mill (feed size: 0.425-0.500 mm).



Figure 5.12: A cylindrical lead fragment recovered from the small ball mill (feed size: 1.18-1.40 mm).



**Figure 5.13:** A flattened lead fragment with smooth shape recovered from the small ball mill (feed size: 0.850-1.000 mm).



**Figure 5.14:** A flattened lead fragment with smooth shape recovered from the small ball mill (feed size: 0.850-1.000 mm).

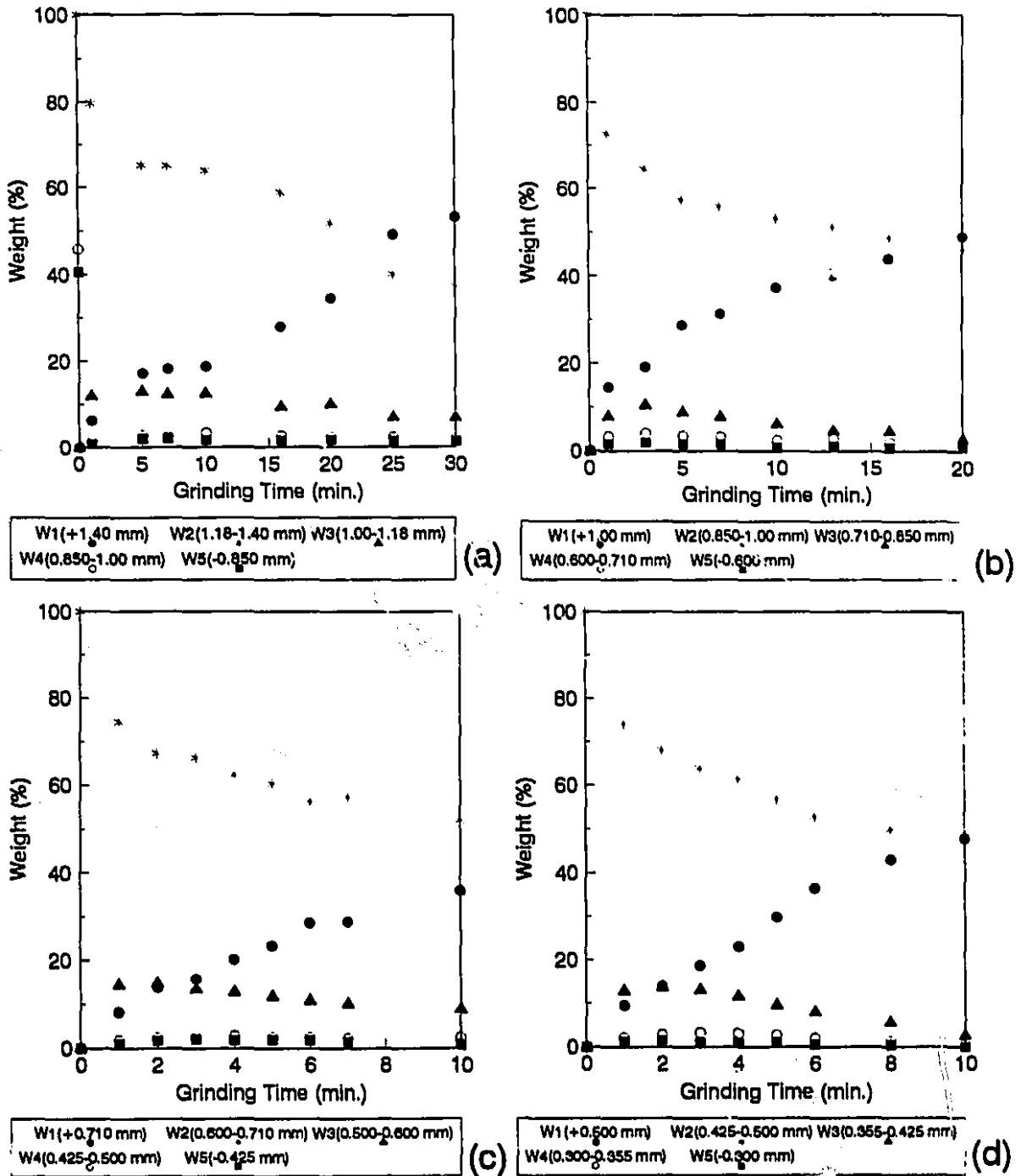


**Figure 5.15:** Size distribution of lead fragments as a function of grinding time in the small ball mill tests; a: 1.18-1.40 mm, b: 0.850-1.000 mm, c: 0.600-0.710 mm, d: 0.425-0.500 mm.

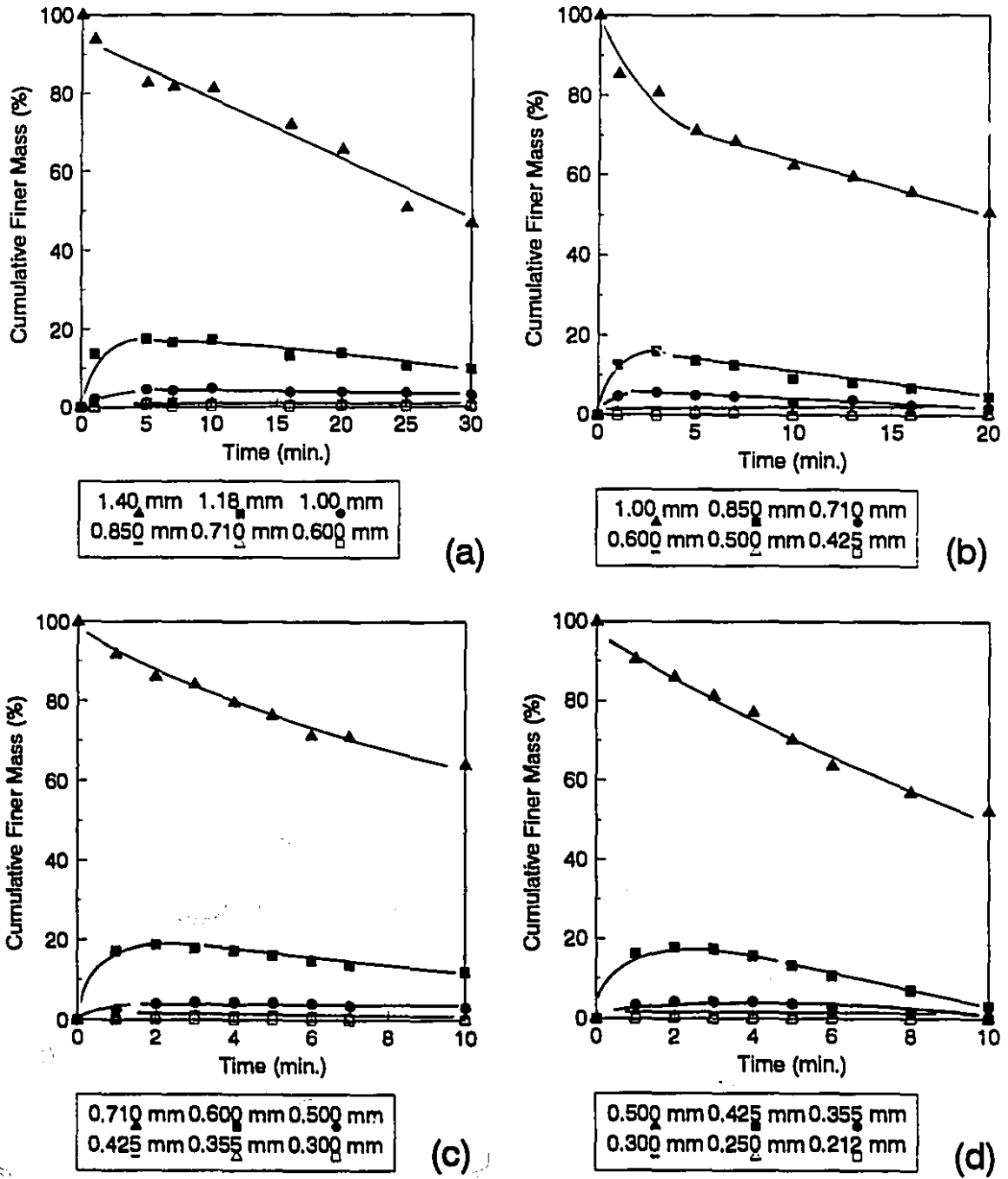
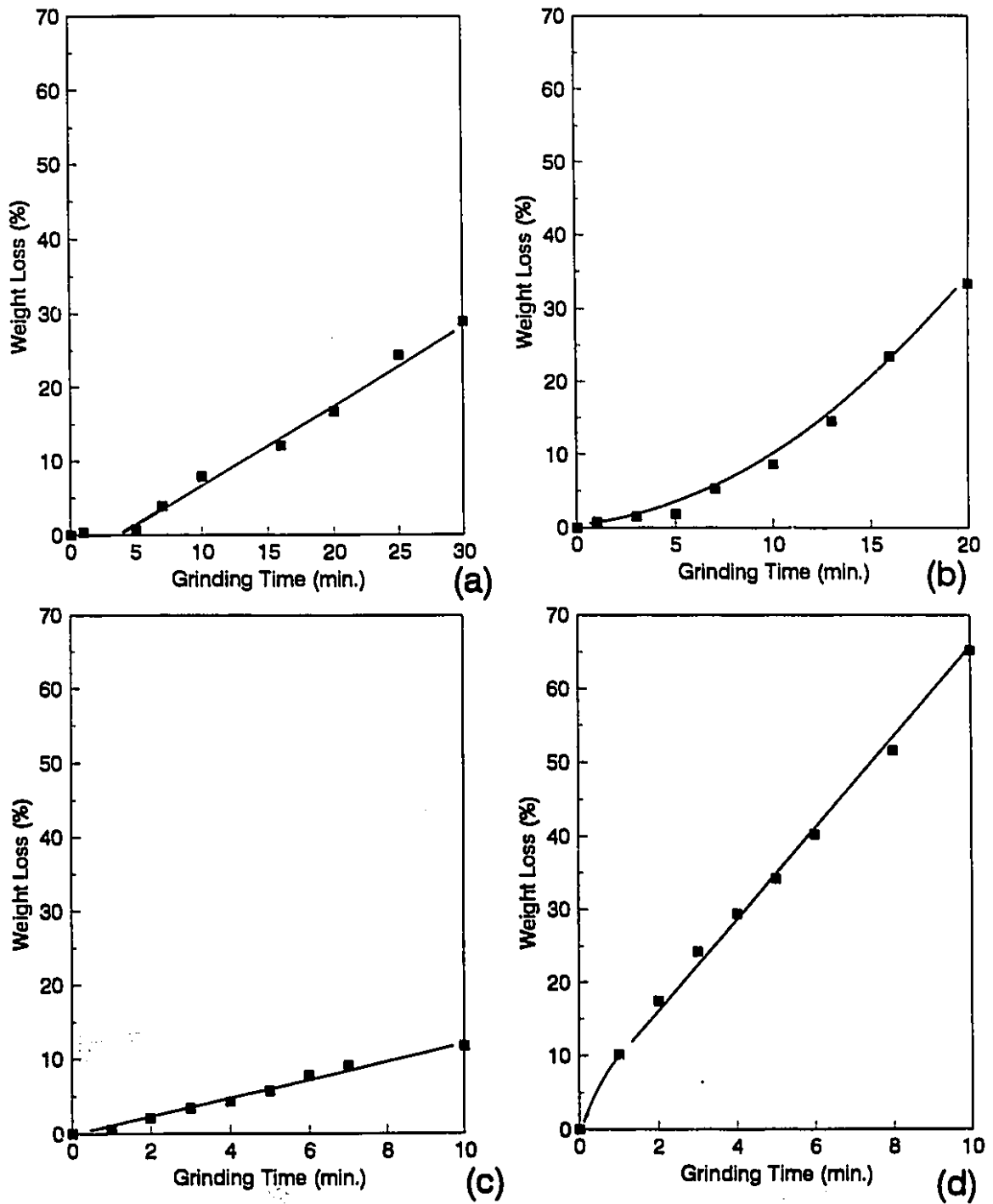


Figure 5.16: Fines production as a function of time in the small ball mill (Feed:lead fragments; a: 1.18-1.40 mm, b: 0.850-1.000 mm, c: 0.600-0.710 mm, d: 0.425-0.500 mm).



**Figure 5.17:** Lost weight of lead fragments as a function of grinding time in the small ball mill tests; a: 1.18-1.40 mm, b: 0.850-1.000 mm, c: 0.600-0.710 mm, d: 0.425-0.500 mm.

**Table 5.3:** Estimated rate constants (all in  $\text{min}^{-1}$ ) for the small ball mill test, flattening and folding without breakage model (feed: 0.600-0.710 mm lead fragments).

Rate Constants	Three Size classes ( $w_1, w_2, w_3$ )	Four Size classes ( $w_1, w_2, w_3, w_4$ )	Five Size classes ( $w_1, w_2, w_3, w_4, w_5$ )
$r_{1,2}$	0.1	0.1	0.1
$r_{2,1}$	0.1	0.1	0.1
$r_{2,3}$	0.5	0.9	0.8
$r_{3,2}$	1.8	4.6	4.3
$r_{3,4}$	-	0.6	0.7
$r_{4,3}$	-	1.8	3.7
$r_{4,5}$	-	-	19.5
$r_{5,4}$	-	-	28.9
SS	44	47	47
MSS	0.9	0.7	0.6
$S_r$	0.9	0.8	0.8

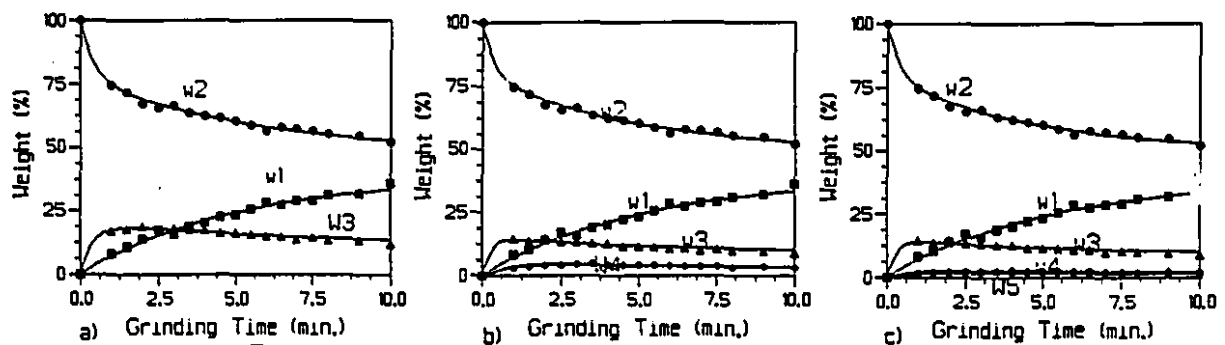


**Figure 5.18:** Fit of the flattening and folding model (no breakage) for the small ball mill test (feed: 0.600-0.710 mm lead fragments); a: 3 size classes, b: 4 size classes, c: 5 size classes.

**Bond Rod Mill:** Figures 5.19 to 5.22 show SEM photographs of the fragments recovered from the Bond rod mill tests. Particles flattened (Figure 5.19, and 5.21) and folded (Figure 5.20, and 5.22), thus reporting to size classes coarser and finer than their initial size classes.

Figure 5.23 shows the size distribution of the mass recovered from the mill as a function of grinding time. Visual observation indicated that as soon as grinding started, particles began to break and report to finer size classes. Flattening also takes place, as significant mass reports to size class 1 (Figure 5.23). The extent of flattening decreases slightly with decreasing fragment size, as the maximum mass percent in size class 1 decreases from 34% in Test 1 (Figure 5.23 (a), point A) to 19% in Test 4 (Figure 5.23 (d), point B). In all tests the production of fines, size class 5, is very significant.

Figure 5.24 confirms the extent of breakage, and shows zero order production of fines, which is typical of breakage. Breakage is clearly less extensive for Test 3 (Figures 5.23(c), and 5.24(c)) and especially for Test 4 (Figures 5.23(d), and 5.24(d)), which is consistent with the general observation that the selection function decreases with decreasing particle size, for brittle minerals.

Figure 5.25 shows the extent of smearing, which increases slightly with finer feeds (in size class 2), as for the two other mills tested. We notice that the extent of smearing is not directly correlated with breakage kinetics, as Test 4, with the slowest zero order production of fines, displays the largest smearing losses.

As Figures 5.23 and 5.24 show, breakage is dominant for these tests. As a result, the flattening, folding and explicit breakage model (Equation 3.14) was used. As the production of fines followed zero order kinetics, it was used to estimate the breakage function, shown in Table 5.4 for all parent classes.

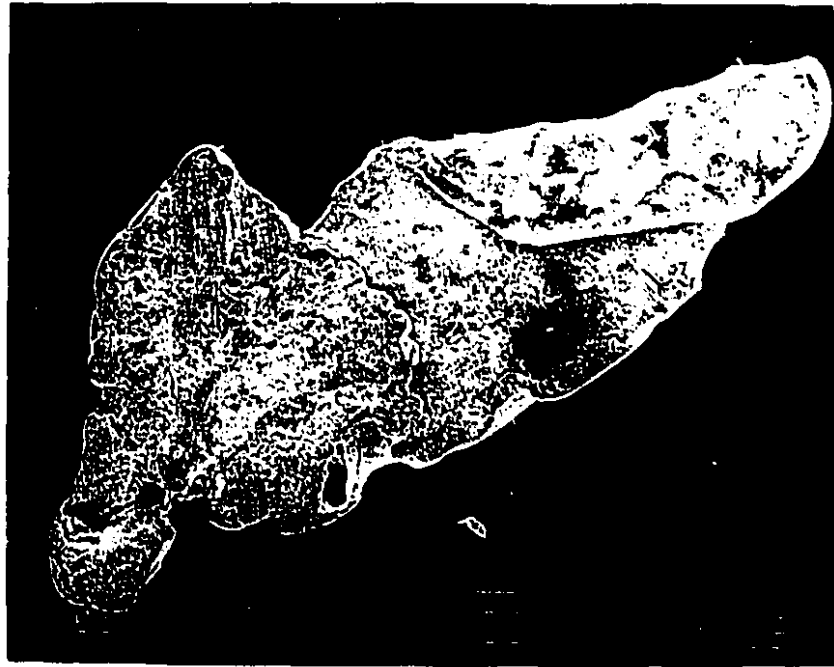
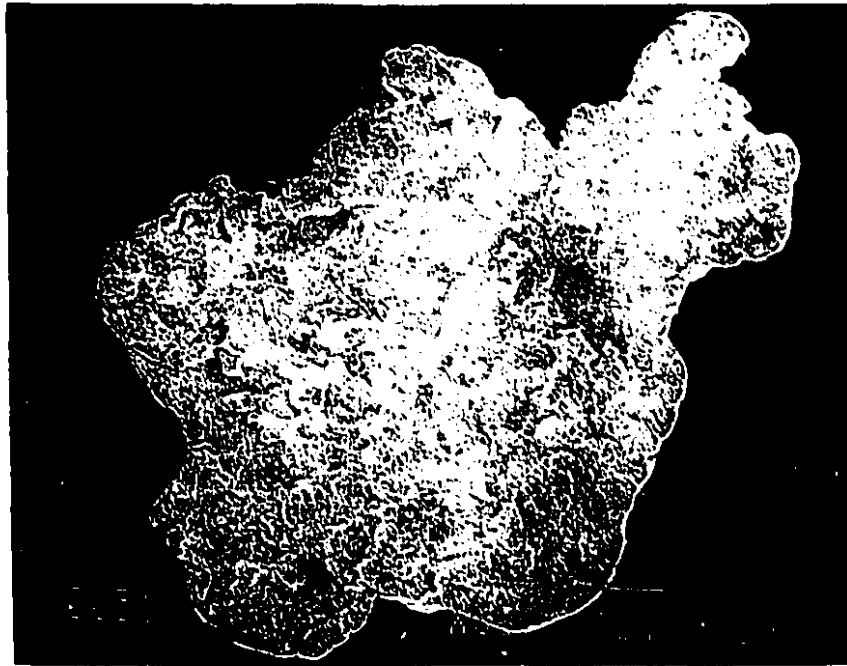


Figure 5.19: A flattened lead fragments recovered from the Bond rod mill (feed size: 0.850-1.000 mm).



Figure 5.20: A cylindrical lead fragment recovered from the Bond rod mill (feed size: 1.18-1.40 mm).



**Figure 5.21:** A flattened lead fragment recovered from the Bond rod mill (feed size: 0.600-0.710 mm).



**Figure 5.22:** A folded and flattened lead fragment recovered from the Bond rod mill (feed size: 0.850-1.000 mm).

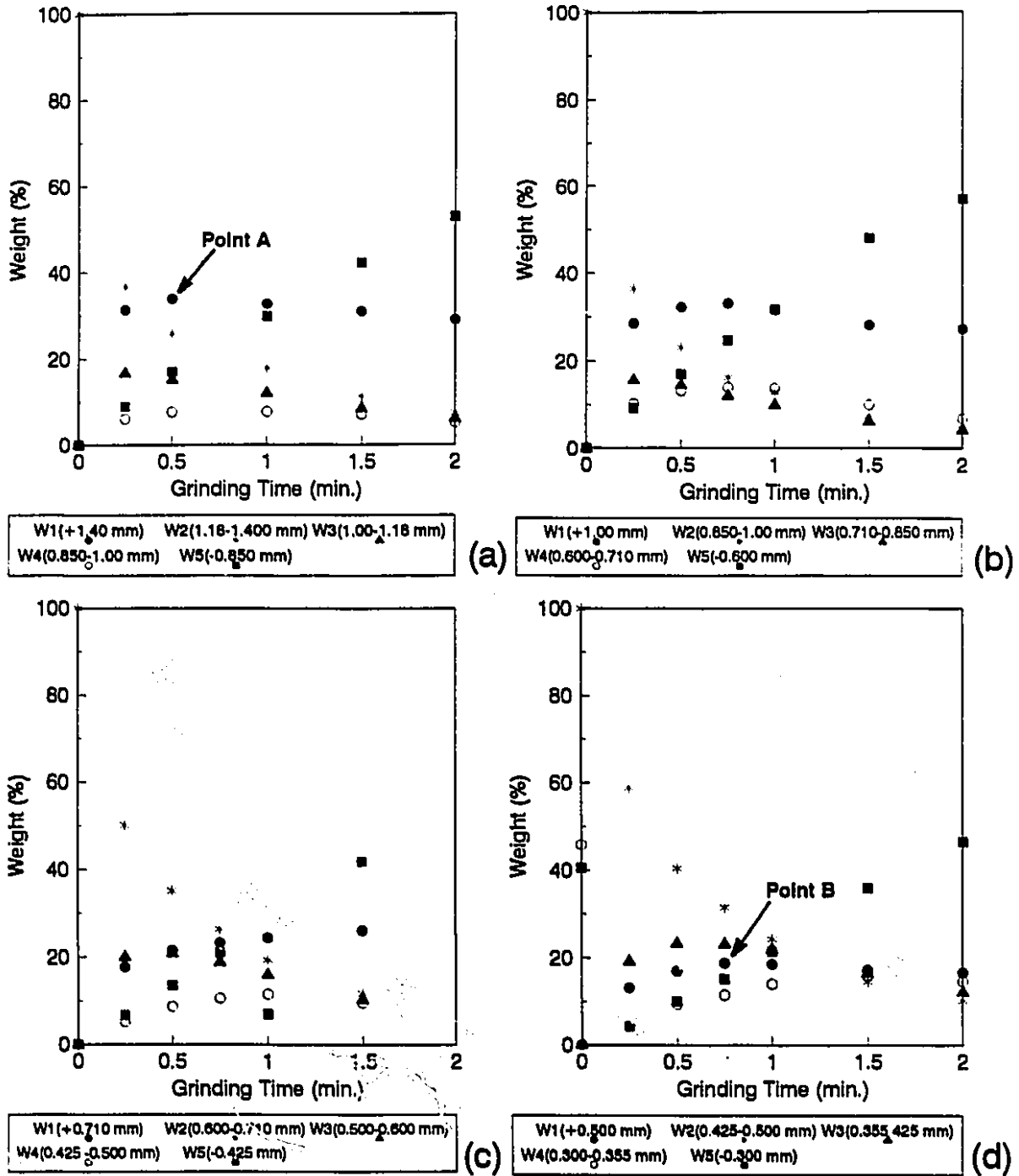


**Figure 5.23:** Size distribution of lead fragments as a function of grinding time in the Bond rod mill tests; a: 1.18-1.40 mm, b: 0.850-1.000 mm, c: 0.600-0.710 mm, d: 0.425-0.500 mm.

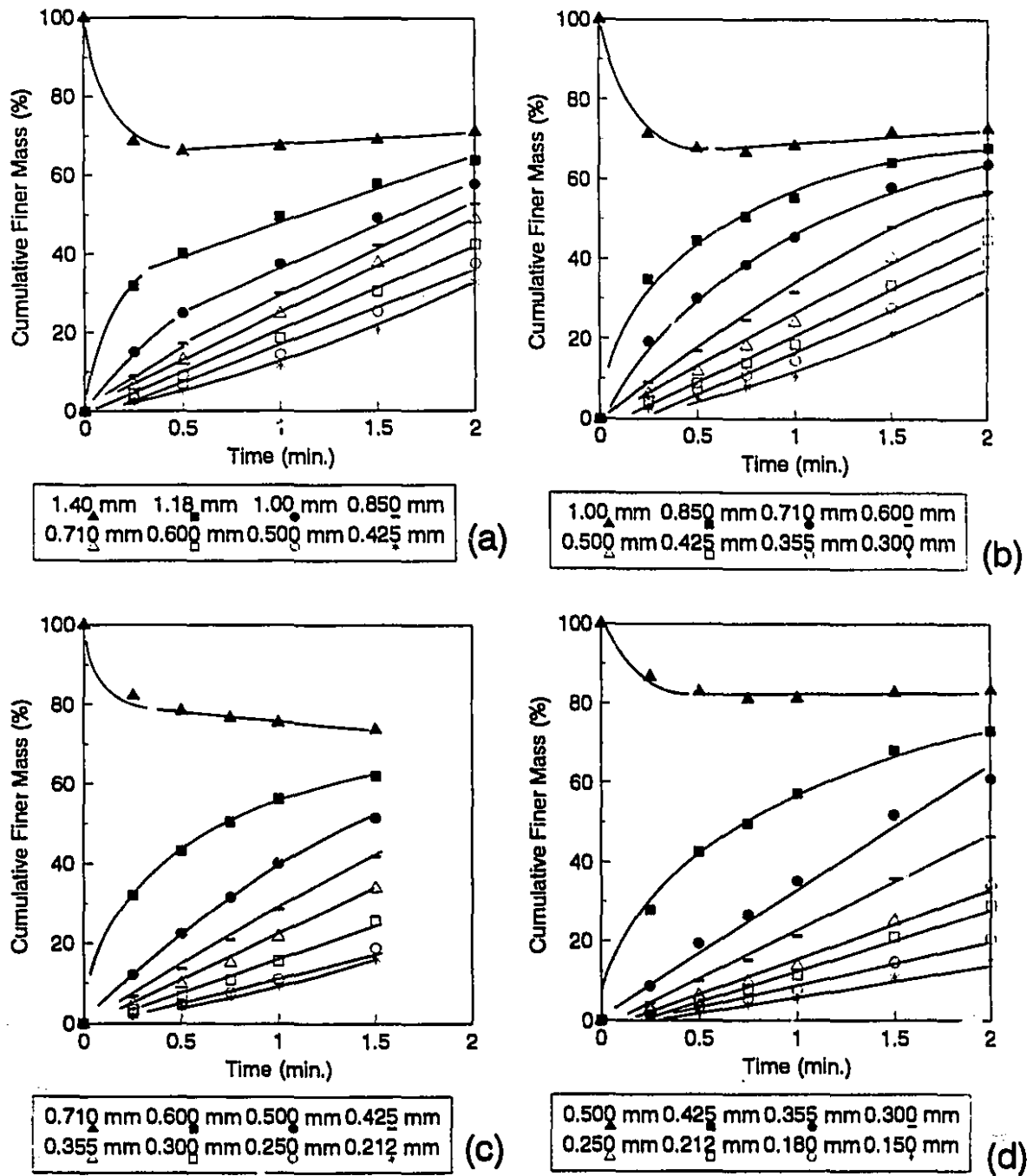
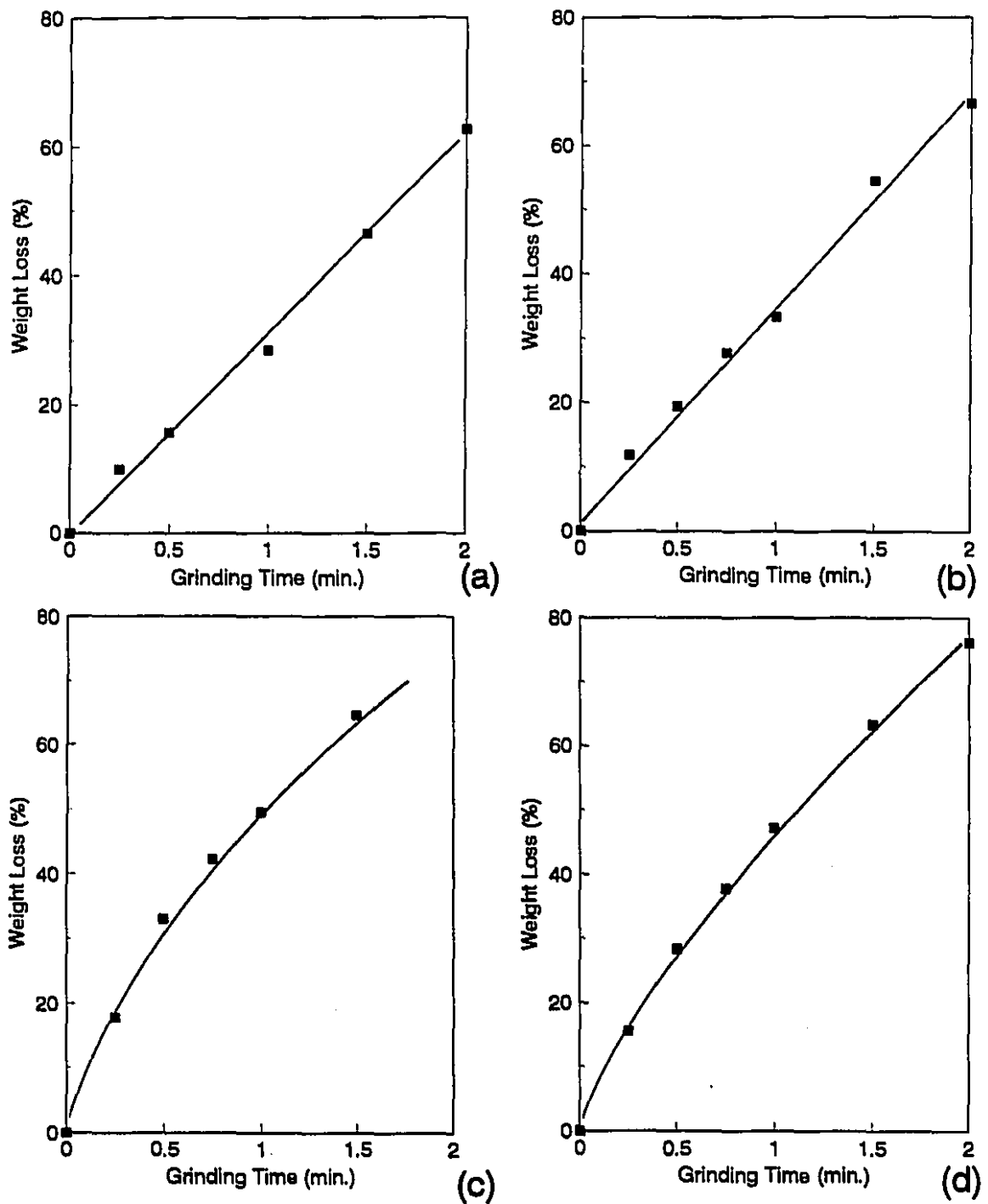


Figure 5.24: Fines production as a function of time in the Bond rod mill (Feed: lead fragments; a: 1.18-1.40 mm, b: 0.850-1.000 mm, c: 0.600-0.710 mm, d: 0.425-0.500 mm).



**Figure 5.25:** Lost weight of lead fragments as a function of grinding-time in the Bond rod mill tests; a: 1.18-1.40 mm, b: 0.850-1.000 mm, c: 0.600-0.710 mm, d: 0.425-0.500 mm

Table 5.4: Estimated breakage function (BF) of lead for the Bond rod mill tests.

Size classes (mm)	Breakage Function Values for the Feed Size of:			
	1.18-1.40	0.850-1.00	0.600-0.710	0.425-0.500
1.180	-	-	-	-
1.000	0.388	-	-	-
0.850	0.033	-	-	-
0.710	0.036	0.415	-	-
0.600	0.071	0.025	-	-
0.500	0.058	0.055	0.432	-
0.425	0.056	0.061	0.103	-
0.355	-	0.061	0.091	0.508
0.300	-	0.072	0.091	0.115
0.250	-	-	0.077	0.098
0.212	-	-	0.031	0.045
0.180	-	-	-	0.068
0.150	-	-	-	0.042

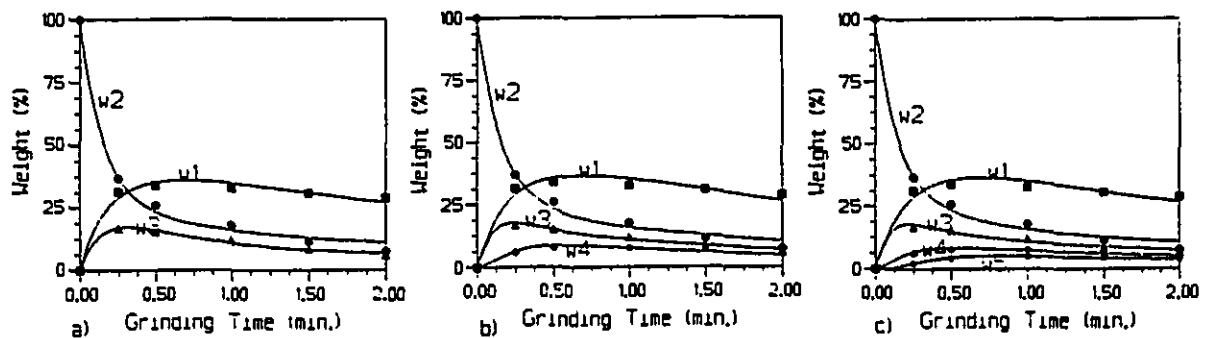


Figure 5.26: Fit of the flattening, folding and explicit breakage model for the Bond rod mill test (feed: 1.18-1.40 mm lead fragments); a: 3 size classes, b: 4 size classes, c: 5 size classes.

**Table 5.5:** Estimated rate constants (all in  $\text{min}^{-1}$ ) for the Bond rod mill test, flattening, folding and explicit breakage model (feed: 1.18-1.40 mm lead fragments).

Size classes	Feed size: 1.18-1.40 mm		
Rate constants	Three Size classes: $w_1, w_2, w_3$	Four size classes: $w_1, w_2, w_3, w_4$	Five size classes: $w_1, w_2, w_3, w_4, w_5$
$s_1$	0.0	0.9	1.2
$s_2$	1.6	0.9	0.5
$s_3$	0.5	0.0	0.0
$s_4$	-	0.0	0.0
$s_5$	-	-	0.0
$\Gamma_{1,2}$	1.2	0.4	0.1
$\Gamma_{2,1}$	2.3	2.4	2.4
$\Gamma_{2,3}$	1.1	2.5	3.2
$\Gamma_{3,2}$	2.7	5.3	6.3
$\Gamma_{3,4}$	-	2.7	4.1
$\Gamma_{4,3}$	-	4.6	7.3
$\Gamma_{4,5}$	-	-	3.2
$\Gamma_{5,4}$	-	-	5.6
SS	46.0	50.0	53.0
MSS	4.2	3.6	3.1
$S_f$	2.0	1.9	1.8

Figure 5.26 shows the good fit of the model, with standard errors of 1.8 to 2.0% (Table 5.5). These are relatively high because of the low degrees of freedom of the tests (because of the larger number of parameters). The large number of parameters also make their accurate estimation very difficult. For example, only the two coarsest size classes yield an estimate of the selection function. The flattening and folding rate

constants are very high, and again assume a 2:1 ratio (flattening to folding). Appendix II (Table II.3) presents the model fit of the other three size classes, which is generally better than that of the 1.18-1.40 mm (standard errors of 1.1 to 1.7%). Again flattening rate constants are generally higher than their corresponding folding rate constants.

### 5.3.2 Second series of tests: Grinding lead fragments mixed with silica

**Bond Ball Mill:** Figure 5.29 presents the size distribution of lead fragments in the Bond ball mill tests. Separation of lead fragments from silica with the MLS was easily achieved, as each size class was processed individually and most classes were of a particle size easily treated by gravity (+0.075 mm with the MLS v-shaped tray).

Figure 5.29 to 5.31 summarize results, which are strikingly different from those obtained without silica. For example, from 51 to 92% of the mass reports to size class 5 after only 20 minutes of grinding. Figure 5.29 also shows some flattening, but to a lesser extent than without silica, as the maximum mass reporting to size class 1 is 15 to 28%, after only 5 minutes of grinding, compared to 65 to 84% in size class 1 after 120 minutes of grinding without silica. It is unclear, however, whether or not flattening kinetics are different. Breakage rates are obviously much higher in the presence of silica, as confirmed by Figure 5.30, which displays zero order production of fines, typical of breakage (rather than folding). Both Figures 5.29 and 5.30 show that for Tests 2 to 4 breakage does not begin at time zero, but after about 2 minutes of grinding.

Figure 5.31 shows the weight loss in the Bond ball mill tests as a function of grinding time. Losses to the mill inner shell and balls are low, 3 to 10%. These losses also include potential losses during the MLS separation of lead from silica. Figures 5.27 and 5.28 show the lead fragments retrieved from the mill and confirm that folding and flattening did occur.

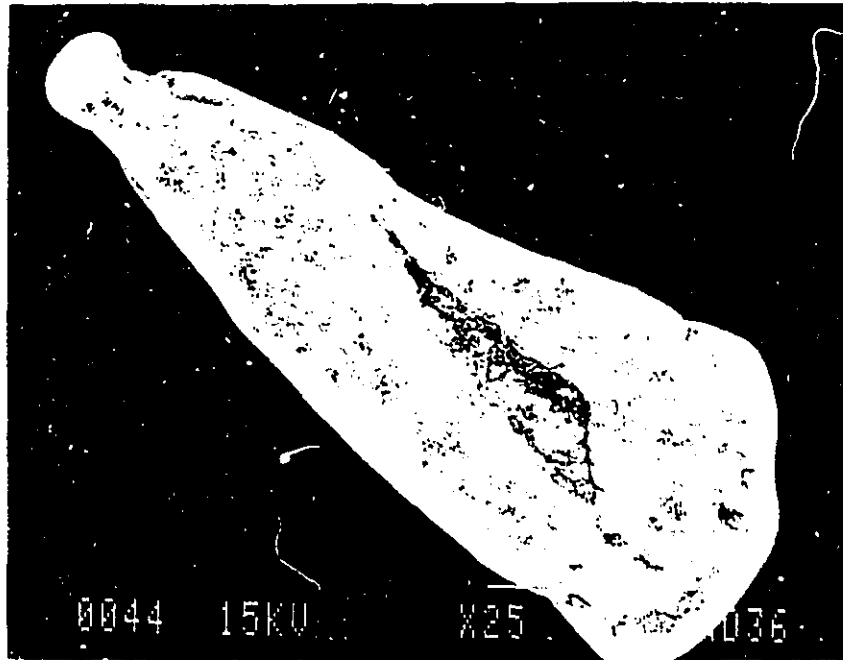


Figure 5.27: A lead fragment recovered from the Bond ball mill (feed size: 1.18-1.40 mm).

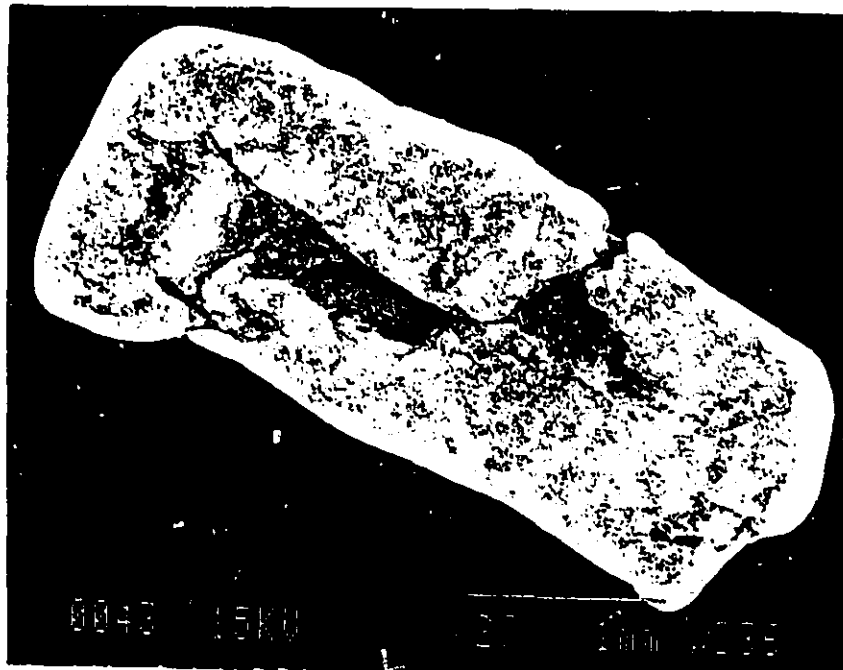
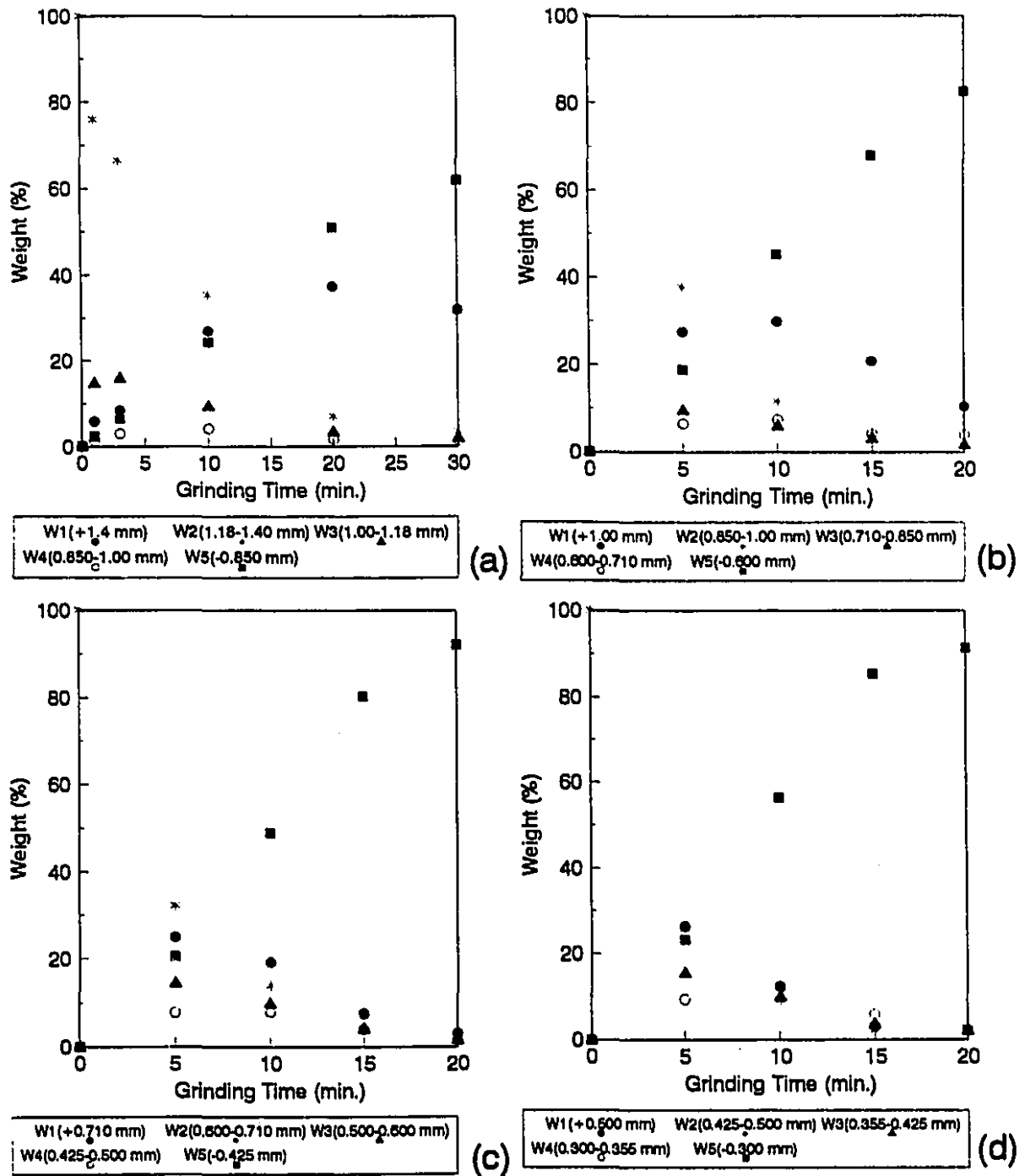


Figure 5.28: A lead fragment recovered from the Bond ball mill (feed size: 0.600-0.710 mm).



**Figure 5.29:** Size distribution of lead fragments as a function of grinding time in the Bond ball mill tests (lead fragments mixed with silica); a: 1.18-1.40 mm, b: 0.850-1.000 mm, c: 0.600-0.710 mm, d: 0.425-0.500 mm.

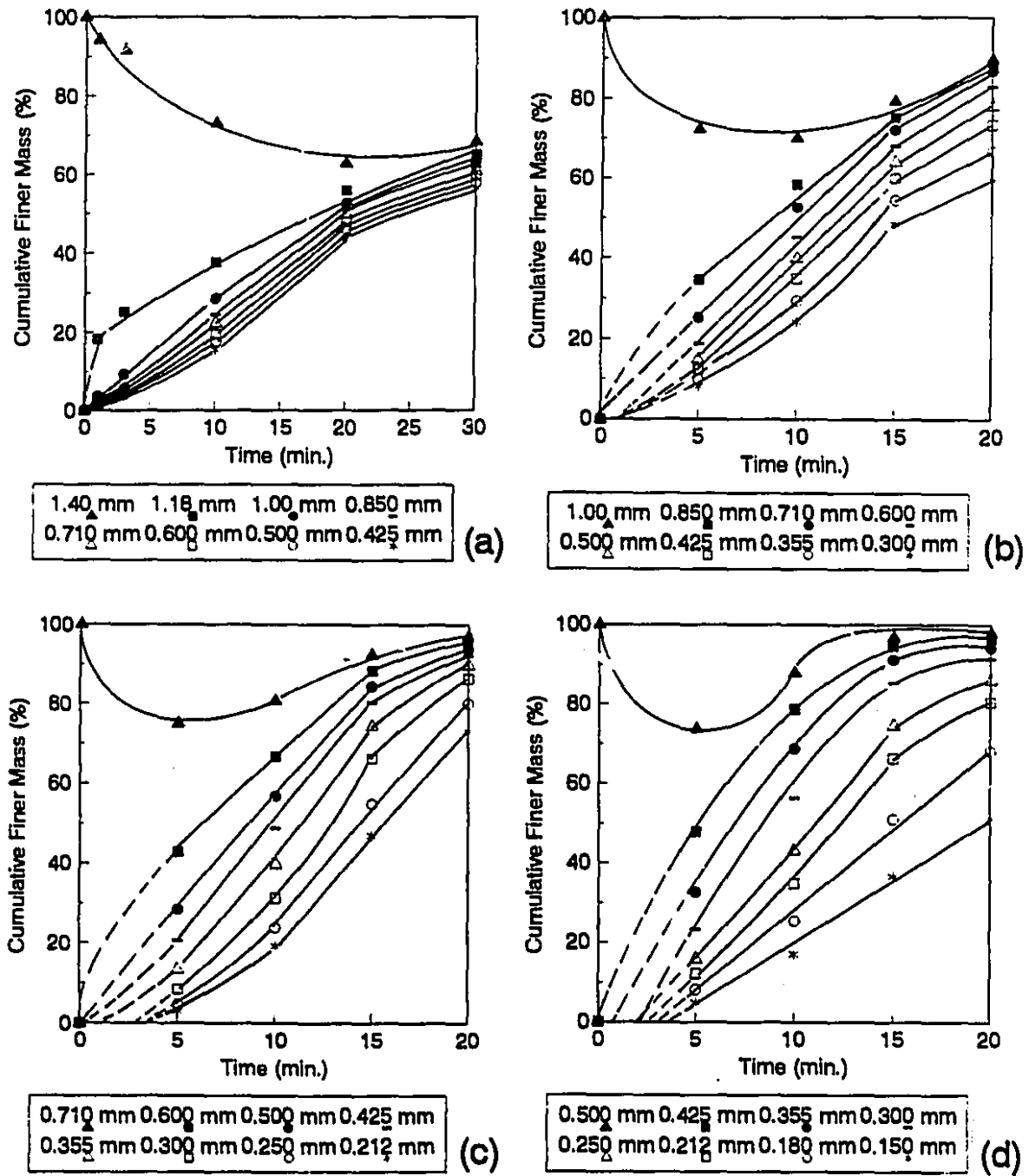
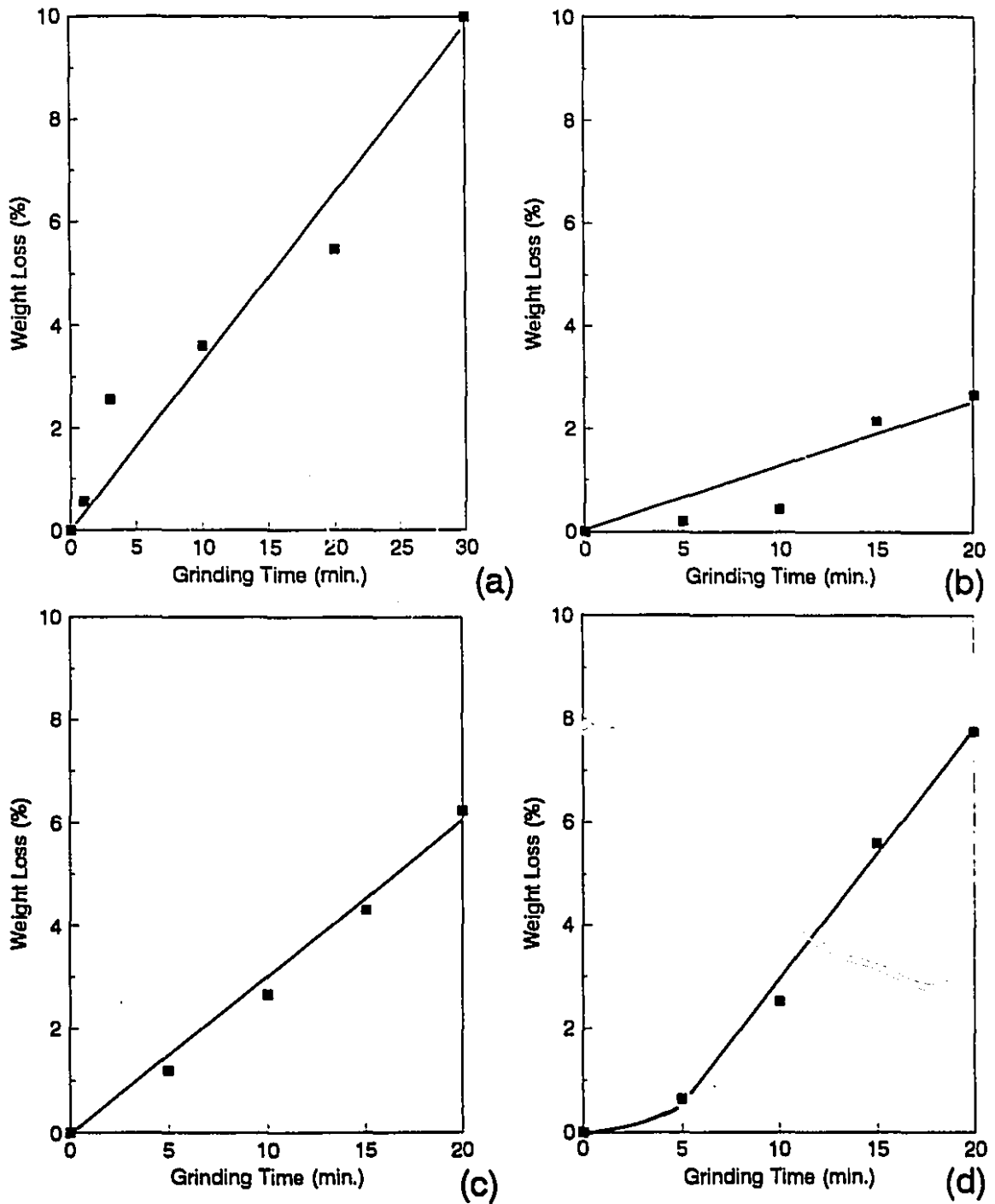


Figure 5.30: Fines production as a function of time in the Bond ball mill (Feed: lead fragments mixed with silica; a: 1.18-1.40 mm, b: 0.850-1.000 mm, c: 0.600-0.710 mm, d: 0.425-0.500 mm).



**Figure 5.31:** Lost weight of lead as a function of grinding time in the Bond ball mill (lead fragments mixed with silica); a: 1.18-1.40 mm, b: 0.850-1.000 mm, c: 0.600-0.710 mm, d: 0.425-0.500 mm

Because breakage is so important, the flattening, folding and explicit breakage model was used to fit experimental data. The zero order production of fines made it possible to estimate the breakage functions, which are shown in Table 5.6. Model fit is shown in Table 5.7 and Figure 5.32. Fit is generally good (standard errors of 2.0 to 2.5%). Rate constant estimation yielded erratic results, because of the numerical difficulty of distinguishing between breakage and folding. Breakage rate constants for two of the coarsest size classes are high, of values comparable to the flattening rate constants.

**Table 5.6:** Estimated breakage function (BF) of lead for the Bond ball mill tests (lead fragments mixed with silica).

Size classes (mm)	Breakage Function Values for the Feed Size of:			
	1.18-1.40	0.850-1.00	0.600-0.710	0.425-0.500
1.180	-	-	-	-
1.000	0.322	-	-	-
0.850	0.002	-	-	-
0.710	0.007	0.615	-	-
0.600	0.013	0.000	-	-
0.500	0.019	0.012	0.682	-
0.425	0.017	0.015	0.000	-
0.355	-	0.027	0.005	0.719
0.300	-	0.031	0.013	0.002
0.250	-	-	0.026	0.016
0.212	-	-	0.026	0.018
0.180	-	-	-	0.041
0.150	-	-	-	0.051

Results for all four size classes are shown in Appendix II (Table II.4). Fit is comparable to that of the 1.18-1.40 mm size class, but improves significantly when the first data points (at a time of 0) are dropped, to focus on the actual breakage phase (which begins after about 2 minutes). Table II.4.1, in Appendix II, presents the results of rate constants estimates with point zero, for the two finest size classes, 0.600-0.710 mm and 0.425-0.500 mm which shows higher standard errors than without point zero (Table II.4).

**Table 5.7:** Estimated rate constants (all in  $\text{min}^{-1}$ ) for the Bond ball mill test, flattening, folding and explicit breakage model (feed: 0.850-1.000 mm lead fragments mixed with silica).

Size classes	Feed size: 0.850-1.000 mm		
	Three Size classes: $w_1, w_2, w_3$	Four size classes: $w_1, w_2, w_3, w_4$	Five size classes: $w_1, w_2, w_3, w_4, w_5$
$s_1$	0.13	0.87	1.21
$s_2$	0.72	0.88	0.50
$s_3$	0.82	0.00	0.00
$s_4$	-	0.00	0.00
$s_5$	-	-	0.00
$\Gamma_{1,2}$	0.00	0.00	0.17
$\Gamma_{2,1}$	0.42	0.45	0.47
$\Gamma_{2,3}$	0.00	0.00	0.00
$\Gamma_{3,2}$	0.91	0.93	1.429
$\Gamma_{3,4}$	-	0.00	0.78
$\Gamma_{4,3}$	-	0.36	0.00
$\Gamma_{4,5}$	-	-	0.06
$\Gamma_{5,4}$	-	-	0.52
SS	49.0	42.0	49.0
MSS	6.1	4.2	4.1
$S_r$	2.5	2.0	2.0

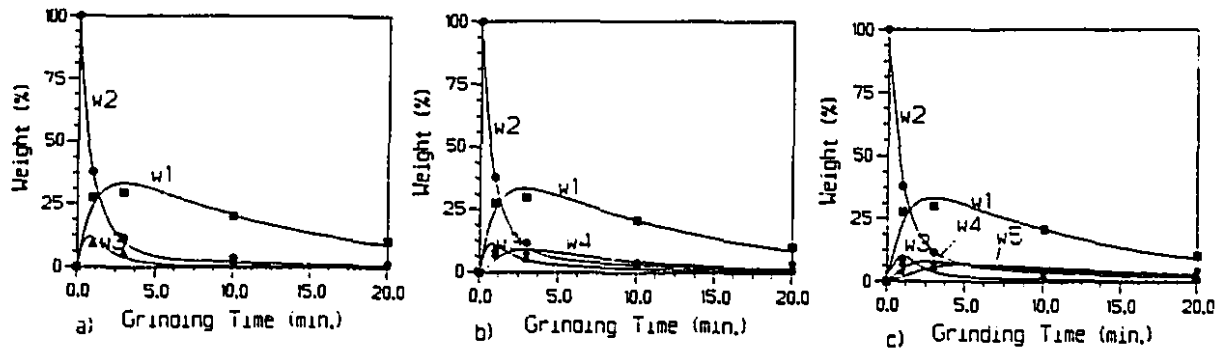


**Figure 5.32:** Fit of the flattening, folding and explicit breakage model for the Bond ball mill test (feed: 0.850-1.000 mm lead fragments mixed with silica); a: 3 size classes, b: 4 size classes, c: 5 size classes.

**Small Ball Mill:** Figures 5.33 to 5.35 present the size distribution, cumulative percent finer and weight loss of lead in the small ball mill. Without silica breakage was almost undetectable. Weight losses were significant, up to 65% after 10 to 30 minutes. Silica causes significant breakage (Figure 5.34), and minimizes weight losses to the mill shell and grinding media, which never exceed 7%, even after 20 minutes of grinding (Figure 5.35). However, flattening remains significant (Figure 5.33), as a significant weight appears in size class 1.

The Bond ball mill modelling approach was also used here. Breakage functions are shown in Table 5.8. Figure 5.36 and Table 5.9 show the fit for the 1.18-1.40 mm size class. Fit is reasonable, with standard errors of 2.1 to 2.4%. Breakage rate constants have low or null values, compared to the flattening rate constants. However, the 1.18-1.40 mm experienced the least breakage. Appendix II (Table II.5) shows that for the finest size class, 0.425-0.500 mm, some breakage rate constants are of the same order of magnitude as the flattening rate constants. The model yielded a standard error of 2.2 to 3.9% for the four size classes tested.

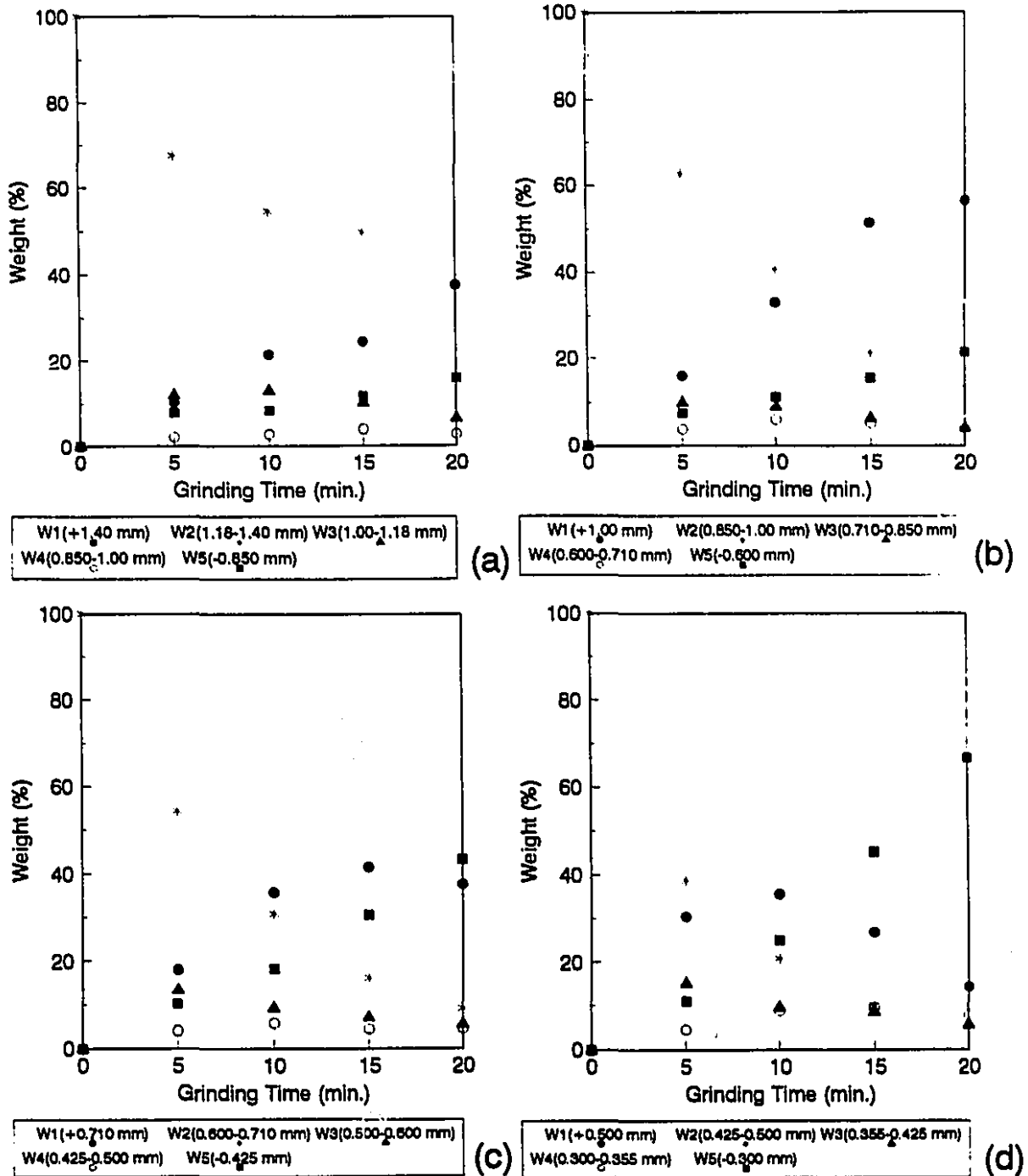


**Figure 5.33:** Size distribution of lead fragments as a function of grinding time in the small ball mill tests (lead mixed with silica); a: 1.18-1.40 mm, b: 0.850-1.000 mm, c: 0.600-0.710 mm, d: 0.425-0.500 mm.

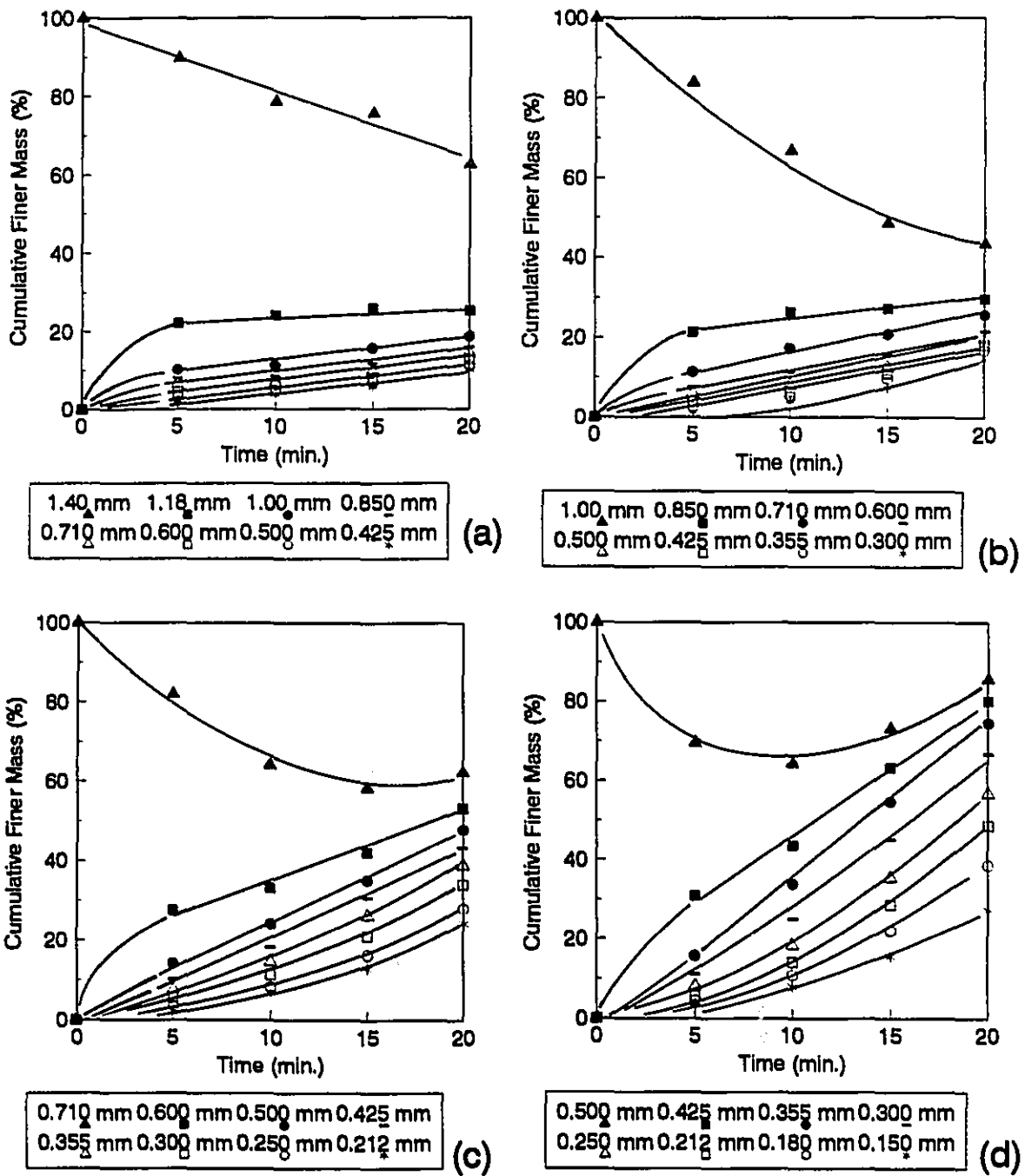
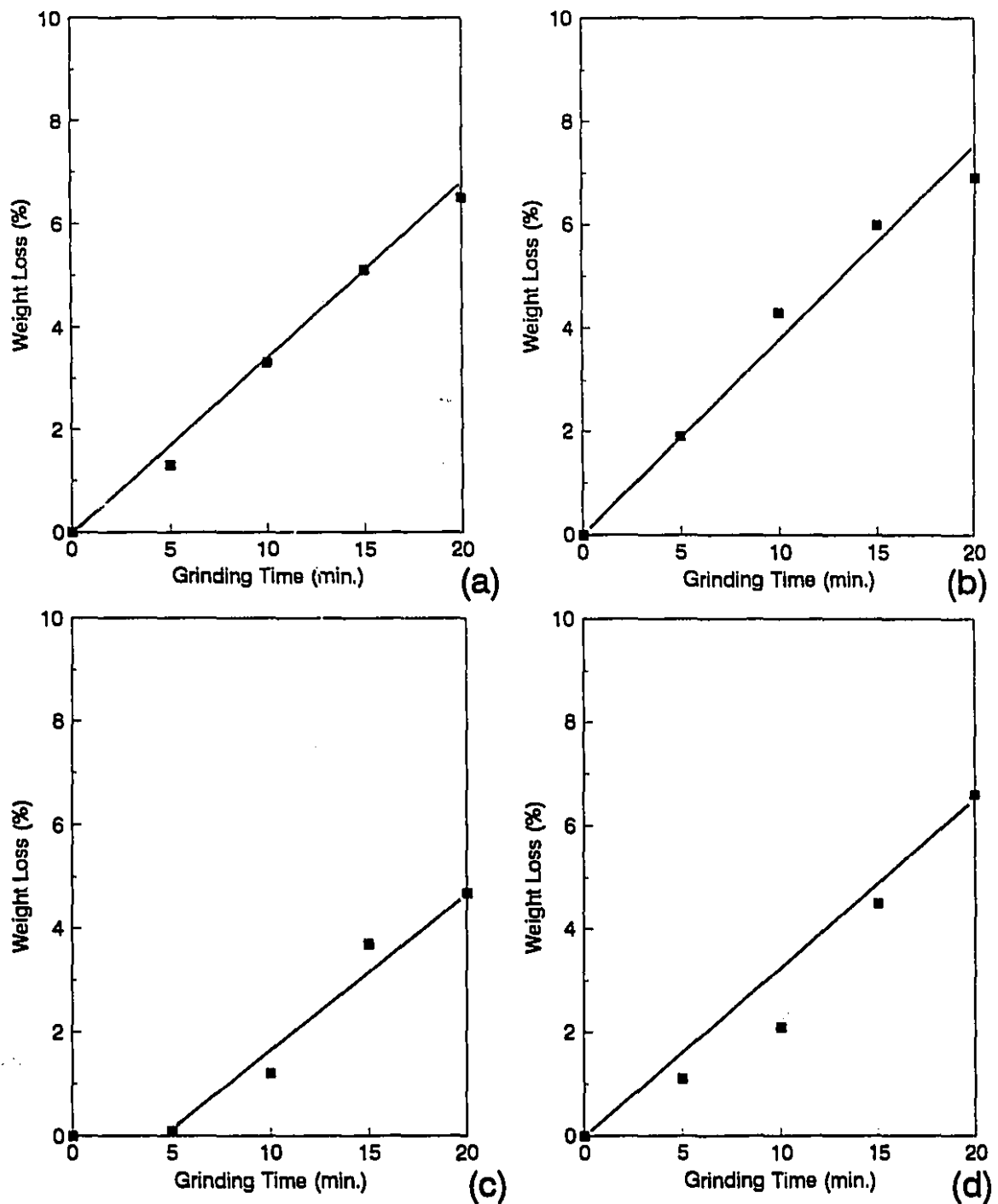


Figure 5.34: Fines production as a function of time in the small ball mill (Feed: lead fragments mixed with silica; a: 1.18-1.40 mm, b: 0.850-1.000 mm, c: 0.600-0.710 mm, d: 0.425-0.500 mm).



**Figure 5.35:** Lost weight of lead fragments as a function of grinding time in the small ball mill tests (lead fragments mixed with silica); a: 1.18-1.40 mm, b: 0.850-1.000 mm, c: 0.600-0.710 mm, d: 0.425-0.500 mm

Table 5.8: Estimated breakage function (BF) of lead for the small ball mill tests (lead fragments mixed with silica).

Size classes (mm)	Breakage Function Values for the Feed Size of:			
	1.18-1.40	0.850-1.00	0.600-0.710	0.425-0.500
1.180	-	-	-	-
1.000	0.320	-	-	-
0.850	0.118	-	-	-
0.710	0.054	0.225	-	-
0.600	0.041	0.012	-	-
0.500	0.055	0.066	0.333	-
0.425	0.031	0.033	0.054	-
0.355	-	0.035	0.062	0.514
0.300	-	0.069	0.073	0.053
0.250	-	-	0.085	0.069
0.212	-	-	0.054	0.053
0.180	-	-	-	0.066
0.150	-	-	-	0.073

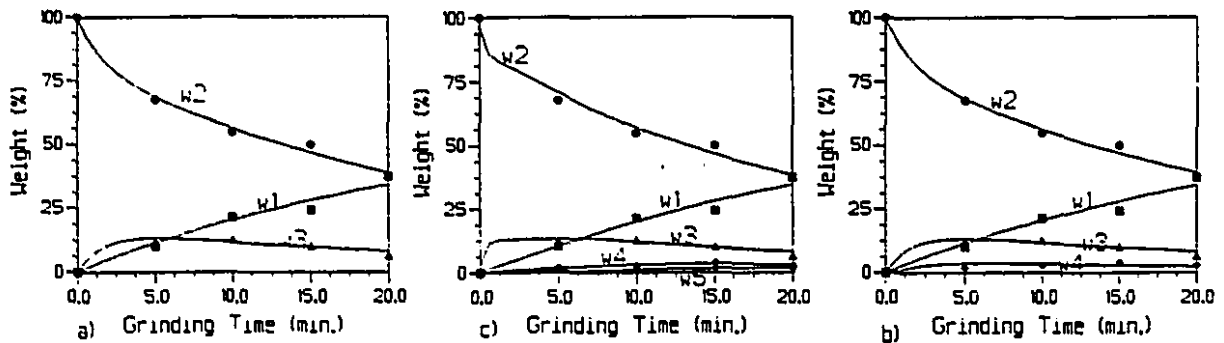


Figure 5.36: Fit of the flattening, folding and explicit breakage model for the small ball mill test (feed: 1.18-1.40 mm lead fragments mixed with silica); a: 3 size classes, b: 4 size classes, c: 5 size classes.

**Table 5.9:** Estimated rate constants (all in  $\text{min}^{-1}$ ) for the small ball mill test, flattening, folding and explicit breakage model (feed: 1.18-1.40 mm lead fragments mixed with silica).

Size classes	Feed size: 1.18-1.40 mm		
Rate constants	Three Size classes: $w_1, w_2, W_3$	Four size classes: $w_1, w_2, w_3, W_4$	Five size classes: $w_1, w_2, w_3, w_4, W_5$
$s_1$	0.00	0.00	0.00
$s_2$	0.02	0.00	0.01
$s_3$	0.00	0.00	0.00
$s_4$	-	0.28	0.16
$s_5$	-	-	0.07
$r_{1,2}$	0.00	0.00	0.00
$r_{2,1}$	0.03	0.03	0.03
$r_{2,3}$	0.09	0.13	0.65
$r_{3,2}$	0.49	0.56	3.08
$r_{3,4}$	-	0.40	0.05
$r_{4,3}$	-	1.09	0.00
$r_{4,5}$	-	-	0.00
$r_{5,4}$	-	-	0.00
SS	47.0	50.0	52.0
MSS	5.9	5.0	4.3
$S_r$	2.4	2.2	2.1

**Bond Rod Mill:** In the Bond rod mill, extrapolation of the Bond ball mill results would suggest that breakage overwhelmingly dominates. Figures 5.42 to 5.44 confirms this hypothesis to the extent that flattening and folding could be almost ignored (although

the presence of up to 18% mass in size class 1, Test 4, testifies to at least some flattening). Weight loss to mill liner and rods and the MLS separation, is only 6 to 10% after 10 minutes, compared to 46 to 65% after 1.5 minutes without silica. Figures 5.37 to 5.41 show SEM photographs of several flattened and broken lead fragments: much damage shows, evidence of the combined effect of rod impact and the scouring of silica.

Using the same approach as the first two mills, breakage functions were estimated (Table 5.10), as the flattening, folding and explicit breakage model fitted. Figure 5.45 shows that for the 1.18-1.40 mm, the fit is excellent. Table 5.11 confirms the low standard error, 1.0%, and the importance of breakage, especially for size classes 1 and 3. Table 5.11 illustrates some of the numerical difficulties of combining explicit breakage to flattening and folding. In this case, the parameters  $s_2$  and  $r_{2,3}$  have a very similar impact on the model, i.e. to describe the migration of lead from size class 2 to finer size classes. The SCIENTIST software chooses to describe this with folding for the three and four size class model, but with breakage for the five size class model.

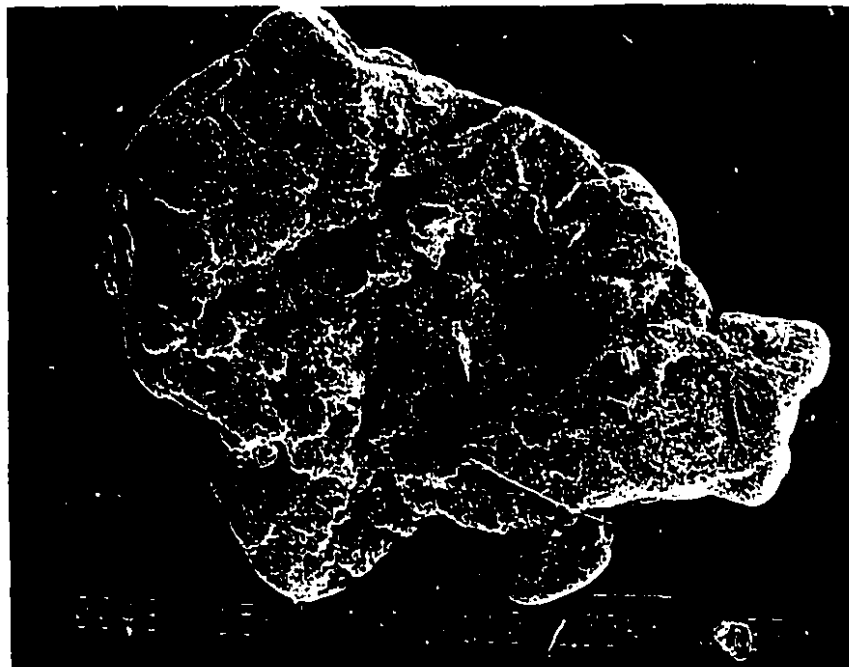


Figure 5.37: A lead fragment recovered from the Bond rod mill (feed size: 0.850-1.00 mm).

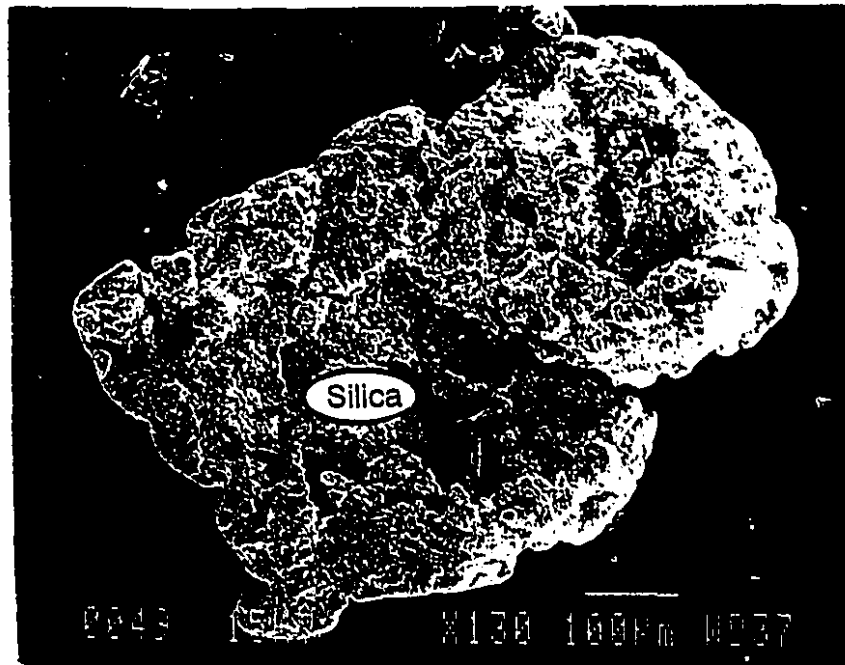


Figure 5.38: A lead fragment recovered from the Bond rod mill (feed size: 0.850-1.00 mm).



Figure 5.39: A lead fragment recovered from the Bond rod mill (feed size: 1.18-1.40 mm).

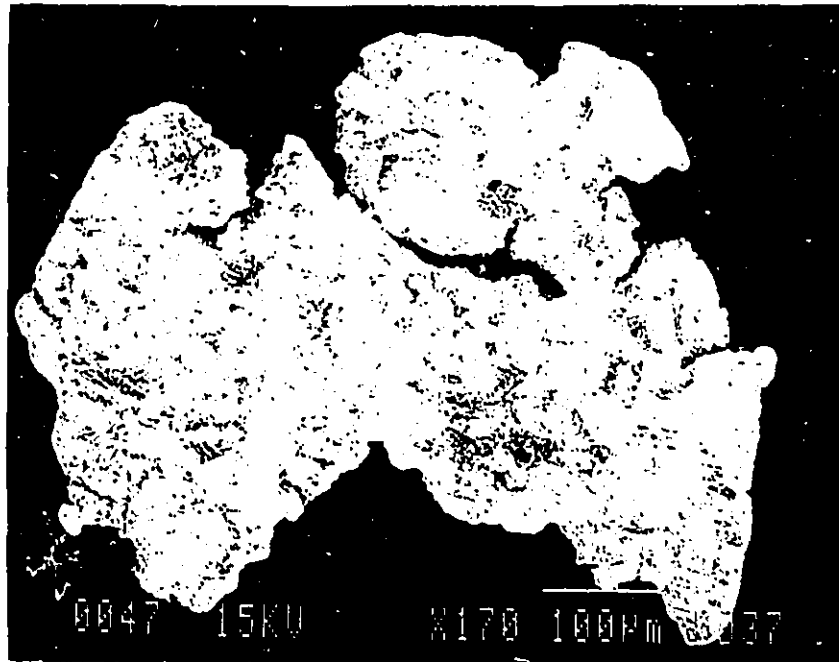
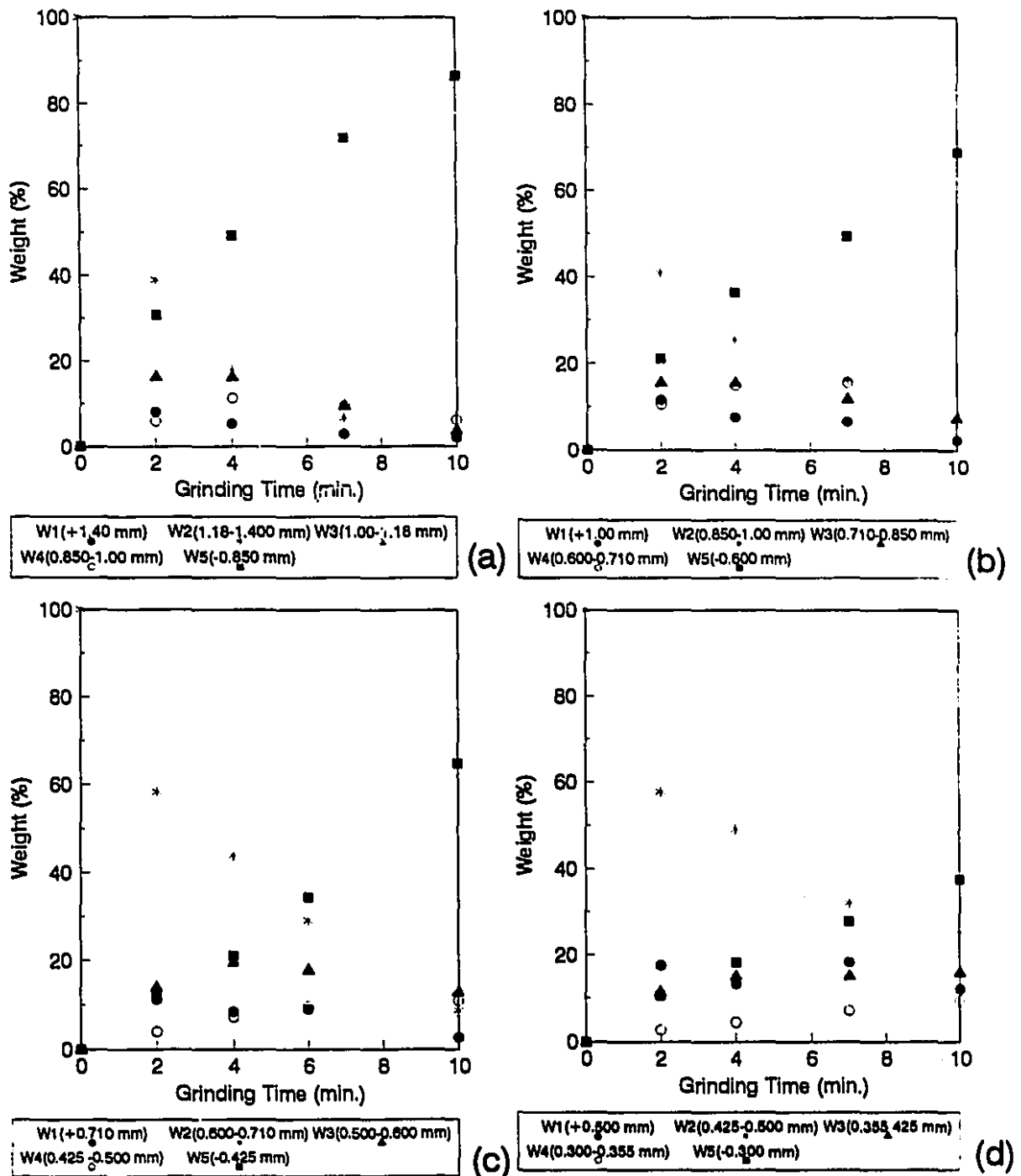


Figure 5.40: A lead fragment recovered from the Bond rod mill (feed size: 1.18-1.40 mm).



Figure 5.41: A lead fragment recovered from the Bond rod mill (feed size: 0.600-0.710 mm).



**Figure 5.42:** Size distribution of lead fragments as a function of grinding time in the Bond rod mill tests (lead fragments mixed with silica); a: 1.18-1.40 mm, b: 0.850-1.000 mm, c: 0.600-0.710 mm, d: 0.425-0.500 mm.

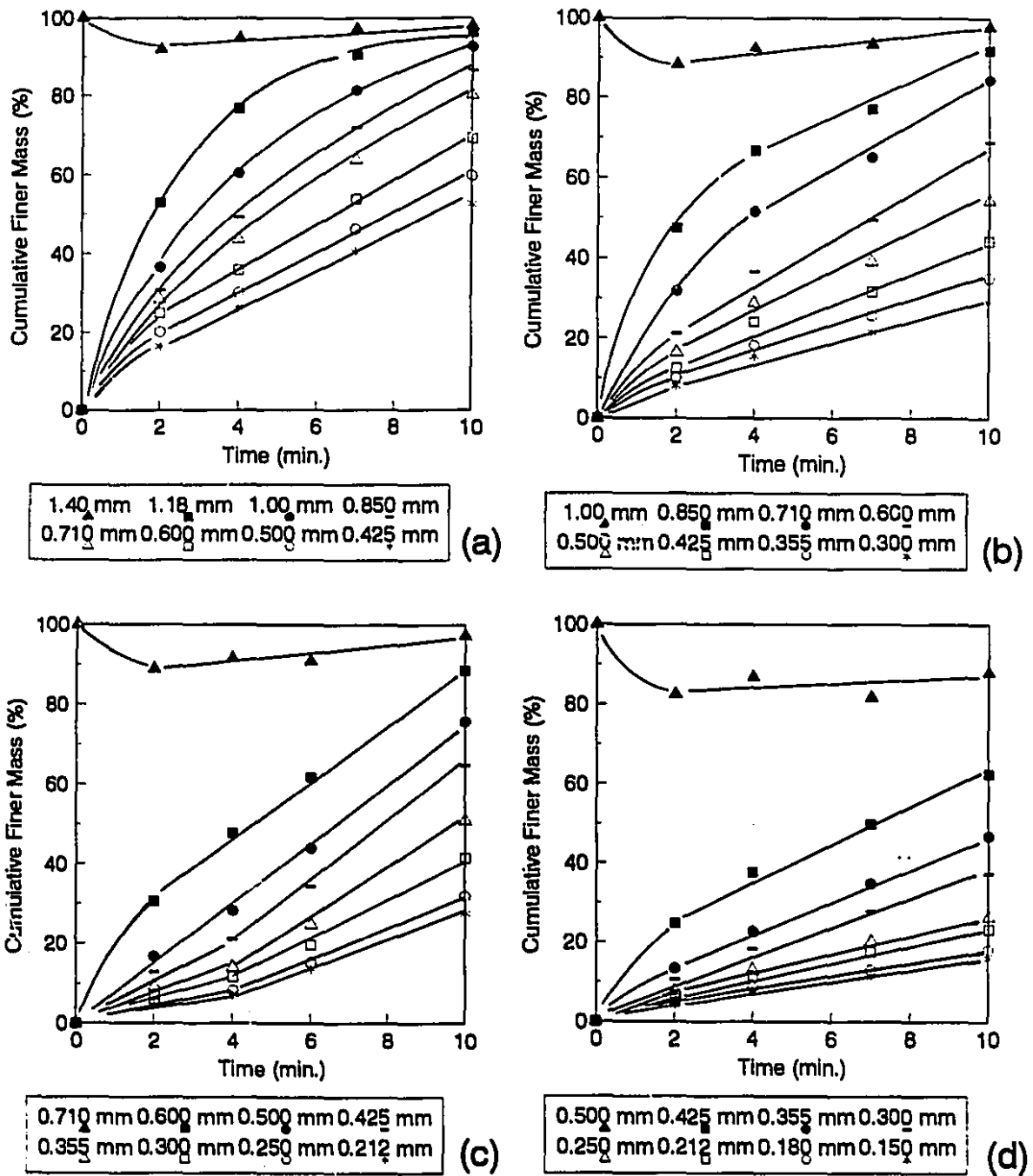
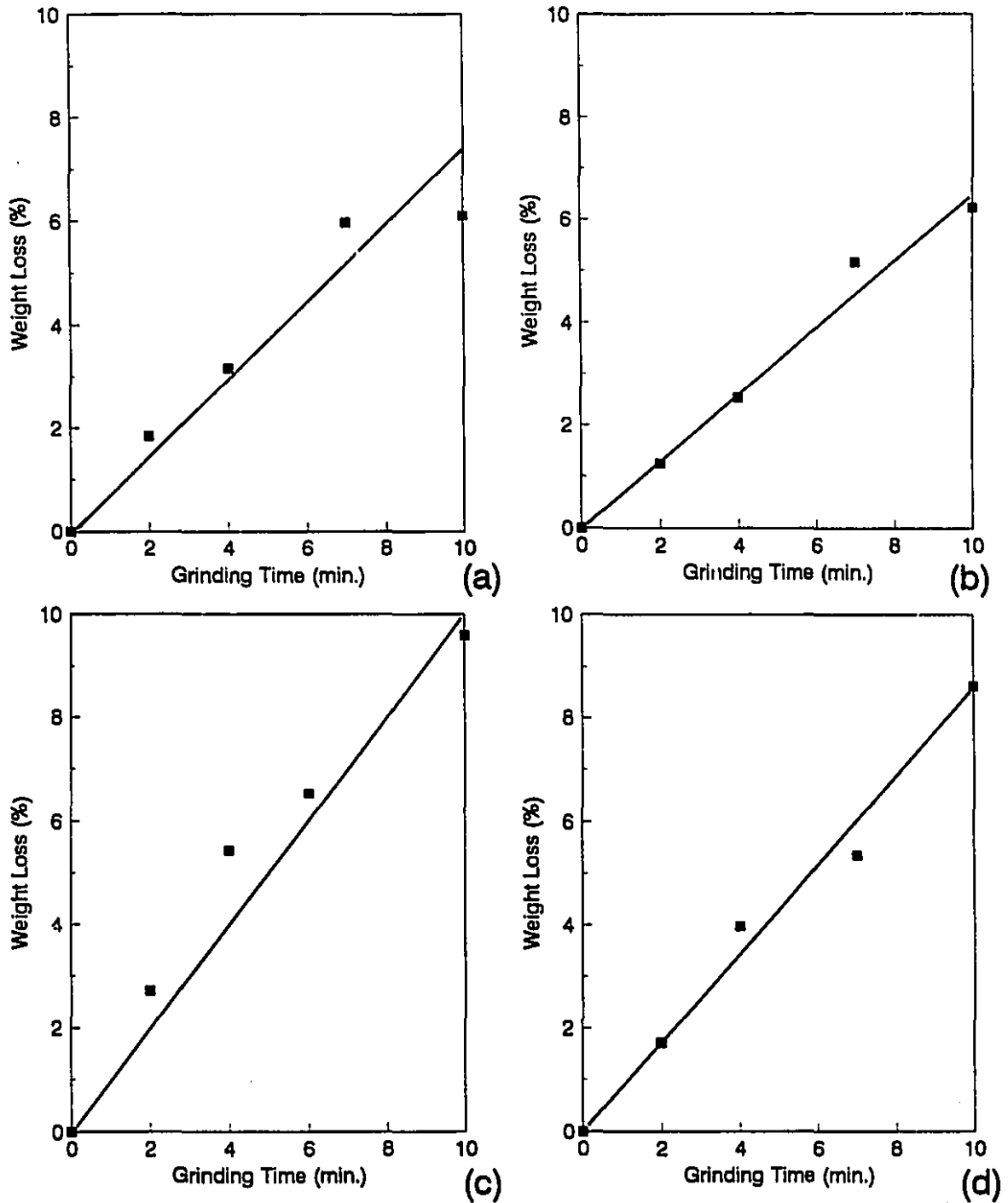


Figure 5.43: Fines production as a function of time in the Bond rod mill (Feed: lead fragments mixed with silica; a: 1.18-1.40 mm, b: 0.850-1.000 mm, c: 0.600-0.710 mm, d: 0.425-0.500 mm).



**Figure 5.44:** Lost weight of lead fragments as a function of grinding time in the Bond rod mill tests (lead fragments mixed with silica); a: 1.18-1.40 mm, b: 0.850-1.00 mm, c: 0.600-0.710 mm, d: 0.425-0.500 mm.

As this is the system where breakage is most dominant, an additional model was tested, explicit breakage with a single flattening transfer, from size class 2 to size class 1 ( $r_{2,1}$ ). Folding was assumed negligible, as was flattening from all size classes finer than size class 2. Table 5.12 shows that the sum of squared residuals is similar to that of the much more cumbersome flattening, folding and explicit breakage model. The standard error is lower, because the fewer parameters yield more degrees of freedom.

**Table 5.10:** Estimated breakage function (BF) of lead for the Bond rod mill tests (lead fragments mixed with silica).

Size classes (mm)	Breakage Function Values for the Feed Size of:			
	1.18-1.40	0.850-1.00	0.600-0.710	0.425-0.500
1.180	-	-	-	-
1.000	0.728	-	-	-
0.850	0.020	-	-	-
0.710	0.021	0.661	-	-
0.600	0.034	0.057	-	-
0.500	0.026	0.059	0.647	-
0.425	0.020	0.040	0.051	-
0.355	-	0.037	0.065	0.516
0.300	-	0.024	0.044	0.098
0.255	-	-	0.044	0.112
0.212	-	-	0.020	0.033
0.180	-	-	-	0.056
0.150	-	-	-	0.020

**Table 5.11:** Estimated rate constants (all in  $\text{min}^{-1}$ ) for the Bond rod mill test, flattening, folding and explicit breakage model (feed: 1.18-1.40 mm lead fragments mixed with silica).

Size classes	Feed size: 1.18 - 1.40 mm		
	Three Size classes: $w_1, w_2, w_3$	Four size classes: $w_1, w_2, w_3, w_4$	Five size classes: $w_1, w_2, w_3, w_4, w_5$
$s_1$	4.44	4.29	2.88
$s_2$	0.00	0.00	0.29
$s_3$	0.36	0.38	0.38
$s_4$	-	0.37	0.00
$s_5$	-	-	0.52
$r_{1,2}$	0.00	0.00	0.00
$r_{2,1}$	0.95	0.92	0.60
$r_{2,3}$	0.19	0.21	0.00
$r_{3,2}$	0.00	0.00	0.00
$r_{3,4}$	-	0.00	0.00
$r_{4,3}$	-	0.00	0.00
$r_{4,5}$	-	-	0.36
$r_{5,4}$	-	-	0.00
SS	9.0	10.0	12.0
MSS	1.0	1.0	1.0
$S_r$	1.0	1.0	1.0

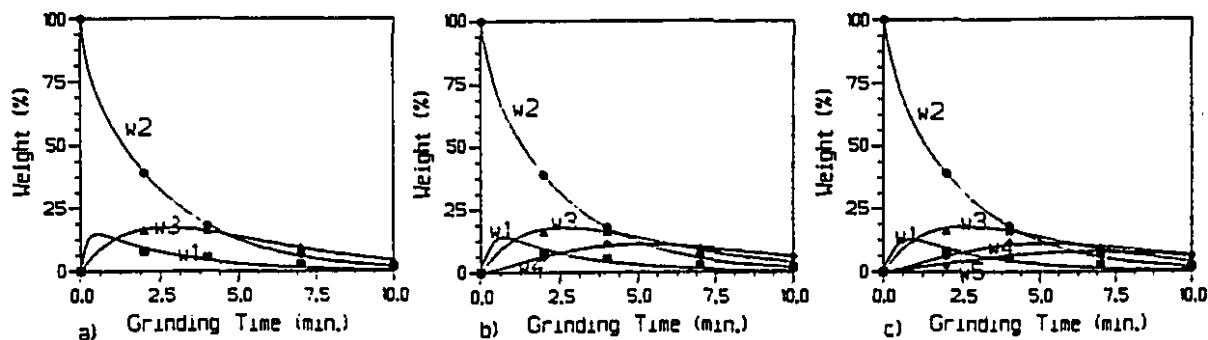


**Figure 5.45:** Fit of the flattening, folding and explicit breakage model for the Bond rod mill test (feed: 1.18-1.40 mm lead fragments mixed with silica); a: 3 size classes, b: 4 size classes, c: 5 size classes.

**Table 5.12:** Estimated rate constants (all in  $\text{min}^{-1}$ ) for the Bond rod mill test, flattening, folding and explicit breakage model with only  $r_{2,1}$ , and breakage rate constants (feed: 1.18-1.40 mm lead fragments mixed with silica).

Size classes	Feed size: 1.18-1.40 mm		
Rate constants	Three Size classes: $w_1, w_2, w_3$	Four size classes: $w_1, w_2, w_3, w_4$	Five size classes: $w_1, w_2, w_3, w_4, w_5$
$s_1$	3.19	2.99	2.92
$s_2$	0.27	0.28	0.28
$s_3$	0.36	0.38	0.38
$s_4$	-	0.36	0.36
$s_5$	-	-	0.37
$r_{2,1}$	0.66	0.61	0.60
SS	8.0	9.0	11.0
MSS	0.7	0.6	0.6
$S_r$	0.8	0.8	0.8

## 5.4 Conclusions

Grinding lead fragments in the three mills yielded a variety of responses, from the virtual absence of breakage (small ball mill, no silica) to its absolute dominance (Bond rod mill with silica). In all cases, a judicious choice of model yielded a reasonable fit to the data, although individual rate constant estimates were generally unreliable. These rate constants, taken as a whole, did give quantitative measure of the importance of flattening and folding versus breakage, and of flattening versus folding.

In the most cases, flattening was approximately twice as likely to occur than

folding, and much more likely than breakage. Even in the most aggressive environments, the Bond rod mill with silica, when breakage becomes dominant over flattening, the flattening rate constant of size class 2 ( $r_{2,1}$ ) is numerically higher than the corresponding breakage rate constant ( $s_2$ ). In this type of environment, classical breakage, coupled with a single flattening rate constant, yields an acceptable description of grinding.

The phenomenon of smearing is highly variable, and is quite distinct from particle breakage. It can be very significant when the mill shell is rough, even when collisions have low energy levels (small ball mill). It is also extremely significant when impact energy is high (Bond rod mill). It increases whenever fragments begin to break, an indication that smearing is probably related to the surface area of the smeared substances.

**Chapter 6: The Behaviour of Copper Fragments in  
Tumbling Mills**

## 6.1 Introduction

After lead, a relatively soft metal, we will now turn to a harder one, copper, to assess its grinding behaviour. The case of copper is an interesting one: unlike lead, it is a relatively common native metal, such as in the Keweenaw Peninsula, Michigan<sup>(3)</sup>. Metallic copper is also milled in the converter slag at the Horne Smelter, Rouyn-Noranda, Quebec. Thus, although lead is similar to gold in softness and density, investigating the grinding of metallic copper has more direct applications in mining and metallurgy.

The approach used will be similar to that of the work described for lead. In particular, the relative importance of flattening, folding and breakage will be assessed, and the applicability of Equations 3.7, 3.14, 3.22, and 3.23 evaluated.

The study will be limited to copper fragments, that most approach copper particles found in grinding circuits either as native copper or copper droplets entrained in slag in the Noranda process<sup>(192)</sup>.

## 6.2 Experimental

**Apparati and Feed:** The grinding mills and media used were identical to those of the lead work (Table 5.1), as were the screens. Copper fragments in four specific size classes, 1.18-1.40 mm, 0.850-1.000 mm, 0.600-0.710 mm and 0.425-0.500 mm, were obtained by grinding of copper shots, from Fisher Scientific, 2.80-3.35 mm in diameter, in the Bond rod mill.

**Methodology:** Test procedure was identical to that of lead fragments in the first series

of tests in chapter 5. The feed was ground and its product screened, weighed and mixed to be used for the next grinding increment. The grinding times were different for each of these three mills. In the Bond ball mill, copper fragments were ground up to 120 minutes in 10, 15, and 20 minute increments. In the small ball mill, grinding times were up to 70 minutes, with 5 to 25 minute increments. In the Bond rod mill, total grinding time was 10 minutes for each test with 0.5, 1, 2, and 4 minute increments. The initial copper mass was 25 g for the Bond ball mill, 10 g for the small ball mill, and 50 g for the Bond rod mill.

### 6.3 Results and Discussion

**Bond Ball Mill:** Figures 6.1 and 6.2 show the size distribution of the mass recovered from the mill in the four tests. The coarsest, 1.18-1.40 mm (Figure 6.1(a), and 6.2(a)) displayed virtually no change after 120 minutes of grinding, apart from an initial (after 10 minutes) shift of mass of 13% to the 1.00-1.18 mm, which was attributed to folding (no breakage was observed, and virtually no mass reported to the 0.850-1.00 mm). By comparison, the finest size class, 0.425-0.500 mm, displayed the classical folding and flattening behaviour, with the predominance of flattening. Thus, after 120 minutes, more than 50% of the mass recovered from the mill reported to the +0.500 mm.

Figure 6.2, which shows the production of fines (or rather the lack thereof), confirms the absence of significant breakage for all four size classes. Figure 6.3 shows that the loss of copper to the mill inner shell and grinding media was modest, 6 to 8% after 120 minutes.

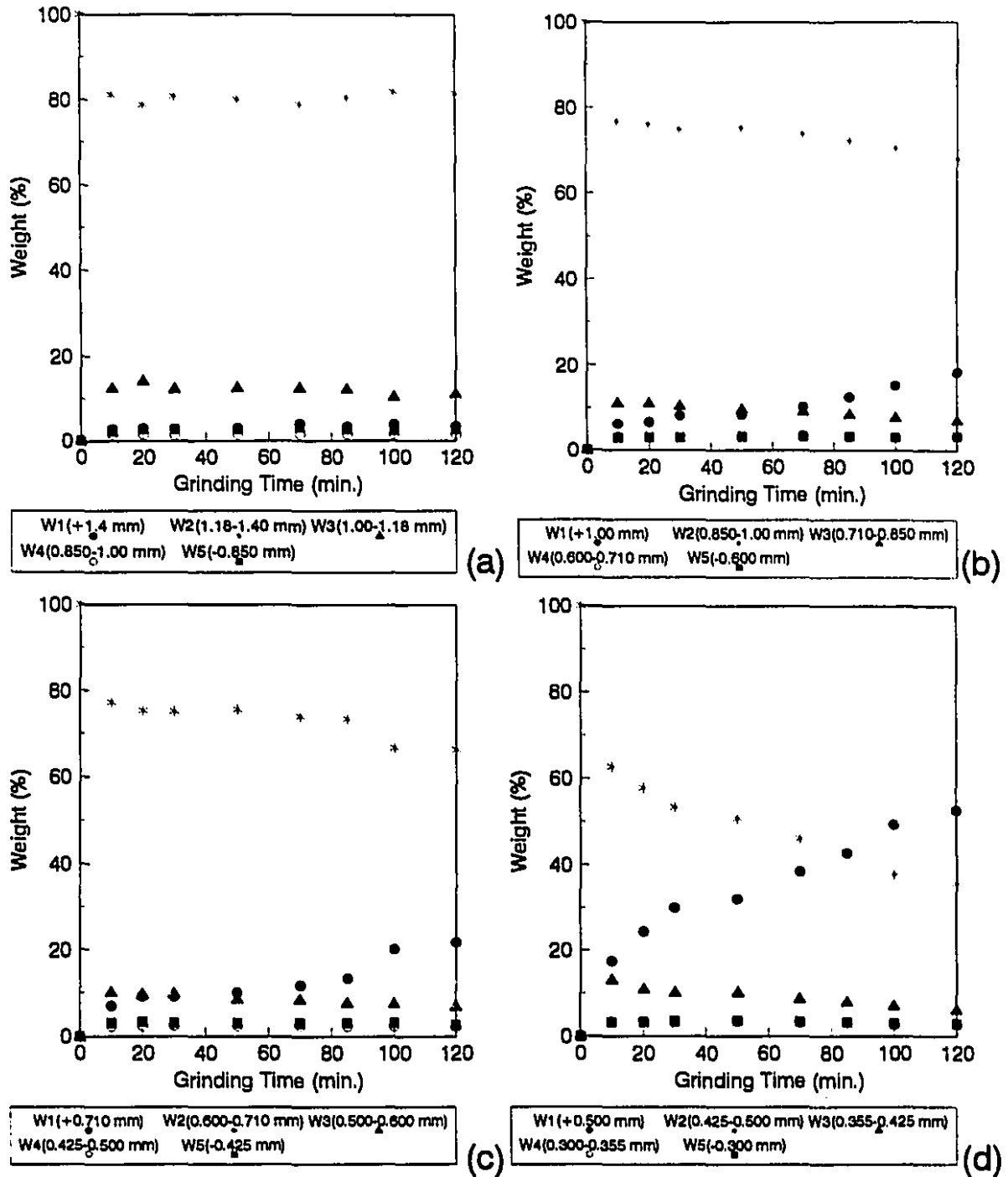


**Figure 6.1:** Size distribution of copper fragments as a function of grinding time in the Bond ball mill tests: a: 1.18-1.40 mm, b: 0.850-1.000 mm, c: 0.600-0.710 mm, d: 0.425-0.500 mm.

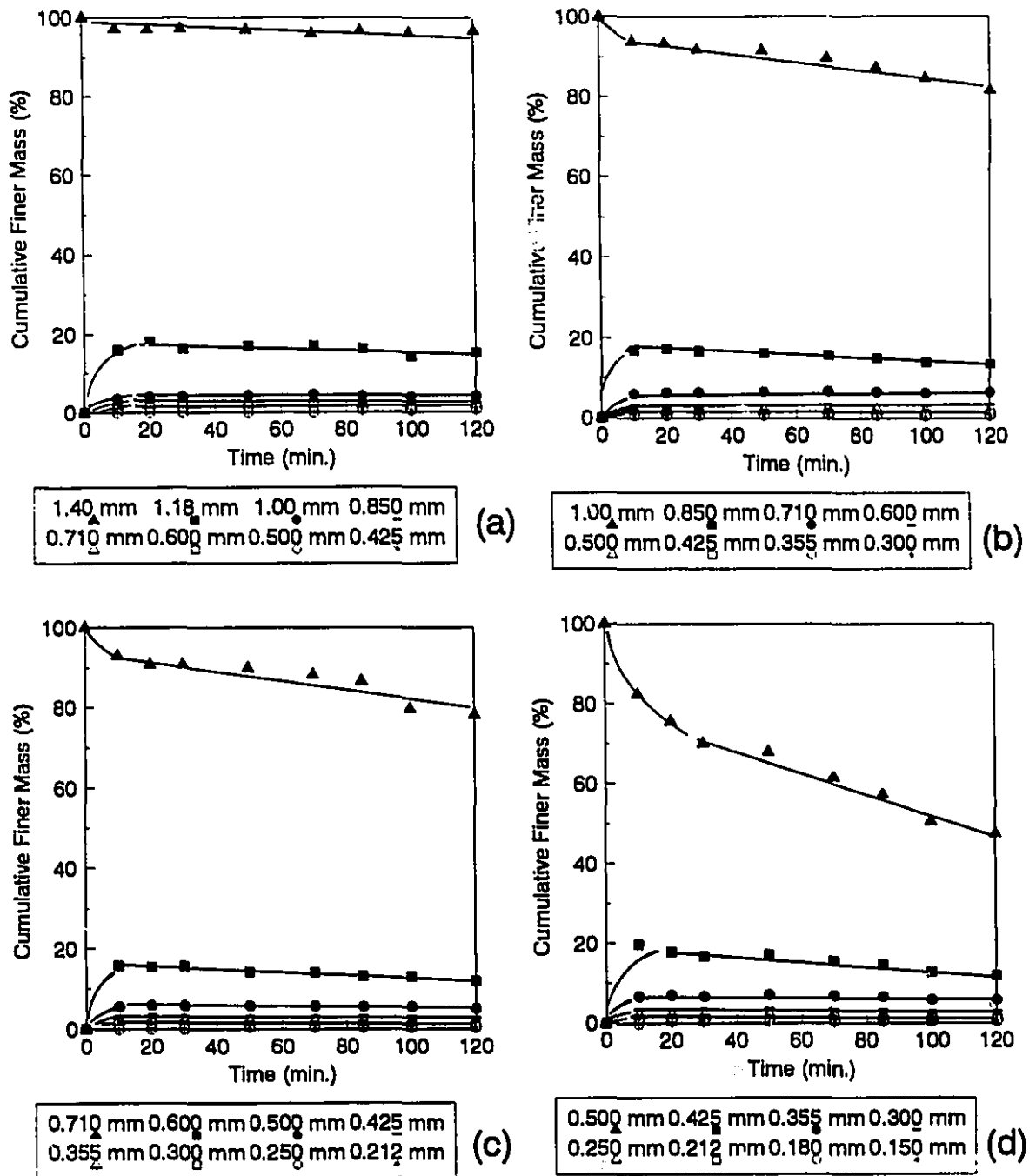


**Figure 6.2:** Fines production as a function of time in the Bond ball mill (Feed: copper fragments; a: 1.18-1.40 mm, b: 0.850-1.000 mm, c: 0.600-0.710 mm, d: 0.425-0.500 mm).

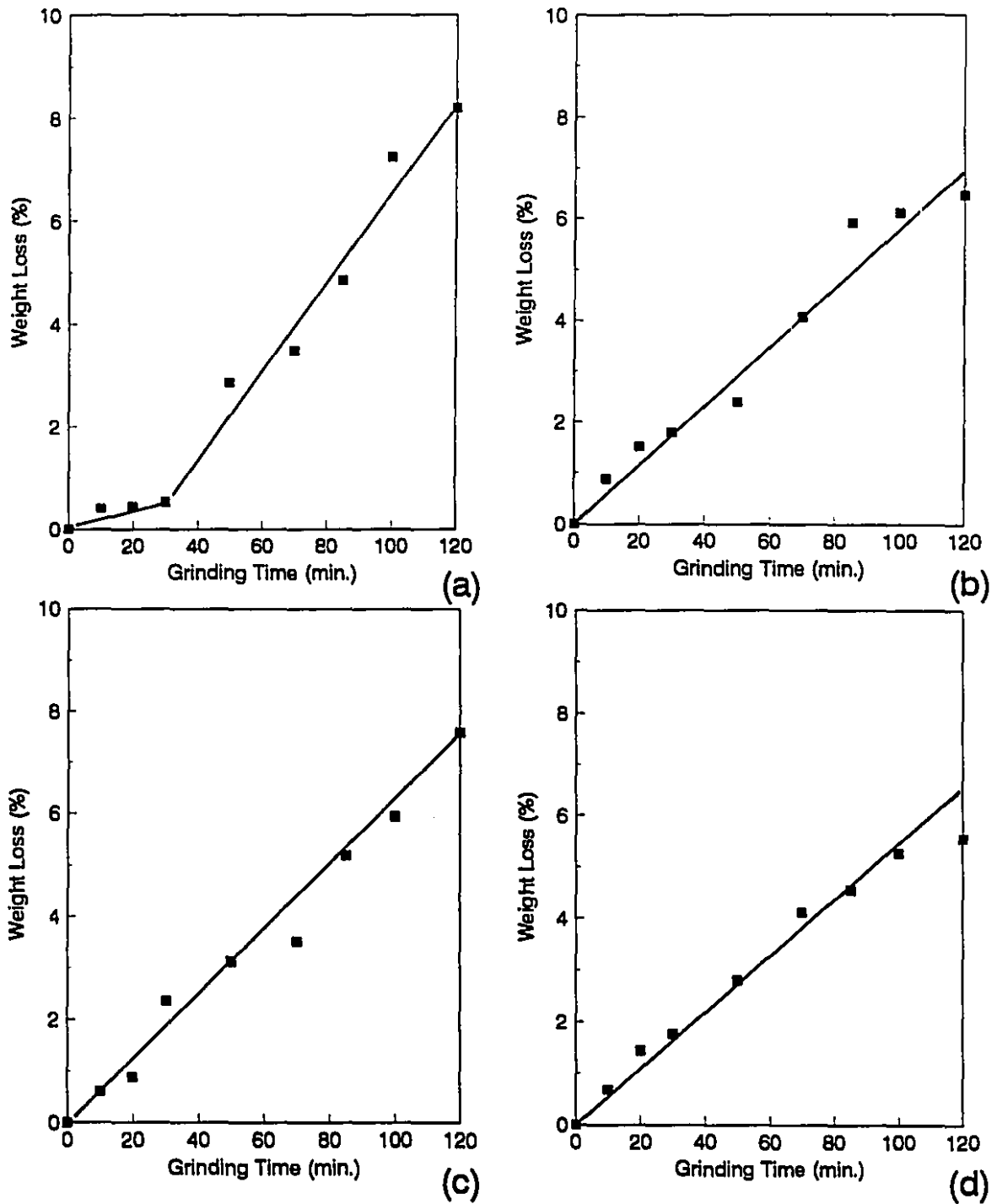


**Figure 6.3:** Lost weight of copper fragments as a function of grinding time in the Bond ball mill tests; a: 1.18-1.40 mm, b: 0.850-1.000 mm, c: 0.600-0.710 mm, d: 0.425-0.500 mm.

The flattening and folding model (no breakage) was used to fit the curves to the results in the Bond ball mill tests. First a simple model of three size classes was used:  $w_2$  (the original size class),  $W_1$  (the coarsest) and  $W_3$  (all copper finer than size class 2). In a second step,  $W_3$  was divided into two size classes,  $w_3$  and  $W_4$ . Finally, five size classes were used, as  $W_4$  was split into  $w_4$  and  $W_5$ .

**Table 6.1:** Estimated rate constants (all in  $\text{min}^{-1}$ ) for the Bond ball mill test, flattening and folding without breakage model (feed: 0.425-0.500 mm copper fragments).

Rate Constants	Three Size classes ( $w_1, w_2, W_3$ )	Four Size classes ( $w_1, w_2, w_3, W_4$ )	Five Size classes ( $w_1, w_2, w_3, w_4, W_5$ )
$r_{1,2}$	0.01	0.01	0.01
$r_{2,1}$	0.02	0.02	0.02
$r_{2,3}$	0.07	0.08	0.09
$r_{3,2}$	0.21	0.39	0.46
$r_{3,4}$	-	1.40	0.73
$r_{4,3}$	-	2.00*	2.00*
$r_{4,5}$	-	-	2.00*
$r_{5,4}$	-	-	2.00*
SS	175.0	175.0	171.0
MSS	7.6	5.8	4.6
$S_r$	2.8	2.4	2.1

(\*: 2.00 was the upper search limit.)

All rate constant estimations are presented in Appendix II (Table II.7). Table 6.1 and Figure 6.4 show the results of one test, with the 0.425-0.500 mm feed. The fit is reasonable; standard errors vary between 2.1 and 2.8%, some of which is due to experimental scatter rather than model lack-of-fit. Because of the absence of breakage, estimation of the flattening and folding rate constants is more reliable, and confirm the

preponderance of flattening over folding.

For the three other size classes, Table II.7 shows even lower standard errors, 0.8 to 2.3%. However, rate constant estimates differ from those of the 0.425-0.500 mm, in that the  $r_{1,2}$  (folding) rate constants are systematically higher than the  $r_{2,1}$  (flattening). For the finer size classes (e.g.  $r_{2,3}$  and  $r_{3,2}$ ), the usual trend (i.e.  $r_{3,2} > r_{2,3}$ ) returns.

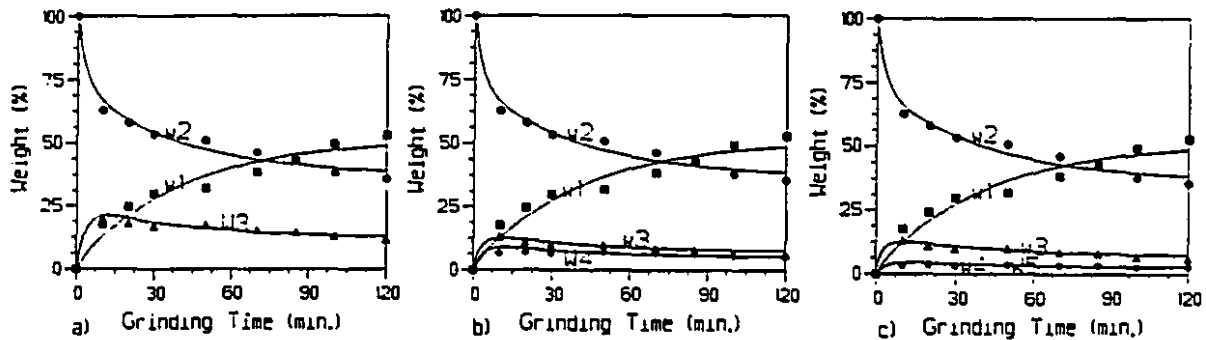


**Figure 6.4:** Fit of the flattening and folding without breakage model for the Bond ball mill test (feed: 0.425-0.500 mm copper fragments), a: 3 size classes, b: 4 size classes, c: 5 size classes.

**Small Ball Mill:** Figures 6.5 and 6.6 present the percent retained and cumulative finer weight of the small ball mill tests. As expected, the gentler grinding environment results in slower kinetics, mostly flattening to size class 1, and virtually no fines production. Subtle differences appear; for example, after 5 minutes of grinding, all tests show a sudden increase in the mass of size class 3. This increase is not repeated again. Flattening results in the other major shift in size distribution, from the initial to the coarsest size class; its importance increases with decreasing initial particle size, from 12% with the 1.18-1.40 mm to 23% with the 0.425-0.500 mm (after 70 minutes).

Figure 6.7 shows the weight loss to the balls and mill. After 70 minutes of grinding, it is significant, 16% for the coarsest fragments down to 9% for the finest, but remains much below that of lead (12 to 65% after 10 to 30 minutes of grinding).

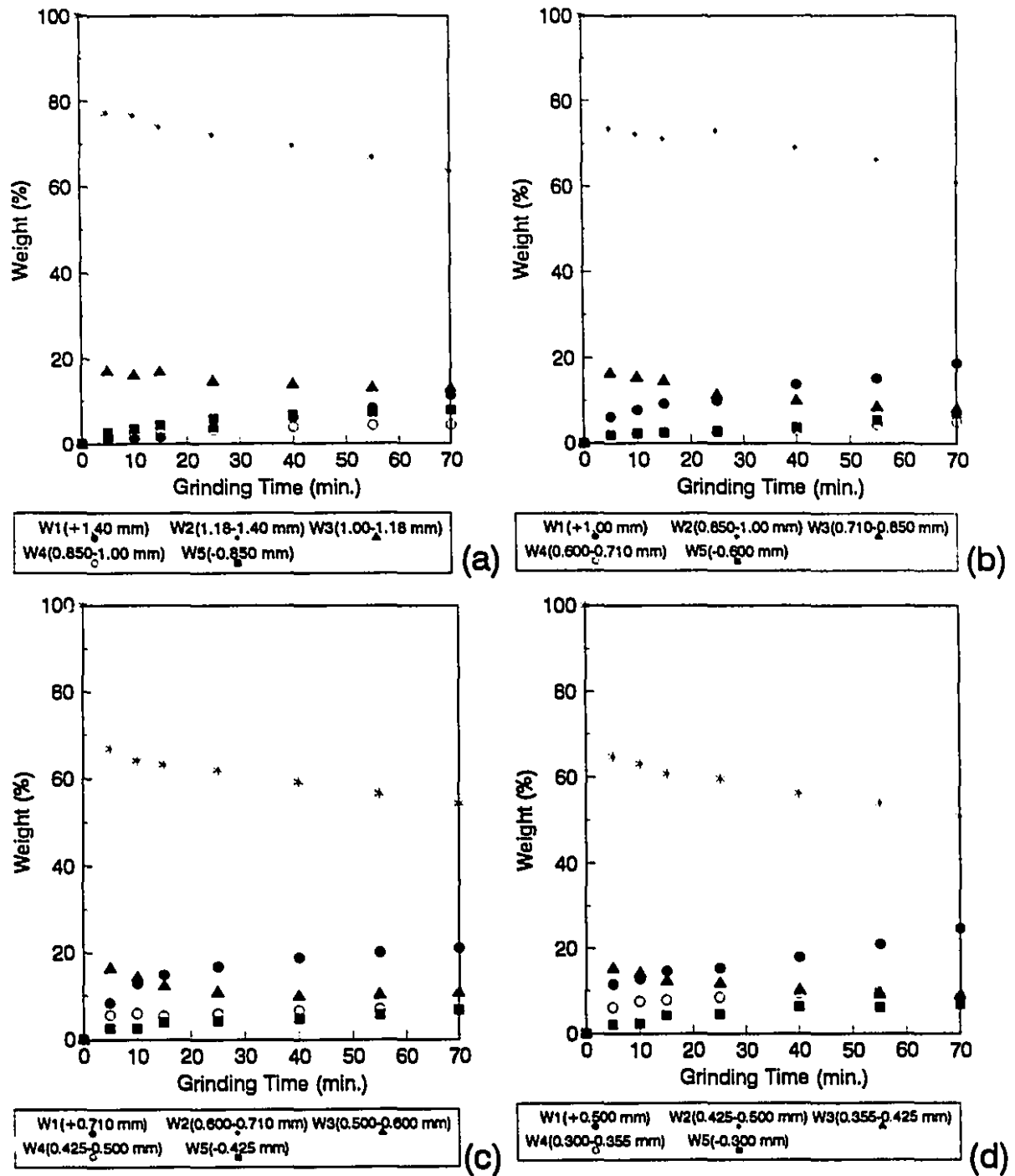


**Figure 6.5:** Size distribution of copper fragments as a function of grinding time in the small ball mill tests; a: 1.18-1.40 mm, b: 0.850-1.000 mm, c: 0.600-0.710 mm, d: 0.425-0.500 mm.

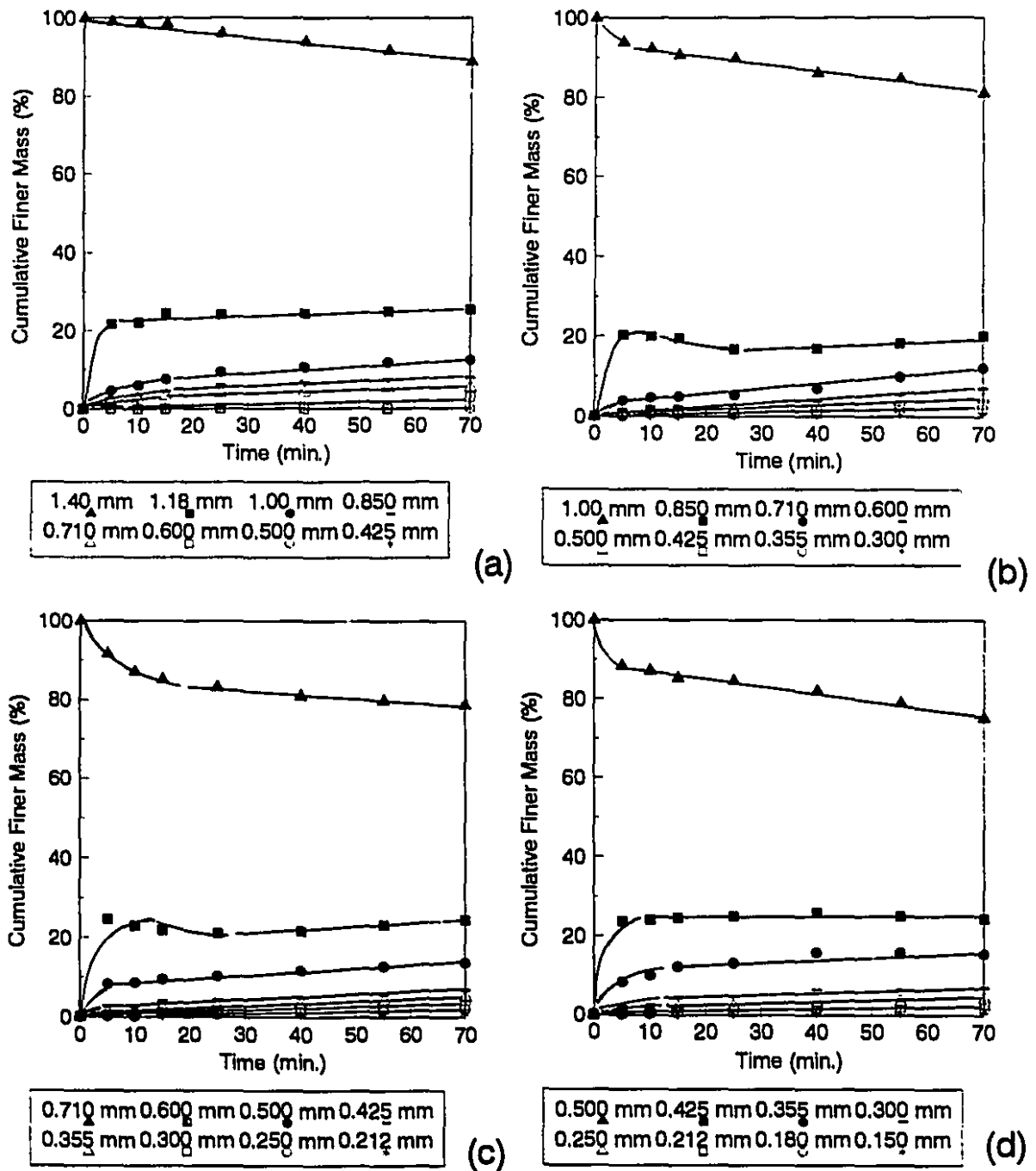


**Figure 6.6:** Fines production as a function of time in the small ball mill (Feed: copper fragments; a: 1.18-1.40 mm, b: 0.850-1.000 mm, c: 0.600-0.710 mm, d: 0.425-0.500 mm).

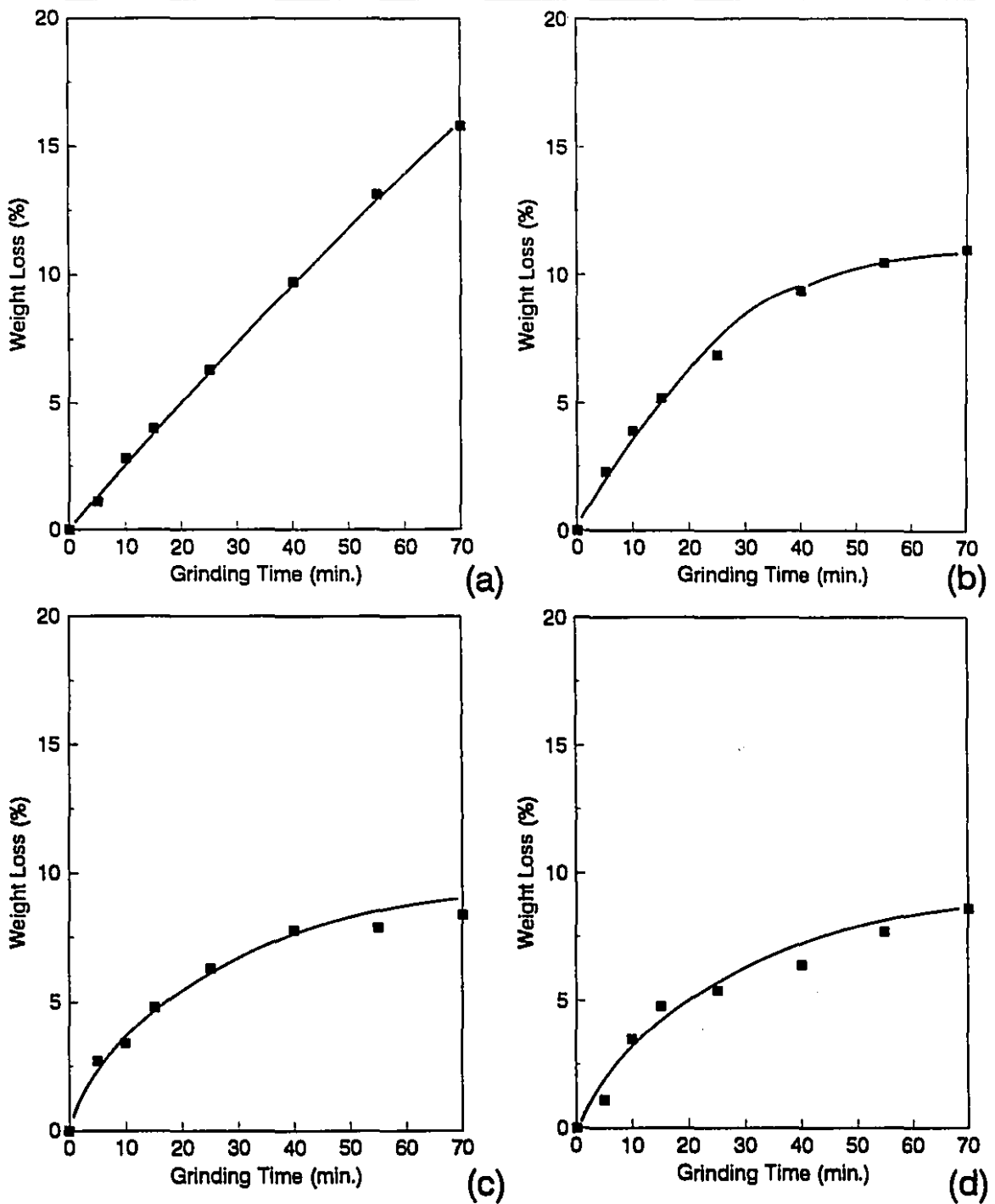
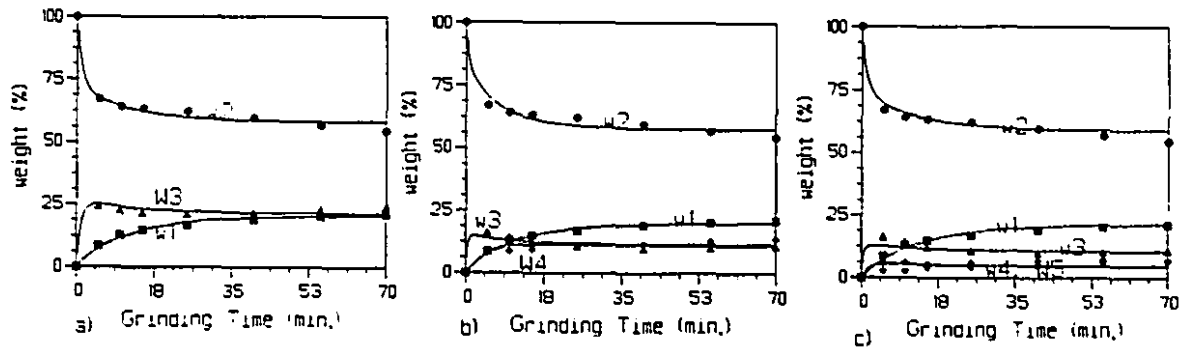


Figure 6.7: Lost weight of copper fragments as a function of grinding time in the small ball mill tests; a: 1.18-1.40 mm, b: 0.850-1.000 mm, c: 0.600-0.710 mm, d: 0.425-0.500 mm.

Obviously the flattening and folding model (no breakage) was chosen to fit data. Table 6.2 and Figure 6.8 present the results of the 0.600-0.710 mm feed size class, and Table II.8 in Appendix II presents the rate constant estimates for all feed sizes. Goodness of fit is comparable to that of the Bond ball mill tests. As for the 0.600-0.710 mm class, folding is more significant than flattening between size classes 1 and 2, especially for the 0.425-0.500 mm feed. However, transfers between finer size classes (e.g. 2 and 3) show the usual higher flattening rate constant. For the two coarsest feeds tested, so little flattening and folding takes place between size classes 1 and 2 that the respective rate constants can not be estimated reliably.

**Table 6.2:** Estimated rate constants (all in  $\text{min}^{-1}$ ) for the small ball mill test, flattening and folding without breakage model (feed: 0.600-0.710 mm copper fragments).

Rate Constants	Three Size classes ( $w_1, w_2, W_3$ )	Four Size classes ( $w_1, w_2, w_3, W_4$ )	Five Size classes ( $w_1, w_2, w_3, w_4, W_5$ )
$r_{1,2}$	0.07	0.07	0.06
$r_{2,1}$	0.02	0.02	0.02
$r_{2,3}$	0.25	0.41	0.40
$r_{3,2}$	0.68	2.01	2.21
$r_{3,4}$	-	0.18	0.87
$r_{4,3}$	-	0.19	1.99
$r_{4,5}$	-	-	2.20
$r_{5,4}$	-	-	2.12
SS	44.0	79.0	81.0
MSS	2.2	3.0	2.5
$S_r$	1.5	1.7	1.6



**Figure 6.8:** Fit of the flattening and folding without breakage model for the small ball mill test (feed: 0.600-0.710 mm copper fragments); a: 3 size classes, b: 4 size classes, c: 5 size classes.

**Bond Rod Mill:** The Bond rod mill had been used to generate the copper fragments by breakage of coarser shots, and therefore it was expected to break them effectively. Figures 6.9 and 6.10 show how the size distribution of the copper fragments evolved with time. The breakage of copper fragments in the Bond rod mill is confirmed, inclusive of zero order production of fines. Some flattening does happen, and the maximum weight in size class 1, which varies between 24% and 35%, is reached very early in each test, before a grinding time of 2 minutes. Figure 6.11 shows the weight loss to the mill shell and grinding medium, which is modest, 5 to 7% after 10 minutes (compared to 63 to 76% after 1.5 to 2 minutes for lead).

As Figures 6.9 and 6.10 show, breakage is dominant for these tests. As a result, the flattening, folding and explicit breakage model was used. The breakage function values were first estimated, and are presented in Table 6.3. Model parameters were then estimated. Model fit is excellent. Rate constants, however, are not easily estimated, again because of the large number of fragments. For the three other feed size classes, fit remains good (standard errors of 0.9 to 2.1%). Table 6.4 and Figure 6.12 present the results of the 0.600-0.710 mm feed size class. Rate constant estimates are also erratic (Table II.9, Appendix II).

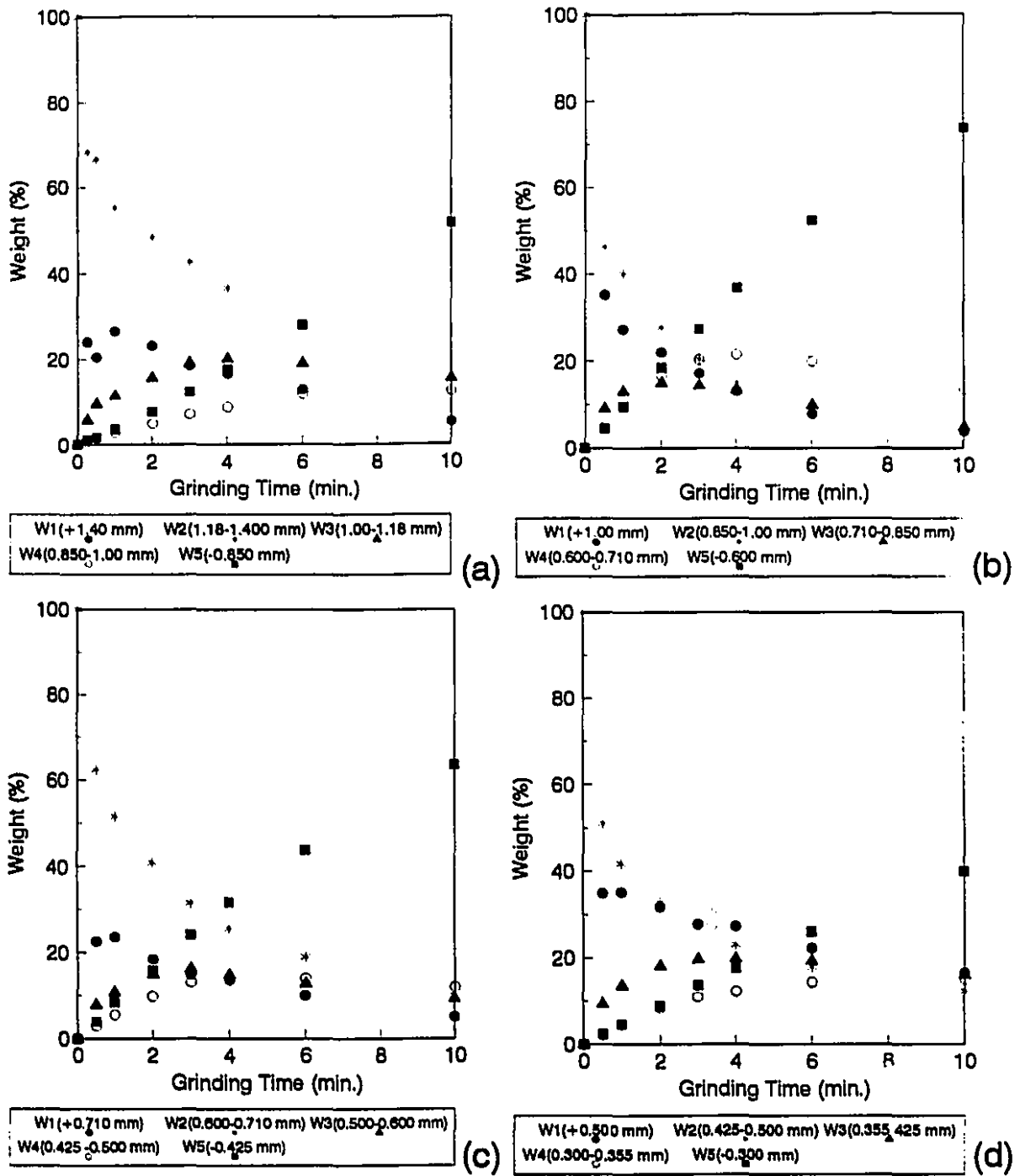


**Figure 6.9:** Size distribution of copper fragments as a function of grinding time in the Bond rod mill tests; a: 1.18-1.40 mm, b: 0.850-1.000 mm, c: 0.600-0.710 mm, d: 0.425-0.500 mm.

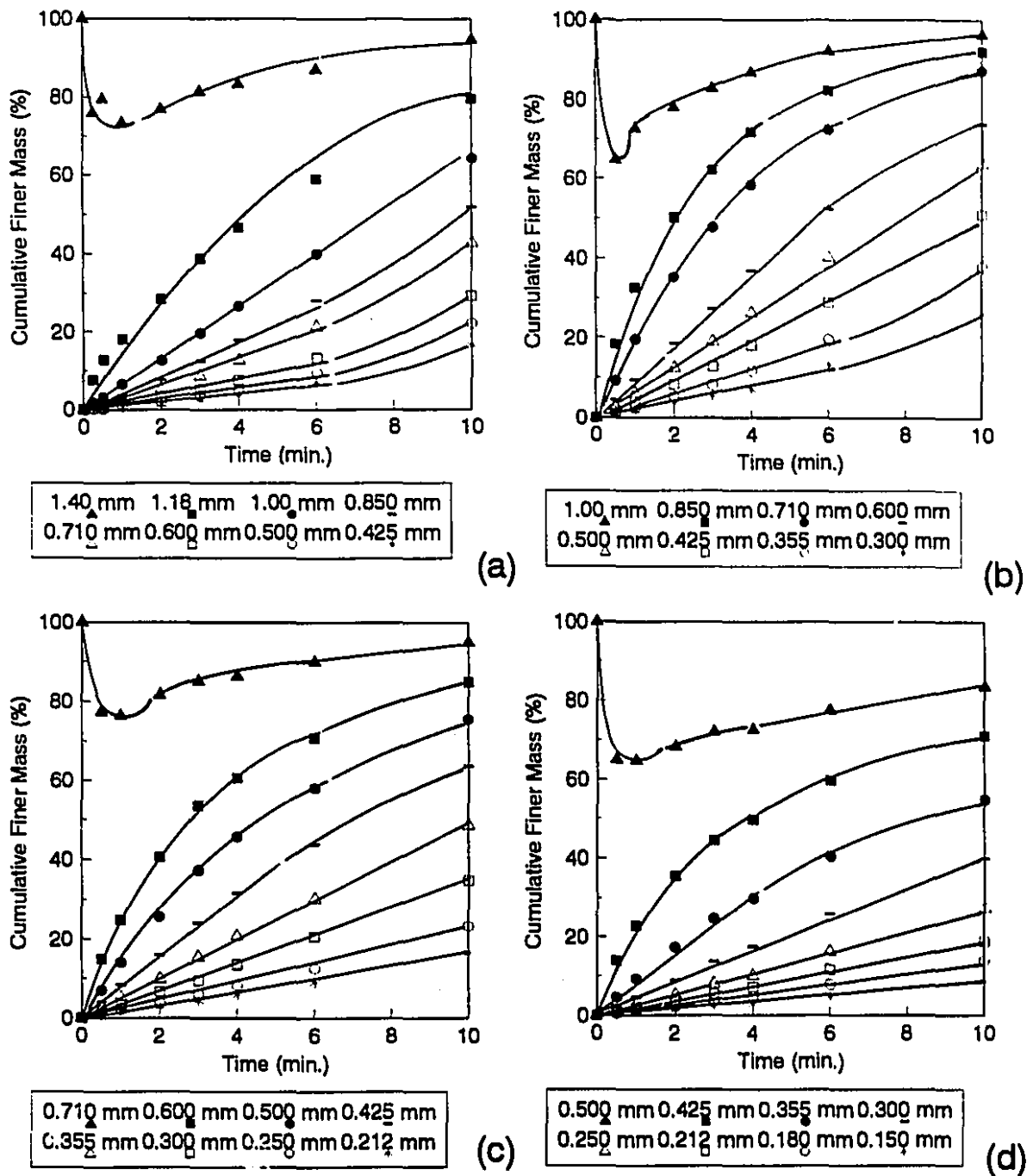


**Figure 6.10:** Fines production as a function of time in the Bond rod mill (Feed: copper fragments; a: 1.18-1.40 mm, b: 0.850-1.000 mm, c: 0.600-0.710 mm, d: 0.425-0.500 mm).

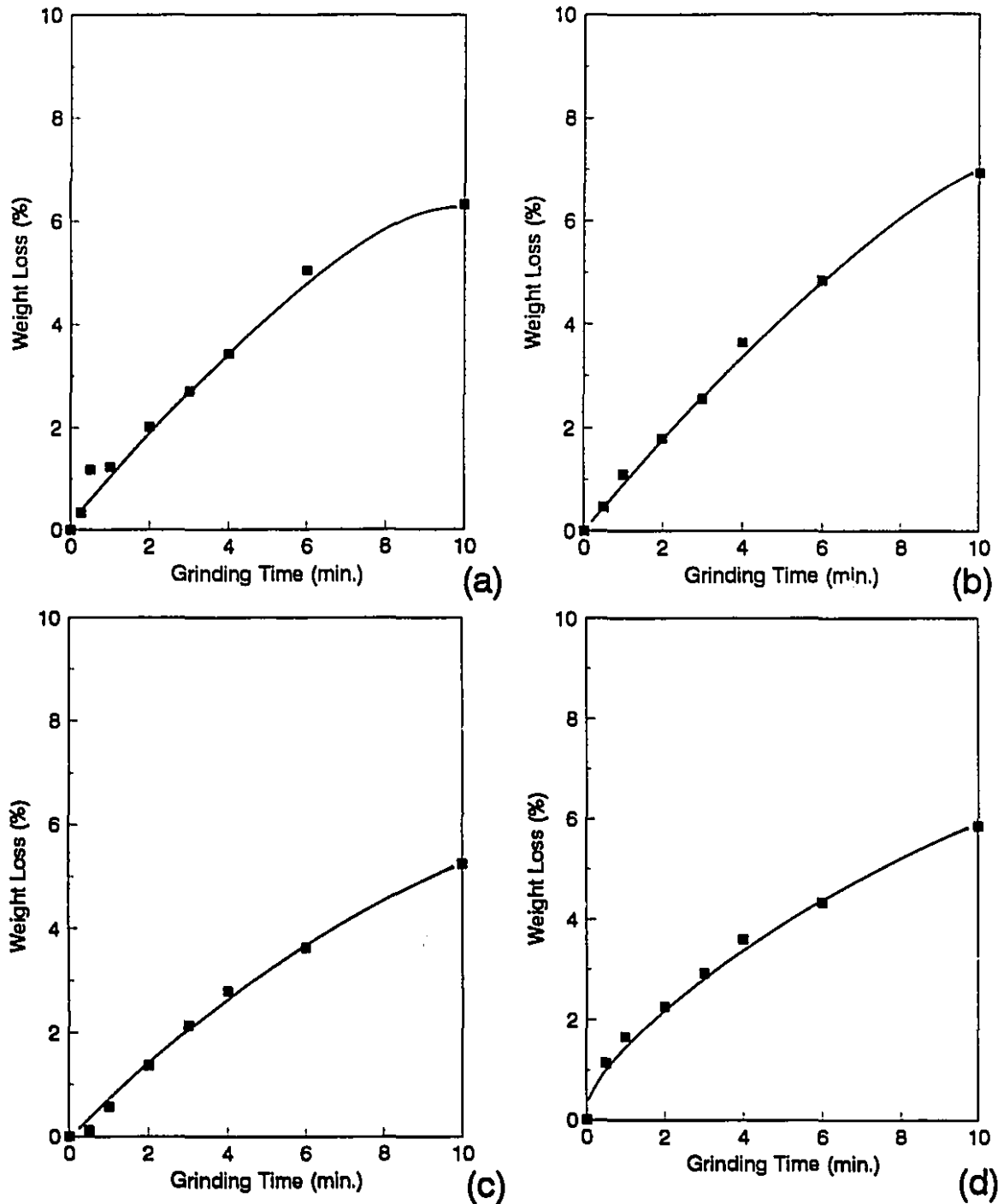


**Figure 6.11:** Lost weight of copper fragments as a function of grinding time in the Bond rod mill tests; a: 1.18-1.40 mm, b: 0.850-1.000 mm, c: 0.600-0.710 mm, d: 0.425-0.500 mm.

**Table 6.3:** Estimated breakage function (BF) of copper for the Bond rod mill tests.

Size classes (mm)	Breakage Function Values for the Feed Size of:			
	1.18-1.40	0.850-1.00	0.600-0.710	0.425-0.500
1.180	-	-	-	-
1.000	0.576	-	-	-
0.850	0.088	-	-	-
0.710	0.063	0.653	-	-
0.600	0.089	0.048	-	-
0.500	0.046	0.043	0.591	-
0.425	0.035	0.053	0.061	-
0.355	-	0.054	0.084	0.543
0.300	-	0.048	0.076	0.123
0.250	-	-	0.064	0.106
0.212	-	-	0.036	0.069
0.180	-	-	-	0.043
0.150	-	-	-	0.044

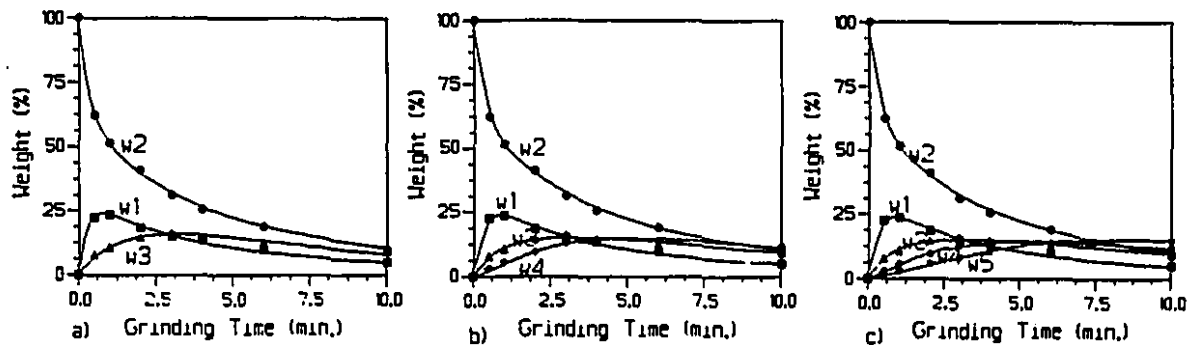


**Figure 6.12:** Fit of the flattening, folding and explicit breakage model for the Bond rod mill test (feed: 0.600-0.710 mm copper fragments); a: 3 size classes, b: 4 size classes, c: 5 size classes.

**Table 6.4:** Estimated rate constants (all in  $\text{min}^{-1}$ ) for the Bond rod mill test, flattening, folding and explicit breakage model (feed: 0.600-0.710 mm copper fragments).

Size classes	Feed size: 0.600-0.710 mm		
	Three Size classes: $w_1, w_2, w_3$	Four size classes: $w_1, w_2, w_3, w_4$	Five size classes: $w_1, w_2, w_3, w_4, w_5$
$s_1$	0.65	0.21	0.00
$s_2$	0.33	0.31	0.33
$s_3$	0.10	0.00	0.00
$s_4$	-	0.24	0.12
$s_5$	-	-	0.18
$r_{1,2}$	1.84	2.47	2.74
$r_{2,1}$	1.09	1.17	1.20
$r_{2,3}$	0.00	0.07	0.09
$r_{3,2}$	0.31	0.26	0.24
$r_{3,4}$	-	0.66	0.84
$r_{4,3}$	-	0.44	0.57
$r_{4,5}$	-	-	0.33
$r_{5,4}$	-	-	0.19
SS	3.0	12.0	12.0
MSS	0.6	0.5	0.4
$S_r$	0.8	0.7	0.6

## 6.4 Conclusions

Copper with higher hardness yielded the expected results. Very little breakage took place in the Bond and small ball mills; weight loss to smearing was also low.

Fitting to the flattening and folding model yielded good results. However, the harder copper flakes showed increased resistance to flattening. The flattening rate constants are systematically lower than the corresponding flattening rate constants for the two coarsest size classes of each test. This had not been observed with lead. For the Bond rod mill, breakage was significant, to the extent that the explicit breakage model (with flattening and folding) yielded an excellent fit.

**Chapter 7: Cascadography- An Attempt at  
Characterizing the Shape of Lead Fragments**

## 7.1 Introduction

Density, shape and size of particles are three important properties which can characterize flowing, packing, reacting, sintering, compressibility and segregating of particles<sup>(193, 194)</sup>. The shape of a particle is physically defined as the recognized pattern of relationships among all of the points which constitute the external surface<sup>(195)</sup>. The shape of particles is not only important in the mineral industries, but also in several other fields such as dentistry, concrete, and abrasives<sup>(196)</sup>.

Particle shape has been linked to the natural structure of materials and the type of comminution process and unit used<sup>(196, 197)</sup> to produce the particle i.e. its "history". For example, it has been reported that product angularity increases with mill type in the order: ball mill, ring roll mill, hammer mill<sup>(196)</sup>.

Ground gold flakes display various shapes<sup>(9, 10)</sup> from very serrated thin flakes to nearly perfect spheres. Gold particle shape is as important as mass, in their deposition in alluvials and their recovery<sup>(198, 199)</sup>, most particularly by gravity methods. This can in part be linked to initial settling velocity<sup>(124, 200)</sup>, although recent work suggests that shape also affects the ability of flakes to percolate a bed of gangue<sup>(201)</sup>. There is, as a result, almost as much incentive to characterize particle shape as particle size.

Particles can also be segregated according to their shape, as a means to achieve more uniform products of greater value. This has been effected with the use of gravitational, centrifugal and vibrational forces<sup>(202, 203)</sup>. This shape-based separation also provides an indirect means of characterizing particle shape (i.e. by inference). Various separation approaches have been used, including:

- The particle velocity on a tilted solid wall
- The time the particle passes through a mesh aperture

- The particle cohesive force to a solid wall
- The particle settling velocity in liquid

In the first group, several methods are classified on the basis of the particle shape and velocity on any sort of wall: shape separation by tilted plate<sup>(202, 203)</sup>, tilted rotating disk<sup>(204, 205, 206)</sup>, tilted rotating cylinder<sup>(207, 208, 209, 210)</sup>, tilted vibrating trough, and tilted chute<sup>(202)</sup>. In the second group, the shape of particles is correlated by how long they take to pass through a mesh aperture<sup>(211, 212)</sup>. There are several methods in this group such as: tilted vibrating screen, vibrating stacked screens (sieve-cascadograph)<sup>(202, 213)</sup>, and rotating cylindrical sieve<sup>(202, 214)</sup>. One other way to separate particles based on their shape is the settling velocity method. Particles in a fluid which encounter a drag force, whose coefficient,  $C_D$ , depends on the particle shape, as well as the particle Reynolds number,  $Re$ <sup>(202, 215)</sup>.

For the purpose of studying gold particles, indirect methods are attractive, as they eliminate the need to extract and measure individual particles, which may prove nearly impossible for samples containing only a few ppms of gold. From the above indirect methods, cascadography is the most attractive for this work, as it most closely resembles screening, the other characterization which was extensively used. In this study the response of two lead fragments samples to cascadography will be correlated to their recoverability by gravity, as measured with a Mozley Laboratory Separator (MLS)<sup>(216)</sup>. If the cascadography response can be correlated with the gravity response, it could prove very useful for future studies.

## 7.2 Theory of Cascadography

Cascadography, a form of particle chromatography, is a method to separate particles based on their physical shape differences, which can be easily applied on a lab-

scale<sup>(217, 218)</sup>. Cascadographs are specifically designed to characterize powders, abrasives and comminuted material, food grains such as wheat and corn, and other material like, sands and soils<sup>(219)</sup>. The range of particle sizes that can be analyzed is in the 0.075-2 mm, but minor modification of equipment should extend this range, potentially with upper size range of 10 cm<sup>(220)</sup>.

Cascadography characterizes the particle shape distribution in a sample of particles by measuring the rate at which they pass through a column of identical sieves<sup>(219, 221)</sup>. A cascadograph is made from stack of "n" identical sieves which is shaken in vibrating Ro-Tap machine. Feed particles from one size class are placed on the top sieve and shaking is started. Particles exit the cascadograph from the last sieve at the bottom, and at regular interval times, the pan content is extracted<sup>(220)</sup>. Figure 7.1 shows a cascadograph consists of a stack of "n" sieves, all of the same mesh size.

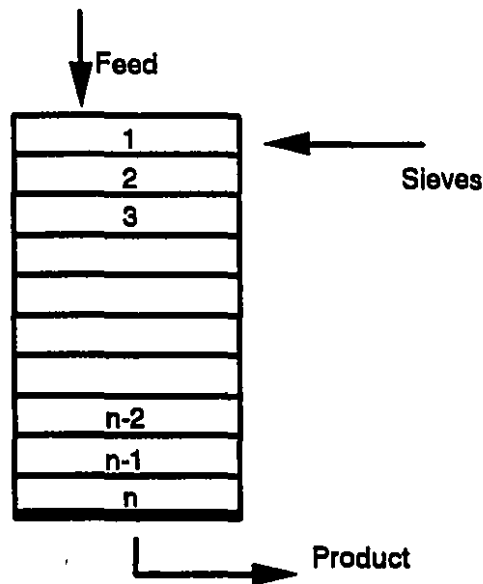


**Figure 7.1:** A schematic of a cascadograph (Adapted from Meloy & Durney<sup>(220)</sup>).

The fundamentals of cascadography are based on the residence time of each particle during the screening or sieving. Each particle has its average residence time on

an individual sieve, which is correlated to its shape. Thus, two particles of identical size but different shape would pass through a sieve at different rates<sup>(219)</sup>. This difference can be amplified if  $n$  screens, rather than a single one, are used. Measuring the accumulation of particles in the pan as a function of time would define a residence time distribution for the whole stack, or the flowrate whose peaks identify a group of particles with similar residence times as shown in Figure 7.2.

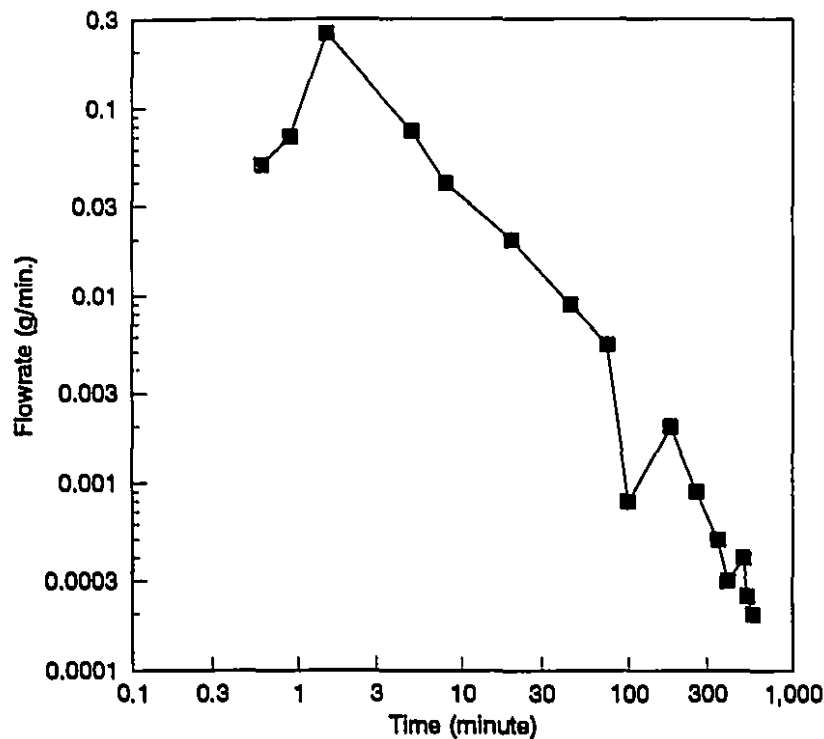


**Figure 7.2:** A typical plot of mass flowrate vs. residence time of a cascadograph test (Adapted from Meloy & Durney<sup>(220)</sup>).

It is argued<sup>(220)</sup> that monoshaped and sized particles would not display such peaks, which are then an evidence of non-homogeneous material. To understand better how a non-homogeneous material responds to cascadography, it is appropriate to begin with a theoretical analysis of how monosized and shaped particles behave. Considering a single screen, the rate at which particles go through can be written as follows:

$$\frac{N}{N_o} = e^{(-s_{rc}t)} \quad (7.1)$$

If n-1 such screens are stacked (i.e. the pan in  $n^{\text{th}}$  position), a similar equation can be derived:

$$\frac{dN_n}{dt} = \frac{N_o}{(n-2)!} s_{rc}^{(n-1)} t^{(n-2)} e^{(-s_{rc}t)} \quad (7.2)$$

where N is the current number of particle on the sieve, and  $N_o$  is the original number of particles on the sieve,  $s_{rc}$  is the sieve rate constant, which is characteristic both of the particle and the operating conditions of the sieve, t is the time, and  $N_n$  is the amount of material in a pan placed below n-1 sieves. This equation is analogous to a residence time distribution for n-1 identical perfect mixers in series<sup>(222)</sup>. Integration of Equation 7.2 yields the following equation in which the number of terms is equivalent to the number of the sieves in the cascadograph:

$$N_n = -\frac{N_o e^{s_{rc}t}}{(n-2)! s_{rc}} \left[ t^{(n-2)} - \frac{(n-2)t^{(n-3)}}{(-s_{rc})^{-1}} + \frac{(n-2)(n-3)t^{(n-4)}}{(-s_{rc})^{-2}} - \dots + \frac{(-1)^{(n-2)}(n-2)!}{(-s_{rc})^{(n-2)}} \right] \quad (7.3)$$

If the material on the sieve is not homogeneous (heterogeneously shaped particles), there is a variety of sieving rates for each of the different type of particle, and the above equations do not hold, since  $s_{rc}$  will vary with particle shape<sup>(219, 221)</sup>.

## 7.3 Experimental Section

### 7.3.1 Apparatus & procedure

Two samples of lead fragments, 46.81 g of 1.00-1.18 mm, and a 20.87 g of 0.710-0.850 mm, were used in a cascadograph made of ten 1.18 mm screens for the first sample and ten 0.850 mm screens for the second. A standard Ro-Tap machine was used to vibrate the cascadograph.

The two samples were first fed to a Mozley Laboratory Separator (MLS) equipped with a v-shape tray. The MLS was operated to produce one tail and three concentrates, of approximately similar weight. The four products were then characterized using the cascadograph in twenty one-minute increments.

#### 7.4 Results and Discussion

Figures 7.3 to 7.10 show SEM photos of flakes recovered from the various products of the two tests. It is immediately apparent that there is a large variety of shape, from very regular flaked, folded flakes, rolled-up flakes into cylindrical and cigar shapes, and even spherical particles. These few particles are only part of the much larger sample size examined. There was no particular trend as to where particles of various shapes reported, i.e. spheres were encountered in the tails as well as the third concentrate of either tests.

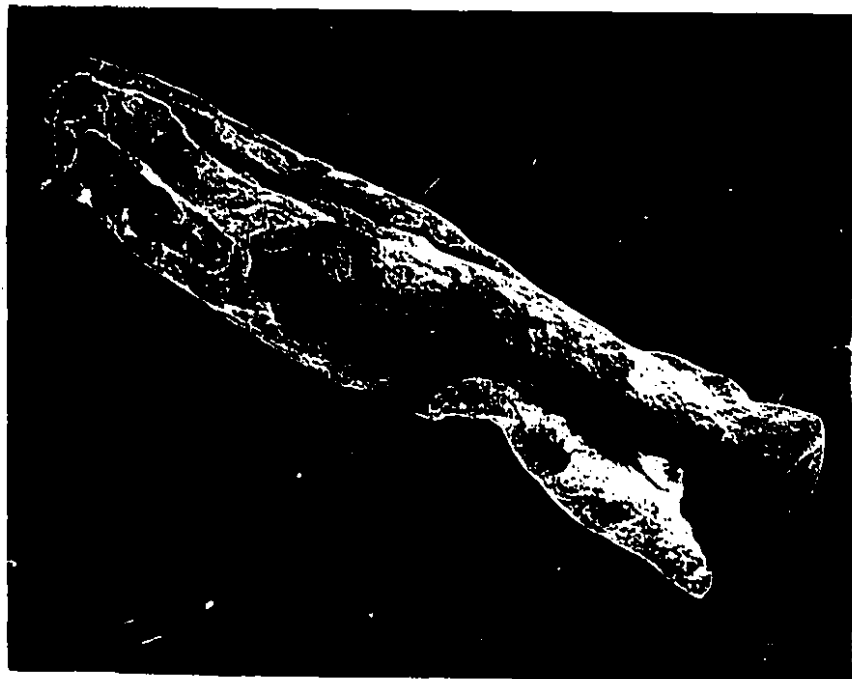


Figure 7.3: An elongated particle, 3<sup>rd</sup> concentrate of MLS test, (feed: 0.710-0.850 mm).

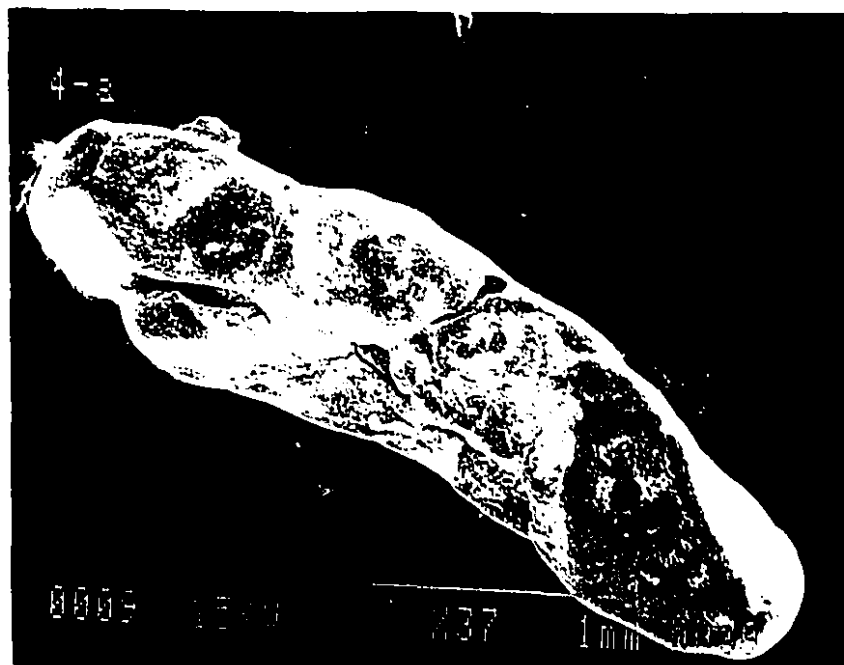


Figure 7.4: An elongated particle, 1<sup>st</sup> concentrate of MLS test, (feed: 0.710-0.850 mm).



Figure 7.5: A flattened particle, tail of MLS test, (feed: 0.710-0.850 mm).

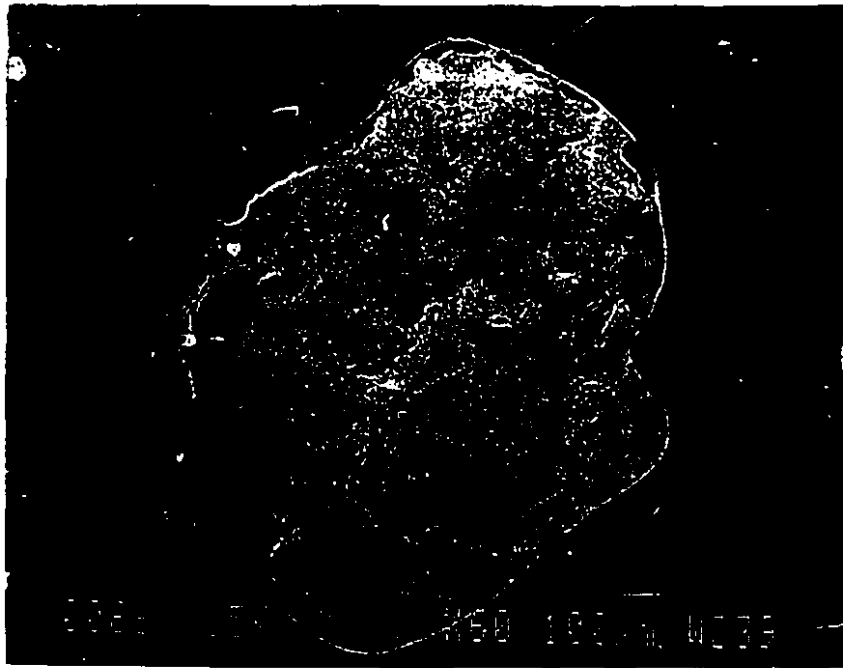


Figure 7.6: A flattened particle, 3<sup>rd</sup> concentrate of MLS test, (feed: 0.710-0.850 mm).



Figure 7.7: An elongated particle, 1<sup>st</sup> concentrate of MLS test, (feed: 1.00-1.18 mm).

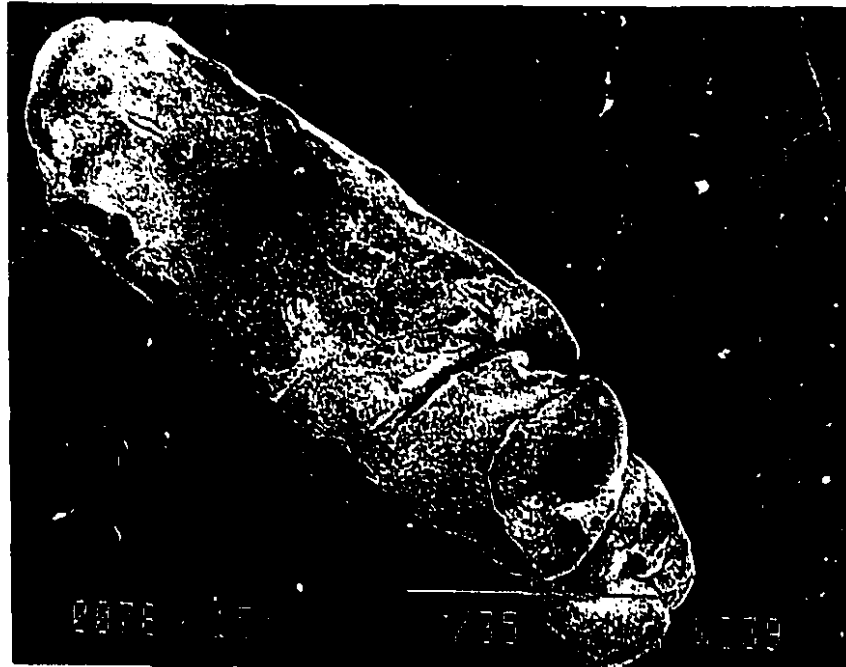


Figure 7.8: An elongated particle, 3<sup>rd</sup> concentrate of MLS test, (feed: 1.00-1.18 mm).

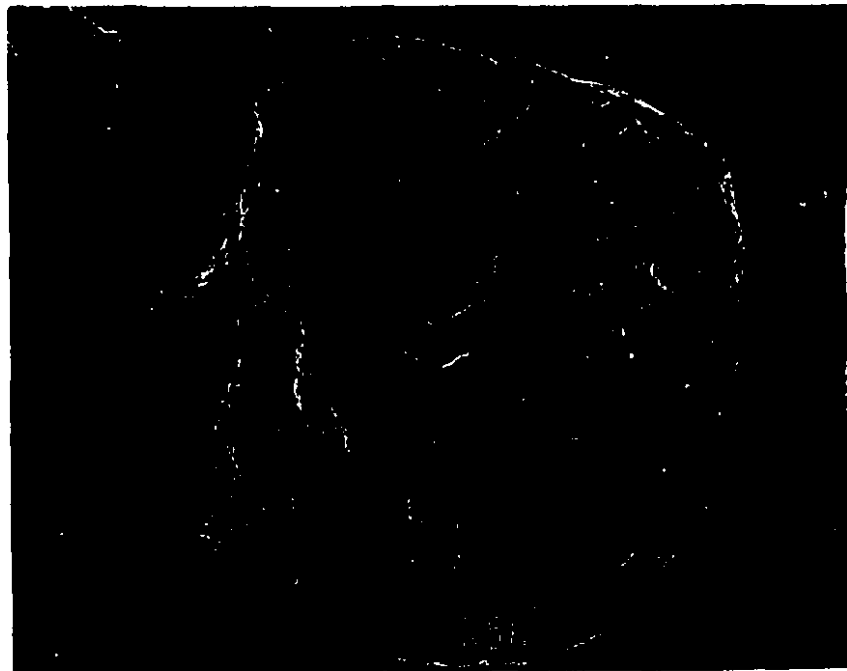
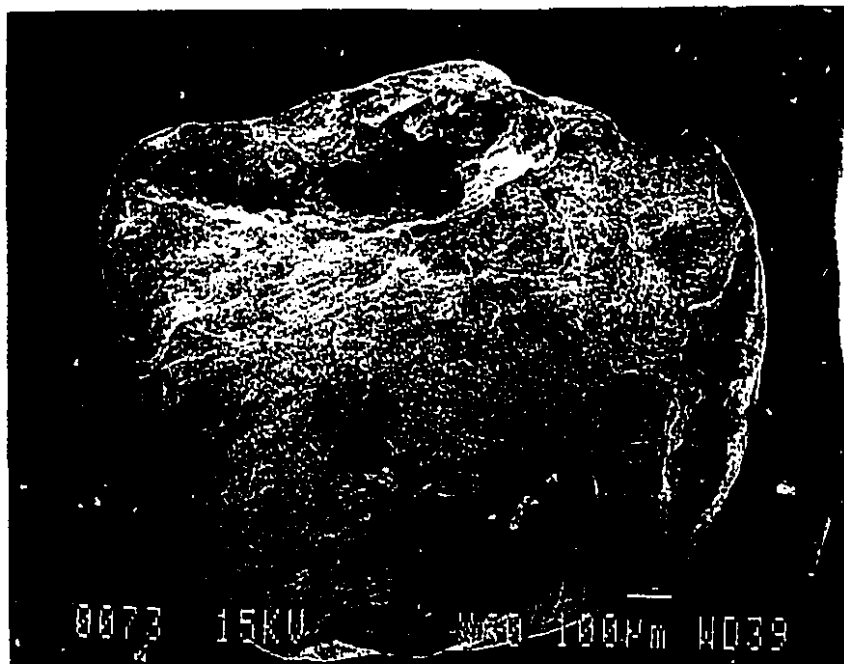


Figure 7.9: A flattened particle, 2<sup>nd</sup> concentrate of MLS test, (feed: 1.00-1.18 mm).



**Figure 7.10:** A flattened particle, 3<sup>rd</sup> concentrate of MLS test, (feed: 1.00-1.18 mm).

Table 7.1 presents the results of MLS test for both samples. The cascadography results are presented in Table 7.2 for sample 1, and Table 7.3 for sample 2. For the 0.710-0.850 mm sample, about 50% of the mass of each MLS product had left the cascadograph after 1 minute. After 20 minutes between 85-89% of the mass had been recovered in the pan. For the 1.00-1.18 mm sample, even more material left during the first minute. After 20 minutes, between 94-98% of the material had been recovered.

**Table 7.1:** The results of MLS tests for each sample.

Feed Size (mm)	MLS Feed (g)	MLS Products (g)			
		Tail	1 <sup>st</sup> Conc.	2 <sup>nd</sup> Conc.	3 <sup>rd</sup> Conc.
0.710-0.850	20.87	8.41	3.13	4.08	4.20
1.000-1.180	46.81	12.91	10.84	9.50	11.42

Figure 7.11 presents the cascadowgraph curves of the first test (0.710-0.850 mm sample) in the format suggested by Meloy and Durney<sup>(220)</sup>. It is difficult to detect any significant differences between the four products. Figure 7.12 shows the same curves for the second test (1.00-1.18 mm sample), much with the same conclusions. Both tests show "peaks" in the 10 to 20 minute range, but these are due to the low number of particles leaving the cascadowgraph, as opposed to sudden changes in shape.

Because of the presence of noise, it was decided to examine the data differently. The data were converted to cumulative mass percent discharged as a function of time i.e. much as a residence time distribution. Two working hypotheses were made. First, it was assumed that all mass that leaves the cascadowgraph had done so after 20 minutes (as in Table 7.4 and Figure 7.13(c), and 7.13(d)). Second, it was assumed that all mass would eventually leave the cascadowgraph. Table 7.5 and Figure 7.13(a), and 7.13(b) give the resulting residence time distribution (RTD) for the two tests and two hypotheses.

Figure 7.13 is difficult to analyze. The two hypotheses do not yield very different conclusions. In any of the four presentations, the differences between the four MLS products are small. There seems to be a loose link between recoverability and response, but the link is inverted for the two tests. Thus, for the 0.710-0.850 mm, the third concentrate leaves the cascadowgraph more slowly, whereas for the 1.000-1.180 mm, it is the fastest to leave. In all fairness to cascadowgraphy, given the complexity of MLS separation, and the lack of apparent link between shape and response to MLS separation, a strong correlation between cascadowgraphy and MLS responses would have been surprising. In general individual particles weight did not show very significant difference. Figure 7.14 shows the average particle weight of cascadowgraphy test using 1.00-1.18 mm sample which slightly decreases with increasing sieving time.

Table 7.2: Cascadography tests results on MLS products, (feed: 0.710-0.850 mm).

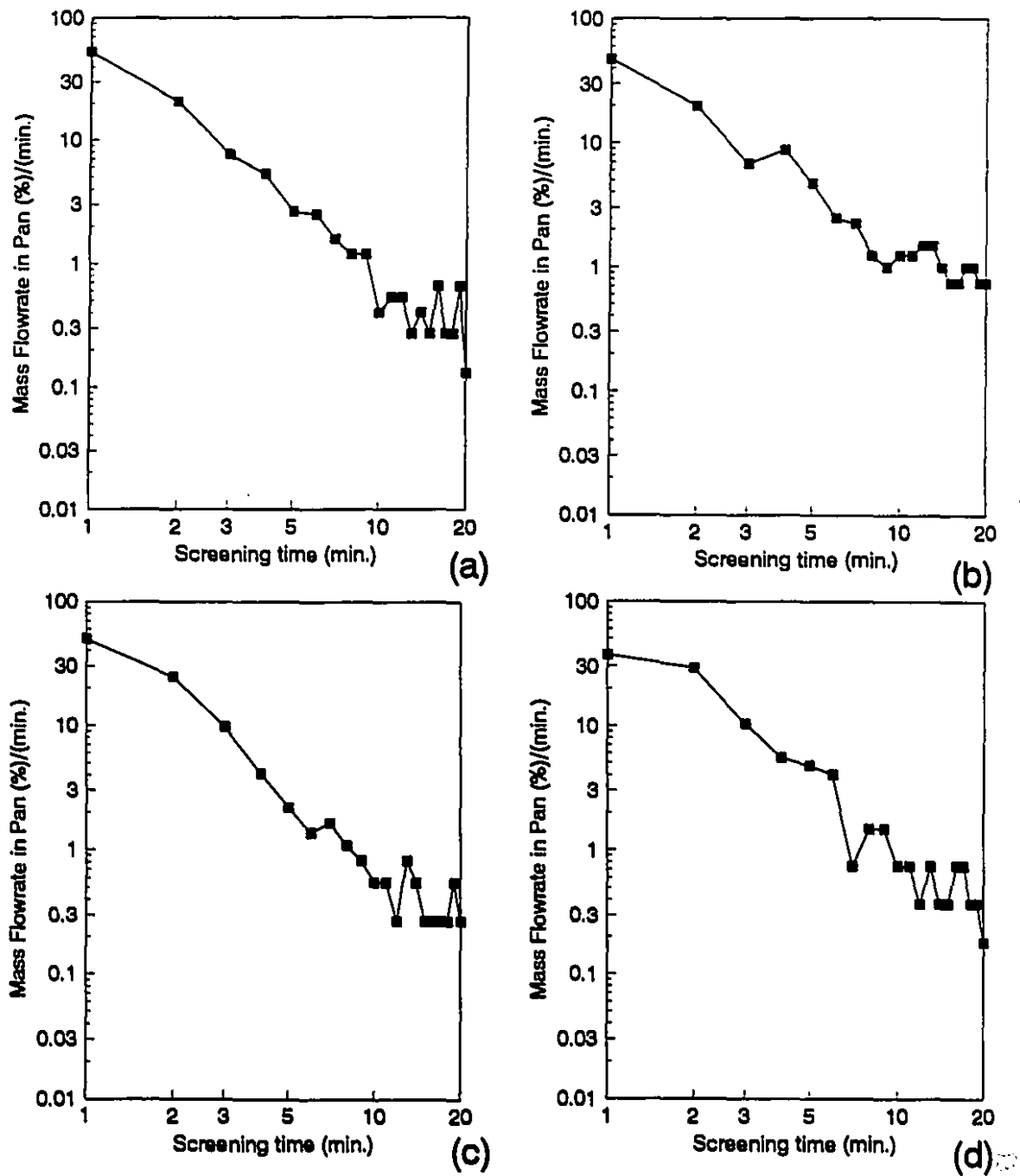
Sieving Time (minute)	Weight on Pan (%) or Mass Flowrate (%)/(minute)			
	Tail	1 <sup>st</sup> Conc.	2 <sup>nd</sup> Conc.	3 <sup>rd</sup> Conc.
1	52.92	36.83	49.73	47.25
2	20.56	29.10	24.59	19.75
3	7.69	10.31	9.84	8.75
4	5.31	5.52	4.10	4.75
5	2.65	4.79	2.19	2.50
6	2.52	4.05	1.37	2.25
7	1.59	0.74	1.64	1.25
8	1.19	1.47	1.09	1.00
9	1.19	1.47	0.82	1.25
10	0.40	0.74	0.55	1.25
11	0.53	0.74	0.55	1.50
12	0.53	0.37	0.27	1.50
13	0.27	0.74	0.82	1.00
14	0.40	0.37	0.55	0.75
15	0.27	0.37	0.27	0.75
16	0.66	0.74	0.27	1.00
17	0.27	0.74	0.27	1.00
18	0.27	0.37	0.27	1.00
19	0.66	0.37	0.55	0.75
20	0.13	0.18	0.27	0.75
Weight on Sieve (%)	10.61	14.73	11.48	12.50
Total	100.00	100.00	100.00	100.00

Table 7.3: Cascadography tests results on MLS products, (feed: 1.00-1.18 mm).

Sieving Time (minute)	Weight on Pan (%) or Mass Flowrate (%)/(minute)			
	Tail	1 <sup>st</sup> Conc.	2 <sup>nd</sup> Conc.	3 <sup>rd</sup> Conc.
1	64.90	62.07	62.79	76.60
2	18.65	22.30	20.20	13.79
3	6.76	6.95	5.82	3.47
4	2.36	2.80	3.51	1.60
5	1.71	1.45	1.98	1.16
6	0.73	1.06	1.54	0.71
7	0.65	0.68	0.88	0.89
8	1.22	0.58	0.66	0.18
9	0.57	0.10	0.44	0.44
10	0.33	0.29	0.66	0.18
11	0.41	0.29	0.11	0.36
12	0.16	0.10	0.33	0.18
13	0.24	0.10	0.11	0.00
14	0.08	0.19	0.22	0.00
15	0.24	0.29	0.11	0.00
16	0.24	0.10	0.11	0.09
17	0.24	0.29	0.22	0.09
18	0.24	0.10	0.11	0.09
19	0.08	0.10	0.11	0.09
20	0.16	0.19	0.11	0.09
Weight on Sieve (%)	5.70	4.83	4.39	1.51
Total	100.00	100.00	100.00	100.00







**Figure 7.11:** Mass flowrate percent in pan vs. sieving time in cascadography tests (feed: 0.710-0.850 mm), for four different products of Mozley Laboratory Separator; a: Tail, b: 3<sup>rd</sup> concentrate, c: 2<sup>nd</sup> concentrate, d: 1<sup>st</sup> concentrate.

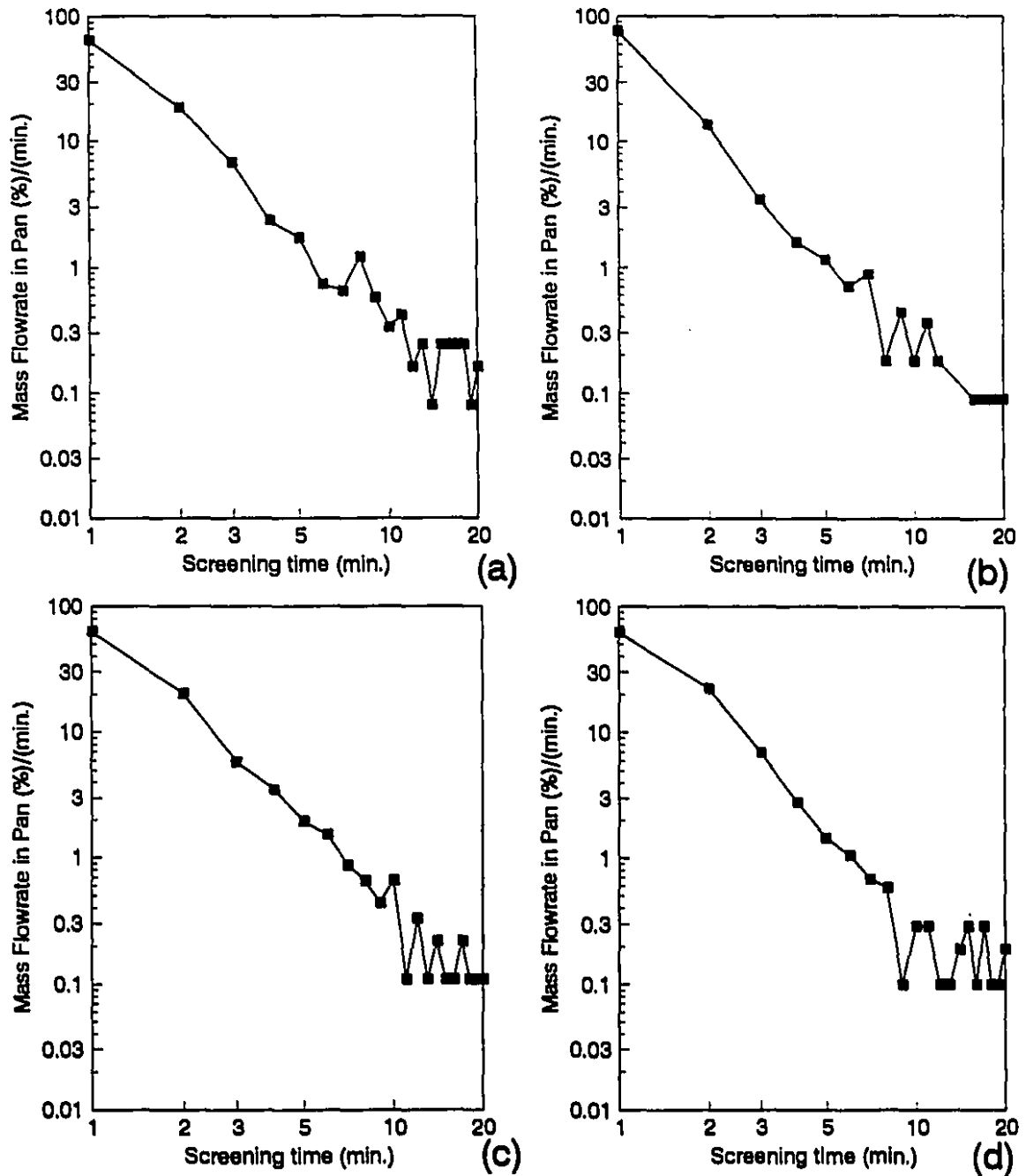


**Figure 7.12:** Mass flowrate percent in pan vs. sieving time in cascadography tests (feed: 1.00-1.18 mm), for four different products of Mozley Laboratory Separator; a: Tail, b: 3<sup>rd</sup> concentrate, c: 2<sup>nd</sup> concentrate, d: 1<sup>st</sup> concentrate.

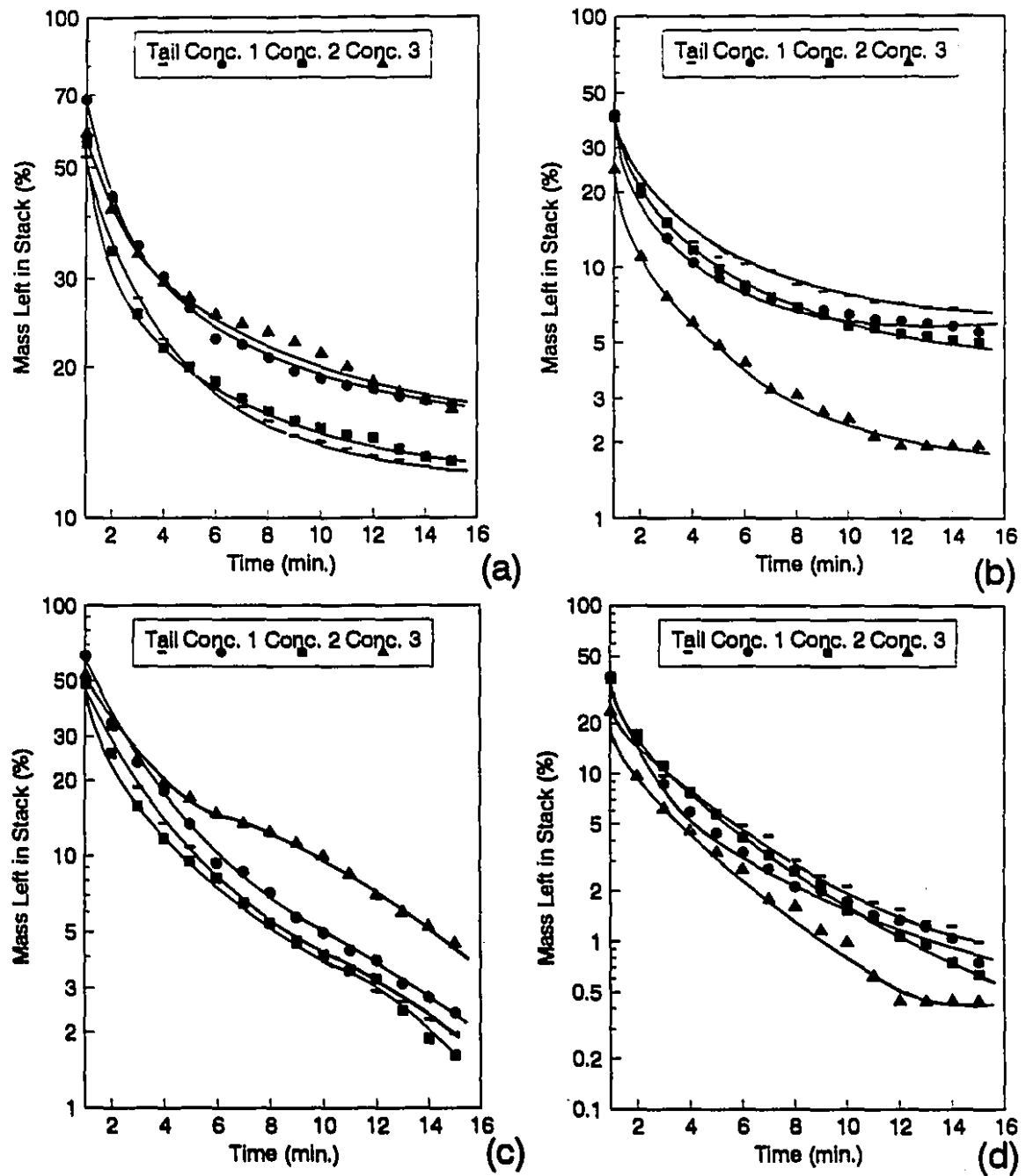


Figure 7.13: Mass left in stack vs. sieving time in cascadography tests; a: 2<sup>nd</sup> assumption, and 0.710-0.850 mm feed, b: 2<sup>nd</sup> assumption, and 1.000-1.180 mm feed, c: 1<sup>st</sup> assumption, and 0.710-0.850 mm feed, d: 1<sup>st</sup> assumption, and 1.000-1.180 mm feed.

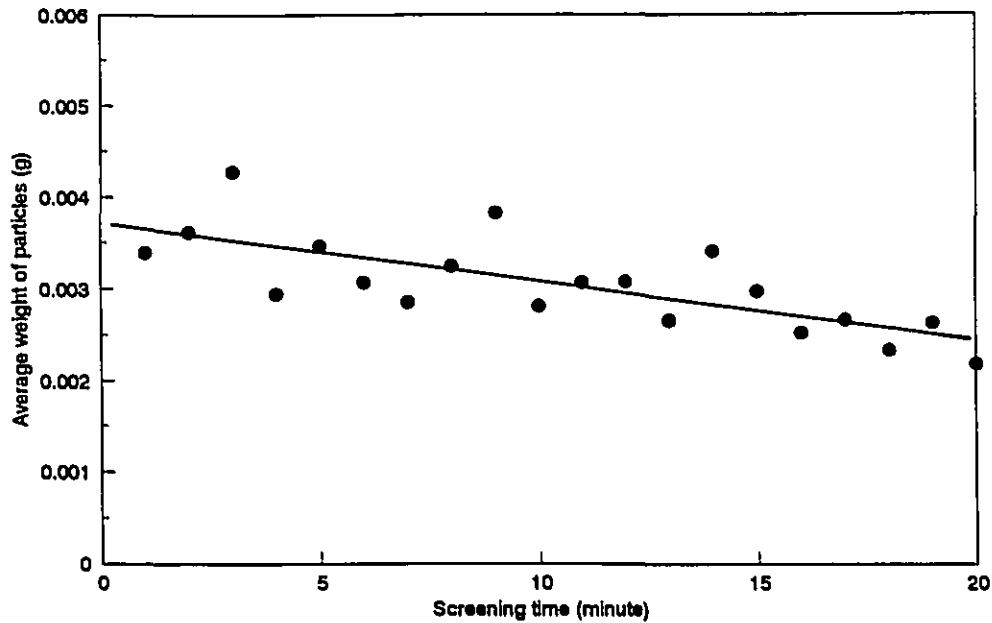


Figure 7.14: Average weight of particles in cascadography test (feed: 1.00-1.18 mm).

## 7.5 Conclusions

The attempt at correlating cascadography and gravity separation (i.e. the effect of shape on separation performance) was probably doomed, but such is often the fate of exploratory work. The simple cascadography test did demonstrate the ability of cascadography to effect a slight separation which could be correlated with particle weight. The probability analysis of the cascadography response is far more complex, and would probably require a more powerful approach than what was suggested by Meloy and Durney<sup>(220)</sup> (such as a Fourier transform), to generate a continuous probability density function (PDF) of sieve rate constants, rather than a discrete one. This would also represent more realistically the continuum of variation in particle shape.

Future work would do well to consider the complexity of the problem and rely first on experimental work with synthetic, well defined and extremely mono-sized material. From the perspective of gold gravity-based research, cascadography does not

offer much potential, which probably explains why it was not considered in earlier work

(124, 198, 200)

**Chapter 8: Breakage Function and Recoverability of  
Free Gold**

## 8.1 Introduction

The behaviour of gold in industrial grinding circuits, and more specifically how its malleability decreases its specific rate of breakage, is now a well established fact<sup>(10)</sup>, which prompted this investigation. In chapters 4 and 5, the grinding of lead shots, flakes and fragments clearly reflected the impact of malleability, as particles displayed a higher propensity for flattening than breaking, especially in a less energy intensive tumbling environment (i.e. small ball mill). Folding was also observed, but is not as frequently as flattening. However, when silica was added to the mill charge, lead's behaviour was dramatically altered, and very significant breakage took place, even in the low energy grinding environment.

In chapter 6, we saw that copper fragments displayed a similar behaviour, although copper's hardness, being greater than lead's, slowed down the overall kinetics of all transfers, and prevented significant breakage from taking place in the Bond ball mill, i.e. the unit of intermediate specific energy, and any detectable breakage from occurring in the small ball mill.

Gold, of hardness intermediate between that lead and copper, should display an intermediate behaviour. However, its behaviour in a grinding unit will be significantly affected by the presence of gangue. Laboratory studies aimed at understanding this behaviour should include a gangue phase. This work should also generate a characterization of how gold fragments and their progeny respond to gravity recovery, as one of the primary objectives of this work is to generate data that can be used in a simulator of gold gravity recovery in grinding circuits.

To understand the grinding and recoverability of gold we will consider limited breakage (i.e. the so-called "single breakage event") and measure: a) the rate of

disappearance from the parent class, b) the distribution of fragments in the other size classes, both coarser and finer than the parent class, and c) what proportion of the progeny and unbroken material is gravity recoverable. The first concept corresponds to the selection function, the second to the breakage function, and the third is relatively new.

The reader might wonder why gravity recovery is specifically considered. The economic incentive for gold gravity recovery has been discussed elsewhere<sup>(11, 12, 223, 224)</sup>. Suffice to say, gold's very special behaviour dictates that gravity recovery be used on the circulating load of grinding circuits, which makes the interaction between gravity and grinding particularly important.

The above discussion is a useful guide to develop the experimental methodology that will be used in this chapter. First, the study will focus on gold particles that are liberated and can be concentrated into a relatively high grade product. This corresponds to the concept of *Gravity Recoverable Gold (GRG)*, which has been developed and investigated by other members of the McGill gold gravity research group<sup>(11, 12)</sup>. Thus, feedstock for this work will be either gold that has been recovered by gravity in industrial circuits (Hemlo) or pre-concentrated by Laboratory Knelson Concentrator, LKC, (Casa Berardi and Snip).

The Knelson Concentrator (KC) is a centrifugal device designed to recover semi-continuously the heavy minerals<sup>(225)</sup>, consisting of a rotating bowl with rings that are partially fluidized by water injection<sup>(225, 226, 227)</sup>. A centrifugal force of the order of 60 times the force of gravity acts on the particles. Information on the Knelson Concentrator performance has been presented in several papers<sup>(228, 229, 230, 231)</sup> and is not detailed here. A scaled-down version of the production units, the LKC, has been extensively used at McGill, in particular to isolate GRG from a large sample (5-120 kg) into a relatively

small mass, typically 100 g, that can be screened and assayed for gold content<sup>(232)</sup>. Figure 8.1 shows a diagram of the laboratory LKC, which will be used for this work. It has been extensively studied<sup>(227, 232)</sup>, and shown to give reliable estimates of GRG, if operated optimally.

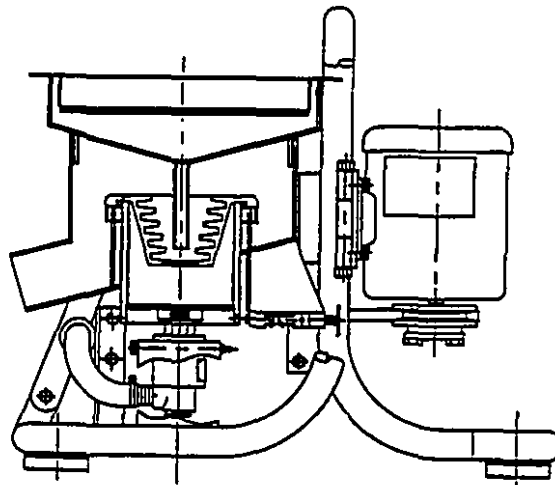


**Figure 8.1:** The schematic diagram of the Laboratory Knelson Concentrator (reprinted with permission from Knelson International Sales Inc. manual<sup>(229)</sup>).

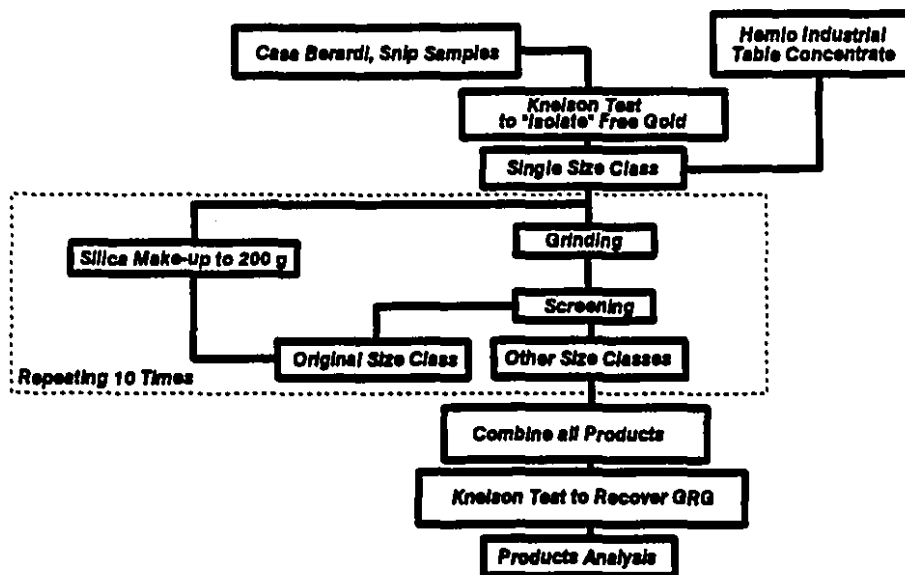


**Figure 8.2:** The schematic of the methodology of the tests.

### 8.2 Methodology

The basic methodology was based on three steps, namely the isolation of GRG, its incremental grinding and recovery. This basic approach is shown in Figure 8.2. Figure 8.3 shows more detail specific to the Casa Berardi tests. The boxed procedure (Figure 8.3) is at heart of the test. Both upstream and downstream manipulations are aimed at isolating GRG.

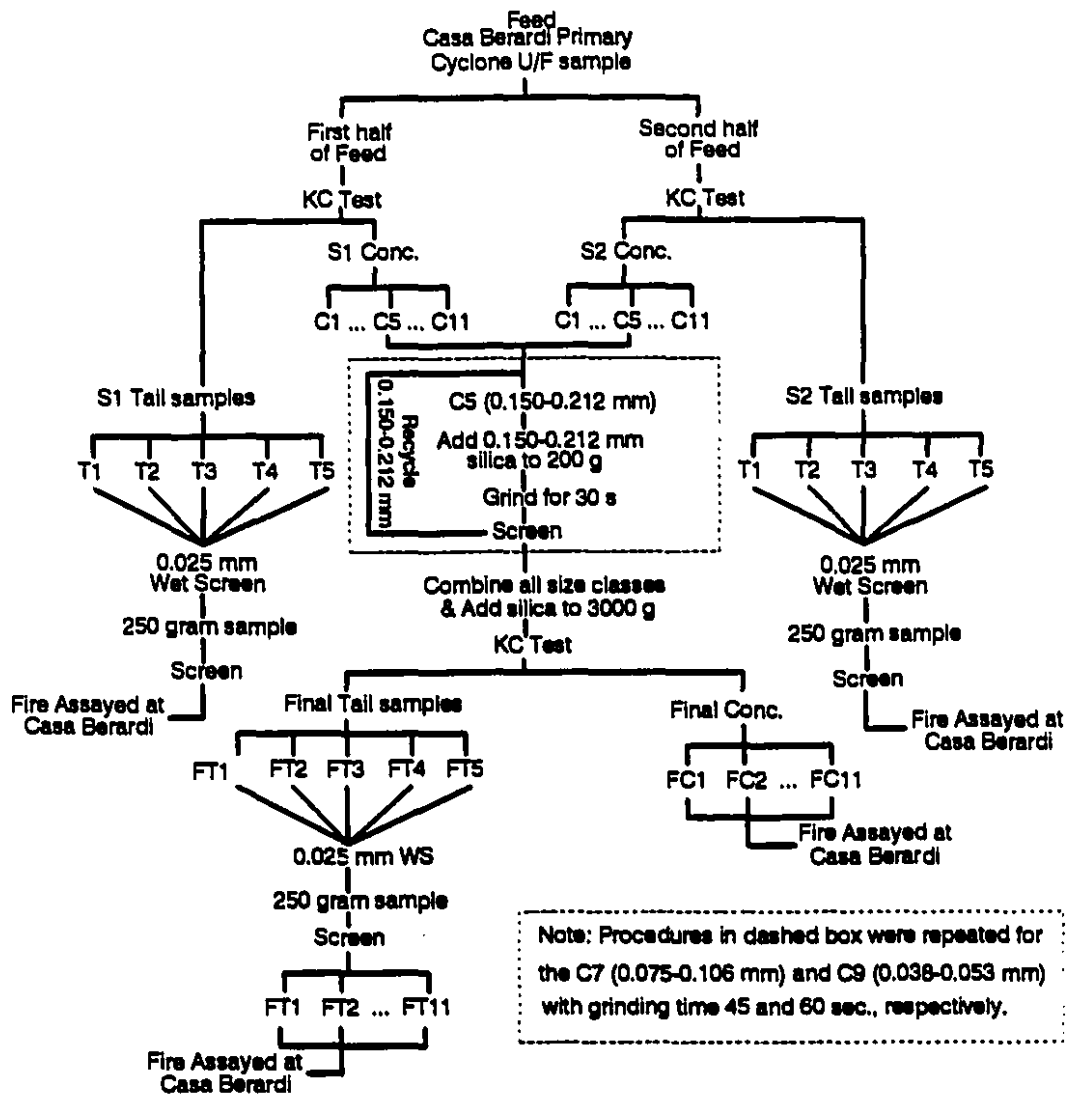


Figure 8.3: A typical flowsheet of Casa Berardi sample tests.

### 8.2.1 Isolating GRG

For the Casa Berardi tests GRG was isolated by processing a 10.5 kg sample of primary cyclone underflow with a Laboratory Knelson Concentrator (LKC). To maximize GRG recovery, the sample was halved and each half processed separately. The LKC concentrates and samples of the tails were then screened. The two concentrates were combined for the 0.150-0.212 mm, 0.075-0.106 mm, and 0.038-0.053 mm size classes. The other concentrate samples and all tails size classes were fire assayed for gold at the Casa Berardi laboratory.

For the Snip ore, a 3.8 kg sample of jig concentrate from the first hatch was processed with the LKC. All of the concentrate and 250 g of tails were screened from 1.18 to 0.025 mm. Most concentrate size fractions were used for further testing. The unused concentrate fractions and all of the tails fractions were assayed for the gold at Snip.

The Hemlo tests were performed to supplement the rather noisy Casa Berardi and Snip tests results. To minimize errors, substantially larger gold masses were used. As it would have been impractical to generate so much gold with a LKC, screened fractions of a table concentrate sample were used. As most fractions graded more than 70% gold, it was not necessary to isolate their GRG. The fractions were re-screened individually and into subsamples, the coarsest being 1.18-1.70 mm, and the finest -0.025 mm.

### 8.2.2 The grinding tests

Using the size fractions as prepared in section 8.2.1, each sample was first combined with silica sand from Daubois Inc. of the same size class to a total mass of 200 g. Material was then incrementally ground either in the small or the Bond ball mills.

After each increment, the ground product was dry screened and all material other than that in the original size class was set aside and replaced with silica sand, to make up the original 200 g for the next increment.

For the three Casa Berardi tests, incremental grinding times were different, 30 seconds for the 0.150-0.212 mm sample, 45 seconds for the 0.075-0.106 mm, and 60 seconds for the 0.038-0.053 mm sample. The incremental grinding times for the Snip tests were also different for each test, from 30 seconds to 60 seconds, as shown in Table 8.1. For all Hemlo tests, the incremental grinding time was increased to 5 minutes for all tests, to a total grinding time of 50 minutes (to achieve more grinding than for the first two tests series). Significant gold quantities were used, as shown in Table 8.2.

**Table 8.1:** Incremental grinding times for the Snip tests.

Size Classes (mm)	Incremental Grinding Time (s)	
	Small Ball Mill	Bond Ball Mill
0.600-0.850	45	-
0.425-0.600	45	30
0.300-0.425	45	-
0.212-0.300	60	60
0.150-0.212	45	-
0.106-0.150	45	-
0.075-0.106	45	-
0.053-0.075	45	-
0.038-0.053	45	-

Table 8.2: Table concentrate weight used for the Hemlo tests.

Size Class (mm)	Sample Weight (g)	
	First Test	Repeated Test
1.180-1.700	1.08	-
0.600-0.850	1.50	-
0.300-0.425	3.00	-
0.150-0.212	3.00	6.00
0.053-0.075	3.00	-
0.038-0.053	3.00	3.00
0.025-0.038	3.00	-
-0.025	3.00	-

### 8.2.3 Recovery of GRG

After incremental grinding, all samples were mixed and silica from the initial size class was added to obtain a 3 kg sample. The rationale of this step is to minimize yield for the subsequent KC test, to insure that gold recovered is truly gravity recoverable<sup>(227)</sup>. This sample was then processed with a LKC, whose concentrate and tails were analyzed with the standard McGill procedure<sup>(233)</sup> i.e. screening of the concentrate and part of the tails from 0.025 mm to 0.600 mm, and fire assaying of each size class at the respective mine sites.

## 8.3 Results and Discussion

### 8.3.1 Casa Berardi tests

Table 8.3 shows the metallurgical balance of one of the Casa Berardi test. The

3 kg sample assays 30.36 g/t (i), but comes originally from 10.19 g of S1 and 12.92 g of S2 (Appendix III, Page A58). Thus, the original LKC concentrates of the two tests averaged 3941.1 g/t in the 0.150-0.212 mm size class. After grinding, 60.36% of the gold remains in the original size class (ii); only 2.37% has moved to the adjacent coarser size class (iii). The remainder has moved to finer size classes, of which most is in the 0.105-0.150 mm, 16.82% (iv). Most of the gold, 91.87% (v) remains gravity recoverable. Gold still in the original size class is virtually all gravity recoverable, 99.80% (vi), but recoverability drops to 50.27% for the -0.025 mm (vii).

Table 8.3: A typical metallurgical balance for the Casa Berardi first test.

Size (um)	CONCENTRATE				TAILS				FEED			
	Weight (g)	% Weight	Grade g/t	Rec. (%)	Weight (g)	% Weight	Grade g/t	Rec. (%)	Weight (g)	% Weight	Grade g/t	Rec. (%)
600	1.87	2.01	96.43	97.71	0	0.02	9.09	2.29	2	0.08	79.03	0.20
420	2.44	2.62	16.84	53.71	4	0.13	9.09	46.29	6	0.21	12.08	0.08
300	7.13	7.66	3.21	66.80	99	3.41	0.12	33.20	106	3.54	0.32	0.04
210	17.36	18.65	119.00	95.87	668	23.00	0.13	4.13	686	22.86	3.14	2.37
150	22.23	23.89	2468.00	99.80	812	27.95	0.13	0.20	835	27.82	65.86	60.36
105	16.41	17.63	918.00	98.35	633	21.79	0.40	1.65	650	21.66	23.58	16.82
75	11.79	12.67	187.00	92.36	391	13.44	0.47	7.64	403	13.42	5.93	2.62
53	6.46	6.94	290.00	87.68	162	5.57	1.63	12.32	168	5.61	12.69	2.35
37	3.47	3.73	497.00	61.20	65	2.22	16.93	38.80	68	2.27	41.41	3.09
25	2.17	2.33	833.00	53.44	22	0.74	73.12	46.56	24	0.79	142.67	3.71
-25	1.74	1.87	2200.00	50.27	30	1.74	75.00	49.73	52	1.74	145.79	8.36
Total	93.07	100.00	899.07	91.87	2907	100.00	2.55	8.13	3000	100.00	30.36	100.00

(v)
(vii)
(vi)
(i)

Feed grade before starting grinding times = 3941.1 g/t

Table 8.4 shows the gold recovery and distribution for all three Casa Berardi tests (i.e. the last concentrate and feed columns of the metallurgical balances, Table 8.3). The highlighted cells correspond to the parent class of each test. Most gold remained in its original size class, 60%, 77% and 78% for the 0.150-0.212 mm, 0.075-0.105 mm, and

0.037-0.053 mm, respectively. Most material leaving the parent class reports to the adjacent size classes, especially the finer one. The weight reporting to the adjacent coarser size class increases dramatically with decreasing size (of the parent class), 2.4% for the 0.150-0.212 mm to the 8.0% for the 0.037-0.053 mm.

Most of the gold is still gravity recoverable, especially if it remains in the parent size class (95.7 to 99.8% gravity recoverable) or reports to adjacent classes (95.7 to 99.6% gravity recoverable). Generally gravity recoverability decreases as the parent size class gets finer or the progeny class gets much finer than the parent class.

**Table 8.4:** The distribution of recoveries to the concentrate and feed distribution of the Casa Berardi tests.

Parent size:→ Progeny size:↓ (µm)	0.150-0.212 mm		0.075-0.105 mm		0.037-0.053 mm	
	Conc. Rec. (%)	Dist. (%)	Conc. Rec. (%)	Dist. (%)	Conc. Rec.(%)	Dist. (%)
0.600-0.850	97.7	0.2	100.0	0.0	100.0	0.0
0.425-0.600	53.7	0.1	100.0	0.0	46.6	0.0
0.300-0.425	66.8	0.0	100.0	0.0	83.0	0.0
0.212-0.300	95.9	2.4	95.4	0.4	90.2	0.2
0.150-0.212	99.8	60.4	91.6	0.9	90.3	0.4
0.105-0.150	98.4	16.8	98.3	4.3	90.6	0.4
0.075-0.105	92.4	2.6	99.8	76.7	89.5	0.7
0.053-0.075	87.7	2.4	99.6	11.7	95.7	8.0
0.037-0.053	61.2	3.1	95.3	1.6	95.7	77.9
0.025-0.037	53.4	3.7	97.0	1.5	96.6	9.9
-0.025	50.3	8.4	92.0	3.0	77.0	2.5
Total	91.9	100.0	99.3	100.0	95.2	100.0

The breakage function of gold was calculated using the two assumptions that 1)

all material in size classes finer than the parent class could be considered broken and 2) grinding increments were small enough to consider secondary breakage negligible. Figure 8.4 shows the cumulative breakage function of gold for the three Casa Berardi tests. The crossing of the lines is suspicious (as it implies that coarser parent particles would yield a finer progeny), and is probably the result of experimental scatter, which comes from the relatively low mass of gold used for each test, 0.569 to 0.091 g. Figure 8.5 shows the selection function of gold, which increases with increasing particle size.

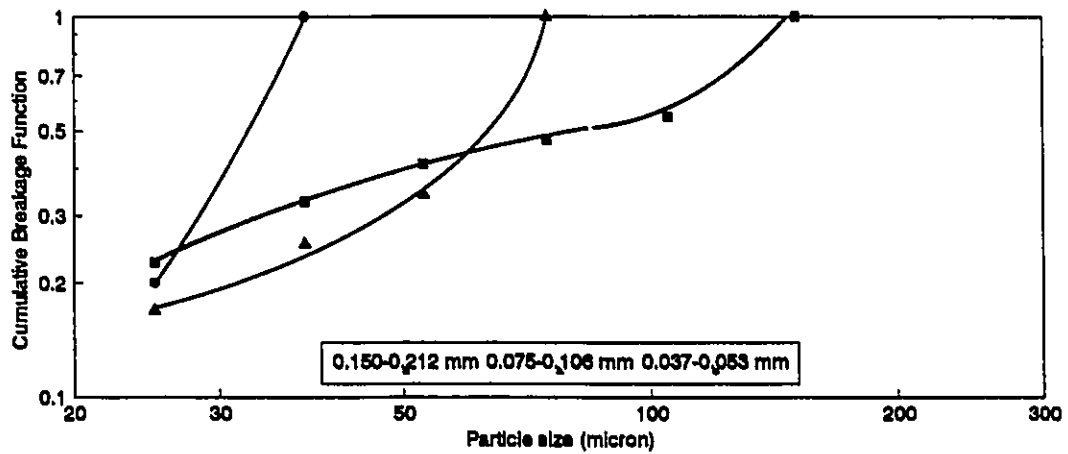


Figure 8.4: Calculated cumulative breakage functions for the Casa Berardi tests.

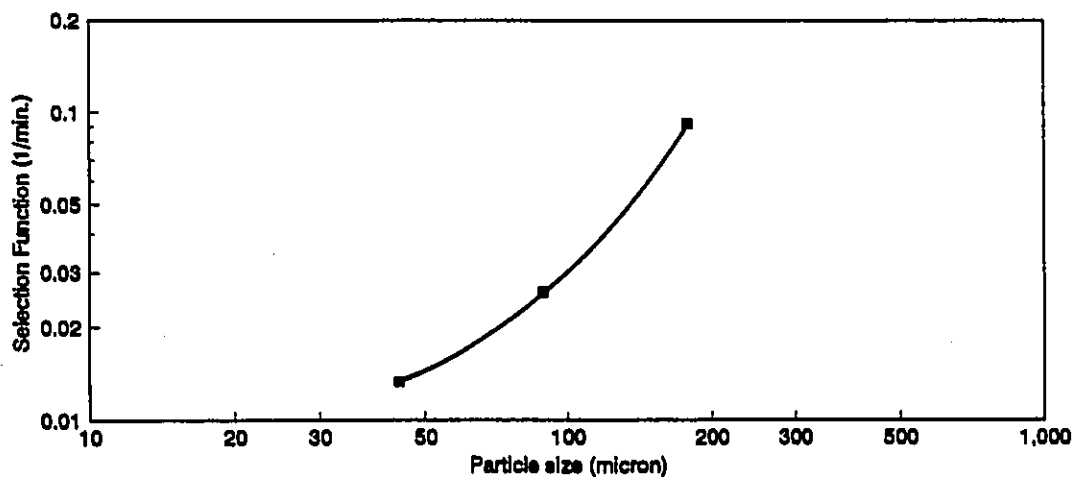


Figure 8.5: Estimated selection functions for the Casa Berardi tests.

## 8.3.2 Snip tests

Table 8.5: The distribution of concentrates recoveries for the Snip tests.

Parent size:→ Progeny size: ↓ (mm)	Recovery of concentrates of different size classes (%)								
	0.600	0.425	0.300	0.212	0.150	0.105	0.075	0.053	0.038
1.180	-	0.0	-	-	-	34.9	-	-	-
0.850	100.0	41.7	100.0	-	-	0.5	-	-	-
0.600	98.8	13.4	0.1	100.0	0.4	0.4	0.4	-	2.1
0.425	98.3	97.4	99.3	0.2	0.6	0.6	48.2	2.2	6.8
0.300	30.7	97.5	99.6	99.8	0.7	97.2	1.0	3.0	2.2
0.212	34.9	60.4	90.1	99.6	98.2	86.2	51.4	2.8	65.6
0.150	91.2	13.7	83.6	94.1	99.8	98.8	92.1	38.5	42.2
0.105	46.9	53.4	57.0	92.1	99.0	99.9	99.1	87.9	51.2
0.075	83.6	87.2	49.7	80.2	90.0	99.3	99.1	90.8	88.7
0.053	51.6	10.1	21.5	55.3	89.7	90.5	92.4	98.6	91.6
0.038	26.6	23.1	30.8	41.5	67.7	89.4	84.6	-*	98.6
0.025	30.5	-*	16.1	29.9	-*	72.2	-*	-*	-*
-0.025	24.4	28.4	37.4	17.3	-*	-*	-*	-*	-*
Total	91.1	77.5	96.3	97.4	98.2	98.6	98.2	94.8	93.1

(\*: No assay available, Note: only the lower end of the progeny classes is shown).

Table 8.5 shows, as Table 8.4 did for Casa Berardi, that unbroken gold is still overwhelmingly gravity recoverable, 97.4% to 99.9%. Recovery appears maximum in the 0.075 to 0.425 mm range, but drops only slightly at both ends. Some assays were unavailable, and as a result, some recoveries could not be calculated, but in general results confirm those of Casa Berardi, in that the lowest recoveries were observed for progeny particles much finer than their parent size class, essentially the -0.075 mm when

the parent class is coarser than 0.212 mm. The gold distribution is shown in Table 8.6. Screening and assaying difficulties generated uncertain results, especially in the finer size classes for the 0.425-0.600 mm parent class. Nevertheless, the overwhelming conclusion is that most gold remains gravity recoverable (over 90%), especially when it remains in the parent size class. There is again a strong indication that fine fragments are much less gravity recoverable, but this conclusion is marred by experimental errors and assaying problems. GRG does show its resilience, as 35 to 89% of gold remained in the parent size class. Significant flattening took place, as testified by the gold reporting to the coarser adjacent size class (0.2 to 41.7%).

Table 8.6: The distribution of feeds for the Snip tests.

Parent size:→ Progeny size:↓ (mm)	Percentages of feeds in different size classes after grinding (%)								
	0.600	0.425	0.300	0.212	0.150	0.105	0.075	0.053	0.038
1.180	0.0	6.1	0.0	0.0	0.0	0.0	0.0	0.0	0.0
0.850	0.2	0.8	0.5	0.0	0.0	0.1	0.0	0.0	0.0
0.600	65.0	2.8	0.2	1.3	0.0	0.2	0.0	0.0	0.4
0.425	21.1	44.4	16.7	0.0	0.2	0.1	0.1	0.6	0.4
0.300	1.9	30.4	71.5	41.7	0.2	2.1	0.1	0.2	1.8
0.212	1.2	1.4	6.0	35.1	8.1	0.4	0.1	0.3	2.6
0.150	1.6	4.3	1.4	18.7	78.7	13.9	0.9	0.3	0.9
0.105	1.9	1.1	1.0	0.8	10.2	72.0	16.9	0.8	0.9
0.075	0.9	1.0	0.6	0.7	1.2	8.3	77.5	6.9	3.1
0.053	0.8	3.9	0.6	0.5	0.3	0.8	3.3	89.0	6.4
0.038	1.4	1.2	0.5	0.3	0.4	0.5	1.0	0.8*	83.1
0.025	1.7	1.3*	0.5	0.4	0.2*	0.4	0.1*	0.4*	0.4*
-0.025	2.3	1.4	0.6	0.5	0.6*	0.3*	0.2*	0.8*	0.3*
Total	100.0	100.0	100.0	100.0	100.0	100.0	100.0	100.0	100.0

(\*: No LKC concentrate assay, Note: only the lower end of the classes is shown).

**Table 8.7:** The distribution of recoveries to the concentrate and feed distribution for the Snip tests with the Bond ball mill.

Parent size:→ Progeny size:↓ (mm)	0.425-0.600		0.212-0.300	
	GRG (%)	Distribution	GRG (%)	Distribution
1.180-1.700	0.4	0.1	-	0.0
0.850-1.180	1.1	0.4	-	0.0
0.600-0.850	0.4	1.3	100.0	0.0
0.425-0.600	99.8	53.9	0.1	0.1
0.300-0.425	99.6	29.3	99.9	14.3
0.212-0.300	95.6	4.4	99.5	46.1
0.150-0.212	98.1	3.5	99.0	25.3
0.105-0.150	90.1	3.9	78.1	1.9
0.075-0.105	77.1	1.4	85.7	1.1
0.053-0.075	66.9	0.6	76.5	0.7
0.038-0.053	59.0	0.6	43.9	1.1
0.025-0.038	-*	0.3**	11.0	1.7
-0.025	-*	0.3**	5.0	7.6
Total	95.9	100.0	89.3	100.0

(\*: No assay available, \*\*: No LKC concentrate assay).

Table 8.7 shows the gold concentrates and distribution for the Bond ball mill tests. For the 0.425-0.600 mm size class, recovery is much higher than that of the small ball mill test, but in line with other small ball mill results. This confirms the unreliability of the small ball mill 0.425-0.600 mm results. For the 0.212-0.300 mm, results are in reasonable agreement with those of the small ball mill, although recoveries in the fine sizes are lower. The cumulative breakage function of the various classes, shown in Figure 8.6, shows some crossing-over, which suggests the improbable

production of a finer progeny from a coarser size class. The weight of gold used for these tests, 0.016 g to 0.205 g, might still have been too small to minimize sampling and assaying errors. Figure 8.7 shows a monotonic relationship between particle size and selection function of gold, except for the 0.300-0.425 mm class, which had also yielded suspicious recoveries (Table 8.5). This further confirms that this test should be disregarded.

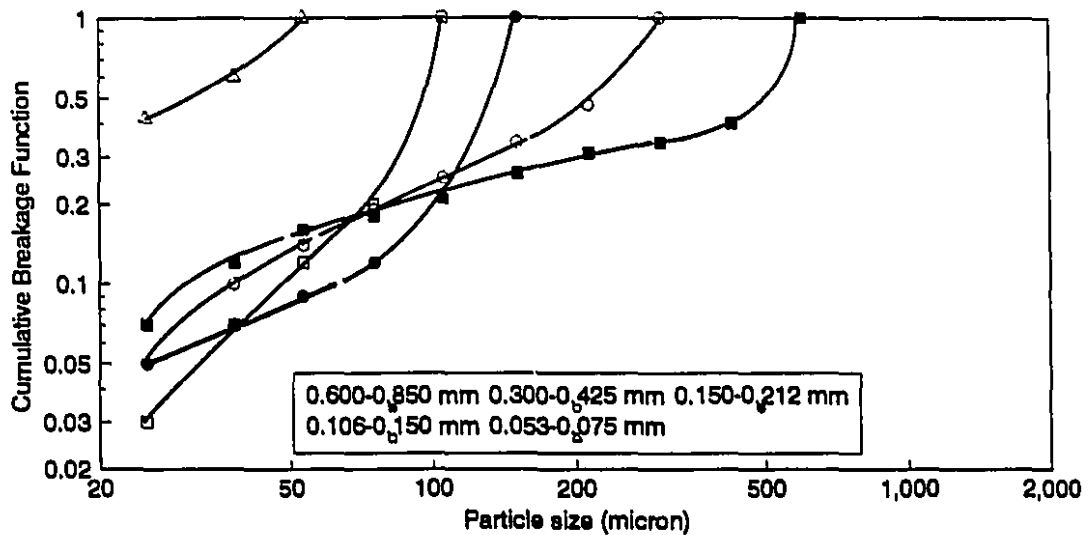


Figure 8.6: Calculated cumulative breakage functions for the Snip tests.

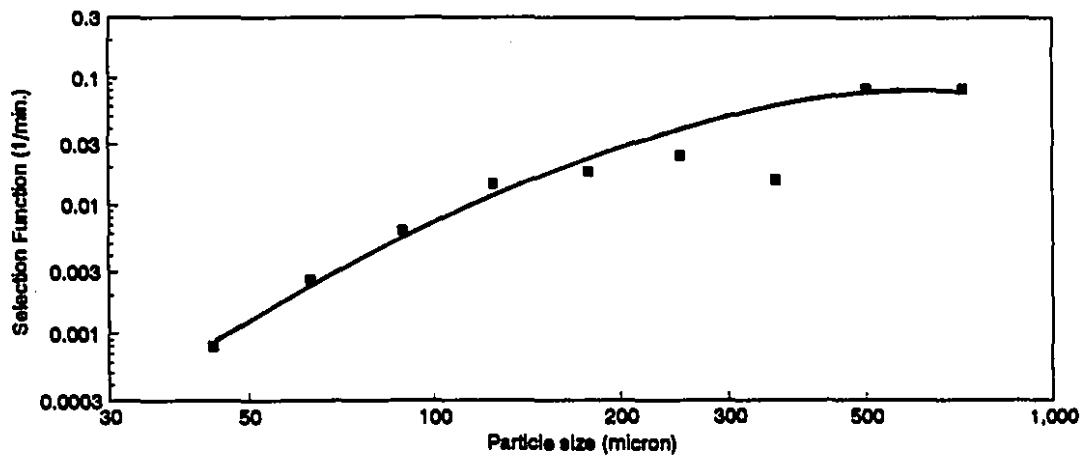


Figure 8.7: Estimated selection functions for the Snip tests.

### 8.3.3 Hemlo tests

Although the Snip tests yielded more consistent data than Casa Berardi's, evidence of random errors was still present. The Hemlo test series was less ambitious, in that a single grinding environment was tested, but a large weight of gold was used, 1 to 6 g per test, to minimize experimental errors.

**Table 8.8:** The distribution of recoveries to the concentrate for the Hemlo tests.

Parent size:→ Progeny size:↓ (mm)	Recovery of concentrates of different size classes (%)									
	1.18	0.600	0.300	0.150		0.053	0.038		0.025	-0.025
				1 <sup>st</sup> Test	Repeat		1 <sup>st</sup> Test	Repeat		
1.700	1.4	-	-	-	-	-	-	-	-	-
1.180	99.4	-	-	-	-	-	-	-	-	-
0.850	100.0	45.7	-	-	-	-	-	-	-	-
0.600	100.0	99.9	-	-	-	-	-	-	-	-
0.425	99.4	99.9	99.9	-	-	-	21.8	100.0	6.5	6.7
0.300	99.9	99.6	99.9	100.0	100.0	100.0	83.4	100.0	57.6	96.6
0.212	99.6	93.6	99.7	100.0	99.9	100.0	95.7	100.0	78.4	94.6
0.150	85.9	80.6	99.7	99.7	99.6	100.0	76.0	90.0	83.0	84.6
0.105	93.6	78.4	99.4	99.8	99.7	99.1	70.7	91.0	81.4	75.9
0.075	93.4	75.6	99.3	99.9	99.2	99.3	84.9	96.3	69.1	82.6
0.053	74.3	61.9	96.1	97.7	98.1	99.6	92.8	98.2	69.8	45.6
0.038	72.1	56.5	98.0	98.6	96.6	99.3	99.5	99.2	93.2	58.9
0.025	63.4	57.8	94.2	93.7	92.6	89.6	83.0	41.2	69.3	92.9
-0.025	-*	62.7	42.1	44.5	31.0	37.7	42.6	34.6	74.1	97.5
Total	98.4	95.5	98.6	99.0	98.6	98.2	92.2	95.7	89.2	89.1

(\*: No assay available, Note: only the lower end of the progeny classes is shown).

Table 8.9: The feed distribution for the Hemlo tests .

Parent size:→ Prog. size: ↓ (mm)	Percentages of feeds in different size classes after grinding (%)									
	1.18	0.600	0.300	0.150		0.053	0.038		0.025	-0.025
				1 <sup>st</sup> Test	Repeat		1 <sup>st</sup> Test	Repeat		
1.700	0.5	-	-	-	-	-	-	-	-	-
1.180	97.7	-	-	-	-	-	-	-	-	-
0.850	38.6	3.8	-	-	-	-	-	-	-	-
0.600	11.3	25.1	-	-	-	-	-	-	-	-
0.425	4.7	54.9	17.5	-	-	-	-	0.1	0.0	0.0
0.300	3.9	9.1	32.1	1.5	2.2	0.0	0.0	0.1	0.0	0.0
0.212	0.9	2.3	37.7	38.0	24.4	0.1	0.2	0.1	0.2	0.2
0.150	0.5	1.4	6.9	36.9	41.7	0.7	0.3	0.1	0.2	0.3
0.105	0.2	0.7	2.1	16.0	22.2	1.9	0.5	0.3	0.2	0.3
0.075	0.3	0.4	1.1	3.3	4.5	19.3	1.1	1.5	0.1	0.2
0.053	0.1	0.2	0.6	1.4	1.6	6.4	8.9	9.5	0.3	0.2
0.038	0.2	0.5	0.5	1.2	1.4	14.0	32.5	37.7	15.6	1.6
0.025	0.6	0.7	0.2	0.4	0.6	0.7	3.3	3.8	15.6	36.8
-0.025	0.7	1.1	1.5	1.3	1.4	1.9	2.9	1.3	4.3	67.6
Total	100	100	100	100	100	100	100	100	100	100

(\*: No LKC concentrate assay, Note: only the lower end of the classes is shown).

Table 8.8 and Figure 8.8 show the recovery of gold for the various tests, and its distribution is shown in Table 8.9. Snip results are largely confirmed, and gold still reporting to the parent class is largely recoverable by gravity, 97.4 to 99.9% above 0.053 mm. Recovery below 0.053 mm dips slightly, from 94.5% in the 0.038-0.053 mm to 87.8% below 0.025 mm. Fragments recovery shows less dependence on distance from the parent size class (i.e. the  $x_i/x_j$  ratio), and more on the absolute fragment size. Recovery for flattened particles (reporting mostly to the size class immediately coarser than the parent class) is high for parent particles between 0.075 and 0.600 mm, above

99%, but dips to the low nineties below 0.075 mm. Above 0.600 mm not enough gold is flattened to yield reliable recovery data. Table 8.8 incorporates two repeat tests that show reasonable reproducibility for the breakage function.

Table and Figure 8.8 raise the issue of reproducibility. Clearly gold fire-assaying is challenging, and can yield erratic results. For example, the low recovery of the 0.025-0.038 mm size class, in the second test with 0.038-0.053 mm feed, is based on a single tail assay, 114.5 g/t (page A81), which is anomalous, when compared to that of other size classes. What is more significant is the low recovery of the progeny of the tests with the two coarsest parent classes. There is some uncertainty associated with the low initial gold weight, 1.1 and 1.5 g, and the relatively low number of gold particles. This clearly warrants further work, as it is important to ensure that breakage of these coarser fragments does not result in a significant proportion of the progeny being non-gravity recoverable.

The data of the Table and Figure 8.8 was modelled with a modified Rosin-Rammler equation:

$$R_{GRG} = 98.5 * \left( 1 - e^{-0.693 \left( \frac{x}{0.019} \right)^{2.9}} \right) \quad (8.1)$$

which states that the maximum recovery of fragments, 98.5%, decreases to reach half this value at a fragment size of 0.019 mm. The lack of fit of this equation is significant, a standard error of 10%, and comes mostly from data generated with the two finest parent size classes, 0.025-0.038 mm and -0.025 mm (not shown in Figure 8.8). These two classes show higher recoveries, 74 to 89%, because most gold particles have not been broken.

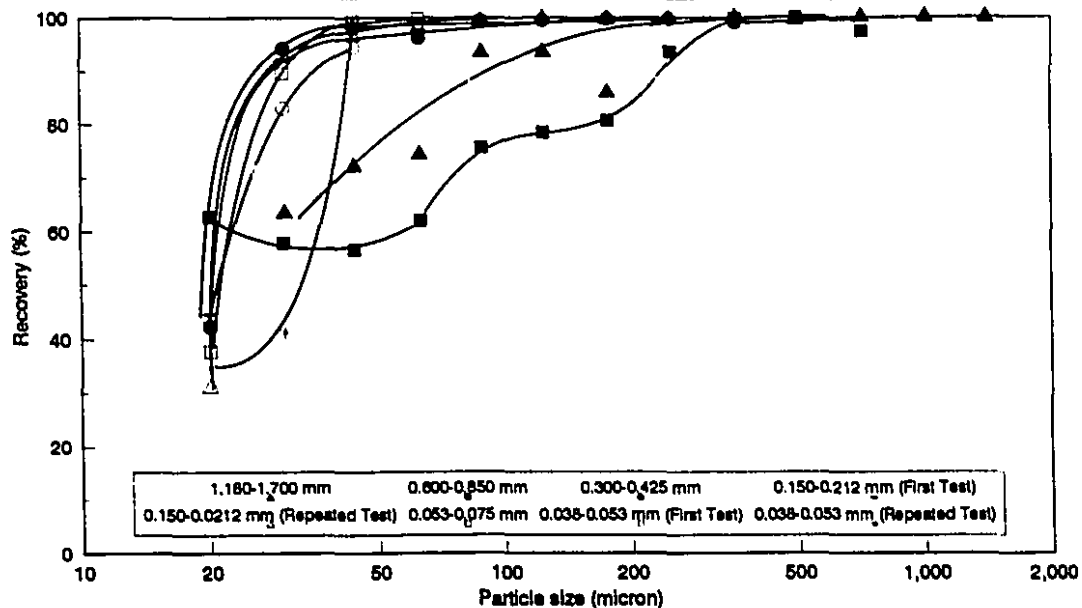


Figure 8.8: Recovery of the progeny as a function of particle size for the Hemlo tests.

The two coarsest parent classes show very different results, with recoveries dropping at much coarser progeny size, below 0.212 mm for the 0.600-0.850 mm and below 0.075 mm for the 1.18-1.70 mm. When the two size classes are dropped, the lack-of-fit of Equation 8.1 improves markedly (standard error of 3%), without significant change in its parameters:

$$R_{GRG} = 98.5 * \left( 1 - e^{-0.693 \left( \frac{x}{0.022} \right)^4} \right) \tag{8.2}$$

This equation yields the GRG data shown in Table 8.10 which can be used to model gold recovery in grinding circuits.

Table 8.10: Amount of GRG predicted by Equation 8.2.

Size (mm)	-0.025*	0.025-0.037	0.037-0.053	+0.053
GRG (%)	37.1	89.5	98.5	98.5

(\* mean size of the -0.025 mm assumed to be 0.020 mm).

Table 8.11 shows the calculated head grade of the final LKC step of the Hemlo tests. This grade was used, in turn, to calculate the grade of the table concentrate provided by Hemlo Gold Mines. These grades show no obvious discrepancies, and confirm the high grade of the product.

**Table 8.11:** Calculated head grades of the Hemlo tests.

Size class (mm)		Final LKC step (g/t)	First step (%)
1.180-1.700		212	58.9
0.600-0.850		364	72.8
0.300-0.425		718	71.8
0.150-0.212	1 <sup>st</sup> Test	830	83.0
	Repeat	1685	84.3
0.053-0.075		532	53.2
0.038-0.053	1 <sup>st</sup> Test	716	71.6
	Repeat	762	76.2
0.025-0.038		475	47.5
-0.025		736	73.6

(Final step grade: Grade of the 3000 g sample processed at the end of each test; First step grade: Grade of the initial table concentrate from Hemlo).

For all tests above 0.150 mm, the coarsest size class of silica used was the parent size class of gold. Its selection function can be easily estimated using Equation 2.30, and is shown in Figure 8.9 and Table 8.12. In principle, the selection functions should be time (or grinding increment) invariant, and this is largely confirmed by Figure 8.9. Figure 8.10 compares the selection functions of gold and silica; that of gold is

considerably lower than silica's, as noted in earlier work, both at laboratory<sup>(10)</sup> and plant scale<sup>(170)</sup>.

Table 8.12: Estimates of average selection functions of silica used in the Hemlo tests.

Size class (mm)	Average of Selection Function (minute) <sup>-1</sup>	
	Selection Function	Standard Deviation
1.180-1.700	0.984	0.082
0.600-0.850	1.132	0.056
0.300-0.425	0.703	0.016
0.150-0.212	0.258	0.004

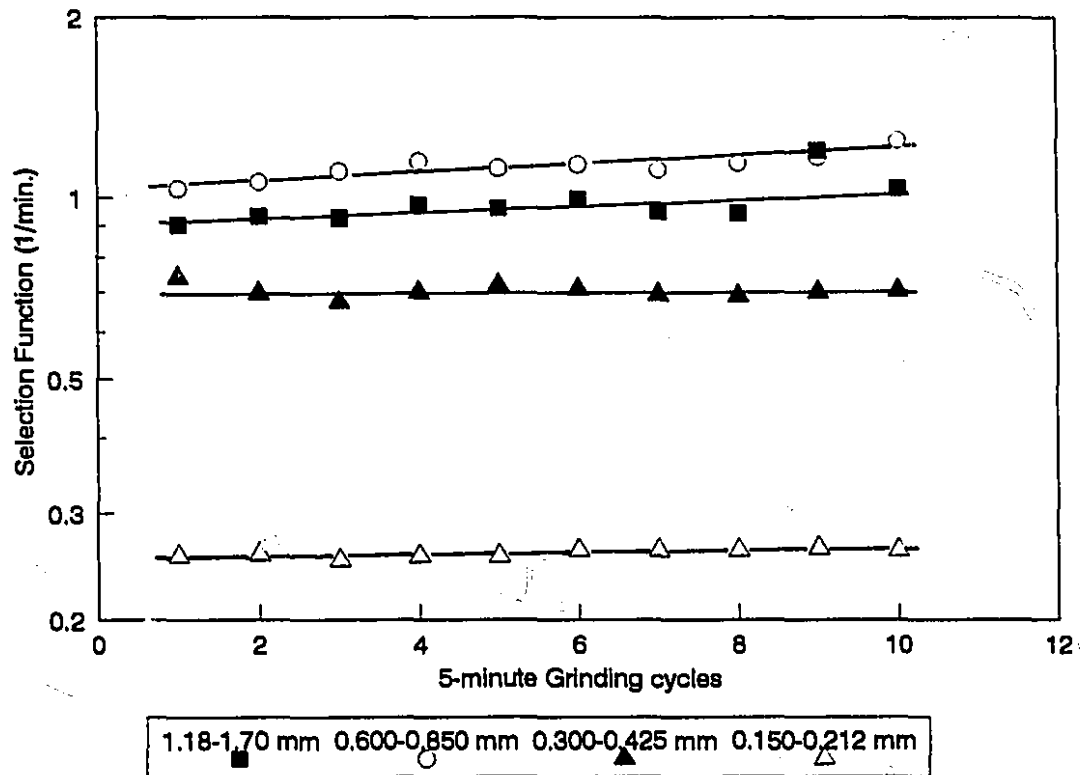


Figure 8.9: The variation of silica selection functions in grinding increments for the Hemlo samples.

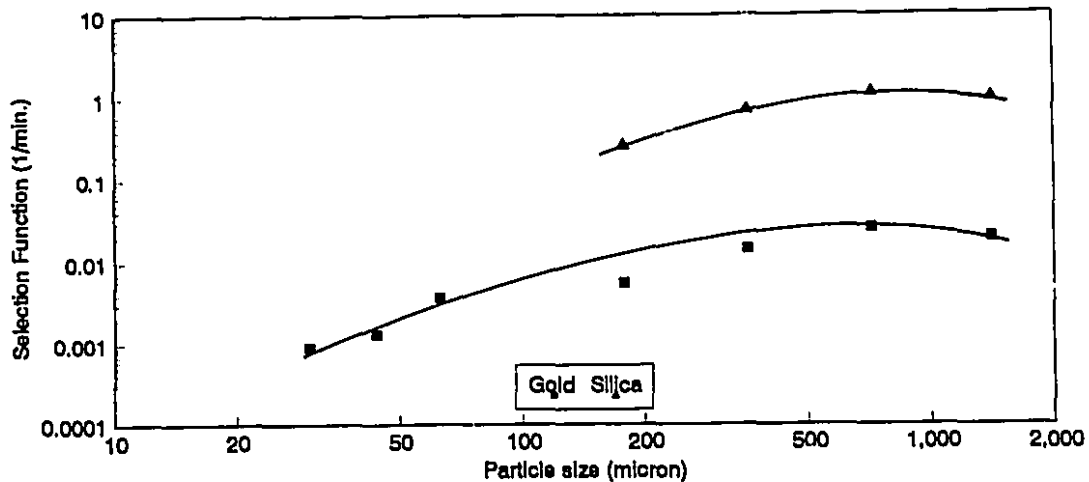


Figure 8.10: Estimated selection functions for gold and silica for the Hemlo tests.

Table 8.9 shows the distribution of gold at the end of each test. The amount remaining in the parent size class generally increases with decreasing particle size, from 25% for the 0.600-0.850 mm to 79% for the 0.025-0.038 mm. This would be expected, as the selection function decreases with particle size, and the total grinding time was equal for all tests. The importance of flattening first appears unrelated to particle size, but in fact, when considering only the material leaving the parent class, the weight fraction reporting to the coarser size classes steadily increases with decreasing parent particle size. In other words, the finer the particle, the more it will flatten rather than fold or break. Most of the mass moving to coarser size classes is found in the adjacent size class (i.e. class  $j-1$ ).

The breakage function of GRG was calculated using the same assumptions as for Casa Berardi and Snip tests, and is shown in Figure 8.11. The data of Figure 8.11 are well behaved, as cumulative breakage functions do not cross (compare to Figure 8.6 for the Snip tests). In fact, the progressive increase in the initial slope of each curve with decreasing particle size is a typical characteristic of breakage function families for the same material<sup>(234)</sup>. These curves are well fitted by the following equation, and the

parameters obtained from a least-square fit are shown in Table 8.13:

$$B_{i,j} = \phi_j \left( \frac{x_{i-1}}{x_j} \right)^\gamma + (1 - \phi_j) \left( \frac{x_{i-1}}{x_j} \right)^\beta, \quad 0 \leq \phi_j \leq 1 \quad (8.3)$$

The parameters in Table 8.13 show modest scatter, but the following points are clear:

- The lower exponent values of  $\beta$  are in the range of 0.6 to 1.2 (except for one repeat at 1.7), not unlike values reported for brittle minerals.
- The higher exponent value,  $\gamma$ , is in the range of 3 to 7 (except for the 0.053-0.075 mm class), which is slightly higher than reported values in the literature<sup>(100)</sup>.
- The major difference is that the relative importance of the distribution decay component,  $\phi_j$ , varies between 0.6 and 0.9 (except for 1.18-1.70 mm at 0.2), and is much higher than reported for brittle minerals.

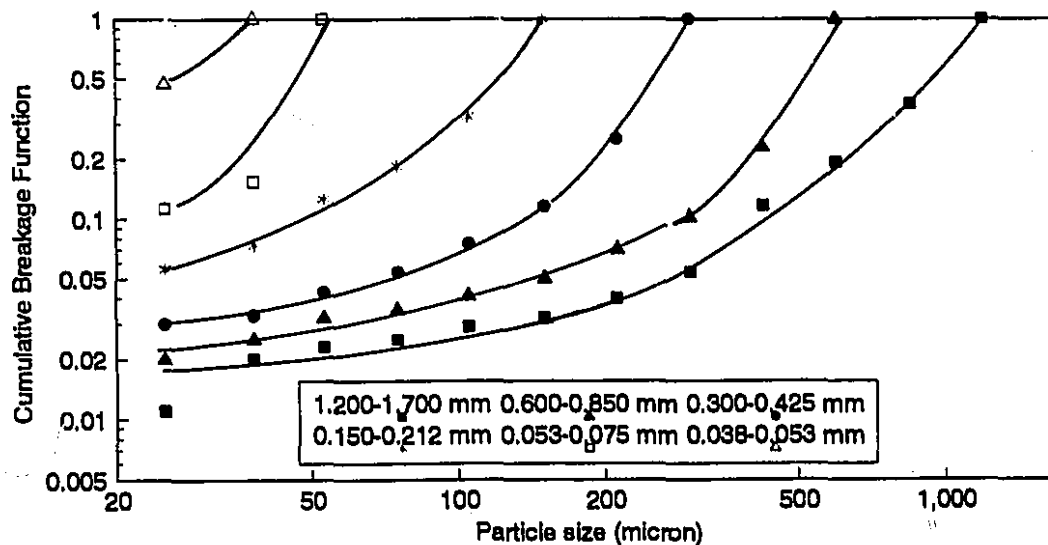


Figure 8.11: Calculated cumulative breakage functions for the Hemlo tests.

The above observations reflect the fact that for all parent classes, the  $B_{j+1,j}$  values are high, i.e. much material reports to the adjacent progeny class. Thus, the  $b_{j+1,j}$  values are high. This is by far the most significant difference between the breakage function

of gold and that of most minerals.

If gold behaves as lead does, the probability of flattening is approximately twice that of the folding. Table 8.9 shows that the amount of gold reporting to size class  $j-1$  (the size class adjacent to the parent class but coarser) is significant. Assuming that half of this amount reports to size class  $j+1$  because of folding would account for a significant proportion of the  $b_{j+1,j}$  terms and explain the major difference between the breakage function of gold (Figure 8.11) and those reported in the literature for brittle minerals.

**Table 8.13:** Estimated values of  $\phi$ ,  $\beta$ , and  $\gamma$  on the basis of breakage function calculation for the Hemlo tests.

Size class (mm)		$\phi$	$\beta$	$\gamma$
1.180-1.700		0.21	0.85	3.62
0.600-0.850		0.88	0.62	5.54
0.300-0.425		0.85	0.73	5.34
0.150-0.212	1 <sup>st</sup> Test	0.59	1.18	7.07
	Repeated Test	0.65	1.21	6.53
0.053-0.075		0.83	0.63	11.78
0.037-0.053	1 <sup>st</sup> Test	0.75	0.57	3.03
	Repeated Test	0.68	1.71	6.00

Figures 8.12 to 8.17 give evidence of the transfer of gold between size classes and its modes of occurrence. What they show is similar to photographs of lead fragments (chapter 5), yet gold particles look even more serrated, evidence of gold's greater malleability.



Figure 8.12: Gold flake, originally in 0.150-0.212 mm, moved into two coarser size class, 0.300-0.425 mm, after flattening.



Figure 8.13: Gold flake, originally in 0.300-0.425 mm, moved into two coarser size class, 0.600-0.850 mm, after flattening.

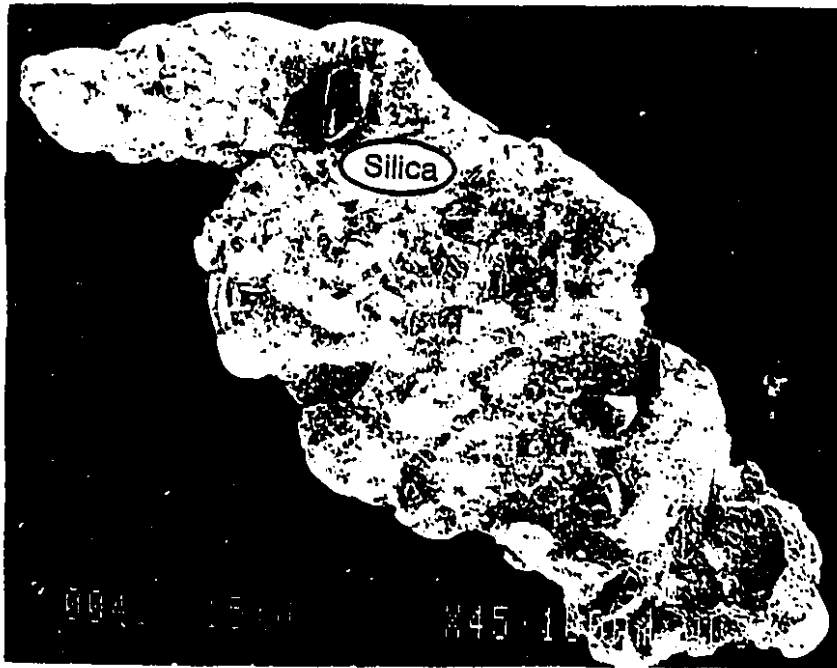


Figure 8.14: Gold flake, originally in 0.300-0.425 mm, moved into two finer size class, 0.150-0.212 mm, after folding and possibly breakage.

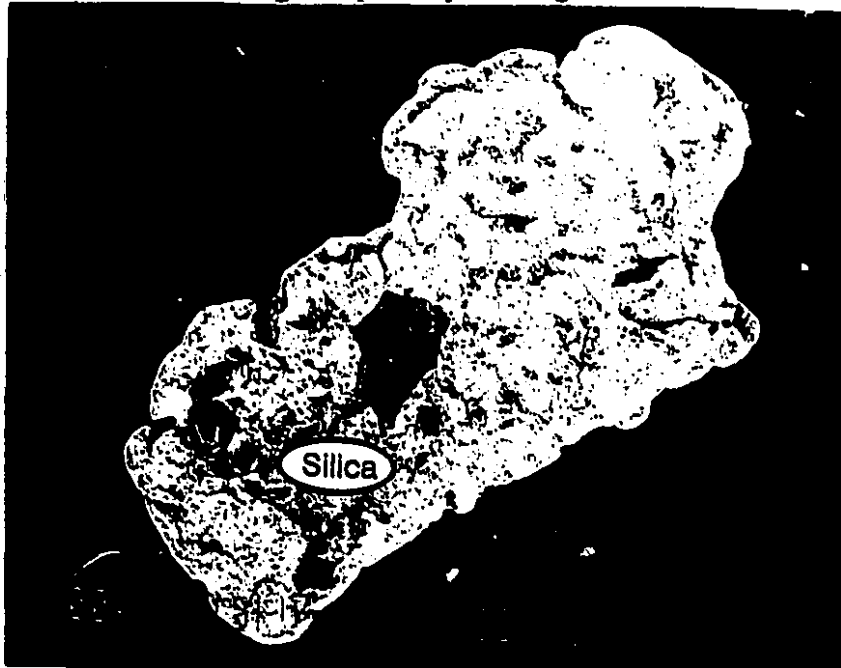
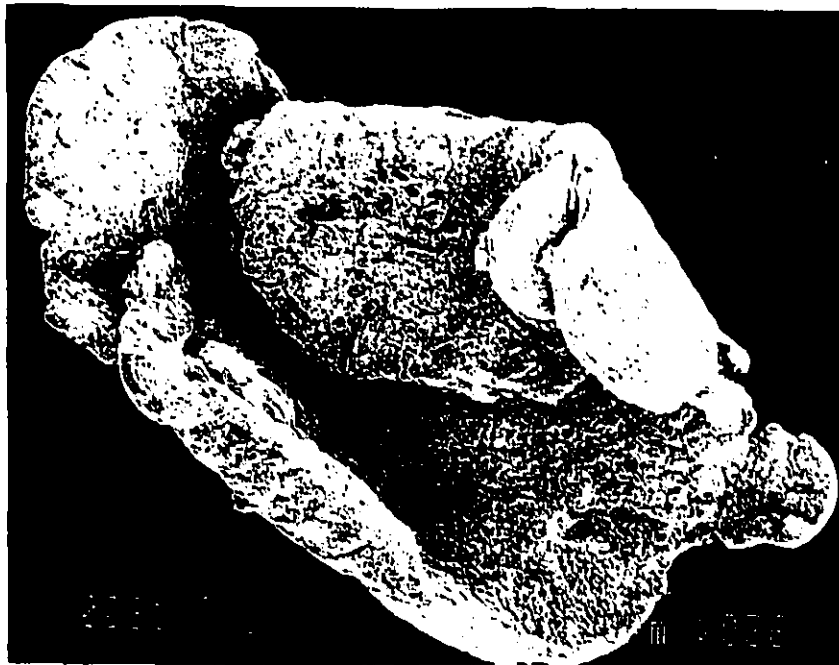


Figure 8.15: Gold flake, originally in 0.300-0.425 mm, moved into two finer size class, 0.150-0.212 mm, after folding and possibly breakage.



**Figure 8.16:** Gold flake, originally in 1.18-1.70 mm, moved into one finer size class, 0.850-1.180 mm, after folding and possibly breakage.



**Figure 8.17:** Gold flake originally in 1.18-1.70 mm, moved into two finer size class, 0.600-0.850 mm. after folding and possibly breakage.

## 8.4 Conclusions

The present work verified what had been found by others<sup>(9, 166)</sup> namely, that gold grinds quite slowly (here silica sand was used as a standard), and does flatten significantly, especially for finer particles. Evidence of folding is not so readily generated (as transfers to finer size classes can also be caused by breakage), but some photographic evidence and the very large data base of the lead work give it complete support.

The recoverability and breakage function work yielded some surprising results. First, it proved far more difficult to generate reliable data than expected. This is in large part due to the assaying step, which was unconventional, as very small weights were generated, especially in the concentrate fines. Fire assaying normally uses larger samples, especially at mine site laboratories, used for the present work. The experimental methodology also required refinements, such as the very large grinding times of the Hemlo work.

Another difficulty proved to be of statistical nature, i.e. breaking enough gold fragments. Reproducible data were finally generated when 2 g of gold or more were used for each test (Hemlo tests). Above 0.600 mm, uncertainty persisted, and future work, in the feed masses of about 10 g for each test, will be required. This is an indirect justification of the approach used in this work, namely, the use of lead as the main stock material for testing. Using a combination of gold and fire assaying would have been far too slow (with the turn-around time for analysis), error-prone, and costly.

Second, fragment recoverability for Hemlo proved far less dependent on parent size classes than early work on Casa Berardi and Snip would have suggested. In retrospect, this should have been expected. It adds a measure of simplicity to modelling

of gold gravity recovery.

Third, the breakage function itself proved similar to that of other minerals (Figure 8.11, in that its initial slope (i.e.  $b_{j+1,j}$ ) increases with decreasing parent size ( $x_j$ ). The observation of others<sup>(9)</sup> that  $b_{2,1}$  is equal to 0.7 is verified (within experimental error). An analysis of the shape of the breakage function suggests that the major difference is due to folding into the finer, adjacent, size class.

## Chapter 9: Discussion and Conclusions

## 9.1 Overall Discussion

The bulk of the experimental work was performed with copper, lead, and lead-silica charges in three tumbling mills representing three different grinding intensity levels. These, as well as the different charges, yielded very different behaviour. Table 9.1 is an attempt to summarize and classify these in terms of transfer mechanisms: flattening, folding, breakage, and smearing. The model which offered the best and simplest fit is also identified, and generally corresponds to the dominant mechanisms observed.

The importance of breakage (compared to flattening and folding) increases from the top left to the bottom right corner (Table 9.1). Thus, no breakage was observed with copper fragments in the small ball mill, whereas the grinding of lead and silica in the Bond rod mill was successfully modelled with the conventional breakage model and a single flattening rate constant. The table shows that an increase in the grinding intensity (i.e. power factor), a decrease in the size of the fragments, and the presence of a brittle phase which can act as secondary grinding medium promote breakage. The selection function, however, remains low in comparison to that of brittle minerals.

Table 9.1 also shows that at lower energy intensity the behaviour of malleable metals can be complex, with as many as three very different phases. The first phase is flattening and folding without breakage; the second phase is dominated by superflake formation, a cold-working form of agglomeration; finally, the third phase yields actual breakage of the superflakes. The breakage is caused by the propagation of cracks from the edge of the flakes. The flakes are rendered brittle because the cold welding is incomplete, and prevents recrystallization across its different layers (each layer originates from the normal flakes formed during phase 1).

Table 9.1: Summary of the results.

	Copper Fragments	Lead shots	Flattened Lead shots	Lead Fragments	
				without Silica	with silica
Small Ball Mill	-FF model, S <sub>e</sub> : 0.7-2.7% -ML: 9-16% after 70 min. -Fla. > Fol.			-FF model, S <sub>e</sub> : 0.8-3.0% -ML: 65% after 30 min. -Fla. >> Fol.	-FFWEB model, S <sub>e</sub> : 2.1-3.9% -ML: 5-7% after 20 min. -Fla. > Fol., Bre. > Fol., Fla. + Fol. > Bre.
Bond Ball Mill	-FF model, S <sub>e</sub> : 0.8-2.4% -ML: 6-8% after 120 min. -Fla. > Fol.	Phase I: FF model, S <sub>e</sub> : 2.1-4.6% Phase II: AG model, S <sub>e</sub> : 1.9-2.3% Phase III: FFWLB model, S <sub>e</sub> : 2.7-3.3% -ML: 18% after 120 min. Phase I: Fla. > Fol. Phase II: only Fla. Phase III: Fla. = Fol.	Phase I: FF model, S <sub>e</sub> : 0.3-0.5% Phase II: FFWLB model, S <sub>e</sub> : 1.8-2.3% -ML: 35% after 80 min. Phase I: Fol. > Fla. Phase II: Fla. > Fol., Fla. + Fol. > Bre.	-FFWLB model, S <sub>e</sub> : 1.7-3.1% -ML: 5-19% after 160 min. -Fla. > Fol., Fla. + Fol. > Bre.	-FFWEB model, S <sub>e</sub> : 0.9-3.1% -ML: 3-10% after 30 min. -Fla. > Fol., Bre. > Fol., Fla. + Fol. > Bre.
Bond Rod Mill	-FFWEB model, S <sub>e</sub> : 0.6-2.1% -ML: 5-7% after 10 min. -Fol. > Fla., -Fol. > Bre. -Fla. + Fol. > Bre.	Phase I: FF model, S <sub>e</sub> : 1.4-2.0% Phase II: FFWLB model, S <sub>e</sub> : 3.3-4.0% -ML: 48% after 20 min. Phase I: Fla. > Fol. Phase II: Fla. > Fol., Bre. > Fla. + Fol.	-FFWLB model, S <sub>e</sub> : 1.1-1.6% -ML: 19% after 120 min. -Fla. >> Fla., Fol. = Bre.	-FFWEB model, S <sub>e</sub> : 1.1-2.0% -ML: 63-76% after 2 min. -Fla. > Fol., Fla. + Fla. > Bre., Fol. = Bre.	-FFWEB model, S <sub>e</sub> : 1.0-3.1% -ML: 6-10% after 10 min. -Fol. > Fla., Bre. > Fol., Bre. > Fla. + Fol. -EBWOF model (just for 1.18-1.40 mm feed size), S <sub>e</sub> : 0.8% Bre. > Fla.

FF: Flattening and folding model, FFWLB: Flattening, folding and limited breakage model, FFWEB: Flattening, folding and explicit breakage model, AG: Agglomeration model, EBWOF: Explicit breakage model with only one flattening rate constant, S<sub>e</sub>: Standard error, ML: Mass Loss, Fla.: Flattening rate constants, Fol.: Folding rate constants, Bre.: Breakage rate constants.

This behaviour was observed in particular for lead shots, and would probably have been observed for copper, had very long grinding times been used. With smaller lead fragments, no cold welding was observed, and breakage was readily achieved. However, breakage still requires many impacts, and even in the harshest grinding environment (i.e. the Bond rod mill), a short induction time between the beginning of grinding and the onset of breakage was observed. This suggests that the first-order kinetics models used are convenient approximation rather than accurate representations of the observed transfer mechanisms. Indeed, first-order kinetics can be easily justified when particulate damage can be described by Griffith's theory, which is not the case with malleable metals.

A model of progressive damage would be more appropriate to describe how grinding affects malleable metals, as the induction time probably results from the fact that multiple blows are often needed to effect a transfer, be it progressive flattening (of lead shots, for example) or breakage of fragments. Hardness measurements of lead flakes showed that no work-hardening had taken place, as would be expected from the recrystallization temperature of lead ( $-4\text{ }^{\circ}\text{C}$ ). Thus, the induction time, in the case of breakage, probably corresponds to the average number of blows required for cracks to form at the edges of flakes and propagate until progeny is formed. This has been reported by others<sup>(160)</sup>.

Given the limitations of the phenomenological models used, they were able to describe data sets remarkably well. This is in part due to the large number of rate constants used, whose main drawback was often the poor reliability of individual estimates. However, the large body of data, when examined as a whole, shows that folding and flattening rate constants are generally higher than the selection function of the some parent size classes, even when breakage dominates. This is because breakage is final (i.e. irreversible), whereas the folding and flattening transfers are quite

reversible. Another general observation is that rate constants are generally higher than their folding counterpart, in a proportion of 2:1 to 3:1. This is intuitively correct, as fragment populations are made of predominantly flakes, the result of flattening, rather than spheres and cylinders, the end products of folding.

Weight loss was observed in all systems; in fact, it proved a hindrance to the study of folding and flattening (many tests had to be cut short as weight loss became excessive). Coating of lead could be observed onto the mill shell and grinding media. Factors contributing to this smearing mechanism (also a transfer, from the charge to the grinding medium and mill shell) are also quite complex. In many systems it was linked to the onset of breakage (the third phase when grinding lead shots in the Bond ball mill, the second phase with flattened lead shots in the Bond ball and rod mill tests), but it was also quite important in the small ball mill, in the absence of actual breakage. It was in this case attributed to the rough surface of the mill porcelain shell. It was very significant in the environment of highest intensity (i.e. the Bond rod mill). Adding a gangue phase minimized the importance of smearing, but it is not clear that this phenomenon was abated as much as the smeared material scoured off the surface onto which it had smeared.

The impetus for this work was the importance of the breakage of gold flakes in industrial tumbling mills. Other less important applications can be found in the grinding of copper slag containing droplets of metallic copper and the remediation of sites containing metallic lead i.e. old firing ranges. For all three applications, smearing of the malleable phase in either the grinding media and mill shell or the non-malleable gangue can have adverse effects. For gold, it results in unliberation and can cause a loss of recovery. Gold inclusions into mill shells have been informally reported by scrap dealers, and scouring of old mill equipment to dislodge smeared gold practised commercially. Gold smeared onto the grinding media is eventually liberated again when

the grinding media wears down, but may be unresponsive to flotation, or even possibly passivated by galvanic interaction. Some grinding media is eventually discarded because it is too small or angular (colloquially called skats), and would have its own gold content.

The smearing of gold onto mill shell may be less significant in large diameter mills because of their much smaller liner surface to charge volume ratio than the three much smaller mills used in this study (although the total amount of gold smeared would be higher because the surface area, in absolute terms, is much higher). This is not the case of the small mills used for the regrinding of table tails, which makes this practice objectionable. Furthermore, studies<sup>(235)</sup> have shown that gold in these products was largely liberated, but fine, and would be recovered effectively by screening and processing the undersize with a centrifuge unit. Gold's grinding behaviour simply suggests that as it should be ground as little as possible.

In the case of metallic copper, downstream recovery is likely to be by flotation, and the impact of smearing, overgrinding, the excessive retention time in the grinding circuit is not known. The possibility of gravity recovery in this case has never been investigated, to the knowledge of the author. Copper is the hardest of the three metals investigated, thus the least susceptible to smearing. However, its selection function would be even lower than that of gold, and it would accumulate in grinding circuits, as its density,  $8.96 \text{ g/cm}^3$ , is significantly higher than that of most mineral gangues,  $2.8 \text{ g/cm}^3$ , and fayalite slag ( $\text{FeSiO}_3$ ),  $3.5 \text{ g/cm}^3$ .

In the case of lead decontamination, the cheapest recovery method is gravity, and lead's ability to smear, which can be linked to its very low hardness, is more likely to be a problem. Thus comminution circuits should use very low grinding intensities (e.g. scrubbers) and emphasize gravity recovery as early as possible in the flowsheet. The use of cyclones to classify mill discharges should be avoided whenever possible.

When modelling the gravity recovery of gold its grinding must also be modelled. Should the folding and flattening transfers be incorporated into the simulator? The results of this thesis argue strongly against it, as breakage rapidly becomes the dominant transfer as: i) grinding energy intensity increases, ii) fragment size decreases, and iii) grinding takes place in the presence of a brittle but harder gangue phase. The first condition is met in the large diameter mills used industrially. The second, in that most gold accumulates below 0.300 mm in grinding circuits. Finally, gold ores contain typically 5 to 30 ppm of gold, yielding circulating loads (ball mill feeds) of 25 to 500 ppm of gold. This presents a very low concentration of malleable metal or, conversely a very high concentration of scouring material. All three conditions make breakage mechanisms more significant than folding and flattening.

Pure gold, which recrystallizes at room temperature, is postulated not to work-harden during grinding, much like lead. Commercial gold and even more so native gold, are not nearly as pure, and have much higher activation energies and recrystallization temperatures. It is therefore expected that they will not recrystallize at room temperature. Yet their malleability is retained. This could be the case for platinum, with an even higher recrystallization temperature<sup>(191)</sup> than pure gold or lead. Recovery (the reordering of dislocations to lower their energy) is likely to be the mechanism which explains why impure gold retains its malleability in the absence of recrystallization.

Table 9.1 is a thorough summary of the grinding work with lead and copper, but not a user-friendly presentation. Figures 9.1 and 9.2 attempt to present the same information, but from a less quantitative, more phenomenological perspective. Figure 9.1 depicts a conceptual view of the transfers across size classes, with and without silica (i.e. the dominant, brittle gangue phase).

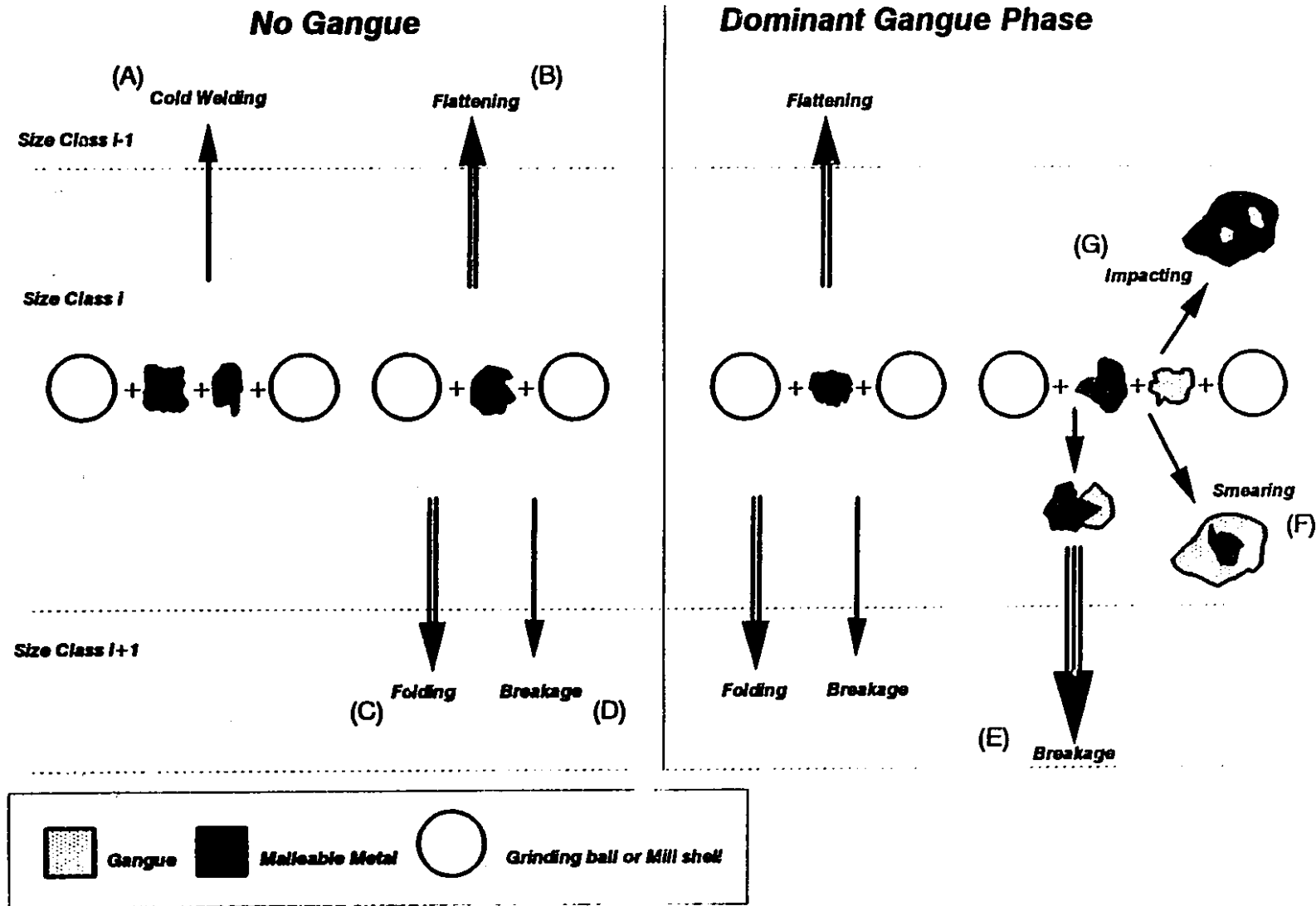


Figure 9.1: A conceptual view of the transfers across size classes.

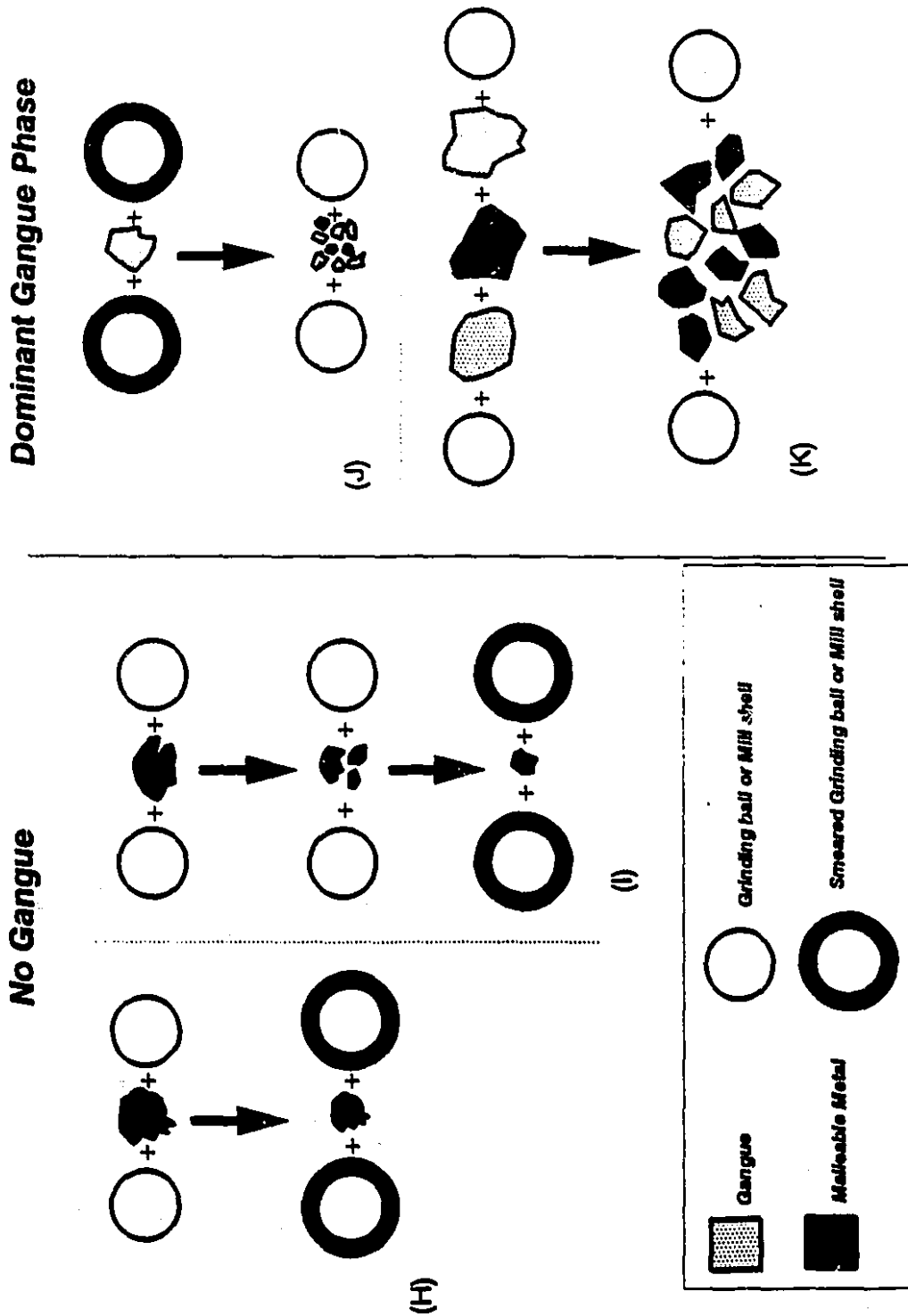


Figure 9.2: A conceptual view of smearing.

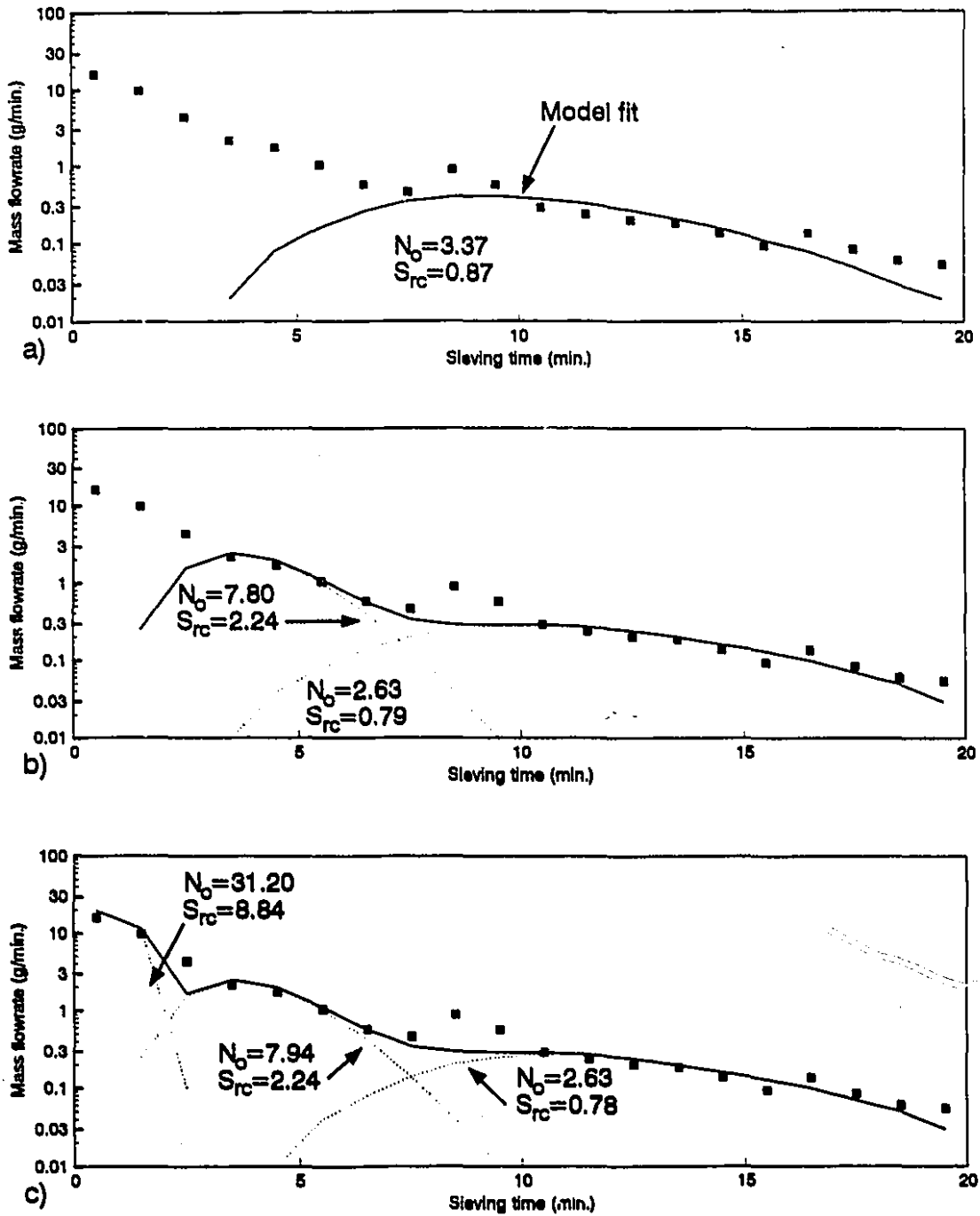


Figure 9.3: Fit of the cascadoigraphy response of the 1<sup>st</sup> concentrate of MLS product of the 0.710-0.850 mm sample to Equation 7.2 using a) one, b) two and c) three particle types (each with a single screening rate constant).

In the absence of silica (Figure 9.1), the first phenomenon to be depicted is agglomeration by cold-welding (A). This phenomenon was observed mostly with shots and flattened shots, only in the Bond ball mill with larger diameter balls. It can be postulated that a more energy intensive environment like the Bond rod mill would yield impacts that can break rather than weld particles. Finer lead particles did not yield cold welding, presumably because their smaller size lowers the probability of quadruple collision (ball-lead-lead-ball or mill shell). The second phenomenon depicted in the absence of gangue is flattening (B), which dominated many systems. Folding (C) was one half to one third less likely than flattening, except in the system of very low grinding intensity with respect to fragment hardness (i.e. copper fragments in the small ball mill). In this last case, it can be postulated that impacts could occasionally bend particle edges, but were not capable of flattening. Breakage (D) can be virtually absent (copper fragments in small ball mill) to very significant (lead fragments in the Bond rod mill).

When a dominant brittle hard phase is added to mimic gold ores, the phenomena observed in the absence of gangue are still present with virtually the same kinetics, except for agglomeration, which was not observed. The major difference is that the brittle particles act as wedges in the malleable fragments, significantly increasing the kinetics of breakage (E). Secondary phenomena include the smearing of the malleable metal onto the brittle mineral (F), and the impacting of small mineral fragments into the malleable metal (G).

Figure 9.2 is a conceptual representation of the smearing of the malleable metal onto the grinding media and mill shell. In the absence of brittle gangue, the phenomenon can be extremely significant, especially with softer malleable metals and rougher surfaces. Although fast smearing kinetics have been observed in the absence of breakage (H), in all cases smearing significantly increased at the onset of breakage (I), presumably because progeny was more susceptible to smearing than parent particles. When gangue

is added, the impact of smearing is considerably decreased. A first, obvious mechanism is the removal of smearing material by the scouring action of the mineral (J). As the loss of weight of material in the coarser size classes due to smearing is also decreased, a second mechanism must be evoked. The dominance of the brittle phase makes it likely that it will be present between the grinding media and the malleable fragments upon impact, and will decrease direct contact of the medium with the metal (K). Evidence of this mechanism is, at this point, only circumstantial.

One last point to be discussed has to do with cascadowgraphy. It was argued in the conclusion of chapter 7 that analysis of cascadowgraphy results must be more powerful than the mere detection of peaks on the flow rate plots proposed by Meloy and Durney<sup>(220)</sup>. Figure 9.3 (a) to (c) propose a least-square fit to Equation 7.2 based on the assumptions of unimodal, bimodal and trimodal populations, respectively. The goodness of fit obviously improves as the number of particle types used (each with its unique probability of screening) increased. This suggests that a small number of particle types should yield an excellent fit. To limit the degrees of freedom of the fit, this should be achieved using relatively simple probability functions, much like what was proposed in flotation<sup>(236)</sup>. The potential of cascadowgraphy would then be improved significantly.

## 9.2 Contributions to Knowledge

- The transfer of malleable metals (lead and copper) between size classes was investigated in different grinding environments. Phenomena of breakage, flattening, and folding were modelled using an extension of the classical grinding model.
- The effect of grinding intensity, the size and hardness of the malleable phase and presence of a brittle harder gangue phase on the relative importance of the various transfers was identified.

---

- The breakage function of gold was determined in a realistic grinding environment (i.e. in the presence of a dominant brittle phase), and linked to recoverability by gravity. This information has since been incorporated in a simulator of gold recovery by gravity. The main difference between the breakage function of gold and that of brittle minerals has been conclusively linked to the folding mechanism.

- Hardness measurements showed that lead does not work harden during grinding at room temperature. This would be expected from published values of lead's recrystallization temperature and activation energy, but experimental evidence on grinding products had not been found in the literature.

### 9.3 Suggestions for Future Research

This investigation, as would be expected of exploratory work, has raised as many questions (and probably more) as it has answered. The following topics are of particular interest:

- The assumption that first order kinetics can represent the transfer mechanisms observed is a convenient analytical tool. However, it can not predict the various phases that were observed, and is clearly incapable of accounting for the induction times observed before the onset of breakage. Other models should be investigated.

- The relative importance of smearing has been demonstrated. It is much less significant in the presence of a hard, brittle phase. This would be expected if the brittle phase scours the smeared phase, but the brittle phase could also act as a barrier between the grinding medium and the mill shell. Which mechanism is dominant has yet to be determined.

- 
- The importance of smearing suggests that the presence of gold should be detectable in steel discarded from grinding circuits. This should be tested with actual samples, either directly (e.g. SEM work) or indirectly (e.g. cyanidation of skats).
  
  - Determination of the breakage function of coarse gold yielded uncertainty, as weights in excess of 10 g of gold should have been used. This should be completed, using the procedure tested with the Hemlo samples.
  
  - The results of cascadowgraphy were inconclusive, but at least identified some discrimination (i.e. relative to particle weight). The analytical approach suggested by Meloy<sup>(220)</sup> must be refined. Only then could the potential of cascadowgraphy be tapped.
  
  - The breakage function work, particularly that of gold, showed that the  $b_{j+1,j}$  terms contain a significant folding contribution. Significant weight also reports to the size class immediately coarser than the parent class. The impact of these transfers on the modelling of gold's behaviour in grinding circuits has yet to be determined.
  
  - Just as the gravity recovery of gold can be in part justified by its grinding behaviour, it may be attractive in plants that process materials containing malleable metals such as lead and copper. In particular, the use of centrifuge units such as the Knelson Concentrator could be investigated.
  
  - Work hardening of lead was not detected; this would be expected from its recrystallization temperature ( $-1^{\circ}\text{C}$ ), the case of gold and copper is more interesting, as their recrystallization temperature is much higher, with no apparent effect on their malleability. It was postulated that this can be explained by dynamic recovery (the re-organization of dislocations to minimize their energy). Obviously this warrants a closer examination.

## References

---

**References:**

- [1] Letchworth, G., (1934), "Getting acquainted with minerals", McGraw Hill, New York.
- [2] Jensen, D.E., (1958), "Getting acquainted with minerals", McGraw-Hill Book Company, New York.
- [3] Berry, L.G., Mason, B., (1959), "Mineralogy, concepts, descriptions, determinations", W.H. Freeman and Company, San Francisco.
- [4] Pough, F.G., (1960), "A field guide to rocks and minerals", Houghton Mifflin Company, Boston.
- [5] Vanders, I., Kerr, P.F., (1967), "Mineral recognition", John Wiley & Sons, New York.
- [6] Sinkankas, J., (1964), "Mineralogy for amateurs", D. Van Nostrand Company, Inc., London.
- [7] Jones, M.P., Fleming, M.G., (1965), "Identification of mineral grains", Elsevier Publishing Company, New York.
- [8] Battey, M.H., (1972), "Mineralogy for students", Oliver & Boyd, Edinburgh.
- [9] Banisi, S., (1990), "An investigation of the behaviour of gold in grinding circuits", M.Eng. Thesis, Mining & Metallurgical Engineering Department, McGill University, Montreal, Canada.

- 
- [10] Banisi, S., Laplante, A.R., Marois, J., (1991), "The behaviour of gold in Hemlo Mines Ltd. grinding circuit", CIM Bulletin, Vol. 84, No. 955, pp. 72-78.
- [11] Laplante, A.R., Vincent, F., Noaparast, M., Woodcock, F., Boulet, A., Dubé, G., Robitaille, J., (1995), "Predicting gold recovery by gravity", Proceedings of the 19<sup>th</sup> International Mineral Processing Congress, San Francisco, Vol. 4, pp. 19-26.
- [12] Laplante, A.R., Woodcock, F., Noaparast, M., (1995), "Predicting gravity separation gold recoveries", Minerals and Metallurgical Processing, Vol. 12, No 2, May 1995, pp. 74-79.
- [13] Quantinez, M., Schafer, R.J., Smeal, C.R., (1962), "The production of submicron metal powders by ball milling with grinding aids", NASA TN-D-879, March 1962.
- [14] Quantinez, M., Schafer, R.J., Smeal, C.R., (1961), "The production of submicron metal powders by ball milling with grinding aids", Transactions of the Metallurgical Society, Vol. 221, pp. 1105-1110.
- [15] Sureshan, M.K., Vedaraman, R., Ramanujam, M., (1982), "Investigation on the mechanism of grinding of metal powders", International Symposium on Recent Advances in Particulate Science and Technology, Indian Institute of Technology, Madras, pp. 185-194.
- [16] Olbrich, M., (1944), "Superfine grinding of metal powders", Light Metals, Vol. 7, No. 75, April 1944, pp. 157-160.

- 
- [17] Goetzl, C.G., (1949), "Treatise on powder metallurgy, Volume I: Technology of metal powders and their products", Interscience Publishers, New York.
- [18] Small, M.J., Nunn, A., Forslund, B.L., Daily, D.A., (1995), "Source attribution of elevated residential soil lead near a battery recycling site", *Environmental Science & Technology*, Vol. 29, No. 4, pp. 883-895.
- [19] Sureshan, M.K., Vedaraman, R., Ramanujam, M., (1983), "Effects of grinding aids on vibration milling of aluminum", *Particulate Science and Technology*, Vol. 1, No. 1, pp. 55-65.
- [20] Vedaraman, R., Chandrasekaran, R.M., (1979), "Studies in grinding of aluminum powder by vibration mill", *Chemical Engineering World*, Vol. 14, No. 7, pp. 55-60.
- [21] Alfa AESAR Catalog, (1995-96), "The right chemicals, the right chemistry", Johnson Matthey, pp. 647, 671.
- [22] Laplante, A.R., Huang, L., Noaparast, M., Nickoletopoulos, N., (1995), "A philosopher's stone: Turning tungsten and lead into gold- The use of synthetic ores to study gold gravity separation", 27<sup>th</sup> Annual meeting of CMP, Paper No. 28, Ottawa.
- [23] Olsen, K.B., Wang, J., Setiadji, R., Lu, J., (1994), "Field screening of chromium, cadmium, zinc, copper and lead in sediments by stripping analysis", *Environmental Science & Technology*, Vol. 28, No. 12, pp. 2074-2079.
- [24] Kysriss, K., (1993), "Lead and copper rules complicate matters for water

- 
- systems", *Water-Engineering and Management*, May 1993, pp. 28-30.
- [25] Herbst, J.A., Fuerstenau, D.W., (1968), "The zero order production of fine sizes in comminution and its implications in simulation", *AIME Transactions*, Vol. 241, pp. 538-548.
- [26] Everell, M.D., (1972), "Empirical relations between grinding selection functions and physical properties of rocks", *AIME Transactions*, Vol. 252, pp. 300-306.
- [27] Gill, C.B., (1991), "Materials beneficiation", Springer-Verlog. New York.
- [28] Lowrison, G.C., (1974), "Crushing and grinding, the size reduction of solids materials", CRC press, Inc., Cleveland.
- [29] Lowrison, G.C., (1977), "Crushing and grinding, the future for comminution", *The Chemical Engineer*, No. 325, pp. 699-701.
- [30] Hukki, R.T., (1975), "The principles of comminution: An analytical summary", *Engineering and Mining Journal*, Vol. 176, pp. 106-110.
- [31] Austin, L.G., (1984), "Size reduction of solids: Crushing and grinding equipment", in: *Handbook of powder science and technology*, Editors: Fayed, M.E., Otton, L., Van Nostrand Reinhold Company, New York, Chapter 13, pp. 562-606.
- [32] Austin, L.G., (1971/72), "A review, introduction to the mathematical description of grinding as a rate process", *Powder Technology*, Vol. 5, pp. 1-17.

- 
- [33] Klimpel, R.R., Austin, L.G., (1984), "The back-calculation of specific rates of breakage from continuous mill data", *Powder Technology*, Vol. 38, pp. 77-91.
- [34] Kanda, Y., Abe, Y., Yamaguchi, M., Endo, C., (1988), "A fundamental study of dry and wet grinding from the viewpoint of breaking strength", *Powder Technology*, Vol. 56, pp. 57-62.
- [35] Fuerstenau, D.W., Sullivan, D.A., (1961), "Size distributions and energy consumption in wet and dry grinding", *AIME Transactions*, Vol. 220, pp. 397-402.
- [36] Crabtree, D.D., Kinasevich, R.S., Mular, A.L., Meloy, T.P., Fuerstenau, D.W., (1964), "Mechanisms of size reduction in comminution systems, Part I. Impact, abrasion and chipping grinding", *AIME Transactions*, Vol. 229, pp. 201-206.
- [37] Kinasevich, R.S., Crabtree, D.D., Mular, A.L., Meloy, T.P., Fuerstenau, D.W., (1964), "Mechanisms of size reduction in comminution systems, Part II. Interpreting size distribution curves and the comminution event hypothesis", *AIME Transactions*, Vol. 229, pp. 207-210.
- [38] Richards, R.H., Locker, C.E., Schuhmann, R., (1940), "Textbook of ore dressing", McGraw-Hill Book Company, New York.
- [39] Kelly, E.G., Spottiswood, D.J., (1982), "Introduction to mineral processing", John Wiley & Sons, New York.
- [40] Austin, L.G., Rogers, R.S.C., (1985), "Powder technology in industrial size reduction", *Powder Technology*, Vol. 42, pp. 91-109.

- 
- [41] Menacho, J.M., (1986), "Some solutions for the kinetics of combined fracture and abrasion breakage", Powder Technology, Vol. 49, pp. 87-96.
- [42] Schuhmann, R., (1940), "Principles of comminution, I. Size distribution and surface calculations", AIME Technical Publication No. 1189, pp. 1-11.
- [43] Schuhmann, R., (1960), "Energy input and size distribution in comminution". AIME Transactions, Vol. 217, pp. 22-25.
- [44] Gaudin, A.M., Meloy, T.P., (1962), "Model and a comminution distribution equation for single fracture", AIME Transactions, Vol. 232, pp. 40-50.
- [45] Gilvarry, J.J., (1961), "Fracture of brittle solids, I. Distribution function for fragment size in single fracture (theoretical)", Journal of Applied Physics, Vol. 32, pp. 391-399.
- [46] Gaudin, A.M., (1926), "An investigation of crushing phenomena", AIME Transactions, Vol. 73, pp. 253-316.
- [47] Harris, C.C., (1969), "A method for determining the parameters of the 3-parameter size distribution equation", AIME Transactions, Vol. 244, pp. 187-190.
- [48] Bennett, J.G., (1936), "Broken coal", Journal of Institute of Fuel, Vol. 10, pp. 22-39.
- [49] Epstein, B., (1948), "Logarithmico-normal distribution in breakage of solids", Industrial and Engineering Chemistry, Vol. 40, No. 12, pp. 2289-2291.

- 
- [50] Rosin, P., Rammler, E., (1933), "The laws governing the fineness of powdered coal", *Journal of Institute of Fuel*, Vol. 7, pp. 29-36.
- [51] Mular, A.L., (1962), "Relationship among size modulus, size ratio and the integral rate at which fines are produced", *AIME Transactions*, Vol. 223, pp. 422-427.
- [52] Klimpel, R.R., Austin, L.G., (1965), "The statistical theory of primary breakage distributions for brittle materials", *AIME Transactions*, Vol. 232, pp. 88-94.
- [53] Broadbent, S.R., Callcott, T.G., (1956), "Coal breakage processes, I. A new analysis of coal breakage processes", *Journal of the Institute of Fuel*, Vol. 29, pp. 524-528.
- [54] Gilvarry, J.J., Bergstrom, B.H., (1961), "Fracture and comminution of brittle solids (theory and experiment)", *AIME Transactions*, Vol. 220, pp. 380-389.
- [55] Gilvarry, J.J., Bergstrom, B.H., (1962), "Fracture and comminution of brittle solids: Further experimental results", *AIME Transactions*, Vol. 223, pp. 412-419.
- [56] Griffith, A.A., (1920), "The phenomena of rupture and flow in solids", *Royal Society of London Philosophical Transactions, Series A*, Vol. 221, pp. 163-198.
- [57] Oka, Y., Majima, H., (1970), "A theory of size reduction involving fracture mechanics", *Canadian Metallurgical Quarterly*, Vol. 9, No. 2, pp. 429-439.
- [58] Harris, C.C., (1968), "The application of size distribution equations to multi-event comminution processes", *AIME Transactions*, Vol. 241, pp. 343-358.

- 
- [59] Charles, R.J., (1957), "Energy-size reduction relationships in comminution", AIME Transactions, Vol. 208, pp. 80-88.
- [60] Bond, F.C., (1961), "Crushing & grinding calculations, Part I", British Chemical Engineering, Vol. 6, No. 6, pp. 378-385.
- [61] Holmes, J.A., (1957), "A contribution to the study of comminution-A modified form of Kick's law", Transactions Institution of Chemical Engineers, Vol. 35, pp. 125-156.
- [62] Bond, F.C., (1952), "The third theory of comminution", AIME Transactions, Vol. 193, pp. 484-494.
- [63] Bond, F.C., (1960), "Confirmation of the third theory", AIME Transactions, Vol. 217, pp. 139-153.
- [64] Bond, F.C., Wang, J.T. (1950), "A new theory of comminution", AIME Transactions, Vol. 187, pp. 871-878.
- [65] Bond, F.C., (1953), "Mathematics of crushing and grinding", in: Recent developments in mineral dressing; A symposium arranged by the Institution of Mining and Metallurgy held on 23<sup>rd</sup>-25<sup>th</sup> Sep. 1952, London, Session 2, Size reduction and screening, Institution of Mining and Metallurgy, London.
- [66] Hukki, R.T., (1961), "Proposal for a Solomonic settlement between the theories of Von Rittinger, Kick, and Bond", AIME Transactions, Vol. 220, pp. 403-408.
- [67] Agar, G., Charles, J., (1961), "Size distribution shift in grinding", AIME

- 
- Transactions, Vol. 220, pp. 390-394.
- [68] Walker, W.H., Lewis, W.K., McAdams, W.H., Gilliland, E.R., (1937), "Principles of chemicals engineering", McGraw-Hill, New York, pp. 251-288.
- [69] Berlioz, L.M., Fuerstenau, D.W., (1967), "A test of the Charles energy-size reduction relationship", AIME Transactions, Vol. 238, pp. 282-284.
- [70] Flament, F., Del villar, R., Lanthier, R., (1991), "Computer aided design of a control strategy for an industrial grinding circuit", Proceeding of 2<sup>nd</sup> Conference of Computer Applications in the Mineral Industry, pp. 337-348.
- [71] Pauw, O.G., (1988), "Optimization of individual events in grinding mills during which breakages occur", Powder Technology, Vol. 55, pp. 247-256.
- [72] Rajamani, R.K., Herbst, J.A., (1991), "Optimal control of a ball mill grinding circuit-I. Grinding circuit modelling and dynamic simulation", Chemical Engineering Science, Vol. 46, No. 3, pp. 861-870.
- [73] Rajamani, R.K., Herbst, J.A., (1991), "Optimal control of a ball mill grinding circuit-II. Feedback and optimal control", Chemical Engineering Science, Vol. 46, No. 3, pp. 870-879.
- [74] Austin, L.G., Rogers, R.S.C., Brame, K.A., Stubican, J., (1988), "A rapid computational procedure for unsteady-state ball mill circuit simulation", Powder Technology, Vol. 56, pp. 1-11.

- 
- [75] Flintoff, B.C., Edwards, R.P., (1992), "Process control in crushing", 1992 of SME, Phoenix, pp. 505-515.
- [76] Bascur, O.A., (1990), "Profit-based grinding controls", Minerals & Metallurgical Processing, Feb. 1990, pp. 9-15.
- [77] Bourassa, M., Roy, P., (1993), "Supervisory control in the grinding circuit at Les Mines D'OR Kiena", 25<sup>th</sup> Annual meeting of CMP, Paper No. 33, Ottawa.
- [78] Birch, P.R., (1972), "An introduction to the control of grinding circuits closed by hydrocyclones", Minerals Science and Engineering, Vol. 4, No. 3, pp. 55-66.
- [79] Roberts, E.J., (1950), "The probability theory of wet ball milling and its application", AIME Transactions, Mining Engineering, Vol. 187, pp. 1267-1272.
- [80] Arbiter, N., Harris, C.C., (1965), "Particles size distribution/time relationships in comminution", British Chemical Engineering, Vol. 10, No. 4, pp. 240-247.
- [81] Bowdish, F.W., (1960), "Theoretical and experimental studies of the kinetics of grinding in a ball mill", AIME Transactions, Vol. 217, pp. 194-202.
- [82] Arbiter, N., Bhrany, U.N., (1960), "Correlation of production size, capacity, and power in tumbling mills", AIME Transactions, Vol. 217, pp. 245-252.
- [83] Fuerstenau, D.W., Somasundaran, P., (1963), "Comminution kinetics", Proceedings of the 6<sup>th</sup> International Mineral Processing Congress, pp. 25-34.
- [84] Harris, C.C., (1968), "Batch grinding kinetics", AIME Transactions, Vol. 241,

---

pp. 359-364.

- [85] Harris, C.C., (1968), "Size reduction-time relationships of batch grinding", AIME Transactions, Vol. 241, pp. 449-453.
- [86] Nijman, I.J., (1958), "Ball-mill grinding- Part I", British Chemical Engineering, February 1958, pp. 77-80.
- [87] Gardner, R.P., Austin, L.G., (1962), "The use of a radioactive tracer technique and a computer in the study of the batch grinding of coal", Journal of the Institute of Fuel, Vol. 35, pp. 173-177.
- [88] Gardner, R.P., Austin, L.G., (1962), "A chemical engineering treatment of batch grinding", Parts I and II, 1<sup>st</sup> European symposium on size reduction, Editor: Rumpf, H., Verlag Chemie, Wein/Bergstr., pp. 217-248.
- [89] Austin, L.G., Klimpel, R.R., (1964), "The theory of grinding", Industrial and Engineering Chemistry, Vol. 56, No. 11, pp. 18-29.
- [90] Epstein, B., (1947), "The mathematical description of certain breakage mechanisms leading to the logarithmico-normal distribution", Journal of the Franklin Institute, Vol. 244, pp. 471-477.
- [91] Reid, K.J., (1965), "A solution to the batch grinding equation", Chemical Engineering Science, Vol. 20, pp. 953-963.
- [92] Broadbent, S.R., Callcott, T.G., (1956), "Coal breakage processes, II. A matrix representation of breakage", Journal of the Institute of Fuel, Vol. 29, pp. 528-

539.

- [93] Lynch, A.J., (1977), "Mineral crushing and grinding circuits, their simulation, optimization, design and control", Elsevier Scientific Publishing Company, New York.
- [94] Broadbent, S.R., Callcott, T.G., (1956), "A matrix analysis of processes involving particle assemblies", Royal Society of London Philosophical Transactions, Series A, Vol. 249, pp. 99-123.
- [95] Sedlatschek, K., Bass, L., (1953), "Contribution to the theory of milling processes", Powder Metallurgy Bulletin, Vol. 6, No. 5, pp. 148-153.
- [96] Austin, L.G., Klimpel, R.R., Beattie, A.N., (1967), "Solutions of equations of grinding", 2<sup>nd</sup> European symposium on size reduction, Editor: Rumpf, H., Verlag Chemie, Wein/Bergstr., pp. 281-312.
- [97] Furuya, M., Nakajima, Y., Tanaka, T., (1971), "Theoretical analysis of closed-circuit grinding system based on comminution kinetics", Industrial & Engineering Chemistry Process Design and Development, Vol. 10, No. 4, pp. 449-456.
- [98] Austin, L.G., Luckie, P.T., Klimpel, R.R., (1972), "Solutions of the batch grinding equation leading to Rosin-Rammler distributions", AIME Transactions, Vol. 252, pp. 87-94.
- [99] Gurevitch, L.S., Kremer, Y.B., Fidin, A.Y., (1992), "Batch grinding kinetics", Powder Technology, Vol. 69, pp. 133-137.

- 
- [100] Austin, L.G., Klimpel, R.R., Luckie, P.T., (1984), "Process engineering of size reduction: Ball milling", Society for Mining Engineers. AIME Inc., New York.
- [101] Austin, L.G., Shoji, K., Luckie, P.T., (1976), "The effect of ball size on mill performance", Powder Technology, Vol. 14, pp. 71-79.
- [102] Gupta, V.K., Kapur, P.C., (1974), "Empirical correlations for the effects of particulate mass and ball size on the selection parameters in the discretized batch grinding equation", Powder Technology, Vol. 10, pp. 217-223.
- [103] Morrell, S. (1990), "Effect of ball size on ball mill breakage rates", Julius Kruttschnitt Mineral Research centre (JKMRC), Sep. 1990, Australia, pp. 1-15.
- [104] Kelsall, D.F., Reid, K.J., Restarick, C.J., (1967/68), "Continuous grinding in a small wet ball mill, Part I. A study of the influence of ball diameter", Powder Technology, Vol. 1, pp. 291-300.
- [105] Herbst, J.A., Fuerstenau, D.W., (1972), "Influence of mill speed and ball loading on the parameters of the batch grinding equation", AIME Transactions, Vol. 252, pp. 169-176.
- [106] Herbst, J.A., Grandy, G.A., Fuerstenau, D.W., (1973), "Population balance models for the design of continuous grinding mills", Proceedings of the X<sup>th</sup> International Mineral Processing Congress, London, pp. 23-45.
- [107] Shoji, K., Lohrasb, S., Austin, L.G., (1980), "The variation of breakage parameters with ball and powder loading in dry ball milling", Powder Technology, Vol. 25, pp. 109-114.

- 
- [108] Austin, L.G., Bhatia, V.K., (1971/72), "Experimental methods for grinding studies in laboratory mills", *Powder Technology*, Vol. 5, pp. 261-266.
- [109] Kelsall, D.F., Stewart, P.S.B., Weller, K.R., (1973), "Continuous grinding in a small wet ball mill, Part IV. A study of the influence of media load and density", *Powder Technology*, Vol. 7, pp. 293-301.
- [110] Kelsall, D.F., Stewart, P.S.B., Weller, K.R., (1973), "Continuous grinding in a small wet ball mill, Part V. A study of the influence of media shape", *Powder Technology*, Vol. 8, pp. 77-83.
- [111] Herbst, J.A., Lo, Y.C., (1989), "Grinding efficiency with balls or cones as media", *International Journal of Mineral Processing*, Vol. 26, pp. 141-151.
- [112] Hasegawa, M., Honma, T., Kanda, Y., (1990), "Effect of mill diameter on the rate of initial grinding in vibration ball mills", *Powder Technology*, Vol. 60, pp. 259-264.
- [113] Gupta, V.K., Zouit, H., Hodouin, D., (1985), "The effect of ball and mill diameters on grinding rate parameters in dry grinding operation", *Powder Technology*, Vol. 42, pp. 199-208.
- [114] Nomura, S., Tanaka, T., (1989), "Analysis of mill capacity using a theoretically derived selection function applied to ball and Hardgrove mills", *Powder Technology*, Vol. 58, pp. 117-124.
- [115] Gao, M.W., Forssberg, E., (1989), "The effect of powder filling on selection and breakage functions in batch grinding", *Powder Technology*, Vol. 59, pp. 275-283.

- 
- [116] Austin, L.G., Bagga, P., (1981), "An analysis of fine dry grinding in ball mills", Powder Technology, Vol. 28, pp. 83-90.
- [117] Bérubé, M.A., Bérubé, Y., (1978), "A semi-empirical relationship between selection function and particle load in batch ball milling", Powder Technology, Vol. 19, pp. 89-92.
- [118] Le Houillier, R., Van Neste, A., Marchand, J.C., (1977), "Influence of charge on the parameters of the batch grinding equation and its implications in simulation", Powder Technology, Vol. 16, pp. 7-15.
- [119] Kelsall, D.F., Reid, K.J., Restarick, C.J., (1968/69), "Continuous grinding in a small wet ball mill, Part II. A study of the influence of hold-up weight", Powder Technology, Vol. 2, pp. 162-168.
- [120] Austin, L.G., Klimpel, R.R., (1985), "A note on the prediction of specific rates of breakage for an equilibrium ball charge", Powder Technology, Vol. 43, pp. 199-201.
- [121] Austin, L.G., Barahona, C.A., Weymont, N.P., Suryanarayanan, K., (1986), "An improved simulation model for semi-autogenous grinding", Powder Technology, Vol. 47, pp. 265-283.
- [122] Nomura, S., Hosoda, K., Tanaka, T., (1991), "An analysis of the selection function for mills using balls as grinding media", Powder Technology, Vol. 68, pp. 1-12.
- [123] Austin, L.G., Bagga, P., Celik, M., (1981), "Breakage properties of some

- 
- materials in a laboratory ball mill", *Powder Technology*, Vol. 28, pp. 235-241.
- [124] Cook, D.J., Rao, P.D., (1979), "Influence of particle shape and size on recovery of gold", in: *Conference on Alaskan Placer Mining, Focus: Gold Recovery Systems*, Mineral Industry Research Laboratory, Report No. 43, University of Alaska, Fairbanks, Alaska, pp. 1-19.
- [125] Dieter, Jr, G.E., (1961), "Mechanical metallurgy", McGraw-Hill Book Company, New York.
- [126] Hodouin, D., Bérubé, M.A., Everell, M.D., (1978), "Modelling industrial grinding circuits and applications in design", *CIM Bulletin*, Vol. 71, No. 797, pp. 138-146.
- [127] Austin, L.G., Barahona, C.A., Menacho, J.M., (1987), "Investigations of autogenous and semi-autogenous grinding in tumbling mills", *Powder Technology*, Vol. 51, pp. 283-294.
- [128] Austin, L.G., Shoji, K., Bell, D., (1982), "Rate equations for non-linear breakage in mills due to material effects", *Powder Technology*, Vol. 31, pp. 127-133.
- [129] Austin, L.G., Shoji, K., Everett, M.D., (1973), "An explanation of abnormal breakage of large particle sizes in laboratory mills", *Powder Technology*, Vol. 7, pp. 3-7.
- [130] Gardner, R.P., Austin, L.G., (1975), "The applicability of the first-order grinding law to particles having a distribution of strengths", *Powder Technology*, Vol. 12, pp. 65-69.

- 
- [131] Austin, L.G., Trimarchi, T., Weymont, N.P., (1977), "An analysis of some cases of non-first-order breakage rates". Powder Technology, Vol. 17, pp. 109-113.
- [132] Zhang, Y., (1992), "Simulation of comminution and classification in cement manufacture", Ph.D. Thesis, Department of Mining and Metallurgical Engineering, University of Queensland, Australia.
- [133] Herbst, J.A., Fuerstenau, D.W., (1980), "Scale-up procedure for continuous grinding mill design using population balance models", International Journal of Mineral Processing, Vol. 7, pp. 1-3.
- [134] Klimpel, R.R., Austin, L.G., (1970), "Determination of selection-for-breakage functions in the batch grinding equation by nonlinear optimization", Industrial & Engineering Chemistry Fundamentals, Vol. 9, No. 2, pp. 230-236.
- [135] Laplante, A.R., Finch, J.A., Del Villar, R., (1987), "Simplification of grinding equation for plant simulation", Transactions of the Institution of Mining and Metallurgy, Section C: Mineral Processing and Extractive Metallurgy, Vol. 96, June 1987, pp. C108-C112.
- [136] Laguitton, D., Leung, J., Gupta, V.K., Hodouin, D., Spring, R., (1983), "Program for breakage and selection functions determination in kinetic model of ball mills", SPOC Manual, Chapter 7.2, Report SP85-1/7.2E, CANMET, Energy, Mines and Resources Canada.
- [137] Zhang, Y.M., Kavetsky, A., (1993), "Investigation of particle breakage mechanisms in a batch mill using back-calculation", International Journal of Mineral Processing, Vol. 39, pp. 41-60.

- 
- [138] Kelly, E.G., Spottiswood, D.J., (1990), "The breakage function: What is it really?", *Minerals Engineering*, Vol. 3, No. 5, pp. 405-414.
- [139] Laplante, A.R., (1991), "Presentation on the modelling of grinding", Professional Development Seminars, Mining and Metallurgical Engineering Department, McGill University, Montreal, Canada.
- [140] Narayanan, S.S., Whiten, W.J., (1988), "Determination of comminution characteristics from single particle breakage tests and its application to ball-mill scale-up", *Transactions of the Institution of Mining and Metallurgy, Section c: Mineral Processing & Extractive Metallurgy*, Vol. 97, pp. C115-C124.
- [141] Krogh, S.R., (1979), "Determination of crushing and grinding characteristics based on testing of single particles", *AIME Transactions*, Vol. 266, pp. 197-1962.
- [142] Narayanan, S.S., (1987), "Modelling the performance of industrial ball mills using particle breakage data", *International Journal of Mineral Processing*, Vol. 20, pp. 211-228.
- [143] King, R.P., (1994), "Comminution and liberation of minerals", *Minerals Engineering*, Vol. 7, Nos. 2/3, pp. 129-140.
- [144] Austin, L.G., Luckie, P.T., (1971/72), "Methods for determination of breakage distribution parameters", *Powder Technology*, Vol. 5, pp. 215-222.
- [145] Austin, L.G., Luckie, P.T., (1971/72), "The estimation of non-normalized breakage distribution parameters from batch grinding tests", *Powder Technology*, Vol. 5, pp. 267-271.

- 
- [146] Hurlbut, Jr, C.S., (1967), "Minerals and how to study them", John Wiley & Sons, New York, pp. 69-138.
- [147] Read, H.H., (1947), "Rutley's elements of mineralogy", Thomas Murby & Co., London.
- [148] Hurlbut Jr., C.S., (1971), "Dana's manual of mineralogy", John Wiley & Sons, New York.
- [149] Hausner, H.H., (1973), "Handbook of powder metallurgy", Chemical Publishing Co. Inc., New York.
- [150] Trent, E.M., (1958), "Mechanical methods of powder production as used in the carbide industry", Powder Metallurgy, No. 1/2, pp. 65-72.
- [151] Amin, H.S., (1952), "Production of aluminum powder and paste in India", Indian Institute of Metals-Transactions, Vol. 6., pp. 285-295.
- [152] Noel, D.O., Shaw, J.D., Gebert, E.B., (1938), "Production and some testing methods of metal powders", AIME Transactions, Vol. 128, pp. 37-57.
- [153] Andrade, E.N.C., Randall, R.F.Y., Makin, M.J., (1950), "The Rehbinder effect", London Physical Society Proceedings, Vol. 63B, pp. 990-995.
- [154] Klimpel, R.R., Austin, L.G., (1982), "Chemical additives for wet grinding of minerals", Powder Technology, Vol. 31, pp. 239-253.
- [155] Hall, J.E., (1926), "Process and method of disintegrating metals in a ball mill or

- 
- the like", U.S. Patent, No. 1569484.
- [156] Hall, J.E., (1935), "Bronze, bronze powders, and method of making the same", U.S. Patent, No. 2002891.
- [157] Huttig, G.F., Sales, H., (1954), "The grinding of metal powders", Powder Metallurgy, Group I, pp. 8-10.
- [158] Smith, E.A., (1970), "Comminuting very hard and soft solids", Metals and Materials, October 1970, pp. 426-428.
- [159] Rees, G.J., Young, B., (1972), "The milling of hard metal alloy powders", South African Mechanical Engineer, Vol. 22, pp. 81-87.
- [160] Hopkins, D.W., Brooks, R.G., (1976), "Some observations on the milling behaviour of nitrogen-atomized cobalt powder", Powder Metallurgy, Vol. 19, No. 1, pp. 46-48.
- [161] Hashimoto, H., Watanabe, R., (1990), "Model simulation of energy consumption during vibratory ball milling of metal powder", Materials Transactions, JIM, Vol. 31, No. 3, pp. 219-224.
- [162] Snow, R.H., Luckie, P.T., (1976), "Annual review of size reduction-1974", Powder Technology, Vol. 13, pp. 33-48.
- [163] Tripathi, K.C., Groszek, A.J., (1973), "Effect of hydrocarbons on milling of aluminum powder" Aluminum, Vol. 149, No. 9, pp. 612-615.

- 
- [164] Moothedath, S.K., Sastry, K.V.S., (1993), "Solution and experimental validation of a mathematical model for vibration milling of metal powders". Powder Technology, Vol. 75, pp. 89-96.
- [165] Sastry, Kal V.S., Moothedath, S.K., (1990), "A mathematical model for vibration milling of metal powders", Proceedings of 2<sup>nd</sup> of World Congress Particle Technology, Kyoto, Japan, Sep. 19-22, pp. 447-454.
- [166] Yeen, W.. (1985), "Experimental abrasion of detrital gold", in: Conference on Alaskan Placer Mining (7<sup>th</sup>), Mineral Industry Research Laboratory, University of Alaska, Fairbanks, Alaska, pp. 1-8.
- [167] Liu, L., (1989), "An investigation of gold recovery in the grinding and gravity circuits at Les Mines Camchib Inc.", M.Eng. Thesis, Mining & Metallurgical Engineering Department, McGill University, Montreal, Canada.
- [168] Laplante, A.R., Liu, L., Cauchon, A., (1990), "Gold gravity recovery at the mill of Les Mines Camchib Inc., Chibougamau, Quebec", 22<sup>nd</sup> Annual meeting of CMP, Paper No. 22, Ottawa.
- [169] Woodcock, F.C., (1994), "Use of a Knelson unit to quantify gravity recoverable gold in an ore", M.Eng. Thesis, Mining & Metallurgical Engineering Department, McGill University, Montreal, Canada.
- [170] Buonvino, M., (1993), "A study of the Falcon Concentrator", M.Eng. Thesis, Mining & Metallurgical Engineering Department, McGill University, Montreal, Canada.

- 
- [171] Laplante, A.R., Vincent, F., Luisntra, W.F., (1996), "A laboratory procedure to determine the amount of gravity recoverable gold- A case study at Hemlo Gold Mines", 28<sup>th</sup> Annual meeting of CMP, Paper No. 6, Ottawa.
- [172] Bronson, R., (1973), "Modern introductory differential equations", Schaum's Outline Series, Mcgraw-Hill Book Company, New York.
- [173] Software Manual, (1993), "Scientist, mathematical modelling/differential and nonlinear equations", Micromath Scientific Software Company.
- [174] Callister Jr., W.D., (1991), "Materials science and engineering", John Wiley & Sons Inc., New York.
- [175] Avner, S.H., (1974), "Introduction to physical metallurgy", McGraw-Hill Book Company, New York.
- [176] ASTM, (1992), "Annual book of ASTM standards, metals test methods and analytical procedures", American Society for Testing and Materials, Vol. 3.01, E18, pp. 184-197.
- [177] ASTM, (1992), "Annual book of ASTM standards, metals test methods and analytical procedures", American Society for Testing and Materials, Vol. 3.01, E10, pp. 177-183.
- [178] ASTM, (1992), "Annual book of ASTM standards, general products, chemical specialties, and end use products", American Society for Testing and Materials, Vol. 15.02, C849, pp. 284-287.

- 
- [179] ASTM, (1992), "Annual book of ASTM standards, metals test methods and analytical procedures", American Society for Testing and Materials, Vol. 3.01, E384, pp. 484-497.
- [180] John, V., (1992), "Testing of materials", Macmillan, London.
- [181] Cahn, R.W., (1965), "Physical metallurgy", John Wiley & Sons Inc., New York.
- [182] Chalmers, B., (1959), "Physical metallurgy", John Wiley & Sons Inc., New York.
- [183] Sheager, A.M., (1969), "Elementary metallurgy and metallography", Dover Publications Inc., New York.
- [184] Savitsky, E., Polyakova, V., Gorina, N., Roshan, N., (1978), "Physical metallurgy of platinum metals", Mir Publishers, Moscow.
- [185] Ross, R.B., (1977), "Handbook of metal treatments and testing", John Wiley & Sons, New York.
- [186] Allen, D.K., (1969), "Metallurgy theory and practice", American Technical Society, Chicago.
- [187] Sietz, F., (1943), "The physics of metals", McGraw-Hill Book Company, Inc., New York.
- [188] Smithells, C.J., Brandes, E.A., (1976), "Metals reference book", Butterworths, London.

- 
- [189] Samuels, L.E., (1988). "Metals engineering, a technical guide". ASM International, Metals park, Ohio.
- [190] Boyer, H.E., Gall, T.L., (1985), "Metals handbook, Desk Edition", American Society for Metals, Metals Park, Ohio.
- [191] Dalton, W.K., (1994), "The technology of metallurgy". Macmillan Publishing Company, New York.
- [192] Kim, J., Noranda Technology Centre, Montreal, Canada, Personal Communication.
- [193] Meloy, T.P., Clark, N., Durney, T.E., Pitchumani, B., (1985), "Measuring the particle shape mix in a powder with the cascadowgraph", Chemical Engineering Science, Vol. 40, No. 7, pp. 1077-1085.
- [194] German, R.M., (1984), "Powder metallurgy science", Metal Powder Industries Federation, Princeton.
- [195] Luerkens, D.W., Beddow, J.K., Vetter, A.F., (1987), "Structure and morphology- the science of form applied to particles characterization", Powder Technology, Vol. 50, pp. 93-101.
- [196] Holt, C.B., (1981), "The shape of particles produced by comminution. A review", Powder Technology, Vol. 28, pp. 59-63.
- [197] Durney, T.E., Meloy, T.P., (1986), "Particles shape effects due to crushing method and size", International Journal of Mineral Processing, Vol. 16, pp. 109-

- 
- 123.
- [198] Lashley, W.C., (1983), "The flatness factor", California Mining Journal, Part I: October 1983, pp. 14-19, Part-II: November 1983, pp. 38-40.
- [199] Tourtelot, H.A., Riley, L.B., (1971), "Size and shape of gold and platinum grains", Ores Sediments, International Sedimentological Congress (8<sup>th</sup>), pp. 307-319.
- [200] Walsh, D.E., Rao, P.D., (1988), "A study of factors suspected of influencing the settling velocity of fine gold particles", MIRL Repot No. 76, Mineral Industry Research Laboratory, University of Alaska, Fairbanks, Alaska.
- [201] Laplante, A.R., Shu, Y., Marios, J., (1996), "Experimental characterization of a centrifugal separation", Canadian Metallurgical Quaterly, Vol. 35, No. 1, pp. 23-29.
- [202] Furuuchi, M., Gotoh, K., (1992), "Shape separation of particles", Powder Technology, Vol. 73, pp. 1-9.
- [203] Shinohara, K., (1986), "Fundamental analysis on gravitational separation of differently shaped particles on inclined plates", Powder Technology, Vol. 48, pp. 151-159.
- [204] Riley, G.S. (1968/69), "An examination of the separation of differently shaped particles", Powder Technology, Vol. 2, pp. 311-314.
- [205] Viswanathan, K., Aravamudhan, S., Mani, B.P., (1984), "Separation based on

- shape. Part I: Recovery efficiency of spherical particles", *Powder Technology*, Vol. 39, pp. 83-91.
- [206] Aravamudhan, S., Premkumar, N., Yerrapragad, S.S., Mani, B.P., Viswanathan, K., (1984), "Separation based on shape, Part II: Newton's separation efficiency", *Powder Technology*, Vol. 39, pp. 93-98.
- [207] Nakagawa, M., Furuuchi, M., Yamahata, M., Gotoh, K., Beddow, J.K., (1985), "Shape classification of granular materials by rotating with blades", *Powder Technology*, Vol. 44, pp. 195-202.
- [208] Waldie, B., (1973), "Separation of particles according to shape", *Powder Technology*, Vol. 7, pp. 244-246.
- [209] Furuuchi, M., Gotoh, K., (1988), "Continuous shape separation of binary mixture of granular particles", *Powder Technology*, Vol. 54, pp. 31-37.
- [210] Furuuchi, M., Nakagawa, M., Suzuki, M., Tsuyumine, H., Gotoh, K., (1987), "Optimal performance of a shape classifier for binary mixtures of granular materials", *Powder Technology*, Vol. 50, pp. 137-145.
- [211] Roberts, T.A., Beddow, J.K., (1968/69), "Some effects of particle shape and size upon blinding during sieving", *Powder Technology*, Vol. 2, pp. 121-124.
- [212] Ludwick, J.C., Henderson, P.L., (1968), "Particle shape and inference of size from sieving", *Sedimentology*, Vol. 11, pp. 197-235.
- [213] Orr, C., (1987), "An exploration of dry powder chromatography", *Powder*

- 
- Technology, Vol. 50, pp. 217-220.
- [214] Furuuchi, M., Yamada, C., Gotoh, K., (1993), "Shape separation of particulate by a rotary horizontal sieve drum", Powder Technology, Vol. 75, pp. 113-118.
- [215] Murali, C., Pitchuman, B., Clark, N.N., (1986), "A settler for continuous particle shape separation", International Journal of Mineral Processing, Vol. 18, pp. 237-249.
- [216] Sivamohan, R., Forssberg, E., (1985), "Principles of tabling", International Journal of Mineral Processing, Vol. 15, pp. 281-295.
- [217] Durney, T.E., Meloy, T.P., (1985), "Experimental proof: residence time distribution in cascadography", International Journal of Mineral Processing, Vol. 14, pp. 313-317.
- [218] Meloy, T.P., Williams, M.C., Ferrara, G., Guimaraes, C.A., (1992), "Continuous sieve cascadography, very narrow band sizing", in: Comminution-Theory and Practice, Editor: Kawatra, S.K., Society for Mining Engineers, AIME Inc., Colorado, Chapter 49, pp. 677-688.
- [219] Meloy, T.P., Makino, K., (1983), "Characterizing residence times of powder samples on sieves", Powder Technology, Vol. 36, pp. 253-258.
- [220] Meloy, T.P., Durney, T.E., (1983), "Particle shape chromatography-the sieve cascadograph", International Journal of Mineral Processing, Vol. 11, pp. 101-113.

- 
- [221] Clark, N.N., Meloy, T.P., (1988), "Particle sample shape description with an automated cascadograph particle analyzer", Powder Technology, Vol. 54, pp. 271-277.
- [222] Levenspiel, O., (1972), "Chemical reaction engineering", John Wiley & Sons, New York.
- [223] Agar, G.E., (1993), "Assessment of gravity recoverable gold", 25<sup>th</sup> Annual meeting of CMP, Paper No. 13, Ottawa.
- [224] Laplante, A.R., Putz, A., Huang, L., Vincent, F., (1994), "Practical considerations in the operations of gold gravity circuits", 26<sup>th</sup> Annual meeting of CMP, Paper No. 23, Ottawa.
- [225] Forssberg, E., Nordquist, T., (1987), "Pilot plant trials of new gravity concentration equipment", Minerals and Metallurgical Processing, Technical Note, May 1987, pp. 87-89.
- [226] Laplante, A.R., (1993), "A comparative study of two centrifugal concentrators", 25<sup>th</sup> Annual meeting of CMP, Paper No. 5, Ottawa.
- [227] Woodcock, F., Laplante, A.R., (1993), "A laboratory method for determining the amount of gravity recoverable gold", Randol Gold Seminar, Beaver Creek, Sep. 1993.
- [228] Knelson, B., (1992), "The Knelson Concentrator. Metamorphosis from crude beginning to sophisticated world wide acceptance", Minerals Engineering, Vol. 5, Nos. 10/12, pp. 1091-1097.

- 
- [229] Knelson International Sales Inc., "Operating guidelines for the 3" Knelson Concentrator", manual prepared by: Knelson International Sales Inc.
- [230] Knelson, B., Jones, R., (1994), "A new generation of Knelson Concentrators, A totally secure system goes on line", Minerals Engineering, Vol. 7, Nos., 2/3, pp. 201-207.
- [231] Sanders, D., Sanders, R., (1985), "A study on fine gold recovery and the Knelson Concentrator", Golden Nugget Mining Operation on Olive Creek, Livengood.
- [232] Laplante, A.R., Shu, Y., (1992), "The use of a laboratory centrifugal separator to study gravity recovery in industrial circuits", 24<sup>th</sup> Annual meeting of CMP, Paper No. 12, Ottawa.
- [233] Laplante, A.R., Putz, A., Huang, L., (1993), "Sampling and sample processing for gold gravity circuits", Professional Development Seminars, Gold recovery by Gravity, Mining and Metallurgical Engineering Department, McGill University, Montreal, Canada.
- [234] Del villar, R., Laplante, A.R., (1985), "Grinding simulation in Applesoft Basic", CIM Bulletin, Volume 78, No. 883, pp. 62-65.
- [235] Huang, L., (1996), "Upgrading of gold gravity concentrates", Ph.D. Thesis, Department of Mining and Metallurgical Engineering, McGill University, Canada, in preparation.
- [236] Mazumdar, M., (1994), "Statistical discrimination of flotation models based on batch flotation data", International Journal of Mineral Processing, Vol. 42, pp.

53-73.

---

**Appendix I: Analytical & Numerical Solutions of the  
Proposed Models**

## I.1 Introduction

In this chapter analytical and numerical solutions for the proposed model for malleable materials, Equations 3.7, in chapter 3 are presented.

## I.2 Analytical Solution

Proposed models are analytically solved using the ODE (ordinary differential equation) solution for a system and initial conditions. When the number of size classes increases the analytical solution is not simple, and therefore numerical solutions are used. In this chapter, the analytical solutions for the simplest case which is a system consisting of three size classes is presented.

### I.2.1 Case 1: Folding & flattening and no breakage

Based on this model for malleable material a system consisting of three size classes has three differential equations as follows:

$$dw_1/dt = -r_{1,2}w_1 + r_{2,1}w_2$$

$$dw_2/dt = r_{1,2}w_1 - (r_{2,1} + r_{2,3})w_2 + r_{3,2}w_3$$

$$dw_3/dt = -r_{3,2}w_3 + r_{2,3}w_2$$

and, the analytical solution for this system is as follows;

$$dw_1/dt = -r_{1,2}w_1 + r_{2,1}w_2$$

$$dW_2/dt = r_{1,2}w_1 - (r_{2,1} + r_{2,3})w_2 + r_{3,2}w_3$$

$$w_1 + w_2 + w_3 = 100 (\%)$$

Therefore,

$$dw_1/dt = -r_{1,2}w_1 + r_{2,1}w_2$$

$$dw_2/dt = r_{1,2}w_1 - (r_{2,1} + r_{2,3})w_2 + r_{3,2}(1 - w_1 - w_2)$$

and

$$dw_1/dt = -r_{1,2}w_1 + r_{2,1}w_2$$

$$dw_2/dt = (r_{1,2} + r_{3,2})w_1 - (r_{2,1} + r_{2,3} + r_{3,2})w_2 + r_{3,2}$$

using the differential operator "D", yields:

$$(D + r_{1,2})w_1 - r_{2,1}w_2 = 0$$

$$(D + r_{2,1} + r_{2,3} + r_{3,2})w_2 - (r_{3,2} - r_{1,2})w_1 = r_{3,2}$$

Solving the above equations for  $w_1$  and  $w_2$ ,

$$\text{for } w_1: (D^2 + (r_{1,2} + r_{2,1} + r_{2,3} + r_{3,2})D + (r_{1,2}r_{2,3} + r_{1,2}r_{3,2} + r_{2,3}r_{3,2}))w_1 = r_{3,2}$$

$$\text{for } w_2: (D^2 + (r_{1,2} + r_{2,1} + r_{2,3} + r_{3,2})D + (r_{1,2}r_{2,3} + r_{1,2}r_{3,2} + r_{2,3}r_{3,2}))w_2 = r_{1,2}r_{3,2}$$

If suppose the  $r_1$  and  $r_2$  are the roots of the above equations, therefore the general solution of differential equations will be:

$$w_1 = c_1e^{-r_1t} + c_2e^{-r_2t} + l_1$$

$$w_2 = c_3e^{-r_1t} + c_4e^{-r_2t} + l_2$$

In order to calculate the exact answer, the coefficients of  $l_1$ ,  $l_2$ ,  $c_1$ ,  $c_2$ ,  $c_3$  and  $c_4$  must be calculated. To do that, at  $t = \infty$ :

$$dw_1/dt = dw_2/dt = 0$$

and,

$$w_1 = l_1, w_2 = l_2$$

Therefore,

$$-r_{1,2}l_1 + r_{2,1}l_2 = 0$$

$$(r_{1,2} - r_{3,2})l_1 - (r_{2,1} + r_{2,3} + r_{3,2})l_2 = -r_{3,2}$$

Finally, by solving for the  $l_1$  and  $l_2$  in the above system,

$$l_1 = (r_{2,1}r_{3,2}) / (r_{1,2}r_{2,3} + r_{1,2}r_{3,2} + r_{2,1}r_{3,2})$$

$$l_2 = (r_{1,2}r_{3,2}) / (r_{1,2}r_{2,3} + r_{1,2}r_{3,2} + r_{2,1}r_{3,2})$$

$c_1$ ,  $c_2$ ,  $c_3$  and  $c_4$  are calculated from the initial conditions. As an example we will choose  $w_2(0) = 1$ , therefore:

$$w_1(0) = 0, w_3(0) = 0$$

Substituting the above initial conditions in the general answers of the differential

equations yield:

$$l_1 + c_1 + c_2 = 0 \quad (i)$$

$$l_2 + c_3 + c_4 = 1 \quad (ii)$$

and at  $t=0$ ,

$$w_1 = 0, w_2 = 1, w_3 = 0$$

Substitution these values in the original differential equations yields:

$$(dw_1/dt)_{t=0} = r_{2,1}$$

$$(dw_2/dt)_{t=0} = -(r_{2,1} + r_{2,3})$$

Now, if we derive from the general answers at  $t=0$ ,

$$r_1 c_1 + r_2 c_2 = r_{2,1} \quad (iii)$$

$$r_1 c_3 + r_2 c_4 = -(r_{2,1} + r_{2,3}) \quad (iv)$$

After solving the system of equations (i), (ii), (iii) and (iv), the coefficients are equal to:

$$c_1 = -l_1 + ((r_1 l_1 + r_{2,1}) / (r_1 - r_2))$$

$$c_2 = (-r_1 l_1 - r_{2,1}) / (r_1 - r_2)$$

$$c_3 = 1 - l_2 - ((r_1 - r_1 l_2 + r_{2,1} + r_{2,3}) / (r_1 - r_2))$$

$$c_4 = (r_1 - r_1 l_2 + r_{2,1} + r_{2,3}) / (r_1 - r_2)$$

### I.3 Numerical Solution

A numerical method for solving an initial-value problem is a procedure which produces approximate solutions at particular points using only the operations of addition, subtraction, multiplication, division and function evaluations. All numerical methods will involve finding approximate solutions at different steps of independent variables, where the difference between any two successive independent values is a constant (for example if  $x$  is independent variable, then  $h = x_{n+1} - x_n$ ).

The step value of two successive independent iterations is arbitrarily chosen, and in general, the smaller step gives the more accurate the approximate solution. There are

different numerical methods, such as Euler's, Heun's, Nystrom's, and Runge-Kutta's. A numerical method is of order  $n$ , where  $n$  is a positive integer, if the method is exact for polynomials of  $n$  or fewer degrees. In other words, if the true solution of initial-value problem is a polynomial of degree  $n$  or less, the approximate solution and the true solution will be identical for a method of order  $n$ .

In general, the higher the order, the more accurate the method. For example, Euler's method is of first order and both Heun's and Nystrom's methods are of second order. Runge-Kutta has two sub-groups as third-order and fourth-order methods. Here, the fourth-order Runge-Kutta method is defined for the three size classes system which was used to illustrate analytical solutions. In this part, the numerical solution based on the fourth order of Runge-Kutta method is only used for the folding and flattening model of malleable material and the other models are solved in a same procedures.

### I.3.1 Case 1: Folding & flattening and no breakage

The differential equations of this model for a system consisting of three size classes are the same as section I.2.1, the step value of two successive iterations,  $h$ , is a time increment, the values of dependent variables in new iteration will be calculated by using several coefficients based on the shape of each equation. If we use the parameters of  $l_1$  to  $l_4$  for  $w_1$ ,  $k_1$  to  $k_4$  for  $w_2$  and  $j_1$  to  $j_4$  for  $w_3$  (four parameters for each mass), therefore the solutions will be as follows:

$$dw_1/dt = -r_{1,2}w_1 + r_{2,1}w_2$$

$$dw_2/dt = r_{1,2}w_1 - (r_{2,1} + r_{2,3})w_2 + r_{3,2}w_3$$

$$dw_3/dt = r_{2,3}w_2 - r_{3,2}w_3$$

Therefore,

$$l_1 = h*(-r_{1,2}w_1 + r_{2,1}w_2)$$

$$k_1 = h*(r_{1,2}w_1 - (r_{2,1} + r_{2,3})w_2 + r_{3,2}w_3)$$

$$j_1 = h^*(r_{2,3}w_2 - r_{3,2}w_3)$$

$$l_2 = h^*(-r_{1,2}(w_1 + 0.5l_1) + r_{2,1}(w_2 + 0.5k_1))$$

$$k_2 = h^*(r_{1,2}(w_1 + 0.5l_1) - (r_{2,1} + r_{2,3})(w_2 + 0.5k_1) + r_{3,2}(w_3 + 0.5j_1))$$

$$j_2 = h^*(r_{2,3}(w_2 + 0.5k_1) - r_{3,2}(w_3 + 0.5j_1))$$

$$l_3 = h^*(-r_{1,2}(w_1 + 0.5l_2) + r_{2,1}(w_2 + 0.5k_2))$$

$$k_3 = h^*(r_{1,2}(w_1 + 0.5l_2) - (r_{2,1} + r_{2,3})(w_2 + 0.5k_2) + r_{3,2}(w_3 + 0.5j_2))$$

$$j_3 = h^*(r_{2,3}(w_2 + 0.5k_2) - r_{3,2}(w_3 + 0.5j_2))$$

$$l_4 = h^*(-r_{1,2}(w_1 + l_3) + r_{2,1}(w_2 + k_3))$$

$$k_4 = h^*(r_{1,2}(w_1 + l_3) - (r_{2,1} + r_{2,3})(w_2 + k_3) + r_{3,2}(w_3 + j_3))$$

$$j_4 = h^*(r_{2,3}(w_2 + k_3) - r_{3,2}(w_3 + j_3))$$

and the new masses are:

$$(w_1)_{n+1} = (w_1)_n + (1/6)(k_1 + 2k_2 + 2k_3 + k_4)$$

$$(w_2)_{n+1} = (w_2)_n + (1/6)(l_1 + 2l_2 + 2l_3 + l_4)$$

$$(w_3)_{n+1} = (w_3)_n + (1/6)(j_1 + 2j_2 + 2j_3 + j_4)$$

---

**Appendix II: Complete Set of the Estimated Rate  
Constants & Fitted Curves of Chapters 5 & 6**

**Table II.1: Estimated rate constants (all in min<sup>-1</sup>) for the Bond ball mill tests (lead fragments tests): flattening, folding and limited breakage model.**

Feed Size (mm)	1.18-1.40, w <sub>1</sub>			0.850-1.00, w <sub>2</sub>			0.600-0.710, w <sub>3</sub>			0.425-0.500, w <sub>4</sub>			
	Products (No. of Size Classes):			Products (No. of Size Classes):			Products (No. of Size Classes):			Products (No. of Size Classes):			
	(3)	(4)	(5)	(3)	(4)	(5)	(3)	(4)	(5)	(3)	(4)	(5)	
r <sub>1,2</sub>	0.000	0.000	0.000	0.000	0.000	0.000	0.000	0.000	0.000	0.001	0.001	0.000	
r <sub>2,2</sub>	0.005	0.004	0.003	0.003	0.003	0.002	0.003	0.004	0.003	0.003	0.003	0.002	
r <sub>1,3</sub>	0.000	0.000	0.000	0.000	0.000	0.000	0.000	0.000	0.000	0.000	0.000	0.000	
r <sub>2,3</sub>	-	0.004	0.000	-	0.000	0.000	-	0.000	0.000	-	0.000	0.000	
r <sub>1,4</sub>	-	-	0.000	-	-	0.000	-	-	0.000	-	-	0.000	
r <sub>2,4</sub>	0.008	0.012	0.011	0.009	0.013	0.012	0.007	0.011	0.011	0.005	0.009	0.009	
r <sub>3,1</sub>	0.036	0.047	0.045	0.063	0.090	0.087	0.066	0.093	0.092	0.089	0.139	0.139	
r <sub>4,1</sub>	0.041	0.104	0.129	0.021	0.076	0.071	0.022	0.099	0.101	0.026	0.333	0.086	
r <sub>3,2</sub>	0.106	0.237	0.297	0.118	0.380	0.344	0.163	0.673	0.677	0.138	0.004	0.346	
r <sub>4,2</sub>	-	0.005	0.005	-	0.005	0.008	-	0.002	0.004	-	0.000	0.000	
r <sub>3,3</sub>	-	0.013	0.000	-	0.000	0.000	-	0.000	0.000	-	0.001	0.000	
r <sub>4,3</sub>	-	-	0.012	-	-	0.006	-	-	0.009	-	-	0.010	
r <sub>3,4</sub>	-	-	0.000	-	-	0.000	-	-	0.000	-	-	0.000	
SS of:	w <sub>1</sub>	33	75	71	119	179	166	112	149	151	28	52	54
	w <sub>2</sub>	43	87	58	100	132	127	129	159	154	45	70	69
	w <sub>3</sub>	31	23	33	15	13	15	10	8	9	7	6	7
	w <sub>4</sub>	-	7	7	-	8	5	-	1	1	-	2	1
	w <sub>5</sub>	-	-	5	-	-	2	-	-	1	-	-	1
	w <sub>6</sub>	3	3	5	9	3	1	5	7	8	6	6	6
	Total	110	192	179	243	335	316	256	324	327	86	136	138
MSS	3.8	5.5	4.4	8.4	9.6	7.7	7.3	7.9	4.0	3.0	3.9	3.4	
S <sub>1</sub>	1.9	2.3	2.1	2.9	3.1	2.8	2.7	2.8	2.0	1.7	2.0	1.8	

**Table II.2: Estimated rate constants (all in min<sup>-1</sup>) for the small ball mill tests (lead fragments tests); flattening and folding model (no breakage).**

Feed Size (mm)		1.18-1.40, w <sub>2</sub>			0.850-1.00, w <sub>2</sub>			0.600-0.710, w <sub>2</sub>			0.425-0.500, w <sub>2</sub>		
Rate Constants		Products (Sizes)			Products (Sizes)			Products (Sizes)			Products (Sizes)		
		(3)	(4)	(5)	(3)	(4)	(5)	(3)	(4)	(5)	(3)	(4)	(5)
r <sub>1,2</sub>		0.000	0.000	0.000	0.116	0.118	0.117	0.112	0.116	0.116	0.039	0.039	0.042
r <sub>2,1</sub>		0.030	0.030	0.030	0.112	0.113	0.121	0.093	0.095	0.095	0.101	0.097	0.099
r <sub>2,3</sub>		0.313	0.442	0.337	0.417	0.484	2.710	0.475	0.901	0.823	0.751	0.882	3.467
r <sub>3,2</sub>		1.233	2.347	1.791	2.060	3.685	20.000	1.838	4.649	4.253	3.312	5.150	20.000
r <sub>3,4</sub>		-	0.745	0.749	-	11.779	8.920	-	0.594	0.741	-	4.262	3.687
r <sub>4,3</sub>		-	1.989	3.299	-	20.175	20.000	-	1.767	3.697	-	13.007	15.752
r <sub>4,5</sub>		-	-	2.965	-	-	0.000	-	-	19.497	-	-	7.902
r <sub>5,4</sub>		-	-	4.903	-	-	0.000	-	-	28.935	-	-	20.000
SS of:	w <sub>1</sub>	143	144	148	82	84	96	21	22	22	36	39	39
	w <sub>2</sub>	103	100	110	46	42	58	15	15	15	49	45	45
	w <sub>3</sub>	13	6	5	50	28	32	9	7	7	94	52	52
	w <sub>4</sub>	-	6	2	-	6	6	-	2	1	-	9	5
	w <sub>5</sub>	-	-	1	-	-	15	-	-	2	-	-	1
	Total	259	256	266	178	160	207	44	47	47	179	145	142
MSS		8.9	6.7	5.7	6.8	4.7	4.9	0.9	0.7	0.6	4.4	2.7	2.1
S <sub>r</sub>		3.0	2.6	2.4	2.6	2.2	2.2	0.9	0.8	0.8	2.1	1.6	1.4

**Table II.3: Estimated rate constants (all in min<sup>-1</sup>) for the Bond rod mill tests (lead fragments tests); flattening, folding and explicit breakage model.**

Feed Size (mm)	1.18-1.40, w <sub>2</sub>			0.850-1.00, w <sub>2</sub>			0.600-0.710, w <sub>2</sub>			0.425-0.500, w <sub>2</sub>			
	Products (No. of Size Classes):			Products (No. of Size Classes):			Products (No. of Size Classes):			Products (No. of Size Classes):			
	(3)	(4)	(5)	(3)	(4)	(5)	(3)	(4)	(5)	(3)	(4)	(5)	
s <sub>1</sub>	0.000	0.865	1.212	0.000	0.000	0.000	0.000	0.000	0.000	0.001	0.001	1.076	
s <sub>2</sub>	1.602	0.880	0.497	0.003	0.003	0.002	0.003	0.004	0.003	0.003	0.003	0.188	
s <sub>3</sub>	0.536	0.000	0.000	0.000	0.000	0.000	0.000	0.000	0.000	0.000	0.000	0.000	
s <sub>4</sub>	-	0.000	0.000	-	0.000	0.000	-	0.000	0.000	-	0.000	0.000	
s <sub>5</sub>	-	-	0.000	-	-	0.000	-	-	0.000	-	-	0.857	
r <sub>1,2</sub>	1.217	0.411	0.060	0.889	0.000	0.000	0.628	0.000	0.000	0.849	0.000	0.000	
r <sub>2,1</sub>	2.259	2.390	2.398	1.933	2.032	2.025	0.917	0.950	0.969	0.678	0.694	0.860	
r <sub>2,3</sub>	1.127	2.518	3.205	0.770	2.466	2.849	1.294	1.675	1.969	1.020	1.260	2.052	
r <sub>3,2</sub>	2.730	5.299	6.329	2.197	5.417	4.756	1.962	3.315	2.915	0.611	1.223	2.182	
r <sub>3,4</sub>	-	2.668	4.088	-	3.945	4.734	-	1.171	1.624	-	1.160	1.230	
r <sub>4,1</sub>	-	4.559	7.279	-	3.576	3.593	-	1.585	1.290	-	0.441	0.530	
r <sub>4,3</sub>	-	-	3.227	-	-	1.103	-	-	1.834	-	-	1.681	
r <sub>4,4</sub>	-	-	5.634	-	-	0.667	-	-	1.072	-	-	1.324	
SS of:	w <sub>1</sub>	17	22	23	13	13	20	11	12	13	4	5	10
	w <sub>2</sub>	27	23	24	21	22	16	15	18	12	15	12	28
	w <sub>3</sub>	2	3	4	1	8	6	1	5	3	1	2	8
	w <sub>4</sub>	-	2	2	-	4	5	-	4	1	-	3	2
	w <sub>5</sub>	-	-	0	-	-	2	-	-	1	-	-	1
	Total	46	50	53	35	47	49	27	39	30	20	22	49
MSS	4.2	3.6	3.2	2.5	2.6	2.2	2.5	2.8	1.8	1.4	1.2	2.2	
S <sub>1</sub>	2.0	1.9	1.8	1.6	1.6	1.5	1.6	1.7	1.3	1.2	1.1	1.5	

Table II.4: Estimated rate constants (all in  $\text{min}^{-1}$ ) for the Bond ball mill tests (lead fragments mixed with silica); flattening, folding and explicit breakage model (point zero for the two finest feed sizes, 0.600-0.710, and 0.425-0.500 nm was considered).

Feed Size (mm)	1.18-1.40, $w_1$			0.850-1.00, $w_2$			0.600-0.710, $w_3$			0.425-0.500, $w_4$			
Rate Constants	Products (No. of Size Classes):												
	(3)	(4)	(5)	(3)	(4)	(5)	(3)	(4)	(5)	(3)	(4)	(5)	
$s_1$	0.011	0.010	0.012	0.126	0.148	0.000	0.566	0.461	0.391	0.196	0.318	0.373	
$s_2$	0.000	0.000	0.000	0.718	0.743	0.877	0.081	0.000	0.000	0.609	0.000	0.000	
$s_3$	0.298	0.446	0.292	0.820	1.037	0.000	0.192	0.000	0.000	0.309	0.000	0.036	
$s_4$	-	0.000	0.000	-	0.000	0.753	-	0.438	0.000	-	0.446	0.000	
$s_5$	-	-	0.369	-	-	0.000	-	-	0.468	-	-	0.363	
$r_{12}$	0.000	0.000	0.000	0.000	0.000	0.161	0.000	0.000	0.000	0.000	0.000	0.000	
$r_{21}$	0.051	0.051	0.054	0.417	0.448	0.468	0.637	0.484	0.383	0.026	0.179	0.250	
$r_{31}$	0.412	0.535	1.400	0.000	0.000	0.000	0.000	0.129	0.160	0.155	0.321	0.303	
$r_{32}$	1.646	2.257	6.219	0.913	0.932	1.419	0.000	0.000	0.000	0.382	0.000	0.000	
$r_{34}$	-	0.000	0.000	-	0.000	0.780	-	0.296	0.342	-	0.446	0.392	
$r_{43}$	-	2.019	0.000	-	0.355	0.000	-	0.000	0.000	-	0.000	0.000	
$r_{44}$	-	-	0.207	-	-	0.060	-	-	0.499	-	-	0.420	
$r_{54}$	-	-	0.000	-	-	0.518	-	-	0.000	-	-	0.000	
SS of:	$w_1$	31	32	28	27	23	22	6	7	8	3	3	3
	$w_2$	68	73	68	7	3	1	10	11	11	2	2	2
	$w_3$	9	11	10	15	5	11	3	2	2	1	1	1
	$w_4$	-	20	1	-	11	4	-	1	1	-	1	1
	$w_5$	-	-	1	-	-	11	-	-	1	-	-	1
	Total	108	136	108	49	42	49	19	21	23	6	7	8
MSS	9.8	9.7	6.3	6.1	4.2	4.1	3.8	3.5	3.3	1.2	1.0	0.9	
$S_1$	3.1	3.1	2.5	2.5	2.0	2.0	1.9	1.9	1.8	1.1	1.0	0.9	

Table II.4.1: Estimated rate constants (all in  $\text{min}^{-1}$ ) for the Bond ball mill tests (lead fragments mixed with silica) for the two 0.600-0.710 mm, and 0.425-0.500 mm feed sizes; flattening, folding and explicit breakage model. (point zero was considered in fitting).

Feed Size (mm)		0.600-0.710, $w_2$			0.425-0.500, $w_2$		
Rate Constants		Products (No. of Size Classes):			Products (No. of Size Classes):		
		(3)	(4)	(5)	(3)	(4)	(5)
$s_1$		0.258	0.302	0.293	0.586	0.573	0.528
$s_2$		0.146	0.000	0.000	0.000	0.000	0.000
$s_3$		0.255	0.000	0.000	0.270	0.000	0.000
$s_4$		-	0.528	0.000	-	0.312	0.000
$s_5$		-	-	0.473	-	-	0.281
$r_{1,2}$		0.000	0.000	0.000	0.000	0.000	0.000
$r_{2,1}$		0.179	0.209	0.203	0.470	0.456	0.411
$r_{2,3}$		0.000	0.136	0.138	0.139	0.143	0.153
$r_{3,2}$		0.000	0.000	0.000	0.000	0.000	0.000
$r_{3,4}$		-	0.341	0.347	-	0.278	0.300
$r_{4,3}$		-	0.000	0.000	-	0.000	0.000
$r_{4,5}$		-	-	0.541	-	-	0.344
$r_{5,4}$		-	-	0.000	-	-	0.000
SS of:	$w_1$	21	19	19	9	10	11
	$w_2$	32	34	33	18	18	18
	$w_3$	6	3	3	4	3	3
	$w_4$	-	2	3	-	6	7
	$w_5$	-	-	1	-	-	3
	Total	59	58	59	31	37	42
MSS		7.4	5.8	4.9	3.9	3.7	3.5
$S_1$		2.7	2.4	2.2	2.0	1.9	1.9

Table II.5: Estimated rate constants (all in  $\text{min}^{-1}$ ) for the small ball mill tests (lead fragments mixed with silica); flattening, folding and explicit breakage model.

Feed Size (mm)	1.18-1.40, $w_2$			0.850-1.00, $w_2$			0.600-0.710, $w_2$			0.425-0.500, $w_2$			
	Products (No. of Size Classes):			Products (No. of Size Classes):			Products (No. of Size Classes):			Products (No. of Size Classes):			
	(3)	(4)	(5)	(3)	(4)	(5)	(3)	(4)	(5)	(3)	(4)	(5)	
$s_1$	0.000	0.000	0.000	0.000	0.000	0.000	0.000	0.000	0.000	0.119	0.123	0.124	
$s_2$	0.024	0.000	0.011	0.000	0.000	0.000	0.000	0.000	0.000	0.000	0.000	0.000	
$s_3$	0.000	0.000	0.000	0.192	0.000	0.000	0.258	0.000	0.000	0.211	0.194	0.169	
$s_4$	-	0.277	0.157	-	0.267	0.234	-	0.474	0.474	-	0.132	0.000	
$s_5$	-	-	0.068	-	-	0.058	-	-	0.156	-	-	0.131	
$r_{1,2}$	0.000	0.000	0.000	0.000	0.000	0.000	0.000	0.000	0.000	0.000	0.000	0.000	
$r_{2,1}$	0.029	0.029	0.031	0.059	0.059	0.069	0.055	0.056	0.057	0.142	0.151	0.152	
$r_{2,3}$	0.088	0.125	0.645	0.035	0.037	0.081	0.065	0.066	0.066	0.076	0.076	0.076	
$r_{3,2}$	0.493	0.561	3.080	0.000	0.115	0.216	0.000	0.000	0.000	0.000	0.000	0.000	
$r_{3,4}$	-	0.380	0.046	-	0.192	0.173	-	0.251	0.251	-	0.011	0.036	
$r_{4,3}$	-	1.088	0.000	-	0.000	0.000	-	0.000	0.000	-	0.000	0.000	
$r_{4,5}$	-	-	0.000	-	-	0.000	-	-	0.000	-	-	0.149	
$r_{5,4}$	-	-	0.000	-	-	0.000	-	-	0.000	-	-	0.000	
SS of:	$w_1$	26	26	24	109	104	67	49	48	47	43	39	39
	$w_2$	15	14	19	14	14	13	1	1	2	13	12	12
	$w_3$	6	6	7	2 <sup>a</sup>	2	1	4	5	5	5	7	7
	$w_4$	-	4	1	-	1	1	-	4	4	-	1	1
	$w_5$	-	-	1	-	-	5	-	-	1	-	-	1
	Total	47	50	52	125	121	87	54	58	59	61	59	60
MSS	5.9	5.0	4.3	15.6	12.1	7.3	6.8	5.8	4.9	7.6	5.8	4.9	
$S_2$	2.4	2.2	2.1	3.9	3.5	2.7	2.6	2.4	2.2	2.8	2.4	2.2	

**Table II.6:** Estimated rate constants (all in min<sup>-1</sup>) for the bond rod mill tests (lead fragments mixed with silica); flattening, folding and explicit breakage model.

Feed Size (mm)	1.18-1.40, w <sub>1</sub>			0.850-1.00, w <sub>2</sub>			0.600-0.710, w <sub>3</sub>			0.425-0.500, w <sub>4</sub>			
	Products (No. of Size Classes):			Products (No. of Size Classes):			Products (No. of Size Classes):			Products (No. of Size Classes):			
	(3)	(4)	(5)	(3)	(4)	(5)	(3)	(4)	(5)	(3)	(4)	(5)	
s <sub>1</sub>	4.435	4.292	2.884	2.150	1.922	0.861	1.551	1.152	1.633	0.000	0.000	0.000	
s <sub>2</sub>	0.000	0.000	0.291	0.000	0.000	0.259	0.000	0.000	0.000	0.138	0.089	0.114	
s <sub>3</sub>	0.360	0.383	0.383	0.327	0.383	0.371	0.245	0.765	0.000	0.126	0.372	0.260	
s <sub>4</sub>	-	0.368	0.000	-	0.194	0.000	-	0.000	0.000	-	0.000	0.000	
s <sub>5</sub>	-	-	0.515	-	-	0.213	-	-	0.289	-	-	0.000	
r <sub>1,2</sub>	0.000	0.000	0.000	0.000	0.000	0.000	0.000	0.000	0.000	0.501	0.553	0.541	
r <sub>2,1</sub>	0.948	0.922	0.598	0.615	0.549	0.239	0.292	0.215	0.308	0.182	0.200	0.195	
r <sub>3,1</sub>	0.189	0.207	0.000	0.136	0.164	0.000	0.111	0.137	0.105	0.016	0.049	0.039	
r <sub>3,2</sub>	0.000	0.000	0.000	0.000	0.000	0.000	0.000	0.000	0.000	0.064	0.000	0.058	
r <sub>3,4</sub>	-	0.000	0.000	-	0.000	0.000	-	0.000	0.228	-	0.000	0.000	
r <sub>4,1</sub>	-	0.000	0.000	-	0.000	0.000	-	0.934	0.000	-	0.368	0.229	
r <sub>4,3</sub>	-	-	0.362	-	-	0.178	-	-	1.139	-	-	0.296	
r <sub>4,4</sub>	-	-	0.000	-	-	0.000	-	-	0.672	-	-	0.251	
SS of:	w <sub>1</sub>	7	7	7	20	20	13	10	9	11	36	41	38
	w <sub>2</sub>	1	1	1	51	55	50	33	35	33	25	23	23
	w <sub>3</sub>	1	1	1	2	5	4	1	7	1	2	2	1
	w <sub>4</sub>	-	1	1	-	5	16	-	10	1	-	2	1
	w <sub>5</sub>	-	-	2	-	-	6	-	-	3	-	-	1
	Total	9	10	12	73	95	89	44	61	49	63	68	64
MSS	1.0	1.0	1.0	9.1	9.5	7.3	5.5	6.5	4.0	7.9	6.9	5.6	
S <sub>1</sub>	1.0	1.0	1.0	3.0	3.1	2.7	2.3	2.5	2.0	2.8	2.6	2.4	

**Table II.7: Estimated rate constants (all in min<sup>-1</sup>) for the Bond ball mill tests (copper fragments tests): flattening and folding (no breakage) model.**

Feed Size (mm)		1.18-1.40, w <sub>1</sub>			0.850-1.00, w <sub>2</sub>			0.600-0.710, w <sub>3</sub>			0.425-0.500, w <sub>4</sub>		
		Products (Sizes)			Products (Sizes)			Products (Sizes)			Products (Sizes)		
		(3)	(4)	(5)	(3)	(4)	(5)	(3)	(4)	(5)	(3)	(4)	(5)
r <sub>1,1</sub>		0.165	2.074	5.162	0.014	0.013	0.013	0.011	0.011	0.010	0.013	0.012	0.012
r <sub>2,1</sub>		0.004	0.085	0.211	0.004	0.004	0.004	0.004	0.004	0.004	0.017	0.017	0.017
r <sub>3,1</sub>		0.064	0.303	1.308	0.102	0.232	0.106	0.089	0.241	0.095	0.068	0.077	0.089
r <sub>4,1</sub>		0.316	2.002	8.643	0.469	1.800	0.827	0.454	2.000	0.800	0.208	0.394	0.458
r <sub>5,1</sub>		-	0.071	0.236	-	0.532	2.572	-	0.463	1.711	-	1.404	0.726
r <sub>6,1</sub>		-	0.208	2.023	-	0.767	7.052	-	0.700	5.530	-	2.000	2.000
r <sub>7,1</sub>		-	-	1.378	-	-	3.294	-	-	5.047	-	-	2.000
r <sub>8,1</sub>		-	-	0.745	-	-	3.496	-	-	4.117	-	-	2.000
SS of:	w <sub>1</sub>	1	2	2	31	31	31	61	61	61	108	109	110
	w <sub>2</sub>	9	9	9	24	24	23	57	56	55	54	51	50
	w <sub>3</sub>	11	9	9	4	8	8	3	4	3	13	5	5
	w <sub>4</sub>	-	1	0	-	2	1	-	1	1	-	10	3
	w <sub>5</sub>	-	-	1	-	-	1	-	-	1	-	-	3
	Total	21	21	21	59	65	64	121	122	121	175	175	171
MSS		0.9	0.7	0.6	2.6	2.2	1.7	5.3	4.1	3.3	7.6	5.8	4.6
S <sub>i</sub>		0.9	0.8	0.8	1.6	1.5	1.3	2.3	2.0	1.8	2.8	2.4	2.1

**Table II.8:** Estimated rate constants (all in min<sup>-1</sup>) for the small ball mill tests (copper fragments tests); flattening and folding (no breakage) model.

Feed Size (mm)	1.18-1.40, w <sub>1</sub>			0.850-1.00, w <sub>2</sub>			0.600-0.710, w <sub>3</sub>			0.425-0.500, w <sub>4</sub>			
	Products (Sizes)			Products (Sizes)			Products (Sizes)			Products (Sizes)			
	(3)	(4)	(5)	(3)	(4)	(5)	(3)	(4)	(5)	(3)	(4)	(5)	
r <sub>1,2</sub>	0.000	0.000	0.000	0.035	0.079	0.030	0.065	0.066	0.060	0.055	0.063	0.061	
r <sub>2,1</sub>	0.002	0.002	0.002	0.000	0.017	0.009	0.023	0.023	0.022	0.022	0.024	0.239	
r <sub>2,3</sub>	0.100	0.424	0.425	0.240	1.058	0.355	0.253	0.405	0.400	0.130	0.415	0.409	
r <sub>3,2</sub>	0.290	2.000	2.010	0.880	6.072	2.000	0.683	2.010	2.211	0.304	1.987	1.995	
r <sub>3,4</sub>	-	0.048	0.049	-	0.074	0.563	-	0.175	0.868	-	0.141	1.042	
r <sub>4,3</sub>	-	0.059	0.168	-	0.015	1.965	-	0.187	1.987	-	0.111	1.488	
r <sub>4,5</sub>	-	-	2.001	-	-	2.000	-	-	2.195	-	-	0.036	
r <sub>5,4</sub>	-	-	1.150	-	-	2.000	-	-	2.121	-	-	0.038	
SS of:	w <sub>1</sub>	2	2	2	14	32	16	5	4	7	43	44	49
	w <sub>2</sub>	20	8	8	38	78	37	23	39	21	35	62	29
	w <sub>3</sub>	15	4	4	13	46	43	16	15	16	18	13	12
	w <sub>4</sub>	-	3	1	-	34	11	-	21	11	-	12	21
	w <sub>5</sub>	-	-	1	-	-	27	-	-	26	-	-	2
	Total	37	17	16	65	190	134	44	79	81	96	131	113
MSS	1.9	0.7	0.5	3.3	7.3	4.2	2.2	3.0	2.5	4.8	5.0	3.5	
S <sub>i</sub>	1.4	0.8	0.7	1.8	2.7	2.0	1.5	1.8	1.6	2.2	2.2	1.9	

**Table II.9: Estimated rate constants (all in min<sup>-1</sup>) for the Bond rod mill tests (copper fragments tests): flattening, folding and explicit breakage model.**

Feed Size (mm)	1.18-1.40, w <sub>1</sub>			0.850-1.00, w <sub>2</sub>			0.600-0.710, w <sub>3</sub>			0.425-0.500, w <sub>4</sub>			
	Products (No. of Size Classes):			Products (No. of Size Classes):			Products (No. of Size Classes):			Products (No. of Size Classes):			
	(3)	(4)	(5)	(3)	(4)	(5)	(3)	(4)	(5)	(3)	(4)	(5)	
s <sub>1</sub>	0.000	0.000	0.000	0.948	0.000	0.000	0.653	0.210	0.000	0.000	0.000	0.000	
s <sub>2</sub>	0.147	0.000	0.011	0.494	0.589	0.569	0.325	0.310	0.329	0.363	0.264	0.238	
s <sub>3</sub>	0.244	0.000	0.000	0.204	0.000	0.000	0.100	0.000	0.000	0.076	0.000	0.000	
s <sub>4</sub>	-	0.277	0.157	-	0.253	0.000	-	0.236	0.120	-	0.152	0.033	
s <sub>5</sub>	-	-	0.068	-	-	0.415	-	-	0.178	-	-	0.155	
r <sub>1,2</sub>	4.901	15.386	14.737	22.727	8.757	8.865	1.842	2.465	2.738	1.499	1.637	1.748	
r <sub>2,1</sub>	2.066	6.496	6.232	17.297	6.376	6.482	1.091	1.174	1.202	1.417	1.547	1.653	
r <sub>3,1</sub>	0.114	0.221	0.193	0.000	0.109	0.133	0.000	0.074	0.085	0.083	0.191	0.225	
r <sub>3,2</sub>	0.094	0.112	0.118	0.384	0.306	0.307	0.310	0.257	0.236	0.252	0.263	0.273	
r <sub>3,4</sub>	-	0.000	0.000	-	1.177	1.239	-	0.662	0.838	-	0.329	0.400	
r <sub>4,1</sub>	-	0.528	0.265	-	0.456	0.489	-	0.439	0.571	-	0.284	0.365	
r <sub>4,3</sub>	-	-	0.100	-	-	0.265	-	-	0.331	-	-	0.294	
r <sub>4,4</sub>	-	-	0.000	-	-	0.000	-	-	0.194	-	-	0.234	
SS of:	w <sub>1</sub>	47	56	54	7	9	9	3	4	4	24	26	27
	w <sub>2</sub>	25	26	26	5	3	3	4	3	3	19	18	19
	w <sub>3</sub>	17	13	14	3	2	2	3	2	2	2	1	1
	w <sub>4</sub>	-	6	3	-	4	5	-	3	1	-	2	1
	w <sub>5</sub>	-	-	3	-	-	5	-	-	2	-	-	1
	Total	89	100	100	15	18	24	10	12	12	45	47	49
MSS	4.5	3.9	3.1	0.9	0.8	0.9	0.6	0.5	0.4	2.7	2.1	1.9	
S <sub>1</sub>	2.1	1.9	1.8	0.9	0.9	0.9	0.8	0.7	0.6	1.6	1.4	1.3	

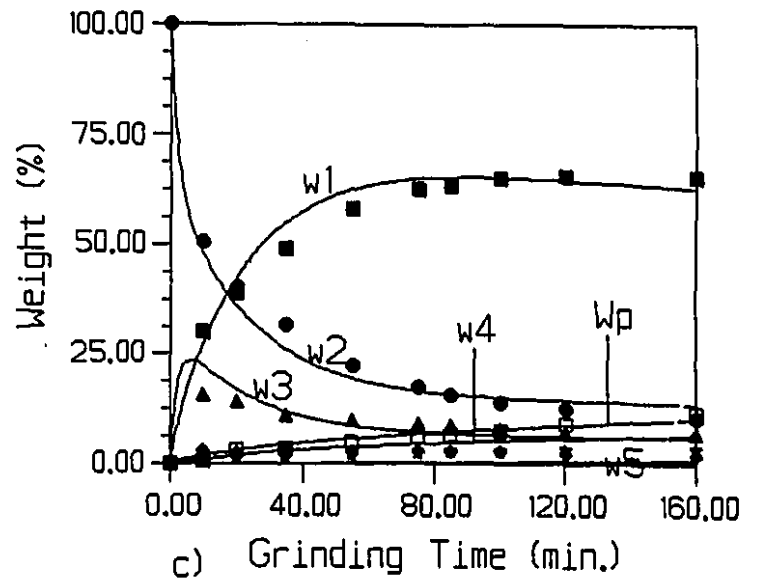
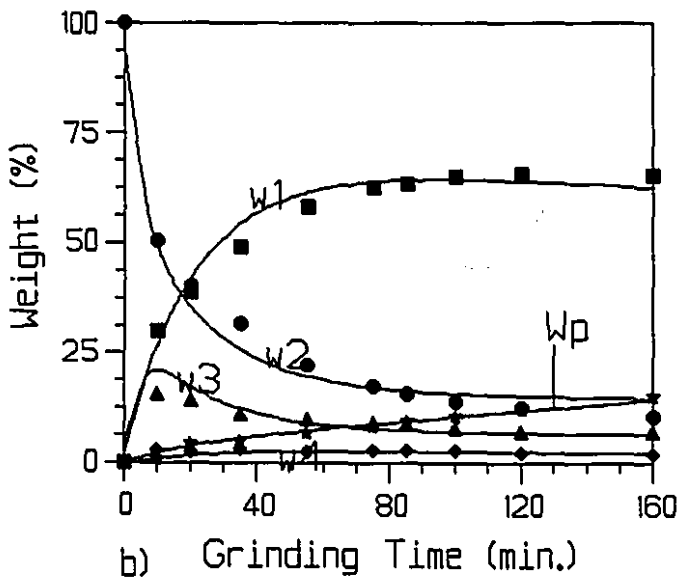
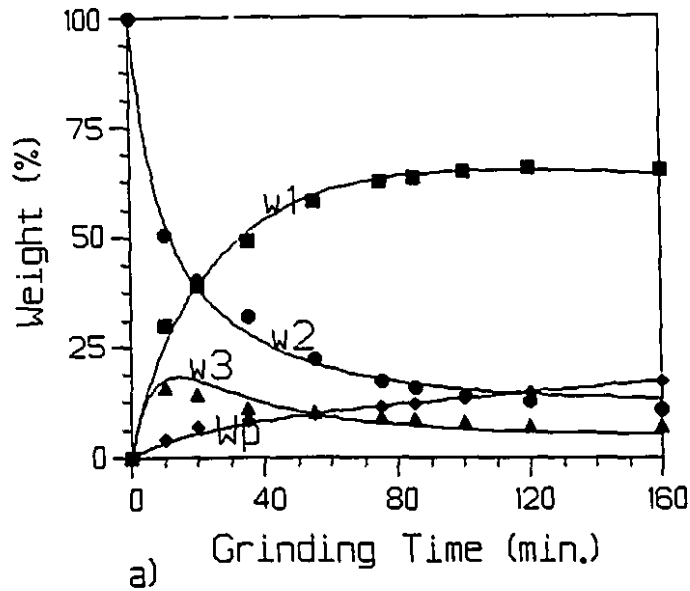


**Figure II.1:** Fit of the folding, flattening and limited breakage model for the Bond ball mill test (lead fragments tests), using 1.18-1.40 mm feed size; a: 3 size classes, b: 4 size classes, c: 5 size classes.

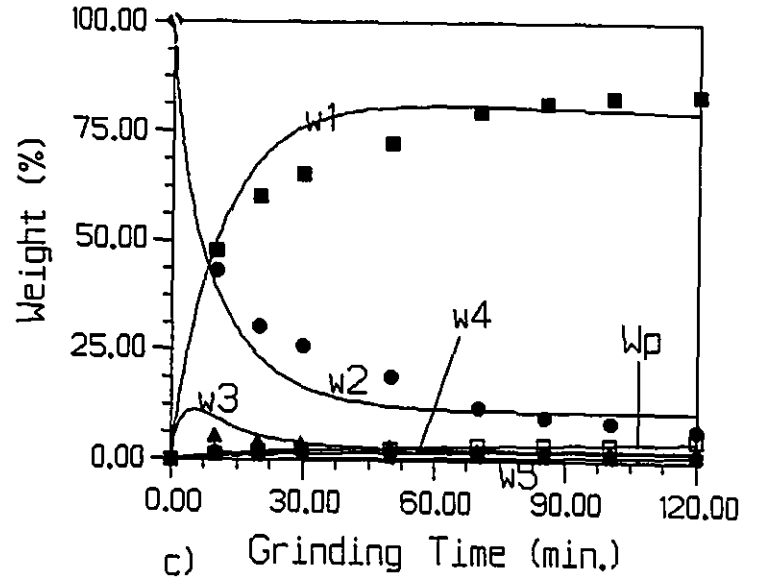
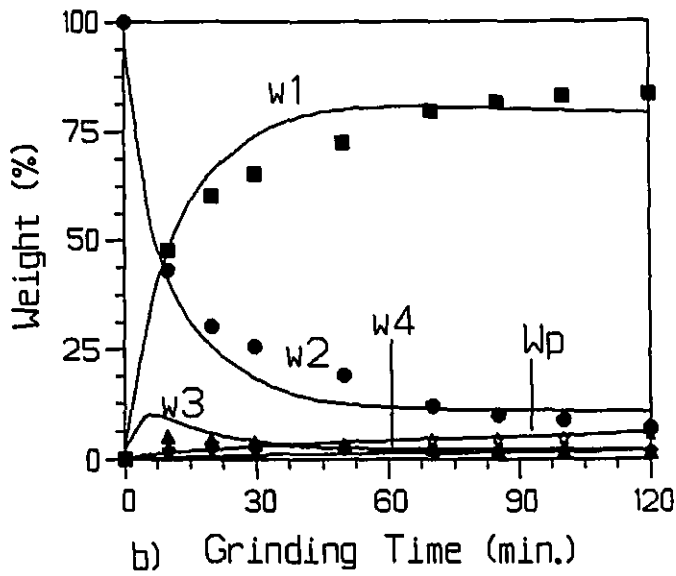
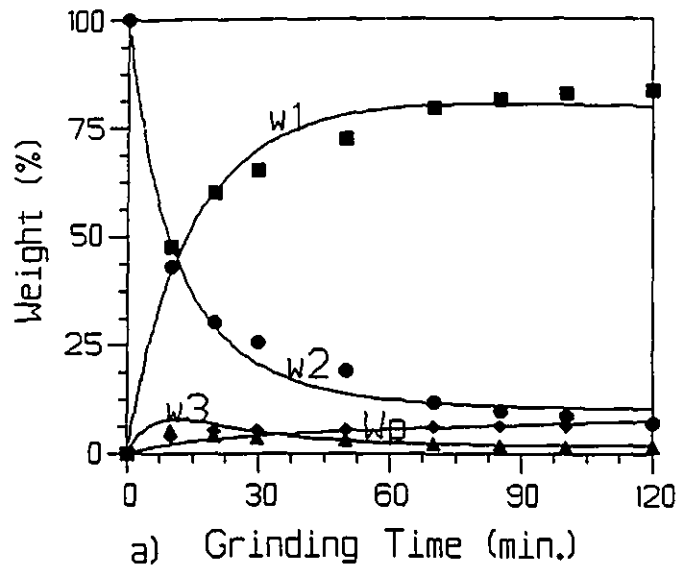


**Figure II.2:** Fit of the folding, flattening and limited breakage model for the Bond ball mill test (lead fragments tests), using 0.850-1.00 mm feed size; a: 3 size classes, b: 4 size classes, c: 5 size classes.

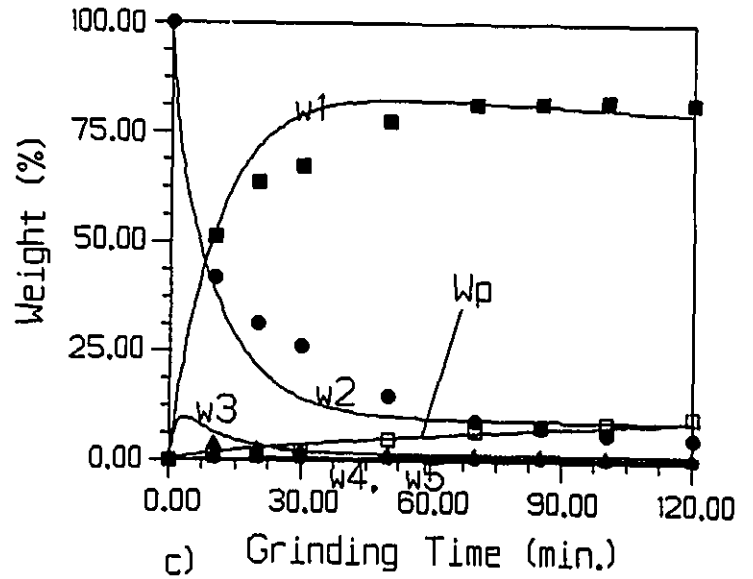
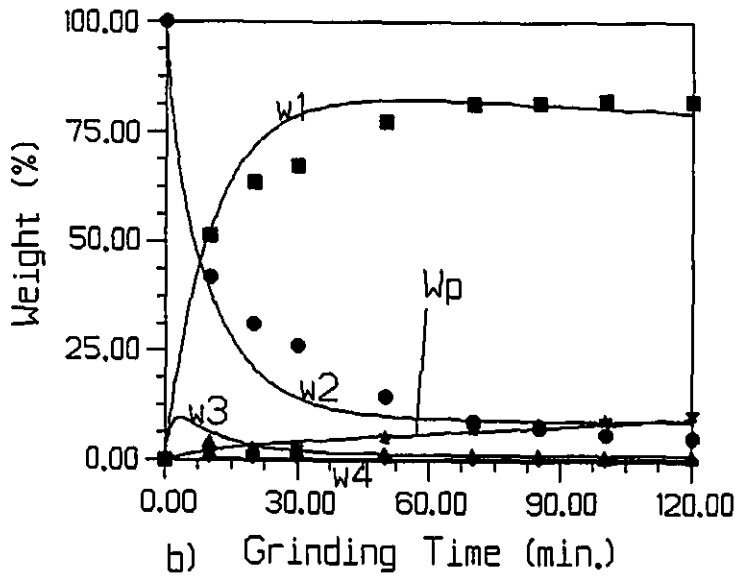
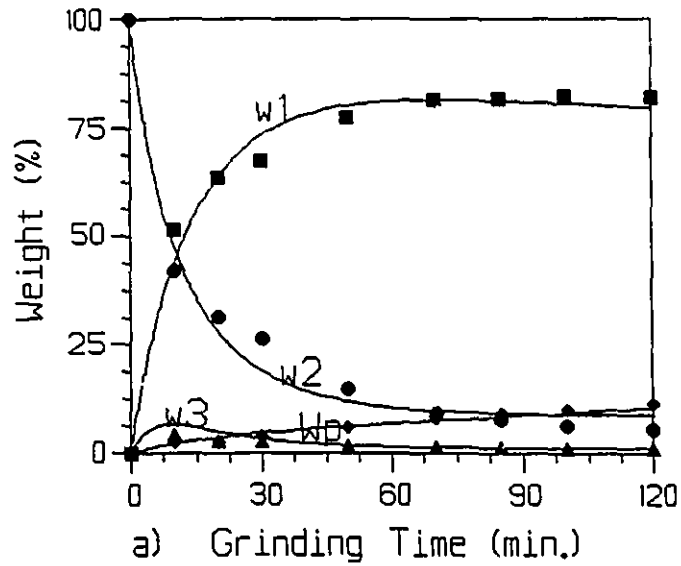


**Figure II.3:** Fit of the folding, flattening and limited breakage model for the Bond ball mill test (lead fragments tests), using 0.600-0.710 mm feed size; a: 3 size classes, b: 4 size classes, c: 5 size classes.

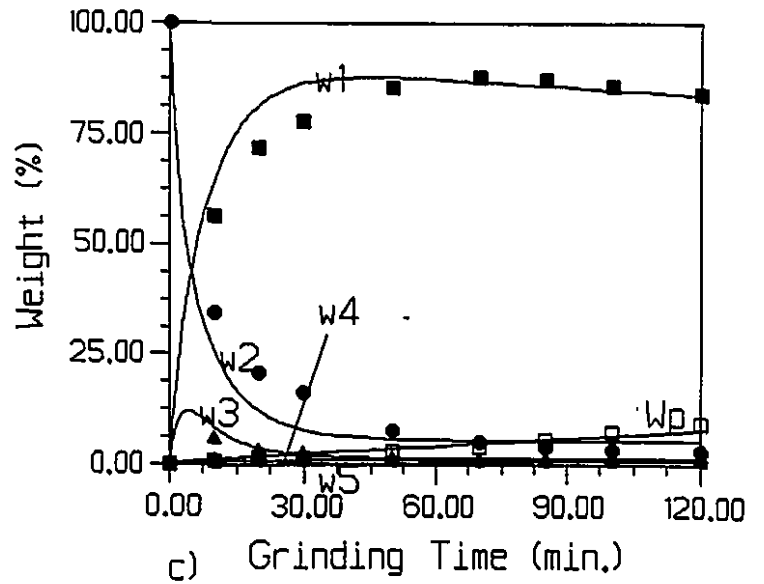
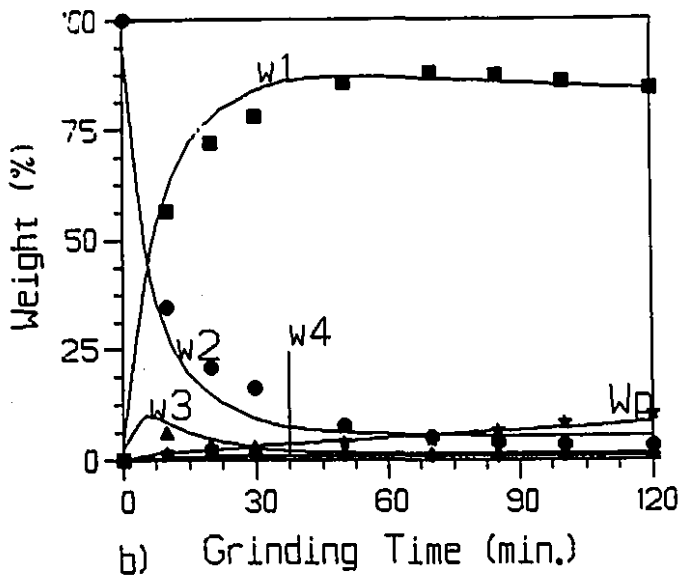
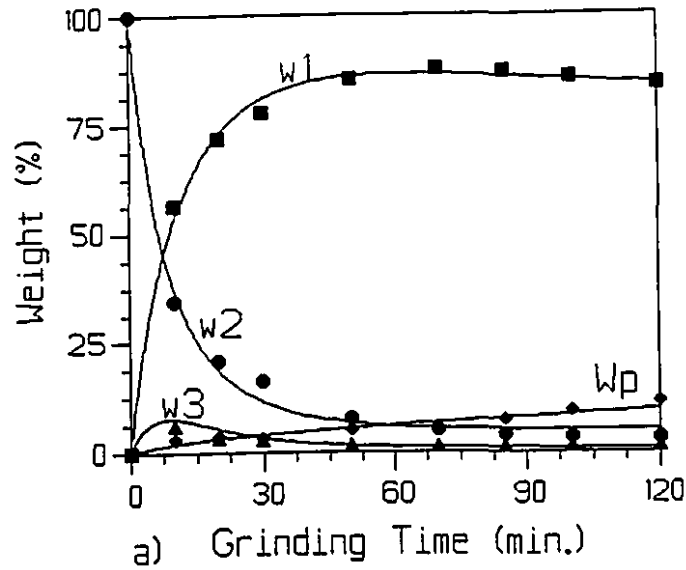


**Figure II.4:** Fit of the folding, flattening and limited breakage model for the Bond ball mill test (lead fragments tests), using 0.425-0.500 mm feed size; a: 3 size classes, b: 4 size classes, c: 5 size classes.

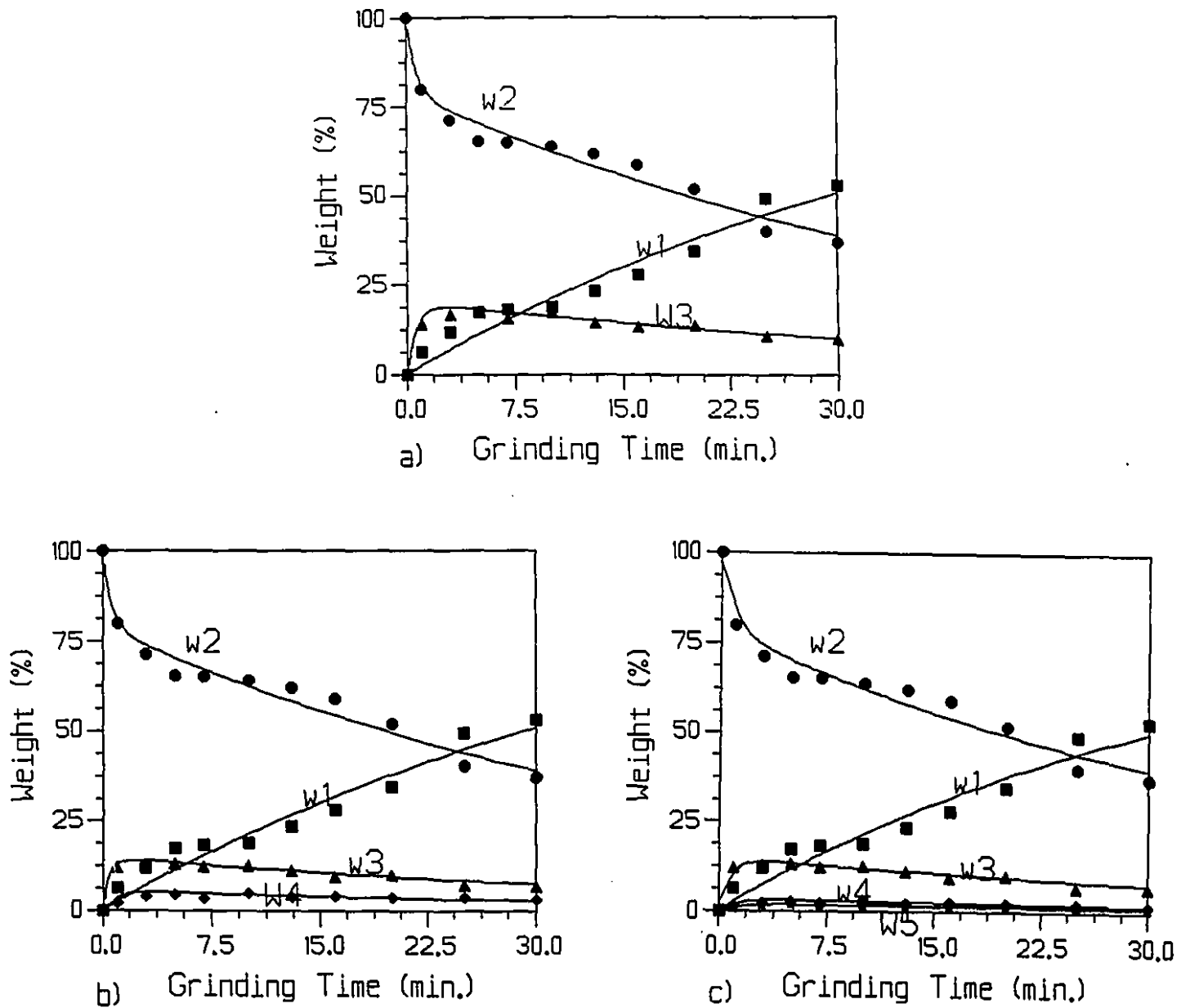


**Figure II.5:** Fit of the folding and flattening (no breakage) model for the small ball mill test (lead fragments tests), using 1.18-1.40 mm feed size; a: 3 size classes, b: 4 size classes, c: 5 size classes.

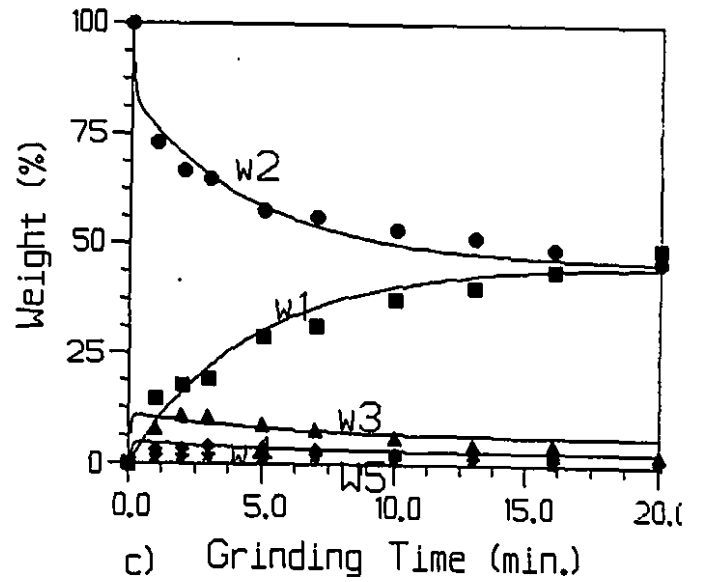
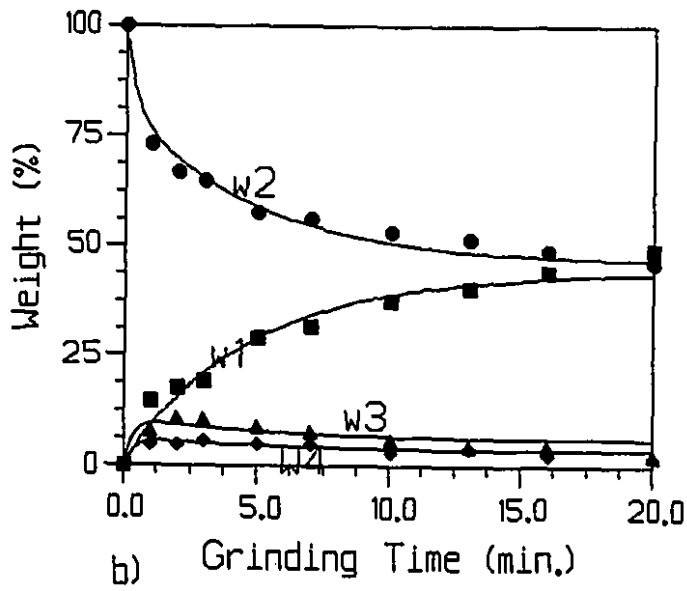
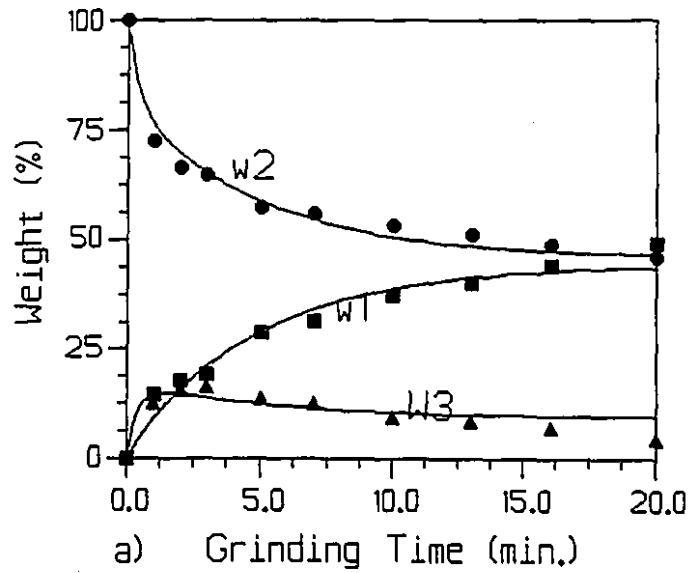


**Figure II.6:** Fit of the folding and flattening (no breakage) model for the small ball mill test (lead fragments tests), using 0.850-1.00 mm feed size; a: 3 size classes, b: 4 size classes, c: 5 size classes.

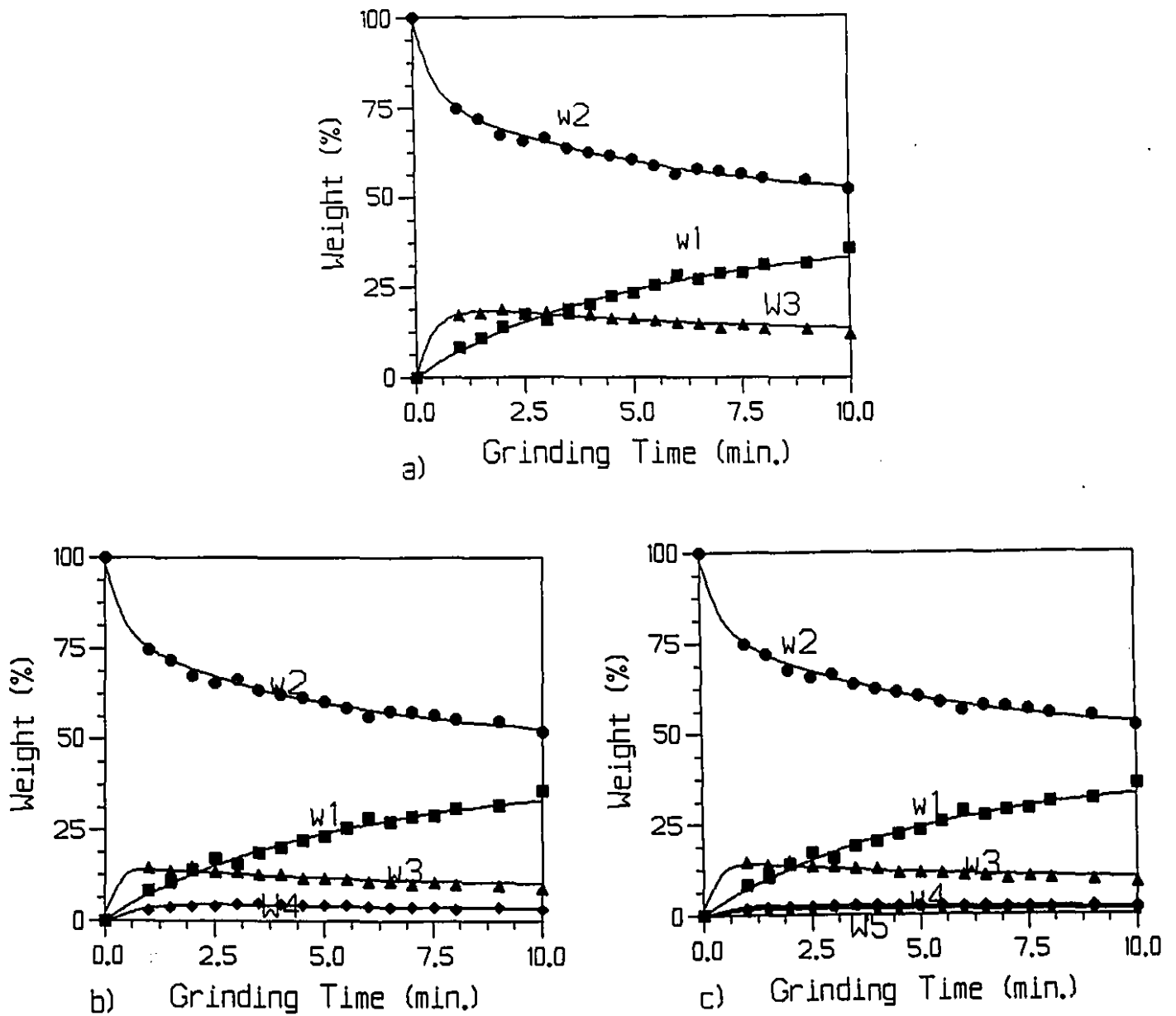


**Figure II.7:** Fit of the folding and flattening (no breakage) model for the small ball mill test (lead fragments tests), using 0.600-0.710 mm feed size; a: 3 size classes, b: 4 size classes, c: 5 size classes.

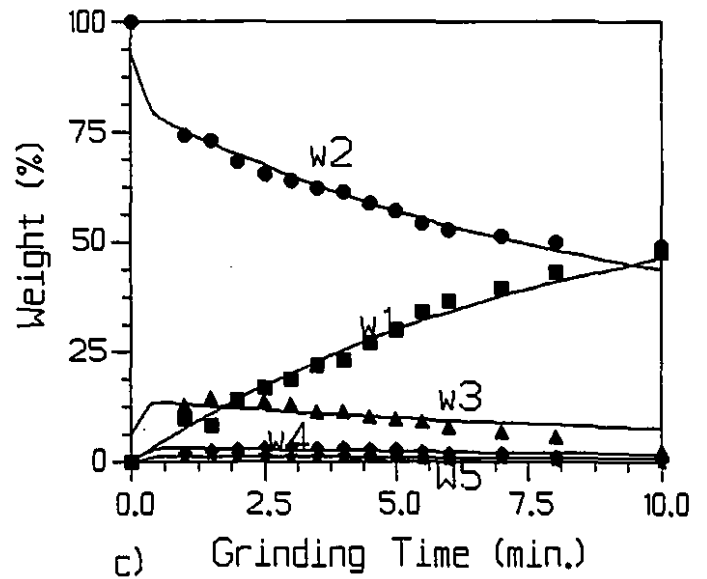
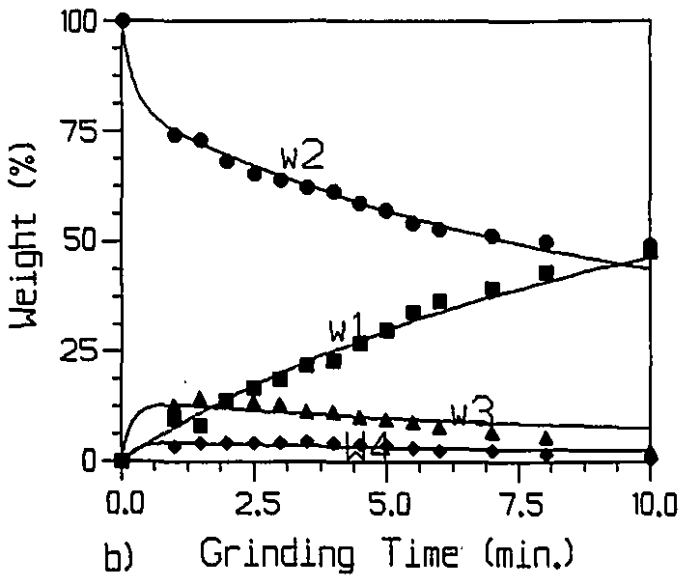
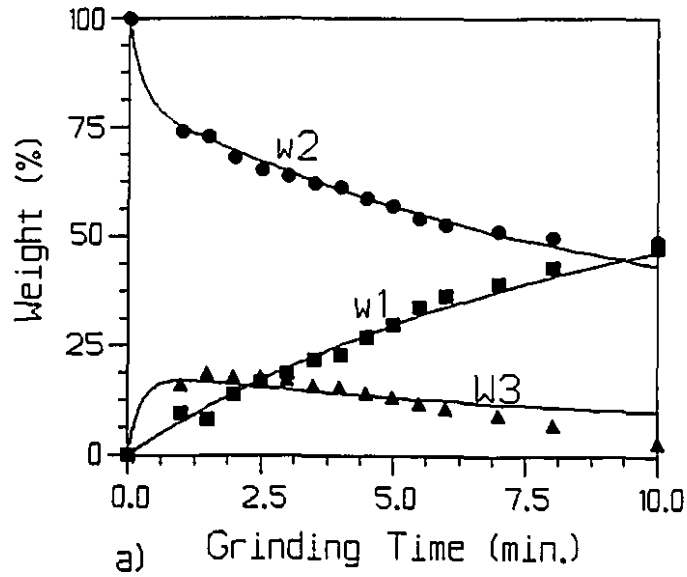


**Figure II.8:** Fit of the folding and flattening (no breakage) model for the small ball mill test (lead fragments tests), using 0.425-0.500 mm feed size; a: 3 size classes, b: 4 size classes, c: 5 size classes.

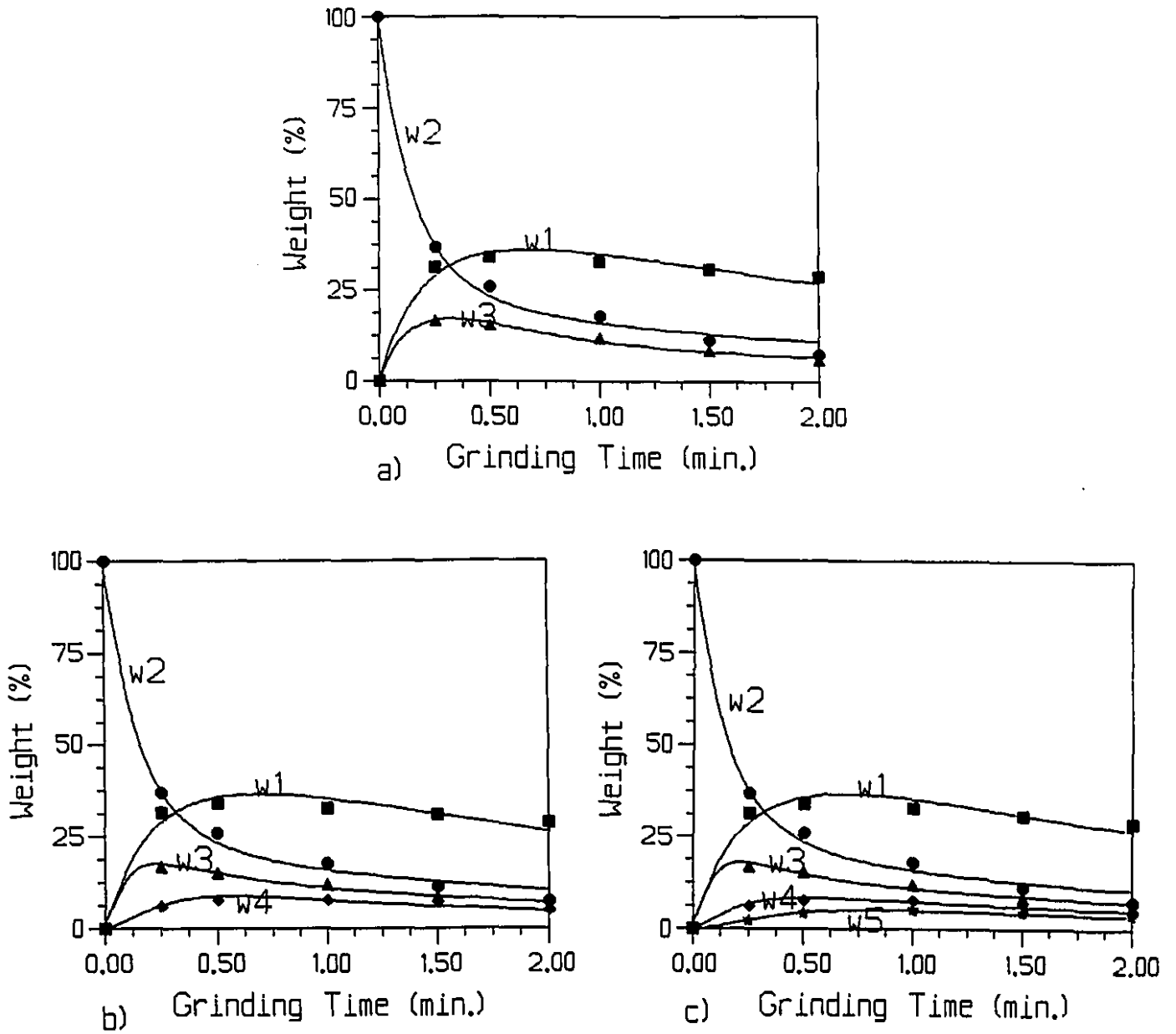


**Figure II.9:** Fit of the folding, flattening and explicit breakage model for the Bond rod mill test (lead fragments tests), using 1.18-1.40 mm feed size; a: 3 size classes, b: 4 size classes, c: 5 size classes.

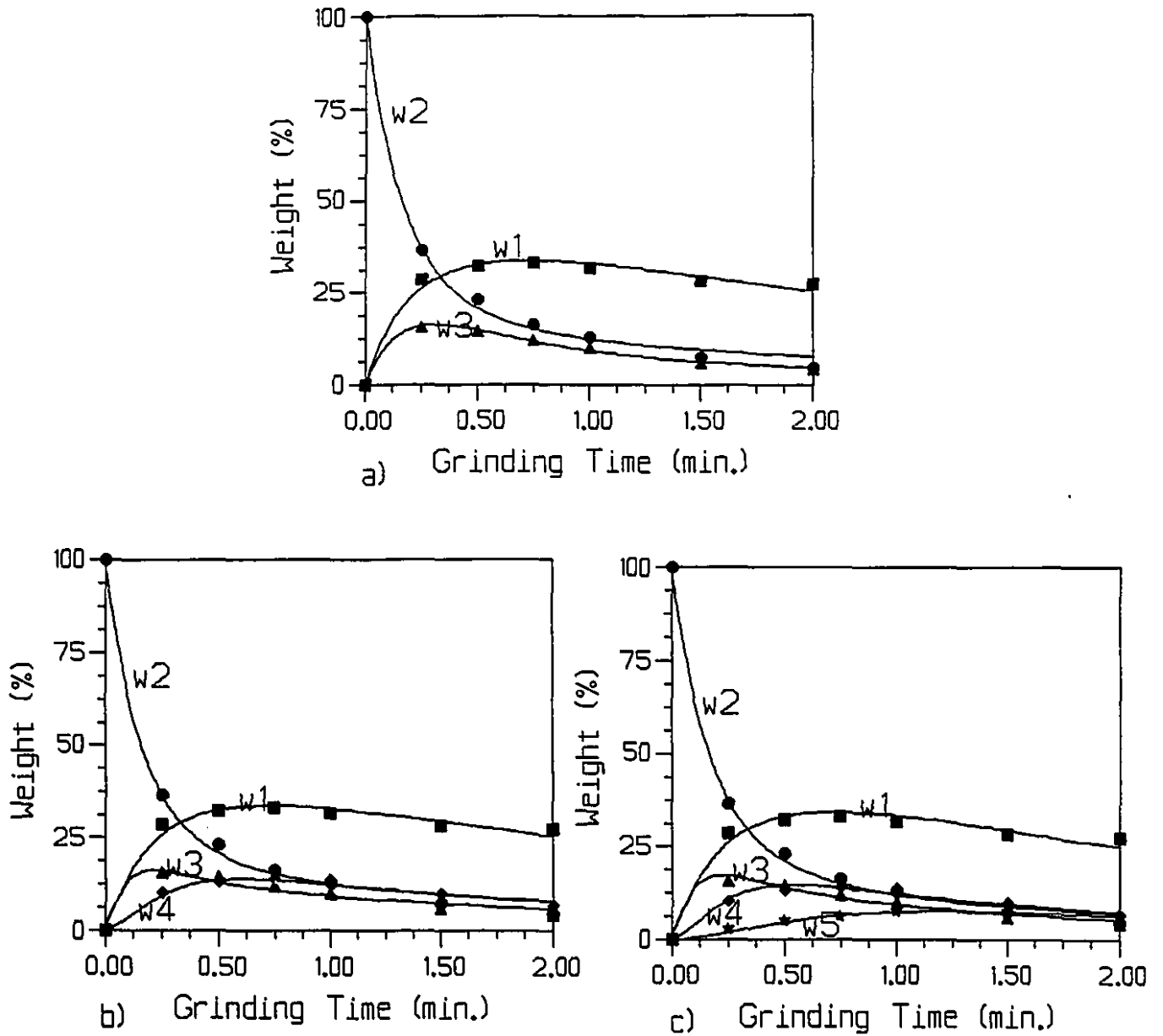


**Figure II.10:** Fit of the folding, flattening and explicit breakage model for the Bond rod mill test (lead fragments tests), using 0.850-1.00 mm feed size; a: 3 size classes, b: 4 size classes, c: 5 size classes.

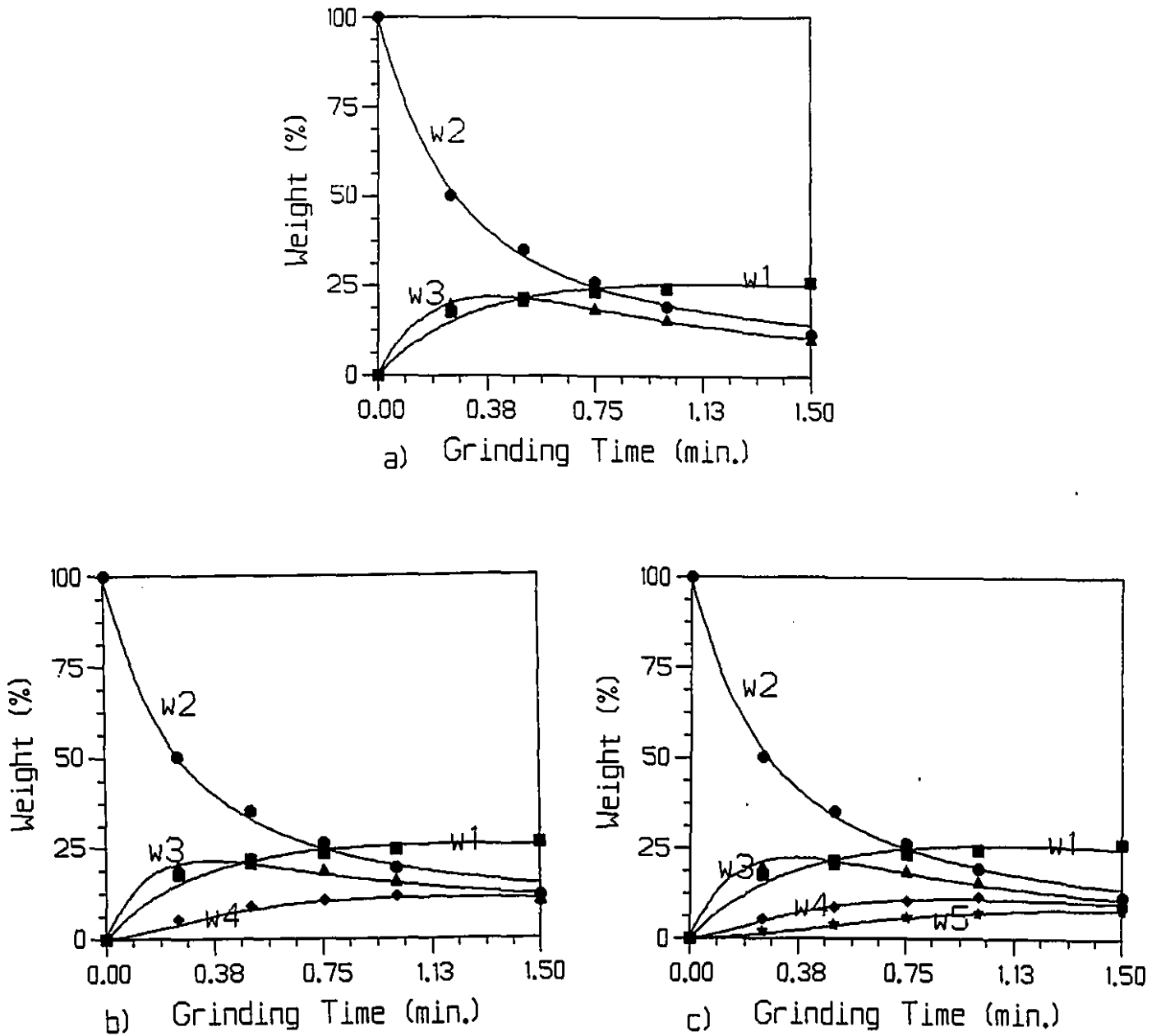


**Figure II.11:** Fit of the folding, flattening and explicit breakage model for the Bond rod mill test (lead fragments tests), using 0.600-0.710 mm feed size; a: 3 size classes, b: 4 size classes, c: 5 size classes.

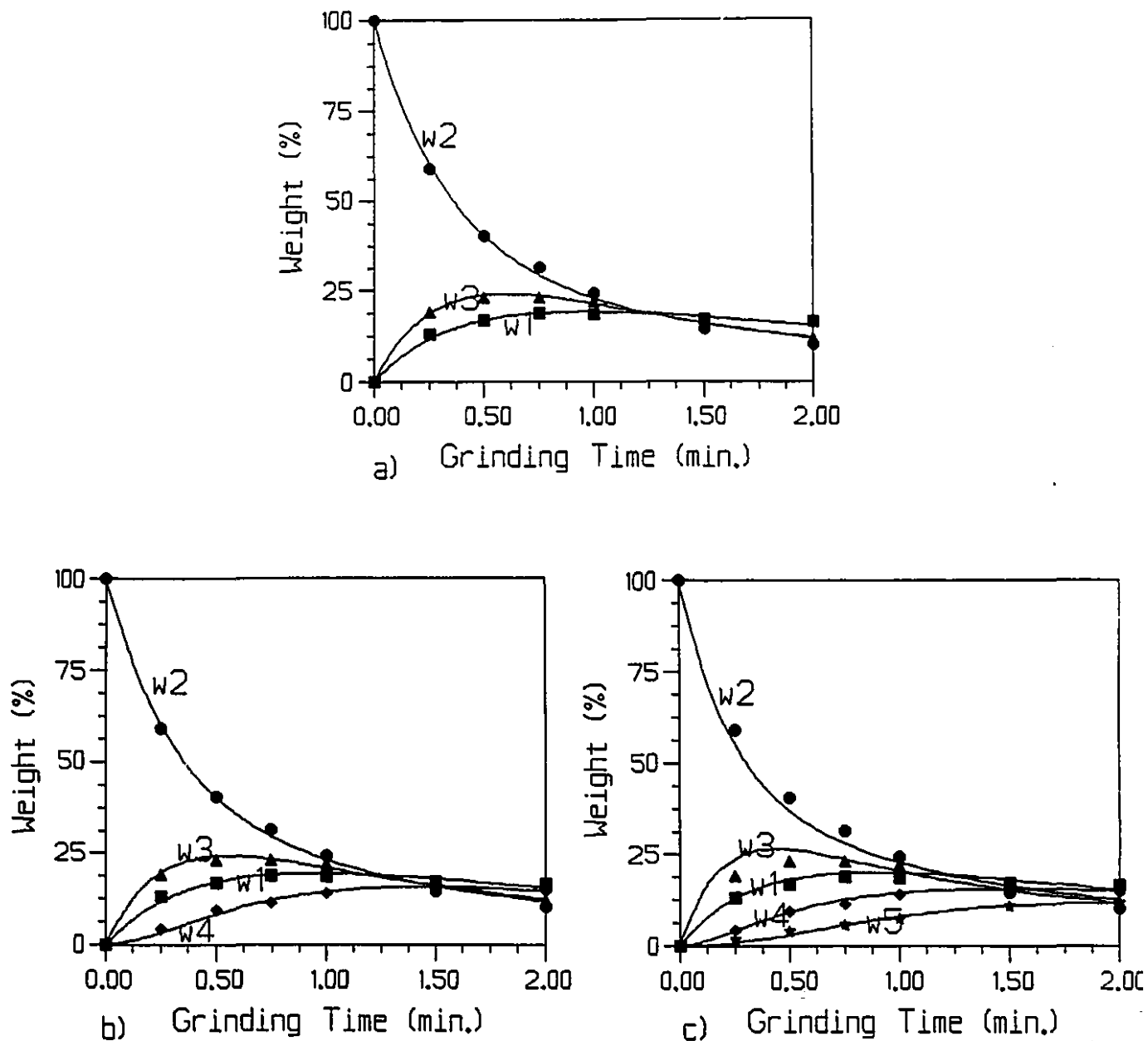


**Figure II.12:** Fit of the folding, flattening and explicit breakage model for the Bond rod mill test (lead fragments tests), using 0.425-0.500 mm feed size; a: 3 size classes, b: 4 size classes, c: 5 size classes.

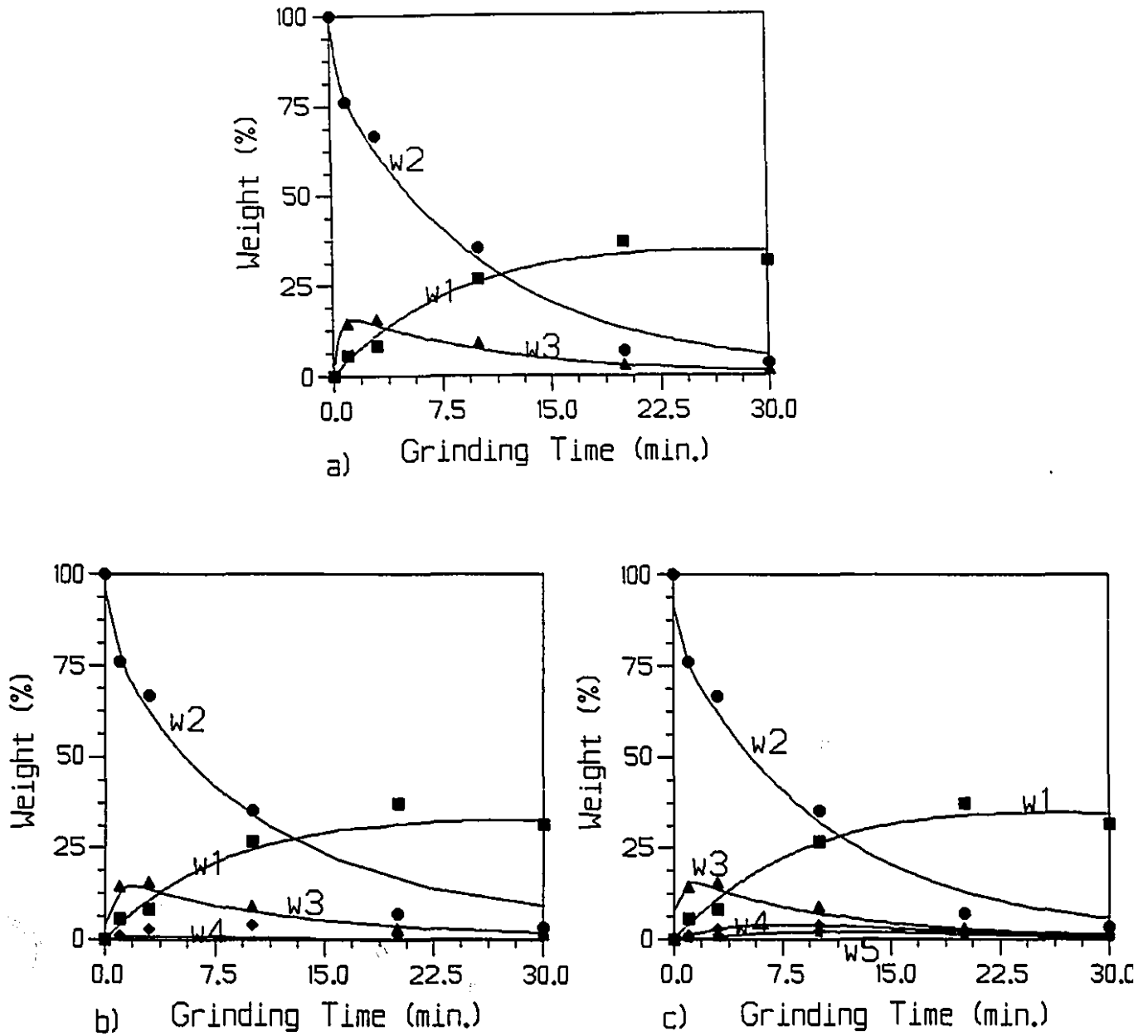


**Figure II.13:** Fit of the folding, flattening and explicit breakage model for the Bond ball mill test (lead fragments mixed with silica tests), using 1.18-1.40 mm feed size; a: 3 size classes, b: 4 size classes, c: 5 size classes.

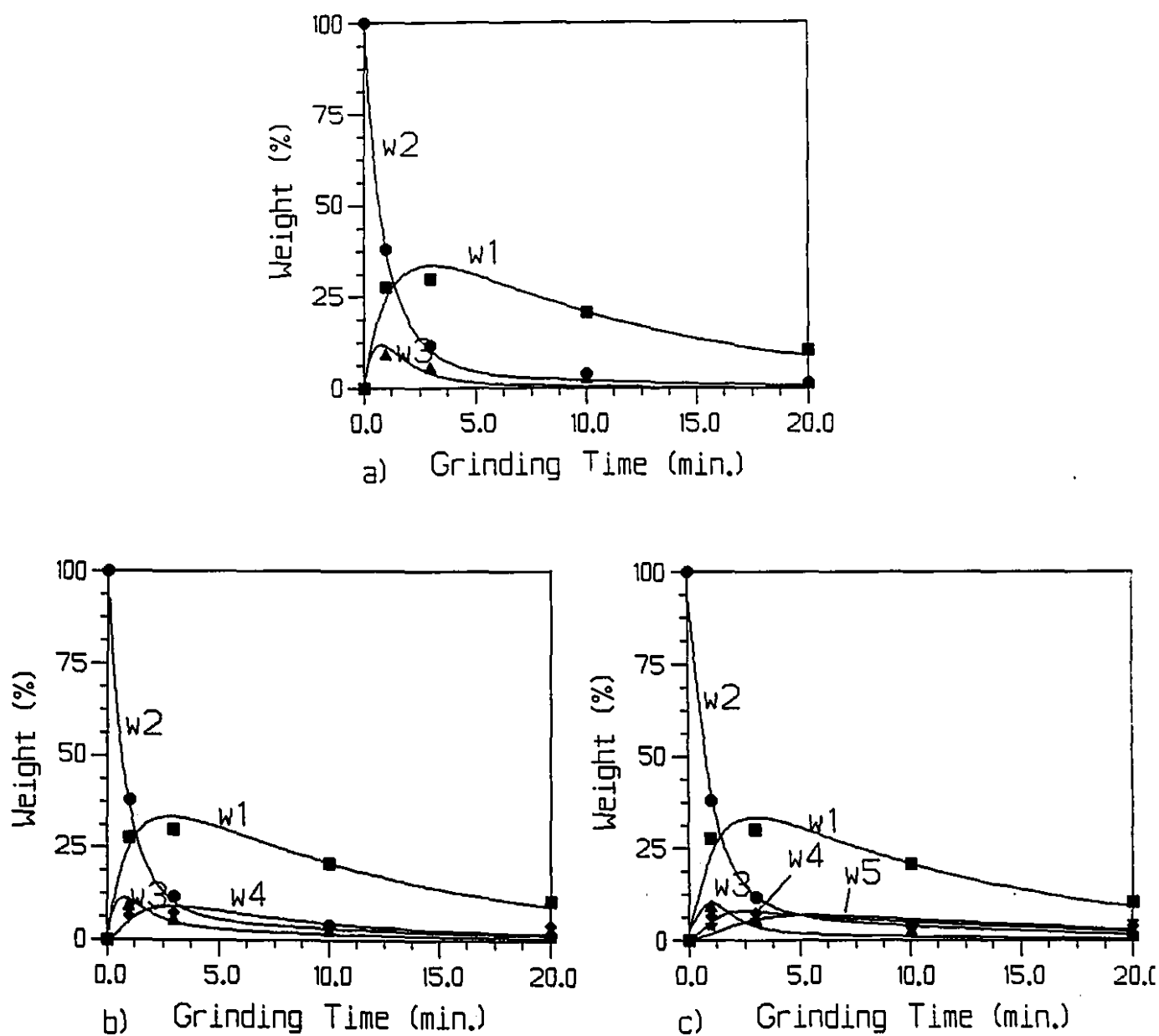


**Figure II.14:** Fit of the folding, flattening and explicit breakage model for the Bond ball mill test (lead fragments mixed with silica tests), using 0.850-1.00 mm feed size; a: 3 size classes, b: 4 size classes, c: 5 size classes.

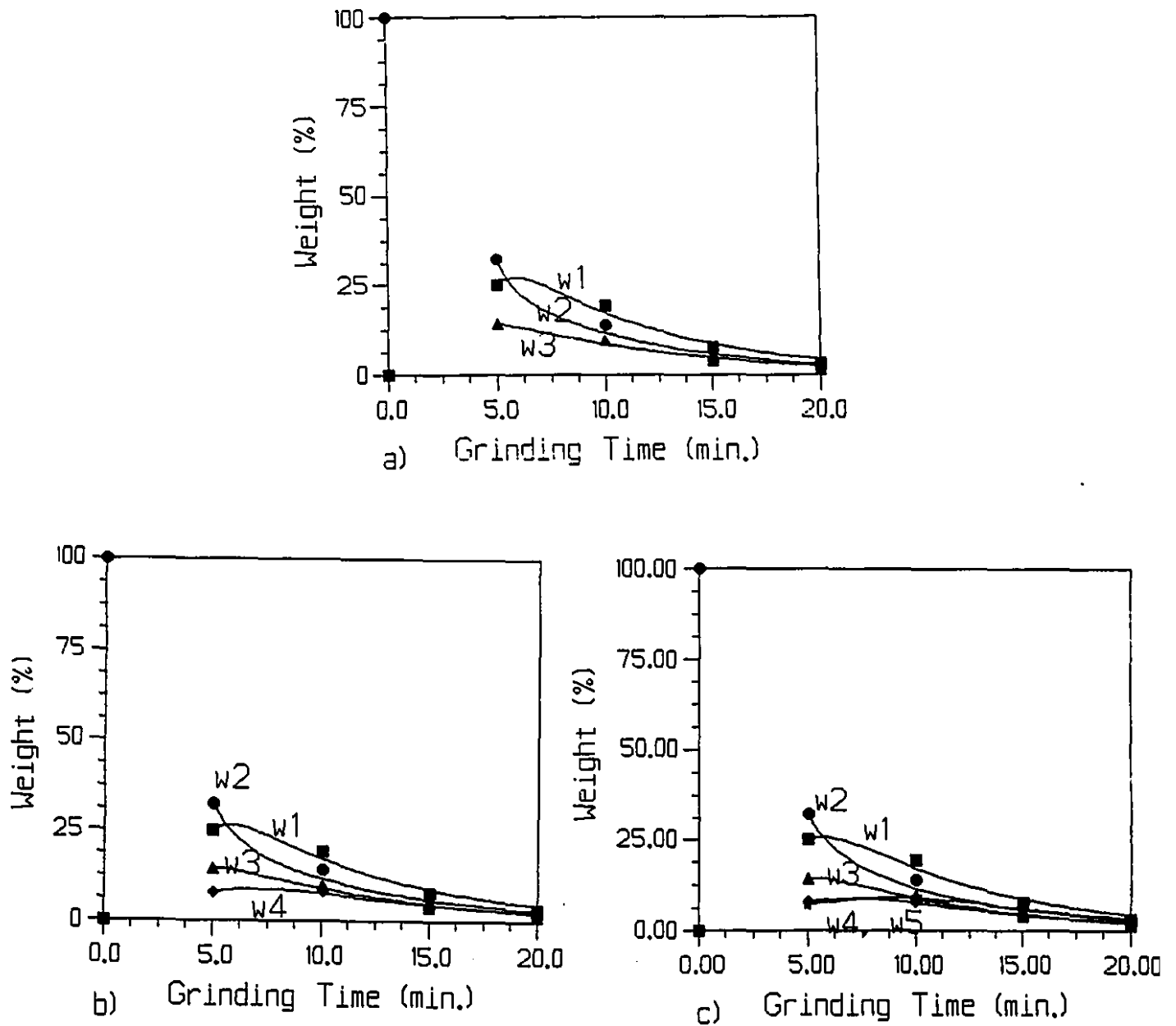


**Figure II.15:** Fit of the folding, flattening and explicit breakage model for the Bond ball mill test (lead fragments mixed with silica tests), point zero was not considered, using 0.600-0.710 mm feed size; a: 3 size classes, b: 4 size classes, c: 5 size classes.

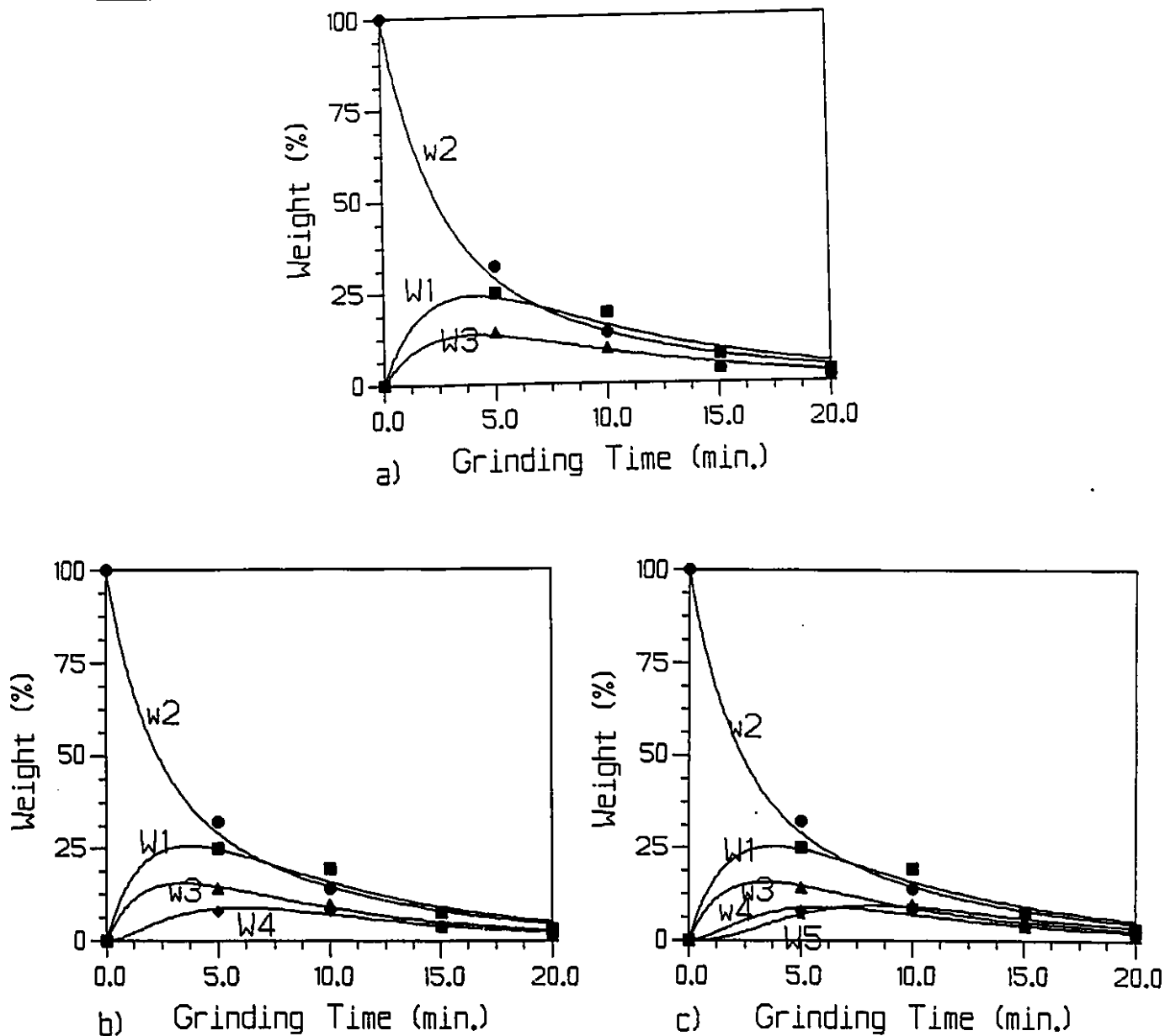


**Figure II.15.1:** Fit of the folding, flattening and explicit breakage model for the Bond ball mill test (lead fragments mixed with silica tests), point zero was considered, using 0.600-0.710 mm feed size; a: 3 size classes, b: 4 size classes, c: 5 size classes.

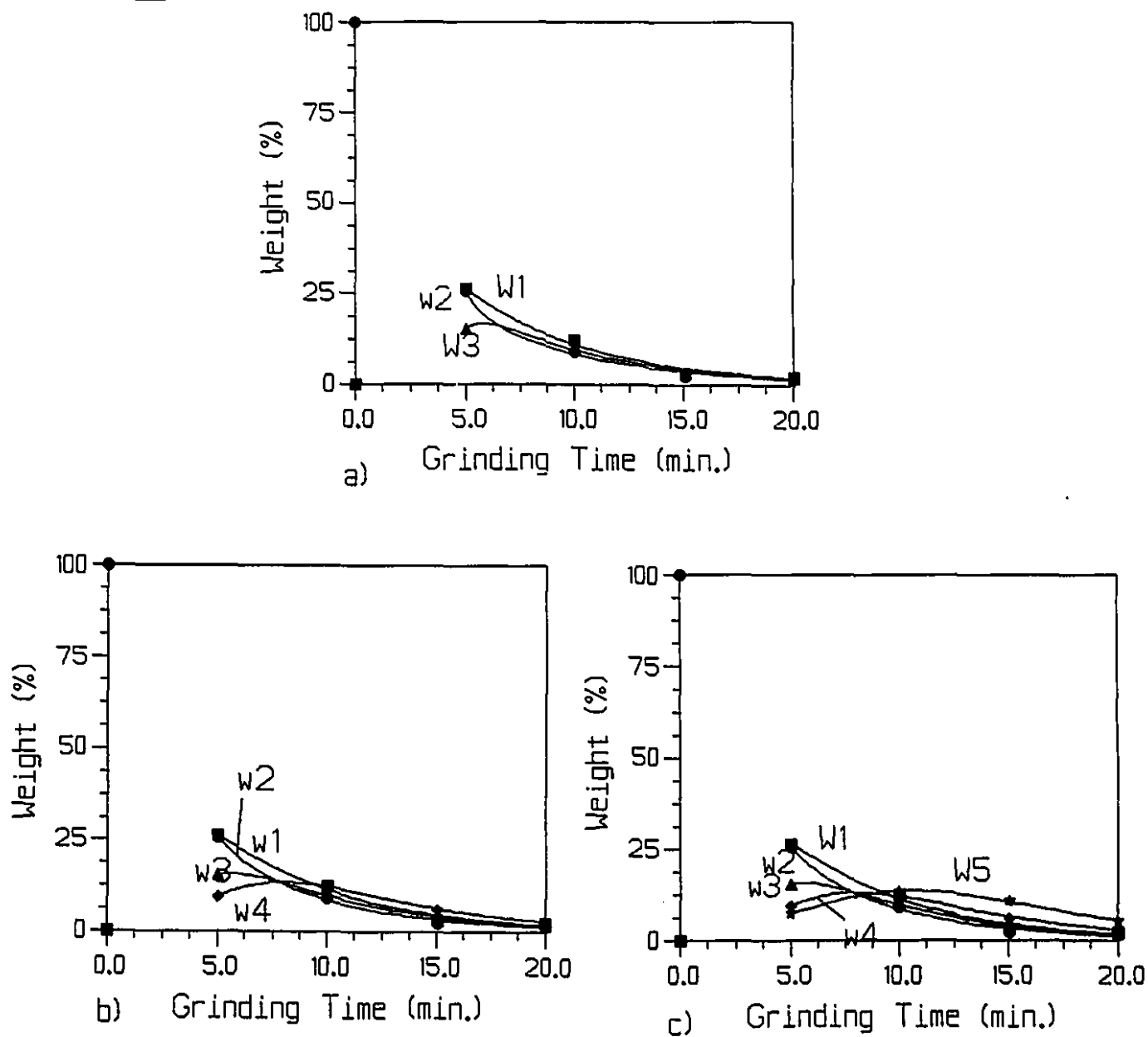


**Figure II.16:** Fit of the folding, flattening and explicit breakage model for the Bond ball mill test (lead fragments mixed with silica tests), point zero was not considered, using 0.425-0.500 mm feed size; a: 3 size classes, b: 4 size classes, c: 5 size classes.

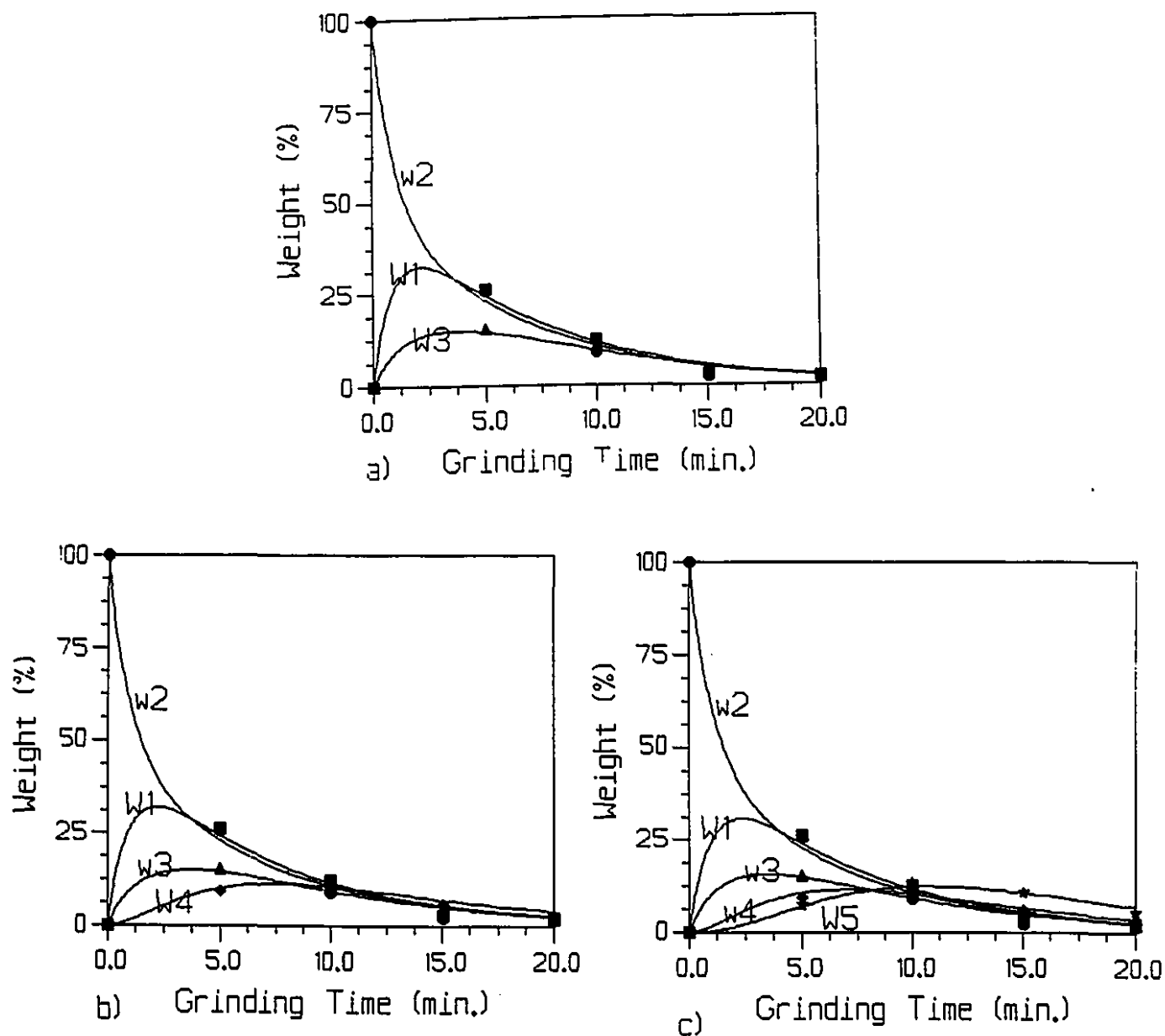


**Figure II.16.1:** Fit of the folding, flattening and explicit breakage model for the Bond ball mill test (lead fragments mixed with silica tests), point zero was considered, using 0.425-0.500 mm feed size; a: 3 size classes, b: 4 size classes, c: 5 size classes.

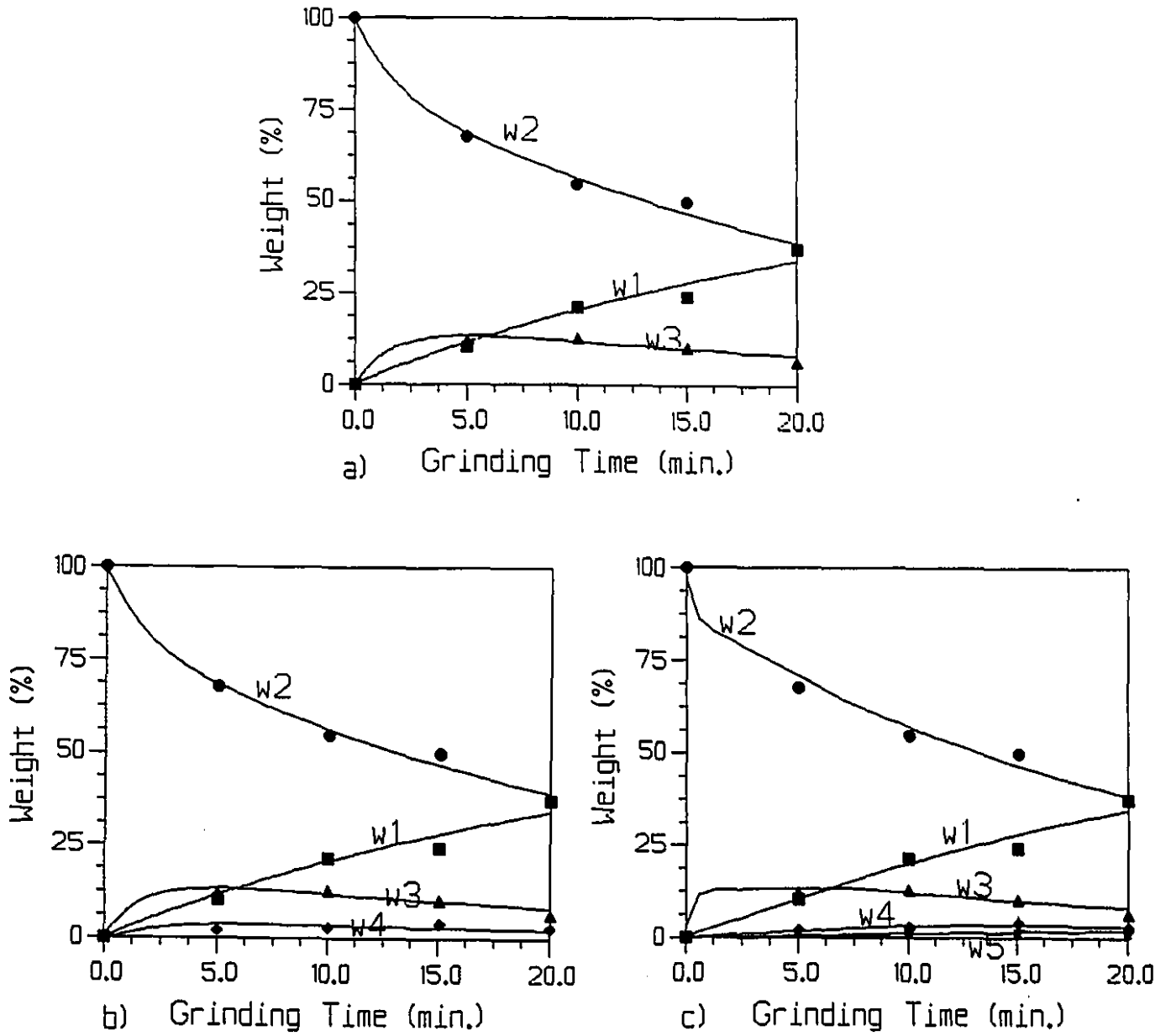


**Figure II.17:** Fit of the folding, flattening and explicit breakage model for the small ball mill test (lead fragments mixed with silica tests), using 1.18-1.40 mm feed size; a: 3 size classes, b: 4 size classes, c: 5 size classes.

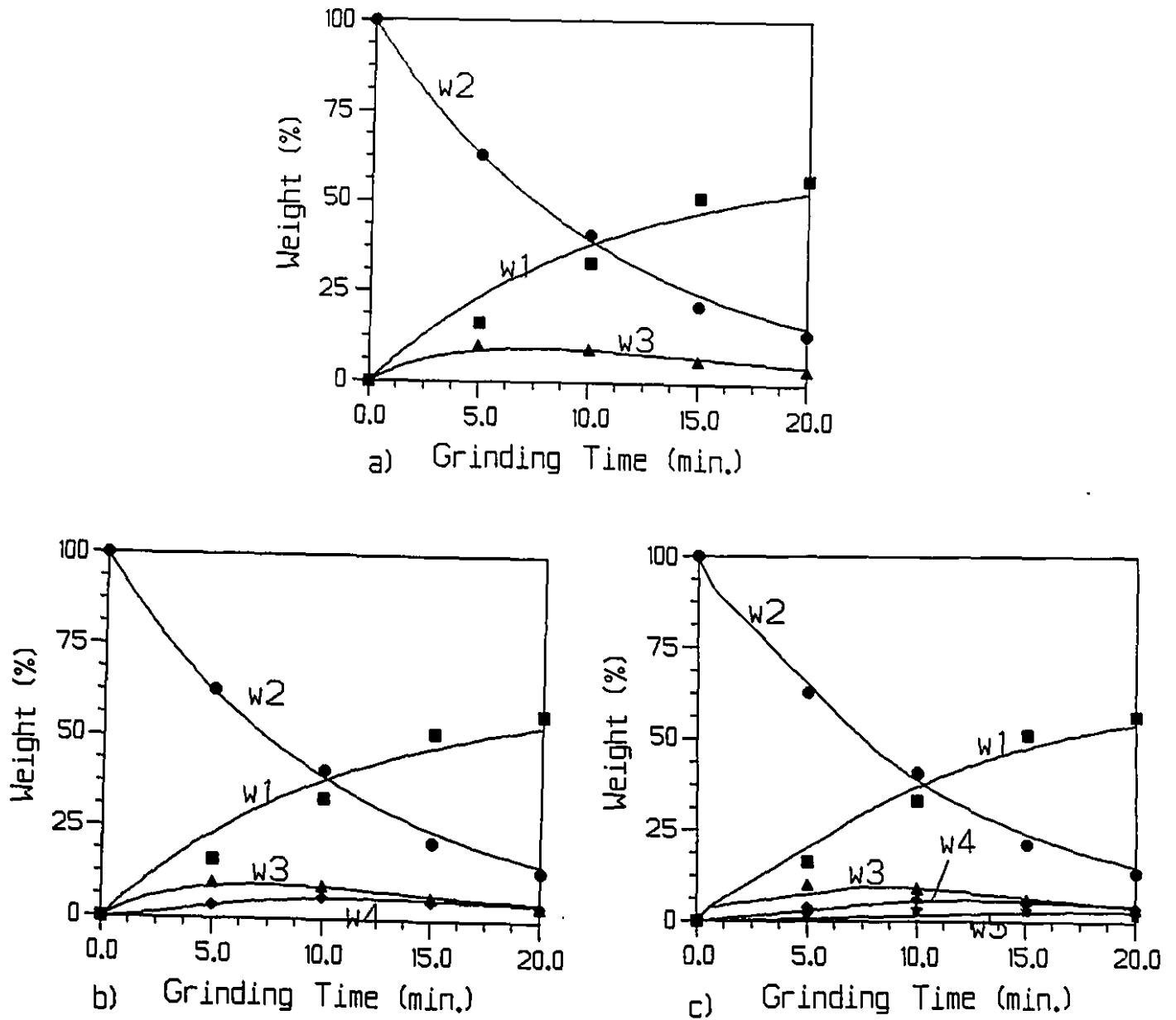


**Figure II.18:** Fit of the folding, flattening and explicit breakage model for the small ball mill test (lead fragments mixed with silica tests), using 0.850-1.00 mm feed size; a: 3 size classes, b: 4 size classes, c: 5 size classes.

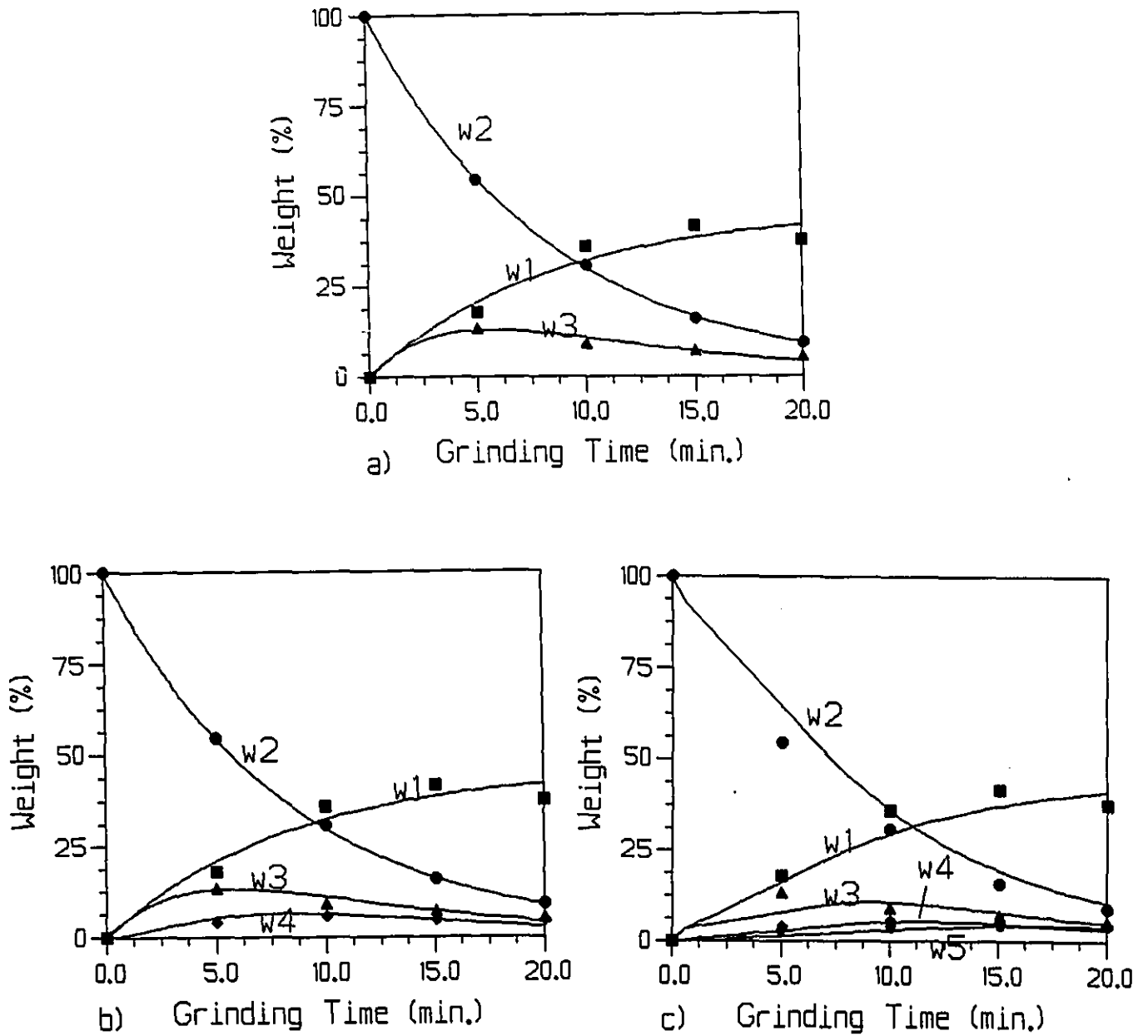


**Figure II.19:** Fit of the folding, flattening and explicit breakage model for the small ball mill test (lead fragments mixed with silica tests), using 0.600-0.710 mm feed size; a: 3 size classes, b: 4 size classes, c: 5 size classes.

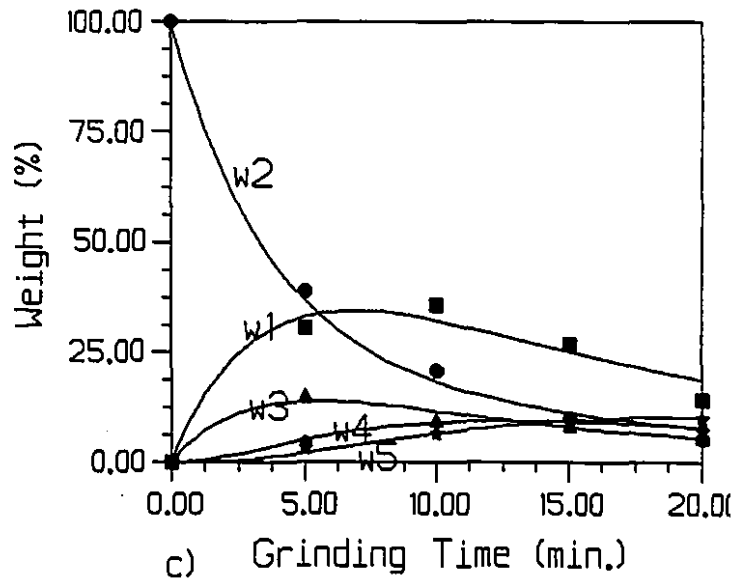
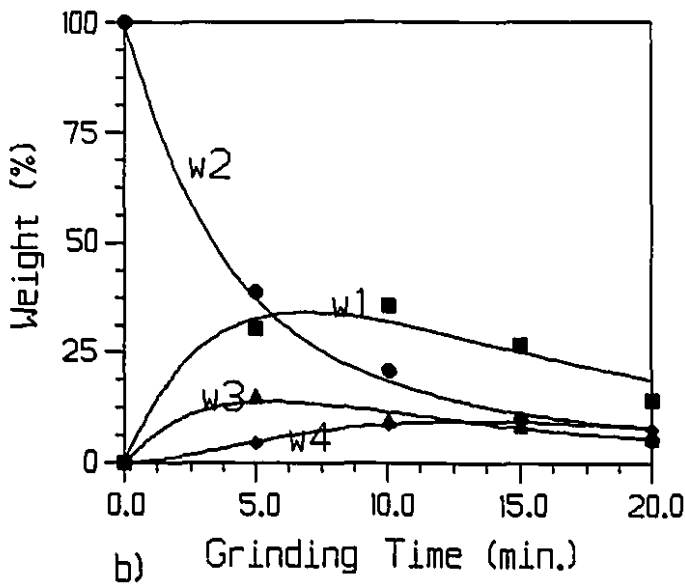
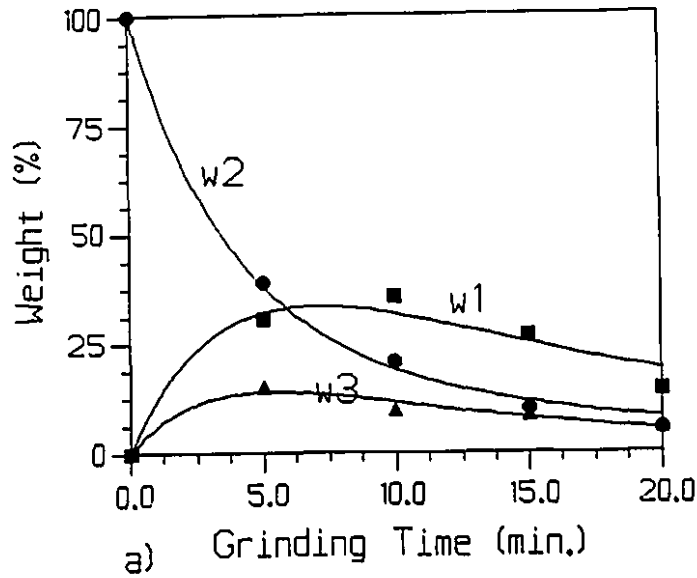


**Figure II.20:** Fit of the folding, flattening and explicit breakage model for the small ball mill test (lead fragments mixed with silica tests), using 0.425-0.500 mm feed size; a: 3 size classes, b: 4 size classes, c: 5 size classes.

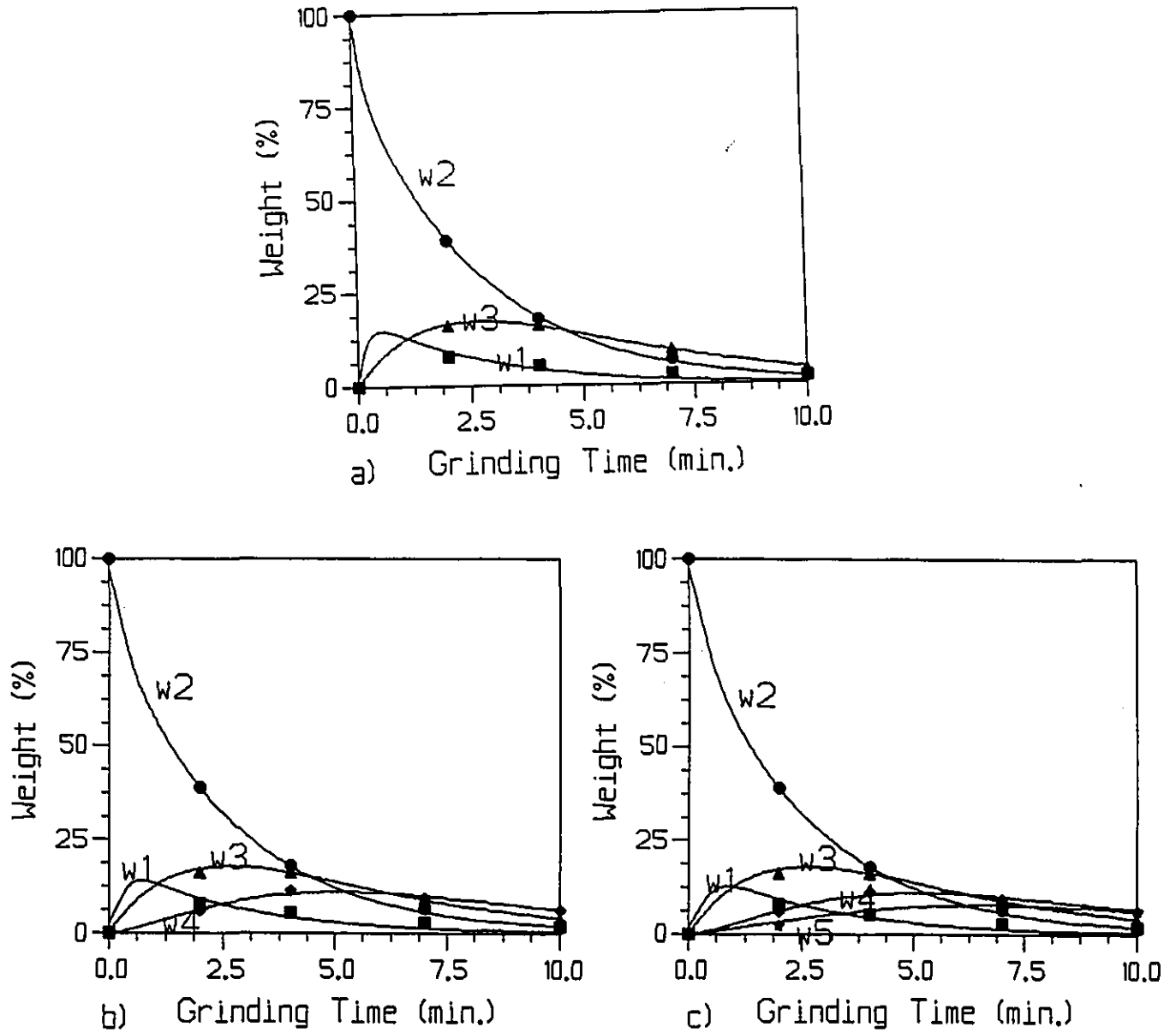


**Figure II.21:** Fit of the folding, flattening and explicit breakage model for the Bond rod mill test (lead fragments mixed with silica tests), using 1.18-1.40 mm feed size; a: 3 size classes, b: 4 size classes, c: 5 size classes.

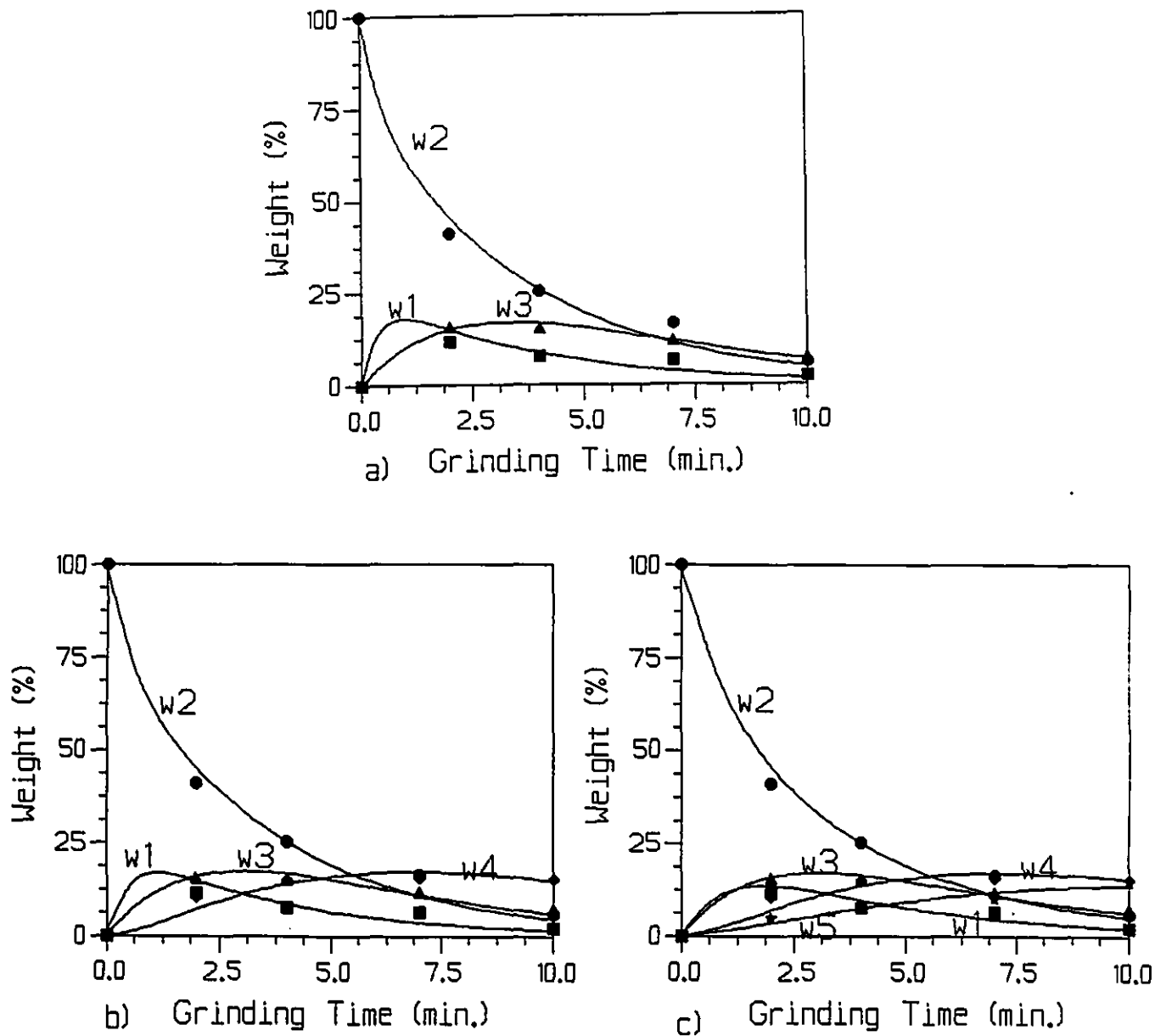


**Figure II.22:** Fit of the folding, flattening and explicit breakage model for the Bond rod mill test (lead fragments mixed with silica tests), using 0.850-1.00 mm feed size: a: 3 size classes, b: 4 size classes, c: 5 size classes.

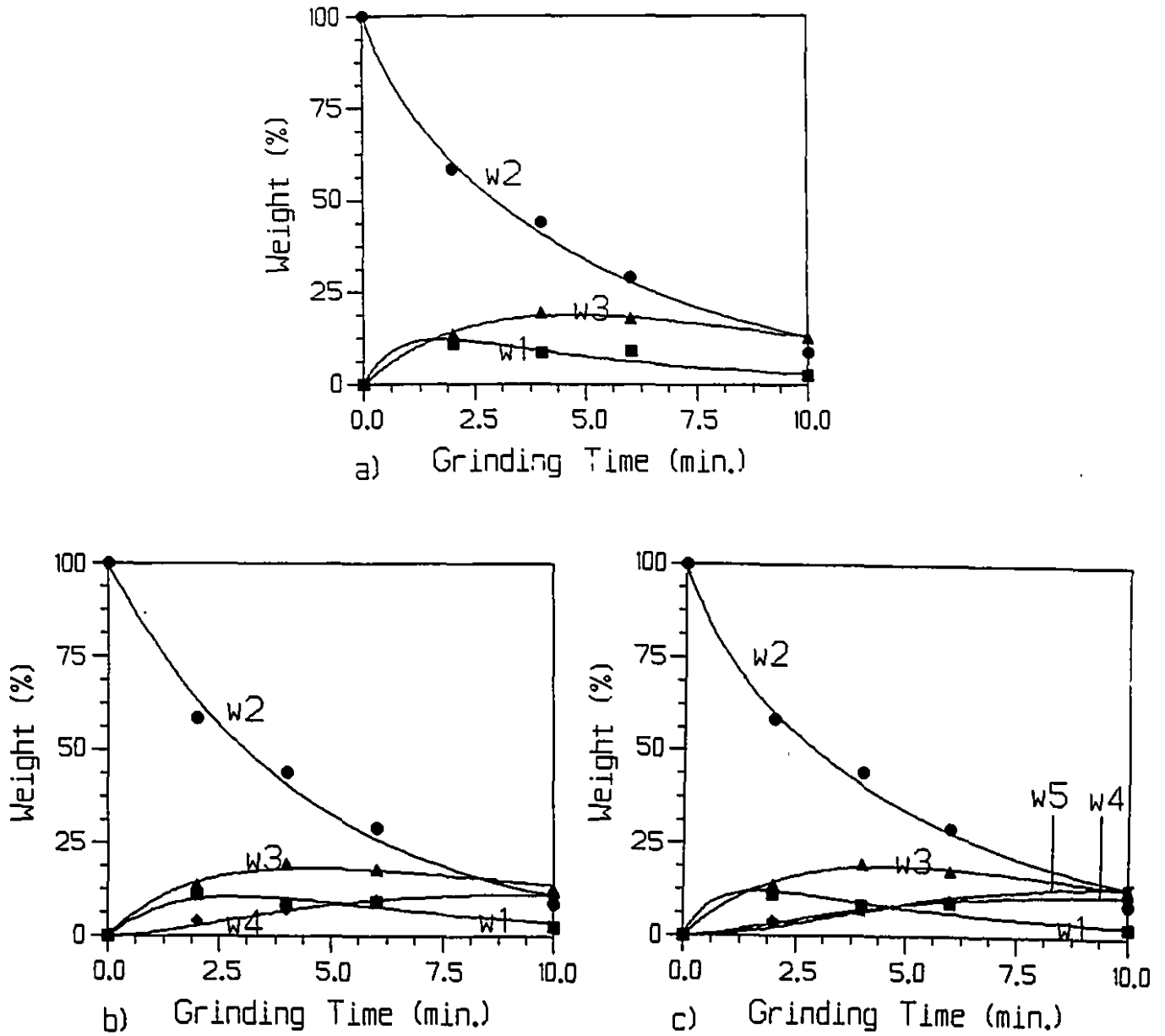


**Figure II.23:** Fit of the folding, flattening and explicit breakage model for the Bond rod mill test (lead fragments mixed with silica tests), using 0.600-0.710 mm feed size; a: 3 size classes, b: 4 size classes, c: 5 size classes.

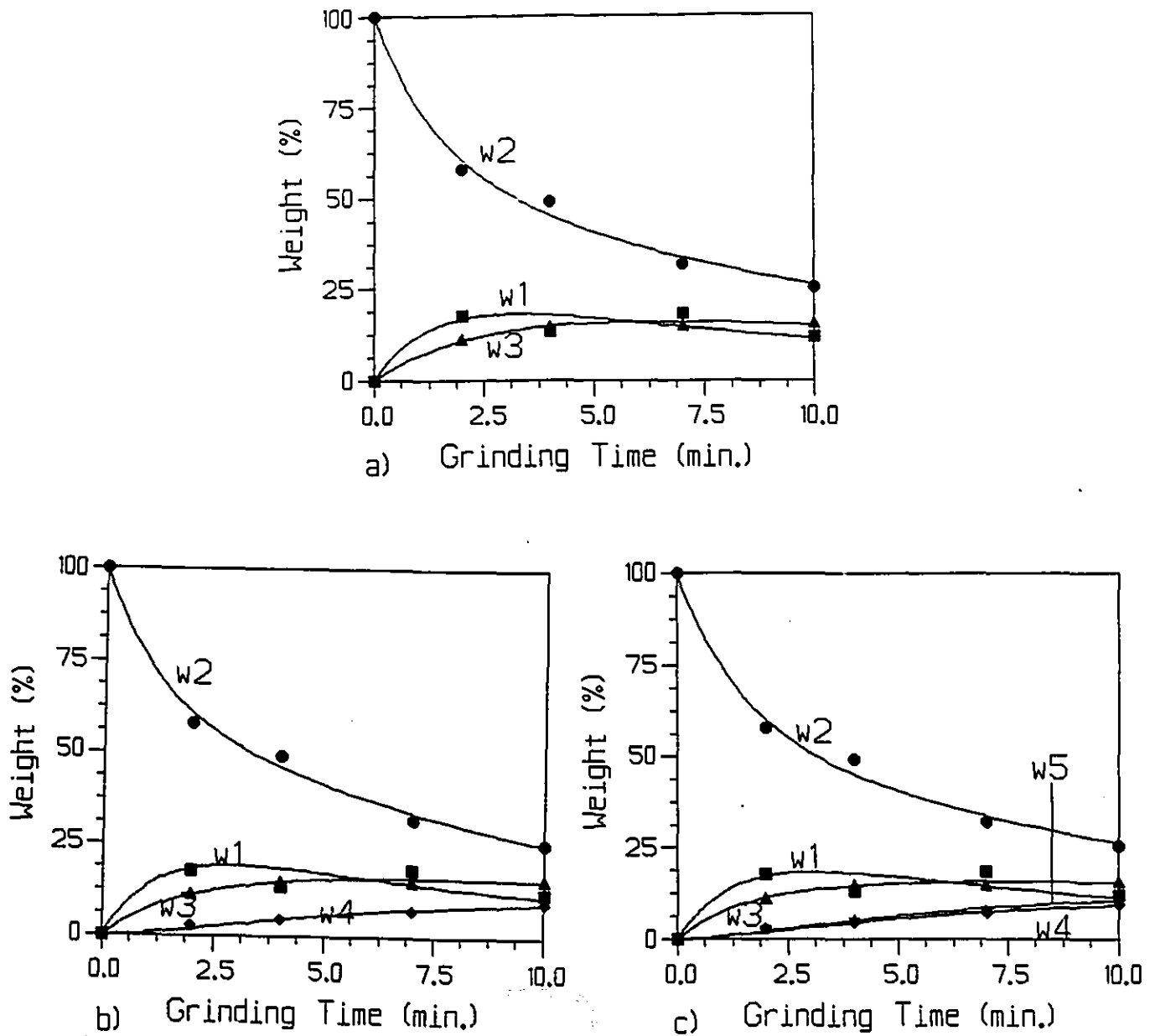


**Figure II.24:** Fit of the folding, flattening and explicit breakage model for the Bond rod mill test (lead fragments mixed with silica tests), using 0.425-0.500 mm feed size; a: 3 size classes, b: 4 size classes, c: 5 size classes.

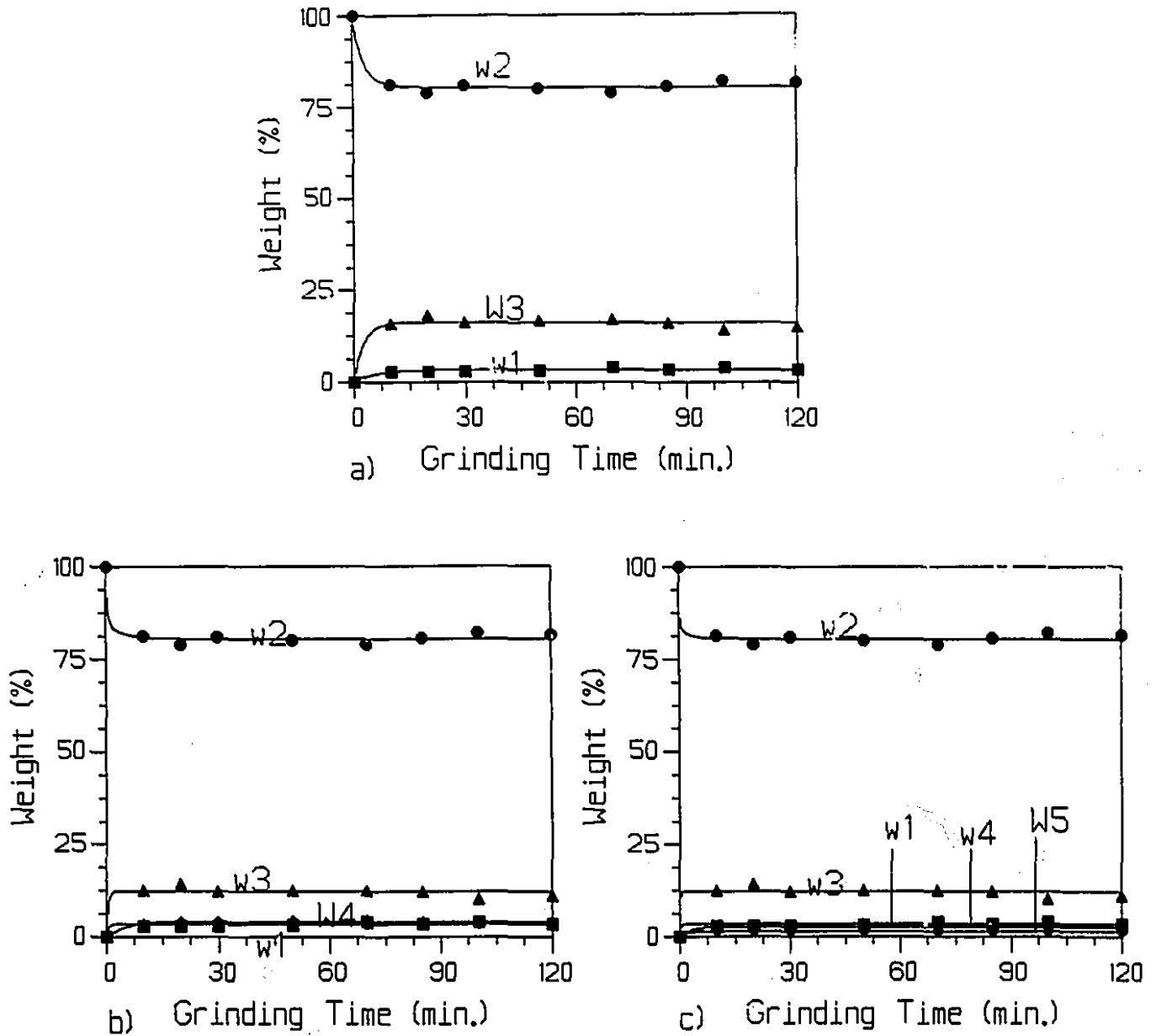


**Figure II.25:** Fit of the folding and flattening (no breakage) model for the Bond ball mill test (copper fragments tests), using 1.18-1.40 mm feed size; a: 3 size classes, b: 4 size classes, c: 5 size classes.

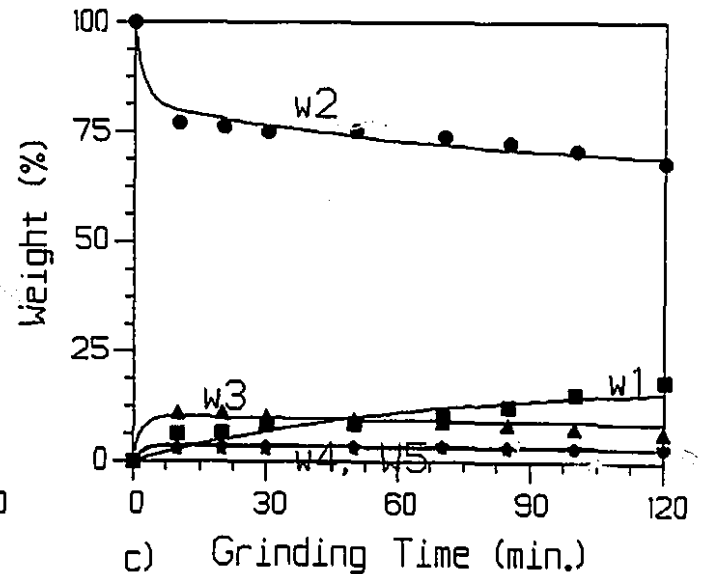
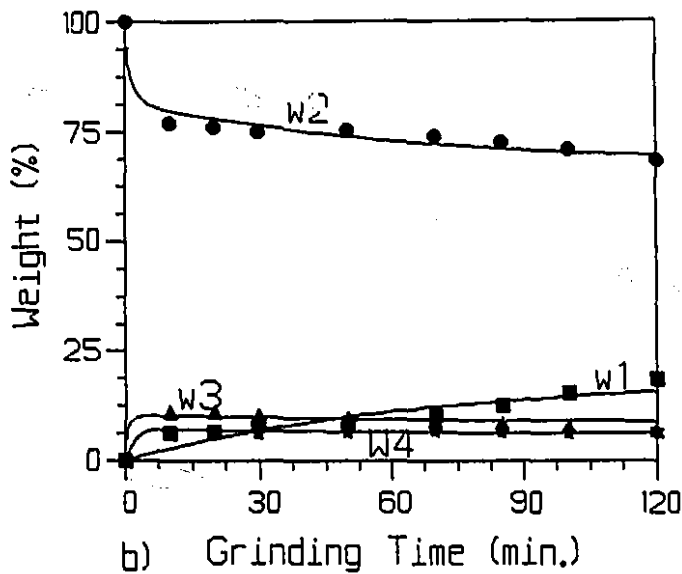
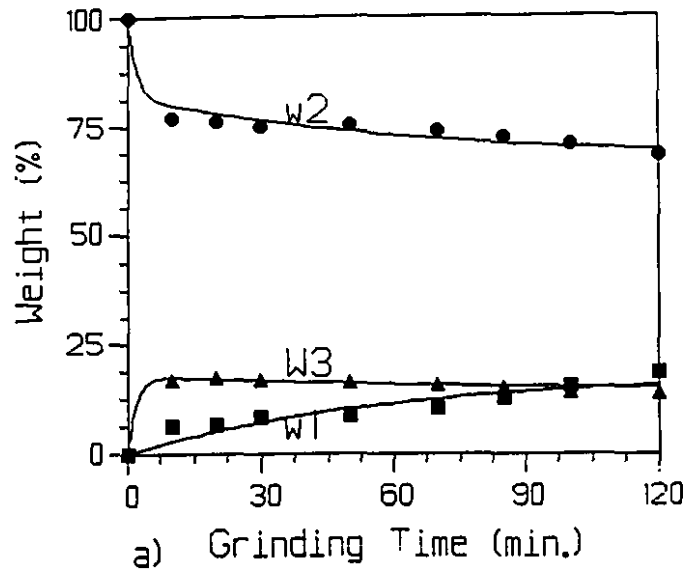


**Figure II.26:** Fit of the folding and flattening (no breakage) model for the Bond ball mill test (copper fragments tests), using 0.850-1.00 mm feed size; a: 3 size classes, b: 4 size classes, c: 5 size classes.

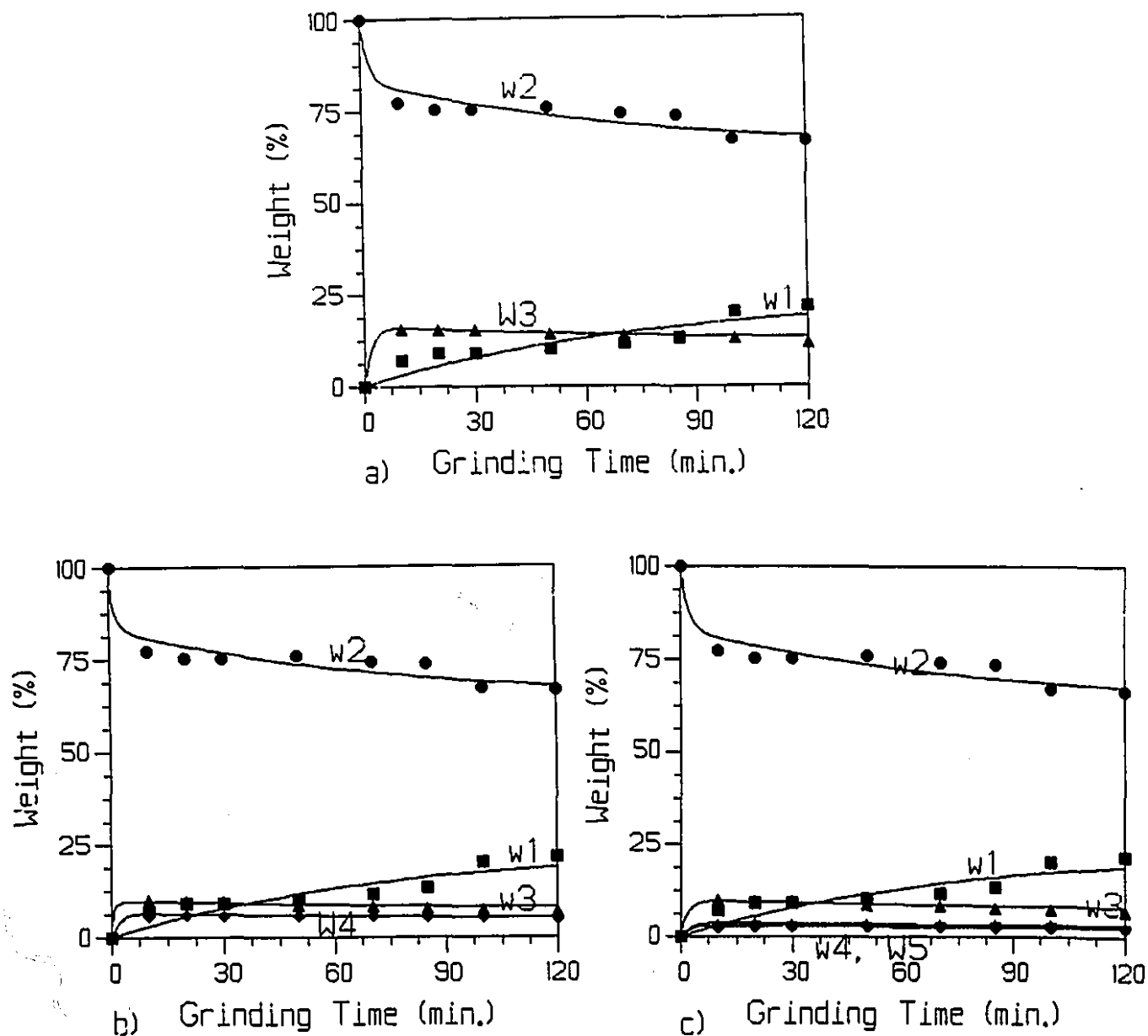


**Figure II.27:** Fit of the folding and flattening (no breakage) model for the Bond ball mill test (copper fragments tests), using 0.600-0.710 mm feed size; a: 3 size classes, b: 4 size classes, c: 5 size classes.

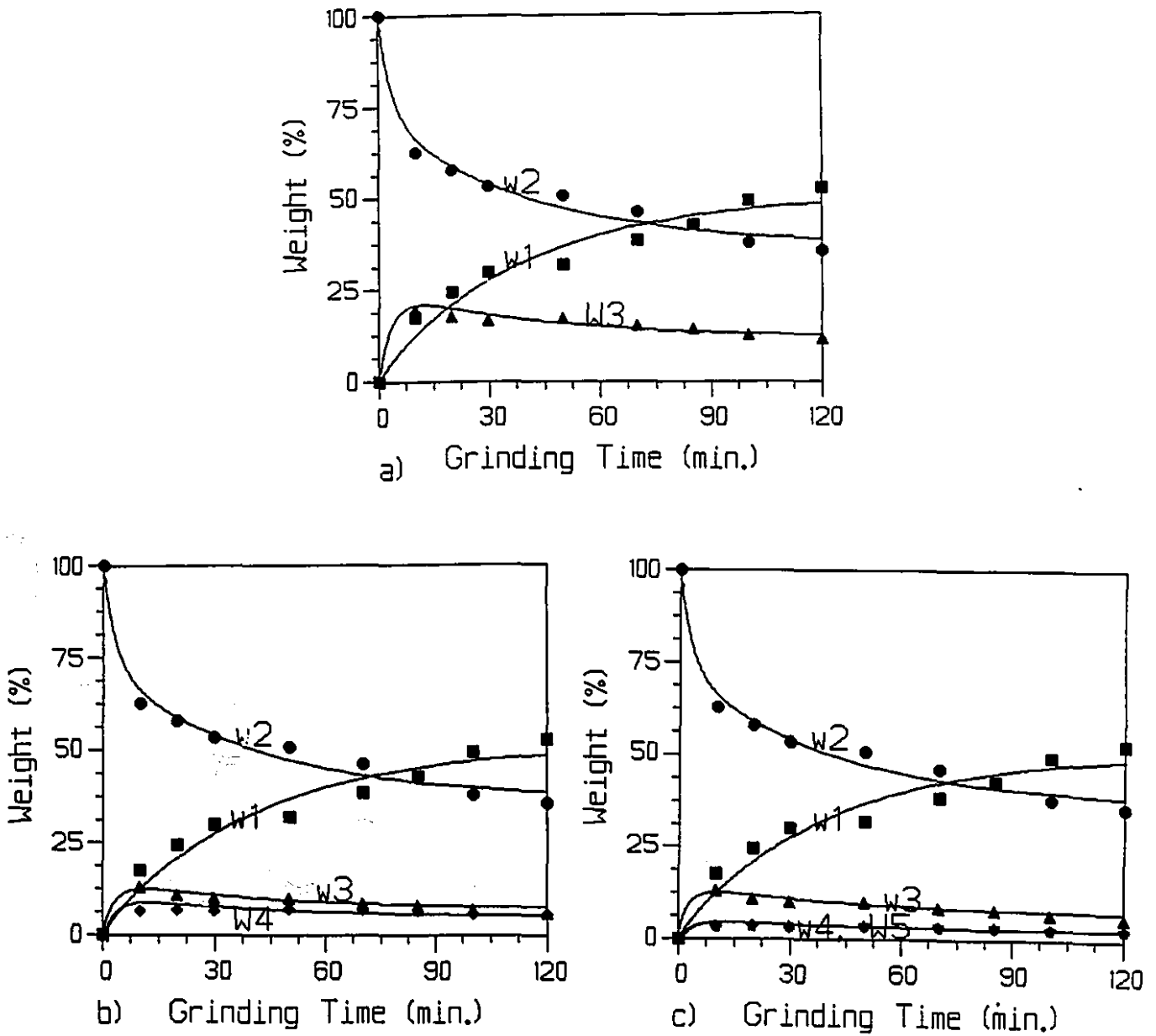


**Figure II.28:** Fit of the folding and flattening (no breakage) model for the Bcnd ball mill test (copper fragments tests), using 0.425-0.500 mm feed size; a: 3 size classes, b: 4 size classes, c: 5 size classes.

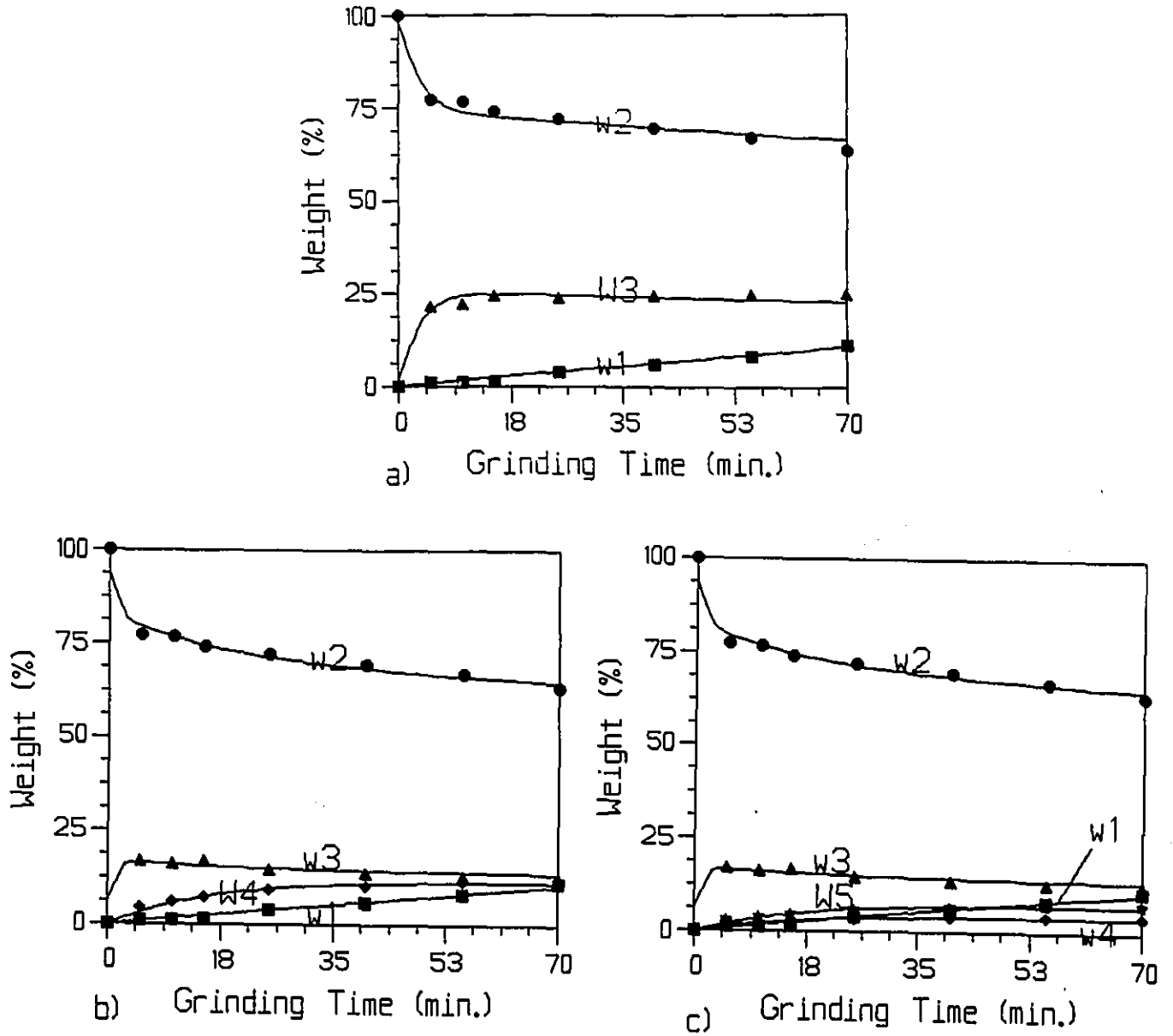


**Figure II.29:** Fit of the folding and flattening (no breakage) model for the small ball mill test (copper fragments tests), using 1.18-1.40 mm feed size; a: 3 size classes, b: 4 size classes, c: 5 size classes.

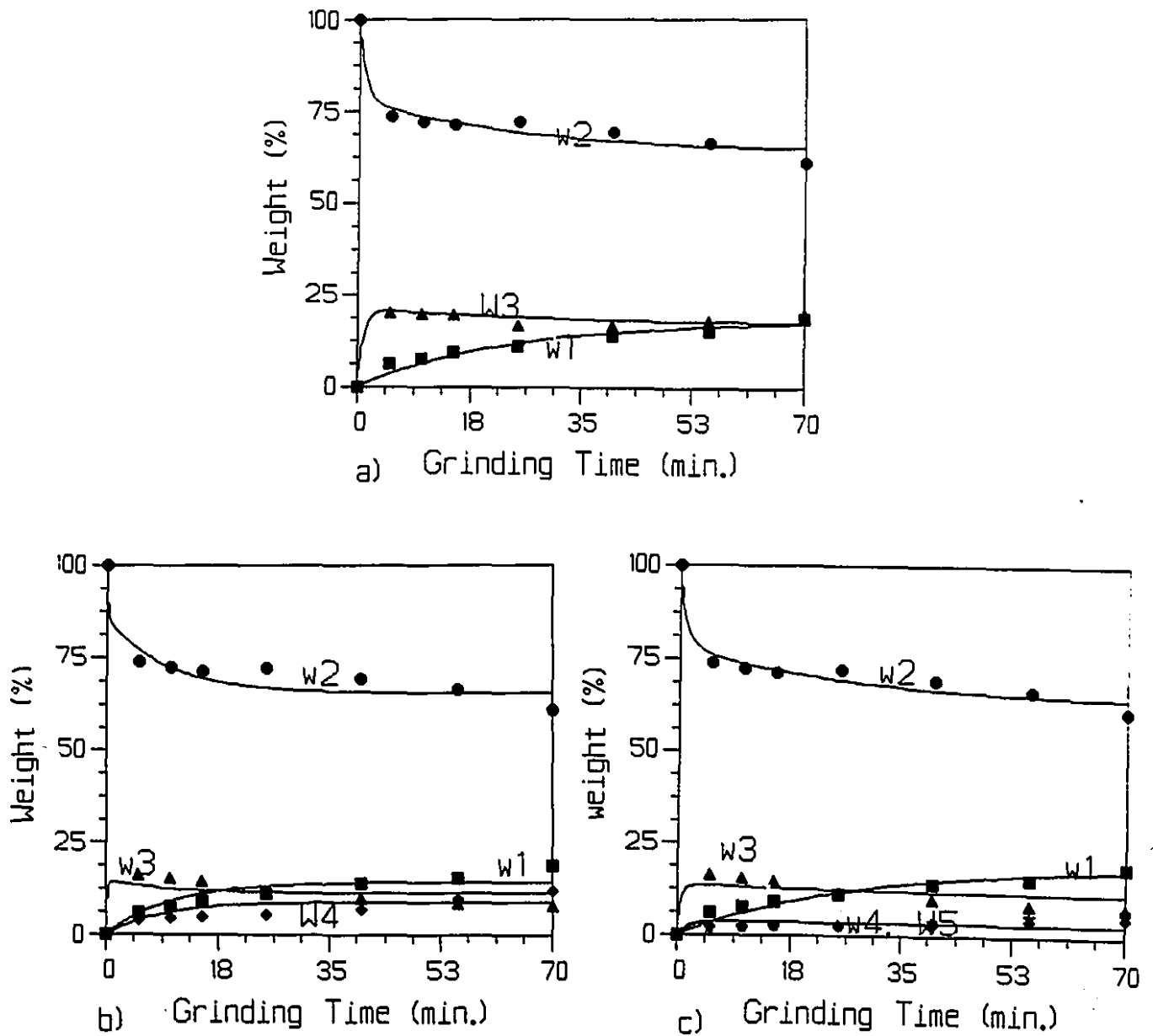


**Figure II.30:** Fit of the folding and flattening (no breakage) model for the small ball mill test (copper fragments tests), using 0.850-1.00 mm feed size; a: 3 size classes, b: 4 size classes, c: 5 size classes.

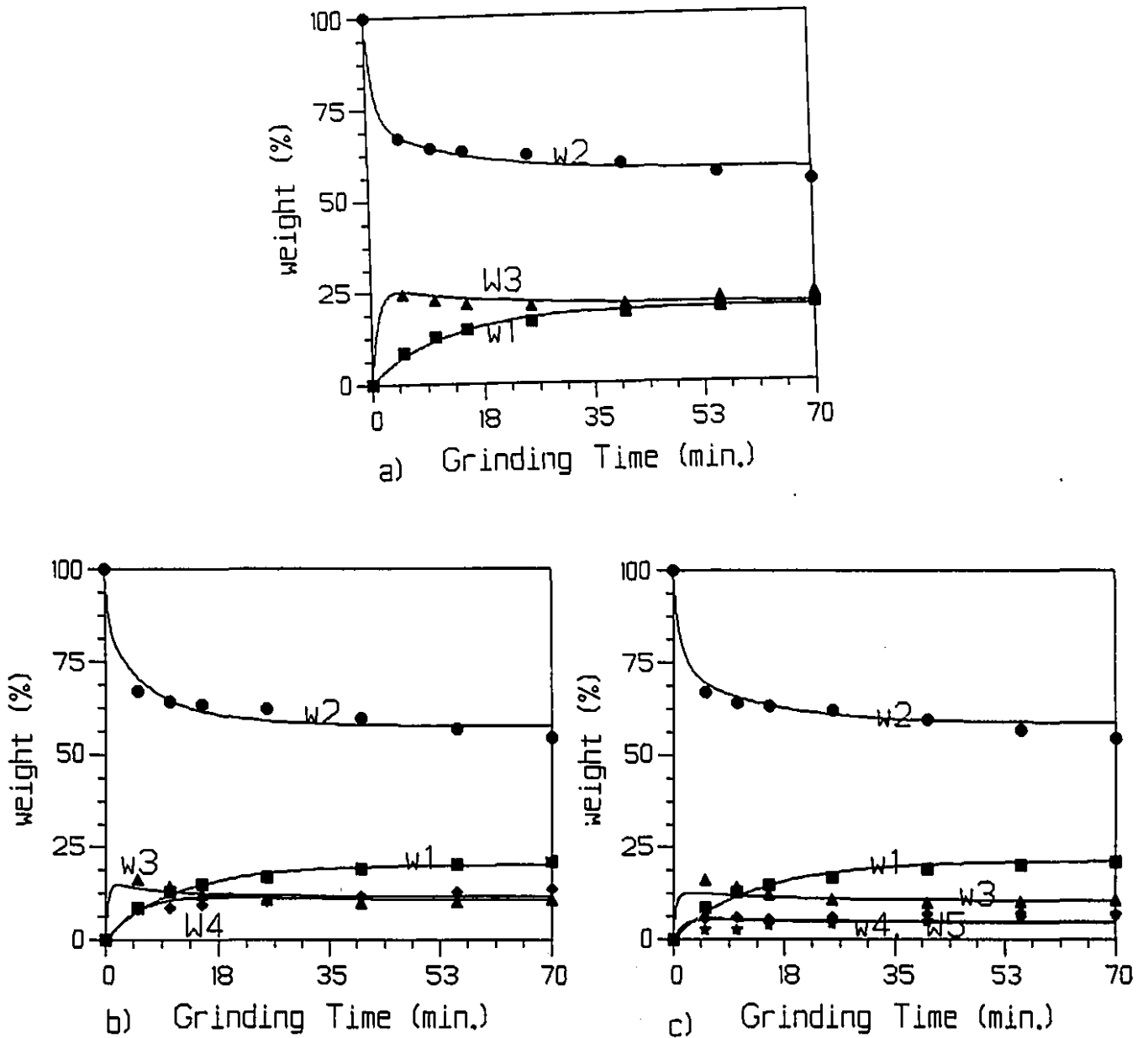


**Figure II.31:** Fit of the folding and flattening (no breakage) model for the small ball mill test (copper fragments tests), using 0.600-0.710 mm feed size; a: 3 size classes, b: 4 size classes, c: 5 size classes.

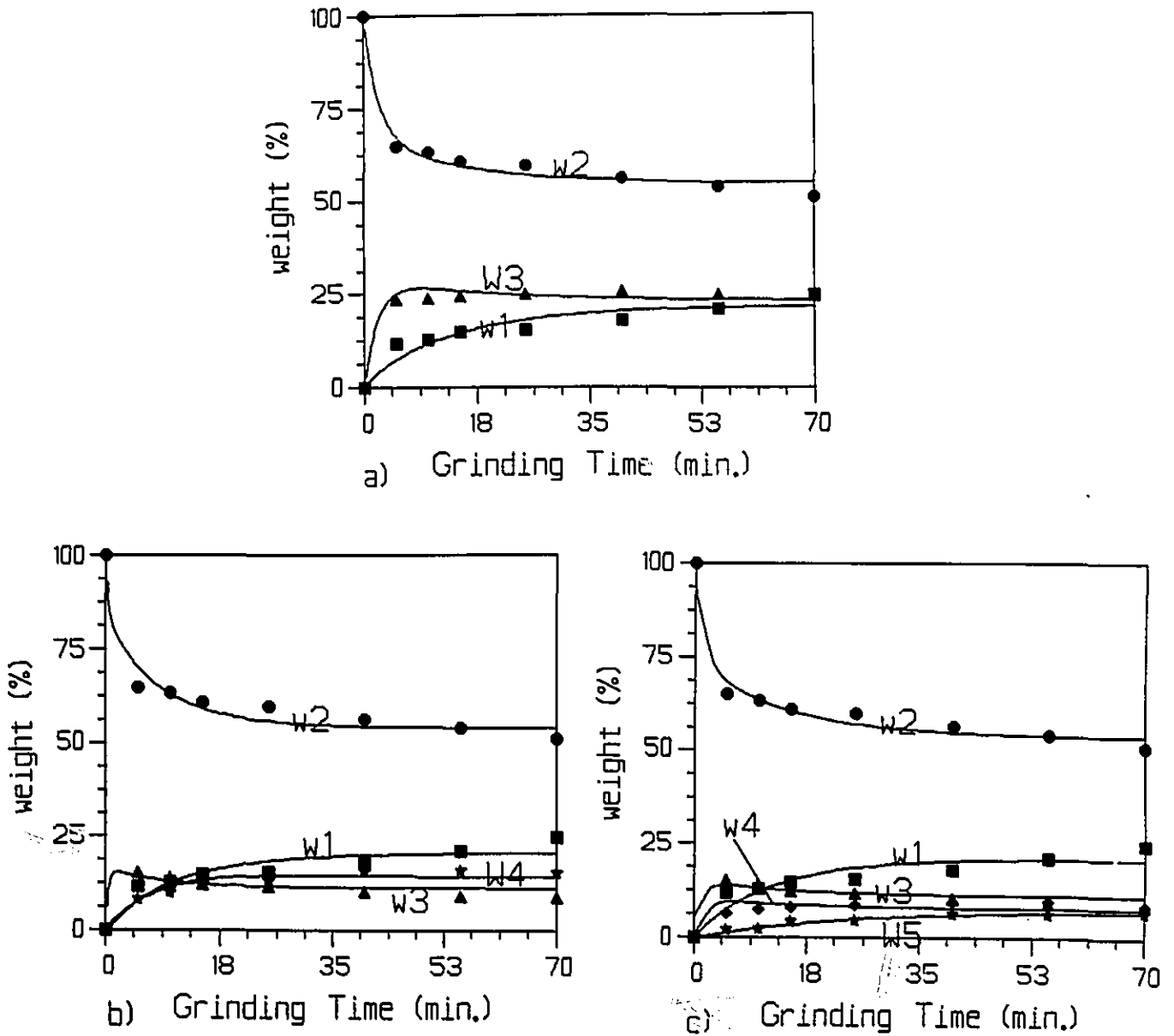


**Figure II.32:** Fit of the folding and flattening (no breakage) model for the small ball mill test (copper fragments tests), using 0.425-0.500 mm feed size; a: 3 size classes, b: 4 size classes, c: 5 size classes.

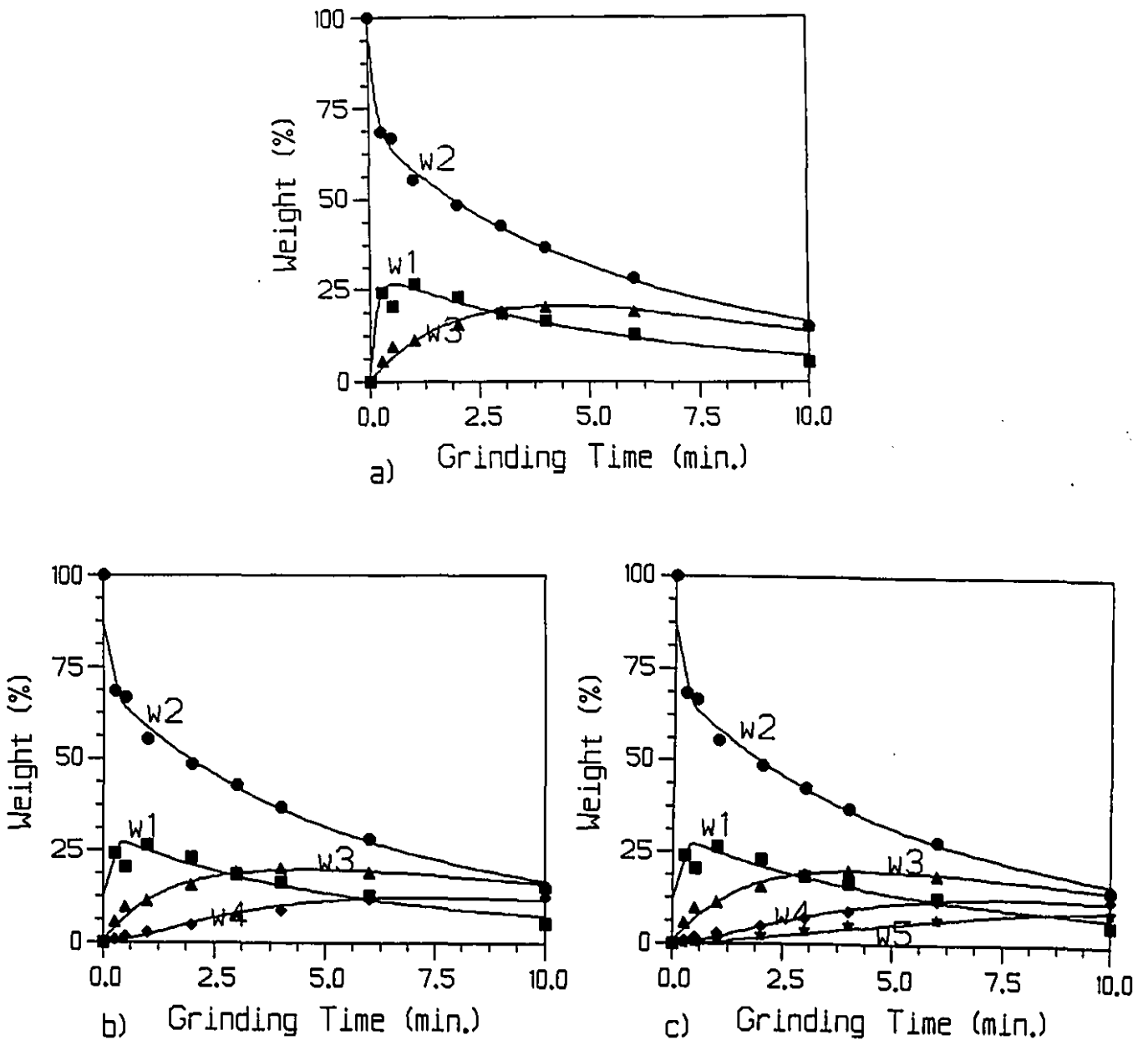


**Figure II.33:** Fit of the folding, flattening and explicit breakage model for the Bond rod mill test (copper fragments tests), using 1.18-1.40 mm feed size; a: 3 size classes, b: 4 size classes, c: 5 size classes.

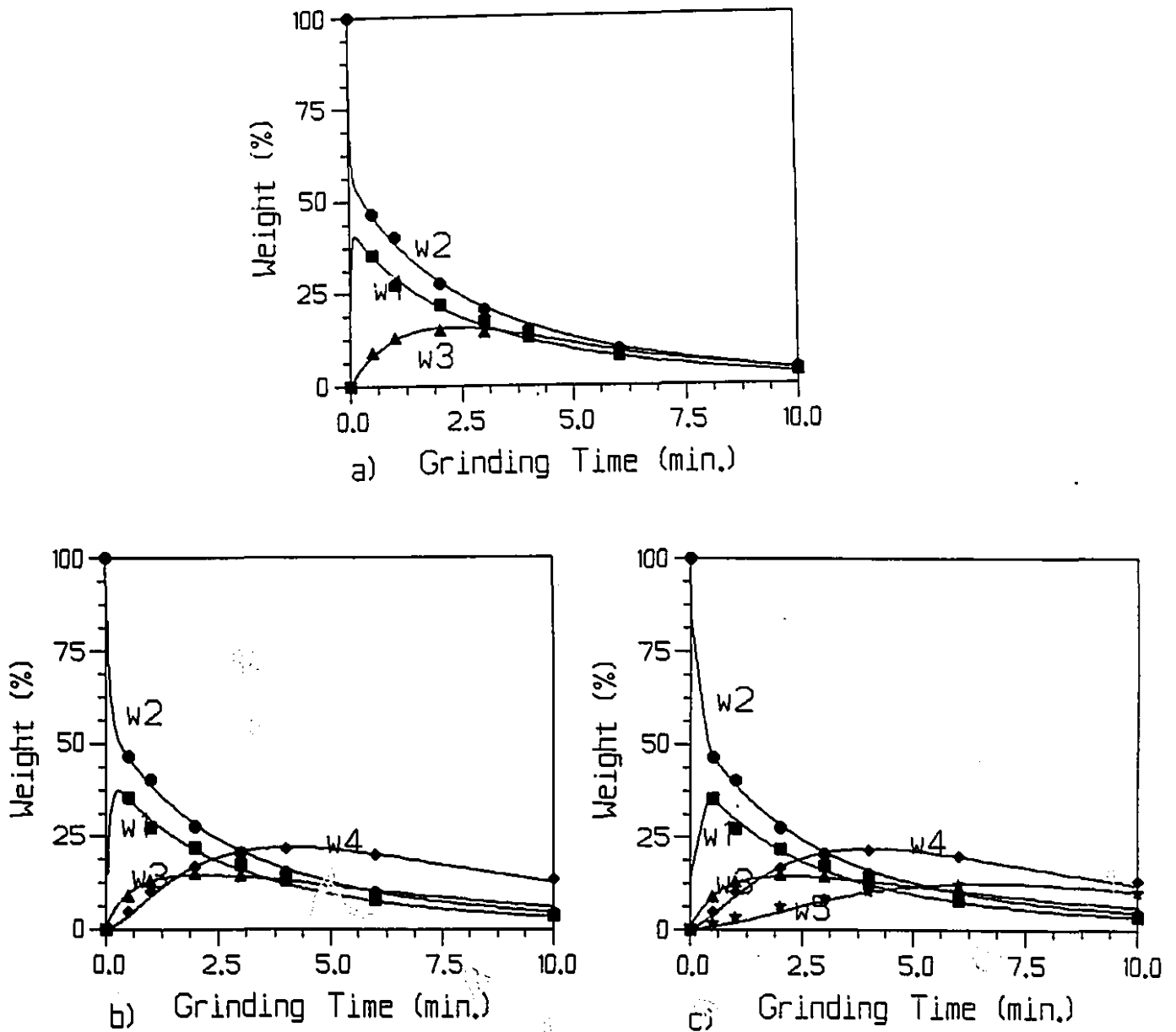


**Figure II.34:** Fit of the folding, flattening and explicit breakage model for the Bond rod mill test (copper fragments tests), using 0.850-1.00 mm feed size; a: 3 size classes, b: 4 size classes, c: 5 size classes.

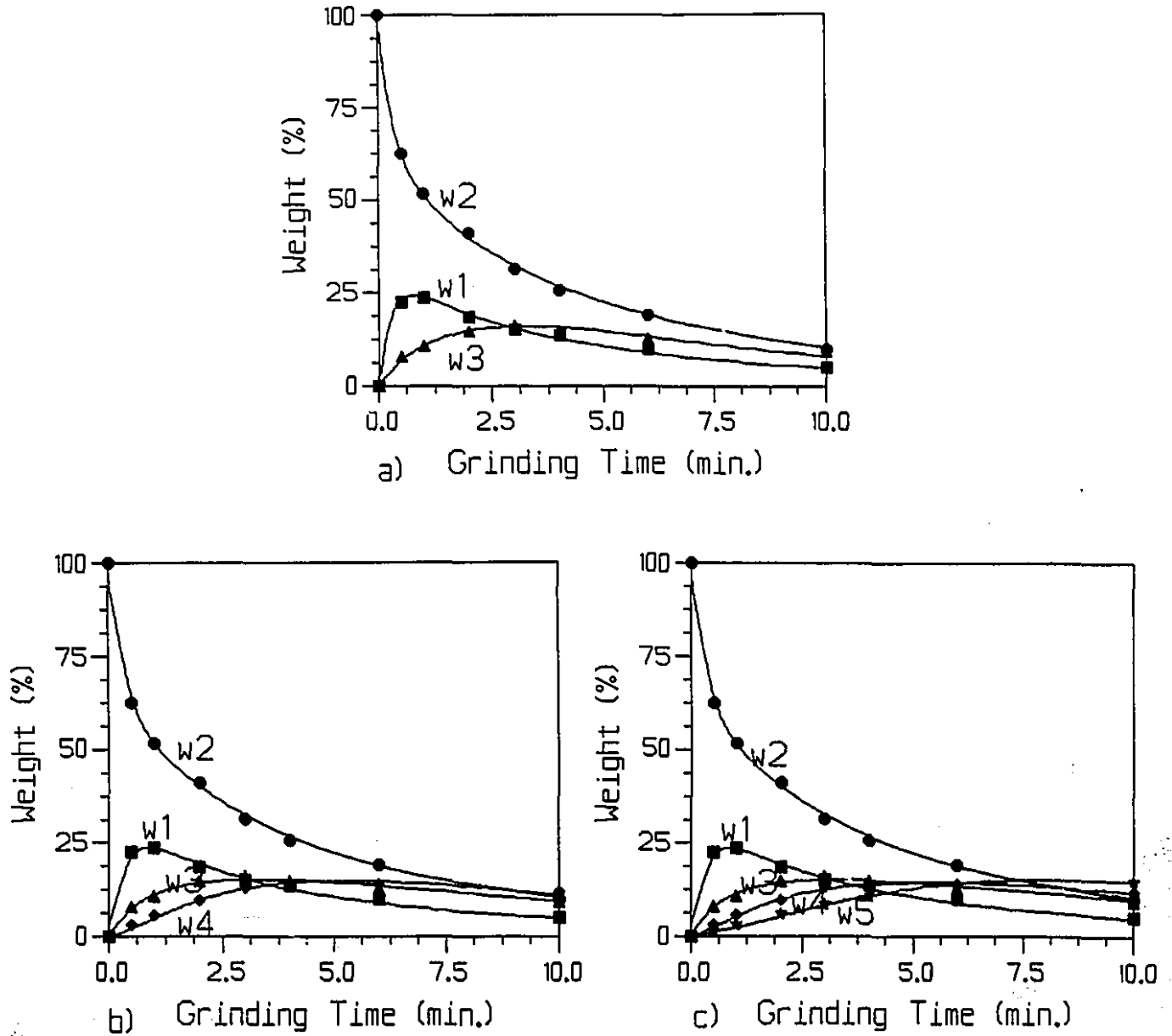


**Figure II.35:** Fit of the folding, flattening and explicit breakage model for the Bond rod mill test (copper fragments tests), using 0.600-0.710 mm feed size; a: 3 size classes, b: 4 size classes, c: 5 size classes.

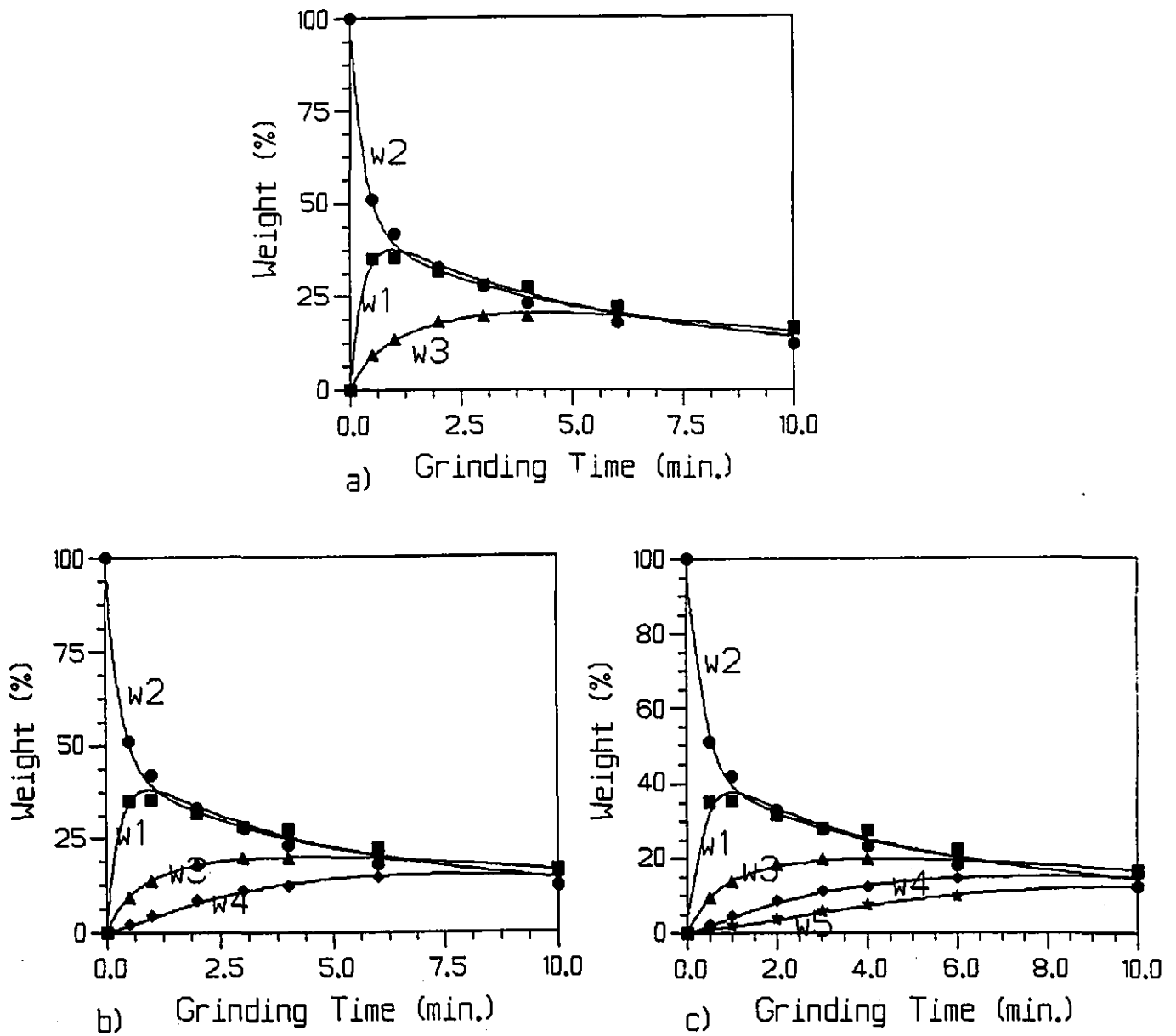


**Figure II.36:** Fit of the folding, flattening and explicit breakage model for the Bond rod mill test (copper fragments tests), using 0.425-0.500 mm feed size; a: 3-size classes, b: 4 size classes, c: 5 size classes.

---

**Appendix III: Experimental Data & Assaying Results,  
Charts and Tables of Chapters 4, 8**

Individual size class grinding, up to 56 minutes/ Chapter 4/ Test 1.

Grinding Time min. Size Class	Feed	1	2	4	8	16	24	32	40	48	56
+4.00 mm (W1)	-	-	-	0.2	0.2 0.3	0.3 0.5 0.5	1.3 4.4 2.6	7.8 9.9 1.5	18.5 12.6 0.2	28.5 9.6 0.4	38.1 8.1 0.3
3.35-4.00 mm (W2)	-	-	1.1 0.4	1.4 7.5 2.2	9.9 8.4 0.3	0.2 15.3 12.5 1.8	22.1 17.4	0.5 28.0 12.7 0.5	0.7 27.4 8.1 0.2	0.8 24.6 8.0 0.6	0.8 24.7 4.3
2.80-3.35 mm (W3)	100	78.9	52.1 6.9	37.5 22.6	0.7 39.7 11.5	2.6 33.9 15.0	2.5 29.9 5.1	0.2 1.5 23.0 4.8	0.8 19.9 1.7	1.4 12.8 3.7	0.01 1.5 12.5 2.3
2.38-2.80 mm (W4)	-	21.2	25.9 13.8	13.4 15.3	0.2 11.8 16.5	0.3 4.9 11.4 0.3	0.2 0.7 10.9 0.2	0.2 0.2 6.4 0.7	1.2 5.4 0.2	0.7 4.6	0.2 3.1
2.00-2.38 mm (W5)	-	-	-	-	0.7	0.3	0.7 0.2	0.2 0.2	0.2 0.2	0.03 0.3	0.01

Casa Berardi Primary Cyclone Underflow sample/ First half (s1)/ 300 g/min/ 2.5 psi/ Chapter 8/

Size (um)	CONCENTRATE				TAILS				FEED			
	Weight (g)	% Weight	Grade g/t	Rec. (%)	Weight (g)	% Weight	Grade g/t	Rec. (%)	Weight (g)	% Weight	Grade g/t	Rec. (%)
600	27.31	25.68	138.00	3.57	679	13.10	150.00	96.43	706	13.35	149.54	4.12
420	11.96	11.25	253.00	3.96	496	9.56	148.00	96.04	508	9.59	150.47	2.98
300	11.48	10.79	510.00	6.53	599	11.55	140.00	93.47	610	11.54	146.96	3.50
210	8.69	8.17	1321.00	15.26	550	10.60	116.00	84.74	558	10.55	134.76	2.94
150	10.19	9.56	3941.11	36.68	673	12.98	103.00	63.32	683	12.91	160.25	4.27
105	9.94	9.35	10084.00	48.02	670	12.92	162.00	51.98	680	12.85	307.10	8.15
75	9.57	9.00	21905.20	54.97	540	10.42	318.00	45.03	550	10.39	693.92	14.88
53	7.80	7.33	36188.00	55.53	289	5.58	782.00	44.47	297	5.61	1712.19	19.84
37	5.40	5.06	49541.10	60.12	166	3.20	1068.00	35.97	171	3.24	2594.41	17.36
25	2.46	2.31	55135.00	59.56	85	1.65	1078.00	40.44	88	1.66	2591.09	8.89
-25	1.55	1.46	71838.00	33.22	437	8.43	512.00	66.78	439	8.29	763.98	13.08
Total	106.35	100.00	11010.12	45.69	5184	100.00	268.48	54.31	5290	100.00	484.43	100.00

Casa Berardi Primary Cyclone Underflow sample/ Second half (s2)/ 300 g/min/ 2.5 psi/ Chapter 8/

Size (um)	CONCENTRATE				TAILS				FEED			
	Weight (g)	% Weight	Grade g/t	Rec. (%)	Weight (g)	% Weight	Grade g/t	Rec. (%)	Weight (g)	% Weight	Grade g/t	Rec. (%)
600	23.11	20.33	131.00	2.83	693	13.39	150.00	97.17	716	13.54	149.39	3.53
420	10.42	9.17	190.00	2.24	499	9.65	173.00	97.76	510	9.63	173.35	2.92
300	11.69	10.28	340.00	4.45	601	11.61	142.00	95.55	613	11.58	145.78	2.95
210	10.21	8.98	1082.00	13.86	545	10.53	126.00	86.14	555	10.50	143.58	2.63
150	12.22	11.37	3941.11	39.96	640	12.53	118.00	60.04	661	12.50	192.69	4.21
105	13.02	11.45	7880.00	48.06	626	12.10	177.00	51.94	639	12.09	333.87	7.05
75	12.25	10.78	21905.20	59.40	501	9.68	366.00	40.60	513	9.70	879.97	14.92
53	9.14	8.04	31423.00	56.23	278	5.37	805.00	43.77	287	5.42	1720.59	16.87
37	6.09	5.36	49541.10	61.69	165	3.18	1139.00	38.31	171	3.22	2866.90	16.16
25	2.85	2.51	47051.00	59.40	86	1.66	1066.00	40.60	89	1.68	2541.39	7.46
-25	1.98	1.74	48422.00	14.87	534	10.31	1028.00	85.13	536	10.13	1203.17	21.29
Total	113.68	100.00	11090.49	41.65	5176	100.00	341.25	58.35	5290	100.00	572.25	100.00

Casa Berardi sample/ 230 g/min/ 2.5 psi/ 100% 0.150-0.212/ chapter 8/

Size (um)	CONCENTRATE				TAILS				FEED			
	Weight (g)	% Weight	Grade g/t	Rec. (%)	Weight (g)	% Weight	Grade g/t	Rec. (%)	Weight (g)	% Weight	Grade g/t	Rec. (%)
600	1.87	2.01	96.43	97.71	0	0.02	9.09	2.29	2	0.08	79.03	0.20
420	2.44	2.62	16.84	53.71	4	0.13	9.09	46.29	6	0.21	12.08	0.08
300	7.13	7.66	3.21	66.80	99	3.41	0.12	33.20	106	3.54	0.32	0.04
210	17.36	18.65	119.00	95.87	668	23.00	0.13	4.13	686	22.86	3.14	2.37
150	22.23	23.89	2468.00	99.80	912	27.95	0.13	0.20	835	27.82	65.86	60.36
105	16.41	17.63	918.00	98.35	633	21.79	0.40	1.65	650	21.66	23.58	16.82
75	11.79	12.67	187.00	92.36	391	13.44	0.47	7.64	403	13.42	5.93	2.62
53	6.46	6.94	290.00	87.68	162	5.57	1.63	12.32	168	5.61	12.69	2.35
37	3.47	3.73	497.00	61.20	65	2.22	16.93	38.80	68	2.27	41.41	3.09
25	2.17	2.33	833.00	53.44	22	0.74	73.12	46.56	24	0.79	142.67	3.71
-25	1.74	1.87	2200.00	50.27	50	1.74	75.00	49.73	52	1.74	145.79	8.36
Total	93.07	100.00	899.07	91.87	2907	100.00	2.55	8.13	3000	100.00	30.36	100.00

Feed grade of initial concentrate= 3941.1 g/t

Casa berardi Primary Cyclone U/F sample/ 100% 0.150-0.212 mm/ chapter 8/  
 Selection & breakage functions estimation:

Total of 10 times grinding time (min.) = 5

Size classes	Geo. size	Sel. Func.	Feed Rec.	Bij	BijCalc.	Res.	bij	Conc. Rec.
600	714	-	0.20	-	-	-	-	97.71
420	499	-	0.08	-	-	-	-	53.71
300	357	-	0.04	-	-	-	-	66.80
210	250	-	2.37	-	-	-	-	95.87
150	175	0.0423	80.38	1.000	1.000	0.000	-	99.80
105	125	-	18.82	0.545	0.575	0.001	0.455	98.35
75	99	-	2.82	0.474	0.454	0.000	0.071	92.36
53	83	-	2.35	0.410	0.378	0.001	0.084	87.68
37	44	-	3.09	0.327	0.318	0.000	0.084	81.20
25	30	-	3.71	0.228	0.285	0.002	0.100	53.44
-25	20	-	8.38	-	-	-	-	50.27
Total			38.95			0.00398		

Beta 0.51  
 Gamma 8.48  
 Phi 0.38

Case Berardi sample/ 230 g/min/ 2.5 psi/ 100% 0.075-0.105 mm/ Chapter8/

Size (um)	CONCENTRATE				TAILS				FEED			
	Weight (g)	% Weight	Grade g/t	Rec. (%)	Weight (g)	% Weight	Grade g/t	Rec. (%)	Weight (g)	% Weight	Grade g/t	Rec. (%)
600	1.79	1.87	3.13	100.00	0	0.01	0.00	0.00	2	0.07	2.77	0.00
420	2.93	3.07	0.72	100.00	2	0.08	0.00	0.00	5	0.18	0.40	0.00
300	7.89	8.25	8.66	100.00	90	3.09	0.00	0.00	98	3.25	0.70	0.01
210	16.60	17.37	108.00	95.40	650	22.38	0.13	4.60	667	22.22	2.82	0.39
150	21.09	22.06	182.00	91.63	877	30.18	0.40	8.37	898	29.93	4.67	0.88
105	14.04	14.69	1452.00	98.31	584	20.11	0.60	1.69	598	19.94	34.66	4.34
75	14.92	15.61	24514.00	99.77	339	11.66	2.53	0.23	354	11.79	1036.69	76.70
53	8.27	8.65	6706.00	99.60	186	6.40	1.20	0.40	194	6.47	286.88	11.65
37	3.89	4.07	1819.00	95.27	85	2.91	4.16	4.73	88	2.95	84.01	1.55
25	2.39	2.50	2865.00	95.98	29	1.01	7.26	3.02	32	1.06	221.96	1.48
-25	1.78	1.86	7400.00	92.02	63	2.16	18.18	7.98	65	2.15	221.57	2.99
Total	95.59	100.00	4962.82	99.25	2904	100.00	1.23	0.75	3000	100.00	159.32	100.00

Feed grade of initial concentrate= 21905 g/t

Case berardi Primary Cyclone U/F sample/ 100% 0.075-0.105 mm/chapter8/  
Selection & breakage functions estimation:

Total of 10 times grinding time (min.) = 7.5

Size classes	Geo. size	Sel. Func.	Feed Rec.	Bij	BijCalc	Res.	bij	Conn. Rec.
800	714	-	0.00	-	-	-	-	100.00
420	499	-	0.00	-	-	-	-	100.00
300	357	-	0.01	-	-	-	-	100.00
210	250	-	0.39	-	-	-	-	95.40
150	178	-	0.88	-	-	-	-	91.83
105	125	-	4.34	-	-	-	-	98.31
75	88	0.0259	76.70	1.000	1.000	0.000	-	99.77
53	63	-	11.85	0.341	0.347	0.000	0.859	99.88
37	44	-	1.55	0.253	0.238	0.000	0.088	95.27
25	30	-	1.48	0.189	0.179	0.000	0.084	98.98
-25	20	-	2.99	-	-	-	-	92.02
Total			17.87			0.000389		

Beta 0.79  
Gamma 7.98  
Phi 0.59

Casa Berardi sample/ 230 g/min/ 2.5 psi/ 100% 0.038-0.053 mm/ Chapter 8/

Size (um)	CONCENTRATE				TAILS				FEED			
	Weight (g)	% Weight	Grade g/t	Rec. (%)	Weight (g)	% Weight	Grade g/t	Rec. (%)	Weight (g)	% Weight	Grade g/t	Rec. (%)
600	1.77	1.90	8.70	100.00	5	0.16	0.00	0.00	6	0.21	2.44	0.00
420	3.00	3.22	13.08	46.55	2	0.06	25.00	53.45	5	0.16	17.55	0.01
300	7.28	7.80	15.22	82.96	73	2.51	0.31	17.04	80	2.67	1.67	0.02
210	14.72	15.78	72.38	90.16	581	20.00	0.20	9.84	596	19.87	1.98	0.21
150	20.56	22.03	105.00	90.32	866	29.81	0.27	9.68	887	29.56	2.69	0.42
105	14.66	15.71	133.00	90.59	608	20.91	0.33	9.41	623	20.75	3.46	0.38
75	11.74	12.58	298.00	89.49	411	14.14	1.00	10.51	423	14.09	9.25	0.69
53	6.78	7.27	6408.00	95.73	184	6.33	10.53	4.27	191	6.36	237.96	7.97
37	7.87	8.43	43924.00	95.73	72	2.49	261.00	4.27	80	2.68	5516.25	77.88
25	2.90	3.11	18837.00	96.58	31	1.05	63.26	3.42	33	1.12	1689.50	9.94
-25	2.03	2.18	5349.00	76.94	74	2.55	44.00	23.06	76	2.53	185.69	2.48
Total	93.31	100.00	5810.22	95.24	2907	100.00	9.31	4.76	3000	100.00	189.74	100.00

Feed grade of initial concentrate = 49541 g/t

Casa berardi Primary Cyclone U/V sample/ 100% 0.038-0.053 mm/ chapter 8/  
Selection & breakage functions estimation:

Total of 10 times grinding time (min.) =

Size classes	Geo. size	Sel. Func.	Feal Rec.	Bij	BijCalc.	Res.	bij	Conc. Rec.
600	714	-	0.00	-	-	-	-	100.00
420	499	-	0.01	-	-	-	-	48.55
300	357	-	0.02	-	-	-	-	82.98
210	250	-	0.21	-	-	-	-	90.16
150	178	-	0.42	-	-	-	-	90.32
105	125	-	0.38	-	-	-	-	90.59
75	89	-	0.89	-	-	-	-	89.49
53	63	-	7.97	-	-	-	-	95.73
37	44	0.0133	77.88	1.000	1.000	0.000	-	95.73
25	30	-	9.94	0.200	0.200	0.000	0.800	96.58
-25	20	-	2.48	-	-	-	-	76.94
Total			12.42			2.83E-08		

Beta 4.59  
Gamma 4.99  
Phi 0.17

Snip jig's concentrate sample (3.8 kg/ 230 g/min/ 2 psi/ Chapter 8/

Size (um)	CONCENTRATE				TAILS				FEED			
	Weight (g)	% Weight	Grade g/t	Rec. (%)	Weight (g)	% Weight	Grade g/t	Rec. (%)	Weight (g)	% Weight	Grade g/t	Rec. (%)
1180	0.33	0.58	226.99	14.62	9.07	0.31	48.26	85.38	9.40	0.31	54.54	0.05
850	1.53	2.71	5859.97	85.36	49.69	1.69	30.96	14.64	51.22	1.71	205.10	0.98
600	5.55	9.81	2816.22	52.57	197.30	6.70	71.47	47.43	202.85	6.76	146.57	2.79
420	4.42	7.81	6617.65	44.32	316.39	10.75	116.15	55.68	320.81	10.69	205.73	6.18
300	7.60	13.44	6994.74	61.29	512.16	17.40	65.55	38.71	519.76	17.33	166.87	8.13
210	8.07	14.27	9516.73	62.21	525.64	17.86	88.75	37.79	533.71	17.79	231.31	11.57
150	11.05	19.54	9714.03	62.11	614.24	20.87	106.60	37.89	625.29	20.84	276.38	16.19
105	8.46	14.96	22390.07	80.55	364.28	12.38	129.55	19.95	372.74	12.42	634.79	22.17
75	7.02	12.41	29188.03	81.07	266.32	9.05	179.70	18.93	273.34	9.11	924.69	23.68
53	1.94	3.43	8195.88	45.80	61.99	2.11	303.57	54.20	63.93	2.13	543.07	3.25
37	0.36	0.64	77500.00	89.92	11.95	0.41	261.80	10.08	12.31	0.41	2520.53	2.91
25	0.15	0.27	57707.32	70.92	3.47	0.12	1022.12	29.08	3.62	0.12	3368.84	1.14
-25	0.08	0.14	95967.74	74.82	10.98	0.37	235.29	25.18	11.06	0.37	927.81	0.96
Total	56.56	100.00	13183.77	69.86	2943.44	100.00	109.28	30.14	3000.00	100.00	355.78	100.00

Snip sample/ 230 g/min/ 2 psi/ 100% 0.600-0.850 mm/ Chapter 8/

Size (um)	CONCENTRATE				TAILS				FEED			
	Weight (g)	% Weight	Grade g/t	Rec. (%)	Weight (g)	% Weight	Grade g/t	Rec. (%)	Weight (g)	% Weight	Grade g/t	Rec. (%)
1180	0.00	0.00	0.00	ERR	0.00	0.00	0.00	ERR	0.00	0.00	ERR	0.00
850	0.06	0.08	441.90	100.00	0.00	0.00	0.00	0.00	0.06	0.00	441.90	0.17
600	0.94	1.25	10671.70	98.77	29.83	1.02	419	1.23	30.77	1.03	330.04	64.95
420	10.30	13.71	315.20	98.33	366.48	12.53	0.15	1.67	376.78	12.56	8.76	21.11
300	26.64	35.45	3.40	30.72	1021.36	34.92	0.20	69.28	1048.00	34.93	0.28	1.89
210	21.17	28.17	3.20	34.91	842.07	28.79	0.15	65.09	863.24	28.77	0.22	1.24
150	11.25	14.97	20.00	91.21	433.76	14.83	0.05	8.79	445.01	14.83	0.55	1.58
105	2.98	3.97	45.80	46.88	132.20	4.52	1.17	53.12	135.18	4.51	2.15	1.86
75	1.04	1.38	117.90	83.56	43.87	1.50	0.55	16.44	44.91	1.50	3.27	0.94
53	0.30	0.40	217.20	51.57	19.30	0.66	3.17	48.43	19.60	0.65	6.45	0.81
37	0.31	0.41	129.50	26.61	16.67	0.57	9.72	73.39	16.98	0.57	13.00	1.41
25	0.10	0.13	812.50	30.47	4.97	0.17	37.29	69.53	5.07	0.17	52.57	1.71
-25	0.05	0.07	1777.80	24.37	14.33	0.49	19.25	7.03	14.38	0.48	25.36	2.33
Total	75.14	100.00	189.53	91.07	2924.86	100.00	0.48	8.93	3000.00	100.00	5.21	100.00

Snip sample/ 100% 0.800-0.850 mm/ chapter 8/  
Selection & breakage functions estimation:

Total of 10 times grinding time (min.) = 5.25

Size classes	Geo. size	Sel. Func.	Feed Rec.	Bij	BijCalc.	Res.	bij	Conc. Rec.
1180	1403	-	0.00	-	-	-	-	-
850	1011	-	0.17	-	-	-	-	100.00
600	714	0.0817	54.95	1.0000	1.0000	0.0000	-	98.77
420	499	-	21.11	0.395	0.457	0.004	0.605	98.33
300	357	-	1.89	0.341	0.324	0.000	0.054	30.72
210	250	-	1.24	0.305	0.288	0.001	0.038	34.91
150	178	-	1.58	0.280	0.231	0.001	0.045	91.21
105	125	-	1.88	0.208	0.200	0.000	0.053	46.88
75	89	-	0.94	0.179	0.173	0.000	0.027	83.56
53	83	-	0.81	0.158	0.151	0.000	0.023	51.57
37	44	-	1.41	0.118	0.131	0.000	0.040	26.61
25	30	-	1.71	0.087	0.114	0.002	0.049	30.47
-25	20	-	2.33	-	-	-	-	24.37
Total			34.88			0.00883		

Beta 0.41  
Gamma 5.00  
Phi 0.60

Snip sample/250 g/min/ 2 psi/ 100% 0.425-0.600 mm/ Chapter 8/

Size (um)	CONCENTRATE				TAILS				FEED			
	Weight (g)	% Weight	Grade g/t	Rec. (%)	Weight (g)	% Weight	Grade g/t	Rec. (%)	Weight (g)	% Weight	Grade g/t	Rec. (%)
1180	1.21	1.57	0.00	0.00	45.60	1.56	38.79	100.00	46.81	1.56	37.79	6.05
850	14.56	18.90	6.60	41.67	538.12	18.41	0.25	58.33	552.68	18.42	0.42	0.79
600	19.02	24.69	5.80	13.42	790.66	27.05	0.90	86.58	809.68	26.99	1.02	2.81
425	11.03	14.22	1148.00	97.48	487.27	16.53	0.70	2.60	494.20	16.47	26.31	44.44
300	14.18	18.41	610.80	97.40	446.63	15.28	0.50	2.51	460.81	15.36	19.28	30.37
210	6.99	9.07	36.20	60.42	236.76	8.10	0.70	39.58	243.75	8.13	1.72	1.43
150	4.97	6.45	34.30	13.73	151.99	5.20	7.05	86.27	156.96	5.23	7.91	4.25
105	2.53	3.28	66.00	53.38	86.81	2.97	1.68	46.62	89.34	2.98	3.50	1.07
75	1.58	2.05	158.40	87.23	52.32	1.79	0.70	12.77	53.90	1.80	5.32	0.98
53	0.43	0.56	270.60	10.13	30.40	1.04	33.95	89.87	30.83	1.03	37.25	3.93
37	0.45	0.58	181.50	23.13	32.74	1.12	8.29	76.87	33.19	1.11	10.64	1.21
25	0.00	0.00	0.00	0.00	10.52	0.36	36.99	100.00	10.52	0.35	36.99	1.33
-25	0.08	0.10	1400.00	28.40	17.25	0.59	16.37	71.60	17.33	0.58	22.76	1.35
Total	77.03	100.00	294.44	77.54	2922.97	100.00	2.25	22.46	3000.00	100.00	9.75	100.00

Snip sample/100% 0.425-0.600 mm/ chapter 8/  
Selection & breakage functions estimation:

Total of 7 times grinding time (min.) =

Size classes	Geo. size	Sel. Func.	Feed Rec.	Bij	BijCalc.	P <sub>ss</sub>	bij	Conc. Rec.
1180	1403	-	6.05	-	-	-	-	0.000
850	1011	-	0.79	-	-	-	-	41.87
600	714	-	2.81	-	-	-	-	13.42
425	489	0.0819	44.44	1.0000	1.000	0.000	-	97.40
300	357	-	30.37	0.3388	0.477	0.019	0.8814	97.49
210	250	-	1.43	0.307	0.314	0.000	0.0311	60.42
150	178	-	4.25	0.215	0.229	0.000	0.0928	13.73
105	125	-	1.07	0.192	0.172	0.000	0.0233	53.38
75	89	-	0.98	0.170	0.129	0.002	0.0213	87.23
53	63	-	3.93	0.085	0.098	0.000	0.0858	10.13
37	44	-	1.21	0.058	0.074	0.000	0.0284	23.13
25	30	-	1.33	0.029	0.058	0.001	0.0290	0.00
-25	20	-	1.35	-	-	-	-	28.40
Total			45.92			0.00341		

Beta 0.81  
Gamma 5.14  
Phi 0.47

Snip sample/250 g/min/ 2 psi/100% 0.425-0.600 mm/Chapter 8/ Repeated Test in the Bond ball mill/

Size (um)	CONCENTRATE				TAILS				FEED			
	Weight (g)	% Weight	Grade g/t	Rec. (%)	Weight (g)	% Weight	Grade g/t	Rec. (%)	Weight (g)	% Weight	Grade g/t	Rec. (%)
1180	1.89	2.54	0.05	0.38	52.37	1.79	0.47	99.62	54.26	1.81	0.46	0.13
850	16.74	22.50	0.05	1.06	518.71	17.73	0.15	98.94	535.45	17.85	0.15	0.42
600	20.88	28.06	0.05	0.41	839.65	28.70	0.30	99.59	860.53	28.68	0.29	1.34
425	12.50	16.89	812.00	99.75	504.06	17.23	6.65	0.25	516.58	17.22	19.70	53.94
300	11.12	14.95	494.20	99.61	433.28	14.81	0.05	0.39	444.40	14.81	12.41	29.25
210	4.95	6.65	159.10	95.64	224.39	7.67	0.16	4.36	229.34	7.64	3.59	4.37
150	2.99	4.02	216.20	98.11	138.67	4.74	0.09	1.89	141.66	4.72	4.65	3.49
105	1.55	2.08	423.60	90.07	81.33	2.78	0.89	9.93	82.88	2.76	8.80	3.86
75	1.03	1.38	194.70	77.10	51.78	1.77	1.15	22.90	52.81	1.76	4.92	1.38
53	0.37	0.50	198.80	66.89	27.79	0.95	1.31	33.11	28.16	0.94	3.90	0.58
37	0.38	0.51	184.20	58.98	31.01	1.06	1.57	41.02	31.39	1.05	3.78	0.63
25	0.00	0.00	0.00	0.00	10.53	0.36	6.14	100.00	10.53	0.35	6.14	0.34
-25	0.00	0.00	0.00	0.00	11.99	0.41	4.24	100.00	11.99	0.40	4.24	0.27
Total	74.40	100.00	243.04	95.85	2925.60	100.00	0.27	4.15	3000.00	100.00	6.29	100.00

Snip sample/100% 0.425-0.600 mm/ chapter 8/ Repeated Test in the Bond ball mill/  
Selection & breakage functions estimation:

Total of 10 times grinding time (min.) =

5

Size classes	Geo. size	Sel. Func.	Feed Rec.	Bij	BjCalc.	Res.	bij	Conc. Rec.
1180	1403	-	0.13	-	-	-	-	0.380
850	1011	-	0.42	-	-	-	-	1.0800
600	714	-	1.34	-	-	-	-	0.4100
425	499	0.1166	53.94	1.0000	1.000	0.000	-	99.75
300	357	-	29.25	0.3378	0.470	0.017	0.8622	99.61
210	250	-	4.37	0.239	0.248	0.000	0.9889	95.64
150	178	-	3.49	0.180	0.139	0.000	0.0790	98.11
105	125	-	3.86	0.072	0.080	0.000	0.0874	90.07
75	89	-	1.38	0.041	0.047	0.000	0.0312	77.10
53	63	-	0.58	0.028	0.028	0.000	0.0131	66.89
37	44	-	0.63	0.014	0.017	0.000	0.0143	58.98
25	30	-	0.34	0.008	0.010	0.000	0.0077	0.00
-25	20	-	0.27	-	-	-	-	0.00
Total			44.17			0.000832		

Beta 1.51  
Gamma 3.97  
Phi 0.38

Snip sample/230 g/min/ 2 psi/ 100% 0.300-0.425 mm/Chapter 8/

Size (um)	CONCENTRATE				TAILS				FEED			
	Weight (g)	% Weight	Grade g/t	Rec. (%)	Weight (g)	% Weight	Grade g/t	Rec. (%)	Weight (g)	% Weight	Grade g/t	Rec. (%)
1180	0.00	0.00	0.00	ERR	0.00	0.00	0.00	ERR	0.00	0.00	ERR	0.00
850	0.10	0.13	2695.65	100.00	0.00	0.00	0.00	0.00	0.10	0.00	2695.65	0.51
600	1.34	1.80	0.05	0.07	50.61	1.73	1.94	99.93	51.95	1.73	1.89	0.18
420	11.16	14.97	787.80	99.29	416.29	14.23	0.15	0.71	427.45	14.25	20.71	16.65
300	20.60	27.64	1838.60	99.64	901.63	30.82	0.15	0.36	922.23	30.74	41.22	71.49
210	22.42	30.08	127.20	90.08	897.53	30.68	0.35	9.92	919.95	30.67	3.44	5.95
150	12.39	16.62	51.40	83.57	417.46	14.27	0.30	16.43	429.85	14.33	1.77	1.43
105	3.73	5.00	80.13	56.97	135.16	4.62	1.67	43.03	138.89	4.63	3.78	0.99
75	1.55	2.08	107.07	49.69	50.61	1.73	3.32	50.31	52.16	1.74	6.40	0.63
53	0.48	0.64	144.61	21.54	20.48	0.70	12.35	78.46	20.96	0.70	15.38	0.61
37	0.54	0.72	149.47	30.75	20.77	0.71	8.75	69.25	21.31	0.71	12.32	0.49
25	0.13	0.17	304.35	16.10	5.27	0.18	39.16	83.90	5.40	0.18	45.55	0.46
-25	0.10	0.13	1200.00	37.43	9.65	0.33	20.78	62.57	9.75	0.33	32.87	0.60
Total	74.54	100.00	686.88	96.29	2925.46	100.00	0.67	3.71	3000.00	100.00	17.72	100.00

Snip sample/100% 0.300-0.425 mm/ chapter 8/  
Selection & breakage functions estimation:

Total of 10 times grinding time (min.) =

7.5

Size classes	Geo. size	Sel. Func.	Feed Rec.	Bij	BijCalc.	Res.	bij	Conc. Rec.
1180	1403	-	0.00	-	-	-	-	-
850	1011	-	0.51	-	-	-	-	100.00
600	714	-	0.18	-	-	-	-	0.0700
420	489	-	18.85	-	-	-	-	99.29
300	367	0.054	21.49	1.000	1.000	0.000	-	99.64
210	250	-	5.95	0.487	0.478	0.000	0.533	90.08
150	178	-	1.43	0.339	0.332	0.000	0.128	83.57
105	125	-	0.99	0.250	0.243	0.000	0.089	56.97
75	89	-	0.83	0.194	0.183	0.000	0.058	49.69
53	83	-	0.81	0.139	0.137	0.000	0.055	21.54
37	44	-	0.49	0.095	0.101	0.000	0.044	30.75
25	30	-	0.48	0.054	0.073	0.000	0.041	16.10
-25	20	-	0.80	-	-	-	-	37.43
Total			11.18			0.00077		

Beta 0.83  
Gamma 6.12  
Phi 0.42

Snip sample/ 220 g/min/ 2 psi/ 100% 0.212-0.300 mm/ Chapter 8/

Size (um)	CONCENTRATE				TAILS				FEED			
	Weight (g)	% Weight	Grade g/t	Rec. (%)	Weight (g)	% Weight	Grade g/t	Rec. (%)	Weight (g)	% Weight	Grade g/t	Rec. (%)
1180	0.00	0.00	0.00	ERR	0.00	0.00	0.00	ERR	0.00	0.00	ERR	0.00
850	0.00	0.00	0.00	ERR	0.00	0.00	0.00	ERR	0.00	0.00	ERR	0.00
600	0.16	0.22	6319.77	100.00	0.00	0.00	0.00	0.00	0.16	0.01	6319.77	1.32
420	0.96	1.32	0.05	0.19	28.39	0.97	0.91	99.81	29.35	0.98	0.88	0.03
300	5.98	8.20	5343.56	99.82	173.87	5.94	0.34	0.18	179.85	6.00	178.00	41.68
210	14.06	19.32	1904.50	99.61	691.09	25.61	0.15	0.39	705.17	23.51	38.17	35.05
150	27.95	38.35	483.50	94.14	990.53	33.84	0.85	5.86	1018.48	33.95	14.10	18.69
105	11.71	16.07	50.70	92.08	510.78	17.45	0.10	7.92	522.49	17.42	1.23	0.84
75	7.71	10.58	54.04	80.23	256.71	8.77	0.40	19.77	264.42	8.81	1.96	0.68
53	2.98	4.09	75.13	55.32	115.91	3.96	1.56	44.68	118.89	3.96	3.40	0.53
37	1.03	1.41	98.91	41.50	85.47	2.92	1.68	58.50	86.50	2.88	2.84	0.32
25	0.26	0.36	317.07	29.93	21.66	0.74	8.91	70.07	21.92	0.73	12.57	0.36
-25	0.07	0.10	968.75	17.28	52.69	1.80	6.16	82.72	52.76	1.76	7.44	0.51
Total	72.89	100.00	1025.95	97.36	2927.11	100.00	0.69	2.64	3000.00	100.00	25.60	100.00

Snip sample/100% 0.212-0.300 mm/ chapter 8/  
 Selection & breakage functions estimation:

Size classes	Geo. size	Sel. Func.	Feed Rec.	Bij	BijCalc.	Res.	bij	Conc. Rec.
1180	1403	-	0.00	-	-	-	-	-
850	1011	-	0.00	-	-	-	-	-
600	714	-	1.32	-	-	-	-	100.00
420	499	-	0.03	-	-	-	-	0.1900
300	357	-	41.88	-	-	-	-	99.82
210	250	0.0217	95.85	1.000	1.000	0.000	-	99.61
150	178	-	18.69	0.148	0.188	0.000	0.852	94.14
105	125	-	0.84	0.109	0.087	0.000	0.038	92.08
75	89	-	0.88	0.078	0.087	0.000	0.031	80.23
53	83	-	0.53	0.054	0.054	0.000	0.024	55.32
37	44	-	0.32	0.040	0.044	0.000	0.015	41.50
25	30	-	0.38	0.023	0.038	0.000	0.016	29.93
-25	20	-	0.51	-	-	-	-	17.28
Total			21.93			0.0012		

Beta 0.60  
 Gamma 7.43  
 Phi 0.88

Snip sample/220 g/min/ 2 psi/ 100% 0.212-0.300 mm/ Chapter 8/ Repeated Test in the Bond ball mill/

Size (um)	CONCENTRATE				TAILS				FEED			
	Weight (g)	% Weight	Grade g/t	Rec. (%)	Weight (g)	% Weight	Grade g/t	Rec. (%)	Weight (g)	% Weight	Grade g/t	Rec. (%)
1180	0.00	0.00	0.00	ERR	0.00	0.00	0.00	ERR	0.00	0.00	ERR	0.00
850	0.00	0.00	0.00	ERR	0.00	0.00	0.00	ERR	0.00	0.00	ERR	0.00
600	0.13	0.18	0.05	100.00	0.00	0.00	0.00	0.00	0.13	0.00	0.05	0.00
420	0.97	1.32	0.05	0.13	19.31	0.66	1.97	99.87	20.28	0.68	1.88	0.06
300	7.22	9.79	1247.75	99.87	148.07	5.06	0.08	0.13	155.29	5.18	58.09	14.33
210	16.21	21.98	1779.00	99.45	639.68	21.86	0.25	0.55	655.89	21.86	44.21	46.08
150	27.87	37.79	566.20	98.95	1050.23	35.89	0.16	1.05	1078.10	35.94	14.79	25.34
105	10.63	14.41	89.40	78.07	533.75	18.24	0.50	21.93	544.38	18.15	2.24	1.93
75	7.02	9.52	86.42	85.70	253.12	8.65	0.40	14.30	260.14	8.67	2.72	1.12
53	2.63	3.57	133.44	76.49	113.54	3.88	0.95	23.51	116.17	3.87	3.95	0.73
37	0.88	1.19	328.47	43.87	89.54	3.06	4.13	56.13	90.42	3.01	7.29	1.05
25	0.15	0.20	803.15	11.01	23.12	0.79	42.12	88.99	23.27	0.78	47.03	1.74
-25	0.04	0.05	6000.00	5.01	55.31	1.89	82.21	94.99	55.35	1.84	86.49	7.61
Total	73.75	100.00	761.82	89.28	2926.25	99.98	2.30	10.72	3000.00	99.98	20.98	100.00

Snip sample/100% 0.212-0.300 mm/ chapter 8/ Repeated Test in the Bond ball mill/  
Selection & breakage functions estimation:

Total of 10 times grinding time (min.) =

Size classes	Geo. size	Sel. Func.	Feed Rec	Bij	BijCalc	Res	bij	Conc. Rec
1180	1403	-	0.00	-	-	-	-	-
850	1011	-	0.00	-	-	-	-	-
600	714	-	0.00	-	-	-	-	100.00
420	499	-	0.08	-	-	-	-	0.13
300	357	-	14.33	-	-	-	-	99.87
210	250	0.0503	49.08	1.000	1.000	0.000	-	99.45
150	178	-	25.34	0.359	0.380	0.000	0.841	98.95
105	125	-	1.93	0.310	0.299	0.000	0.049	78.07
75	89	-	1.12	0.282	0.271	0.000	0.028	85.70
53	63	-	0.73	0.283	0.250	0.000	0.018	78.40
37	44	-	1.05	0.237	0.231	0.000	0.027	43.87
25	30	-	1.74	0.193	0.214	0.000	0.044	11.01
-25	20	-	7.81	-	-	-	-	5.01
Total			39.52			0.00133		

Beta 0.23  
Gamma 8.75  
Phi 0.68

Snip sample/ 250 g/min/ 2 psi/ 100% 0.150-0.212 mm/ Chapter 8/

Size (um)	CONCENTRATE				TAILS				FEED			
	Weight (g)	% Weight	Grade g/t	Rec. (%)	Weight (g)	% Weight	Grade g/t	Rec. (%)	Weight (g)	% Weight	Grade g/t	Rec. (%)
1180	0.00	0.00	0.00	ERR	0.00	0.00	0.00	ERR	0.00	0.00	ERR	0.00
850	0.00	0.00	0.00	ERR	0.00	0.00	0.00	ERR	0.00	0.00	ERR	0.00
600	2.16	2.84	0.05	0.43	47.07	1.61	0.53	99.57	49.23	1.64	0.51	0.02
420	17.49	22.97	0.05	0.56	519.57	17.77	0.30	99.44	537.06	17.90	0.29	0.15
300	24.34	31.96	0.65	0.69	870.43	29.77	0.20	99.31	894.77	29.83	0.20	0.16
210	13.99	18.37	609.20	98.21	621.03	21.24	0.25	1.79	635.02	21.17	13.67	8.08
150	10.31	13.54	8176.00	99.79	441.79	15.11	0.48	0.21	452.10	15.87	186.84	78.69
105	4.98	6.54	2165.79	99.00	241.80	8.27	0.45	1.00	246.78	8.23	44.15	10.15
75	2.12	2.78	557.54	89.97	83.91	2.87	1.57	10.03	86.03	2.87	15.27	1.22
53	0.47	0.62	671.30	89.71	36.55	1.25	0.99	10.29	37.02	1.23	9.50	0.33
37	0.29	0.38	886.08	67.74	32.45	1.11	3.77	32.26	32.74	1.0	11.58	0.35
25	0.00	0.00	0.00	0.00	9.36	0.32	24.10	100.00	9.36	0.31	24.10	0.21
-25	0.00	0.00	0.00	0.00	19.88	0.68	33.83	100.00	19.88	0.66	33.83	0.63
Total	76.15	100.00	1383.58	98.15	2923.85	100.00	0.63	1.85	3000.00	100.00	35.78	100.00

Snip sample/100% 0.150-0.212 mm/ chapter 8/  
Selection & breakage functions estimation:

Total of 10 times grinding time (min.) = 7.5

Size classes	Geo. size	Sel Func	Feed Rec.	Bij	BijCalc	Res	bij	Conc Rec
1180	1403	-	0.00	-	-	-	-	-
850	1011	-	0.00	-	-	-	-	-
600	714	-	0.02	-	-	-	-	0.4300
420	499	-	0.15	-	-	-	-	0.5800
300	357	-	0.18	-	-	-	-	0.8900
210	250	-	8.09	-	-	-	-	98.2100
150	176	0.0134	78.89	1.000	1.000	0.000	-	99.7900
105	125	-	10.15	0.213	0.212	0.000	0.787	99.0000
75	89	-	1.22	0.118	0.120	0.000	0.095	89.9700
53	63	-	0.33	0.092	0.088	0.000	0.028	89.7100
37	44	-	0.35	0.085	0.088	0.000	0.027	87.7400
25	30	-	0.21	0.049	0.050	0.000	0.018	0.0000
-25	20	-	0.83	-	-	-	-	0.0000
Total			12.89			2.7E-05		

Beta 0.81  
Gamma 7.52  
Phi 0.80

Snip sample/ 250 g/min/ 2 psi/ 100% 0.105-0.150 mm/ Chapter 8/

Size (um)	CONCENTRATE				TAILS				FEED			
	Weight (g)	% Weight	Grade g/t	Rec. (%)	Weight (g)	% Weight	Grade g/t	Rec. (%)	Weight (g)	% Weight	Grade g/t	Rec. (%)
1180	2.21	2.63	9.13	34.86	30.91	1.06	1.22	65.14	33.12	1.10	1.75	0.03
850	19.79	23.51	0.05	0.49	367.10	12.59	0.55	99.51	386.89	12.90	0.52	0.11
600	23.95	28.45	0.05	0.35	689.30	23.64	0.50	99.65	713.25	23.77	0.48	0.18
420	16.06	19.08	0.05	0.59	671.51	23.03	0.20	99.41	687.57	22.92	0.20	0.07
300	9.54	11.33	399.20	97.20	438.83	15.05	0.25	2.80	448.37	14.95	8.74	2.07
210	3.50	4.16	198.90	86.18	248.14	8.51	0.45	13.82	251.64	8.39	3.21	0.43
150	2.86	3.40	9092.13	98.78	171.16	5.87	1.88	1.22	174.02	5.80	151.28	13.90
105	3.26	3.97	2293.02	99.99	82.52	2.83	2.60	0.10	85.78	2.86	1608.90	72.86
75	1.75	2.08	8912.35	99.25	75.52	2.59	1.56	0.75	77.27	2.58	203.37	8.30
53	0.54	0.64	2504.97	90.45	45.20	1.55	3.16	9.55	45.74	1.52	32.70	0.79
37	0.60	0.71	1512.06	89.39	49.86	1.71	2.16	10.61	50.46	1.68	20.11	0.54
25	0.13	0.15	4436.36	72.17	17.49	0.60	12.71	27.83	17.62	0.59	45.34	0.42
-25	0.00	0.00	0.00	0.00	28.28	0.97	21.22	100.00	28.28	0.94	21.22	0.32
Total	84.19	100.00	2219.26	98.64	2915.81	100.00	0.89	1.36	3000.00	100.00	63.14	100.00

Snip sample/ 100% 0.105-0.150 mm/ chapter 8/  
Selection & breakage functions estimations

Size classes	Geo. size	Sel. Func.	Feed Rec.	Bij	BijCalc.	Res.	bij	Conc. Rec.
1180	1403	-	0.03	-	-	-	-	34.88
850	1011	-	0.11	-	-	-	-	0.4000
600	714	-	0.18	-	-	-	-	0.3500
420	499	-	0.07	-	-	-	-	0.5000
300	357	-	2.07	-	-	-	-	97.20
210	250	-	0.43	-	-	-	-	86.18
150	178	-	13.90	-	-	-	-	98.78
105	126	0.0148	72.86	1.000	1.000	0.000	-	99.90
75	88	-	8.30	0.200	0.207	0.000	0.800	99.25
53	63	-	0.79	0.123	0.109	0.000	0.078	90.45
37	44	-	0.54	0.071	0.089	0.000	0.052	89.39
25	30	-	0.42	0.031	0.045	0.000	0.041	72.17
-25	20	-	0.32	-	-	-	-	0.00
Total			10.37			0.00047		

Beta 1.25  
Gamma 8.21  
Phi 0.75

Snip sample/ 250 g/min/ 2 psi/ 100% 0.075-0.105 mm/ Chapter 8/

Size (um)	CONCENTRATE				TAILS				FEED			
	Weight (g)	% Weight	Grade g/t	Rec. (%)	Weight (g)	% Weight	Grade g/t	Rec. (%)	Weight (g)	% Weight	Grade g/t	Rec. (%)
1180	0.00	0.00	0.00	ERR	0.00	0.00	0.00	ERR	0.00	0.00	ERR	0.00
850	0.00	0.00	0.00	ERR	0.00	0.00	0.00	ERR	0.00	0.00	ERR	0.00
600	2.15	2.82	0.05	0.42	38.01	1.30	0.67	99.58	40.16	1.34	0.64	0.01
420	17.72	23.21	3.40	48.22	431.24	14.75	0.15	51.78	448.96	14.97	0.28	0.06
300	26.19	34.31	0.05	1.01	858.09	29.35	0.15	98.99	884.28	29.48	0.15	0.06
210	14.61	19.14	9.60	51.39	663.38	22.69	0.20	48.61	677.99	22.60	0.40	0.13
150	8.66	11.34	188.00	92.13	556.37	19.03	0.25	7.87	565.03	18.83	3.13	0.86
105	2.50	3.27	13701.20	99.11	203.19	6.95	1.51	0.89	205.69	6.86	168.02	16.87
75	3.32	4.35	47352.40	99.11	62.85	2.15	22.47	0.89	66.18	2.21	2395.88	77.41
53	0.72	0.94	8626.80	92.39	38.30	1.31	13.35	7.61	39.02	1.30	172.29	3.28
37	0.47	0.62	3545.50	84.59	37.42	1.28	8.11	15.41	37.89	1.26	51.99	0.96
25	0.00	0.00	0.00	0.00	11.69	0.40	18.74	100.00	11.69	0.39	18.74	0.11
-25	0.00	0.00	0.00	0.00	23.39	0.80	20.89	100.00	23.39	0.78	20.89	0.24
Total	76.34	100.00	2635.19	98.18	2923.66	100.01	1.28	1.82	3000.00	100.01	68.30	100.00

Snip sample/100% 0.075-0.105 mm/ chapter 8/  
Selection & breakage functions estimation:

Total of 10 times grinding time (min.) =		7.5							
Size classes	Geo. size	Sel. Func.	Feed Rec.	Bij	BijCalc.	Res.	bij	Conc.	Rec.
1180	1403	-	0.00	-	-	-	-	-	-
850	1011	-	0.00	-	-	-	-	-	-
800	714	-	0.01	-	-	-	-	0.4200	-
420	499	-	0.08	-	-	-	-	48.22	-
300	357	-	0.08	-	-	-	-	1.01	-
210	250	-	0.13	-	-	-	-	51.39	-
150	178	-	0.88	-	-	-	-	92.13	-
105	125	-	16.87	-	-	-	-	99.11	-
75	89	0.0043	77.41	1.000	1.000	0.000	-	99.11	-
53	83	-	3.28	0.285	0.272	0.000	0.715	92.39	-
37	44	-	0.98	0.076	0.101	0.001	0.209	84.59	-
25	30	-	0.11	0.052	0.061	0.000	0.024	0.0000	-
-25	20	-	0.24	-	-	-	-	0.00	-
Total			4.59			0.00089			

Beta 0.02  
Gamma 4.19  
Phi 0.95

Snip sample/ 250 g/min/ 100% 0.053-0.075 mm/ Chapter 8/

Size (um)	CONCENTRATE				TAILS				FEED			
	Weight (g)	% Weight	Grade g/t	Rec. (%)	Weight (g)	% Weight	Grade g/t	Rec. (%)	Weight (g)	% Weight	Grade g/t	Rec. (%)
1180	0.00	0.00	0.00	ERR	0.00	0.00	0.00	ERR	0.00	0.00	ERR	0.00
850	0.00	0.00	0.00	ERR	0.00	0.00	0.00	ERR	0.00	0.00	ERR	0.00
600	0.00	0.00	0.00	ERR	0.00	0.00	0.00	ERR	0.00	0.00	ERR	0.00
420	6.67	8.39	0.30	2.17	180.78	6.19	0.50	97.83	187.45	6.25	0.49	0.58
300	16.69	21.00	0.05	2.97	545.26	18.67	0.05	97.03	561.95	18.73	0.05	0.18
210	27.27	34.32	0.05	2.81	942.46	32.27	0.05	97.19	969.73	32.32	0.05	0.30
150	11.75	14.79	1.60	38.51	600.46	20.56	0.05	61.49	612.21	20.41	0.08	0.31
105	6.79	8.55	16.94	87.89	316.88	10.85	0.05	12.11	323.67	10.79	0.40	0.82
75	3.35	4.22	296.10	90.82	139.31	4.77	0.72	9.18	142.66	4.76	7.60	0.87
53	6.94	8.73	2010.47	98.66	61.67	2.11	3.21	1.40	60.56	2.29	206.39	88.98
37	0.00	0.00	0.00	0.00	61.92	2.12	2.00	100.00	61.92	2.06	2.00	0.78
25	0.00	0.00	0.00	0.00	16.06	0.55	3.60	100.00	16.06	0.54	3.60	0.36
-25	0.00	0.00	0.00	0.00	55.78	1.91	2.33	100.00	55.78	1.86	2.33	0.82
Total	79.46	100.00	189.81	94.84	2920.54	100.00	0.28	5.16	3000.00	100.00	5.30	100.00

Snip sample/ 100% 0.053-0.075 mm/ chapter 8/  
Selection & breakage functions estimation:

Total of 10 times grinding time (min.) = 7.5

Size classes	Geo. size	Sel. Func.	Feed Rec.	Bij	BijCalc	Res	bij	Conc. Rec.
1180	1403	-	0.00	-	-	-	-	-
850	1011	-	0.00	-	-	-	-	-
600	714	-	0.00	-	-	-	-	-
420	499	-	0.58	-	-	-	-	2.17
300	357	-	0.18	-	-	-	-	2.07
210	250	-	0.30	-	-	-	-	2.0100
150	178	-	0.31	-	-	-	-	38.51
105	125	-	0.82	-	-	-	-	87.89
75	89	-	8.87	-	-	-	-	90.82
53	69	0.0026	88.88	1.000	1.000	-	-	98.80
37	44	-	0.78	0.802	0.802	0.000	0.398	0.00
25	30	-	0.38	0.418	0.418	0.000	0.184	0.00
-25	20	-	0.82	-	-	-	-	0.00
Total			1.98			8.2E-15		

Beta 0.11  
Gamma 2.33  
Phi 0.70

Snip sample/ 250g/min/ 2 psi/ 100% 0.037-0.053 mm/ Chapter 8/

Size (um)	CONCENTRATE				TAILS				FEED			
	Weight (g)	% Weight	Grade g/t	Rec. (%)	Weight (g)	% Weight	Grade g/t	Rec. (%)	Weight (g)	% Weight	Grade g/t	Rec. (%)
1180	0.00	0.00	0.00	ERR	0.00	0.00	0.00	ERR	0.00	0.00	ERR	0.00
850	0.00	0.00	0.00	ERR	0.00	0.00	0.00	ERR	0.00	0.00	ERR	0.00
600	1.62	2.15	1.30	2.05	31.59	1.08	3.19	97.95	33.21	1.11	3.10	0.37
420	11.77	15.61	0.60	6.78	323.46	11.06	0.30	93.22	335.23	11.17	0.31	0.37
300	27.39	36.32	0.40	2.24	956.05	32.69	0.50	97.76	983.44	32.78	0.50	1.75
210	19.43	25.77	24.00	65.58	815.67	27.89	0.30	34.42	835.10	27.84	0.85	2.55
150	10.41	13.84	10.00	42.21	476.42	16.29	0.30	57.79	486.86	16.23	0.51	0.89
105	2.92	3.87	42.70	51.20	172.26	5.89	0.69	48.80	175.18	5.84	1.39	0.87
75	1.17	1.55	644.00	88.67	65.51	2.24	1.47	11.33	66.68	2.22	12.74	3.05
53	0.30	0.40	5469.00	91.62	30.12	1.03	4.98	8.38	30.42	1.01	58.86	6.42
37	0.37	0.49	61767.40	98.58	72.23	0.76	14.81	1.42	22.60	0.75	1025.94	83.12
25	0.00	0.00	0.00	0.00	10.82	0.37	8.91	100.00	10.82	0.36	8.91	0.35
-25	0.00	0.00	0.00	0.00	20.76	0.71	3.57	100.00	20.76	0.69	3.57	0.27
Total	75.41	100.00	344.30	93.09	2924.59	100.01	0.66	6.91	3000.00	100.01	9.30	100.00

Snip sample/100% 0.037-0.053 mm/ chapter 8/  
Selection & breakage functions estimation:

Total of 10 times grinding time (min.) = 7.5

Size classes	Geo. size	Sel. Func.	Feed Rec.	Bij	BijCalc.	Res.	bij	Conc. Rec.
1180	1403	-	0.00	-	-	-	-	-
850	1011	-	0.00	-	-	-	-	-
600	714	-	0.37	-	-	-	-	2.05
420	499	-	0.37	-	-	-	-	6.78
300	357	-	1.75	-	-	-	-	2.24
210	250	-	2.55	-	-	-	-	65.58
150	178	-	0.89	-	-	-	-	42.21
105	125	-	0.87	-	-	-	-	51.20
75	89	-	3.05	-	-	-	-	88.87
53	83	-	6.42	-	-	-	-	91.82
37	44	0.0000	03.12	1.000	1.000	0.000	-	98.58
25	30	-	0.35	0.435	0.435	0.000	0.585	0.00
-25	20	-	0.27	-	-	-	-	0.00
Total			0.82			2.4E-15		

Beta 1.31  
Gamma 3.02  
Phi 0.70

Hemlo sample/ 240 g/min/ 2 psi/ 100% 1.18-1.70 mm/ Chapter 8/

Size (um)	CONCENTRATE				TAILS				FEED			
	Weight (g)	% Weight	Grade g/t	Rec. (%)	Weight (g)	% Weight	Grade g/t	Rec. (%)	Weight (g)	% Weight	Grade g/t	Rec. (%)
1700	3.23	4.07	12.80	1.37	85.15	2.92	35.10	98.63	88.38	2.95	34.28	0.48
<b>1180</b>	<b>38.59</b>	<b>48.64</b>	<b>6211.10</b>	<b>99.85</b>	<b>952.34</b>	<b>32.61</b>	<b>0.38</b>	<b>0.15</b>	<b>996.93</b>	<b>33.03</b>	<b>242.28</b>	<b>37.70</b>
850	1.95	2.46	126063.30	100.00	48.96	1.68	0.21	0.00	50.92	1.70	4832.63	38.64
600	2.69	3.39	26658.60	99.98	69.55	2.38	0.20	0.02	72.24	2.41	991.53	11.25
420	4.08	5.14	7347.90	99.44	112.55	3.85	1.50	0.56	116.63	3.89	258.56	4.74
300	6.18	7.78	4015.30	99.85	172.22	5.90	0.22	0.15	178.40	5.95	139.21	3.90
210	6.60	8.31	823.10	99.59	225.39	7.72	0.10	0.41	231.99	7.73	23.50	0.86
150	7.00	8.82	370.80	85.87	266.93	9.14	1.60	14.13	273.93	9.13	11.04	0.47
105	4.57	5.76	220.30	93.60	229.52	7.86	0.30	6.40	234.09	7.80	4.60	0.17
75	2.70	3.40	587.20	93.38	175.45	6.01	0.64	6.62	178.15	5.94	9.52	0.27
53	1.12	1.41	413.20	74.28	123.22	4.22	1.30	25.72	124.34	4.14	5.01	0.10
37	0.58	0.73	1630.40	72.14	152.63	5.23	2.40	27.86	153.21	5.11	8.58	0.21
25	0.07	0.08	34461.40	63.41	73.43	2.51	17.60	36.59	73.50	2.45	48.06	0.55
-25	0.00	0.00	0.00	0.00	233.30	7.99	18.50	100.00	233.30	7.78	18.50	0.68
Total	79.35	100.00	7894.81	98.38	2920.65	100.00	3.54	1.62	3000.00	100.00	212.27	100.00

Hemlo sample/ 100% 1.18-1.70 mm/ chapter 8/  
Selection & breakage functions estimation:

Total of 10 times grinding time (min.) = 50

Size classes	Geo. size	Sel. Func.	Feed Rec.	Bij	BijCalc.	Res.	bij	Conc. Rec.
1700	2022	-	0.48	-	-	-	-	1.37
<b>1180</b>	<b>1403</b>	<b>0.0000</b>	<b>37.70</b>	<b>1.0000</b>	<b>1.0000</b>	<b>0.0000</b>	<b>-</b>	<b>99.850</b>
850	1011	-	38.64	0.375	0.383	0.000	0.8248	100.00
800	714	-	11.25	0.193	0.182	0.000	0.1819	99.99
420	499	-	4.74	0.117	0.108	0.000	0.0768	99.44
300	357	-	3.90	0.054	0.070	0.000	0.0831	99.85
210	250	-	0.88	0.040	0.050	0.000	0.0139	99.59
150	178	-	0.47	0.032	0.037	0.000	0.0076	85.87
105	125	-	0.17	0.029	0.027	0.000	0.0027	93.80
75	89	-	0.27	0.025	0.020	0.000	0.0044	93.38
53	83	-	0.10	0.023	0.015	0.000	0.0016	74.28
37	44	-	0.21	0.020	0.011	0.000	0.0034	72.14
25	30	-	0.55	0.011	0.008	0.000	0.0059	63.41
-25	20	-	0.68	-	-	-	-	0.00
Total			81.84			0.0009		

Beta 0.85  
Gamma 3.82  
Phi 0.21

Hemlo sample/ 240 g/min/ 2 psi/ 100% 0.600-0.850 mm/ Chapter 8/

Size (um)	CONCENTRATE				TAILS				FEED			
	Weight (g)	% Weight	Grade g/t	Rec. (%)	Weight (g)	% Weight	Grade g/t	Rec. (%)	Weight (g)	% Weight	Grade g/t	Rec. (%)
850	1.17	1.56	16207.70	45.66	40.52	1.39	555.20	54.34	41.68	1.39	993.19	3.79
600	27.27	36.47	9767.00	97.39	925.17	31.63	7.70	2.61	952.44	31.75	287.09	25.06
420	5.00	6.69	119602.00	99.87	147.20	5.03	5.30	0.13	152.20	5.07	3934.81	54.88
300	5.12	6.84	19158.20	99.62	164.59	5.63	2.30	0.38	169.71	5.66	579.73	9.02
210	7.52	10.06	3130.30	93.60	268.18	9.17	6.00	6.40	275.69	9.19	91.19	2.30
150	9.41	12.58	1306.50	80.60	347.94	11.89	8.50	19.40	357.35	11.91	42.67	1.40
105	6.98	9.34	817.00	78.35	302.58	10.34	5.21	21.65	309.56	10.32	23.53	0.67
75	5.05	6.76	630.30	75.61	213.98	7.31	4.80	24.39	219.03	7.30	19.22	0.39
53	2.75	3.63	573.00	61.94	156.05	5.33	6.20	38.06	158.80	5.29	16.01	0.23
37	3.04	4.06	987.00	56.51	180.17	6.16	12.80	43.49	183.21	6.11	28.94	0.49
25	0.96	1.28	4433.70	57.82	88.15	3.01	35.10	42.18	89.10	2.97	82.32	0.67
-25	0.51	0.68	14941.80	62.73	90.72	3.10	49.90	37.27	91.23	3.04	133.15	1.11
Total	74.76	100.00	13944.24	95.52	2925.24	100.00	16.70	4.48	3000.00	100.00	363.76	100.00

Hemlo sample/ 100% 0.800-0.850 mm/ chapter 8/  
 Selection & breakage functions estimation:

Total of 10 times grinding time (min.) = 50

Size classes	Geo. size	Sel. Func.	Feed Rec.	Bij	BijCalc.	Res.	bij	Conc. Rec.
1180	1403	-	0.00	-	-	-	-	-
850	1011	-	3.79	-	-	-	-	45.66
600	716	0.0240	25.06	1.0000	1.000	0.000	-	97.39
420	499	-	54.88	0.229	0.229	0.000	0.771	99.87
300	357	-	9.02	0.102	0.100	0.000	0.127	99.62
210	250	-	2.30	0.070	0.088	0.000	0.032	93.60
150	178	-	1.40	0.050	0.054	0.000	0.020	80.60
105	125	-	0.67	0.041	0.043	0.000	0.009	78.35
75	89	-	0.39	0.035	0.035	0.000	0.005	75.61
53	83	-	0.23	0.032	0.028	0.000	0.003	61.94
37	44	-	0.49	0.025	0.023	0.000	0.007	56.51
25	30	-	0.67	0.018	0.018	0.000	0.009	57.82
-25	20	-	1.11	-	-	-	-	62.73
Total			71.16			5.1E-05		

Beta            0.82  
 Gamma        5.54  
 Phi            0.88

Hemlo sample/ 240 g/min/ 2 psi/ 100% 0.300-0.425 mm/ Chapter 8/

Size (um)	CONCENTRATE				TAILS				FEED			
	Weight (g)	% Weight	Grade g/t	Rec. (%)	Weight (g)	% Weight	Grade g/t	Rec. (%)	Weight (g)	% Weight	Grade g/t	Rec. (%)
850	0.00	0.00	0.00	ERR	0.00	0.00	0.00	ERR	0.00	0.00	ERR	0.00
600	0.00	0.00	0.00	ERR	0.00	0.00	0.00	ERR	0.00	0.00	ERR	0.00
420	1.03	1.38	365744.00	99.92	17.38	0.59	16.90	0.08	18.41	0.61	20426.78	17.46
300	22.71	29.41	36166.66	98.95	720.66	24.62	19.10	1.05	742.79	24.76	930.20	32.09
210	16.72	22.39	48413.00	99.65	536.06	18.32	5.30	0.35	552.78	18.43	1469.41	37.73
150	12.16	16.28	12120.00	99.74	423.34	14.47	0.90	0.26	435.50	14.52	339.33	6.86
105	8.13	10.89	5414.00	99.37	308.76	10.55	0.90	0.63	316.89	10.56	139.80	2.06
75	5.19	6.95	4335.00	99.34	213.60	7.30	0.70	0.66	218.78	7.29	103.47	1.05
53	3.27	4.38	3631.00	96.08	142.65	4.88	3.40	3.92	145.92	4.86	84.76	0.57
37	3.36	4.49	3083.00	97.97	178.50	6.10	1.20	2.03	181.86	6.06	58.08	0.49
25	1.22	1.64	3057.00	94.18	76.98	2.63	3.00	5.82	78.20	2.61	50.74	0.18
-25	0.89	1.20	15121.00	42.14	307.97	10.53	60.30	57.86	308.86	10.30	103.92	1.49
Total	74.68	100.00	28416.54	98.57	2925.32	100.00	10.50	1.43	3000.00	100.00	717.63	100.00

Hemlo Sample/100% 0.300-0.425 mm/ chapter 8/  
Selection & breakage functions estimation:

Total of 10 times grinding time (min.) =

50

Size classes	Gen. size	Sel. Func.	Feed Rec.	Bij	BijCalc.	Res.	bij	Conc. Rec.
1180	1403	-	0.00	-	-	-	-	-
850	1011	-	0.00	-	-	-	-	-
600	714	-	0.00	-	-	-	-	-
420	499	-	17.46	-	-	-	-	99.92
300	357	0.0140	32.00	1.0000	1.000	0.000	-	98.95
210	250	-	37.73	0.252	0.252	0.000	0.748	99.85
150	178	-	8.88	0.118	0.114	0.000	0.136	99.74
105	125	-	2.08	0.075	0.075	0.000	0.041	99.37
75	89	-	1.05	0.054	0.057	0.000	0.021	99.34
53	83	-	0.57	0.043	0.044	0.000	0.011	98.08
37	44	-	0.49	0.033	0.034	0.000	0.010	97.97
25	30	-	0.18	0.030	0.028	0.000	0.004	94.18
-25	20	-	1.49	-	-	-	-	42.14

2.25E-05

Total

50.43

Beta 0.73  
Gamma 5.34  
Phi 0.85

Hemlo sample/ 240 g/min/ 2 psi/ 100% 0.150-0.212 mm/ Chapter 8/

Size (um)	CONCENTRATE				TAILS				FEED			
	Weight (g)	% Weight	Grade g/t	Rec. (%)	Weight (g)	% Weight	Grade g/t	Rec. (%)	Weight (g)	% Weight	Grade g/t	Rec. (%)
850	0.00	0.00	0.00	ERR	0.00	0.00	0.00	ERR	0.00	0.00	ERR	0.00
600	0.00	0.00	0.00	ERR	0.00	0.00	0.00	ERR	0.00	0.00	ERR	0.00
420	0.00	0.00	0.00	ERR	0.00	0.00	0.00	ERR	0.00	0.00	ERR	0.00
300	0.08	0.11	462414.00	100.00	0.00	0.00	0.00	0.00	0.08	0.00	462414.00	1.45
210	1.50	2.07	631935.00	99.97	11.03	0.38	28.80	0.03	12.52	0.42	75535.57	37.98
150	42.56	58.93	21501.00	99.66	1491.88	50.96	2.10	0.34	1534.44	51.15	598.37	36.86
105	13.46	18.64	29605.00	99.84	449.81	15.36	1.40	0.16	463.27	15.44	861.68	16.03
75	6.40	8.86	12903.00	99.86	294.79	10.07	0.40	0.14	301.18	10.04	274.42	3.32
53	3.40	4.70	9934.00	97.73	173.95	5.94	4.50	2.27	177.35	5.91	194.72	1.39
37	3.38	4.68	8853.00	98.55	141.67	4.84	3.10	1.45	145.05	4.84	209.25	1.22
25	0.98	1.36	10415.00	93.74	88.53	3.02	7.70	6.26	89.51	2.98	121.58	0.44
-25	0.47	0.65	31741.00	44.49	276.12	9.43	66.20	55.51	276.59	9.22	119.05	1.32
Total	72.22	100.00	34150.93	99.02	2927.78	100.00	8.33	0.98	3000.00	100.00	830.20	100.00

Hemlo sample/100% 0.150-0.212 mm/ chapter 8/  
Selection & breakage functions estimation:

Size classes	Geo. size	Sel. Func.	Feed Rec.	Bij	BijCalc	Res	bij	Conc. Rec.
1180	1403	-	0.00	-	-	-	-	-
850	1011	-	0.00	-	-	-	-	-
800	714	-	0.00	-	-	-	-	-
420	499	-	0.00	-	-	-	-	-
300	357	-	1.45	-	-	-	-	-
210	250	-	37.98	-	-	-	-	-
150	125	0.054	36.86	1.088	1.000	0.000	-	99.86
105	89	-	16.03	0.324	0.324	0.000	0.878	99.84
75	63	-	3.32	0.184	0.188	0.000	0.140	99.86
53	44	-	1.39	0.128	0.121	0.000	0.059	97.73
37	30	-	1.22	0.074	0.080	0.000	0.051	98.55
25	20	-	0.44	0.056	0.053	0.000	0.019	93.74
-25	20	-	1.32	-	-	-	-	44.49
Total			23.72			6.6E-05		
				Beta	1.18			
				Gamma	7.07			
				Phi	0.59			

Herold sample/ 240 g/min/ 2 psi/ 100% 0.150-0.212 mm/ Chapter 8/Repeated Test/

Size (um)	CONCENTRATE				TAILS				FEED			
	Weight (g)	% Weight	Grade g/t	Rec. (%)	Weight (g)	% Weight	Grade g/t	Rec. (%)	Weight (g)	% Weight	Grade g/t	Rec. (%)
550	0.00	0.00	0.00	ERR	0.00	0.00	0.00	ERR	0.00	0.00	ERR	0.00
600	0.00	0.00	0.00	ERR	0.00	0.00	0.00	ERR	0.00	0.00	ERR	0.00
420	0.00	0.00	0.00	ERR	0.00	0.00	0.00	ERR	0.00	0.00	ERR	0.00
300	0.15	0.19	763123.00	100.00	0.00	0.00	0.00	0.00	0.15	0.00	763123.00	2.23
210	1.57	1.98	787699.00	99.87	2.31	0.08	714.00	0.13	3.88	0.13	318696.16	24.44
150	45.78	57.92	45816.00	99.47	1478.49	50.34	7.60	0.53	1516.27	50.54	1390.57	41.70
105	17.26	21.84	64849.00	99.68	515.90	17.66	7.00	0.32	533.16	17.77	2106.49	22.21
75	6.71	8.48	33725.00	99.16	248.12	8.49	7.70	0.84	254.82	8.49	894.97	4.51
53	3.29	4.16	23650.00	98.05	154.96	5.31	10.00	1.95	158.25	5.28	501.49	1.57
37	3.07	3.88	22466.00	96.56	185.71	6.36	13.20	3.44	188.78	6.29	377.94	1.41
25	0.97	1.23	27939.00	92.57	87.17	2.99	24.90	7.43	88.44	2.95	331.23	0.58
-25	0.25	0.31	86077.00	30.96	256.01	8.76	185.00	69.04	256.26	8.54	267.69	1.36
Total	79.03	100.00	63069.13	98.58	2920.97	100.00	24.61	1.42	3000.00	100.00	1685.48	100.00

Herold sample/100% 0.150-0.212 mm/ chapter 8/Repeated Test/  
 Selection & breakage functions estimation:

Total of 10 times grinding time (min.) = 50

Size classes	Geo. size	Sel. Func.	Feed Rec.	Bij	BijCalc.	Res.	bij	Conc. Rec.
1180	1403	-	0.00	-	-	-	-	-
850	1011	-	0.00	-	-	-	-	-
800	714	-	0.00	-	-	-	-	-
420	489	-	0.00	-	-	-	-	-
300	357	-	2.23	-	-	-	-	100.00
210	250	-	24.44	-	-	-	-	99.87
150	170	0.0078	41.70	1.000	1.000	0.000	-	99.47
105	125	-	22.21	0.298	0.298	0.000	0.702	99.88
75	68	-	4.51	0.155	0.158	0.000	0.143	99.16
53	63	-	1.57	0.108	0.100	0.000	0.050	98.05
37	44	-	1.41	0.081	0.085	0.000	0.045	98.58
25	30	-	0.58	0.043	0.043	0.000	0.018	92.57
-25	20	-	1.38	-	-	-	-	30.08
Total			31.84			5.8E-05		

Beta 1.21  
 Gamma 6.53  
 Phi 0.85

Hemlo sample/240 g/min/ 100% 0.053-0.075 mm/ Chapter 8/

Size (um)	CONCENTRATE				TAILS				FEED			
	Weight (g)	% Weight	Grade g/t	Rec. (%)	Weight (g)	% Weight	Grade g/t	Rec. (%)	Weight (g)	% Weight	Grade g/t	Rec. (%)
850	0.00	0.00	0.00	ERR	0.00	0.00	0.00	ERR	0.00	0.00	ERR	0.00
600	0.00	0.00	0.00	ERR	0.00	0.00	0.00	ERR	0.00	0.00	ERR	0.00
420	0.00	0.00	0.00	ERR	0.00	0.00	0.00	ERR	0.00	0.00	ERR	0.00
300	0.09	0.14	4017.00	100.00	0.00	0.00	0.00	0.00	0.09	0.00	4017.00	0.02
210	1.08	1.82	2082.00	100.00	0.00	0.00	0.00	0.00	1.08	0.04	2082.00	0.14
150	6.02	10.11	1865.00	100.00	0.00	0.00	0.00	0.00	6.02	0.20	1865.00	0.70
105	6.34	10.64	4476.00	93.12	8.15	0.28	257.00	6.88	14.49	0.48	2101.92	1.91
75	1.82	3.05	168649.00	99.33	11.36	0.39	182.00	0.67	13.17	0.44	23414.74	19.34
53	6.34	10.64	4476.00	99.64	22.50	7.66	15.70	0.96	231.54	7.72	4227.13	61.37
37	18.67	31.35	11863.00	99.33	829.06	28.19	1.80	0.67	847.73	28.26	262.96	13.98
25	9.68	16.25	998.00	89.59	448.79	15.26	2.50	10.41	458.47	15.28	23.51	0.68
-25	9.51	15.98	1180.00	37.67	1417.90	48.22	13.10	62.33	1427.41	47.58	20.88	1.57
Total	59.54	100.00	26304.47	98.19	2940.46	100.00	9.82	1.81	3000.00	100.00	531.66	100.00

Hemlo sample/100% 0.053-0.075 mm/ chapter 8/  
Selection & breakage functions estimation:

Total of 10 times grinding time (min.) = 50

Size classes	Gen. size	Sel. Func.	Feed Rec.	Bij	BijCalc.	Res.	bij	Conc. Rec.
1180	1403	-	0.00	-	-	-	-	-
850	1011	-	0.00	-	-	-	-	-
600	714	-	0.00	-	-	-	-	-
420	499	-	0.00	-	-	-	-	-
300	357	-	0.02	-	-	-	-	100.00
210	250	-	0.14	-	-	-	-	100.00
150	178	-	0.70	-	-	-	-	100.00
105	125	-	1.91	-	-	-	-	93.12
75	89	-	19.34	-	-	-	-	99.33
53	63	0.0135	61.37	1.000	1.000	-	-	99.64
37	44	-	13.98	0.154	0.154	0.000	0.846	99.33
25	30	-	0.88	0.113	0.113	0.000	0.041	89.59
-25	20	-	1.87	-	-	-	-	37.67
Total			16.53			4.8E-10		

Beta 0.83  
Gamma 11.78  
Phi 0.83

Hemlo sample/ 240 g/min/ 2 psi/ 100% 0.037-0.053 mm/ Chapter 8/

Size (um)	CONCENTRATE				TAILS				FEED			
	Weight (g)	% Weight	Grade g/t	Rec. (%)	Weight (g)	% Weight	Grade g/t	Rec. (%)	Weight (g)	% Weight	Grade g/t	Rec. (%)
850	0.00	0.00	0.00	ERR	0.00	0.00	0.00	ERR	0.00	0.00	ERR	0.00
600	0.00	0.00	0.00	ERR	0.00	0.00	0.00	ERR	0.00	0.00	ERR	0.00
420	0.22	0.30	77.20	21.79	4.94	0.17	12.40	78.21	5.16	0.17	15.18	0.00
300	4.54	6.23	93.80	83.37	132.80	4.54	0.64	16.63	137.34	4.58	3.72	0.02
210	14.91	20.44	256.80	95.69	522.13	17.84	0.33	4.31	537.03	17.90	7.45	0.19
150	19.11	26.21	272.50	75.99	685.31	23.41	2.40	24.01	704.42	23.48	9.73	0.32
105	13.53	18.56	595.70	70.71	538.51	18.40	6.20	29.29	552.04	18.40	20.65	0.53
75	8.96	12.30	2315.90	84.92	326.19	11.14	11.30	15.08	335.15	11.17	72.94	1.14
53	5.49	7.53	32355.40	92.75	193.23	6.60	71.90	7.25	198.72	6.62	963.97	8.92
37	4.58	6.28	26648.00	94.53	119.04	4.07	814.90	5.47	123.63	4.12	14348.80	82.63
25	1.10	1.51	53525.40	82.95	90.18	3.08	134.50	17.05	91.28	3.04	779.27	3.31
-25	0.46	0.63	58692.20	42.75	314.78	10.75	114.50	57.25	315.24	10.51	199.72	2.93
Total	72.90	100.00	27141.91	92.17	2927.10	100.00	57.42	7.83	3000.00	100.00	715.61	100.00

Hemlo Sample/100% 0.037-0.053 mm/ chapter 8/  
Selection & breakage function estimation:

Size classes	Geo. size	Sel. Func.	Feed Rec.	Bij	BijCalc.	Res.	bij	Conc. Rec.
1180	1403	-	0.00	-	-	-	-	-
850	1011	-	0.00	-	-	-	-	-
600	714	-	0.00	-	-	-	-	-
420	489	-	0.00	-	-	-	-	21.79
300	357	-	0.02	-	-	-	-	83.37
210	250	-	0.19	-	-	-	-	95.89
150	178	-	0.32	-	-	-	-	75.99
105	125	-	0.53	-	-	-	-	70.71
75	89	-	1.14	-	-	-	-	84.92
53	83	-	8.92	-	-	-	-	92.75
37	44	0.0013	82.83	1.000	1.000	0.000	-	94.53
25	30	-	3.31	0.470	0.470	0.000	0.530	82.95
-25	20	-	2.93	-	-	-	-	42.75
Total			6.24			3.7E-13		

Beta 0.57  
Gamma 3.03  
Phi 0.75

Hemlo sample/ 240 g/min/ 2 psi/ 100% 0.037-0.053 mm/ Chapter 8/ Repeated Test/

Size (um)	CONCENTRATE				TAILS				FEED			
	Weight (g)	% Weight	Grade g/t	Rec. (%)	Weight (g)	% Weight	Grade g/t	Rec. (%)	Weight (g)	% Weight	Grade g/t	Rec. (%)
850	0.00	0.00	0.00	ERR	0.00	0.00	0.00	ERR	0.00	0.00	ERR	0.00
600	0.00	0.00	0.00	ERR	0.00	0.00	0.00	ERR	0.00	0.00	ERR	0.00
420	0.08	0.13	21086.00	100.00	0.00	0.00	0.00	0.00	0.08	0.00	21086.00	0.07
300	0.23	0.38	11865.00	100.00	0.00	0.00	0.00	0.00	0.23	0.01	11865.00	0.12
210	1.19	1.97	786.00	100.00	0.00	0.00	0.00	0.00	1.19	0.04	786.00	0.04
150	6.57	10.87	299.00	89.76	13.49	0.46	16.60	10.24	20.06	0.67	109.07	0.10
105	7.53	12.46	797.00	90.95	35.12	1.19	17.00	9.05	42.65	1.42	154.75	0.29
75	3.11	5.14	10591.00	96.27	18.97	0.65	67.20	3.73	22.08	0.74	1548.87	1.50
53	2.39	3.95	89287.00	98.15	41.40	1.41	97.20	1.85	43.79	1.46	4965.75	9.51
37	13.34	22.06	141106.00	98.84	574.12	19.53	38.60	1.16	587.46	19.58	3240.75	83.24
25	15.18	25.12	2362.00	41.22	446.59	15.19	114.50	58.78	461.77	15.39	188.39	3.80
-25	10.83	17.92	979.00	34.55	1809.87	61.57	11.10	65.45	1820.70	60.69	16.86	1.34
Total	60.44	100.00	36194.39	95.65	2939.56	100.00	33.85	4.35	3000.00	100.00	762.42	100.00

Hemlo Sample/100% 0.037-0.053 mm/ chapter 8/ Repeated Test/  
 Selection & breakage functions estimation:

Total of 10 times grinding time (min.) =

50

Size classes	Geo. size	Sel. Func.	Feed Rec.	Bij	BijCalc.	Res.	bij	Conc. Rec.
1180	1403	-	0.00	-	-	-	-	-
850	1011	-	0.00	-	-	-	-	-
600	714	-	0.00	-	-	-	-	-
420	499	-	0.07	-	-	-	-	100.00
300	357	-	0.12	-	-	-	-	100.00
210	250	-	0.04	-	-	-	-	100.00
150	178	-	0.10	-	-	-	-	89.76
105	125	-	0.29	-	-	-	-	90.95
75	89	-	1.50	-	-	-	-	96.27
53	63	-	9.51	-	-	-	-	98.15
37	44	0.0011	83.24	1.000	1.000	0.000	-	98.84
25	30	-	3.80	0.261	0.261	0.000	0.739	41.22
-25	20	-	1.34	-	-	-	-	34.55
Total			5.14			5.03E-09		

Beta 1.71  
 Gamma 6.00  
 Phi 0.68

Hemlo sample/ 240 g/min/ 2 psi/ 100% 0.025-0.037 mm/ Chapter 8/

Size (um)	CONCENTRATE				TAILS				FEED			
	Weight (g)	% Weight	Grade g/t	Rec. (%)	Weight (g)	% Weight	Grade g/t	Rec. (%)	Weight (g)	% Weight	Grade g/t	Rec. (%)
850	0.00	0.00	0.00	ERR	0.00	0.00	0.00	ERR	0.00	0.00	ERR	0.00
600	0.00	0.00	0.00	ERR	0.00	0.00	0.00	ERR	0.00	0.00	ERR	0.00
420	0.24	0.32	40.40	6.52	4.82	0.16	29.20	93.48	5.06	0.17	29.74	0.01
300	3.95	5.22	42.70	57.60	112.85	3.86	1.10	42.40	116.80	3.89	2.51	0.02
210	13.32	17.61	129.90	78.36	434.45	14.86	1.10	21.64	447.77	14.93	4.93	0.16
150	21.43	28.32	118.90	83.00	636.63	21.77	0.82	17.00	658.06	21.94	4.67	0.22
105	16.46	21.75	143.90	81.41	540.98	18.50	1.00	18.59	557.44	18.58	5.22	0.20
75	9.63	12.73	128.20	69.11	344.96	11.80	1.60	30.89	354.60	11.82	5.04	0.13
53	4.87	6.44	508.50	69.79	223.51	7.64	4.80	30.21	228.38	7.61	15.55	0.25
37	3.72	4.92	55812.20	93.22	247.90	8.48	60.90	6.78	251.62	8.39	885.34	15.64
25	1.69	2.24	394675.20	89.33	91.74	3.14	1310.20	10.67	93.43	3.11	12058.07	79.09
-25	0.35	0.46	131155.70	74.14	286.50	9.80	55.10	25.86	286.85	9.56	212.78	4.29
Total	75.67	100.00	16780.46	89.15	2924.33	100.00	52.83	10.85	3000.00	100.00	474.78	100.00

Hemlo Sample/100% 0.025-0.037 mm/ chapter 8/  
Selection & breakage functions estimation:

Total of 10 times grinding time (min.) = 50

Size classes	Geo. size	Sel. Func.	Feed Rec.	Bij	BijCalc.	Res.	bij	Conc. Rec.
1180	1403	-	0.00	-	-	-	-	-
850	1011	-	0.00	-	-	-	-	-
600	714	-	0.00	-	-	-	-	-
420	489	-	0.01	-	-	-	-	8.52
300	357	-	0.02	-	-	-	-	57.80
210	250	-	0.16	-	-	-	-	78.36
150	178	-	0.22	-	-	-	-	83.00
105	125	-	0.20	-	-	-	-	81.41
75	89	-	0.13	-	-	-	-	89.11
53	63	-	0.25	-	-	-	-	69.79
37	44	-	15.84	-	-	-	-	93.22
25	30	0.0002	79.09	1.000	1.000	0.000	-	89.33
-25	20	-	4.29	-	-	-	1.000	74.14
Total			83.38			0		

Beta 0.50  
Gamma 0.10  
Phi 0.50

Hemlo sample/ 240 g/min/ 2 psi/ 100% -0.025 mm/ Chapter 8/

Size (um)	CONCENTRATE				TAILS				FEED			
	Weight (g)	% Weight	Grade g/t	Rec. (%)	Weight (g)	% Weight	Grade g/t	Rec. (%)	Weight (g)	% Weight	Grade g/t	Rec. (%)
850	0.00	0.00	0.00	ERR	0.00	0.00	0.00	ERR	0.00	0.00	ERR	0.00
600	0.00	0.00	0.00	ERR	0.00	0.00	0.00	ERR	0.00	0.00	ERR	0.00
420	0.49	0.68	21.70	6.65	4.71	0.16	31.70	93.35	5.20	0.17	30.76	0.01
300	5.99	8.29	95.80	96.64	79.75	2.72	0.25	3.36	85.74	2.86	6.93	0.03
210	13.69	18.93	233.40	94.62	363.11	12.40	0.50	5.38	376.80	12.56	8.96	0.15
150	17.65	24.41	266.70	84.60	658.96	22.51	1.30	15.40	676.61	22.55	8.22	0.25
105	13.05	18.05	351.00	75.88	582.51	19.90	2.50	24.12	595.56	19.85	10.14	0.27
75	8.60	11.90	329.90	82.61	351.38	12.00	1.70	17.39	359.99	12.00	9.54	0.16
53	5.02	6.94	341.90	45.56	227.80	7.78	9.00	54.44	232.82	7.76	16.18	0.17
37	4.17	5.76	4834.60	58.89	244.55	8.35	57.50	41.11	248.71	8.29	137.54	1.55
25	1.94	2.68	389561.80	92.85	94.54	3.23	614.30	7.15	96.47	3.22	8419.16	36.77
25	1.72	2.38	684856.30	87.76	320.30	10.94	311.50	12.24	322.09	10.74	4158.05	60.64
Total	72.32	100.00	27204.07	89.07	2927.68	100.00	82.43	10.93	3000.00	100.00	736.22	100.00

Hemlo Sample/ 100% -0.025 mm/ chapter 8/  
Selection & breakage functions estimation:

Size classes	Geo. size	Sel. Func.	Feed Rec.	Conc. Rec.
1180	1403	-	0.00	-
850	1011	-	0.00	-
600	714	-	0.00	-
420	499	-	0.01	8.85
300	357	-	0.03	96.64
210	250	-	0.15	94.62
150	178	-	0.25	84.60
105	125	-	0.27	75.88
75	89	-	0.16	82.61
53	83	-	0.17	45.56
37	44	-	1.55	58.89
25	30	-	38.77	92.85
25	20	-0.0000	80.84	87.76
Total			0.00	